technische universität dortmund

Max-Planck-Institut
für molekulare Physiologie

DISSERTATION

DISCOVERY AND TARGET IDENTIFICATION OF SMALL MOLECULE AUTOPHAGY INHIBITORS

Zur Erlangung des akademischen Grades eines
Doktors der Naturwissenschaften (Dr. rer. nat.)
von der Fakultät für Chemie und Chemische Biologie
an der Technischen Universität Dortmund

vorgelegt von
Bachelor of Science Lucas Robke
aus Wuppertal / Nordrhein-Westfalen

Dekan:	Prof. Dr. Roland Winter
1.	Prof. Dr. Herbert Waldmann
2.	Prof. Dr. Martin Engelhard

Die vorliegende Dissertation entstand in dem Zeitraum von April 2014 bis September 2017 unter Anleitung von Prof. Dr. H. Waldmann an der Fakultät für Chemie und Chemische Biologie der Technischen Universität Dortmund und dem Max-Planck-Institut für Molekulare Physiologie in Dortmund.

Teile dieser Arbeit wurden bereits in folgendem Beitrag veröffentlicht:

Robke, L. et al. Phenotypic Identification of a Novel Autophagy Inhibitor Chemotype Targeting Lipid Kinase VPS34. Angew. Chem. Int. Ed. 56, 8153–8157 (2017).

Für Ruth und Benni

Dans les champs de l'observation le hasard ne favorise que les esprits préparés.

Louis Pasteur

Lecture, University of Lille, 7 December 1854

Table of Contents

1 Preface

Pharmacologically active substances have been applied in medicine for at least 5300 years.[1] Ever since, mankind has tried to enlarge the assortment of bio-active substances, in order to fight diseases and ultimately maintain health and quality of life. For thousands of years, but especially in the last century, drug discovery has been the scientific key driver for the progression of medicine.[2]

One process that attracts notable attention due to its high potential for the development of new drugs is autophagy.[3] Autophagy is a catabolic process which plays a crucial role in the development, differentiation, homeostasis and survival of cells. It mediates the degradation of cellular components especially under conditions such as starvation, and the misregulation of autophagy is implicated in various diseases, ranging from cancer to microbial infections and neurodegenerative diseases.

Small organic molecules still account for 90% of today's pharmaceuticals and drug-like modulators of biological processes have proven to be valuable reagents and tools for chemical biology.[4] However, to date only a few modulators of autophagy have been reported. Therefore the goal of this work was to identify and characterize new autophagy inhibitors. A cell-based assay was performed to identify inhibitors of autophagic flux. Based on hits from the cellular assay compound libraries were synthesized to provide information regarding structure-activity relationships. The identification of the targets of the inhibitors was achieved through affinity chromatography, mechanistic reasoning and the process of elimination. The examination of the targets' roles in autophagy enlarged our understanding of the autophagic process and allowed us to evaluate their potential as new drug targets. Ultimately, the identified and characterized novel chemotypes for autophagy inhibition provide valuable tools to study their target protein's function as well as the autophagic process more precisely. They can furthermore provide promising starting points for drug discovery focusing on cancer.

2 Introduction

2.1 Historic Prelude

Autophagy is a highly conserved catabolic process, found in eukaryotes, which plays a crucial role in the development, differentiation, homeostasis and survival of cells. The term autophagy or autophagocytosis, was introduced by Christian de Duve, who first discovered lysosomes, in 1963[5] and derives from the Greek words "auto" meaning "self" and "phagein", which is "to eat". The reason for the word autophagy was its descriptive character for the phenomenon that vesicles engulfing cytoplasm and organelles showed different levels of degradation of their content.[6–8] It was not until 1992 that Ohsumi and coworkers demonstrated that autophagy is not only conserved from yeast to mammals but also similar in its morphology.[9] This finding was the foundation for the first genomic studies on autophagy, performed in Ohsumi's laboratory.[10] Further genetic experiments revealed the first **A**u**T**opha**G**y-related-gene (ATG1) in 1997.[11] Since then, many ATGs have been discovered, numbered according to the order of their discovery rather than their function, elucidating the mechanism behind autophagy more and more. The most recent ATG (ATG41) was identified in 2015.[12] For the significant breakthroughs by genetic screens for autophagy mutants, Ohsumi was eventually awarded the Nobel Prize in Physiology and Medicine in 2016.

2.2 Autophagosome Formation

The last decades of research have unraveled several different types of autophagy including macroautophagy,[13] microautophagy,[14] chaperone-mediated autophagy,[15] and mitophagy[16]. Although they can differ substantially in their regulation, selectivity and degradative capacity, a shared feature of all of them is their ability to mediate the degradation of cellular components within specialized subcellular compartments. For macroautophagy, hereafter referred to as autophagy, the degradation takes place via cytosolic vesicles termed autophagosomes. (Figure 3).[17,18] During autophagy the autophagosomes are formed, starting from a double-membrane mantle enwrapping cytosolic components. This open pre-autophagosomal structure is called phagophore and its site of formation is called the phagophore assembly site (PAS, Figure 1).[19] At the beginning of this process, the PAS is not much more than a sack of a membrane double-layer together with a few of the core proteins initiating the metamorphosis to form an autophagosome. Thus, during this metamorphosis the ATGs, or their mammalian equivalents, colocalize with the PAS and the phagophore.

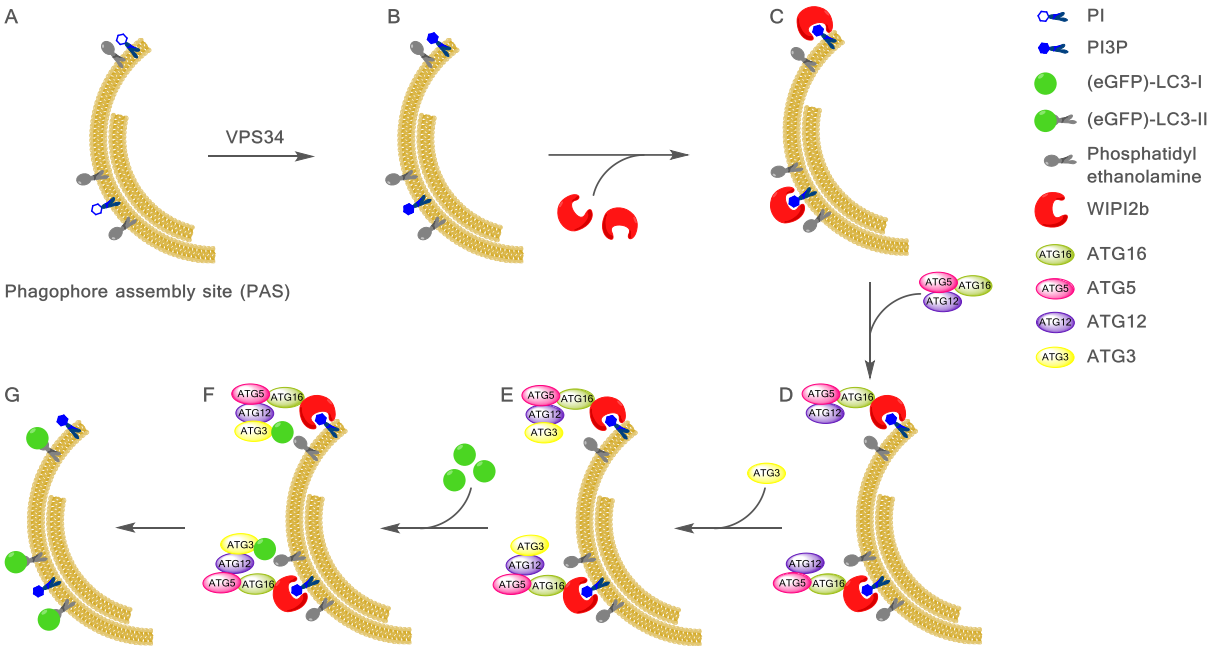

Figure 1: Schematic representation of the phagophore assembly. **A**: The phagophore assembly site (PAS) is an assemblage of membranes with a distinctive lipid pattern, which play a role in the phagophore assembly, and specific proteins. **B**: VPS34, the lipid kinase within the PI3KC3 complex, phosphorylates phosphatidylinositol (PI) to phosphatidylinositol-3-phosphate (PI3P). **C**: WIPI2b binds to and is recruited by PI3P. **D**: WIPI2b itself recruits ATG16, which binds to ATG5, which again is conjugated to ATG12. The ATG16-ATG5-ATG12 complex resembles an E3-like complex of the ubiquitin system. **E**: The recruitment of the E3-like complex follows the recruitment of an E2-like enzyme, ATG3. **F**: ATG3 promotes the lipidation of LC3-I to LC3-II. **G**: The result of the processing cascade is the phagophore containing LC3-II, which is important for the expansion of the phagophore as well as the recruitment of adapter proteins delivering cargo to the eventual autophagosome.

Among these ATGs, only ATG9 is conserved throughout all species, as it possibly possesses the most essential function of all, which is recruiting membrane to the PAS and the phagophore. For this purpose ATG9 shuttles between the PAS and non-PAS structures, which are species dependent and in human are late endosomes and the trans-Golgi network.[20] This return of ATG9 from the PAS is catalyzed by several key proteins, such as ATG1, a serine-threonine protein kinase, in human called ULK1, which it is referred to within this thesis.[21] ULK1's kinase activity, itself controlled by several regulators, with the most conserved one being the regulatory subunit ATG13, controls the magnitude of autophagy. In addition to ULK1, the retrieval of ATG9 from the PAS is facilitated by its interaction with ATG2 and ATG18. The latter is recruited to the PAS by binding to phosphatidylinositol-3-phosphate (PI3P), which is generated by the only member of the class-3-phosphatidylinositol-3-kinase (PI3KC3), VPS34.[22–25] VPS34 acts within two different complexes of different proteins, regulating its activity and localization. These two complexes have different functions. One complex acts in vesicular trafficking including endosomes and lysosomes, whilst the other complex includes ATG6,

(referred to within this thesis as Beclin-1 according to the human nomenclature) and is selectively responsible for autophagy. In contrast to Beclin-1, VPS15, a protein kinase, is present in both complexes, regulating VPS34's association with membranes.

Besides ATG18 in mammalian cells also WD repeat domain phosphoinositide-interacting protein 2b (WIPI2b) binds to and is recruited by PI3P to the autophagosome formation site.[26] WIPI2b recruits several further proteins, which form a complex, functioning similarly to an ubiquitin E3-ligase. This complex consists of ATG16 binding to ATG5, which is conjugated to ATG12. Following the recruitment of the E3-like complex the E2-like ATG3 protein is recruited. Together with the E1-like ATG7 this ubiquitin like system facilitates the conjugation of LC3-I to LC3-II.[27] For this to occur, LC3-I must first be activated by the cysteine protease ATG4, which cleaves off the C-terminus, revealing a C-terminal glycine, which is then conjugated with phosphatidylethanolamine (PE) to form LC3-II.[28] The PE-moiety allows LC3-II to associate itself to the autophagosomal membrane.

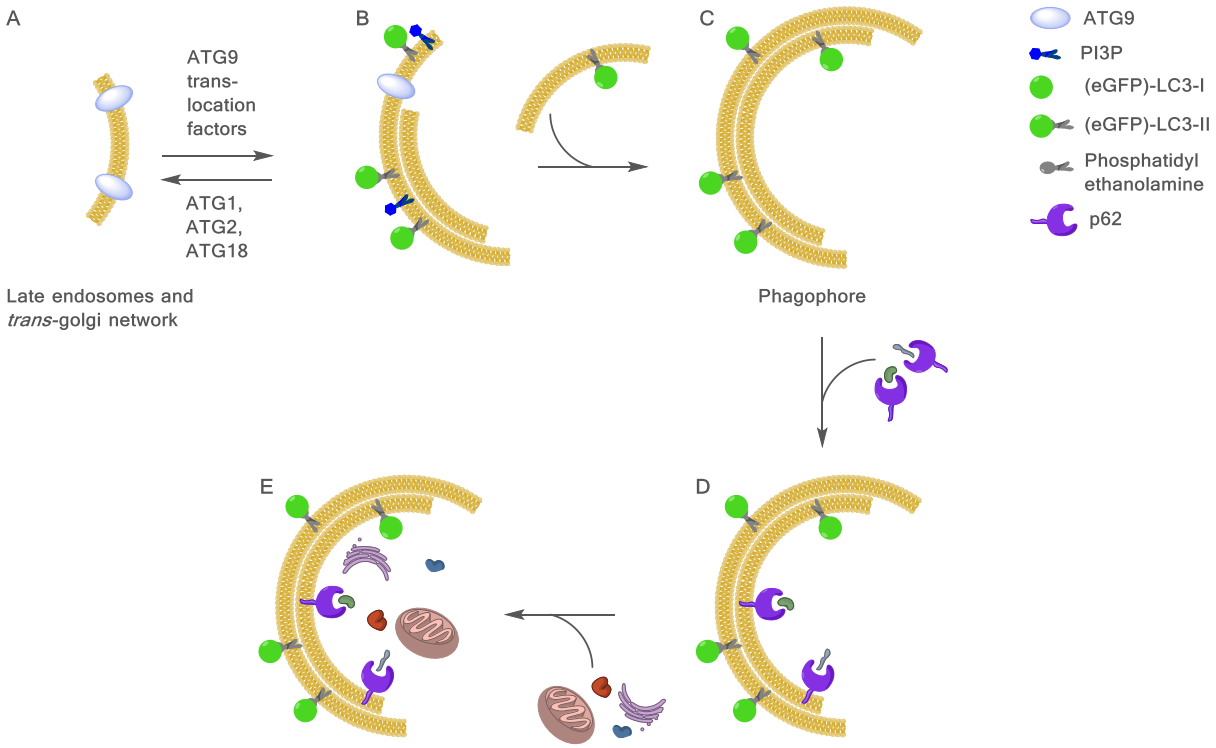

Figure 2: Schematic representation of the phagophore expansion and recruitment of cytosolic components to the growing phagophore by p62. **A**: Shuttling of ATG9 from peripheral membrane sites to the phagophore assembly site (PAS) is promoted by ATG9 translocation factors whereas its retrieval is supported by ATG1, ATG2 and ATG18. ATG18 is recruited to the PAS by PI3P, depicted in blue. **B** and **C**: ATG9's presence at the PAS allows recruitment of more membrane fractions to the PAS forming the phagophore. **D**: The phagophore harbours lipidated LC3 (LC3-II), which binds to p62. Via this binding p62 delivers ubiquinated proteins, to be degraded, which p62 also binds to, to the growing phagophore. **E**: Other adapter proteins recruit more cargo and more cytosolic portions are non-selectively engulfed by the phagophore.

The LC3 family, which in yeast is referred to as ATG8, fulfills several essential functions in autophagy, such as phagophore extension, recruitment of cytosolic components to be degraded and eventually phagophore closure to form the autophagosome.[17]

In addition to LC3-II there are several more proteins, recruiting cargo to be degraded to the phagophore. One of them is sequestosome 1, also known and hereafter referred to as p62. This adapter protein binds to polyubiquitinated aggregates and LC3, thus delivering proteins to be degraded to the autophagosome, by acting like a chaperone.[29]

Autophagosomes, which measure 300 – 900 nm in size, are trafficked along microtubules to meet and ultimately fuse with another membrane enclosed vesicle, termed lysosome.[30] Upon fusion with the autophagosome, the lysosome delivers degradative enzymes into the newly formed vesicle, which is referred to as an autophagolysosome (Figure 3). The hydrolases are activated by the acidic pH of 4.5 – 5. The pH is generated by pumping protons into the lysosome. The proton pump, called V-ATPase, uses ATP in order to maintain the pH gradient across the lysosomal membrane.[31] For reducing the electrochemical gradient across the membrane, while maintaining the proton gradient as strong as possible, other ion pumps release different cations from the lysosomal lumen into the cytosol.

Upon completion of autophagosome formation the ATG16-ATG5-ATG12 complex, which resides mainly on the outer membrane layer, is released into the cytosol. By contrast LC3-II has no preference for any of the two membrane layers of the autophagosome and the LC3-II in the inside of the autophagosome eventually undergoes degradation in the autophagolysosome. The same happens to p62 and its cargo, as well as every other cytosolic portion and the inner membrane layer of the autophagosome.

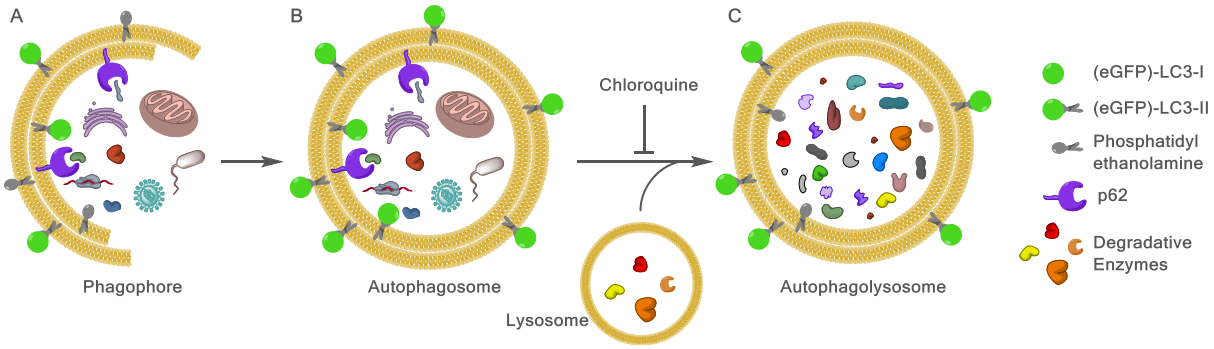

Figure 3: Schematic representation of autophagosome maturation and the autophagy assay principle. **A**: Autophagy induction leads to a lipidation of LC3-I with phosphatidylethanolamine to generate LC3-II. Following LC3 lipidation closure of the phagophore occurs to form the autophagosome. **B**: The cytosolic fractions to be degraded are completely engulfed by the autophagosomal membrane, where LC3-II is found. **C**: Fusion of the autophagosome and the lysosome forms the autophagolysosome. This step is inhibited by the small molecule Chloroquine causing an accumulation of LC3-II at the autophagosomes. In case of an eGFP-LC3 transfected cell line, the autophagosomes are thus visible as green puncta. Autophagy inhibitors are able to revert this accumulation.

2.3 Autophagy Regulation

Although autophagosome biogenesis is mostly observed for cells challenged by stress including starvation, it also occurs at a basal level. The core machinery for the described macroautophagy is also found for different sub-types of autophagy. Nonetheless there can be substantial differences between autophagy induced by starvation, pathogens, other pathological events or even pharmacological treatment.[32]

This illustrates that the multistep process of the formation, maturation and transport of the autophagosomes is also carried out by the tightly regulated interplay of many different proteins (cf. Figure 1-3). The regulation itself is controlled and modulated in its extent by upstream signaling such as growth factors, the concentration of amino acids and the energy level of the cell. Although they are not yet fully elucidated, two major signaling pathways regulating autophagy have been identified (Figure 4). The mammalian target of rapamycin (mTOR) is the lynchpin of one of these pathways (Figure 4, left hand side). One of the various signals controlling mTOR is the pathway that acts via PI3KC1a and Akt.[33]

The class Ia lipid kinase PI3K, activated by growth factors and insulin binding to cell surface receptors, converts phosphatidylinositol-4,5-bisphosphate (PIP_2) to phosphatidylinositol-3,4,5-trisphosphate (PIP_3). Proteins containing a pleckstrin homology (PH) domain, including protein kinase B, also called Akt, bind to these membrane lipids and are recruited by them.[34]

Akt phosphorylates other proteins, among them the tuberous sclerosis complex (TSC), which consists of the two subunits TSC1 and TSC2, which form a heterodimer. TSC1-TSC2 is an upstream regulator of the RAS homolog enriched in brain (RHEB), which directly activates the mTOR complex 1 (mTORC1).[35] Moreover mTOR's function is to integrate many signals, including energy status by means of amino acid and glucose levels as well as growth factors. It controls these signals via its kinase activity to downstream effectors including ULK1, which relays the signal to the PI3KC3 complex. In this regard starvation inhibits mTOR, leading to the initiation of autophagy. In addition to cellular signaling the pharmacological inhibitor Rapamycin also inhibits mTORC1 and thus initiates autophagy.[36] mTORC1 gains its function of sensing energy levels and is regulated by the activity of AMPK, whose activity depends on the AMP/ATP ratio within the cell. Furthermore AMPK inhibits mTOR upon hypoxic conditions thus inducing autophagy.[37]

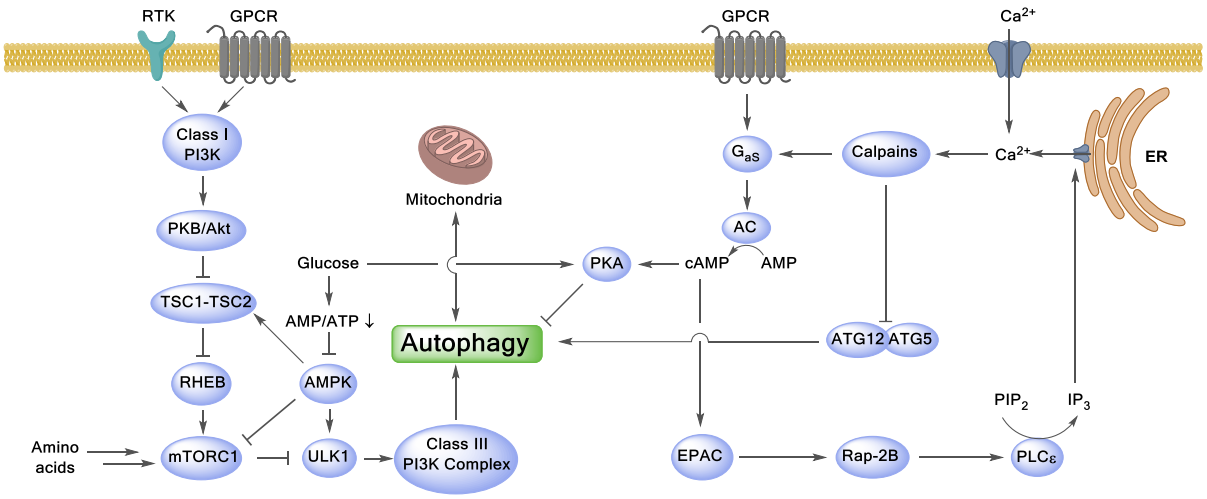

Figure 4: The two major pathways regulating autophagosome formation. Left: The signal transduction acts via mTORC1 as the lynching point. Right: PLCε and calpain dependent signaling pathway. Center: PKA is activated in the presence of cAMP and glucose, leading to autophagy inhibition. Mitochondria and autophagy are highly interconnected in their regulation. RTK: Receptor tyrosine kinase; GPCR: G-protein coupled receptor; PI3K: phosphoinositide 3-kinase; PKB: Protein kinase B; TSC: Tuberous sclerosis complex; Rheb: Ras homolog enriched in brain; AMPK: AMP-activated protein kinase; ULK1: Unc-51 like kinase 1; ER: Endoplasmatic reticulum; $G_{\alpha S}$: α-subunit of the heterotrimeric G-protein of the S-subfamily; AC: Adenylylcyclase; EPAC: Exchange protein directly activated by cAMP; Rap-2B: Ras-related protein 2B; PIP_2: Phosphatidylinositol-4,5-bisphosphate; IP_3: Inositol 1,4,5-trisphosphate. ATG: Proteins expressed by the AuTophaGy-related-genes (ATGs); PKA: Protein kinase A.

In the second pathway an increased concentration of cyclic AMP (cAMP) and Ca^{2+} inhibits autophagy by the activation of calpains (Figure 4, right hand side).[38] In this mTOR independent pathway G_S, cAMP, EPAC, PLC, IP3, Ca^{2+} and calpains are linked. Increased Ca^{2+} levels within the cell inhibit autophagy by activating calpains, Ca^{2+} dependent cysteine proteases, which in return cleave ATG12 from ATG5 and thereby inactivate them.[39] Conversely chemical inhibitors of calpains including calpastatin and calpeptin induce autophagy.[40]
The calcium levels, required for calpain activation, are either resulting from extracellular influx or released from the endoplasmatic reticulum (ER) upon binding of the second messenger inositol-1,4,5-trisphosphate (IP_3) to its receptor IP_3R. IP_3 is generated by the phospholipase C (PLC), which itself is activated by a signaling cascade starting from elevated cAMP levels mediating an activation of the small G protein Rap-2B via EPAC.

During starvation, autophagy is drastically increased compared to its basal level. Besides the mTOR pathway the protein kinase A (PKA) pathway has emerged to be a major sensor of nutrient status, primarily for glucose levels, and a negative regulator of autophagy.[41] In nutrient rich conditions the small Ras GTPases trigger higher cAMP levels leading to the activation of PKA and a constitutively active Ras/PKA pathway has been shown to inhibit mTOR-inhibition induced autophagy, suggesting that the Ras/PKA pathway acts in parallel to the mTOR pathway. To date, several autophagy relevant substrates for PKA have been discussed including ULK1 and LC3.[42,43] However, the mechanism by which PKA controls autophagy is not completely elucidated yet. Conversely autophagy also seems to regulate PKA activity.[44]

In addition to direct metabolites and hormones sphingolipids also regulate autophagy.[45] They are not only a constituent of membranes but also secondary messengers that play important roles in cell signaling, for example by influencing the trafficking and formation of vesicles such as autophagosomes.[46] Within the metabolism of sphingolipids, ceramide is the central molecule, which has effects on cell growth and cell death and the addition of exogenous ceramide as well as an increase of endogenous ceramide levels induce autophagy. Sphingolipid treatment has been shown to reduce the import of nutrients such as amino acids which contributes to their effect of autophagy induction.[47] Another possible mechanism whereby ceramide might induce autophagy is the formation of reactive oxygen species (ROS).[48]

ROS are reactive oxygen containing molecules, such as peroxide, superoxide and hydroxyl radicals. Most ROS are generated by incomplete reduction of oxygen at the electron transport chain. The effect of outbalanced ROS formation causes oxidative stress. For this reason ROS have traditionally been considered as destructive for the cell.

Despite their harmful effects, ROS have also decisive functions in the physiology of the cell, foremost in signaling. This occurs by reactions of ROS with enzymes. For example can ROS oxidize enzymes and thus (in)activate them.[49]

A mechanisms by which ROS might regulate autophagy is the inactivation of ATG4 by oxidation of Cys81, which is essential for its protease activity. ATG4 processes LC3 by cleavage of its C-terminal end, revealing a glycine residue. Besides this function, which appears not to be redox sensitive, ATG4 furthermore delipidates LC3-II on accessible membranes, i.e. the phagophore, autophagosomes and autophagolysosomes. This recycling of LC3 is hindered under oxidative conditions, allowing LC3 to stay lipidated thus initiating autophagy.[50] Despite ATG4's indisputably important role in the effect of ROS on autophagy, there might be several other switches involved that have yet to be elucidated.

In addition to being the major source of ROS formation via the electron transport chain, mitochondria have been shown to be very tightly interconnected with autophagy regulation.[51,52] As well as the formation of ROS in the mitochondria, many metabolites turned over at mitochondria as well as the ATP generated there can influence autophagy. Conversely, autophagy regulates the quality of mitochondria by the selective degradative pathway called mitophagy.[53] Although not completely elucidated, the emerging knowledge of this interplay supports the importance of this organelle within autophagy.

2.4 Disease Relevance

The fact that there are selective and varying forms of autophagy and their regulation illustrates that the purpose of degradation via autophagy is not only to compensate for a temporary lack of nutrients but also for the general survival or homeostasis of the cell by eliminating dispensable, long-lived or even rogue proteins, protein aggregates and cell organelles.
Moreover autophagy has been linked to aging and microbiological infections and the immune system as a whole. Autophagy influences the innate as well as the adaptive immune system and it is tempting to speculate that autophagy evolved from a metabolic pathway to one of the first eukaryotic defense mechanisms. Cellular stress and nutrient deprivation, caused by microbial invasion, might have been the first link between immunity and autophagy followed by the degradation of pathogens through autophagosomes.[54] In mammalian cells the pro-inflammatory signaling by cytokines, such as interleukin-1β (IL-1β) is essential for the immune response towards *Mycobacterium tuberculosis*. Another class of immune effectors are ROS, generated by the NADPH oxidase upon pathogen invasion.[55]

In a similar manner as described for p62, a range of other adaptors, termed sequestosome 1/p62-like receptors (SLRs) are employed by autophagy, in order to capture and eliminate microorganisms including Salmonella and HIV.[56]

Recent studies have proven autophagy to play a crucial role in the degradation of the protein aggregates which cause several neurodegenerative diseases, including Alzheimer's, Huntington's and Parkinson's disease.[57,58] In the case of Parkinson's two mutations have been identified to cause an early onset of the disease. The proteins of the corresponding genes are phosphatase and tensin homolog (PTEN)-induced putative kinase 1 (PINK1) and Parkin. Whereas under healthy conditions PINK1 levels are stable, in the case of depolarized mitochondria PINK1 degradation is inhibited leading to its accumulation and thereby Parkin recruitment. Parkin is an E3 ubiquitin ligase, ubiquitinating outer mitochondrial membrane proteins, leading to the recruitment of p62 and mitophagy. An impairment of this process at any stage or of autophagy in general has been described to cause Parkinson's.[59]
In fact an accumulation of aggregation-prone proteins in general, associated with many neurodegenerative diseases, can be observed when autophagy is inhibited, whereas an activation of autophagy leads to an elimination of these aggregates.[60,61] These findings suggest autophagy upregulation as a potential treatment for several neurodegenerative diseases and indeed lithium, known to increase autophagic turnover, is prescribed in many cases.[62]

Due to its involvement in all these (patho)physiological processes, autophagy is a decisive mechanism for the development, homeostasis and the survival of cells.[63–65]
Although primarily a protective pathway autophagy can be involved in cell death as well. The cell death occurring by excessive autophagy, i.e. the outsized degradation of cellular components, is called autophagic cell death or autosis.[66] In other cases autophagy can lead to the induction of necrosis or apoptosis. However autophagy and apoptosis are usually mutually exclusive: Autophagy generally inhibits the induction of apoptosis whereas activated apoptosis, as assessed by caspase activity, blocks autophagy (Figure 5).[67]

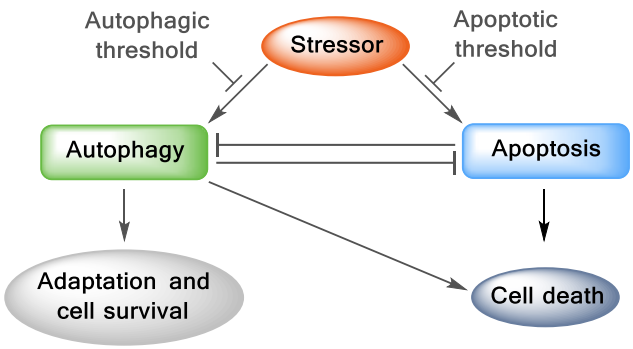

Figure 5: The mutually exclusive relationship between apoptosis and autophagy. Various forms of cellular stress, including toxins, different redox-levels, pathogens and nutrient deprivation can lead to apoptosis or autophagy. The mutual inhibition between both pathways further supports the exclusive activation of one of the two pathways at a time. Adaptation from Maiuri *et al.*[68]

The apparent paradox of a pathway concurrently carrying out protective and destructive purposes is best manifested by autophagy's role in cancer.

By degrading intracellular toxic metabolites and damaged organelles (foremost mitochondria) or misfolded proteins autophagy secures cellular homeostasis as well as integrity of the genome. In this way autophagy is involved in the prevention of cancer.[69] The autophagy promoting functions of several tumor suppressors, including ATG4 and AMPK, further exemplify the tumor suppressing effect of autophagy. Conversely the signaling of PI3K-Akt towards mTOR, found in many different types of cancer, suppresses autophagy.[70] Most evidence suggests that reduced autophagy is a hallmark of cancer.[71]

In addition to its preventive function, autophagy can even kill cancer cells, which have a high apoptotic threshold, due to mutations, by means of autophagic cell death.[72] Induction of autophagy can therefore be beneficial and a therapeutic strategy, in order to kill resistant cancer cells in an established tumor.[70]

However, autophagy's common effect, i.e. described for most tumors, is a pro-survival one. It has been shown to promote the resistance of cancer cells in a tumor towards conditions of cellular stress caused by starvation or cytotoxic agents. In general stress levels in cancer cells are higher, for reasons, which include rapid proliferation, reduced oxygen or nutrient levels within a tumor and higher production of toxic metabolites due to high metabolic demands.[73] For these reasons cancer cells are dependent to a greater extent on autophagy than their non-transformed counterparts, as another way of freeing up necessary energy or dealing with toxic metabolites.[74] In this way autophagy also protects cancer cells from various cytotoxic agents, as applied in chemotherapy (Figure 6).[75]

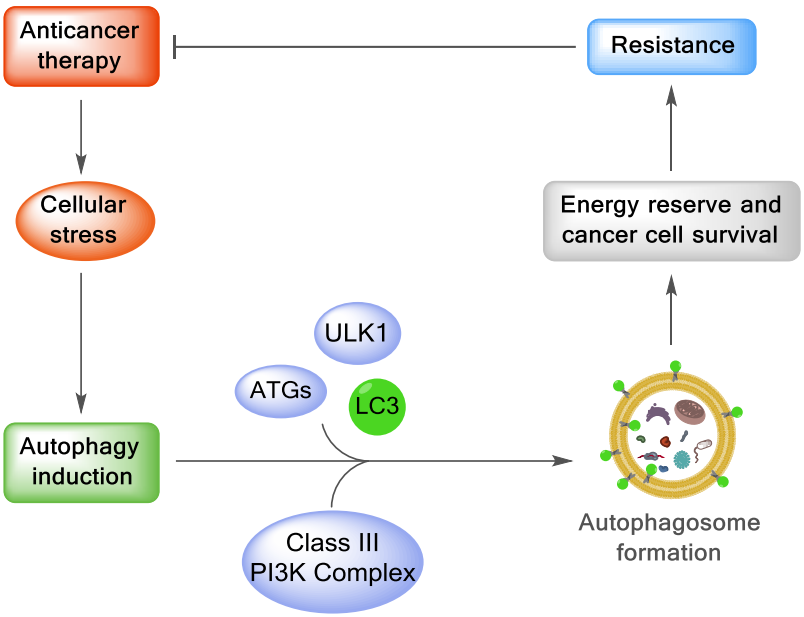

Figure 6: The role of autophagy in anticancer therapy. Chemotherapeutic agents can lead to autophagy-mediated resistance in cancer cells. By inducing protective autophagy the cancer cell is able to deal with the increased stress thus surviving the treatment. Interfering the development of resistance by autophagy inhibitors can sensitize cancer cells towards cytotoxic agents. Adaptation from Chen *et al.*[76]

As a result of these realizations, several pharmacological inhibitors of different steps of the autophagic process have been tested in combinational treatment with chemotherapy as well as radiation. Noteworthy is the match of the expected and observed sensitization of cancer cells by the autophagy inhibitors, suggesting autophagy as an attractive target for cancer treatment.[76] Although cancer cells can be sensitized to chemotherapeutics by means of known autophagy inhibitors, tumors often recover from the treatment and continue to grow. However, the inhibition of autophagy at different stages, such as the autophagosome biogenesis compared to the autophagosome-lysosome fusion, leads to opposing results, when co-treated with cytotoxic agents. This fact underlines that further insights into this pathway are necessary. In this regard it was surprising, that blocking autophagosome formation reduced the potency of Imatinib and Temozolomide as cytotoxic agents whereas the inhibition of autophagosome-lysosome fusion sensitized the cancer cells towards these agents.[77,78] Since the mechanism dependent value of autophagy inhibitors as chemo- or radiation-therapy sensitizers is not fully understood, more studies with different autophagy inhibitors are necessary, in order to rationally design effective anti-cancer therapies. This need is further supported by the side effects of several compounds, especially due to autophagy's involvement and crosstalk in many other biological processes. Since many unanswered questions regarding the double-edged role of autophagy in physiology and pathophysiology remain, there is a strong interest in a deeper understanding of its mechanisms. For this purpose selective autophagy modulators would be valuable reagents.

2.5 Small Molecule Autophagy Modulators

The process of autophagosome biogenesis and maturation is highly regulated by many intra- and extracellular stimuli. Some of them control autophagy by protein expression and long term adaptation can mediate long lasting protective effects for cells suffering from stress.[41] However, autophagy is generally a relatively fast response, occurring within hours to changing circumstances such as nutrient levels. In addition to starvation or ion concentrations, foremost lithium ions, small molecule autophagy regulators have also emerged as valuable tool compounds and potential therapeutics. They can be subdivided into those that induce or enhance autophagy (Table 1), or those that inhibit autophagy (Table 2).

Autophagy inducers might serve as therapeutics against neurodegenerative diseases. The most widely studied autophagy inducer is Rapamycin (Table 1, entry 1), a macrocyclic lactone, which also gave mTOR (the (mammalian) target of Rapamycin) its name. mTOR has several functions and its downstream effects depend strongly on the interaction with effector proteins. For the interaction of mTOR with the regulatory-associated protein of mTOR (Raptor) the complex formed is termed mTORC1. This complex is sensitive to Rapamycin. On the contrary mTORC2, a complex of mTOR with the rapamycin-insensitive companion of mTOR (Rictor), is not inhibited by Rapamycin.[79] The mechanism by which Rapamycin exerts its selectivity for one but not the other mTOR complex is due to the protein FKPB12. Rapamycin first binds to FKBP12 and only the Rapamycin-FKBP12 complex is able to bind to mTOR, specifically blocking its interaction with Raptor but not with Rictor. Thus Rapamycin leaves some of mTOR's functions, i.e. mTORC2's function, unaltered. Small molecule ATP-competitive inhibitors of mTOR's kinase function, such as Torin 1 (Table 1, entry 2), in contrast, directly inhibit mTORC1 and mTORC2, leading to a higher autophagy induction compared to Rapamycin.[80]

The activity of mTOR is furthermore regulated by the signaling of the PI3K-Akt cascade with extracellular input signals from for example receptor tyrosine kinases (RTKs) (Figure 4). In this respect Erlotinib (Table 1, entry 3), an EGFR-antagonist, inhibits the activation of mTOR leading to autophagy induction. In fact, many RTK inhibitors induce autophagy via this pathway, protecting cells, at least partially, against this kind of cancer treatment.[81,82]

Another kinase that can be modulated by small molecules, is AMPK. Metformin, a biguanide, was the first small molecule reported to activate AMPK. Metformin's effect on AMPK was found to be indirect, as a result of inhibition of complex I of the mitochondrial respiration chain and the several accompanied side effects.

Therefore, there are preferable alternatives to Metformin for AMPK activation.[83] Two alternative AMPK activators are A-769662 and AICAR (Table 1, entry 4 and 5), which both target AMPK allosterically.[84–86]

The cyclic pathway of G_S, cAMP, EPAC, PLC, IP_3, Ca^{2+} and calpains (Figure 4, right hand side) regulates autophagy independently of mTOR. Small molecule autophagy inducers that act via this pathway have also been reported. Among them are known pharmacological modulators such as Rilmenidine, Carbamazepine and Verapamil (Table 1, entry 6, 7 and 8), that are already FDA approved. Rilmenidine, already used clinically to treat hypertension, induces autophagy by activating the α_2-adrenergic and imidazoline receptors, thus lowering cAMP levels.[40,87] Inositol-1,4,5-trisphosphate (IP_3) inhibits autophagy in the same cyclic pathway, making compounds lowering IP_3-levels, such as Carbamazepine, autophagy inducers.[40,88] In the same pathway Ca^{2+}-channel inhibitors, such as Verapamil,[40,89] and calpain inhibitors, such as Calpeptin (Table 1, entry 9),[38,40] also block calpain activity, leading to an active ATG5-ATG12 conjugate, which induces autophagy.

Table 1: Selected small molecule autophagy inducers.

Entry	Number	Inhibitor name	Structure	Known targets / Mechanism
1	**1**	Rapamycin[61,90]	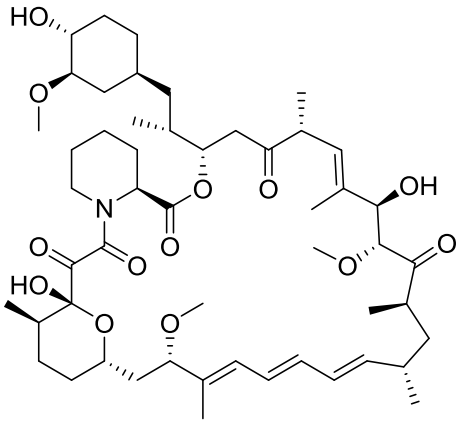	Induces canonical autophagy by inhibiting the formation of mTORC1.
2	**2**	Torin 1[80]	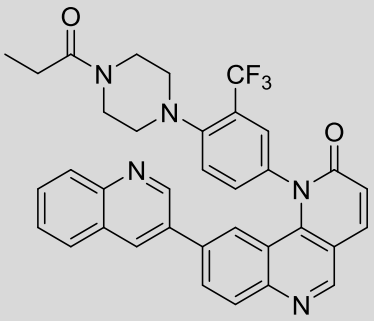	Direct inhibition of mTORC1 and mTORC2 induces autophagy.

3	**3**	Erlotinib[81]	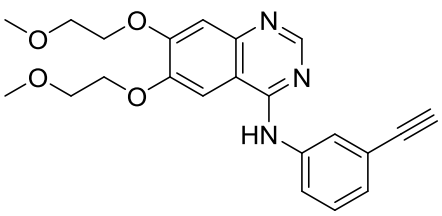	Inhibiting EGFR, thus stimulating the PI3K-Akt-mTOR axis leading to protective autophagy.
4	**4**	A-769662[84,85]	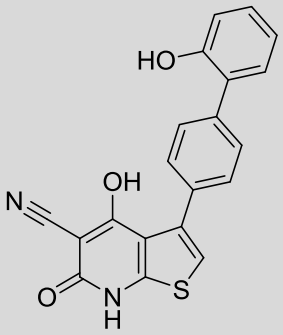	Activates autophagy by allosteric AMPK activation.
5	**5**	AICAR[86]	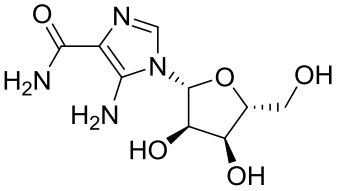	Activates autophagy by allosteric AMPK activation.
6	**6**	Rilmenidine[40,87]	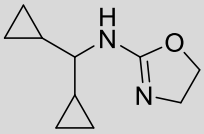	Reduces cAMP levels, leading to induced autophagy.
7	**7**	Carbamazepine[40,88]	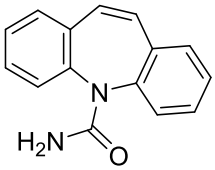	Reduces the intracellular levels of IP_3.
8	**8**	Verapamil[40,89]	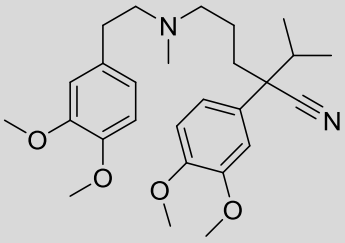	Lowers intracytosolic Ca^{2+} levels by inhibiting L-type Ca^{2+} channels.
9	**9**	Calpeptin[38,40]	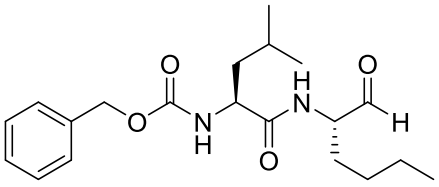	Inhibits calpain-proteases leading to active ATG12-ATG5 conjugates, stimulating autophagosome formation.

Whereas the reported autophagy inducers could potentially serve as treatments against neurodegenerative diseases, several known autophagy inhibitors, alone or in combination with other agents, offer great promise for cancer therapy. Autophagy inhibitors can roughly be subdivided into early-stage inhibitors, i.e. inhibitors of autophagosome formation, and late-stage inhibitors, i.e. inhibitors of the autophagosome-lysosome fusion or autophagolysosome degradation and turnover.

A long known inhibitor of the ATP-dependent vacuolar proton pump (V-ATPase) is Bafilomycin A1 (Table 2, entry 1). By inhibiting the acidification of lysosomes and autophagolysosomes it prevents the degradation of the captured portions to be degraded, thus effectively blocking autophagy.[60,91] The blockade of the degradation leads to an accumulation of autophagolysosomes within the cells.
Another late-stage inhibitor are the very similar compounds Chloroquine and Hydroxychloroquine (Table 2, entry 2 and 3 respectively). Chloroquine has been used for decades against malaria. Although not completely understood it is believed, that (Hydroxy-)chloroquine unfolds its effect as a malaria treatment and as an autophagy inhibitor by accumulating in the lysosomes or their membranes. Lysosomotropic compounds, for example CQ, seem to bind bis(monoacylglycero)phosphates when protonated which stops those from binding sphingolipid hydrolases. This leads to their dissociation from the lysosomal membrane and their subsequent inactivation.[92–95]

The PI3K complex III generates PI3P, which is essential for autophagosome biogenesis. A rather recent study revealed an inhibitor of the ubiquitin-specific peptidases 10 and 13 (USP10 and USP13). These peptidases deubiquitinate a part of the PI3KC3. Thus the first selective and potent autophagy inhibitor (Spautin-1; Table 2, entry 4) leads to an increased degradation of the complex, as the ubiquitinylation signal is no longer suppressed.[96]
Wortmannin, 3-Methyladenine (3-MA), LY294002, SAR405 and VPS34-IN1 inhibit autophagy more directly, though also by affecting PI3P levels (Table 2, entry 5-9). Due to a lack of selective alternatives, Wortmannin, 3-MA and LY 294002 have been used for decades to study the effect of PI3K inhibition. However, they all non-selectively inhibit several isoforms of the PI3K family.[97,98] In addition it has been observed that conditional knockout of VPS34 shows severe differences to 3-MA or Wortmannin treatment, indicating that these inhibitors display VPS34-independent effects, rendering them poor tool compounds for studying autophagy.[22] Recently more potent and selective alternatives have been developed.[99–101] The class III selective PI3K inhibitors SAR405 and VPS34-IN1, developed by Sanofi and Novartis respectively, demonstrate the interest of the pharma industry into the field of autophagy inhibition. Despite the new inhibitors, an expanded toolkit to study autophagy and VPS34 activity would be very beneficial for basic research and potential drug discovery applications.[40,102,103]

Table 2: Selected small molecule autophagy inhibitors.

Entry	Number	Inhibitor name	Structure	Known targets / Mechanism
1	**10**	Bafilomycin A1[60,91]	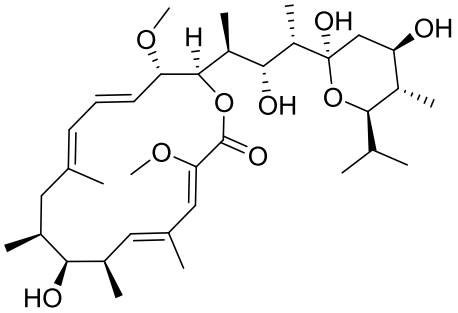	Specific inhibitor of V-ATPase; inhibits autophagosome lysosome fusion.
2	**11**	Chloroquine[92–94]	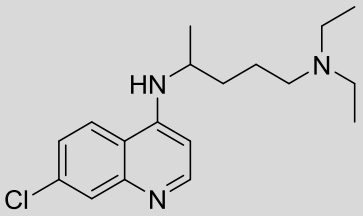	Inhibits autophagosome-lysosome fusion and lysosome acidification.
3	**12**	Hydroxy-chloroquine[94,104]	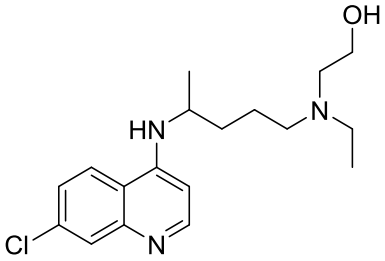	Inhibits autophagosome-lysosome fusion and lysosome acidification.
4	**13**	Spautin-1[96]	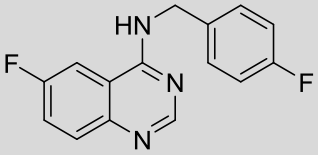	Inhibits USP10 and USP13. Thus lowers beclin 1 levels by promoting its ubiquitylation.
5	**14**	Wortmannin[97,98]	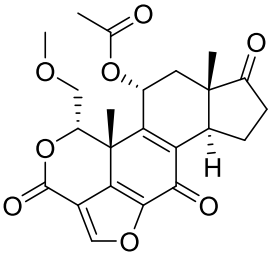	Non-specific, covalent inhibitor of all classes of PI3Ks.
6	**15**	3-Methyl-adenine[97,98]	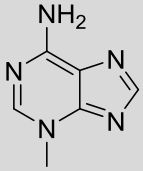	Non-specific inhibitor of class I and III PI3Ks.
7	**16**	LY294002[97,98]	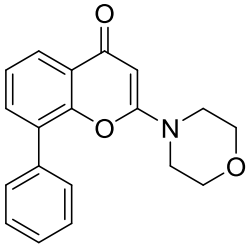	Non-specific inhibitor of class I and III PI3Ks.

8	**17**	SAR405[99,105]	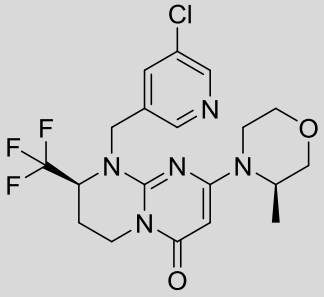	Prevents autophagosome formation by inhibiting VPS34.
9	**18**	VPS34-IN1[100,106]	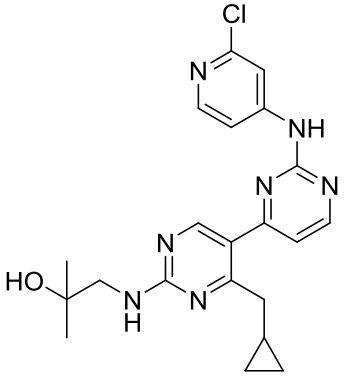	Prevents autophagosome formation by inhibiting VPS34.

Several small molecule modulators of the autophagic process have been identified in the last years and their use has contributed significantly to our understanding of this, in diseases often dysregulated, process. However, there remain many unanswered questions regarding the (patho)physiology of autophagy. For this reason an advanced tool-kit of autophagy modulators is highly desirable and could even present promising starting points for following drug discovery efforts. The need for more chemical tools, in order to study autophagy, is further supported by the diverse off-targets of several small molecules and even diverse biological side effects of selective inhibitors. Bafilomycin A1, for example, has been a valuable tool for studying autophagy. However it has also effects on every other type of lysosomal vesicle, making it difficult to assign biological observations generated with Bafilomycin solely to autophagy. Taken together there is a strong need for new chemical tools modulating the conserved pathway of autophagy.

2.6 Chemical genetics

Chemical genetics aims to investigate biological processes by means of small molecules.[107] In a classical genetic screen organisms or cells are randomly mutated, leading to a different genotype, which is supposed to lead to a different phenotype. A phenotype of interest observed is then examined and the responsible genotype, i.e. mutated gene(s) identified. This extends the understanding of the observed biological process, by connecting phenotype to genotype. In chemical genetics libraries of chemical compounds of low molecular weight, so called small molecules, are employed instead of genetic mutations. Forward chemical genetics, uses small molecules that elicit a desired phenotype to identify the responsible targets for the observed phenotype (Figure 7). Thus the screening is often a phenotypic based screen. Reverse chemical genetics, in contrast, start with a known target (most often a protein) and aims to find novel small molecule modulators for the target of interest, in order to validate it in terms of its disease relevance.

A major advantage of small molecules, in contrary to genetic alterations, is that small molecules allow a better control over the target and thus the biological process in terms of time and magnitude, due to adjustable dosage and reversibility. Additionally small molecules can modulate a specific function of a protein, such as its enzymatic activity or interactions with other proteins, without removing or changing the protein itself.[108] Thus they have benefits as tools for biological studies. Moreover, small molecule tool compounds offer a promising starting point for being developed into drugs. However, chemical genetics also has its drawbacks. An overall drawback is the lack of a general applicability, as some proteins do not have binding sites for small molecule ligands and thus are not druggable.

Out of the lack of ligands new concepts, such as diversity oriented synthesis (DOS) and biology oriented synthesis (BIOS) evolved,[4,109,110] in order to generate more diverse libraries with better rates of biologically active ligands.[108] For reverse chemical genetics one drawback can be the whole process of setting up an assay system for monitoring the effect of the compounds on the protein of interest, including the protein expression, isolation and assay design. A severe drawback and most often the bottleneck for forward chemical genetics is also what makes them often superior over target based screenings; the identification of formerly unknown targets.[111]

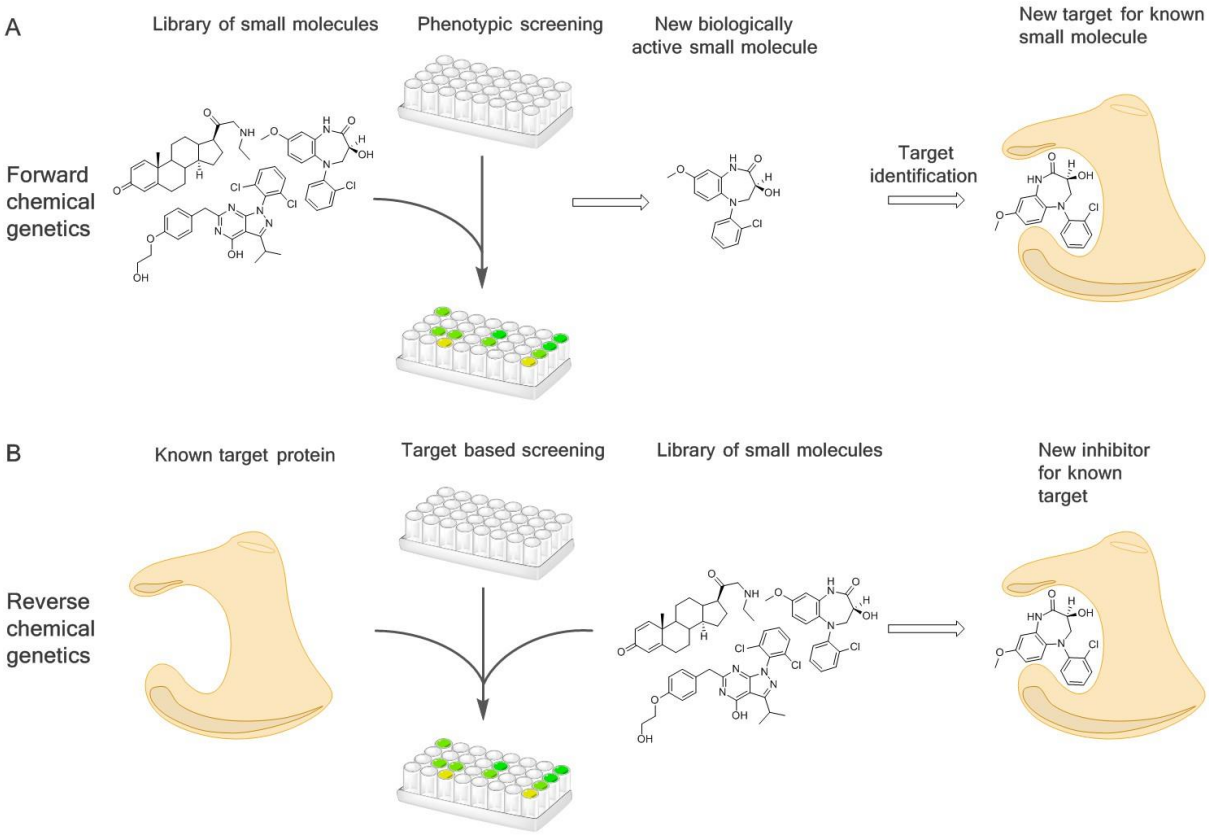

Figure 7: Schematic representation of chemical genetics. **A**: Forward chemical genetics is target agnostic. By phenotypic screening the preconceived aspect is the biological effect. **B**: In reverse chemical genetics, a screen is performed, in order to find new small molecule modulators for a specific protein.

2.6.1 Phenotypic Screening

For the purpose of forward chemical genetics, cell-based screening offers a good starting point for the identification of new biologically active compounds. In the context of cancer, the two most commonly applied cell based assays are reporter-gene or image-based screens.[112]

Disease relevant assays that aim to detect changes in gene expression, not necessarily accompanied by visual morphological or phenotypic changes, are usually carried out as reporter-gene assays. A reporter gene assay measures the expression of one or several proteins of interest by connecting its expression with the expression of the reporter gene. The reporter gene mostly expresses an enzyme catalyzing a reaction leading to a detectable and quantifiable signal, such as the generation of bioluminescent oxyluciferin by the enzyme firefly luciferase. This assay principle has successfully been applied for studies on the developmental pathways, including Wnt, Hedgehog (Hh) and Notch.[113,114]

Image-based screens determine for example changes in cell morphology upon compound treatment, which are detected by means of image analysis. Often applied is a fusion of the green fluorescent protein (GFP) with the protein of interest or the use of fluorescent antibodies.

In both cases the fluorescent signal of GFP or the antibody allows the detection, localization and quantification of the protein of interest within the cell as the readout.[115]
In general phenotypic screening is resurging as an alternative to preconceived target based approaches.[116] By representing a more disease-relevant system, phenotypic screening has a higher chance to reveal compounds possessing a therapeutically-relevant mode of action.[117–119] Moreover hits of a phenotypic screening are already membrane permeable and sample the whole proteome. In this regard it has recently been reported that first-in-class small molecules often derive from phenotypic screens, which further demonstrates the validity of this approach for identifying new druggable targets and lead compounds.[120] On the downside, cell-based SAR studies for hit development as well as target identification provide major challenges.

2.6.2 Target Identification

Following phenotypic screening the target of the small molecule ligand has to be identified. This key step of forward chemical genetics allows the connection between the phenotype and the target protein and the responsible gene. Several approaches for target identification (target-ID) exist, which can be roughly subdivided into genetic-based and affinity-based with the latter one being probably more often used and further advanced.[111] Affinity-based techniques are based on the interaction of the ligand with the target protein. In the first step of the procedure the ligand has to be immobilized to beads or a surface (Figure 8). In the case of affinity chromatography, also referred to as pulldown, cell lysate is added to the immobilized ligand and proteins that bind to the small molecule are retained when the supernatant is removed and the beads are washed, in order to remove non- or unselectively binding proteins. The proteins retained with the biologically active small molecule but not for example with a structurally similar but biologically inactive ligand, are considered to be targets of the small molecule of interest. The detection and identification of retained proteins can be achieved by means of MS/MS based protemics experiments.
By applying the stable isotope labeling by amino acids in cell culture (SILAC) the accuracy of analysis can be increased giving better results. The SILAC version of the pulldown uses different lysates for the positive and the negative control. The different lysates are prepared from cells, which were cultured under either normal conditions or with amino acids containing stable, heavy isotopes, such as ^{13}C and ^{15}N. The heavy isotopes allow the concurrent MS/MS analysis of positive and negative samples, resulting in a better comparison due to possibility of quantification. The quantification is carried out as a ratio between the amount of a retained protein identified, having incorporated heavy amino acids and the protein having the normal, light amino acids incorporated.[121]

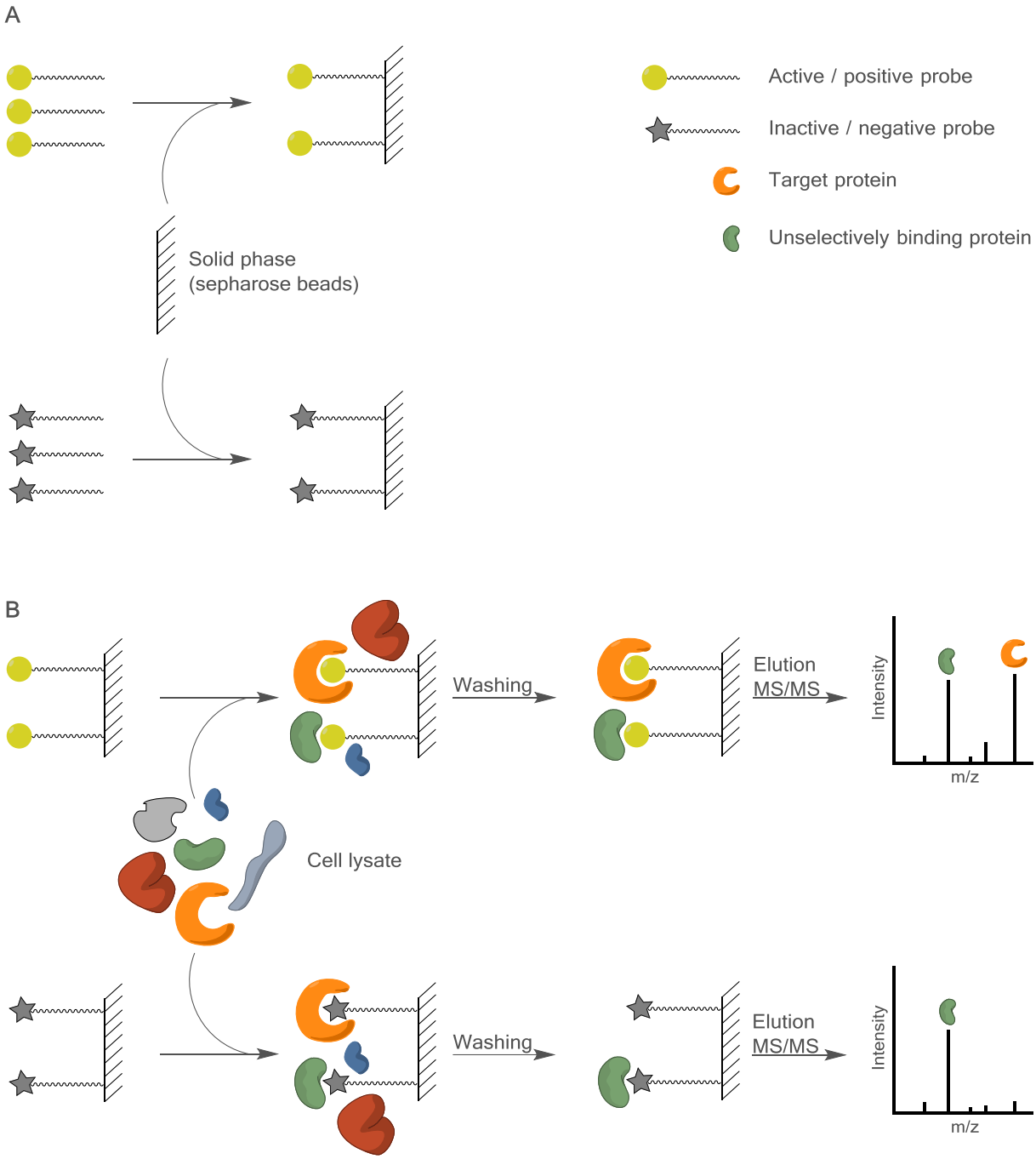

Figure 8: Schematic presentation of the affinity chromatography / pulldown principle. **A**: The active or positive probe, a biologically active compound bearing a linker, and the inactive or negative probe, a biologically inactive, though structurally similar, compound are immobilized to a solid phase, e.g. on sepharaose beads. **B**: The beads are incubated together with cell lysate, allowing the target protein to bind to the probes. Washing removes weakly binding proteins. The comparison of proteins identified by MS/MS analysis for the positive but not for the negative probe are considered as hits.

A drawback of affinity chromatography is often the synthesis of a small molecule derivative that can be immobilized without a loss of affinity towards its target. Experiments that can be performed with the unmodified ligand are based on changed stability towards proteasomal digestion or denaturation induced by heat. Increased temperature leads to the denaturation or melting of proteins. If a small molecule stabilizes or destabilizes its target by binding to it, the melting temperature of the protein changes (Figure 9). Dose and temperature dependent cellular thermal shift analysis (CETSA) can be used for target identification, by performing the assay on a proteome wide level, also referred to as thermal proteome profiling (TPP).[122,123]

In this assay format cell lysates are incubated either with the small molecule of interest or DMSO (as a negative control). Aliquoted lysates are then heated, in order to induce melting of proteins. In this step the compound is expected to affect the stability of its target, while DMSO is supposed to leave the target protein of the compound unaffected. Stabilization of the target protein increases its solubility in the buffer. Denatured and precipitated proteins are separated from still solubilized proteins by a centrifugation step. Subsequently the soluble proteins are digested by proteases and the peptides labeled with isobaric MS-labels, using different labels for each aliquot. Isobaric MS-label have the same mass, but fragment differently in the MS/MS analysis. Thereby they lead to quantifiable differences of same peptides from different samples, which are measured in the same MS/MS analysis. In this way several conditions, such as different temperatures or different compound concentrations, can be analyzed and quantified within one MS/MS analysis. Plotting of the analysis results of the differently treated samples enables the depiction of melting curves. The melting curves for every protein, that melts upon increased temperature (meltome) has to be analyzed. Proteins, that are significantly stabilized or destabilized by the small molecule ligand are counted as hits and considered for further in depth analysis.

After successful discovery of a bio-active compound and target identification, the versatility of the chemical compound is by far not exhausted. It can be used as a valuable tool, in order to study the mechanistic involvement of its target in the pathway of interest and study upstream and downstream signaling of the protein. Additionally, due to the interconnection of several cellular signaling pathways, the repurposing of the small molecule for further studies in different fields further increases the value of chemical tool compounds. In summary chemical genetics offers great possibilities for the discovery of new drug targets and first in class drugs.

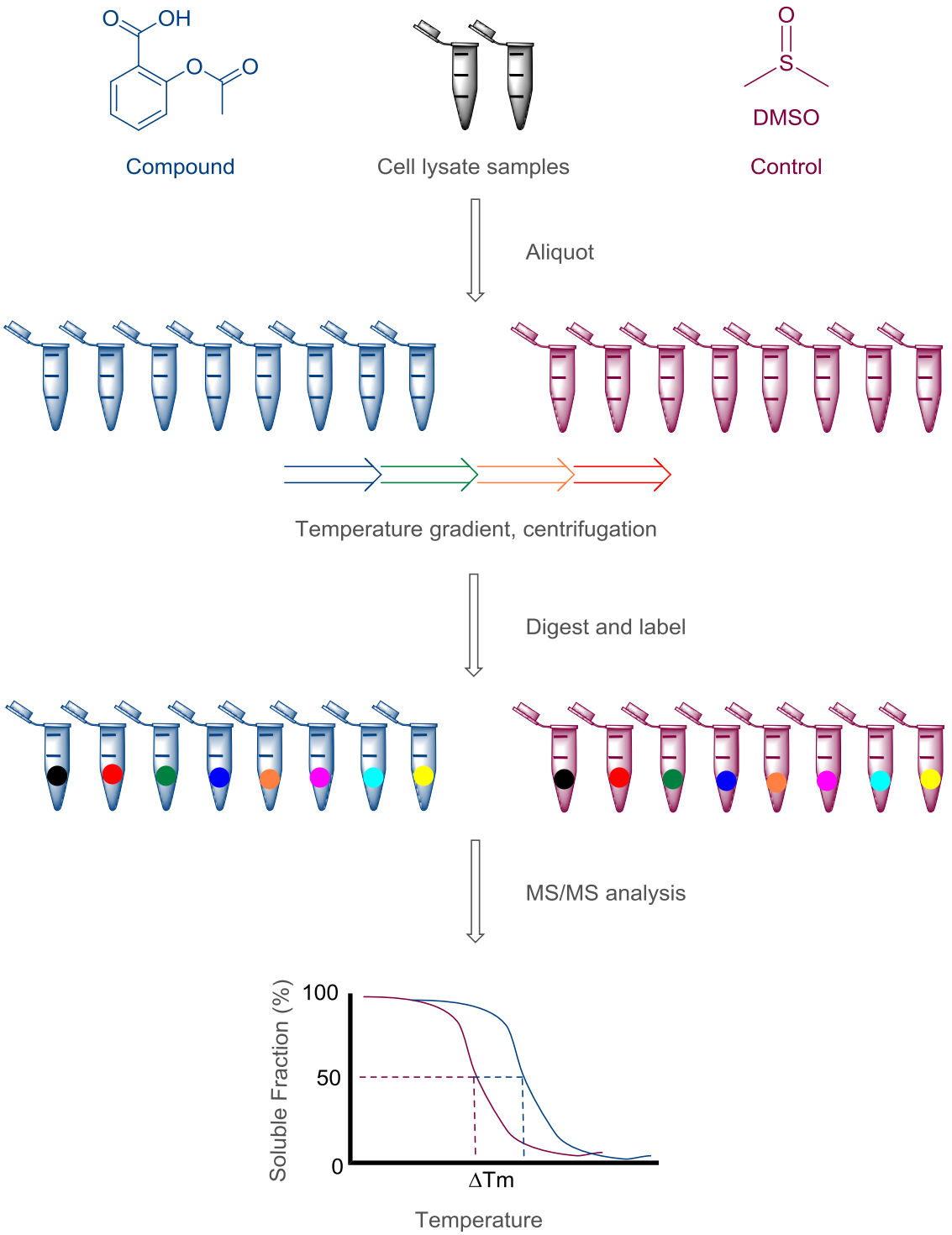

Figure 9: Schematic workflow of the CETSA assay format for target identification purposes. Adapted from Laraia *et al.*[124]

3 Motivation and Aim

Despite the decades of research and great progress in our understanding of autophagy compared to its first report by Christian de Duve in 1963, autophagy is still a process that is not fully understood.

Due to its role in a range of (patho)physiological processes, autophagy is a crucial mechanism for the development, homeostasis and the survival of cells and hence represents an attractive area for drug discovery.[45,125] As its role in many diseases has to be elucidated in more detail, tools to interrogate autophagy at different stages are of major interest, in order to decipher and further study the underlying molecular mechanisms of autophagy. Small molecules that modulate autophagy in a selective and dose-dependent manner would be valuable tools to study this process in more detail and may also lead to the discovery of new drugs for the treatment of cancer as well as neurodegenerative diseases.[96,126–130] Since autophagy is involved in various other developmental pathways, the discovery of a selective modulator remains challenging.[131–134] However, phenotypic screens have proven to offer a good starting point in this regard.[96,99,105]

The aim of this thesis is to discover new small molecule inhibitors of autophagy and identify their targets. For this purpose a cell-based assay will be performed to identify inhibitors of autophagic flux. Based on hits from the cellular assay compound classes will be chosen and compound libraries based on these will be synthesized to provide information regarding structure-activity relationships. This will enable the synthesis of more potent inhibitors and the identification of a position suitable for attaching a linker for immobilizing the inhibitor. An immobilized probe can then be used for affinity-based proteomic profiling to allow the identification of new targets in the autophagic response.

Despite the great advances and successful identifications of new druggable targets in the last years, to date there is still no generally applicable, standardized workflow that guarantees successful target-ID. Hence the affinity chromatography efforts can be accompanied by computational predictions, similarity searches and educated guesses as well as supported by further proteomic-based target-ID methods, such as CETSA (Figure 10).

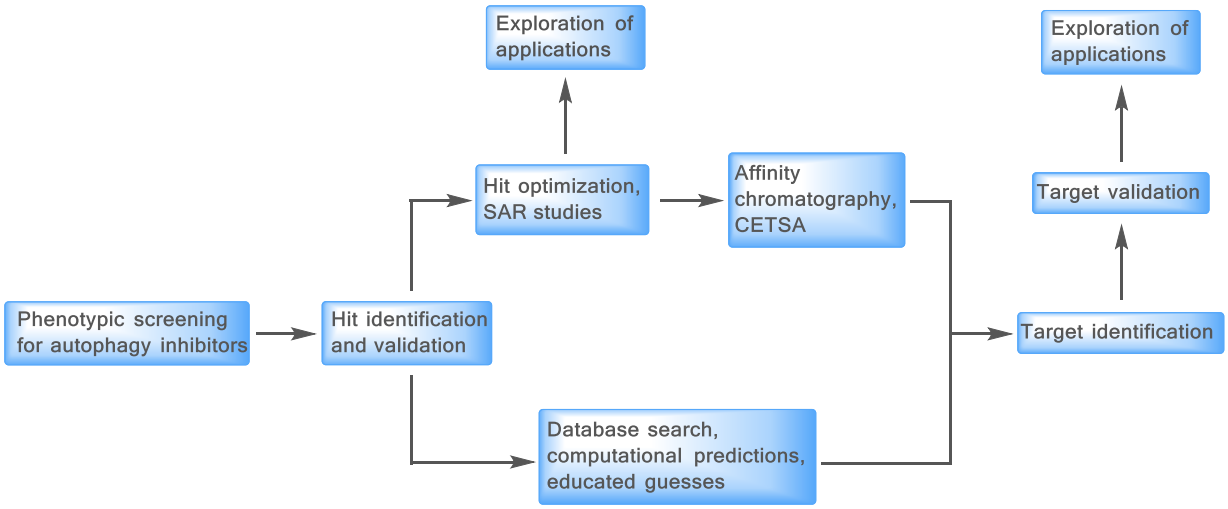

Figure 10: Proposed workflow for the identification and development of new autophagy inhibitors, the identification of their targets and the exploration of potential applications.

Following the identification of the targets the mechanism of the targets' effects on autophagy will be explored and potential applications of the autophagy inhibitors can be examined, including combination treatment of cancer cells with known chemotherapeutic agents. The identification of the targets of the inhibitors and further validation will enlarge our understanding of the autophagic process, which is often misregulated in diseases such as cancer, and allow us to evaluate their potential as new drug targets.

4 Results and Discussion

4.1 Screen for Autophagy Inhibitors

To identify novel autophagy inhibitors, a high-content screening approach previously described by other groups was employed prior to the initiation of the work described within this thesis.[135,136] In brief, autophagy was induced in MCF7 cells stably transfected with eGFP-LC3 (enhanced green fluorescent protein tagged light chain 3) (MCF7-eGFP-LC3 cells) by amino acid starvation using Earle's balanced salt solution (EBSS), or pharmacologically by inhibition of mTOR using Rapamycin. Upon autophagy induction the ubiquitin-like cytosolic protein LC3 is conjugated to phosphatidylethanolamine (PE) and consequently recruited to the autophagosome membrane.[137] Whereas LC3 is distributed throughout the cytoplasm under fed conditions, it accumulates to the autophagosomes after autophagy induction which can be visualized as puncta or "spots". These are detected by automated microscopy and quantified using automated image analysis (Figure 11).[135]

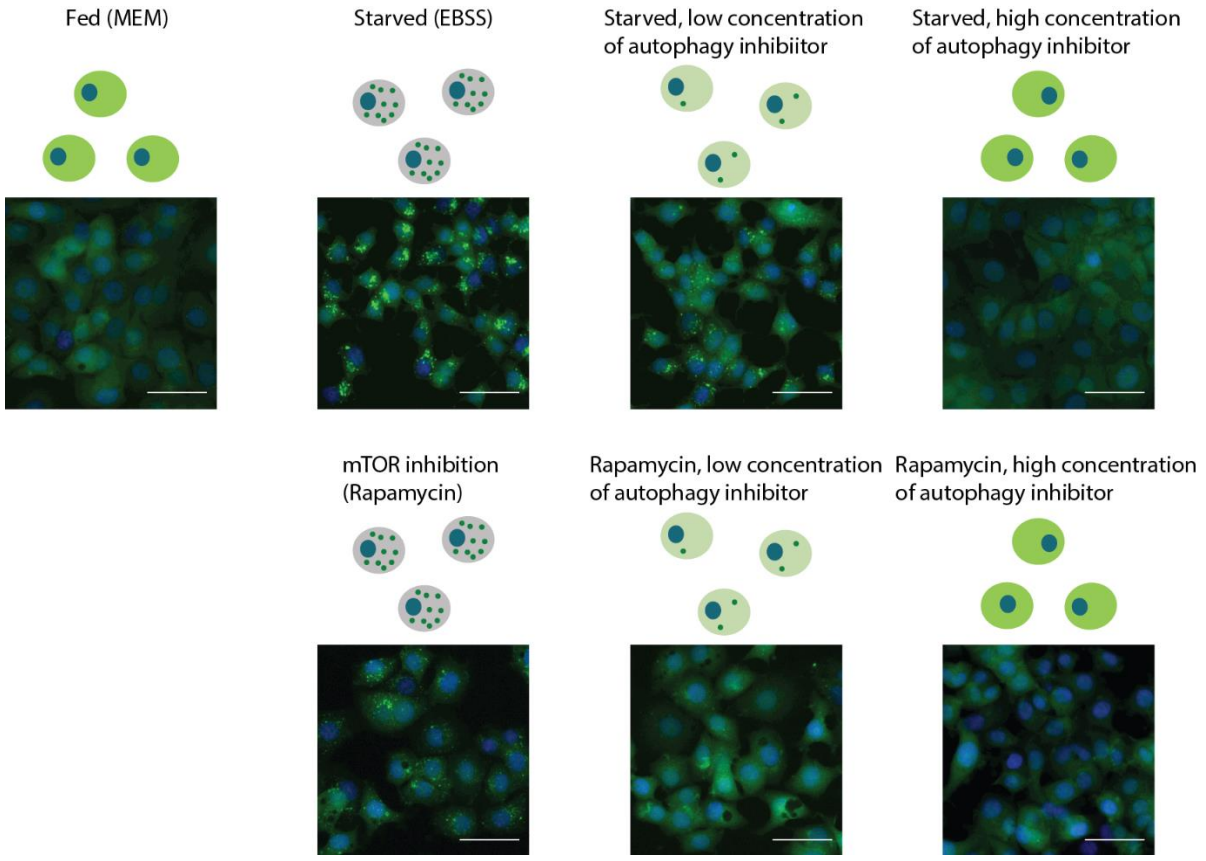

Figure 11: Assay for the identification of autophagy inhibitors. In fed MCF7-eGFP-LC3 cells, incubated in MEM the eGFP-LC3 is distributed throughout the whole cytosol and no green puncta representing autophagosomes are visible. Under starved conditions, i.e. amino acid withdrawal, by means of incubating cells in EBSS or Rapamycin treatment of fed cells autophagosomes are formed, being detectable as puncta due to the accumulation of the fluorescent eGFP-LC3. Inhibitors of autophagy are able to revert this phenotype dose dependently. Scale bar = 50 µm.

Using this assay, a library of about 160,000 compounds was screened for inhibition of starvation-induced autophagy. Approximately 7,000 compounds were able to inhibit autophagosome formation by more than 50% at 10 µM and were thus classed as inhibitors. They were further validated for their ability to inhibit starvation as well as Rapamycin-induced autophagy in a dose dependent manner. Compounds that were active in both screens are predicted to act downstream or independently of mTOR. Hence the parallel screen for rapamycin-induced autophagy inhibition allows for a selection of compounds that act downstream in canonical autophagy regulation or in non-canonical autophagy. From the compound classes found to inhibit autophagy, three promising chemotypes were chosen for further evaluation within the scope of this thesis (Figure 12).

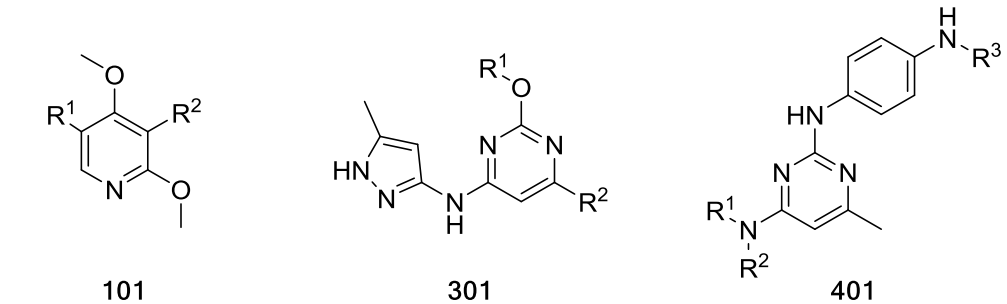

Figure 12: Chosen autophagy inhibiting compound classes for further development and target identification.

The dimethoxypyridine based compound class was chosen because of its rather unusual structure not reported to have biological activity when this thesis was started. The aminopyrimidine and the diaminopyrimidine compound classes stood out because of their potency.

4.2 Dimethoxypyridines

4.2.1 Initial Hits

One of the identified compound classes for autophagy inhibition was a dimethoxypyridine-containing chemotype (DMPs). The DMPs were originally synthetic intermediates of a biology oriented synthesis (BIOS)[4,109] effort to synthesize pyridones based on the natural product Militarinone. These Militarinone-inspired, neuritogenic compounds, were found to be MAP4K4 inhibitors (Figure 13, **102**).[138] At this point in time there were already around 100 analogues in the library containing the dimethoxypyridine core with varying substituents at the 3- and 5-position on the pyridine. The fact that the pyridone analogues were not active in the autophagy screen but neuritogenic compounds and vice versa for the dimethoxypyridines was in line with the BIOS-principle. This intriguing finding that two scaffolds from the same library have different phenotypic effects spurred the follow up of this compound class in more detail and the optimizazion of the dimethoxypyridines towards autophagy inhibition. For this purpose the SAR was analyzed in respect to starvation induced autophagy inhibition and around another 100 compounds were synthesized.

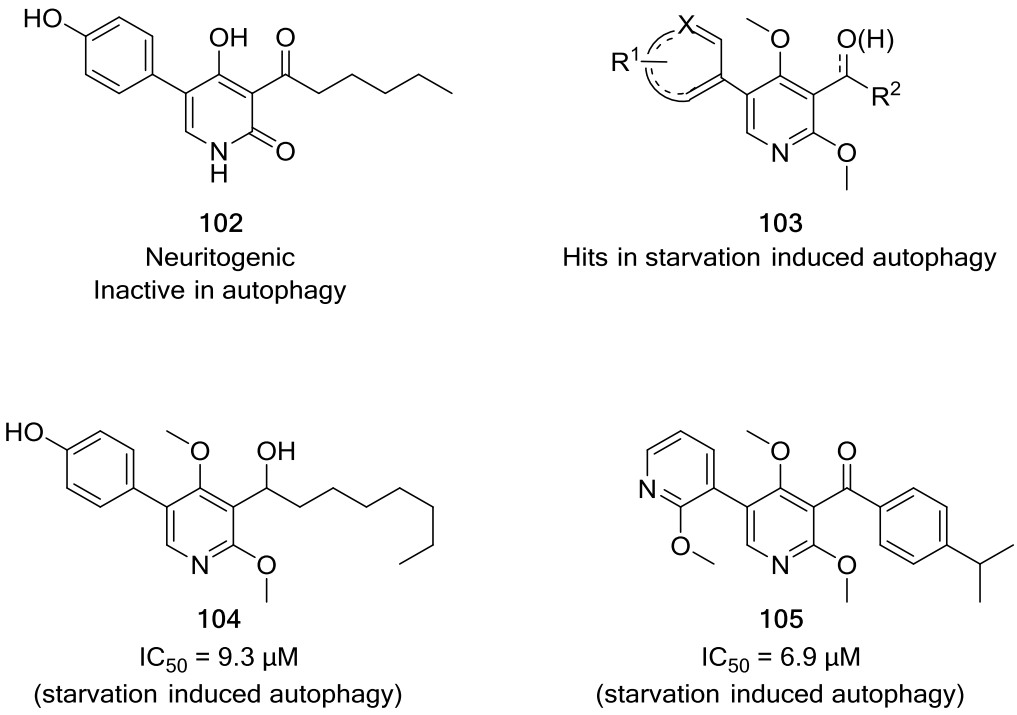

Figure 13: Origin of a new chemotype for autophagy inhibition. The compound class derived from neuritogenic MAP-kinase inhibitors, such as compound **102**, that were developed following the BIOS principle. The general structure of dimethoxypyirdine **103** represents a structural precursor for the neuritogenic MAP-kinase inhibitors of type **102**. Dimethoxypyridines **104** and **105** are representative examples for the first hits found to inhibit autophagy.

4.2.2 Synthesis and SAR Study

In contrast to the recent report,[138] the synthetic route started from 2,4-dimethoxypyridine (106), which was brominated with Br_2 in acetic acid to give the versatile precursor 3,5-dibromo-2,4-dimethoxypyridine (107) in 96% yield (Figure 4, a)). This intermediate was used for synthesizing most of the analogues. Directed *ortho* metalation allowed regioselective metalation of position C3 on the pyridine skeleton *via* a bromine-lithium exchange. By adding an isocyanate or an aldehyde to the lithiated species, the amides of structure **108** were prepared in moderate to good yields (28-65%) and the secondary alcohols with the structure of **110** also in moderate to good yields (20-95%), (Figure 4, b) and d)). The electrophiles were used in an excess in order to achieve the highest possible conversion of the sterically hindered lithiated pyridine. Both the amides and the secondary alcohols were subsequently converted to the bioactive dimethoxypyridines **109** and **113** by Suzuki cross-coupling with boronic acids (Figure 4, c)). In the case of electron-rich aromatics as boronic acids, the Suzuki coupling delivered high yields, while the use of heteroaromatics, such as pyrazole, isoxazole indole, pyridine and pyrimidine resulted in the occurrence of secondary reactions, which necessitated the purification by means of HPLC and led to a low yield. Several benzylpyrazole boronic acid derivatives, were prepared from a nucleophilic substitution of substituted benzyl bromides and pyrazole boronic acid.

For the secondary alcohols **113**, an oxidation with manganese (IV) oxide or with Dess-Martin periodinane followed as the last reaction step. The oxidation by means of manganese (IV) oxide proceeded with high yields in all cases (76-98%), whereas the oxidation with DMP yielded slightly lower yields (68-86%), (Scheme 3, e)).

Replacing the bromine substituent at position C5 with various amines succeeded by means of a Buchwald-Hartwig coupling for the ketones of structure **111.** While the reaction proceeded well in some cases for the ketone as the starting material, only traces of the product could be obtained in the best case for the reaction of the alcohols **110**. A Buchwald-Hartwig amination of the dibromodimethoxypyridine **107** with only one equivalent of the amine gave the desired regioisomer as the main product, due to the steric differentiation of the two bromine substituents, but required the purification of the product by HPLC and thus proved to be unfavourable in comparison with the established route shown in Figure 4 for the preparation of the amines **112**. The synthesized substances of the general structures **109**, **112**, **113** and **114** were investigated as possible inhibitors of autophagy. The compounds and their associated average IC_{50} values are shown in Table 3 and Table 4 and the SAR is discussed below (refer to Appendix-Table 1 – 6 for the full set of all compounds and their IC_{50} values).

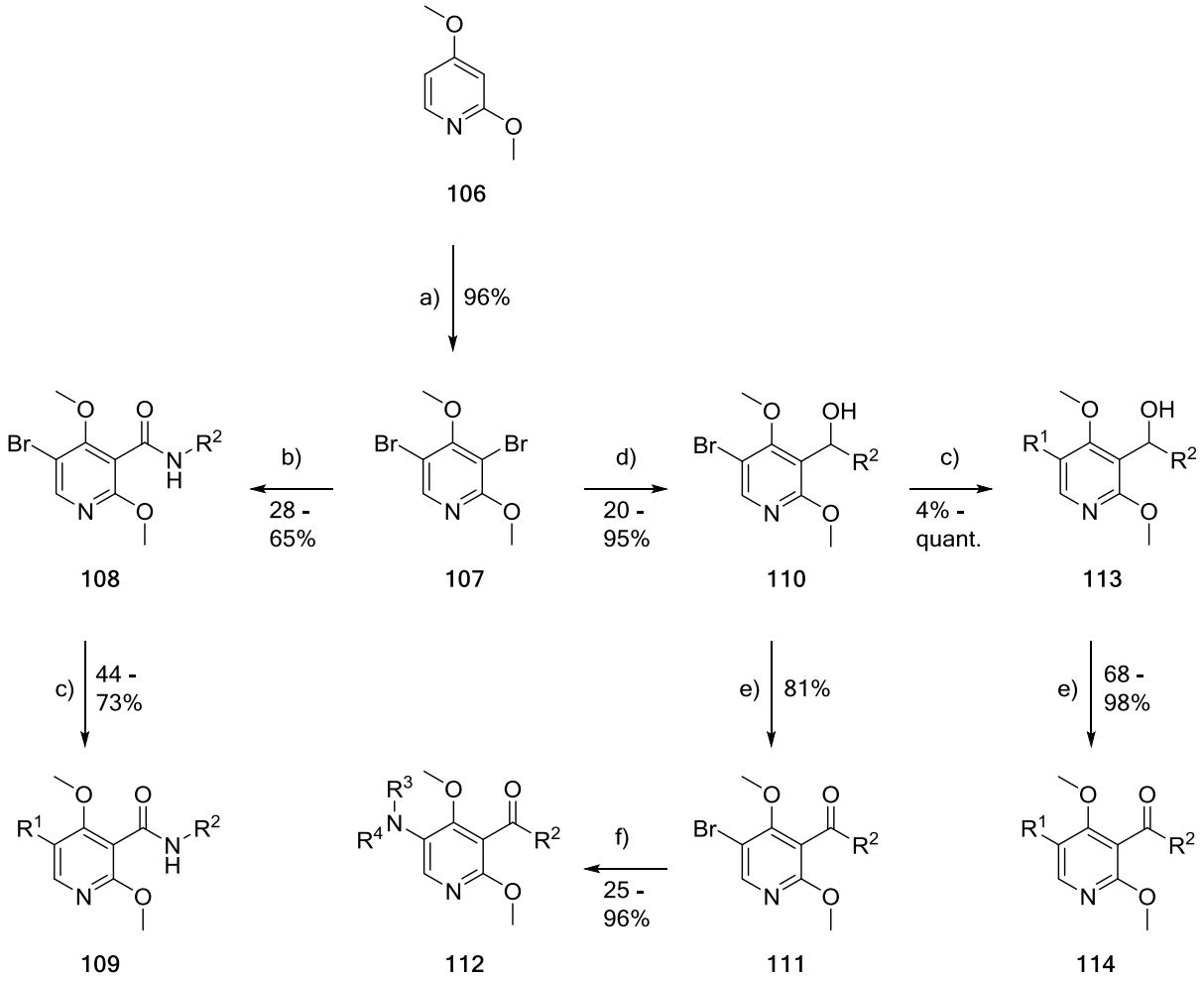

Figure 14: General scheme for the synthesis of the DMPs starting from commercially available **106**. a) Br_2, acetic acid, 80 °C, 16 h; b) *s*-BuLi, THF, -78 °C, 1 h, then isocyanate, -78 °C → rt, overnight; c) Boronic acid, $Pd(PPh_3)_4$, dppf, Na_2CO_3 (aq.), toluene / ethanol, reflux, 16 h; d) *s*-BuLi, THF, -78 °C, 1 h, then aldehyde, -78 °C → rt, overnight; e) MnO_2, DCM, rt, 2 d or Dess–Martin periodinane, DCM, rt, 2 h; f) Amine, *t*BuXPhos, Pd_2dba_3, NaO*t*Bu, Toluene, 80 °C, overnight. DCM = Dichloromethane.

To simplify the discussion of the SAR of a library which comprises more than 200 analogues, only selected analogues are shown and the discussion is subdivided into three parts: The left hand side (R^1) (Table 3), the right hand side (R^2) (Table 4) and the core (Table 5). Substituents for R^1 at the C5-position of the pyridine were indispensable. *N*-heterocycles with larger hydrophobic extensions yielded the most active compounds (Table 3, entry 1-7), whereas it could be observed that compounds without an extension of the aromatic surface of the substituents showed reduced activity (compare benzylpyrazole (Table 3, entry 2) to methylpyrazole (Table 3, entry 15) and quinolone (Table 3, entry 6) to pyridine (Table 3, entry 29). The highest potency was observed for compounds with a pyrazole. While there is an effect on potency for differing substitution patterns on the benzylpyrazole, activity of the compounds with *iso*-butylpyrazole substituent and benzylpyrazole substituent differed only slightly (compare Table 3, entries 1, 2, 4, 11, 14 and 20).

Some phenols (Table 3, entry 8 and 9) and similar to them some phenyls (Table 3, entry 12, 13, 17–19, 25 and 26) as substituents at position C5 of the dimethoxypyridine scaffold also allowed inhibition of autophagy, while, depending on the substitution pattern, some were less active or not active anymore. More polar heterocycles, which were less bulky or contained more heteroatoms, were not active (Table 3, entry entries 21-23, 29 and 31). The introduction of alkyloxy substituents such as methoxy groups did not improve the activity (Table 3, entry 31). The fact that smaller, more polar heterocycles were not active was in line with the finding that a morpholine substituent (Table 3, entry 33) did not allow inhibition. Similarly to the morpholine, replacements of the aromatic substituent at C5, such as an alkene bridging to a phenyl ring (Table 3, entry 24) or a bromine (Table 3, entry 27 and 28) were not sufficient for activity.

Table 3: Inhibition of starvation induced autophagy determined for selected analogues with varying R^1. Activity > 10 = no inhibition at a test concentration > 10 µM. A dashed line signifies that the compound has not been synthesized. Data is mean ± SD, n ≥ 3; if no SD is given, data is mean, n = 2. For a full list of analogues and activities see Appendix-Table 1-6.

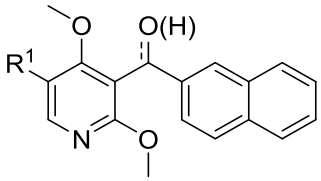

R^1	Number	Entry	Alcohol IC_{50} [µM]	Number	Entry	Ketone IC_{50} [µM]
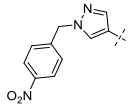	**115**	1	1.3 ± 0.5			—
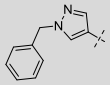	**116**	2	1.9 ± 0.8	**117**	3	6.5 ± 3.2
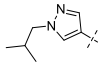	**118**	4	2.2 ± 2.4	**119**	5	4.1
	**120**	6	2.5 ± 0.5	**121**	7	3.9 ± 0.4
	**122**	8	3.8 ± 1.0			—
	**123**	9	3.9	**124**	10	>10
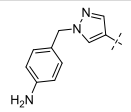	**125**	11	4.4 ± 0.7			—
	**126**	12	4.6 ± 0.6	**127**	13	8.8 ± 0.1
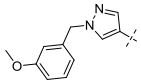	**128**	14	5.5 ± 1.4			—
	**129**	15	6.5 ± 1.6	**130**	16	4.4 ± 1.6

	**131**	17	6.6 ± 1.0	**132**	18	8.3 ± 0.8
	**133**	19	7.0 ± 0.6			—
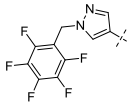	**134**	20	9.2 ± 1.0			—
	**135**	21	>10			—
	**136**	22	>10			—
	**137**	23	>10			—
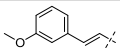	**138**	24	>10			—
	**139**	25	>10	**140**	26	>10
Br	**141**	27	>10	**142**	28	>10
	**143**	29	>10	**144**	30	3.0
	**145**	31	>10	**146**	32	4.2
	**147**	33	>10			—

For R^2, several substituents could be introduced without a drastic change in the activity of the compounds. The characteristics shared by these substituents were aromaticity, the absence of heteroatoms, and their bulkiness (Table 4, entries 1, 2 and 7-9). The combination of these properties of the substituents increased the hydrophobicity of the final compounds. In order to counteract this effect, an attempt was therefore made to introduce polar heteroatoms into the corresponding aromatics. However, most of the corresponding changes either did not improve or lowered the biological activity (Table 4, entries 10-12). The introduction smaller fluorine-containing aromatics yielded active compounds (Table 4, entries 3-5). Further efforts to reduce the hydrophobicity of the compound by changing R^2 led to a slightly less active analogue containing a benzene with an alkyne as a substituent (Table 4, entry 6). Interestingly, there seems to be a favored orientation for the hydrophobic moiety of R^2, as bulky moieties with different orientations reduced activity (Table 4, entries 7-9).

In the case of benzylpyrazole, the secondary alcohols were more beneficial for biological activity, whereas smaller substituents such as pyridine at position C5 of the dimethoxypyridine core showed a higher activity as the corresponding ketone, although the effect was generally not very pronounced (Table 3, compare entries 2-7 versus 29-32). Efforts to derivatise this particular position by replacing the secondary alcohol with a methoxy or fluorine, did not yield active compounds (Appendix-Table 6).

Amides structurally related to the ketones were also synthesized (Table 4, entries 7, 13 and 14). In addition to the introduction of another heteroatom for solubility reasons, the aromatic residue was thus placed at a greater distance from the backbone. This modification was also of interest with regard to the attachment of a linker to this side of the ligand, because if the modification should not cause any or only a minimal change in activity, this would be another indication of the suitability of the large aromatic substituent to bear a linker. Indeed, also for the amides almost only the size of the aromatic residue was decisive for the activity of the compound. This finding confirmed the analysis of the SAR, which could be made with ketones and alcohols.

Table 4: Inhibition of starvation-induced autophagy determined for selected analogues with varying R^2. Activity > 10 = no inhibition at a test concentration of 10 µM. A dashed line signifies that the compound has not been synthesized. Data is mean ± SD, n ≥ 3. For a full list of analogues and activities see Appendix-Table 1-6.

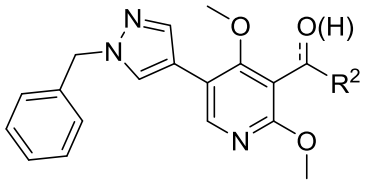

R^2	Number	Entry	Alcohol IC_{50} [µM]	Number	Entry	Ketone IC_{50} [µM]
	**116**	1	1.9 ± 0.8	**117**	2	6.5 ± 3.2
	**148**	3	2.2 ± 2.0			—
	**149**	4	2.4 ± 0.6	**150**	5	6.4 ± 0.6
	**151**	6	3.3 ± 2.5			—
			—	**152**	7	4.0 ± 1.0
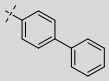	**153**	8	4.2 ± 1.4	**154**	9	>10
	**155**	10	5.9 ± 1.8	**156**	11	3.5 ± 0.3
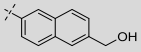	**157**	12	10 ± 6.0			—
			—	**158**	13	>10
			—	**159**	14	>10

Subsequently the SAR studies focused on the core of the scaffold, i.e. the dimethoxypyridine itself. For this purpose a benzene analogue and derivatives with varying methoxy substitution pattern were synthesized, in order to examine their importance for the biological activity. Synthesis was attempted analogously to the established route; however, several adjustments were necessary (Figure 15).

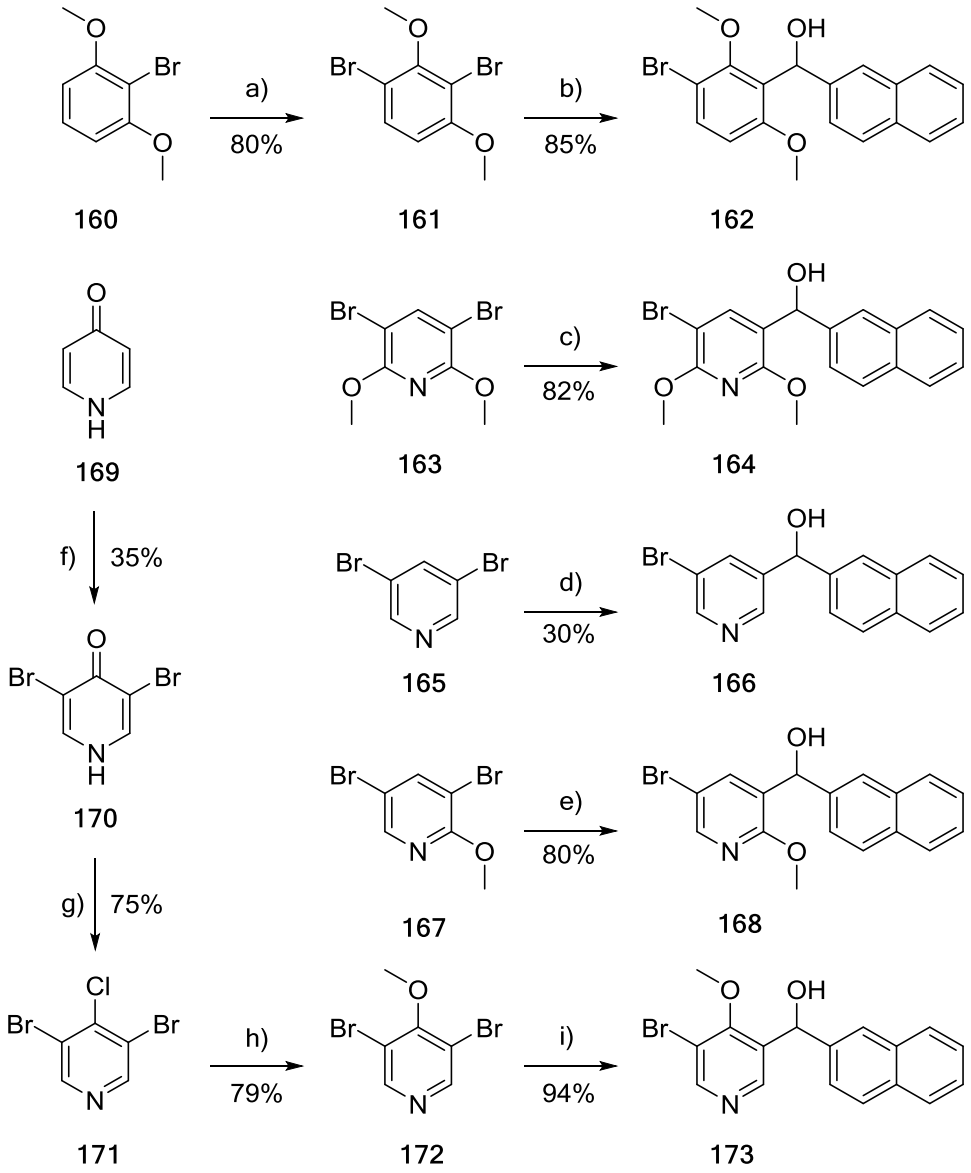

Figure 15: Synthetic scheme for the preparation of different cores. a) NBS, MeCN, 0 °C → rt, 16 h; b) *n*-BuLi, THF, -78 °C, 2 h, then aldehyde, -78 °C, 1 h, then -78 °C → rt, overnight; c) *s*-BuLi, THF, -78 °C, 1 h, then aldehyde, -78 °C → rt, overnight; d) *i*PrMgClLiCl, THF, -78 °C, 1 h, then aldehyde, -78 °C, 2 h, then 78 °C → rt, overnight; e) *s*-BuLi, Et_2O, -100 °C, 1 h, then aldehyde, -100 °C → rt, overnight; f) Br_2, HBr, 0 °C → rt, 1.5 h; g) $POCl_3$, 140 °C, 2.5 h; h) MeONa, MeOH, rt, 6 d; i) *s*-BuLi, THF, -78 °C, 1 h, then aldehyde, -78 °C → rt, overnight.

Synthesis of the benzene analogue **162** proceeded from commercially available 2-bromo-1,3-dimethoxybenzene (160). This was first brominated regioselectively with NBS in MeCN with a yield of 80%. The resulting 1,3-dibromo-2,4-dimethoxybenzene (161) was then regioselectively metalated by means of bromine-lithium exchange with one equivalent of *n*-butyllithium, and then captured with 2-naphthaldehyde in excellent yield. The Suzuki couplings and the oxidations of the secondary alcohols to the ketones were carried out according to the standard procedures for all different cores.

As a starting material for the generation of the 2,6-dimethoxypyridine regioisomers, 3,5-dibromo-2,6-dimethoxypyridine (163) was commercially available, which was transferred into the corresponding alcohol **164** and further derivatised following established reaction conditions.

For the metalation of the commercially available 3,5-dibromopyridine (165), other reaction conditions had to be used. Since the use of *n*-, *s*- and *t*-BuLi was not successful for metalation, *iso*-propyl magnesium chloride—lithium chloride was used, yielding 30% of the desired product **166**. The Suzuki coupling for intermediates **166** and **164** also succeeded according to the established procedures. For the synthesis of compound **168**, commercially available 3,5-dibromo-2-methoxypyridine (167) was reacted with *s*-butyllithium in diethyl ether at -100 °C in 80% yield. An adjusted metalation procedure had to be established since the standard procedure at -78 °C in THF did not deliver regioselective metalation of the starting material by the directing effect of the 2-methoxy group.

The analogue with only one methoxy group in the 4-position **173** was synthesized from commercially available pyridine-4-ol (169). This was dibrominated with bromine in hydrobromic acid. This was followed by the chlorination by phosphorus oxychloride, replacing the tautomeric hydroxy group in **170**. In the next reaction step, the chlorine was replaced by the desired methoxy group by means of sodium methoxide. This synthesis route was applied because methylation of the hydroxy group did not succeed with any of several applied methylation reagents, such as methyl iodide, dimethyl sulfate or trimethyloxonium tetrafluoroborate. The subsequent bromine-lithium exchange was carried out according to the established method. The same applies to the Suzuki coupling as well as to the final oxidation to deliver the final compound.

The analogous compounds with pyridine or benzene as the core (Table 5, entries 1 and 5 respectively) have almost the same inhibitory effect on autophagy. This leads to the speculation that the nitrogen of the pyridine does not form a direct interaction with a potential target protein. Nonetheless the pyridine was retained, as it is predicted to increase polarity and thus solubility.

The two methoxy groups in 2- and 4-position are important for activity. Although the analogue with only one methoxy group at position 4 (Table 5, entry 3) or no methoxy group (Table 5, entry 4) are equally potent autophagy inhibitors, the analogue with only one methoxy group in position 2 of the pyridine (Table 5, entry 2) is still less active than its 2,4-dimethoxy derivative. It appears that both methoxy groups may have a cooperative effect on the activity of the substance class. It is possible to speculate that this effect was steric rather than electronic, as the analogue with two methoxy groups at position 2 and 6 was inactive (Table 5, entry 6). Potentially the two methoxy groups in *ortho* position to the bridging hydroxymethyl group or ketone pre-arrange the bulky hydrophobic aromatics of R^2.

Table 5: Inhibition of starvation induced autophagy determined for selected analogues with a varying core structure. > 10 = no inhibition at a test concentration > 10 µM. Data is mean ± SD, n ≥ 3.

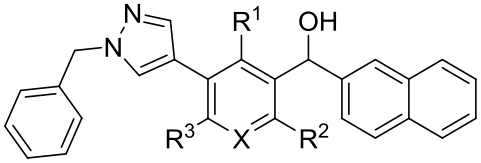

Number	Entry	R^1	R^2	R^3	X	IC_{50} [µM]
116	1	OMe	OMe	H	N	1.9 ± 0.8
174	2	H	OMe	H	N	3.7 ± 1.5
175	3	OMe	H	H	N	6.2 ± 1.2
176	4	H	H	H	N	6.2 ± 2.2
177	5	OMe	OMe	H	C	1.8 ± 0.8
178	6	H	OMe	OMe	N	>10

The corresponding ketones were not active (Table 6, entry 4 and 5) or significantly less active (Table 6, entry 1-3). As a result of these SAR investigations the original core structure was left unaltered.

Table 6: Inhibition of starvation induced autophagy determined for selected analogues with a varying core structure. > 10 = no inhibition at a test concentration > 10 µM. Data is mean ± SD, n ≥ 3.

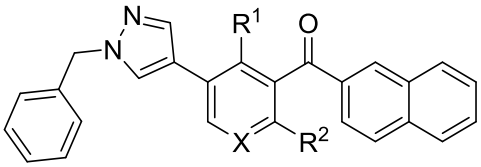

Number	Entry	R^1	R^2	X	IC_{50} [µM]
117	1	OMe	OMe	N	6.5 ± 3.2
179	2	H	OMe	N	5.1 ± 3.3
180	3	OMe	H	N	5.8 ± 3.3
181	4	H	H	N	>10
182	5	OMe	OMe	C	>10

In addition to the dimethoxypyridines that were in the library, medicinal chemistry effort provided further analogues leading to a total of >200 compounds of this class. Overall the generated library allowed a thorough exploration of the SAR of the DMPs, showing the importance of the dimethoxypyridine core unit for activity (Figure 16). It can be speculated that the SAR is rather driven by hydrophobicity than by strong directing interactions such as hydrogen bonds or ionic charges, as the larger hydrophobic groups seem to be indispensable at the left as well as at the right hand side of the dimethoxypyridine core.

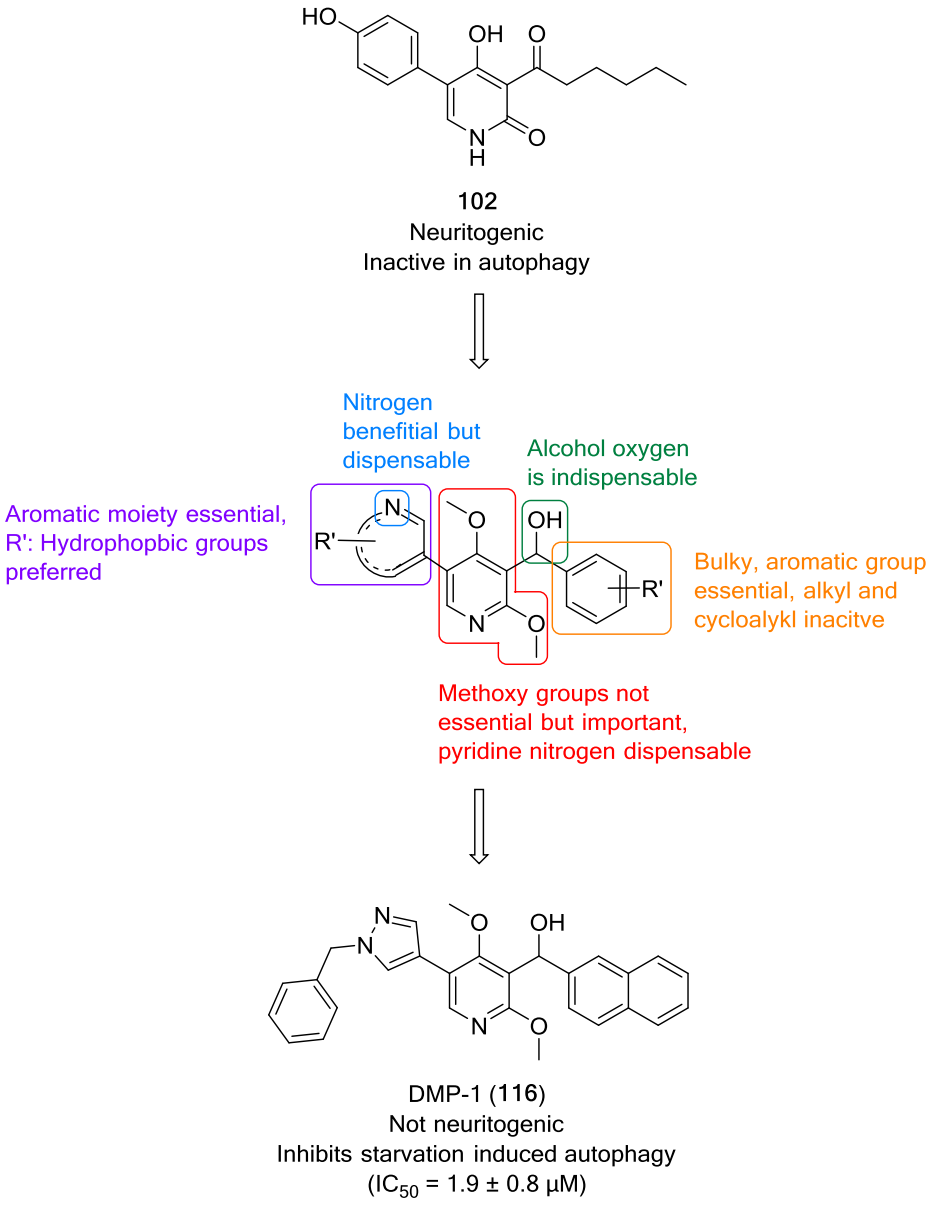

Figure 16: Summary of the development and the SAR of the dimethoxypyridines as a novel chemotype of autophagy inhibitors.

A key takeaway of the extensive SAR investigation is that different large substituents for R^2 all allow activity. This suggested that at this part of the inhibitors, a linker could be attached without affecting the ligand-protein interaction. Based on this observation a pulldown probe was designed and synthesized. As a starting point for the design of the pulldown probe compound **116** was chosen, which was termed DMP-1 —for dimethoxypyridine-1— and characterized further as an autophagy inhibitor.

4.2.3 Biological Validation

DMP-1 inhibited starvation induced autophagy dose dependently (Figure 17A and B) with an IC_{50} of 1.9 ± 0.8 µM. However, neither DMP-1 nor any of its analogues inhibited Rapamycin-induced autophagy, which suggests that they act upstream or independently of mTOR (data not shown).

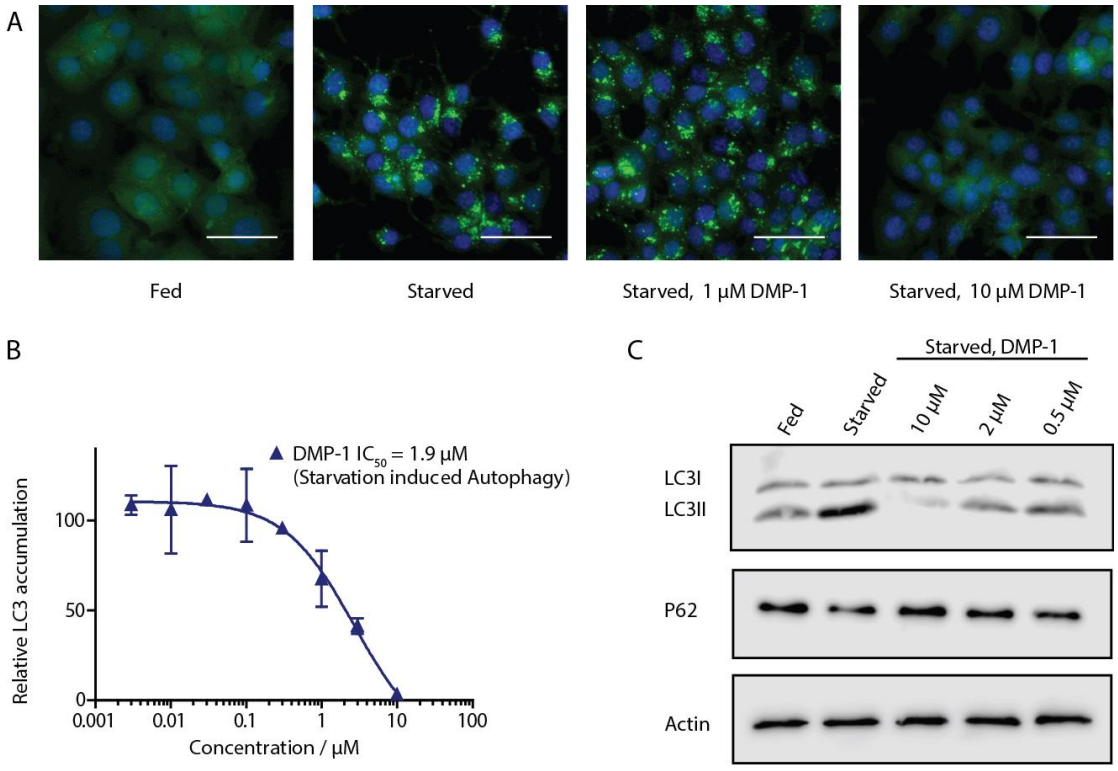

Figure 17: Phenotypic validation of DMP-1 as an autophagy inhibitor. **A**: Fluorescence microscopy images of the starvation induced autophagy screen for inhibition of eGFP-LC3 accumulation. Fed = DMSO control incubated in full media (MEM) as positive control. Starved = Autophagy was induced by amino acid withdrawal (EBSS). DMP-1 reverts the phenotype in a dose dependent manner. Scale bar = 50 µm. **B**: Dose-dependent inhibition of amino acid starvation induced eGFP-LC3 accumulation by DMP-1. Data is mean ± SD, n ≥ 3, representative graph shown. **C**: Inhibition of LC3 lipidation and p62 degradation by DMP-1 in MCF7-eGFP-LC3 cells. Starvation induced autophagy causes lipidation of LC3-I to LC3-II and degradation of p62. DMP-1 inhibits both effects in a dose-dependent manner. n ≥ 3, representative blot shown.

In order to validate DMP-1 as an autophagy inhibitor further, we studied its effect on two key autophagy markers: LC3 lipidation and p62 degradation. After the induction of autophagy, LC3 is lipidated with phosphatidylethanolamine to form LC3-II,[137] an effect that should be reversed by an autophagy inhibitor. DMP-1 inhibited LC3 lipidation dose-dependently as assessed by western blot analysis (Figure 17C). p62 acts as a chaperone to target proteins for degradation by the autophagic machinery, where it is degraded together with its cargo. Autophagy inhibitors are predicted to inhibit this degradation. DMP-1 inhibited the degradation of p62, confirming its ability to inhibit autophagic flux (Figure 17C).

As autophagy is a cytoprotective mechanism which is activated in conditions of cellular stress, autophagy inhibition is reported to render cells more sensitive to the effects of starvation.[96] In line with this expectation DMP-1 selectively inhibited the growth of starved MCF7-eGFP-LC3 cells compared to fed cells as assessed by a WST-1 proliferation assay (Figure 18A). It has been reported that autophagy inhibition causes cells to die *via* apoptosis.[68] MCF7 cells treated with DMP-1 showed apoptotic cell death under fed as well as under starved condition, as assessed by live cell imaging using the Incucyte Zoom of a caspase 3/7 selective probe that releases a DNA intercalating dye which labels the nuclei of apoptotic cells (Figure 18B).

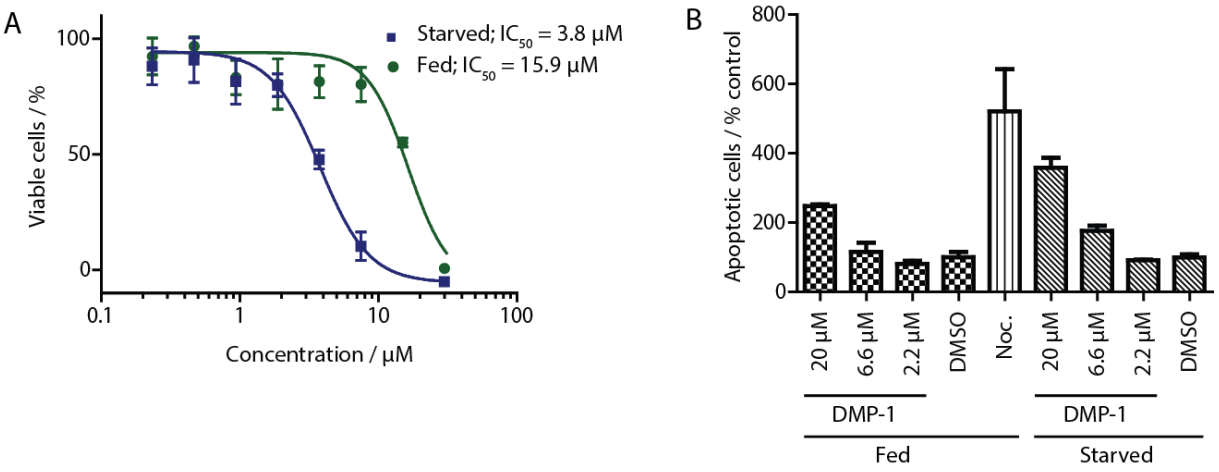

Figure 18: Autophinib induces cell death in starved cells by means of apoptosis. **A**: Treatment of MCF7-eGFP-LC3 cells under starved conditions (EBSS) or fed conditions (MEM) with DMP-1. Under starvation conditions survival is reduced. Cytotoxicity was assessed by means of a WST-1 assay. Data points are mean ± SD, n = 3, representative graphs shown. **B**: DMP-1 dose dependently induces apoptosis. Apoptosis was assessed by using a selective caspase 3/7 probe. The experiment was performed with an Incucyte Zoom instrument. Noc. = Nocodazole (10 µM). Data are presented as a percentage of the DMSO control. Data points are mean ± SD, n ≥ 3, representative experiment shown.

4.2.4 Target Identification

After the discovery, development and the biological validation of the dimethoxypyridine-based autophagy inhibitors, it was of interest to elucidate their mode of action. The identification of a target protein would strengthen our understanding of autophagy and could provide the basis for future drug discovery programs. Since there were no closely related analogues with a known target reported or promising computational predictions available, unbiased proteomics was applied. Initially it was attempted to identify potential protein targets by means of affinity chromatography, hereafter referred to as pulldown.

4.2.4.1 Pulldown

For identifying the protein target of the DMPs from a complex biological system such as a cell lysate, a probe suitable for immobilization (pulldown probe) was synthesized. The insights gained regarding the SAR for this series of compounds enabled the identification of R^2 (Table 4) as suitable for attaching a linker, as a range of substituents were tolerated at this position. For this reason an analogue of DMP-1 was designed, which allowed the attachment of a PEG-linker on the site of the naphthalene, opposite to the hydroxymethyl group (Figure 19, compound **186**). Since attempts to increase the solubility of the compound class by introducing polar groups in and around R^2 led to less active analogues, a methylene unit with an ether was chosen instead of an amide or similar linkage options. This moiety was introduced into the final probe by synthesizing the aldehyde building block, starting from commercially available naphthalene-2,6-diyldimethanol (183). This was mono-TBS-protected in THF giving a low yield of 9% while the starting material could be re-isolated in 87% yield (Figure 19, b)). Varying conditions with more equivalents of TBSCl yielded more product but did not allow the re-isolation of starting material and generated a lot of undesired double protected product. Due to the relatively high costs of the starting material the conditions that gave a low yield, but allowed starting material reisolation were chosen. The reisolated starting material was transformed into the desired mono-protected product **184** in successive reactions. The corresponding aldehyde **185** was generated by oxidation with DMP with a good yield of 90%. This aldehyde was then coupled to the common precursor **107** in the already established manner by means of a butyl-lithium exchange and addition of the aldehyde, to generate intermediate **186**.

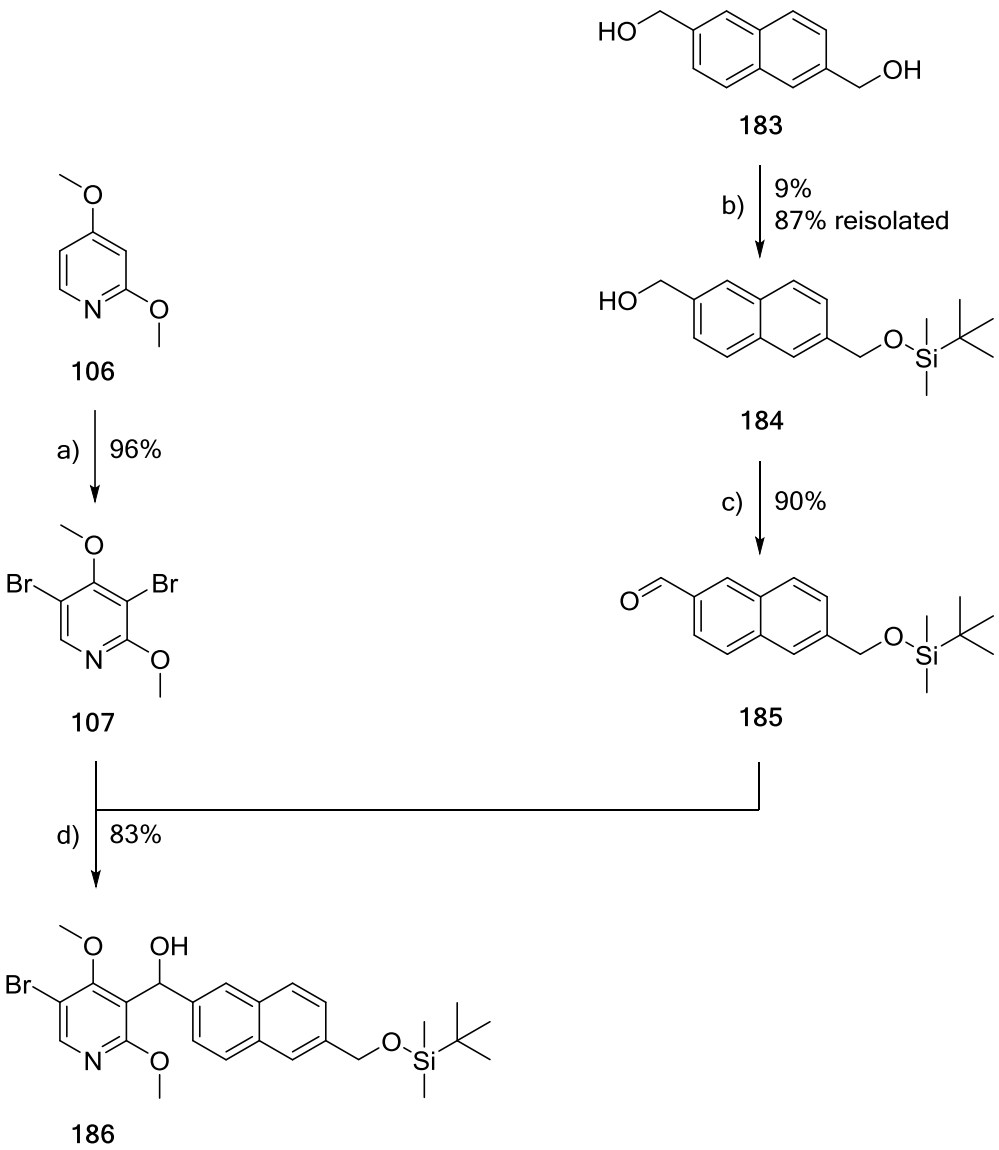

Figure 19: Pulldown probe synthesis Scheme 1. a) Br_2, acetic acid, 80 °C, 16 h; b) imidazole, TBSCl, THF, 0 °C → rt, overnight; c) DMP, DCM, rt, 1 h; d) *s*-BuLi, THF, -78 °C, 1 h, then aldehyde, -78 °C → rt, overnight.

Intermediate **186** was then further derivatized by Suzuki cross coupling reaction (Figure 20, a)). The product **187** was deprotected, in order to yield compound **188**, bearing a primary alcohol. In parallel the PEG-linker **191** was prepared for later attachment to this particular primary alcohol. For this purpose the linker **189** was first mono-Boc protected on the one side and subsequently coupled with bromoacetylbromide, in order to introduce an electrophile into the linker.

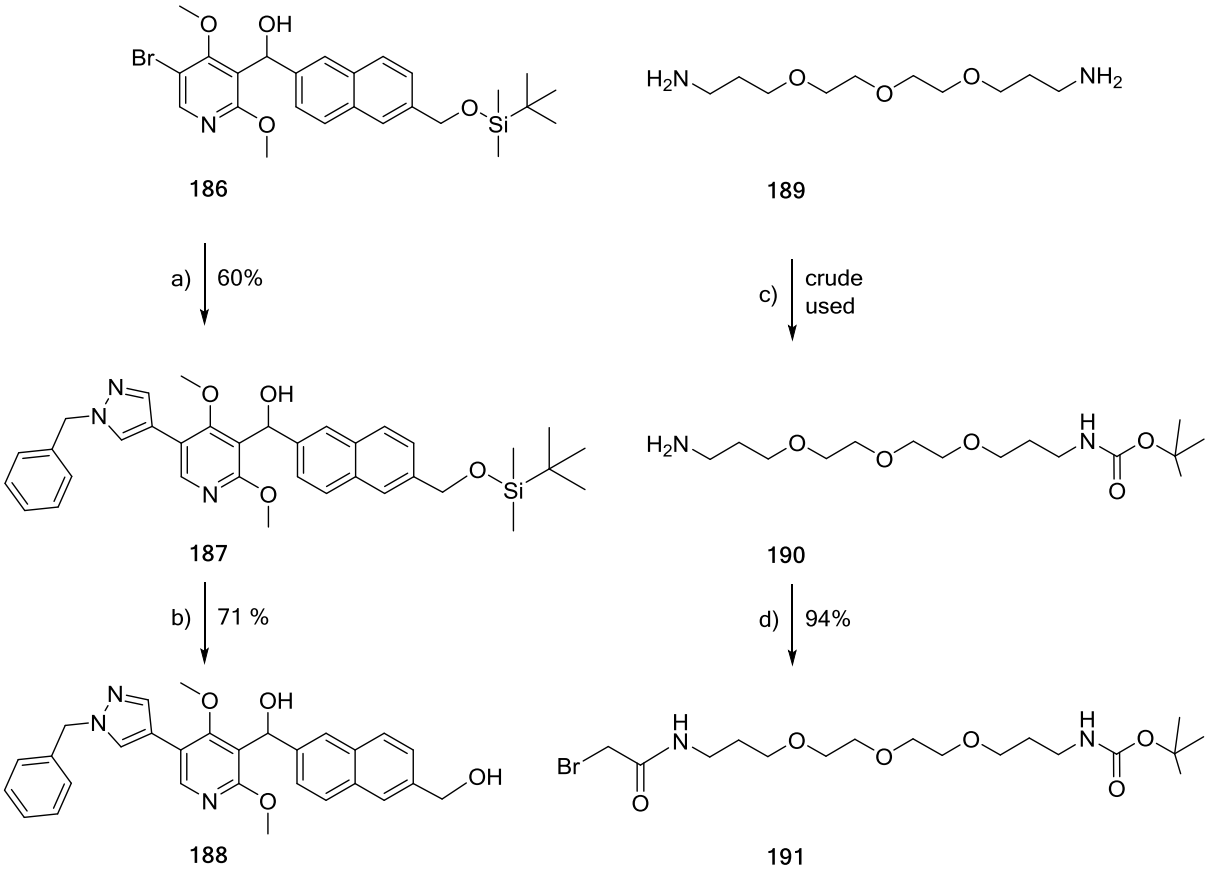

Figure 20: Pulldown probe synthesis scheme 2. a) Boronic acid, $Pd(PPh_3)_4$, dppf, Na_2CO_3 (aq.), toluene / ethanol, reflux, 16 h; b) TBAF, THF, 0 °C, 30 min, then rt; c) Boc_2O, DCM, rt, 16 h, (according to the ^{1}H-NMR the crude contained 60% of the desired product); d) bromoacetylbromide, THF, 0 °C → rt, 1 h.

The alkyl bromide was subsequently coupled to the deprotonated compound **188**. It was assumed that the primary alcohol would possess a higher reactivity for a nucleophilic substitution than the secondary alcohol of the bridging hydroxymethyl group. In contrast to this expectation both alcohols were found to be etherified to a similar extent. Although unplanned this finding held promise of giving access to a negative as well as positive pulldown probe within one step.

Gratifyingly the probe **192** showed only slightly reduced activity compared to the parent molecule (Table 5, entry 1 (DMP-1) and Figure 21), whereas the second probe **193** was found to be inactive in the cellular autophagy assay.

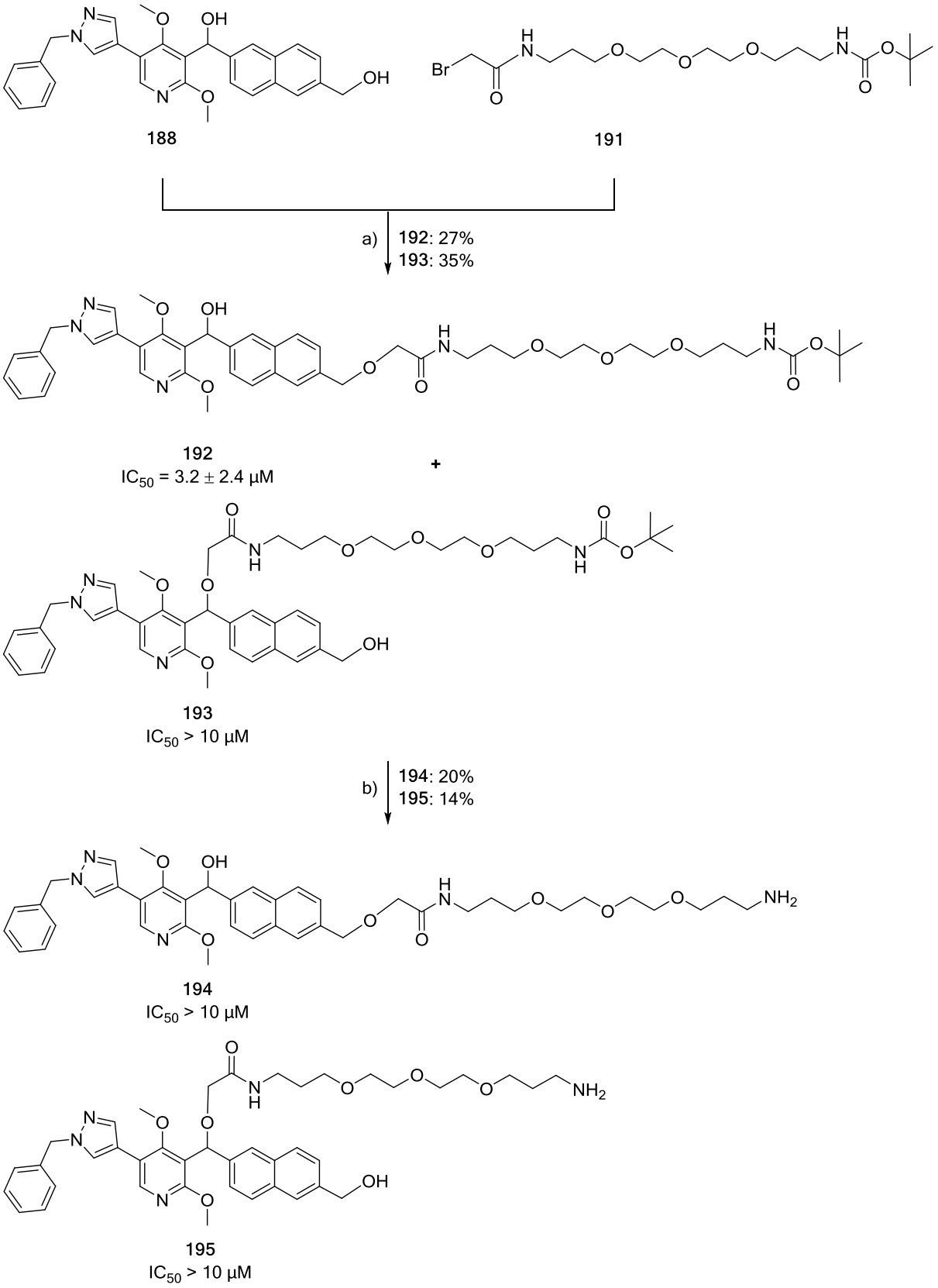

Figure 21: Pulldown probe synthesis scheme 3. a) NaH, THF, 0 °C, 30 min, **191**, -78 °C → rt, overnight; b) 5% (v/v) TFA, 1:1 (v/v) DCM/water, rt. DCM = Dichloromethane.

These findings were in line with the preceding SAR investigations, showing that the secondary alcohol was indispensable for autophagy inhibition, while a derivatization of R^2 was possible without a steep drop in biological activity. The biological activity of the probes were investigated for the Boc-protected analogues, as a primary amine at the end of a PEG-linker could drastically lower the membrane permeability. Unsurprisingly, both deprotected analogues **194** and **195** were found to be inactive in the autophagy assay.

For the pulldown experiment the positive and the negative probe were separately coupled to magnetic NHS-activated sepharose beads (Figure 8). For increasing the reactivity of the NHS-ester the beads were pre-incubated with HCl and then treated with the unprotected pulldown probes **194** and **195** respectively. After coupling the pulldown probe to the solid phase, remaining unreacted NHS-activated esters were quenched by treating them with an excess of ethanolamine. The modified beads were then equilibrated with lysis buffer, which was used to prepare the cell lysate, before incubating them with cell lysate. The lysate was prepared from MCF7-eGFP-LC3 cells, as this cell line was used for the primary screening assay. The protein target of DMP-1 and its analogues was predicted to be present in this cell line and hopefully in its lysate. In addition to lysate prepared from fed MCF7-eGFP-LC3 cells, lysate was generated from cells starved by means of amino acid withdrawal *via* incubation in EBSS for three hours. This treatment represents the conditions used in the starvation induced autophagy assay. By generating conditions that were as similar as possible for the pulldown as for the autophagy assay the chance of successfully identifying the protein target for DMP-1 was considered to be the highest.
After incubation with lysate the beads were washed with lysis buffer with increasing concentrations of magnesium chloride, in order to remove proteins that bind non-specifically. After several additional washing steps with detergent free buffers, in order to remove detergents for following MS-based analyses, the proteins binding to the beads were alkylated, reduced and directly digested on the beads. The resulting peptides were separated from an excess of salts by a short chromatographic purification and submitted for MS/MS analysis.

Each pulldown experiment was performed in technical triplicate, i.e. each condition was performed with the same lysate at the same time thrice. This kind of pulldown was performed twice with lysates from starved cells as well as twice with lysates from fed cells. There was no difference for different lysates, as the four pulldown experiments did not yield any reproducible hits as potential targets for the DMPs. Although proteins were identified, there were no significant differences in the proteins found in the negative and positive probes. These first attempts were performed with unlabeled lysate, i.e. no isotopically labeled amino acids were fed to the cells before lysate preparation. Due to the proven superiority of SILAC compared to unlabeled pulldowns in terms of a better quantification, for the following experiments lysates prepared with stable isotopes of L-arginine-$^{13}C_6{}^{15}N_4$ and L-lysine-$^{13}C_6{}^{15}N_2$ prepared from fed cells, were used.

Unfortunately the SILAC pull-down did not lead to the identification of reproducible protein hits as targets of the DMPs. For this reason several parameters were varied, including the $MgCl_2$ concentration of the washing buffers and the protein concentration of the used lysate. The salt concentration was varied in case that a potential target would only weakly bind to the immobilized probe and being washed away with too stringent washing conditions. An increase of the protein concentration in the lysate was hoped to deliver better results by reducing the amount of non-specific binding by increasing the overall amount of a specific target. Both variations still did not allow the identification of hits. In a next step the digestion protocol was changed. Instead of digesting retained proteins on the solid phase, the captured proteins were eluted by heat induced denaturation and then run into a SDS-PAGE gel, in order to remove the detergents. The gel was subsequently washed and incubated with proteases for digestion. It was speculated that the proteases in the on-bead digestion protocol may not have been able to cleave the target of the immobilized probe and thus did not elute it, because the accessibility near the sepharose surface could be restricted. It was hoped that eluting the protein by heat induced denaturation would change this. However there was no hit identified by the pulldown followed by in-gel digestion.

Conceptually, the pulldown experiment requires a positive probe that binds to the parent compound's target and a negative probe that does not. It was speculated that although the Boc-protected negative probe **193** was determined to be inactive in the cell based autophagy screen, it did not necessarily mean that the respective immobilized probe would not bind to the target in cell lysate. Hence a simplified, negative probe was synthesized consisting just of the naphthalene coupled to the PEG-linker in the same manner (Figure 22).

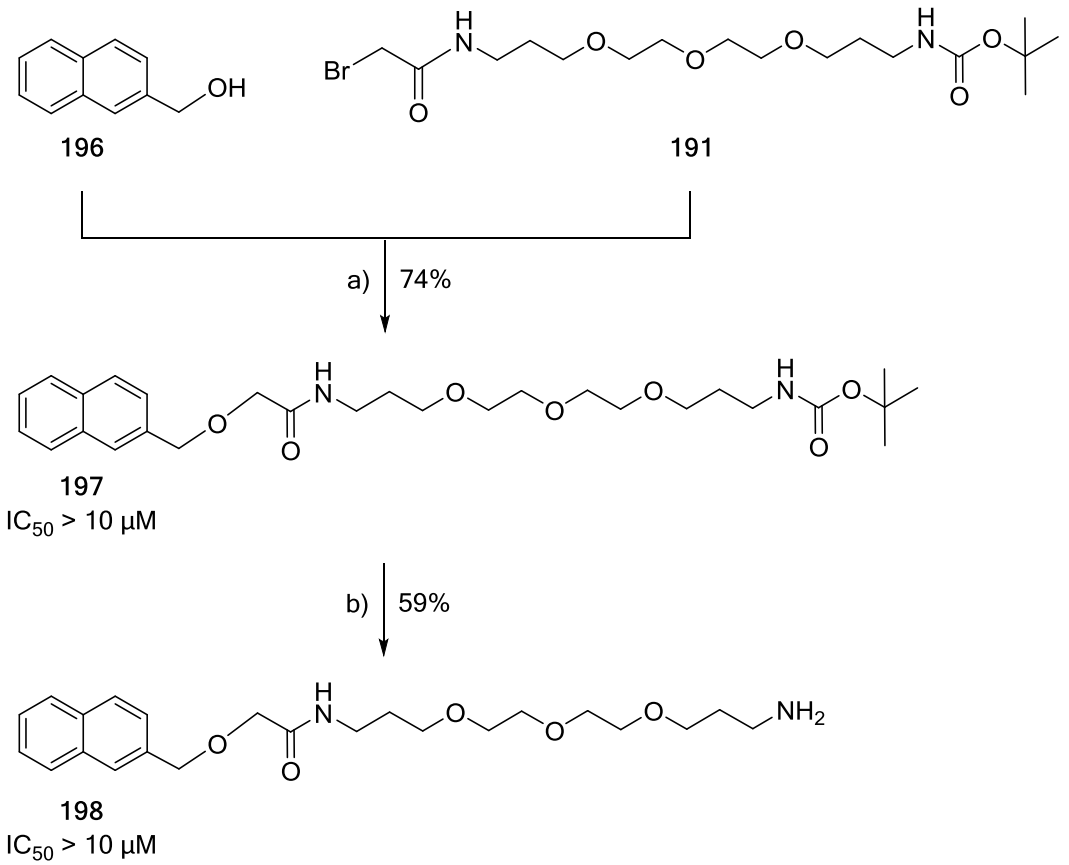

Figure 22: Synthesis of a simplified negative pulldown probe. a) NaH, THF, 0 °C, 30 min, **191**, -78 °C → rt, overnight; b) TFA, DCM, rt.

As expected the Boc-protected simplified negative probe **197** was found to be inactive in the autophagy assay. Hence it represented a promising alternative for the prior negative probe **193 / 195** and was used instead for another pulldown experiment.

Even though the big structural difference between the positive and the negative probe eventually led to the identification of hit proteins, the ratios in which the hits were enriched more by the positive probe than by the simplified negative probe were very weak (Table 7).

Table 7: Proteins identified by means of pulldown. Compound **194** was used as the positive probe while compound **198** was used as the simplified negative probe. The pulldown was performed with lysate containing isotope labeled amino acids by following the SILAC protocol. The ratios represent the fold excess of the protein enriched more by the positive probe than by the negative probe. Frequent hitter, known to be often unspecifically pulled down and identified in MS/MS experiments are not presented in the table. N = 3.

Protein name	Gene name	SILAC ratio	MW / kDa
Receptor expression-enhancing protein 3	REEP3	2.9 ± 0.6	29.3
Receptor expression-enhancing protein 4	REEP4	2.7 ± 0.7	28.2
Protein LYRIC	MTDH	1.9 ± 0.2	63.8

For REEP3 and REEP4 there was no direct link to autophagy known. In contrast the connection between the protein LYRIC, also referred to as MTDH or Astrocyte elevated gene-1 and autophagy has been made already.[139] However the low SILAC-ratios did not deliver a strong enough basis, in order to perform in depth analysis of DMP-1's interaction with MTDH. Thus it was intended to apply another general unbiased approach for identifying protein targets of the DMPs.

Despite the reported successes using standard pulldown protocols, i.e. incubating immobilized small molecules with cell lysate, there are several drawbacks. One of them is that proteins might behave differently in cell lysate than they do within living cells. Reasons for a different behaviour can be a difference in pH, salt concentrations, crowding effects of proteins and the fact that proteins might only exist in compartments or organelles in the cells the small molecule would not reach, for example due to a lack of permeability. Another problem is, that not all proteins can be solubilized in the lysis buffer when preparing the lysate. Membrane proteins for example can be insoluble in their native form in cell lysate and thus would not be identified as hits in the aforementioned pulldown experiments. In order to overcome these potential hindrances a modified pulldown protocol was established.

4.2.4.2 PAL-Pulldown

The Photo-Affinity-Labelling (PAL) pulldown also aims to enrich proteins that bind to the bioactive small molecule. However there are subtle differences. The most prominent feature, which also gave this technique its name, is the covalent labelling of binding proteins by light inducible reactive groups. Diazirines, benzophenones and arylazides are such groups. When irradiated with UV light of a particular wavelength they form radicals that readily react with any kind of Atom—H bond. Such bonds are found in all proteins, for example the Cα—H bond of every amino acid.[140,141]

In addition to the photo-activatable group, the PAL probe should also bear a moiety that allows a click reaction, such as an alkyne or an azide, of which the latter should not be an aryl azide in order to prevent activation and reaction in the UV-induced labelling reaction. This azide or alkyne allows coupling to a fluorophore or the immobilization *via* a biotin-labelled linker. This enables any covalently labelled protein to be tagged. Thus, cells can be treated with a PAL probe and any bound proteins are covalently labelled within the cell. Following cell lysis and a click reaction, potential targets can be enriched and eventually identified.

With the goal of performing a PAL pulldown a derivative of DMP-1 was synthesized, that would carry the necessary groups to make it a suitable PAL probe (Figure 23). For this purpose the benzophenone analogue of the benzylpyrazole boronic acid **201** was prepared by reacting (4-(bromomethyl)phenyl)(phenyl)methanone (199) with pyrazole boronic acid pinacol ester.

The benzophenone-pyrazole was incorporated into the probe by a Suzuki cross coupling with intermediate **204**, which also deprotected the alkyne, leading to the PAL probe **205**.

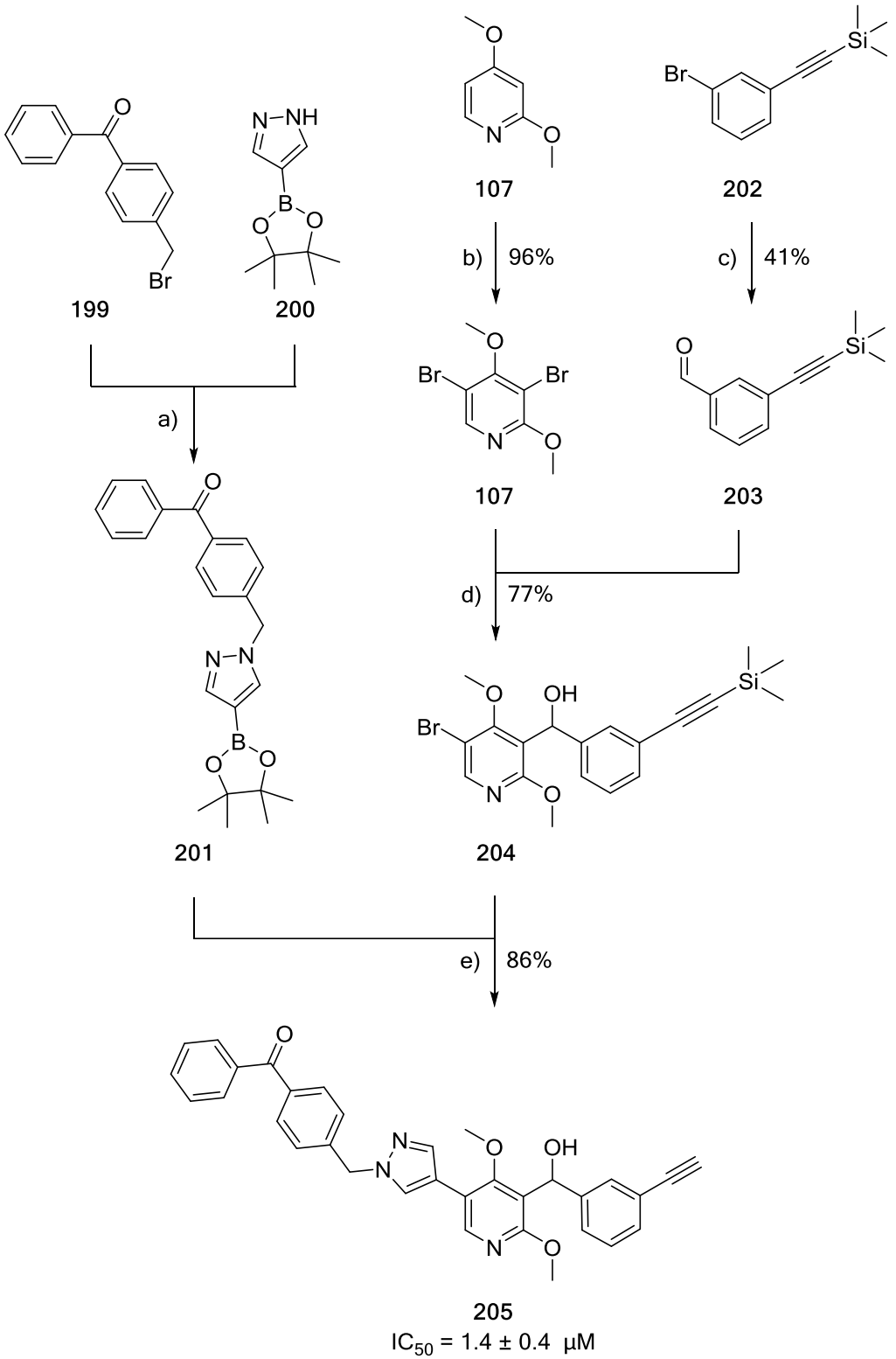

Figure 23: Synthesis of the PAL-pulldown probe **205**. a) Cs_2CO_3, MeCN, rt, 16 h; b) Br_2, acetic acid, 80 °C, 16 h, crude used ;c) *s*-BuLi, THF, -78 °C, 1 h, then DMF, -78 °C → rt, overnight; d) *s*-BuLi, THF, -78 °C, 1 h, then aldehyde, -78 °C → rt, overnight; e) $Pd(PPh_3)_4$, dppf, Na_2CO_3 (aq.), Dioxane, µW, 120 °C, 1 h.

Interestingly PAL probe **205** was found to be slightly more active than its parent compound DMP-1. The small increase in potency by extending the benzylpyrazole to its benzophenone analogue was in line with the observation that bulky hydrophobic substituents favor the activity of the DMPs.

In order to assess the reactivity of the alkyne towards a click-reaction the PAL probe was clicked with an azide-containing PEG-linker (Figure 24). The formation of the product not only showed, that this particular alkyne in general is suitable for a click reaction, but furthermore the fact that the product **207** was found to be active in autophagy further proves that R^2 allows the attachment of a linker without leading to a loss of activity for the DMPs. This finding matched the understanding of the SAR and strengthened the notion that the linker was attached at the right position for the preceding standard pulldown probe.

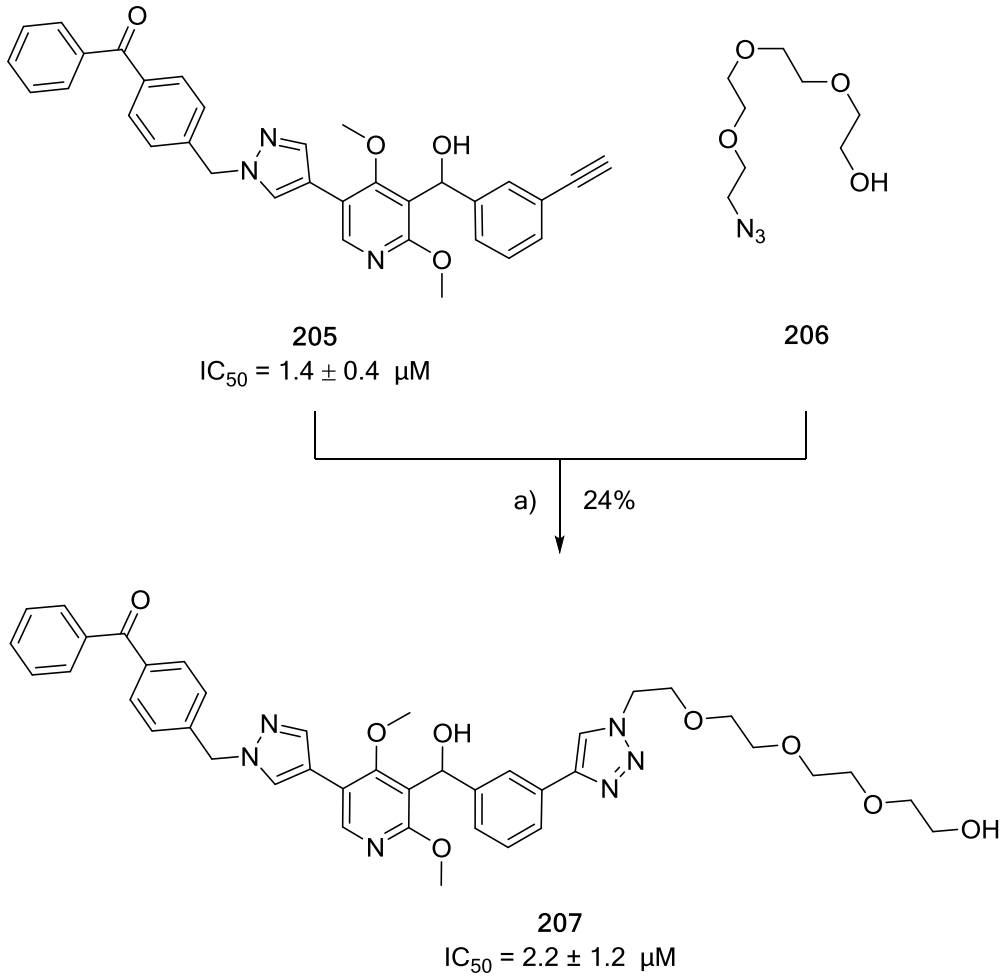

Figure 24: Evaluation of compound **205** as a PAL probe by testing the click reaction of the alkyne. a) (+)-sodium L-ascorbate, $CuSO_4$, TBTA, rt, 1:1 water / *t*-BuOH, rt, overnight.

With these results in hand the PAL pulldown was performed. For this purpose MCF7-eGFP-LC3 cells were treated according to the autophagy assay, i.e. starved by means of amino acid withdrawal by incubating in EBSS and treating with the PAL probe at a concentration of 3 µM. After treating the cells with the probe, the whole dish was irradiated with UV light at a wavelength of 365 nm, in order to induce the photo-activation of the benzophenone (Figure **25**, a)). After labeling of the proteins the cells were lysed and the alkyne was clicked to a trifunctional linker that contained an azide for the click reaction, a biotin for immobilization and a fluorophore for visualization on a gel (Figure 25, b)).

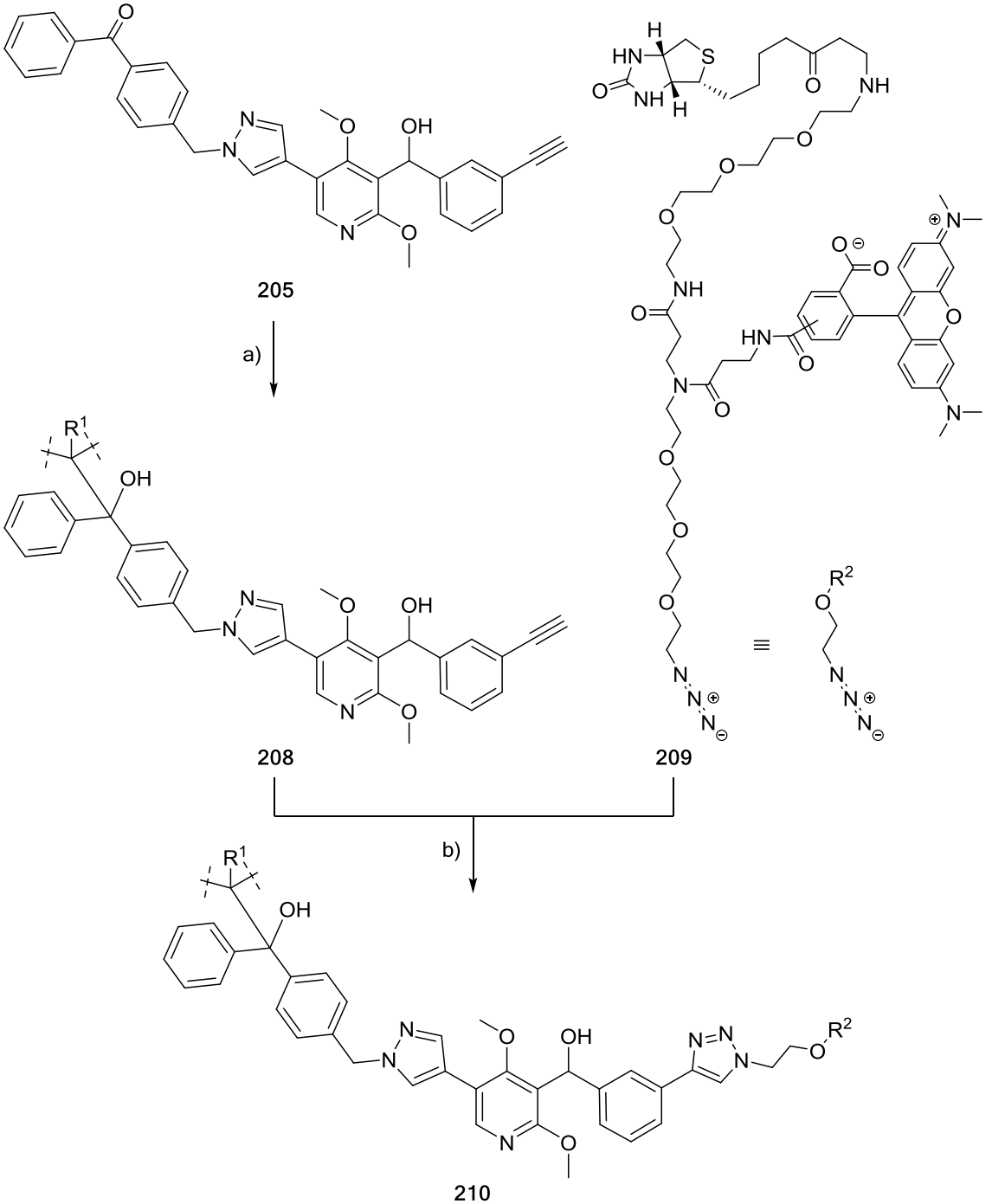

Figure 25: Photo Affinity Labeling (PAL) and click reaction for the PAL-pulldown. a) in cells: UV light (365 nm), 1 h, on ice; b) in lysate: TCEP, CuSO4, TBTA, rt, 5% (v/v) t-BuOH, 1 h.

In control experiments DMP-1 was used as a free competitor in a 5- and 10-fold concentration of the PAL probe, in order to compete the PAL probe off the target protein, to prevent the covalent labeling. Proteins labeled by the PAL probe in the absence of DMP-1 but not labeled in the presence of DMP-1 should therefore be considered as potential targets of the PAL probe and DMP-1.

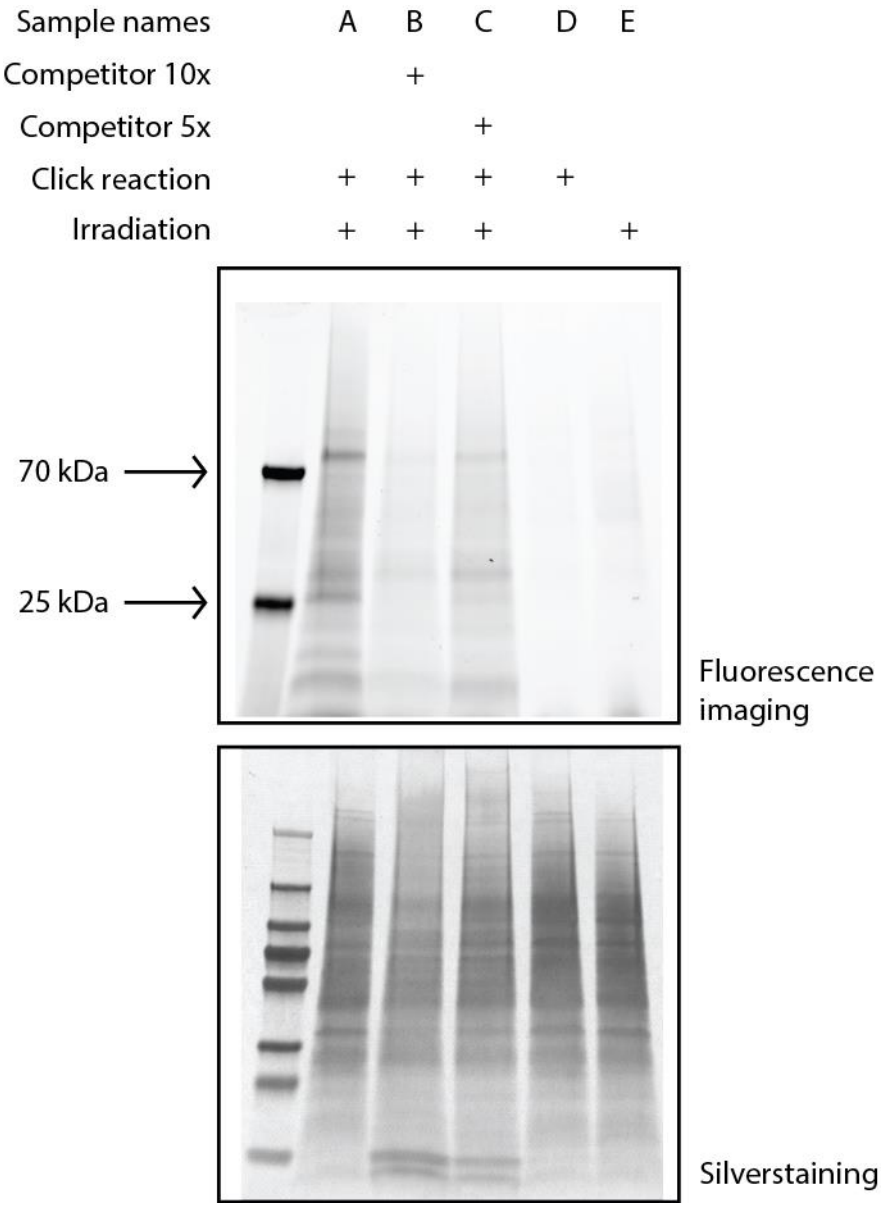

Figure 26: Covalent labeling of proteins with the PAL probe. Proteins were treated with the probe and with or without competitor, irradiated, clicked to the trifunctional linker and run on a SDS-PAGE. Bands in the upper depiction of the gel represent fluorescence of the TAMRA signal. The gel was afterwards silver-stained (bottom depiction of the same gel). Proteins labeled by the PAL probe in the absence (sample A) and presence of DMP-1 (sample B, 10-fold concentration of DMP-1; sample C, 5-fold concentration of DMP-1). Sample D was not irradiated, showing that the labeling is dependent on irradiation. Sample E is the click reaction control, by means of leaving copper out of the click reaction, showing that the visualization *via* the fluorophore only occurs selectively *via* the click reaction. n = 3, representative gel shown.

In another control experiment the feasibility of the photo-induced covalent labeling was assessed by not irradiating one sample, which should result in no covalently labeled proteins. Additionally the practicability of the click reaction in cell lysate was tested by leaving out the copper salts, in order to prevent the click reaction, which led to no fluorescent signal. The result of the experiment and all control experiments were visualized by means of SDS-PAGE, followed by scanning for fluorescence (Figure 26). After visualization of fluorescence the same gel was silver-stained, in order to confirm loading with similar amounts of proteins (Figure 26, bottom depiction of the gel).

The silver staining allows a comparison of the different samples by showing that the amount of proteins loaded onto the gel was similar. The comparison of sample A, B and C indicated dose dependent replacement of the PAL probe by the free competitor DMP-1, proving the general applicability of an experiment using a free competitor as a negative control. The advantage of a free competitor compared to an inactive probe is, that the free competitor was biologically characterized and furthermore does not carry functional groups for the PAL pulldown that could lead to artifacts by altering its binding behavior. The fact that there are no bands visible for the fluorescence imaging for samples D and E prove the specific covalent labeling of proteins by the PAL probe only due to irradiation (sample D) and the specific attachment of a fluorophore only *via* the click reaction (sample E).
After these successful test-experiments showing that every step of the experiment should work, the respective pulldown was performed. Sample type B was chosen as a negative control, because the difference in the intensities in the fluorescence imaging was higher for samples A and B than for samples A and C. Compound treatment, irradiation, lysis and click reaction followed the same protocol. Subsequently the lysate was incubated with streptavidin beads. Due to the tight interaction of Biotin with Streptavidin the covalently labeled proteins were immobilized. The strong binding furthermore allowed stringent washing and thus reduction of not covalently bound proteins. Afterwards the proteins were eluted by heat induced denaturation followed by SDS-PAGE (Figure 27).

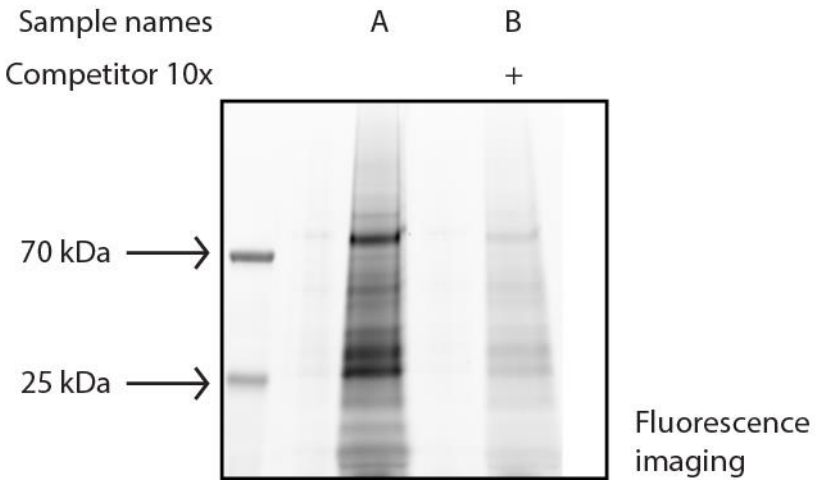

Figure 27: Enrichment of proteins labeled by the PAL probe in the absence (sample A) and presence (sample B) of DMP-1. Proteins were treated with the probe and with or without competitor, irradiated, clicked to the trifunctional linker, immobilized and enriched *via* the biotin on streptavidin-beads, eluted by heat induced denaturation and run on a SDS-PAGE. Bands represent fluorescence of the TAMRA signal. n = 3, representative gel shown.

The bands showing the biggest difference in intensity between sample A and B were cut out of the gel and in-gel digestion was performed. Because there was no significant hit identified by MS/MS analysis, in a follow-up experiment, the whole lane underwent in-gel digestion, in order not to miss any potential target that would not be abundant enough to be visible on the gel but would show a bigger difference in intensity. On-bead digestion was also performed following the same protocol as applied for the preceding standard pulldown. Both pulldown variations employing different digestion methods were performed twice with three technical replicates in each case. The analysis of these four pulldowns did not yield any significant hit. The most outstanding hits, although not significant, are summarized in the Appendix-Table 7. In order to illustrate general complications associated with this experimental setup or potentially even associated to the compound class as such, representative results of the PAL pulldowns were plotted as so called volcano plots (Figure 28).

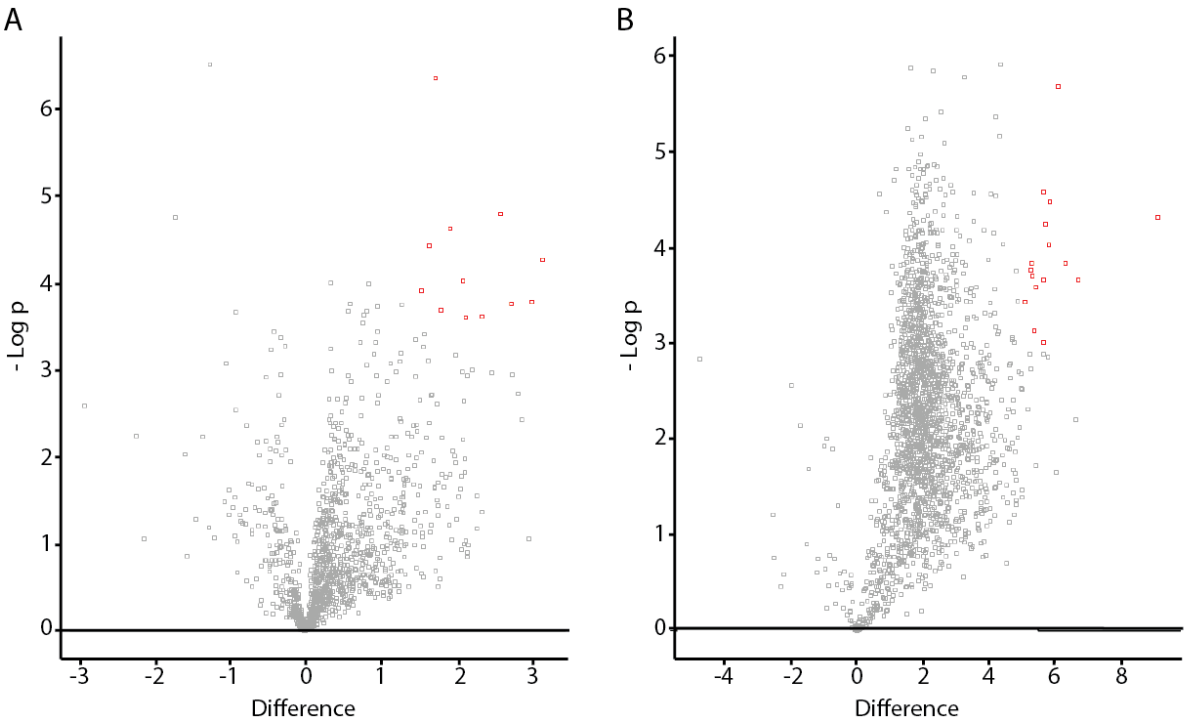

Figure 28: Volcano plots for the MS based PAL pulldowns. Two representative examples are shown. Each grey box represents a protein that was identified. Red boxes represent the strongest outliers. The Y-Axis represents the significance, based on a Student's T-test, of the data. The X-Axis represents the amount with which a protein was found in sample A (positive values, right hand side of 0) or sample B (negative values, left hand side of value 0), based on fold change of intensity-based absolute quantification (iBAQ) values of the MS/MS analysis. iBAQ represents the sum of the measured intensities of all tryptic peptides for each protein, normalized by the number of peptides that can be observed in theory. This allows the label free quantification of proteins.[142–144] Proteins with a difference of 0 are found in equal amounts in the positive as well as in the negative sample, i.e. samples A and B respectively. **A**: Representative example of an experiment processed by on-bead digestion. The red colored outliers are compared to the grey colored outlying boxes not significantly different and can therefore not be considered as hits. **B**: Representative example of an experiment processed by in-gel digestion. The red colored outliers are compared to the grey colored outlying boxes not significantly different and can therefore not be considered as hits.

The volcano plots (Figure 28) as well as the SDS-PAGE gels (Figure 26 and Figure 27), showed that many proteins were not pulled down in the negative sample B which were pulled down in the positive sample A. This indicated that the free competitor DMP-1 replaced the PAL probe from many proteins. This supported the suspicion that the DMPs bind to a relatively large number of different proteins making it difficult to identify single relevant protein targets. Unfortunately there was also no overlap of the proteins identified by the PAL pulldown and the standard pulldown. For this reason the interaction of DMP-1 with any of the identified proteins was not analyzed further.

4.2.4.3 Thermal Proteome Profiling

In order to identify potential targets of the DMPs in a system orthogonal to the pulldowns, thermal proteome profiling was performed. For this purpose lysates of MCF7-eGFP-LC3 cells were prepared and treated with DMP-1. Proteins DMP-1 bound to, were predicted to show altered melting temperatures, either through stabilization or destabilization upon compound binding (Figure 10**).**

The experiment was performed three times and hits showing up in all three single experiments were ordered according to reproducible differences in melting temperature between DMP-1 and DMSO (dT) treated cell lysate (Table 8).

Table 8: Potential protein targets of DMP-1 identified by thermal proteome profiling. Average dT = the average difference in the melting temperature. SD dT = standard deviation of the melting temperature differences determined in different experiments. MW = molecular weight of the respective protein in kDa. The cutoff was chosen to be an average dT of 5 °C. n = 3.

Protein name	Gene name	Average dT / °C	SD dT / °C	MW / kDa
Histone deacetylase complex subunit SAP30	SAP30	5.9	1.6	23.3
Lipoamide acyltransferase component of branched-chain alpha-keto acid dehydrogenase complex, mitochondrial	DBT	5.8	3.3	53.5
Dihydrolipoyllysine-residue acetyltransferase component of pyruvate dehydrogenase complex, mitochondrial; Acetyltransferase component of pyruvate dehydrogenase complex	DLAT	5.3	3.4	69.0
Protein ITFG3	ITFG3	5.3	1.0	59.7
60S ribosomal protein L27a	RPL27A	5.3	2.0	16.6
Protein VPRBP	VPRBP	5.3	0.9	168.9
Nucleoredoxin	NXN	5.2	4.0	48.4
Nuclear receptor-binding factor 2	NRBF2	5.1	3.1	31.0
Target of rapamycin complex subunit LST8	MLST8	5.1	4.0	35.9
Ras-related protein Rab-39A	RAB39A	5.1	2.3	25.0

While there were 10 proteins identified to be reproducibly stabilized by DMP-1 by more than in average 5 °C compared to DMSO, there were 81 proteins in total, which were reproducibly stabilized, with the lowest average dT being 1.9 °C. The findings that DMP-1 was able to stabilize many proteins could be seen as another indication that this compound class binds to many proteins and it is tempting to speculate that DMP-1 acts *via* a polypharmacological mechanism. Since there were no overlapping hits between the preceding pulldowns and the thermal proteome profiling none of the protein hits were further investigated.

4.2.4.4 ChemProteoBase

Due to the fact that no promising protein hit was identified using the aforementioned three independent and unbiased proteome based target identification methods, a different approach was chosen. Although proteome based target-ID methods are among the strongest and there are uncountable examples in which these methods have been successfully applied, there is one common drawback. This drawback is the bias that the target of the small molecule or better its mode of action is to bind to a protein. But there are several biologically active small molecules that unfold there effect by binding to nucleic acids or by perturbing the ion household in the cell, so called ionophores.

In order to include such modes of action, DMP-1 was investigated on a proteome-wide level by comparing it to compounds with known modes of action and known targets (Figure 29 and Table 9). The ChemProteoBase method employs image based proteome analysis by means of 2-D difference gel electrophoresis (DIGE) in comparison to reference compounds.[145–148]

The ChemProteoBase analysis was performed as described in the literature.[145–150] To determine the concentration of the compound for the proteomic analysis, the growth inhibitory activity of DMP-1 against HeLa cells was investigated first. DMP-1 inhibited HeLa cell growth dose dependently after 48 h. According to the established protocol the compound should be used at a concentration that is as close at a concentration of the LD_{100} as possible. For DMP-1 this was determined to be 100 µM against HeLa cells.

Subsequently HeLa cells were treated with 100 µM DMP-1 for 18h and the cells were subjected to the proteomic analysis. ChemProteoBase profiling was performed to estimate the mode of action of the test compound. Using the expression value of the 296 spots measured by 2-D DIGE system, cluster analysis (42 compounds) and calculation of cosine similarity (83 compounds) were performed (Figure 29, Table 9). The spots, whose volume was significantly changed, are listed in Appendix-Table 8.

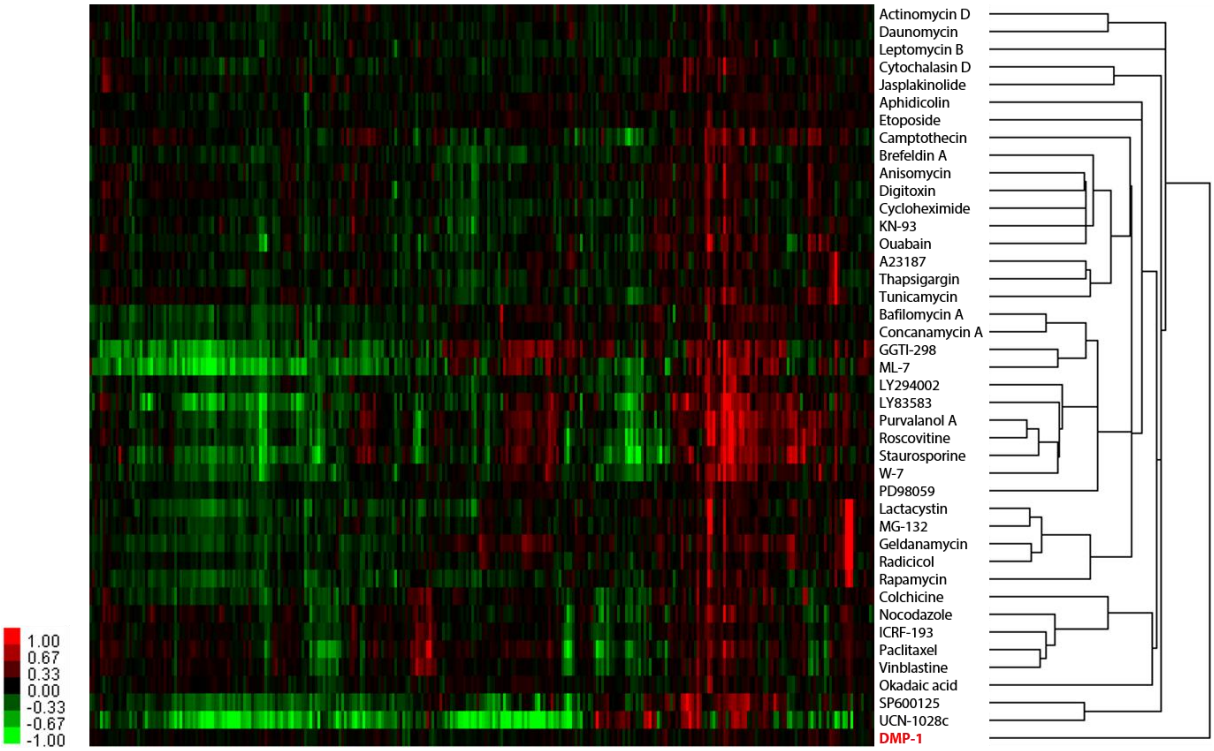

Figure 29: Hierarchical cluster analysis of the ChemProteoBase. HeLa cells were treated with 100 µM DMP-1 for 18 h, and proteomic analysis was done by the 2-D DIGE. Cluster analysis was performed using quantitative data of the 296 common spots (X-axis) derived from DMP-1 and those of 41 well-characterized compounds. In the heat map, log-fold (natural base) of the normalized volume is shown on the colored scale.

Table 9: Similarity of DMP-1 to the 83 compounds in the ChemProteoBase library.

Ranking	Cosine similarity	Compound	Target of compound
1	0.46	A23187	Transmembrane Ca^{2+} concentration
2	0.44	Tunicamycin	N-linked oligosaccharide synthesis
3	0.35	Digitoxin	N/K-ATPase
4	0.35	Cycloheximide	Protein synthesis
5	0.34	Trifluoperazine	Calmodulin
6	0.34	Thapsigargin	ER Ca^{2+} ATPase
7	0.33	MEK Inhibitor I	MEK
8	0.33	Anisomycin	Protein synthesis

Unfortunately also for this target-ID method no significantly similar reference compound (similarity > 0.7) was identified. Thus the mechanism of action of DMP-1 is suggested to be novel. Although the ChemProteoBase did not suggest a specific target for DMP-1, several reference compounds that showed the highest cosine similarity values to DMP-1, are known to influence ion-levels in the cell.

After the unsuccessful proteomic based target-ID efforts it is thus tempting to speculate that DMP-1 does not have a single protein target but acts through a polypharmacological mechanism and determing the relative contribution of each individual target will be challenging.

4.2.5 DMP-1 Summary

Dimethoxypyridine based autophagy inhibitor chemotypes have been discovered. Although not directly derived from natural products but from precursors thereof, the discovery of this compound class shows the versatility of the BIOS principle for the development of biologically active small molecules.
The DMPs expand the toolkit for studying this pathway, which is often misregulated in diseases. However, after several efforts, target-ID remains a challenge for this compound class.

4.3 Pyrazole-aminopyrimidines

4.3.1 Initial Hits

Another compound class identified by the screening of the COMAS library was a class of pyrazole-aminopyrimidines which dose-dependently inhibited autophagosome formation (e.g. **302**; Figure 30 and Table 9). Those compounds were active in both starvation- and Rapamycin-induced autophagy and thus of particular interest, since they were expected to act downstream of mTOR in canonical autophagy regulation or in non-canonical autophagy independent of mTOR.

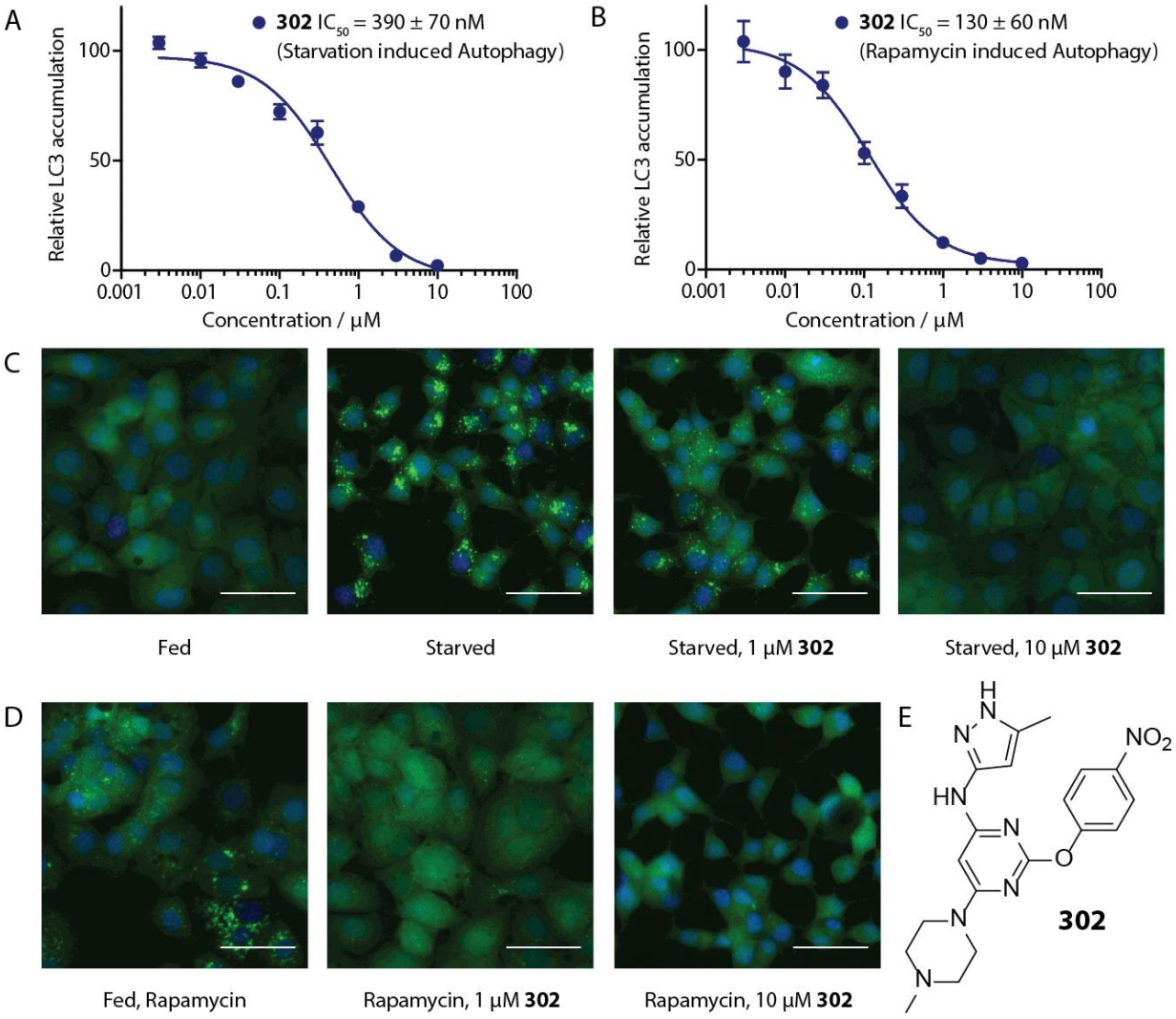

Figure 30: Phenotypic screen for inhibition of LC3 accumulation. **A**: Dose-dependent inhibition of amino acid starvation induced eGFP-LC3 accumulation by 1. **B**: Dose dependent inhibition of Rapamycin induced eGFP-LC3 accumulation by **302**. **C**: Fluorescence microscopy images of the starvation induced autophagy screen. Fed = DMSO control incubated in full media (MEM) as positive control. Starved = Autophagy was induced by amino acid withdrawal (EBSS). **D**: Fluorescence microscopy images of the Rapamycin induced autophagy screen. Rapamycin treated = DMSO control incubated in full media (MEM) together with Rapamycin as a positive control. Compound **302** reverts the phenotype in a dose dependent manner. **E**: Structure of compound **302**. Scale bar = 50 µm. Data is mean ± SD, n ≥ 3, representative graph shown. Reproduced from Robke *et al.*[151]

Autophagy inhibitor **302** and analogues thereof were previously developed as inhibitors of the protein kinase TBK1 by Richters *et al.*[152] However, TBK1 inhibition would result in inhibition of autophagosome maturation, increased autophagosome and eGFP-LC3 puncta formation and, therefore, could not explain the activity of the hit class in the phenotypic autophagy screen.[153] Hence the identification of the target responsible for the inhibition of autophagy was attempted.

An initial SAR analysis of a focused library around **302** revealed that electron withdrawing groups on the phenyl, especially in *para*-position, favored activity (Table 10, entries 1-6). Hydrophobic substituents or an amine substituent allowed only moderate activity or no activity at all (Table 10, entries 7-11).

Table 10: Structure activity relationship of a focused library around **302**. Starvation = starvation induced autophagy assay; Rapamycin = Rapamycin induced autophagy assay; Inactive = no inhibition at a test concentration > 10 µM. Data is mean ± SD, n ≥ 3 for all autophagy IC_{50} values. Reproduced from Robke *et al.*[151]

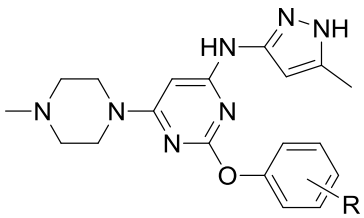

Entry	Number	R	Starvation (IC_{50} [µM])	Rapamycin (IC_{50} [µM])
1	**302**	*p*-NO_2	0.39 ± 0.07	0.13 ± 0.06
2	**303**	*p*-CF_3	1.46 ± 0.40	0.29 ± 0.03
3	**304**	*p*-Cl, *m*-F	1.74 ± 0.30	0.27 ± 0.08
4	**305**	*p*-Cl, *m*-CF_3	3.91 ± 0.30	2.33 ± 0.40
5	**306**	*p*-Cl	4.45 ± 0.40	0.61 ± 0.08
6	**307**	*m*-NO_2	4.98 ± 1.10	1.80 ± 1.00
7	**308**	*p*-^{i}Pr	5.39 ± 0.60	Inactive
8	**309**	*p*-Me	Inactive	5.55 ± 1.70
9	**310**	*p*-^{t}Bu	Inactive	Inactive
10	**311**	*m*-propanamide	Inactive	Inactive
11	**312**	*p*-NH_2	Inactive	Inactive

Due to the high potency of the most active compound of this class it represented a promising starting point for target-ID efforts *via* affinity chromatography. For the purpose of a SAR study more analogues including a few synthetic precursors of the aforementioned compound class were obtained. Remarkably, these precursors happened to be even more active than their respective parent compounds (Table 10, entries 1-7).

Table 11: Structure activity relationship of the obtained precursor of **302** and a few of its analogues. Starvation = starvation induced autophagy assay; Rapamycin = Rapamycin induced autophagy assay; Inactive = no inhibition at a test concentration > 10 µM. Data is mean ± SD, n ≥ 3 for all autophagy IC_{50} values. Reproduced from Robke *et al.*[151]

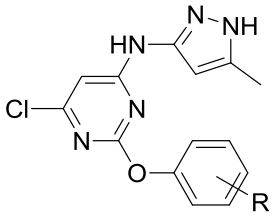

Entry	Number	R	Starvation (IC_{50} [µM])	Rapamycin (IC_{50} [µM])
1	**313**	*p*-NO_2	0.09 ± 0.04	0.04 ± 0.01
2	**314**	*p*-CF_3	0.47 ± 0.02	0.17 ± 0.06
3	**315**	*p*-Cl, *m*-F	0.40 ± 0.25	0.20 ± 0.09
4	**316**	*p*-Cl	0.51 ± 0.27	0.23 ± 0.03
5	**317**	*o*-NO2	1.40 ± 0.20	0.35 ± 0.24
6	**318**	*p*-Cl, *m*-CF_3	1.80 ± 1.40	2.70 ± 1.20
7	**319**	*m*-NO_2	2.00 ± 0.40	0.37 ± 0.14

4.3.2 Synthesis

These observations suggested to base further SAR studies on a chloro-substituent at the 6-position. Thus, for the development of more potent inhibitors, 46 more analogues of the originally intended precursors were synthesized as shown in Figure 31. For this purpose commercially available 4,6-dichloro-2-(methylthio) pyrimidine (320) was subjected to two different synthesis routes to enable diversification at the 2- or 4-position of the pyrimidine core from a respective precursor within one step (Figure 31A). Oxidation of the thioether in **320** by means of *m*-CPBA led to the corresponding sulfone **321** in 96% yield. This was followed by a nucleophilic aromatic substitution with *p*-nitrophenol, leading to intermediate **322** in a yield of 74%. Final compounds of type **325** were generated from intermediate **322** by reacting the latter with nucleophiles, replacing one of the 4-chloro substituents. The yield of this reaction, depended heavily on the type of the nucleophile. In order to explore the SAR around position 2 of the pyrimidine core, an alternative route was established replacing one of the chloro-substituents first, leading to intermediate **323** in 69% yield, followed by oxidation of the thioether to the corresponding sulfone by Oxone, yielding versatile precursor **324** in 59% yield. Intermediate **324** was converted into double substituted pyrimidine **325** by reacting it *via* another nucleophilic aromatic substitution, again showing a broad range of yields, depending on the type of the phenol. For selected analogues the remaining chloride substituent was replaced by secondary amines, leading to compounds **326**, which are more similar to the parent compound.

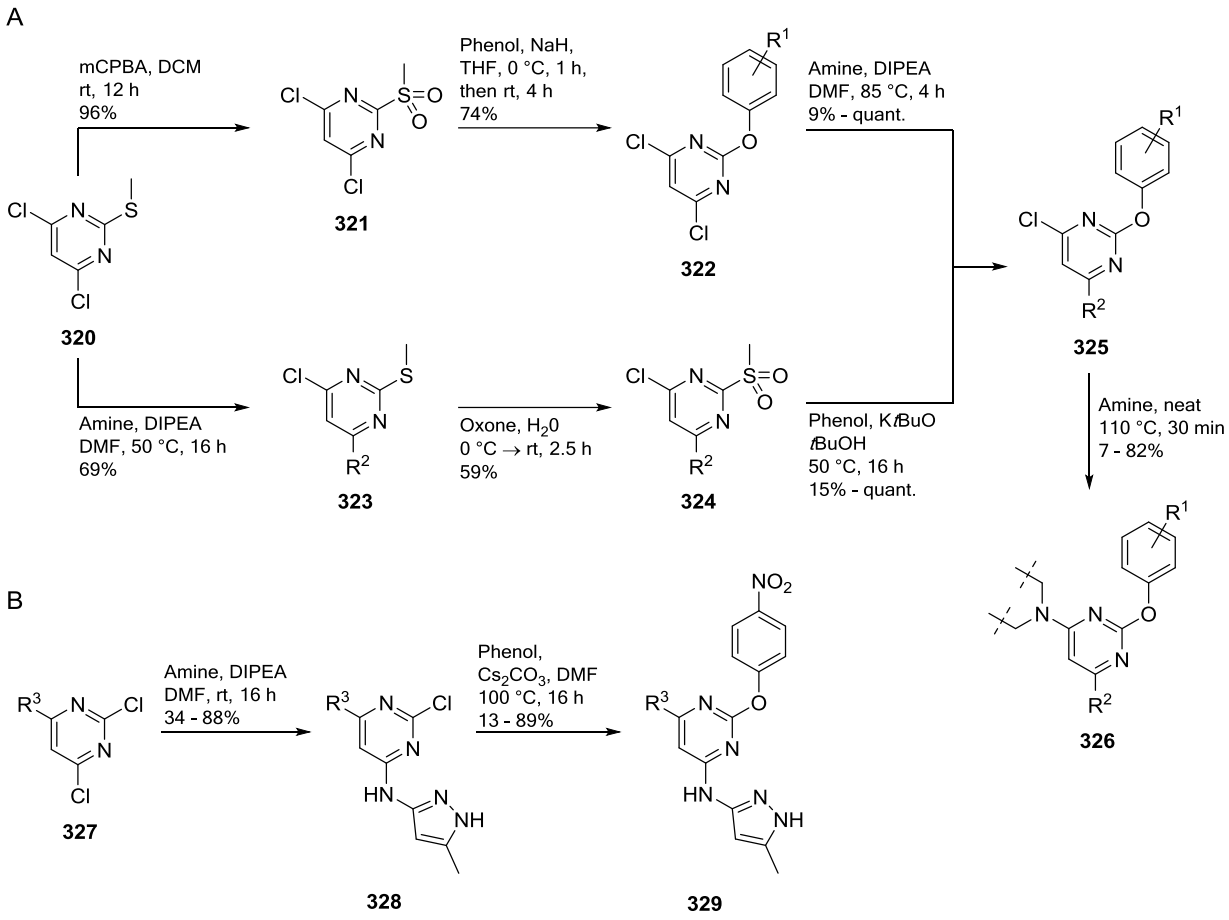

Figure 31: Synthesis of aminopyrimidines. **A**: Positions R^1 and R^2 can be varied by oxidation of the thioether followed by replacement of the methyl sulfone by a nucleophile (upper route for variations of R^2) or by initial replacement of one of the chloro substituents at the pyrimidine 4-position, respectively (bottom route for variations of R^1). **B**: Synthesis of analogues with different R^3. Reproduced from Robke et al.[151]

For the synthesis of compounds bearing a different substituent other than chloride or amines at position 6 of the final pyrimidines, such as CH_3- (Table 12, entry 2) and CF_3-substituents (Table 12, entry 3), the substituent had to be incorporated into the starting material from the beginning on (Figure 31B).

4.3.3 Structure Activity Relationship

The most interesting finding was that introduction of small substituents lacking amino groups (Table 12, entries 1-3) at the 6-position (R^3) led to an increase in inhibitory activity as compared to compound **302 (**Table 12, entry 5**)**. This finding further supported the notion that TBK1 was not the target responsible for autophagy inhibition, as the protonated piperazine moiety generates a key salt bridge with the Asp157 in TBK1 which leads to enhanced potency toward TBK1.[152] This is in line with the finding that replacement of the piperazine by a morpholine (Table 12, entry 4) increases potency as well. More generally, all amine-containing inhibitors, including those containing smaller amines (e.g. Table 12, entry 6), were less potent autophagy inhibitors as compared to the chloro- , methyl- or trifluoromethyl substituted analogues. In this context it is worth mentioning that also the parent compound of the TBK1 inhibitor, Tozasertib, had a methylpiperazine substituent,[154,155] making the fragments a whole new compound class, previously undescribed as possessing biological activity.

Table 12: Structure activity relationship around position 6 on the pyrimidine core. Starvation = starvation induced autophagy assay; Rapamycin = Rapamycin induced autophagy assay; VPS34 = *in vitro* assay for VPS34 activity. Inactive = no inhibition at a test concentration > 10 µM. Data is mean ± SD, data is mean, n ≥ 3 for all autophagy IC_{50} values; n ≥ 2 for all VPS34 inhibition values. Reproduced from Robke *et al.*[151]

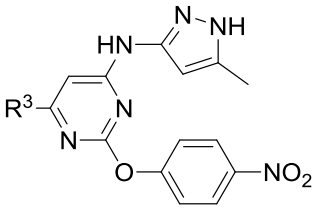

Entry	Number	R^3	Starvation (IC_{50} [µM])	Rapamycin (IC_{50} [µM])	VPS34 (% inhibition @ 0.1µM)
1	**330**	Me	0.07 ± 0.04	0.04 ± 0.02	81
2	**313**	Cl	0.09 ± 0.04	0.04 ± 0.01	80
3	**331**	CF_3	0.19 ± 0.11	0.07 ± 0.03	68
4	**332**		0.23 ± 0.11	0.16 ± 0.06	59
5	**302**		0.39 ± 0.07	0.13 ± 0.06	38
6	**333**		0.45 ± 0.16	0.28 ± 0.12	34

Examination of the heteroatom's effect at the 2-position of the pyrimidine (R^1) was done for CF_3-substituted pyrimidine analogues (Table 13, entry 1), because they were more readily accessible than their respective Cl-substituted counterparts. It was observed that the ether-oxygen of the phenols is indispensable for activity as replacement by the corresponding thiophenol leading to a thioether (Table 13, entry 2) or the aniline, leading to a secondary amine (Table 13, entry 3 and Table 15, entry 9) decreased activity. For this reason the ether oxygen was left in place for studying the SAR at position 4 of the pyrimidine (R^2).

Table 13: The ether oxygen bridging the phenyl ring and the pyrimidine. Starvation = starvation induced autophagy assay; Rapamycin = Rapamycin induced autophagy assay; VPS34 = *in vitro* assay for VPS34 activity. Inactive = no inhibition at a test concentration > 10 µM. Data is mean ± SD, n ≥ 3 for all autophagy IC_{50} values; data is mean, n ≥ 2 for all VPS34 inhibition values. Reproduced from Robke *et al.*[151]

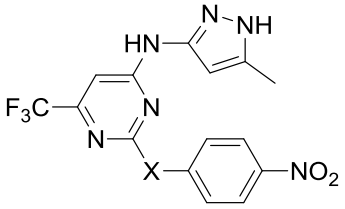

Entry	Number	X	Starvation (IC_{50} [µM])	Rapamycin (IC_{50} [µM])	VPS34 (% inhibition @ 0.1µM)
1	**331**	O	0.19 ± 0.11	0.07 ± 0.03	68
2	**334**	S	0.13 ± 0.00	0.12 ± 0.03	47
3	**335**	NH	0.34 ± 0.16	0.44 ± 0.26	29

At the 4-position of the pyrimidine, replacement of the pyrazole led to a significant loss of activity (Table 13, entries 6 – 11 and 13). This is in line with reported findings that pyrazoles can be involved in key hydrogen bonds to the kinase hinge region.[156] A methyl group on the pyrazole was most advantageous for activity (Table 13, entry 1), whilst the cyclo-propyl group (Table 13, entry 2) lowered cellular activity. A trend also observed for the indazole analogue (Table 13, entry 3) and even more for *tert*-butyl group substituted derivative (Table 13, entry 4) that led to a significant drop in cellular activity. In addition to these steric factors electronic factors or the hydrogen bond donor / acceptor pattern seemed to significantly favor the 3-amino-pyrazole substituent. This is indicated by the loss of activity, when the bridging amine was replaced by an ether (Table 13, entry 5), when an isoxazole was used instead of the pyrazole (Table 13, entry 14) or when the methyl group on the pyrazole was replaced by a hydroxyl group (Table 13, entry 12), leading to a possible tautomerism.

Table 14: Structure activity relationship around position 4 on the pyrimidine core. Starvation = starvation induced autophagy assay; Rapamycin = Rapamycin induced autophagy assay; VPS34 = *in vitro* assay for VPS34 activity. Inactive = no inhibition at a test concentration > 10 µM. Data is mean ± SD, n ≥ 3 for all autophagy IC_{50} values; data is mean, n ≥ 2 for all VPS34 inhibition values. Reproduced from Robke *et al.*[151]

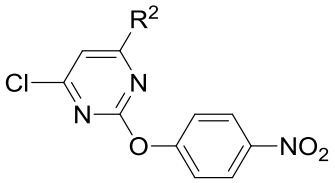

Entry	Number	R^2	Starvation (IC_{50} [µM])	Rapamycin (IC_{50} [µM])	VPS34 (% inhibition @ 0.1µM)
1	**313**		0.09 ± 0.04	0.04 ± 0.01	80
2	**336**		0.13 ± 0.03	0.10 ± 0.02	73
3	**337**		0.18 ± 0.12	0.28 ± 0.09	43
4	**338**		1.40 ± 0.70	2.00 ± 0.80	20
5	**339**		4.20 ± 3.20	4.10 ± 1.40	12
6	**340**		2.80 ± 0.70	9.79 ± 0.20	17
7	**341**		6.30 ± 1.60	Inactive	9
8	**342**		2.30 ± 1.20	Inactive	5
9	**343**		Inactive	Inactive	7
10	**344**		Inactive	Inactive	15
11	**345**		Inactive	Inactive	2
12	**346**		Inactive	Inactive	22
13	**347**		Inactive	Inactive	9
14	**348**		Inactive	Inactive	15

At this point, the SAR around R^1 was evaluated. A nitro group at the *para*-position of the phenyl group at R^1 led to the highest activity of compounds (Table 15, entries 1, 2, 4–7, 9-11), while a nitro group at the *ortho*- or *meta*-position drastically lowered activity (Table 15, entries 20 and 23). Also, replacing the phenyl group by a pyridine (Table 15, entry 24) or hexafluoroisopropanol (Table 15, entry 21), reported to be similar in size and electronic properties,[157] significantly reduced activity. Since it is generally desired to avoid nitro groups in medicinal chemistry, efforts were undertaken to replace it. Whilst it can be notoriously difficult to replace nitro functionalities while retaining activity,[158] the activity of compounds with a nitrile group (Table 15, entry 3) and a sulfonamide (Table 15, entry 13) at the *para*-position respectively, was only slightly lower. Interestingly the pyridine with a spacer of two methylene units away from the ether-oxygen (Table 15, entry 12) also allowed activity and can represent a valuable alternative for replacing nitro phenols. Pyridines with a spacer of only one methylene unit were around tenfold less active (Table 15, entries 26 and 27). Other substituents, mostly in *para*-position, yielded compounds which were active, but less so than their nitrophenol analogues (Table 15, entries 8, 15 – 19, 22 and 25).

Table 15: Structure activity relationship around position 2 on the pyrimidine core: Efforts to replace the nitro-group. Starvation = starvation induced autophagy assay; Rapamycin = Rapamycin induced autophagy assay; VPS34 = *in vitro* assay for VPS34 activity. Inactive = no inhibition at a test concentration > 10 µM. Data is mean ± SD, n ≥ 3 for all autophagy IC_{50} values; data is mean, n ≥ 2 for all VPS34 inhibition values. Reproduced from Robke *et al.*[151]

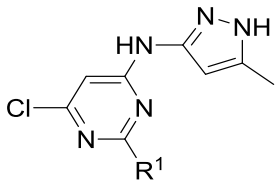

Entry	Number	R^1	Starvation (IC_{50} [µM])	Rapamycin (IC_{50} [µM])	VPS34 (% inhibition @ 0.1µM)
1	**313**	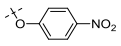	0.09 ± 0.04	0.04 ± 0.01	80
2	**349**	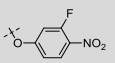	0.17 ± 0.06	0.12 ± 0.03	80
3	**350**	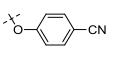	0.13 ± 0.08	0.09 ± 0.08	71
4	**351**	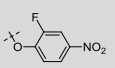	0.20 ± 0.04	0.08 ± 0.03	52
5	**352**		0.20 ± 0.09	0.47 ± 0.27	29
6	**353**	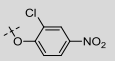	0.17 ± 0.02	0.11 ± 0.02	51

7	**354**	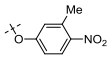	0.19 ± 0.08	0.15 ± 0.07	63
8	**355**	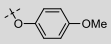	0.41 ± 0.19	0.73 ± 0.40	19
9	**356**	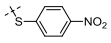	0.24 ± 0.11	0.17 ± 0.05	44
10	**357**	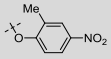	0.26 ± 0.17	0.11 ± 0.06	62
11	**358**	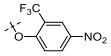	0.31 ± 0.08	0.23 ± 0.08	nd
12	**359**	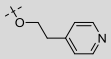	0.38 ± 0.20	0.28 ± 0.13	45
13	**360**	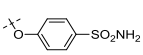	0.45 ± 0.19	0.42 ± 0.17	77
14	**361**	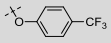	0.47 ± 0.02	0.17 ± 0.06	26
15	**362**	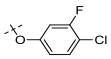	0.40 ± 0.25	0.20 ± 0.09	40
16	**363**	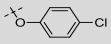	0.51 ± 0.27	0.23 ± 0.03	32
17	**364**	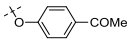	0.48 ± 0.23	0.25 ± 0.14	36
18	**365**	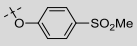	0.67 ± 0.16	0.33 ± 0.10	42
19	**366**	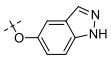	0.80 ± 0.36	0.71 ± 0.32	27
20	**367**		1.40 ± 0.20	0.35 ± 0.24	19
21	**368**		2.20 ± 0.80	8.00 ± 1.50	10
22	**369**	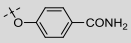	5.80 ± 4.90	5.30 ± 2.30	26
23	**370**		2.00 ± 0.40	0.37 ± 0.14	19
24	**371**	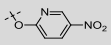	2.20 ± 0.40	2.40 ± 1.00	19
25	**372**	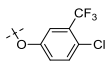	1.80 ± 1.40	2.70 ± 1.20	5
26	**373**		3.50 ± 1.50	2.90 ± 1.10	4
27	**374**		5.50 ± 3.90	3.50 ± 1.20	19

In summary, the SAR of the pyrazole-aminopyrimidine compound class is driven by three major structural features. First, the aminopyrazole is indispensable for the activity. Second, the nitrophenol represents the most active substituent for position C2 at the pyrimidine core, but can be replaced, in order to avoid the nitro group. Third, small substituents like chloro, methyl or trifluoromethyl are favored at the position of the methylpiperazine in the parent compound. Based on the SAR studies (summarized in Figure 32) compound **313** was chosen, and termed Autophinib, for further characterization and target-ID.

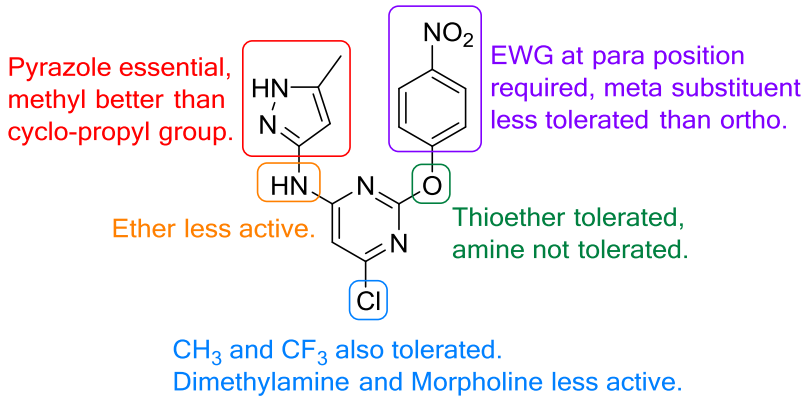

Figure 32: SAR summary of the pyrazole-aminopyrimidine based autophagy inhibitors.

4.3.4 Phenotypic Validation

Autophinib inhibited autophagy induced by amino acid starvation, as well as by Rapamycin, in a dose dependent manner (Figure 33).

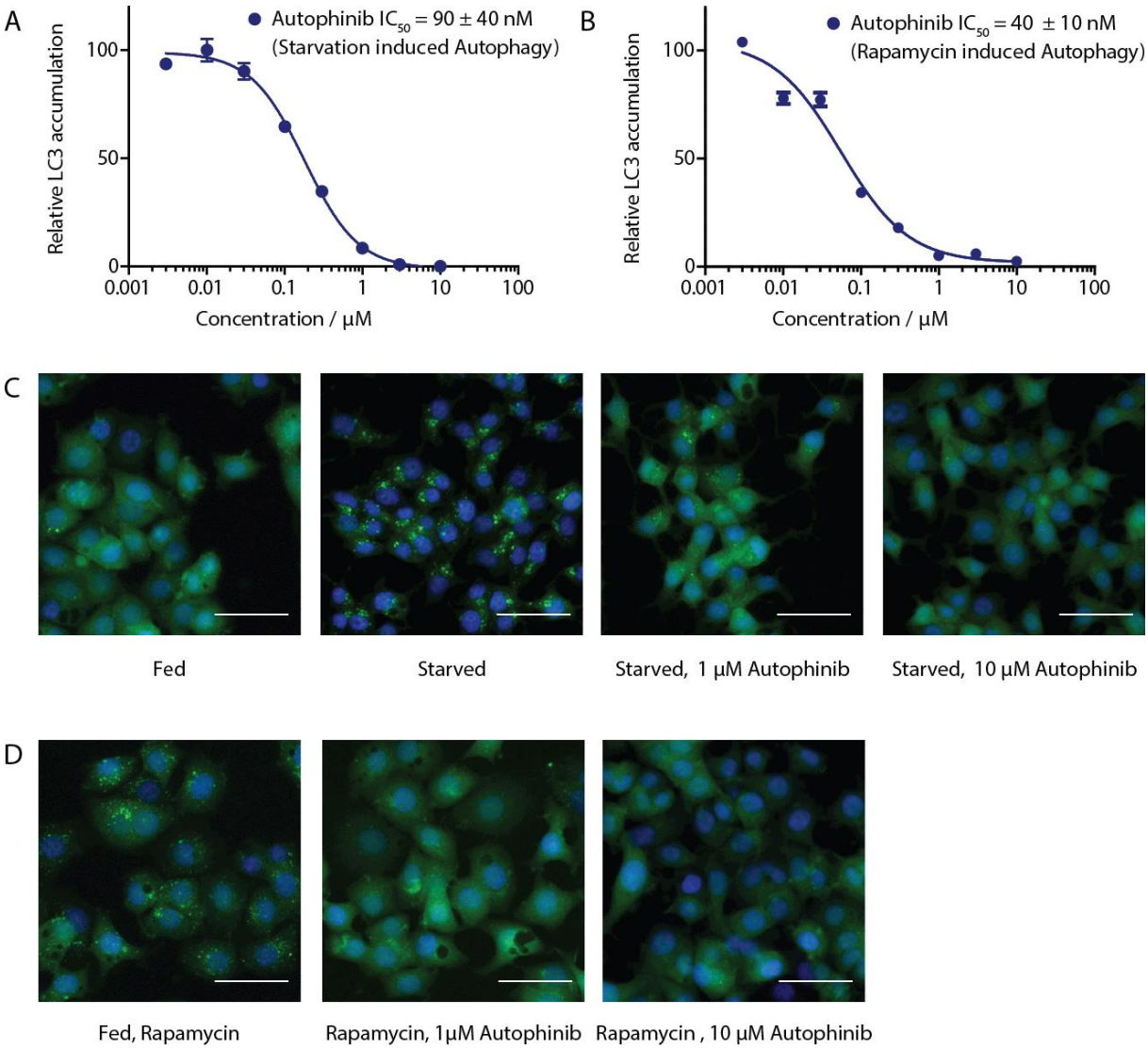

Figure 33: Autophinib inhibits starvation and Rapamycin induced LC3-eGFP accumulation. Fluorescence imaging of the high-content screen for the depletion of LC3 accumulation by Autophinib. **A**: Dose dependent inhibition of amino acid starvation induced LC3-eGFP accumulation by Autophinib. **B**: Dose dependent inhibition of Rapamycin induced LC3-eGFP accumulation by Autophinib. **C**: Images of the starvation induced autophagy high content screen taken by the automated fluorescence microscope. Fed = DMSO control incubated in full media (MEM) as a positive control. Starved = Autophagy was induced by amino acid withdrawal (EBSS). Autophinib reverts the phenotype in a dose dependent manner. **D**: Images of the Rapamycin induced autophagy high content screen taken by the automated fluorescence microscope. Fed, Rapamycin = DMSO control incubated in full media (MEM) together with Rapamycin as a positive control. Autophinib reverts the phenotype in a dose dependent manner. Scale bar = 50 µm. Data is mean ± SD, n ≥ 3, representative graphs and images shown. Reproduced from Robke *et al.*[151]

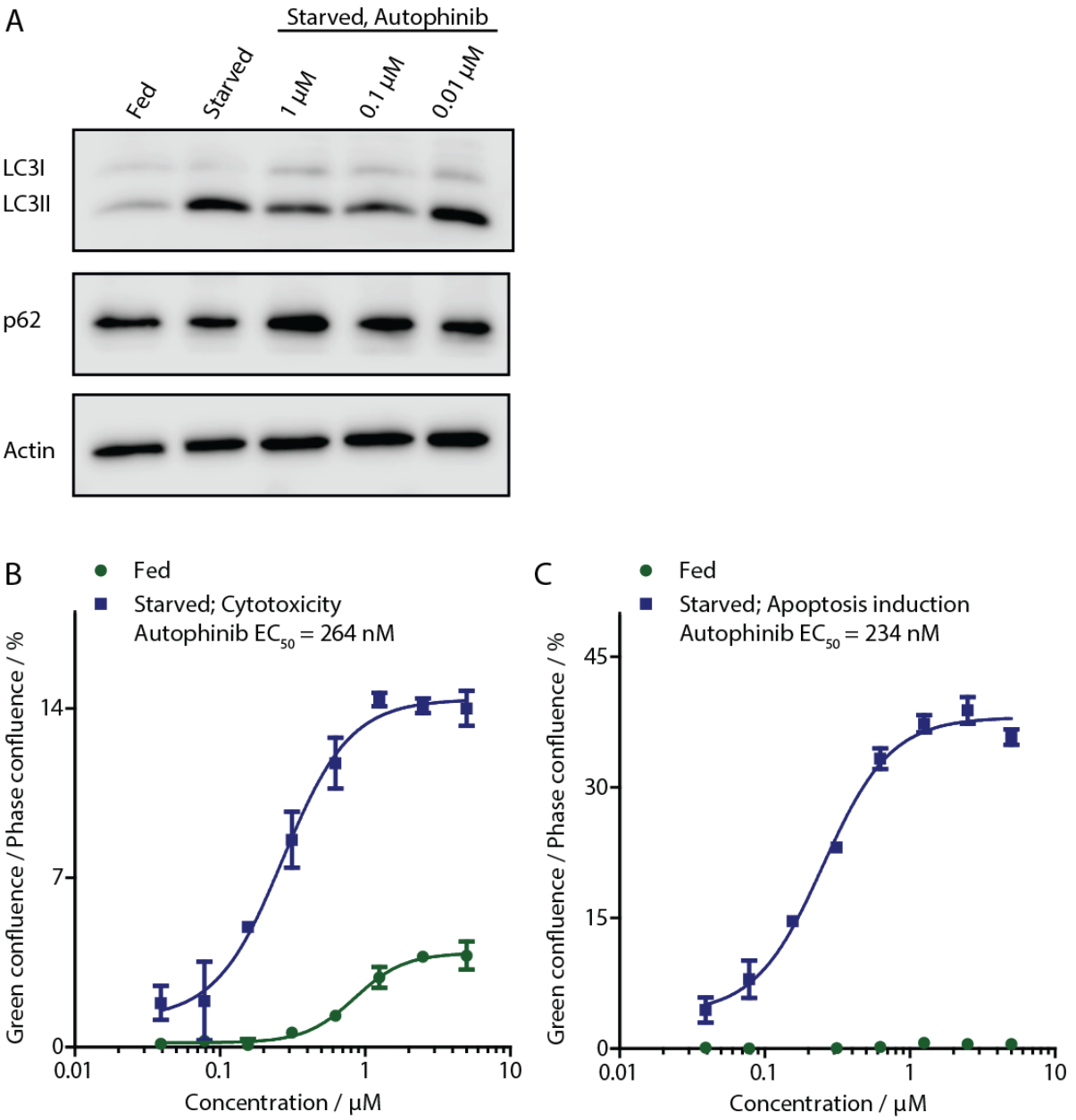

Figure 34: Phenotypic validation of Autophinib as an autophagy inhibitor. **A**: Inhibition of LC3 lipidation and p62 degradation by Autophinib in MCF7-eGFP-LC3 cells. Starvation induced autophagy induces lipidation of LC3-I to LC3-II and degradation of p62. Autophinib inhibits both effects in a dose-dependent manner. n ≥ 3, representative blot shown. **B** and **C**: Autophinib induces cell death in starved cells by means of apoptosis. **B**: Treatment of MCF7 cells under starved conditions (EBSS) or fed conditions (MEM) with Autophinib. Under starvation conditions survival is reduced. Cytotoxicity was assessed by means of the CellTox™ green dye binding to DNA due to cytotoxicity.[159,160] **C**: Autophinib dose dependently induces apoptosis in starved cells. Apoptosis was assessed by using a selective caspase 3/7 probe. The experiments were performed with an Incucyte Zoom instrument. Data are presented as a ratio of green fluorescent area to cellular area as assessed by phase contrast. Data points are mean ± SD, n ≥ 3, representative graphs shown. Reproduced from Robke *et al.*[151]

In order to asses Autophinib's ability to inhibit autophagy in an orthogonal assay, we tested whether Autophinib interferes with the lipidation of LC3. It inhibited LC3 lipidation to form LC3-II in starved MCF7-eGFP-LC3 cells in a dose-dependent manner (Figure 34A), suggesting that it acts upstream of LC3 lipidation in the autophagosome formation. Furthermore the impact of Autophinib on autophagic flux was examined, by means of investigating the levels of the autophagy substrate p62.[161–163] Autophinib inhibited p62 degradation by autophagy dose-dependently in MCF7-eGFP-LC3 cells, which demonstrates that the autophagic flux was inhibited (Figure 34A).

Autophagy is a protective mechanism, known to promote cell survival under stressful conditions, such as nutrient deprivation. In this respect, Autophinib promoted cell death in starved cells as compared to fed cells.[96,164] Moreover the cell death occurred *via* the induction of apoptosis, which was selectively induced by Autophinib in starved cells. Cell viability and induction of apoptosis were assessed by treatment of MCF7 cells with Autophinib in the presence of a caspase 3/7 probe that stains apoptotic cells, (Figure 34C) followed by live-cell imaging using the Incucyte Zoom.

4.3.5 Pathway Deconvolution

In a next step the dissection of the autophagic pathway was attempted, in order to understand Autophinib's mode of action. Since Autophinib inhibited Rapamycin induced autophagy and thus acts downstream or independently of mTOR, the late steps of autophagy were investigated in more detail. Thus a recently reported image based assay of autophagic flux, quantifying the number of autophagosomes as well as autolysosomes (Figure 35), was performed.[134] In this assay MCF7 cells stably transfected with a construct for mCherry-eGFP-LC3 (MCF7-mCherry-eGFP-LC3 cells) were treated with Autophinib under fed or amino acid starvation conditions. While eGFP is acid-sensitive, mCherry is not. Thus, in autophagosomes both fluorophores emit fluorescence (Figure 35A, DMSO-Starved-merged), whereas upon fusion of the autophagosomes with lysosomes the acidification results in quenching of eGFP and thus in the loss of the green fluorescence in autophagolysosomes. A late stage inhibitor of autophagy would therefore present itself by the accumulation of green puncta in this assay (Figure 35A, Bafilomycin A1-Starved-eGFP). As expected Autophinib inhibited the accumulation of autophagosomes under fed as well as starved conditions, but did not significantly (as assessed by student's t-test) alter the number of autolysosomes (Figure 35A, Autophinib-Starved-mCherry and Figure 35C). Taken together with the reduction of LC3 lipidation (Figure 34A) it can be concluded that Autophinib is an inhibitor of autophagosome formation and not an inhibitor of the autophagosome-lysosome fusion. This is in line with the finding that Autophinib acted similarly to Wortmannin, a known autophagosome biogenesis inhibitor, and contrary to Bafilomycin A1, a known late stage inhibitor of autophagy (Figure 35).

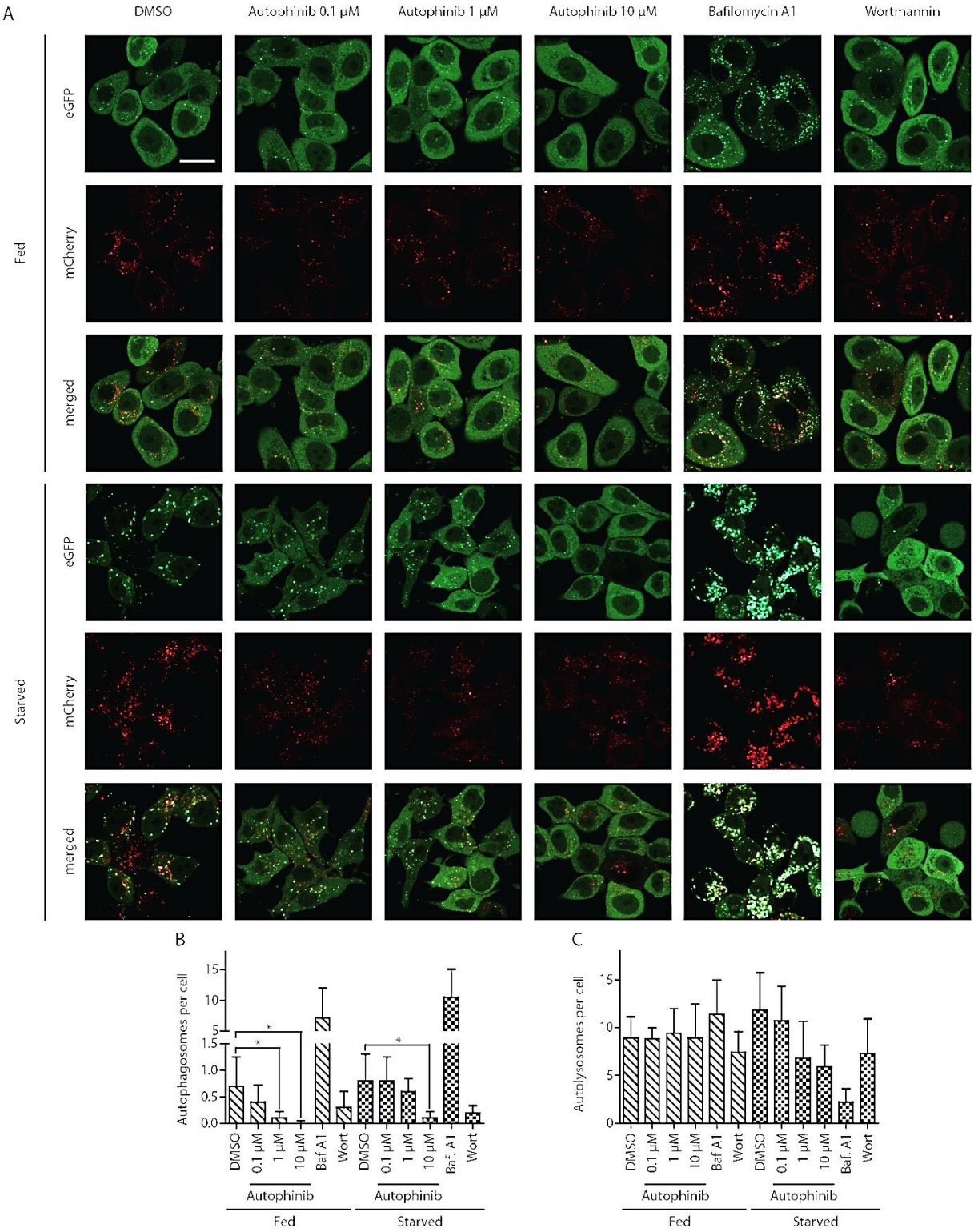

Figure 35: Autophinib inhibits autophagosome but not autolysosome accumulation. **A**: Fluorescence microscopy images of fed and starved MCF7 cells stably expressing mCherry-eGFP-LC3. **B**: Quantification of eGFP puncta showed a dose-dependent reduction of autophagosomes under fed as well as under starved conditions by Autophinib (fed, 1 µM, P = 0.0462; fed, 10 µM, P = 0.0242; starved, 10 µM, P = 0.0372), similarly to the known autophagy inhibitor Wortmannin (500 nM) and the opposite effect of Bafilomycin A1 (Baf. A1, 50 nM). **C**: Quantification of mCherry puncta showed no significant effect of Autophinib on the accumulation of autolysosomes. Scale bar = 20 µm. Statistical analysis was performed using Student's t-test (* = p≤0.05). Data are shown with mean values ± SD. Reproduced from Robke *et al.*[151]

Based on the previous insights regarding Autophinib's mode of action and in order to further narrow down Autophinib's possible target within autophagy regulation, we investigated levels of PI3P upon compound treatment. PI3P, mainly generated by the kinase Vacuolar Protein Sorting 34 (VPS34), is essential for autophagosome biogenesis. One of its functions is to recruit different effector proteins, including WIPI2, to the growing autophagosome. Therefore, eGFP fused to WIPI2b serves as a sensor for autophagosomal PI3P.[26] Hek293 cells, stably expressing eGFP-WIPI2b, showed an increasing number of fluorescent puncta, i.e. accumulation of autophagosomal PI3P, upon starvation. The number of such puncta was decreased dose dependently by Autophinib, suggesting that it lowers PI3P levels (Figure 36 and Appendix-Figure 1).

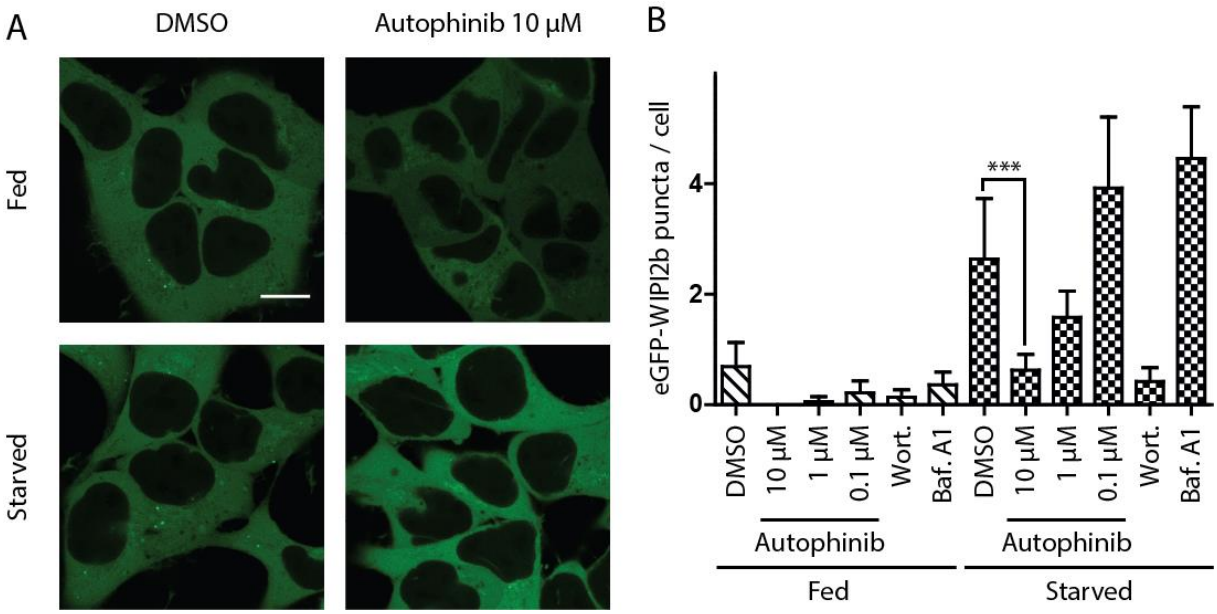

Figure 36: Dissection of autophagy by means of a WIPI2b assay**. A**: Autophinib inhibits formation of PI3P positive vesicles in HEK293A cells stably expressing eGFP-WIPI2b. The WIPI2b domain binds to PI3P leading to fluorescent puncta when PI3P is enriched. Starvation induced autophagy leads to vesicles that contain higher levels of PI3P visible as an increased number of green fluorescent puncta in the microscopy images. **B**: Quantification of the eGFP-WIPI2b assay shown in A. Autophinib reverts the phenotype (starved, 10 µM, $p = 0.0002$) showing a similar effect as Wortmannin (Wort., 500 nM) and the opposite effect of Bafilomycin A1 (Baf. A1, 50 nM). Scale bar = 10 µm. Statistical analysis was performed using Student's t-test (*** = $p \leq 0.001$). Data are shown with mean values ± 95% CI, $N \geq 25$. Reproduced from Robke *et al.*[151]

4.3.6 Target Identification

In order to identify Autophinib's target, we compared it to a set of reference compounds, by the aforementioned ChemProteoBase analysis (Figure 37, Table 16, Appendix-Table 10 and Appendix-Table 11). Unfortunately no significantly similar reference compound (similarity > 0.7) was identified. Although the ChemProteoBase did not suggest a specific target for Autophinib, several reference compounds that showed the highest cosine similarity were kinase inhibitors (Figure 37 and Table 16), among them LY294002, a known PI3K inhibitor. Cosine similarity assesses similarity as the cosine value of the angle between to vectors. If the angle is 90°, the value is 0. If the two vectors are parallel, the value is 1.

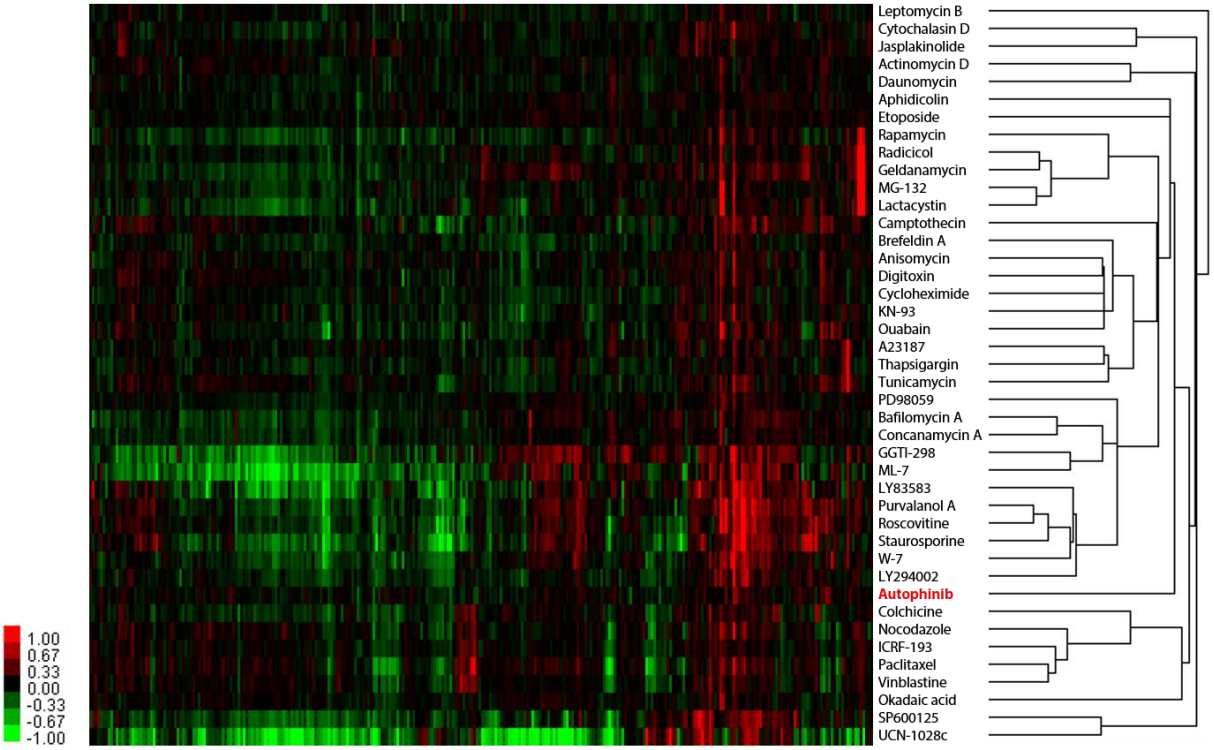

Figure 37: Hierarchical cluster analysis of the ChemProteoBase. HeLa cells were treated with 30 µM Autophinib for 18 h and proteomic analysis was performed by 2-D DIGE. Cluster analysis was carried out using quantitative data of the 296 common spots (X-axis) derived from Autophinib and those of 41 well-characterized compounds. In the heat map, log-fold (natural base) of the normalized volume is shown on the colored scale. Reproduced from Robke *et al.*[151]

Table 16: Similarity of Autophinib to the > 80 compounds in the ChemProteoBase. Reproduced from Robke *et al.*[151]

Ranking	Cosine similarity	Compound	Target of compound
1	0.50	Camptothecin	Topo I
2	0.48	Purvalanol A	Cyclin-dependent kinase (CDK)
3	0.48	Cytotrienin A	protein synthesis
4	0.48	Roscovitine	Cyclin-dependent kinase (CDK)
5	0.47	MEK Inhibitior I	MEK
6	0.44	LY294002	PI3 kinase
7	0.44	Novobiocin	HSP90 GFP
8	0.43	Ethacrynic acid methyl ester	Glutathione S-transferases

The combined results from the ChemProteoBase analysis, the PI3P puncta assay, and the fact that its parent compound is a kinase inhibitor, prompted us to test Autophinib against VPS34. VPS34 (also known as PI3KC3) is the only member of the class III PI3K subfamily. It acts by phosphorylating phosphatidylinositol (PI) to phosphatidylinositol-3-phosphate (PI3P), which is essential for membrane trafficking of proteins by recruiting FYVE, PX or WD-40 domain containing effector proteins, which are important for the formation of autophagosomes by recruiting the PI3P effectors WIPI2b and DFCP1.[165–167] In addition to VPS34's function in the regulation and initiation of autophagosome assembly it has been shown to be involved in endocytosis and mammalian target of rapamycin (mTOR) activation. The various cellular functions of VPS34 are dependent on the subunits of the different complexes it forms and their distinct subcellular localization.[168]

Gratifyingly, Autophinib inhibited VPS34 with IC_{50} values of 19 ± 5 nM at an ATP concentration of 10 µM (≈ K_M) and 51 ± 8 nM at an ATP concentration of 100 µM (Figure 38Figure 37). This ATP dependent shift in the IC_{50} suggests an ATP competitive mode of action for Autophinib.

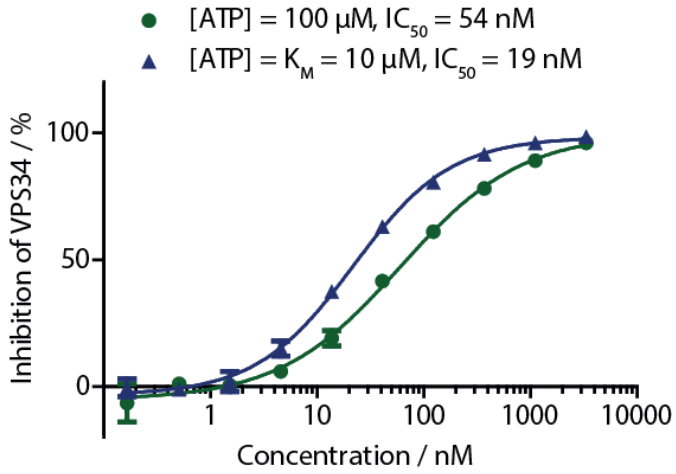

Figure 38: Dose dependent biochemical inhibition of VPS34 / PI3KC3 by Autophinib at different ATP concentrations. Reproduced from Robke *et al.*[151]

At this point a possible correlation of the inhibition of autophagy and the inhibition of VPS34 for analogues of Autophinib was examined. Despite various differences between cellular and biochemical assays, such as different solubility or membrane permeability, the IC_{50} values are expected to correlate. This would further confirm the identified target as the most relevant for the phenotypic activity. In this respect selected analogues were tested in dose-response against VPS34. A clear correlation was observed (Table 17), suggesting VPS34 as a major responsible target for Autophinib's effect on autophagy.

Table 17: Inhibition of autophagy and VPS34 determined for selected analogues. Starvation = starvation induced autophagy assay; Rapamycin = Rapamycin induced autophagy assay; VPS34 = *in vitro* assay for VPS34 activity. Inactive = no inhibition at a test concentration > 10 µM. Data is mean ± SD, n ≥ 3 for all autophagy IC_{50} values; data is mean, n ≥ 2 for all *in vitro* VPS34 IC_{50} values. Reproduced from Robke *et al.*[151]

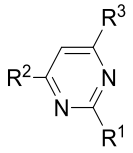

Entry	Number	R^1	R^2	R^3	Starvation (IC_{50} [µM])	Rapamycin (IC_{50} [µM])	VPS34 (IC_{50} [µM])
1	**Autophinib (313)**	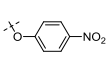		Cl	0.09 ± 0.04	0.04 ± 0.01	0.019
2	**330**	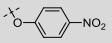		Me	0.07 ± 0.04	0.04 ± 0.02	0.023
3	**331**	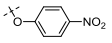		CF_3	0.19 ± 0.11	0.07 ± 0.03	0.078
4	**302**	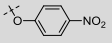			0.39 ± 0.07	0.13 ± 0.06	0.146
5	**332**	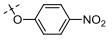			0.23 ± 0.11	0.16 ± 0.06	0.121
6	**333**	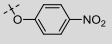			0.45 ± 0.16	0.28 ± 0.12	0.285
7	**338**	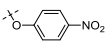		Cl	1.40 ± 0.70	2.00 ± 0.80	0.627
8	**336**	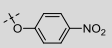		Cl	0.13 ± 0.03	0.10 ± 0.02	0.036
9	**343**	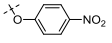		Cl	Inactive	Inactive	Inactive
10	**344**	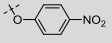		Cl	Inactive	Inactive	Inactive
11	**342**	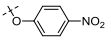		Cl	2.30 ± 1.20	Inactive	Inactive
12	**348**	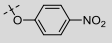		Cl	Inactive	Inactive	Inactive
13	**360**	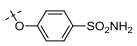		Cl	0.45 ± 0.19	0.42 ± 0.17	0.061
14	**349**	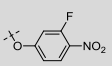		Cl	0.17 ± 0.06	0.12 ± 0.03	0.020
15	**350**	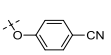		Cl	0.13 ± 0.08	0.09 ± 0.08	0.049
16	**359**	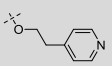		Cl	0.38 ± 0.20	0.28 ± 0.13	0.110
17	**352**	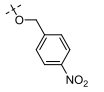		Cl	0.20 ± 0.09	0.47 ± 0.27	0.214
18	**335**	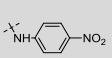		CF_3	0.34 ± 0.16	0.44 ± 0.26	0.310

Since the lipid kinase VPS34 is involved in autophagy,[23,169–172] and conditional knockout of this protein significantly diminishes autophagy[22,173] the finding that an VPS34 inhibitor is a potent inhibitor of autophagy matches our understanding of its regulation. VPS34 is the most downstream kinase in autophagy and thus presents a promising target for selective autophagy modulation with minimal side effects.[174] In this regard it was assessed whether Autophinib could be used or developed as a selective autophagy inhibitor and it was sought to do so by further interrogating its mode of action and its selectivity profile. For this purpose Autophinib was tested against a wide range of kinases. Despite its small size and the similar binding pockets of many lipid kinases, Autophinib did not inhibit other phosphatidylinositol kinases or mTOR at a concentration of 1 µM (Table 18). Also TBK1, the target of the parent compound was not inhibited, which could be explained by the fact that the piperazine in the parent compound, not present in Autophinib anymore, forms an aforementioned key hydrogen bond to TBK1.

Table 18: Selectivity of Autophinib over mTOR, phosphatidylinositol kinases and TBK1 at a concentration of 1 µM. Kinase inhibition is given in %, data is mean, n ≥ 2. Please refer to the Appendix-Table 12 for the full kinase panel. Reproduced from Robke *et al.*[151]

Kinase	Kinase inhibition / %
mTOR	10
PI4K2A	2
PI4K2B	2
PI4KA	-5
PI4KB	17
PIK3C2A	9
PIK3C2B	-21
PIK3C3 (VPS34)	90
PIK3CA/PIK3R1	3
PIK3CA/PIK3R3	10
PIK3CB/PIK3R1	-15
PIK3CB/PIK3R2	-1
PIK3CD/PIK3R1	12
PIK3CG	22
TBK1	8

Of the total >460 tested kinases in the panel (Appendix-Table 12 and Appendix-Table 13) 45 were inhibited ≥ 80% at a concentration of 1 µM. In order to assess which of those could be relevant for Autophinib's inhibitory effect on autophagy, 27 known, selective inhibitors were tested in the autophagy assay (Appendix-Table 14). Among the investigated inhibitors the by far most potent effect on autophagy was observed for two recently reported VPS34 inhibitors, SAR405 and VPS34-IN1 (Table 19).[99,100] This strengthened the hypothesis that VPS34 might be the most relevant target for Autophinib to inhibit autophagy.

Table 19: Characterization of recently reported VPS34 inhibitors in the autophagy assay. Reproduced from Robke *et al.*[151]

Entry	Number	Inhibitor name	Structure	Autophagy Inhibition	
				Starvation IC_{50} [µM]	Rapamycin IC_{50} [µM]
1	**17**	SAR405[99,105]	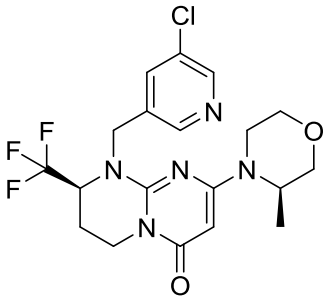	0.053 ± 0.025	0.020 ± 0.000
2	**18**	VPS34-IN1[100,106]	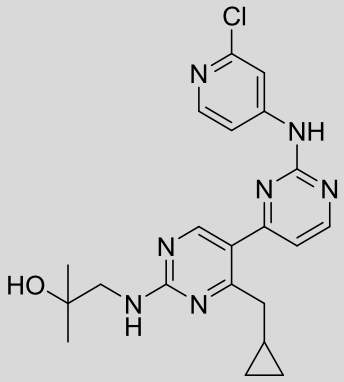	0.013 ± 0.005	0.015 ± 0. 005

In order to further support the hypothesis that VPS34 was the relevant target for autophagy inhibition showing the engagement of VPS34 by Autophinib in a complex biological medium, such as cell lysate was attempted. One of the pursued examinations of target engagements employed was the so called ActiveX assay, which employs a reactive desthiobiotin-labeled ATP-probe.[175,176] The ATP-probe covalently labels ATP binding proteins in a cell lysate with desthiobiotin, thus allowing their pulldown with streptavidin-coated agarose beads. The captured proteins can then be eluted and analyzed. Among the ATP binding proteins are kinases and by pre-treating the lysate with an inhibitor of a specific kinase the labeling of this particular kinase but not all the other kinases is blocked.

This offers the chance of finding the binding target for small molecule kinase inhibitors. In a first experimental set up this assay was performed followed by MS/MS analysis. Of the detected potential hits were a few matching biochemical kinase inhibition found in the kinase panel (Table 20). However, VPS34 was neither detected as a hit nor in general in the control, suggesting that it was either not present or not detectable *via* the performed MS/MS analysis.

Table 20: Identified kinases by the ATP Pulldown (ActiveX ATP Probe). Kinases that were identified as being competed off ATP by Autophinib and thus not pulled down compared to DMSO as the control. HeLa cells were used for preparing the cell lysate. MS: Detection and identification of proteins by means of tandem mass spectrometry.

Kinase	Cell type	Detection Method
AURKA (Aurora A)	MCF7	MS
CDK2	MCF7	MS
CDK5	MCF7	MS
GSK3A (GSK3 alpha)	MCF7	MS
GSK3B (GSK3 beta)	MCF7	MS
MAP2K7	MCF7	MS
MAPK3 (ERK1)	MCF7	MS
MAPK8 (JNK1)	MCF7	MS
RPS6KB2 (p70S6Kb)	MCF7	MS

Via Western blotting, however, it was possible to detect VPS34 in the cell lysate of interest. For this reason the ActiveX assay was performed again, followed by analysis *via* Western blotting. It revealed that Autophinib blocked the labeling of VPS34 with desthiobiotin and thus its capture in a dose-dependent manner. (Figure 39A). This result strengthened the notion that Autophinib engages VPS34 in a biological setting. Moreover the competition of Autophinib with the ATP-probe is also in line with the aforementioned finding that Autophinib inhibits VPS34 ATP-concentration dependently. The combined results indicate that Autophinib's mode of action on VPS34 is ATP competitive. In another effort to show target engagement in an unbiased setting by means of a proteome wide CETSA the same observation was made, that VPS34 could not be detected by MS-based analyses. For this reason an isothermal dose-response fingerprint (ITDRF) was performed, with Western blotting as the readout, that showed VPS34 stabilization towards melting at 50 °C by Autophinib dose dependently at higher concentrations, further confirming target engagement (Figure 39B).[122,123]

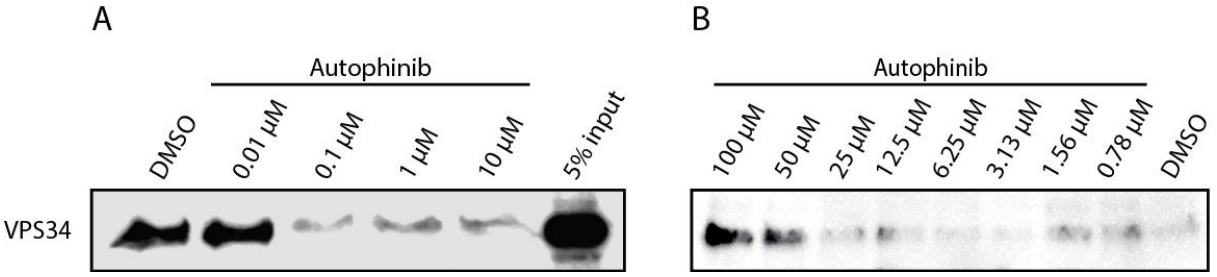

Figure 39: Target engagement of Autophinib towards VPS34. **A**: Evaluation of VPS34 as a target of Autophinib with ATP-biotin probes and readout *via* Western blot (ActiveX assay). Competition of the ATP probes with Autophinib validates binding of Autophinib to VPS34 in cell lysate. 5% input = 5% total protein amount of untreated lysate (100 % used for each reaction). Data is mean ± SD, n ≥ 3, representative blot shown. **B**: Isothermal dose-response fingerprint (ITDRF) experiments at 50 °C with pre-treated MCF7 lysate. Autophinib was used in different concentrations, in order to examine its effect on the melting temperature of VPS34. Pretreated Lysate was heated to 50 °C and denatured proteins were precipitated and removed by centrifugation. The supernatant was resolved by SDS-PAGE and VPS34 was detected by means of immunoblotting. Bands in the blot represent the amount of VPS34 in the supernatant after heat denaturation of the proteins in the lysate. The amount of VPS34 in the supernatant increases at higher concentrations of Autophinib, demonstrating Autophinib's effect to stabilize VPS34 compared to the DMSO control. n = 2, representative blot shown. Adapted from Robke *et al.*[151]

In order to further assess Autophinib's utility as a tool compound, we examined its cytotoxicity by means of a WST-1 assay. MCF7-eGFP-LC3, Panc-1 and Panc-Tu1 cell viability was impeded by the compound with IC_{50} values of 1.1 µM, 3.1 µM and 4.6 µM, respectively. Thus, there is a large concentration window in which Autophinib can be used as an autophagy inhibitor without causing cell death (Figure 40).

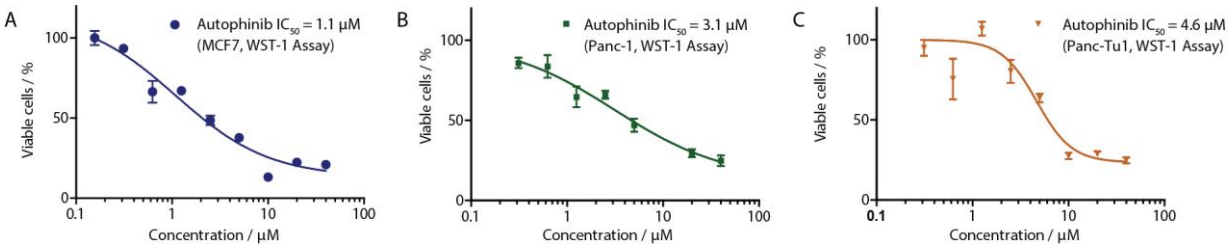

Figure 40: Detection of cytotoxicity by means of a WST-1 assay. Autophinib inhibits the cell growth of **A**: MCF7-eGFP-LC3, **B**: Panc-1 and **C**: Panc-Tu1 cells. The experiments were performed using the WST-1 reagent. Data points are mean ± SD of a representative experiment conducted in triplicate.

4.3.7 Autophinib Summary

Overall Autophinib represents a novel chemotype for the inhibition of autophagy as well as for the lipid kinase VPS34. It was discovered by means of an unbiased phenotypic screening, followed by validation and deconvolution of its effect on the autophagic pathway. Target-ID efforts led to the identification of VPS34 as the evident target. Autophinib is derived from a previously reported TBK1 inhibitor. However, it is completely selective over its parent compound's target as well as all tested phosphatidylinositol kinases and mTOR.

Autophinib potently inhibits autophagy induced by starvation and pharmacologically induced autophagy by Rapamycin. It shows target engagement in cellular models and as such it is a useful tool for studying autophagy and VPS34 activity. Especially since 3-methyladenine (3-MA) and Wortmannin, both known to inhibit several classes of PI3 kinases unselectively, have been used for years.[97] Although selective inhibitors of VPS34 have recently emerged,[99–101] Autophinib offers value by expanding the toolkit for future autophagy studies and for investigating the functions of VPS34. Moreover Autophinib offers ready synthetic accessibility (3 steps, overall yield: 45%) making it an ideal candidate for potential future developments in drug discovery and basic research.

4.4 Diaminopyrimidines

4.4.1 Initial Hits

Among the identified autophagy inhibitors in the primary screen were also compounds of a diaminopyrimidine based substance class (Figure 41). After a first SAR analysis of the 47 compounds in the library 25 additional analogues were bought from a commercial vendor, in order to further investigate the SAR and to obtain more potent inhibitors (Figure 42).

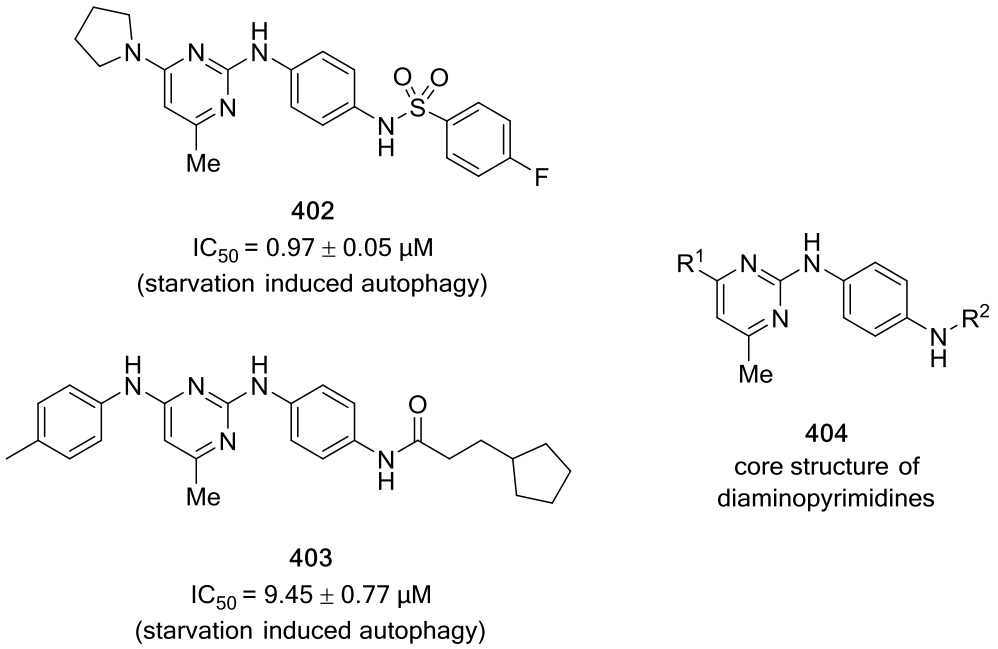

Figure 41: Hits of a diaminopyrimidine based compound class in the autophagy screen. Molecules **402** and **403** are representative examples of the first hits found to inhibit autophagy. The general structure of diaminopyrimidine **404** shows the core and R^1 and R^2 for varied substituents.

4.4.2 Structure Activity Relationship

Overall the SAR was characterized by steep activity cliffs. Comparably small changes had a strong influence on the activity of some of the analogues (Table 21). Different R^1 (left hand side) on position 4 of the pyrimidine ring generally allowed activity, with anilines leading to the most potent compounds (Table 21, entry 1-5). This was particularly clear when changing an aniline to an ethylamine (compare Table 21, entries 2 and 11) or the 4-methoxyaniline to a dimethylamine (compare Table 21, entries 3 and 9). This trend could possibly also explain the big difference in activity between entries 1 and 15, although the difference in electronic properties as a result of the additional *ortho*-fluorine on **419** may play a role.

Although alkylamines at R^1 were generally less active, depending on the amide-derivative (red colored moiety in Figure 42) or R^2, cylcoalkylamines were found to retain some activity (compare Table 21, entries 6, 7, 8 and 11). For the analogues bearing a bridging amide, the activity seemed to depend a lot on R^1 and R^2 (see Appendix-Table 15 for a full set of analogues).

For the right-hand side of the diaminopyrimidines, the most active analogues were obtained for phenyl rings bearing a substituent in *ortho*-position, such as chloro, fluoro or methoxy (Table 21, entries 1, 3 and 4). Substituents in the *para* position were also tolerated (Table 21, entries 2, 7 and 10), where the smaller methoxy was favored compared to the butoxy substituent (Table 21, entries 2 and 10). Substituents on the right hand side, that were not derivatives of benzoic acid, i.e. they had an alkyl substituent or at least an alkyl bridging unit, were generally tollerated, but it was difficult to identify a clear SAR for these examples (Table 21, entries 5, 6, 12, 13 and 14). Sulfonamides instead of the briding amides retained activity (Table 21, entry 7) whereas ureas generally reduced activity (Table 21, entries 8 and 16).

Table 21: Structure activity relationship of the diaminopyrimidines. Starvation = starvation induced autophagy assay; Rapamycin = Rapamycin induced autophagy assay. Inactive = no inhibition at a test concentration of 10 µM. Data is mean ± SD; n ≥ 3 for all values.

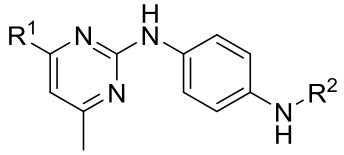

Entry	Number	R^1	R^2	Starvation (IC_{50} [µM])	Rapamycin (IC_{50} [µM])
1	**405**			0.12 ± 0.07	0.24 ± 0.20
2	**406**		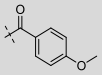	0.37 ± 0.18	1.8 ± 0.90
3	**407**			0.38 ± 0.23	1.8 ± 2.00
4	**408**			0.75 ± 0.11	1.7 ± 0.50
5	**409**			0.80 ± 0.30	0.81 ± 0.68
6	**410**		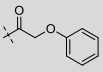	0.81 ± 0.16	0.29 ± 0.18
7	**411**			0.97 ± 0.47	0.16 ± 0.08
8	**412**		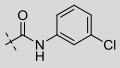	1.6 ± 0.60	4.1 ± 3.00
9	**413**			2.3 ± 1.20	1.3 ± 0.70
10	**414**		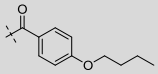	2.7 ± 0.100	1.1 ± 0.50
11	**415**		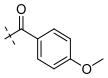	6.9 ± 0.70	2.6 ± 0.90
12	**416**		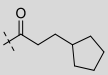	9.45 ± 0.77	4.7 ± 0.30
13	**417**		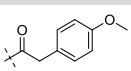	Inactive	Inactive
14	**418**		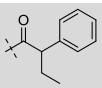	Inactive	Inactive
15	**419**			Inactive	Inactive
16	**420**		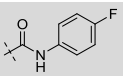	Inactive	Inactive

The SAR for the diaminopyrimidines can be summarized as steep. Small changes for R^1 and R^2 had big impacts on the biological activity. For R^1, anilines were superior over secondary amines. For R^2 phenylrings with substituents in *ortho*-position were favored; especially when the connection to the core was an amide (Figure 42). As an alternative for the amide sulfonamindes retained activity, while ureas were generally less active.

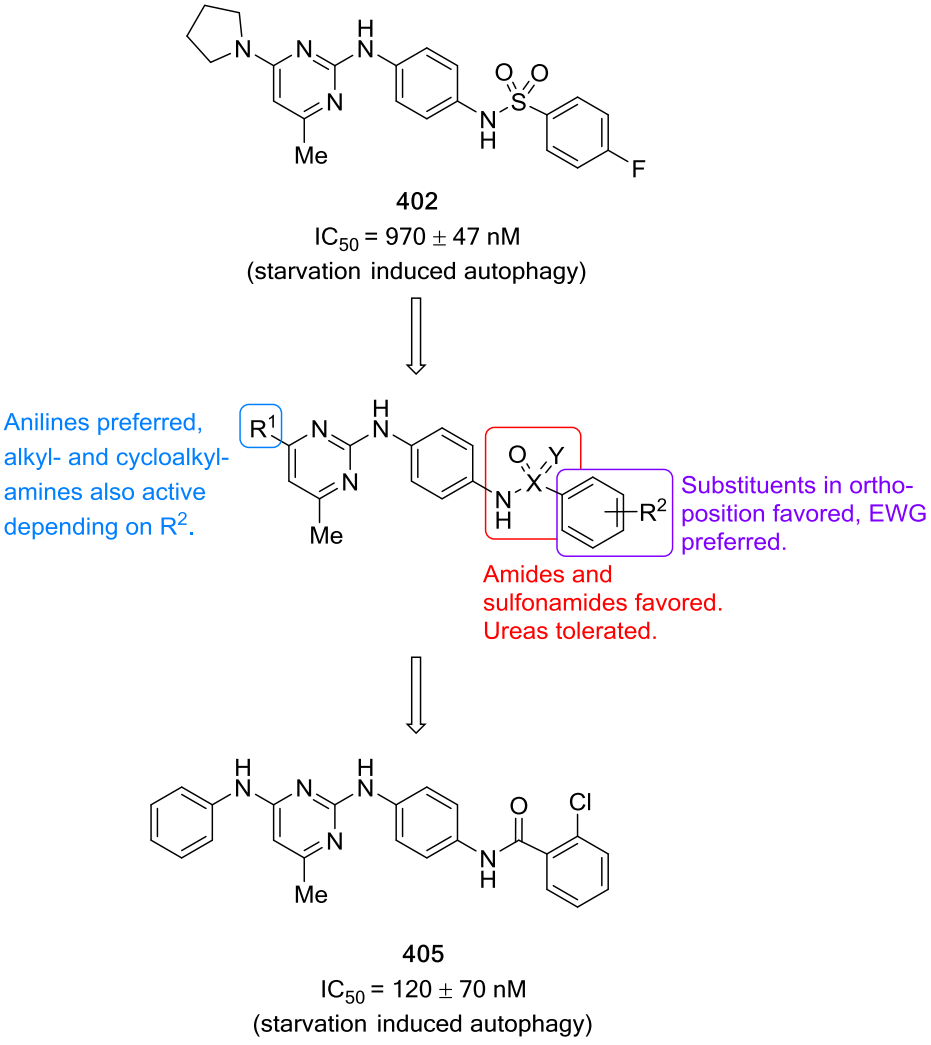

Figure 42: Summary of the development and the SAR of the diamino pyrimidines as a novel chemotype of autophagy inhibitors.

4.4.3 Structure and Activity Validation

Compound **405**, which was termed Aumitin, was chosen as the compound to proceed for further in depth-characterization, as it was the most potent one among this compound class. In order to confirm the structure and activity of the commercially acquired compound, Aumitin was resynthesized (Figure 43).

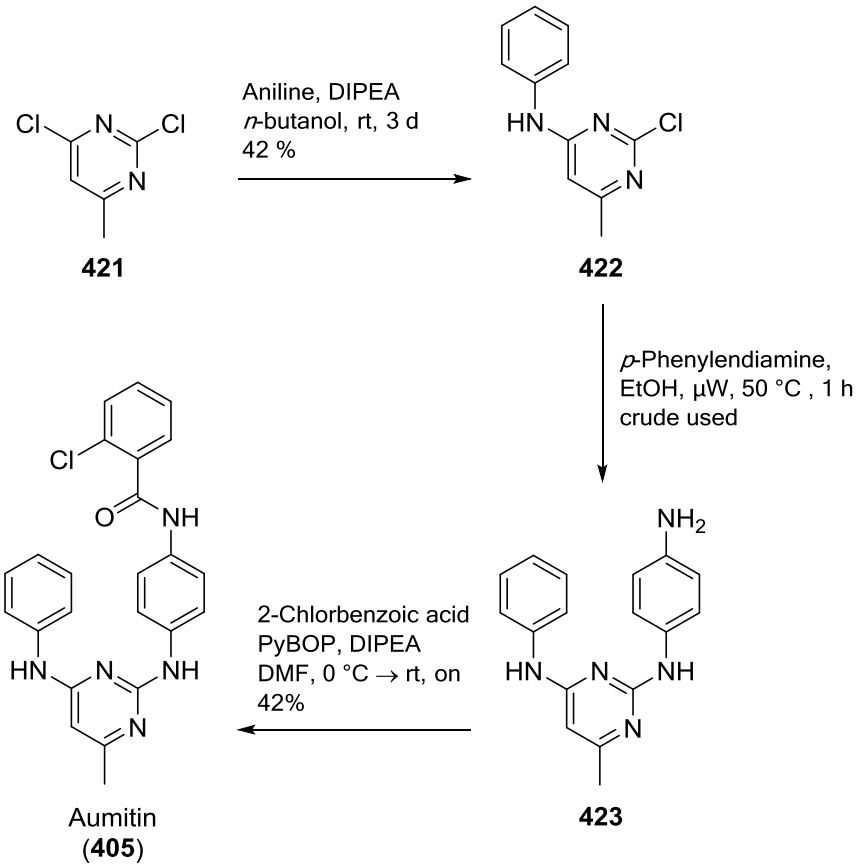

Figure 43: Synthesis of Aumitin. The regioselective replacement of the 4-chloride substituent in the first reaction was achieved by changing the solvent to *n*-butanol.

The synthesis of Aumitin started from commercially available 2,4-dichloro-6-methylpyrimidine (421), which was regioselectively reacted with aniline to replace the 4-chloro substituent. A screen of different bases and solvents revealed *n*-butanol as the superior solvent for the employment of DIPEA as the base. The second nucleophilic substitution on the pyrimidine occurred neatly with *p*-phenylendiamine in ethanol in the microwave. The amide-coupling succeeded following standard conditions using PyBOP.

The resynthesized compound was subsequently tested for its ability to inhibit autophagy by amino acid starvation and direct inhibition of mTOR by Rapamycin (Figure 44). The activity of the resynthesized batch was consistent with the commercial batch, reconfirming the structure.

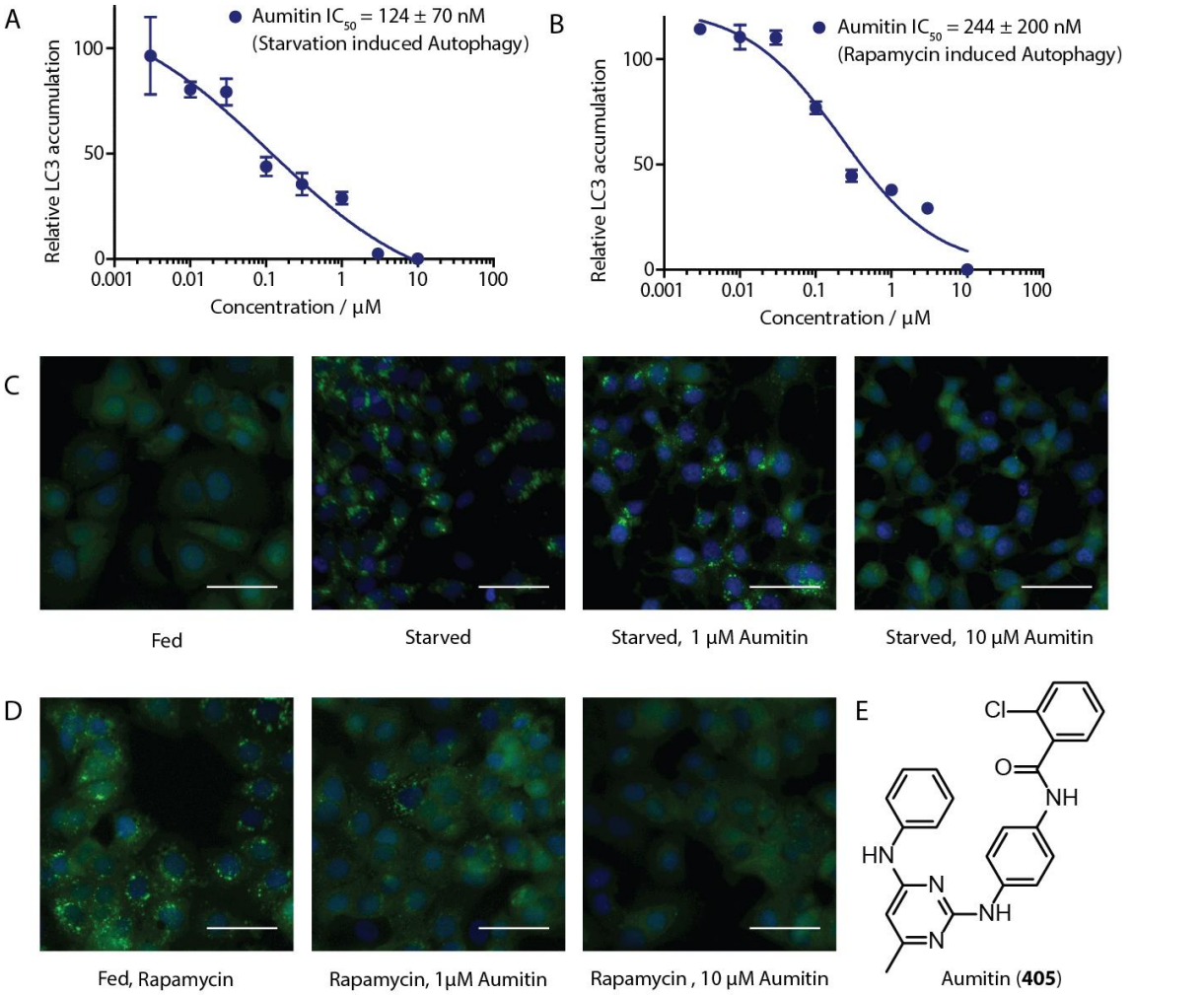

Figure 44: Phenotypic characterization of Aumitin as an autophagy inhibitor. **A**-**D**: Phenotypic screen for inhibition of LC3 accumulation. **A**: Dose-dependent inhibition of amino acid starvation induced eGFP-LC3 accumulation by Aumitin. **B**: Dose dependent inhibition of Rapamycin induced eGFP-LC3 accumulation by Aumitin. **C**: Fluorescence microscopy images of the starvation induced autophagy screen. Fed = DMSO control incubated in full media (MEM) as positive control. Starved = Autophagy was induced by amino acid withdrawal (EBSS). **D**: Fluorescence microscopy images of the Rapamycin induced autophagy screen. Rapamycin treated = DMSO control incubated in full media (MEM) together with Rapamycin as a positive control. Aumitin reverts the phenotype in a dose dependent manner. **E**: Structure of Aumitin. Scale bar = 50 µm. Data is mean ± SD, n ≥ 3, representative graphs and images shown.

4.4.4 Phenotypic Validation and Pathway Dissection

For the purpose of validating Aumitin as an autophagy inhibitor, it was tested in orthogonal assays. Aumitin inhibited LC3 lipidation during autophagy to form LC3-II in a dose-dependent manner in starved and Rapamycin treated MCF7-eGFP-LC3 cells (Figure 45A). To examine the impact of Aumitin on autophagic flux, the levels of the autophagy substrate p62 were investigated.[161–163]

As expected Aumitin inhibited p62 degradation by starvation as well as Rapamycin induced autophagy dose-dependently in MCF7-eGFP-LC3 cells, which is consistent with inhibition of autophagic flux (Figure 45A).

As expected for an autophagy inhibitor, Aumitin enhanced cell death of starved cells as compared to fed cells.[96,164] Treatment of MCF7-eGFP-LC3 cells with Aumitin at varying concentrations in a WST-1 assay (Figure 45B) or together with a caspase 3/7 probe that stains apoptotic cells (Figure 45C) revealed that Aumitin induces cell death by means of apoptosis.

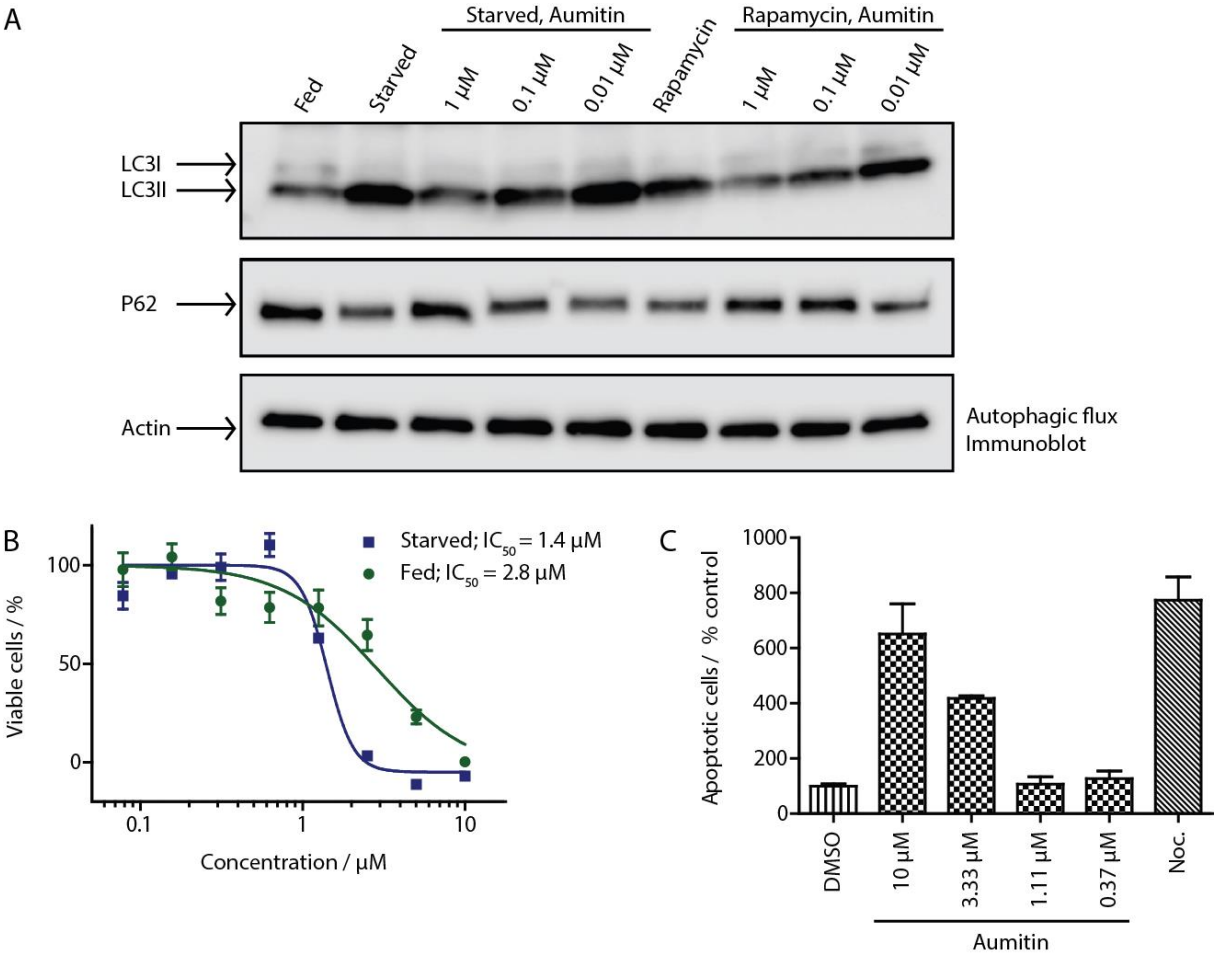

Figure 45: Orthogonal phenotypic validation of Aumitin as an autophagy inhibitor. **A**: Inhibition of LC3-II lipidation and p62 degradation by Aumitin in MCF7-eGFP-LC3 cells. Starvation as well as Rapamycin induced autophagy induces lipidation of LC3-I to LC3-II and degradation of p62. Aumitin inhibits both effects in a dose-dependent manner for starvation as well as Rapamycin induced autophagy. n ≥ 3, representative blot shown. **B** and **C**: Aumitin induces cell death in starved cells by means of apoptosis. **B**: Treatment of MCF7-eGFP-LC3 cells under starved conditions (EBSS) or fed conditions (MEM) with Aumitin. Under starvation conditions survival is reduced. Cytotoxicity was assessed by means of a WST-1 assay. Data points are mean ± SD, n ≥ 3, representative graph shown. **C**: Aumitin dose-dependently induces apoptosis in starved cells. Apoptosis was assessed by using a selective caspase 3/7 probe in starved (EBSS treated) cells in the presence or absence of Aumitin. Noc. = Nocodazole (10 µM). The experiment was performed with an Incucyte Zoom instrument. Data is mean ± SD, n ≥ 3, representative experiments shown.

4.4.5 Target Identification

As Aumitin contained a diaminopyrimidine core, which is found in various protein kinase inhibitors,[177,178] its ability to inhibit a panel of kinases was tested.

Out of 418 tested kinases only the phosphatidyl inositol kinase PI4KB was inhibited by more than 40% at a test concentration of Aumitin of 1 μM (Appendix-Table 16). Due to the similarity of several lipid kinases, Aumitin was furthermore tested against other phosphatidylinositol kinases, revealing PI3KC2G as another weakly inhibited target. Since phosphatidylinositol phosphates and their respective kinases are known to be important for autophagy it was tempting to speculate that these kinases could be the responsible targets of Aumitin for its ability to inhibit autophagy,[169,179,180] despite the fact that Aumitin's IC_{50} in the cellular autophagy assay was lower than for the biochemical kinase inhibition. Although not necessarily so, the inhibitor is predicted to be more active in the biochemical assay.

In order to test whether inhibition of PI4KB or PI3KC2G could lead to inhibition of autophagy, reported small molecule inhibitors of these kinases were synthesized (Table 22).[181,182] In addition, a PI4KB inhibitor, designed and synthesized by Astra Zeneca, was obtained as a kind donation.[183] Inhibition of these kinases by means of small molecules did not inhibit autophagy in our assay, which indicated that the two phosphatidylinositol kinases could be off-targets and thus are unlikely to be relevant for Aumitin's effect on autophagy (Table 22).

Table 22: Examination of the effect of small molecule kinase inhibitors on autophagy. Bought or synthesized literature reported kinase inhibitors, their known targets and their effect in our autophagy assays are shown. The biochemical kinase inhibition by Aumitin was measured in two independent experiments with each datapoint in duplicate. Starvation = starvation induced autophagy assay; Rapamycin = Rapamycin induced autophagy assay. Inactive = no inhibition at a test concentration > 10 µM. Data is mean ± SD, n ≥ 3 for all autophagy inhibition values.

Entry	Compound name (Number)	Structure	Kinase targets		Autophagy Inhibition	
			Kinase name	Biochemical inhibition IC_{50} [µM]	Starvation IC_{50} [µM]	Rapamycin IC_{50} [µM]
1	Aumitin (**405**)	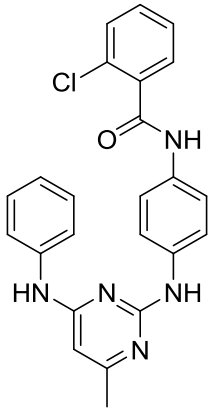	PI4KB PI3KC2G	0.301, 0.426 2.610, 3.670	0.124 ± 0.070	0.244 ± 0.200
2	PI4KB inhibitor 1[183] (**421**)	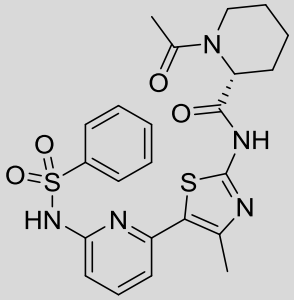	PI4KB	0.016[183]	Inactive	Inactive
3	PI4KB inhibitor 2[181] (**422**)	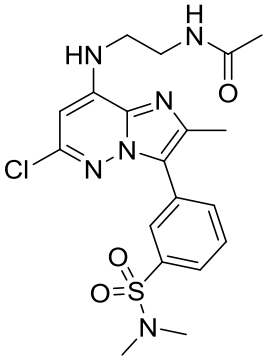	PI4KB	0.054[181]	Inactive	Inactive
4	PIK3C2g inhibitor 1[182,184] (**423**)	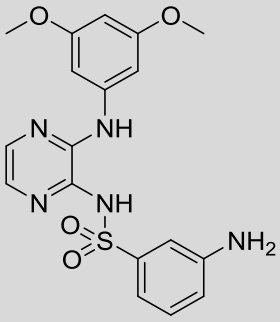	PI3KC2G	0.34[184]	Inactive	Inactive

5	PIK3C2g inhibitor 2[182,184] (**424**)	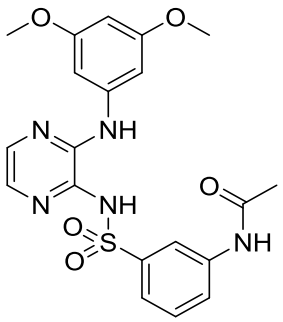	PI3KC2G	3.41[184]	Inactive	Inactive
6	PIK3C2g inhibitor 3[182,184] (**425**)	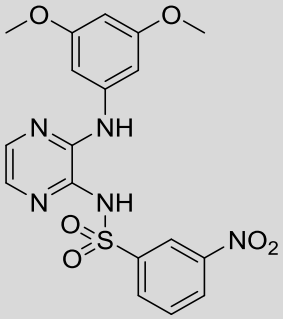	PI3KC2G	23% residual activity at 10 µM[184]	2.40 ± 1.50	Inactive
7	PIK3C2g inhibitor 4[182,184] (**426**)	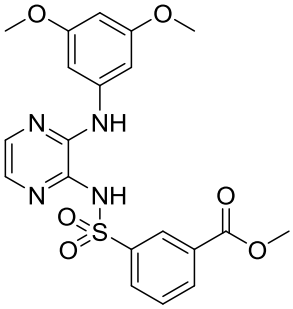	PI3KC2G	14% residual activity at 10 µM[184]	Inactive	Inactive

In order to further devalidate the hypothesis of Aumitin inhibiting autophagy through the inhibition of the phosphatidylinositol kinases, analogues of Aumitin were chosen and tested against the respective kinases (Table 23). The fact that the SAR between the inhibition of the kinases and autophagy did not correlate, further supported the notion that these kinases were not the major responsible targets of Aumitin for its inhibitory effect on autophagy.

Table 23: Correlation of the structure activity relationship between PI4KB and PI3KC2G and autophagy. Inhibition of PI4KB was tested at an ATP concentration of 5 µM ≈ K_M. Inhibition of PI3KC2G was tested at an ATP concentration of 10 µM. Each value shown for the measured inhibition of a kinase represents n = 1, with every data point measured in duplicate. For the single point measurements regarding the inhibition of the kinase the average mean is given. Starvation = starvation induced autophagy assay; Rapamycin = Rapamycin induced autophagy assay. Inactive = no inhibition at a test concentration of 10 µM. Data is mean ± SD; n ≥ 3 for all autophagy inhibition values.

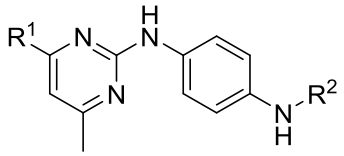

				Kinase inhibition		Autophagy Inhibition	
Entry	**Number**	**R^1**	**R^2**	**PI4KB (IC_{50} [µM])**	**PI3KC2G (% inhibition for 1 µM Aumitin)**	**Starvation (IC_{50} [µM])**	**Rapamycin (IC_{50} [µM])**
1	Aumitin (**405**)			0.301, 0.426	57 ± 2	0.12 ± 0.07	0.24 ± 0.20
2	**409**			0.647	43 ± 2	0.80 ± 0.30	0.81 ± 0.68
3	**410**		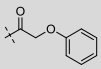	11.400	22 ± 1	0.81 ± 0.16	0.29 ± 0.18
4	**411**			0.874	20 ± 4	0.97 ± 0.47	0.16 ± 0.08
5	**412**		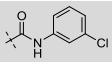	11.100	12 ± 3	1.6 ± 0.60	4.1 ± 3.0
6	**419**			4.430	17 ± 7	Inactive	Inactive

The most prominent role for autophagy is the degradation of cellular components, in order to compensate for a temporary lack of nutrients.[33] In this respect, autophagy is tightly connected to metabolism, nutrient uptake and cellular energy supply by the mitochondria.[185–187] Due to this effect of autophagy, there was an interest to also investigate the effect of autophagy inhibitors on metabolism. Therefore Aumitin was tested in an assay, assessing the cellular ability to take up glucose.[188] However, Aumitin did not inhibit glucose uptake (residual activity > 75 % at 30 µM, n = 4) in HCT116 cells.

Autophagy controls mitochondrial homeostasis by means of mitophagy.[52] Conversely, mitochondria regulate autophagy by generation of ATP and production of reactive oxygen species (ROS).[51]

Therefore, in a next step DMP-1, Autophinib and Aumitin were tested in a mitochondrial respiration assay (Figure 46 and Figure 48). In this test for mitochondrial respiration in a Seahorse XF Extracellular Flux Analyzer two fluorophores, embedded into a polymer are brought into close proximity to the seeded cells. One of the fluorophores is quenched by oxygen. This allows the determination of oxygen consumption, which is a surrogate marker for respiration. The other fluorophore is pH sensitive and is thereby able to determine the acidification of the media around the cells, the extracellular acidification. The extracellular acidification is predicted to correlate with the cells anaerobic glycolysis level, leading to the excretion of lactate. The kinetic measurements of these two factors leads to the measurement of rates, thus oxygen consumption rate (OCR) and extracellular acidification rate (ECAR). Before the addition of an inhibitor the magnitude of the OCR is considered to be the baseline cellular oxygen consumption rate. OCR and ECAR are changed by the addition of an inhibitor of mitochondrial respiration (Figure 46, timepoint a): While oxygen consumption declines, extracellular acidification increases.

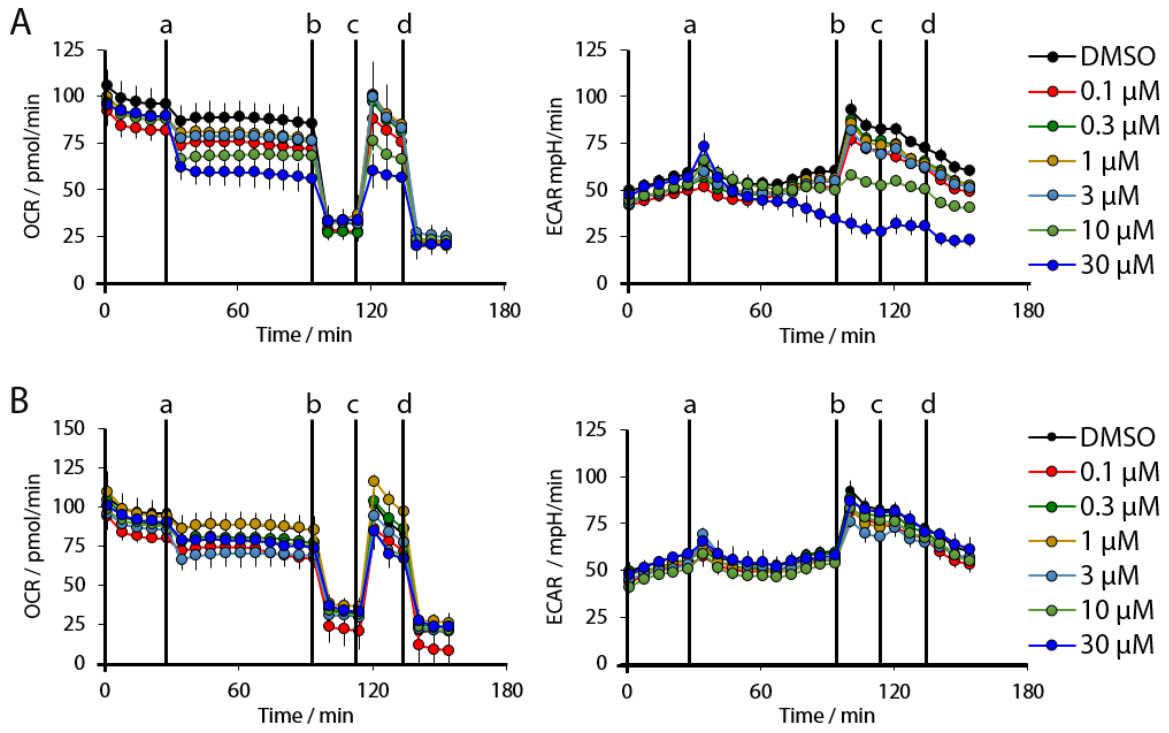

Figure 46: Influence of DMP-1 and Autophinib on mitochondrial respiration. HeLa cells were treated with the respective compound in a Seahorse XF Extracellular Flux Analyzer and oxygen consumption rate (OCR) and extracellular acidification rate (ECAR) were measured dose and time dependently. At timepoint a) the test compound, in this case the autophagy inhibitor was added to the cells. At timepoint b) Oligomycin was added at a concentration of 1 µM. At timepoint c) the decoupling agent FCCP was added in a concentration of 125 nM. At timepoint d) Rotenone and Antimycin were both added to the samples both at a concentration of 1 µM each. **A**: OCR and ECAR determined for DMP-1. **B**: OCR and ECAR determined for Autophinib. All data is mean ± SD, n= 2, representative experiments shown.

The addition of Oligomycin (inhibits complex V, which generates ATP; see Figure 47) to the assay system at timepoint b) reveals ATP-driven respiration, which is the difference in the OCR magnitude for the DMSO control before and after timepoint b). Furthermore, the addition of Oligomycin reveals the extent of proton leak respiration, which is the difference in the OCR of the DMSO control and the highest concentration of Aumitin after timepoint b). The injection of FCCP (Figure 46, timepoint c), a protonophore, reveals the maximal respiratory capacity, as it collapses the proton gradient, which allows maximal respiration. In order to find out the non-mitochondrial respiration, i.e. the lowest possible level for the OCR, at timepoint d) Rotenone (inhibits complex I) and Antimycin (inhibits complex III) are added together.

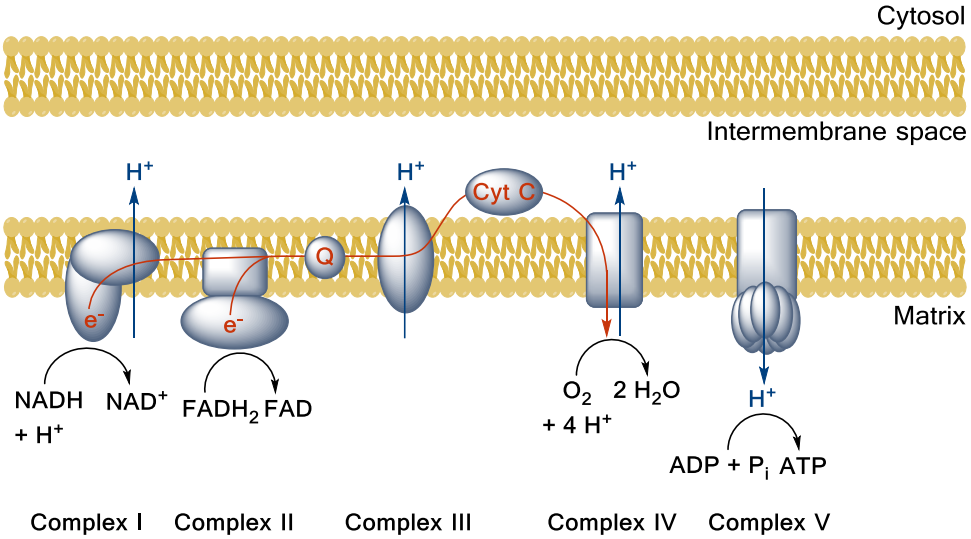

Figure 47: Schematic representation of the mitochondrial respiration chain. The electron transport chain starts with complex I, which oxidizes NADH + H^+ to NAD^+ and passes electrons to coenzyme Q (ubiquinone, labeled Q). Similarly, complex II transfers electrons to ubiquinone from the oxidation of $FADH_2$ to FAD. Ubiqionone passes the electrons to complex III, which transfers them on to complex IV via cytochrome c. Complex IV uses the electrons to reduce molecular oxygen to water. For this reaction complex IV uses the protons that are brought into the matrix of mitochondria by complex V. Importing protons into the mitochondrial matrix lowers the proton gradient across the inner membrane. This allows complex V to generate ATP by the condensation of ADP and phosphate. This proton gradient is built up by the export of protons by the complexes I, III and IV.

Whereas an effect of Autophinib and DMP-1 on mitochondrial respiration could not be observed (Figure 46), Aumitin potently and dose dependently inhibited mitochondrial respiration as assessed by a reduction in oxygen consumption rate (OCR) and an increase in extracellular acidification rate (ECAR) (Figure 48).

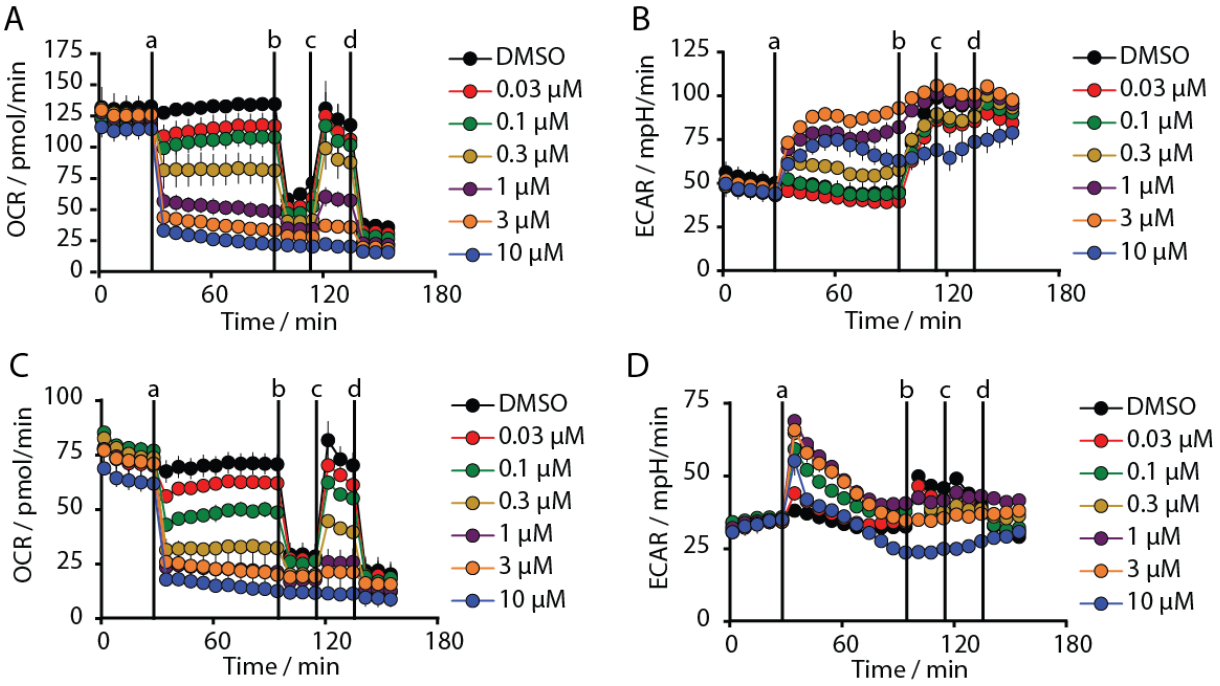

Figure 48: Influence of Aumitin on mitochondrial respiration. Cells were treated with Aumitin in a Seahorse XF Extracellular Flux Analyzer and oxygen consumption rate (OCR) and extracellular acidification rate (ECAR) were measured dose and time dependently. At timepoint a) the test compound, in this case the autophagy inhibitor was added to the cells. At timepoint b) Oligomycin was added at a concentration of 1 µM. At timepoint c) the decoupling agent FCCP was added in a concentration of 125 nM. At timepoint d) Rotenone and Antimycin were both added to the samples both at a concentration of 1 µM each. **A**: OCR measured for Aumitin in MCF7 cells. **B**: ECAR measured for Aumitin in MCF7 cells. **C**: OCR measured for Aumitin in HeLa cells. **D**: ECAR measured for Aumitin in HeLa cells. All data is mean ± SD, n = 3; representative experiments shown.

Although different cell lines can differ significantly in various factors, such as reliance on different pathways for cancer cells and protein expression levels, and different cellular assays are based on different readouts, IC_{50} values are expected to correlate for causal connections. This would strengthen the identified effect on mitochondria as causally connected with autophagy inhibition, instead of attributing it to an off-target effect. Therefore selected analogues of Aumitin were tested regarding their ability to inhibit mitochondrial respiration (Table 24). The observation of a clear correlation between the inhibition of the mitochondrial respiration in MCF7 as well as in HeLa cells and the inhibition of autophagy by Aumitin and its analogues suggested a major role of mitochondrial respiration inhibition for this compound class' on autophagy: Compounds with medium potency in the cell-based autophagy assay (Table 24, entries 2-5) also inhibited mitochondrial respiration less potently than Aumitin and a structurally related but inactive compound in the autophagy assay did not inhibit mitochondrial respiration (Table 24, entry 6). Due to the rapid effect of this compound class on mitochondrial respiration, less than seven minutes after addition to the cells (timepoints 5 and 6 in Figure 48), it was hypothesized that the effect of mitochondrial respiration inhibition caused autophagy and not *vice versa*.

Table 24: Correlation of the structure activity relationship between mitochondrial flux and autophagy. Inhibition of mitochondrial respiration was tested in a Seahorse XF Extracellular Flux Analyzer by means of oxygen consumption rate (OCR) as well as extracellular acidification rate (ECR) in HeLa cells and MCF7 cells. Data is mean ± SD; n = 3. Starvation = starvation induced autophagy assay; Rapamycin = Rapamycin induced autophagy assay. Inactive = no inhibition at a test concentration of 10 µM. Data is mean ± SD; n ≥ 3 for all autophagy inhibition values.

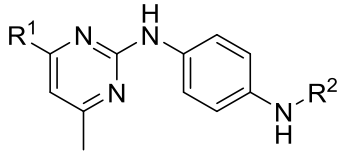

Entry	Number	R^1	R^2	Mitochondrial respiration inhibition		Autophagy Inhibition	
				HeLa cells (IC_{50} [µM])	MCF7 cells (IC_{50} [µM])	Starvation (IC_{50} [µM])	Rapamycin (IC_{50} [µM])
1	Aumitin (**405**)			0.11 ± 0.21	0.44 ± 0.11	0.12 ± 0.07	0.24 ± 0.20
2	**409**			0.92 ± 0.15	1.78 ± 0.15	0.80 ± 0.30	0.81 ± 0.68
3	**410**		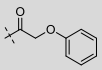	0.38 ± 0.13	0.65 ± 0.09	0.81 ± 0.16	0.29 ± 0.18
4	**411**			0.66 ± 0.08	1.32 ± 0.06	0.97 ± 0.47	0.16 ± 0.08
5	**412**		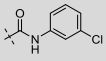	1.23 ± 0.16	8.21 ± 0.05	1.6 ± 0.60	4.1 ± 3.0
6	**419**			Inactive	Inactive	Inactive	Inactive

The influence of Aumitin on mitochondrial respiration was investigated in greater detail by means of the previously reported semi-intact assay, in which the detergent digitonin is employed to semi-permeabilize the plasma membrane. This allows the controlled delivery of mitochondrial substrates, which are usually rather membrane impermeable, to the mitochondria.[189] Inhibition of the different mitochondrial complexes can then be investigated by addition of the distinct substrates. In case of inhibition of a particular mitochondrial complex, only the substrates of the downstream complexes will allow continued mitochondrial respiration as assessed by oxygen consumption. Investigation of Aumitin together with the corresponding substrates of the different mitochondrial complexes revealed that Aumitin exclusively inhibited mitochondrial complex I (Figure 49A). The same result was expected and observed for Rotenone, a known natural product inhibitor of mitochondrial complex I (Figure 49B).[190,191]

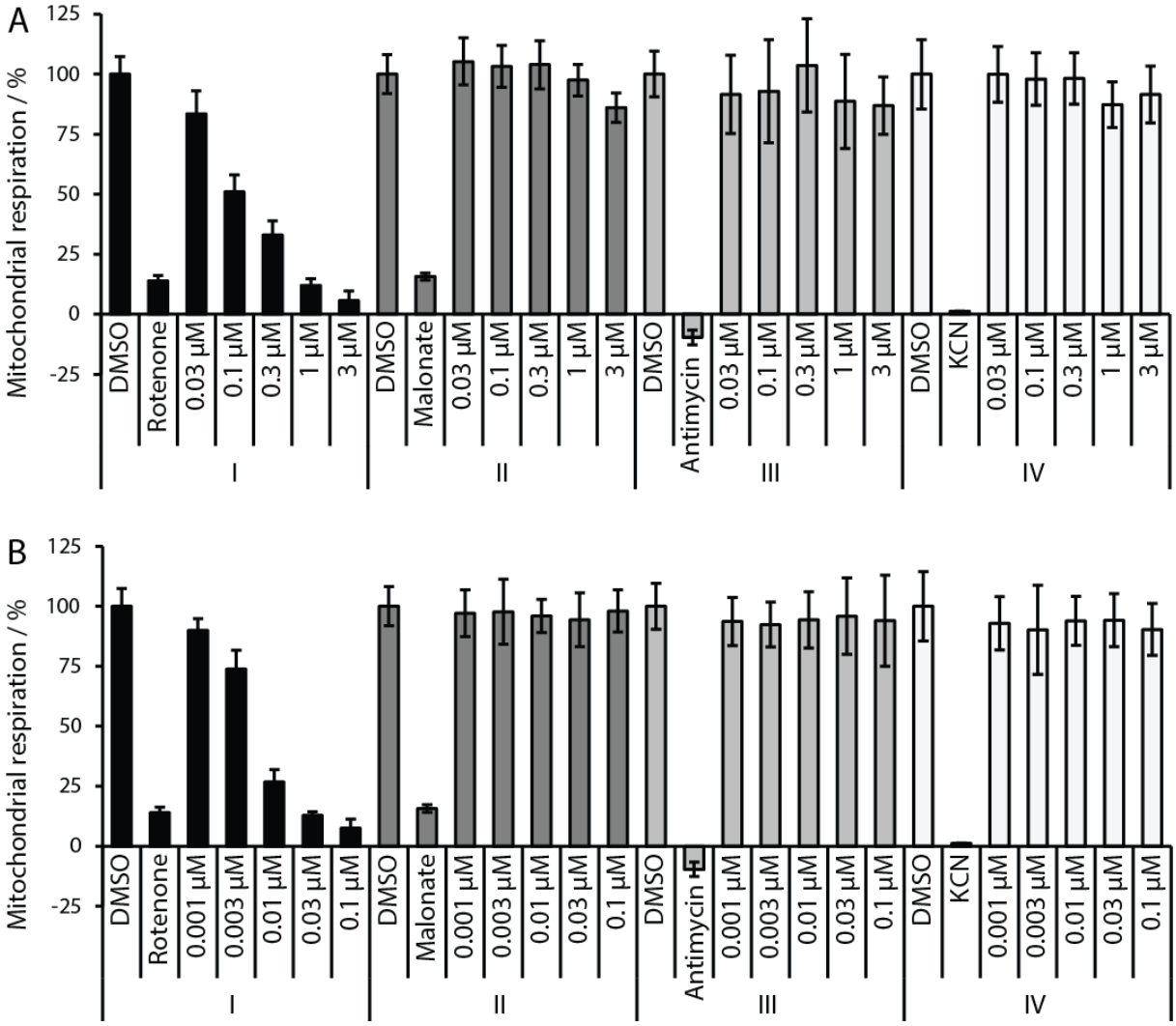

Figure 49: Identification of complex I as the target responsible for Aumitin's ability to inhibit mitochondrial respiration. HeLa cells were semi-permeabilized by digitonin and treated with the specific substrates of each mitochondrial complex. **A**: Aumitin only inhibited the pyruvate / malate-driven respiratory activity of the NADH-CoQ reductase (complex I) activity but did not inhibit the enzymatic activity of any following complex. **B**: Rotenone is also a complex I inhibitor and inhibited as such only the pyruvate / malate-driven respiratory activity of the NADH-CoQ reductase activity but did not inhibit the enzymatic activity of any following complex. All data is mean ± SD, n = 2; representative experiments shown.

Since Aumitin inhibited the activity of complex I it was likely to act through one of two possible mechanisms of action. Aumitin may act similarly to Rotenone and directly inhibited complex I. Aumitin may also disrupt the supply of NADH, which is generated by the pyruvate / malate pathway and which is required for the enzymatic activity of complex I. In order to validate Aumitin as a direct inhibitor of complex I, Aumitin was evaluated in an *in-vitro* NADH-CoQ reductase assay, using isolated mitochondria.

Aumitin inhibited the NADH-CoQ reductase activity directly, revealing that it was a Rotenone-like inhibitor (Figure 50). The observation that IC_{50} values of Aumitin are higher *in vitro* than for the cellular mitochondrial flux inhibition, was made for Rotenone as well (Figure 50) and can be accounted for by the different assay setup or the relatively higher concentration of the target protein in the case for the isolated mitochondria.

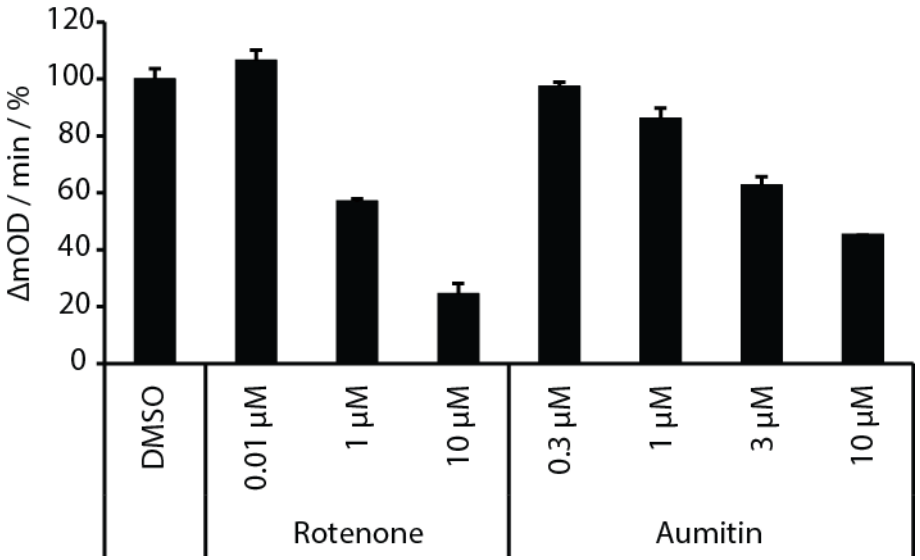

Figure 50: Determination of NADH-CoQ reductase activity inhibition by Aumitin and Rotenone in isolated mitochondria. All data is mean ± SD, n = 2; representative experiment shown.

4.4.6 Selected Viability with or without Glucose

In order to further compare Aumitin and Rotenone, their ability to selectively inhibit cell growth in the absence of glucose was assayed, since autophagy is supposed to compensate for a lack of energy or glucose and it has been reported that glucose depletion sensitizes cells to respiration inhibitors.[192,193] Unsurprisingly, we found Aumitin to be more potent in causing cell death in glucose-starved cells, compared to fed cells (Figure 51), similarly to Rotenone.

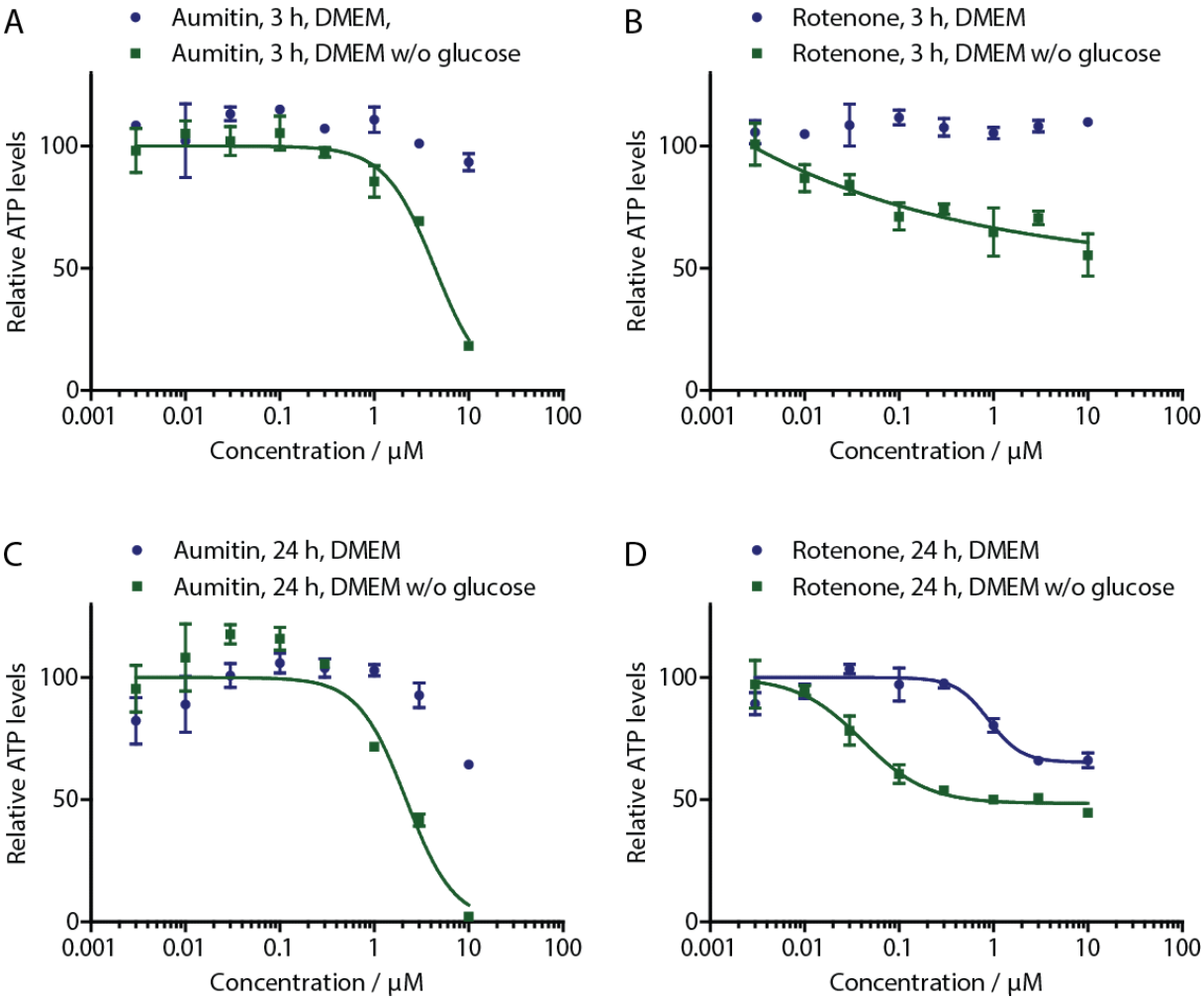

Figure 51: Selective viability of MCF7 cells upon mitochondrial complex I inhibition. Relative ATP levels were determined by means of a CellTiter-Glo® assay and normalized to the ATP levels measured for DMSO treated cells. The ATP levels are considered to be proportional to cell viability. **A**: MCF7 cells were treated for three hours with Aumitin in DMEM with or without glucose. **B**: MCF7 cells were treated for three hours with Rotenone in DMEM with or without glucose. **C**: MCF7 cells were treated for 24 hours with Aumitin in DMEM with or without glucose. **D**: MCF7 cells were treated for 24 hours with Rotenone in DMEM with or without glucose. Data is mean ± SD, n = 3, representative graphs shown.

4.4.7 Mechanistic Investigation

As there is contradicting literature about the effect of mitochondrial respiration inhibitors on autophagy,[194–198] the known respiration inhibitors Rotenone (inhibits complex I), Antimycin (inhibits complex III), Myxothiazol (inhibits complex III), Oligomycin (inhibits complex V), FCCP (de-couples the electro-chemical gradient) and Atractlyoside (inhibits the export of ATP out of the mitochondria) were tested in the autophagy assay (Table 25). Rotenone, Antimycin, Myxothiazol und Oligomycin potently and dose dependently inhibited starvation- as well as Rapamycin induced autophagy in MCF7-eGFP-LC3 cells after 3 hours. The finding that Rotenone inhibited autophagy confirmed that complex I is likely to be the relevant target of Aumitin in regard to its ability to inhibit autophagy. Although Rotenone's role in autophagy is still not fully understood, because there has been contradicting data, it has been reported previously that Rotenone inhibits autophagy.[190,191,194,196,197,199] The fact that as well as complex I inhibitors inhibitors of complex III (Table 25, Antimycin and Myxothiazol, entries 4 and 5 respectively) and complex V (Table 25, Oligomycin, entry 6) also inhibited autophagy suggested a more general involvement of mitochondrial respiration and not only of complex I. Spurred by this discovery, the elucidation of the mechanism by which inhibition of mitochondrial respiration inhibited autophagy was studied further.

Table 25: Examination of pharmacological inhibitors of mitochondrial respiration on autophagy. Literature reported and commercially available inhibitors, their known targets and their effect in the autophagy assays are shown. Starvation = starvation induced autophagy assay; Rapamycin = Rapamycin induced autophagy assay. Inactive = no inhibition at a test concentration > 10 µM. Data is mean ± SD, n ≥ 3 for all autophagy inhibition values.

Entry	Compound name / Number	Structure	Known target / Mechanism	Autophagy Inhibition	
				Starvation IC_{50} [nM]	Rapamycin IC_{50} [nM]
1	Aumitin (**405**)	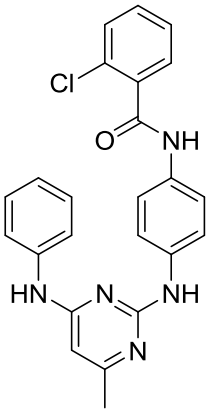	Complex I	124 ± 70	244 ± 200
2	Rotenone (**427**)	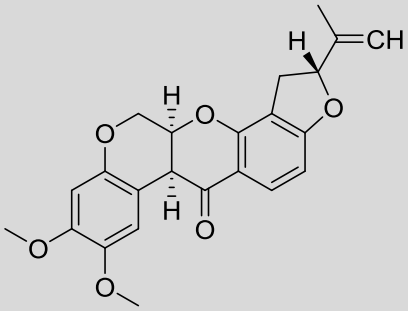	Complex I	3 ± 1	9 ± 2
4	Antimycin A (**428**)	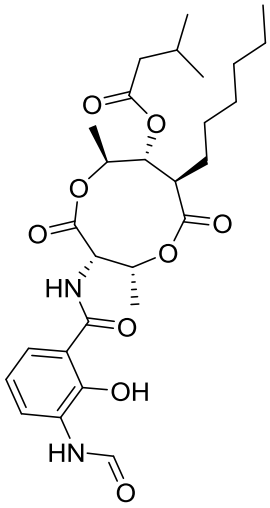	Complex III	< 1.5	6 ± 0.7

5	Myxothiazol (**429**)	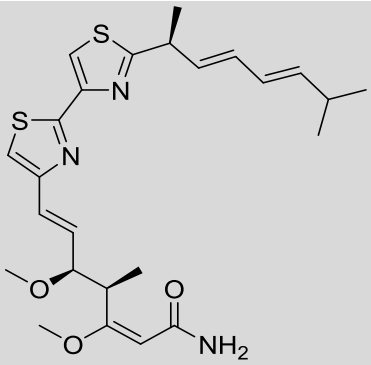	Complex III	35 ± 6	19 ± 3
6	Oligomycin A (**430**)	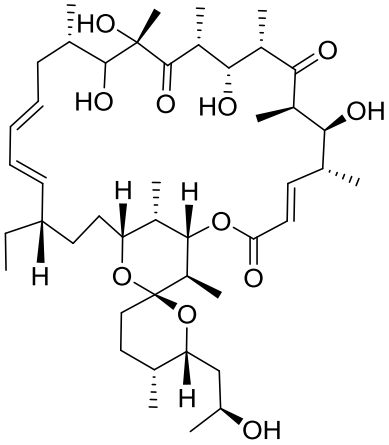	Complex V, ATP synthase	2 ± 0.7	7 ± 0.6
7	FCCP (**431**)	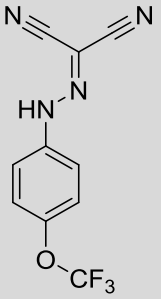	De-couples the electro-chemical gradient	na (please refer to Figure 56)	643 ± 40
8	Atractlyoside (**432**)	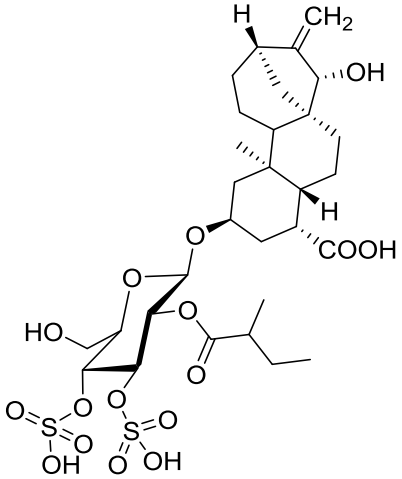	ADP / ATP translocase	Inactive	Inactive

4.4.7.1 Energy depletion

In the framework of investigating the possible mechanism by which mitochondrial respiration inhibitors lead to an inhibition of autophagy, it was hypothesized that a lack of energy upon mitochondrial respiration inhibition might be the reason. Although autophagy serves in regenerating the energy levels of the cell, it needs energy itself, in order to be activated. In this respect, commercially available EBSS, which is used to induce autophagy by amino acid depletion, contains glucose. In order to test the hypothesis MCF7-eGFP-LC3 cells were treated with glucose free EBSS (Figure 52).

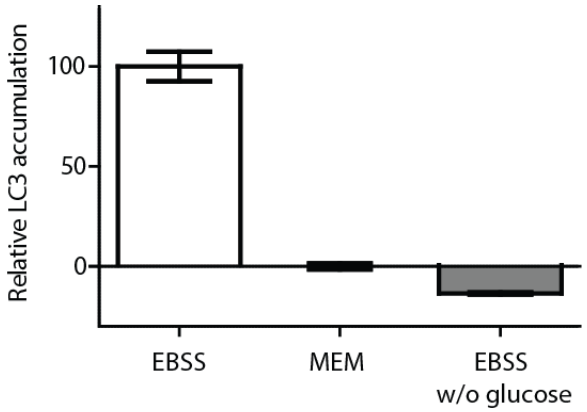

Figure 52: Treatment of MCF7-eGFP-LC3 cells with different media. EBSS, which induces autophagy by amino acid depletion, contains glucose. The extent of autophagy by EBSS induction is set to 100%. MEM, which contains amino acid and glucose, does not lead to starvation induced autophagy. Glucose free EBSS did not lead to an increased number of autophagosomes, but further reduced LC3 containing puncta. Data is mean ± SD, n = 3.

While MEM does not lead to starvation induced autophagy and is thus used as a negative control in many experiments, it does allow basal autophagy to occur. EBSS that does not contain glucose, prevented starvation induced autophagy and led to an even lower number of autophagosomes than MEM. It can be speculated that not even basal autophagy takes place in glucose free EBSS and that the reason for this phenotype is a total lack of any energy source. This initial finding strengthened the hypothesis that a lack of energy, triggered by mitochondrial respiration inhibition could lead to an impaired autophagic response. For that reason we tested ATP levels of MCF7 cells upon treatment with the mitochondrial respiration inhibitors Aumitin, Rotenone, Oligomycin and Antimycin after three hours in EBSS, to resemble the starvation induced autophagy assay (Figure 53).

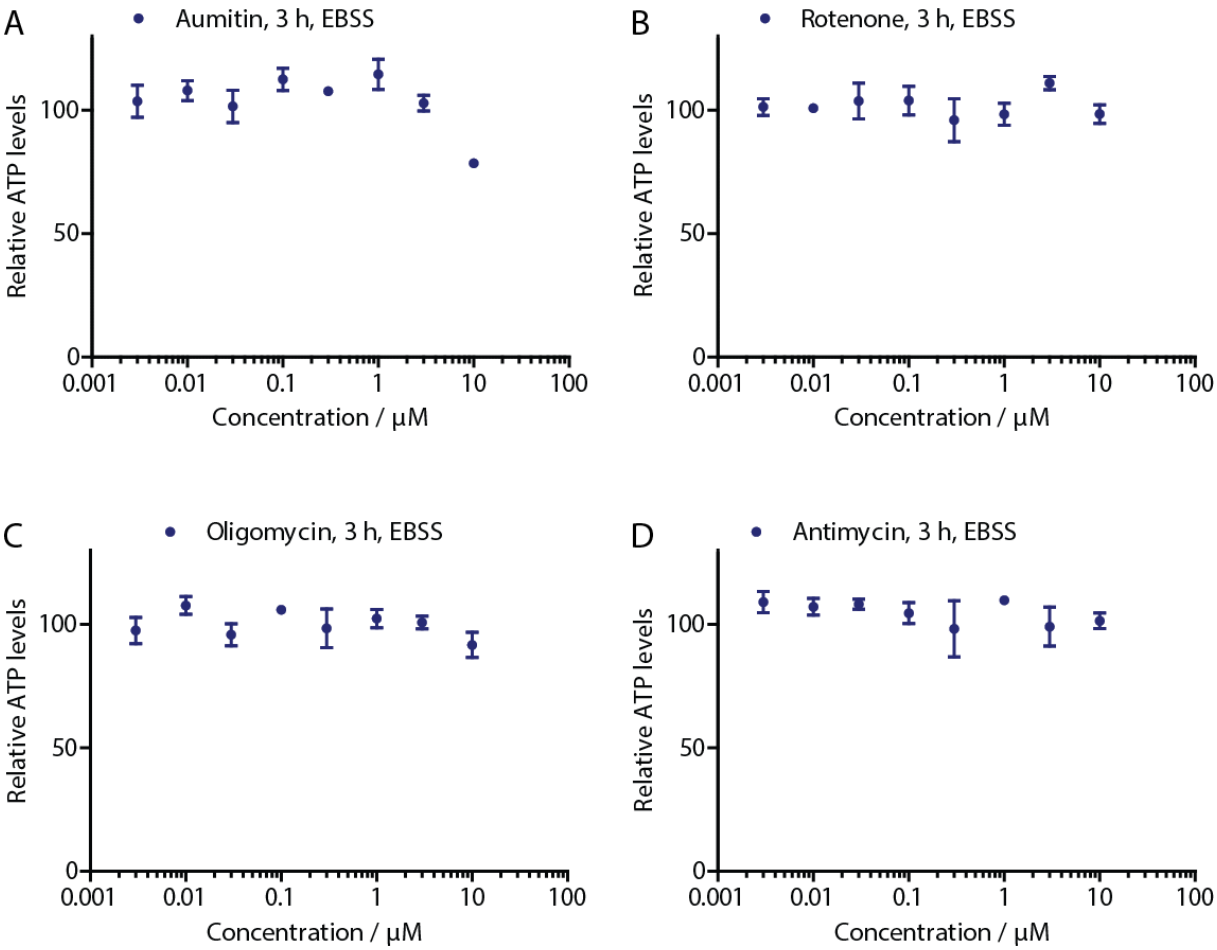

Figure 53: Determination of relative ATP levels upon inhibition of mitochondrial respiration. Relative ATP levels were determined by means of a CellTiter-Glo® assay and normalized to the ATP levels measured for DMSO treated cells. MCF7 cells were treated for three hours with the respective compound in EBSS, starving them by means of amino acid withdrawal. **A**: Aumitin, **B**: Rotenone, **C**: Oligomycin and **D**: Antimycin were used in dose response. Data is mean ± SD; n = 3; representative graphs shown.

The fact that the ATP levels of MCF7 cells under starvation-induced autophagy assay conditions were not reduced by the inhibition of mitochondrial respiration suggested that the tested compounds did not exert their autophagy inhibiting activity by lowering ATP levels. Potentially the anaerobic glycolysis of the glucose contained in the EBSS medium was sufficient to rescue the ATP levels within the assay timeframe even under mitochondrial respiration inhibition conditions. This notion was further supported by the finding that the ADP / ATP translocase inhibitor Atractyloside did not inhibit autophagy (Table 25, entry 8). Thus, a different mechanism than the hypothesized lack of energy appeared to be more likely to be responsible for the respiration inhibitors' effect on autophagy.

4.4.7.2 Induction of Reactive Oxygen Species

Mitochondrial respiration inhibitors are known to induce reactive oxygen species (ROS).[199] ROS itself is known to regulate autophagy by potentially various mechanisms, with the deactivation of the protease ATG4 being potentially the most prominent one (see introduction, section Autophagy Regulation). Therefore, Aumitin was tested in regard of its ability to increase ROS levels in an in-house screen. Aumitin induced ROS in HeLa cells dose dependently with an EC_{50} of 9.4 ± 0.7 µM (n=3). Since respiration inhibitors induce the formation of ROS first of all in mitochondria, levels of mitochondrial ROS but not cytosolic ROS were assessed by means of a MitoSOX™ dye (Figure 54). The assay for investigating mitochondrial ROS levels follows the same principle as the normal ROS assay, but the triphenylphosphine group of the MitoSOX™ dye leads to it localizing mainly in the mitochondria.

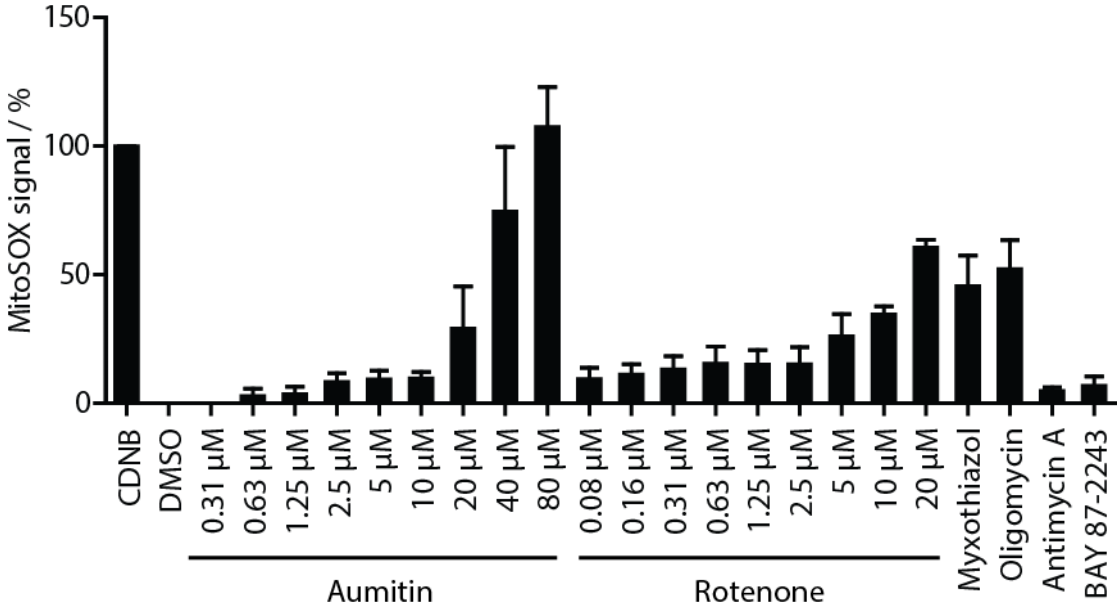

Figure 54: Investigation of the induction of mitochondrial ROS levels. Aumitin and Rotenone were tested in dose response. CDNB (2,4-dinitrochlorobenzene) is a known ROS inducer and was used as the positive control. Data is mean ± SD, n = 3, representative experiment shown.

The necessary concentration of Aumitin to significantly induce ROS was much higher than the concentration required for autophagy inhibition. This is an indication that the induction of mitochondrial as well as cytosolic ROS by Aumitin might not be the reason for autophagy inhibition.

Furthermore, the known ROS inducer L-Buthionine-sulfoximine (BOS) did not inhibit autophagy in our assay, rendering a general ROS induction as a mechanism for autophagy inhibition unlikely. This notion was supported by the finding that 606 small molecules that have recently been found in the COMAS-screening of the in-house library to dose dependently induce ROS, did not consistently show an inhibition of autophagy (Figure 55). Since there was no correlation between these two biological phenomena as assessed by the applied assays, it seemed unlikely that the ROS induction by Aumitin and Rotenone led to the inhibition of autophagy.

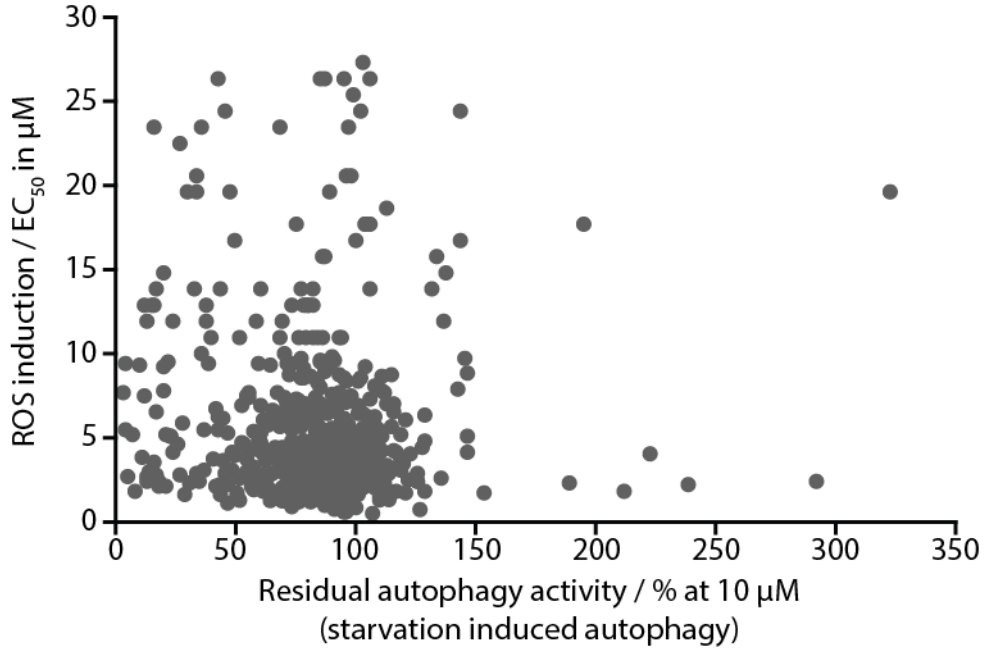

Figure 55: Scatter plot for the correlation of ROS induction and residual autophagy activity. The EC_{50} values of 606 ROS inducers (identified in the COMAS-screening of the in-house library, unpublished) were plotted against the percentual residual activity of starvation induced autophagy at a concentration of 10 µM.

4.4.7.3 Proton Gradient

A possibility of how mitochondria could regulate autophagy different to the two aforementioned hypotheses is *via* the proton gradient across the mitochondrial membrane. This notion was supported by the fact that the uncoupler FCCP (Table 25, entry 7), depending on the dose, inhibits autophagy (Table 25 and Figure 56).

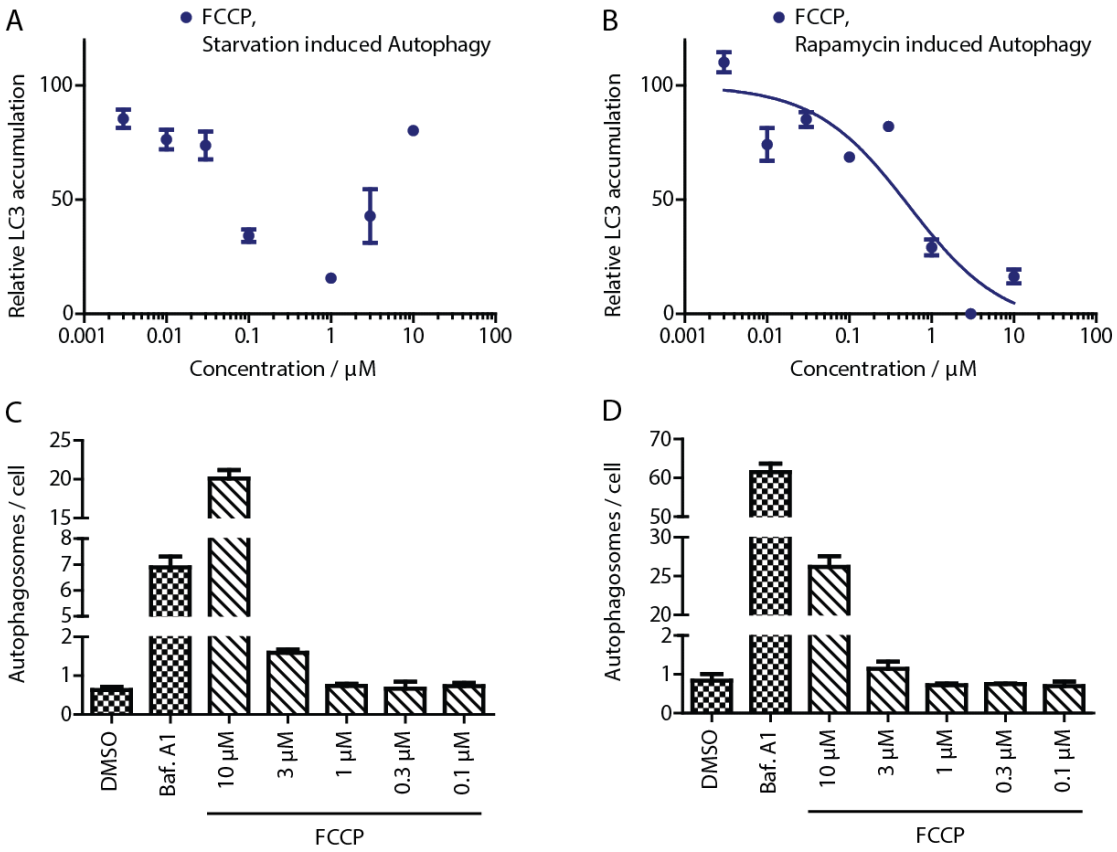

Figure 56: The dose dependent effect of FCCP on autophagy. The effect on autophagy was assessed by means of measuring the number of eGFP-LC3 puncta in the aforementioned MCF7-eGFP-LC3 cell line. **A** and **B**: Examination of FCCP's effect on the number of autophagosomes in the autophagy assay after three hours for the identification of autophagy inhibitors. **A**: Starvation by means of incubation of the cells in EBSS was used for the induction of autophagy. **B**: Rapamycin was used for the induction of autophagy. **C** and **D**: Effect of FCCP on the number of autophagosomes observed in MCF7-eGFP-LC3 cells incubated under fed conditions by means of incubation in MEM. The number of autophagosomes observed for the DSMO treated sample was considered to be accounted for by basal autophagy. Bafilomycin (100 nM) was used as a positive control for an increased number of autophagosomes. **C**: The cells were incubated and treated with the respective compound for three hours. **D**: The cells were incubated and treated with the respective compound for 24 hours. All data is mean ± SD, n = 3; representative experiments shown.

FCCP, which shuttles protons across membranes from low to high pH perturbs the build-up of the proton gradient, which is necessary for the ATP synthase to function. Opposing to that, FCCP has furthermore been reported to impair the acidification of (autophago-)lysosomes.[200,201] This effect of FCCP leads to an impaired maturation and thus clearance of autophagosomal structures and appears as a late-stage inhibitor of autophagy, thus leading to an increased number of autophagosomes in the assay. As a result, depending on the dose, FCCP might lead either to a reduction or to an increase of autophagic puncta visible in the assay (Figure 56).
It is worth mentioning that the concentration dependent effect of FCCP seems to vary within the two different autophagy inhibition assays, i.e. starvation or Rapamycin induced autophagy (Figure 56A and B). It is furthermore worth noting that regardless of the assay format, i.e. under induced autophagy as well as under basal autophagy, only at higher concentrations, FCCP seems to increase the number of LC3-containing puncta only at higher concentrations, whereas at lower concentrations it seems to inhibit autophagy. Many literature reports however use FCCP at high concentrations (from 10 μM).

4.4.8 Aumitin Summary

Aumitin was developed as a new tool compound for interrogating autophagy and mitochondrial respiration by means of complex I inhibition and, consequently, modulation of the proton gradient across the mitochondrial membrane. More generally, diverse inhibitors of mitochondrial respiration have been shown to potently inhibit autophagy independently of their mode of action and mitochondrial target complex. However, only if those compounds interfere with the proton gradient, which is the case for all complex I, III and V inhibitors, including Rotenone and Aumitin. In this respect the experiments suggest that a correct proton gradient seems to be essential for functional autophagy. Aumitin is a useful alternative to Rotenone, and defines a novel chemotype for complex I inhibition. Rotenone has been used extensively as a chemical tool compound for the study of various pathways and for the investigation of Parkinson's disease. However, Rotenone also appears to have activity independent of mitochondrial complex I inhibition.[202–204] Thus new tool compounds targeting complex I may open up novel opportunities to unravel its role in (patho)physiological processes.

5 Summary

In the framework of this thesis, three novel chemotypes for autophagy inhibitors have been identified by means of phenotypic screening. The in-depth characterization of these small molecules, in their regard to inhibit autophagy, validates them as probes for future research. Thus they expand the toolkit for investigating this conserved but still not fully understood cellular process, which is often misregulated in diseases. The elucidation of their molecular targets helped to further understand this process and provides an even better basis for using the presented small molecules as tool compounds or as a promising starting point for potential drug discovery programs.

One of the discovered compound classes is based on a dimethoxypyridine core. It has been developed from precursors of previously reported Militarinone inspired MAP4K4 inhibitors to obtain DMP-1, which was chosen for further in depth analysis. Its ability to inhibit autophagy was proven in orthogonal assays. DMP-1 inhibited starvation- but not rapamycin-induced autophagic flux, suggesting that it acts upstream or independently of mTOR. In an effort to optimize this compound class for its ability to inhibit autophagy >100 further analogues have been prepared. The information obtained regarding the SAR also allowed the design and synthesis of a pulldown probe, which retained biological activity. The respective pulldown, however, did not yield promising hit proteins. For this reason a PAL-probe was synthesized containing a benzophenone and an alkyne. This probe was used in a PAL-pulldown, using DMP-1 as a free competitor. However, DMP-1 was able to compete off the PAL-probe from many proteins, suggesting that DMP-1 binds to many different proteins. In a third attempt to identify target proteins of DMP-1, a proteome wide CETSA was performed, revealing >80 proteins that are stabilized towards heat-induced denaturation by DMP-1. Finally, DMP-1 was tested in the ChemProteoBase, in order to identify similar bioactive molecules on a proteome level. However no significantly similar compound was identified.

DMP-1 and analogues thereof expand the toolkit of pharmacological autophagy inhibition for studying this highly regulated pathway in disease relevant settings including cancer or neurodegenerative diseases. However, the identification of its target or mode of action remains a challenge.

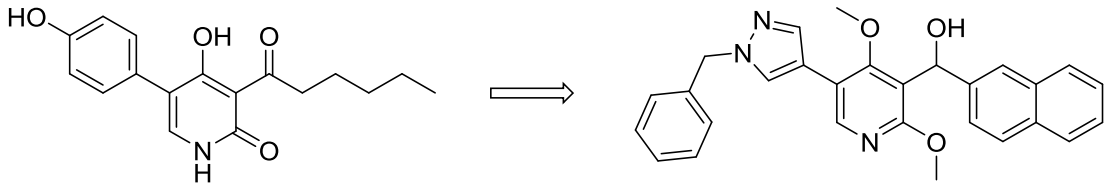

102
Neuritogenic
Inactive in autophagy

DMP-1 (116)
Not neuritogenic
Inhibits starvation induced autophagy

Figure 57: Development of the novel autophagy inhibitor DMP-1 out of neuritogenic MAP4K4 inhibitors.

The second compound class represents a novel chemotype for the inhibition of autophagy as well as for the lipid kinase VPS34. Medicinal chemistry efforts elucidated the SAR of this compound class by synthesizing 46 additional analogues. The SAR investigation was followed by validation and deconvolution of its effect on the autophagic pathway. This deconvolution revealed a particularly interesting effect of the key representor of this compound class, Autophinib: the formation of PI3P containing puncta was inhibited. PI3P is mainly generated by the phosphatidylinositol kinase VPS34 and subsequent target-ID efforts, supported by the ChemProteoBase led to the identification of VPS34 as Autophinib's responsible target for autophagy inhibition. Structurally, Autophinib is derived from a previously reported TBK1 inhibitor. However, it is completely selective over its parent compound's target as well as all tested phosphatidylinositol kinases and mTOR.

Autophinib potently inhibits autophagy induced by starvation and Rapamycin and shows target engagement in cellular models and as such it is a useful tool for studying autophagy and VPS34 activity. This is particularly important as 3-methyladenine (3-MA) and Wortmannin, both known to inhibit all classes of PI3 kinases nonselectively, have been used for years. Moreover Autophinib offers a ready synthetic accessibility (3 steps, overall yield: 45%) making it an ideal candidate for potential future developments in drug discovery and basic research.

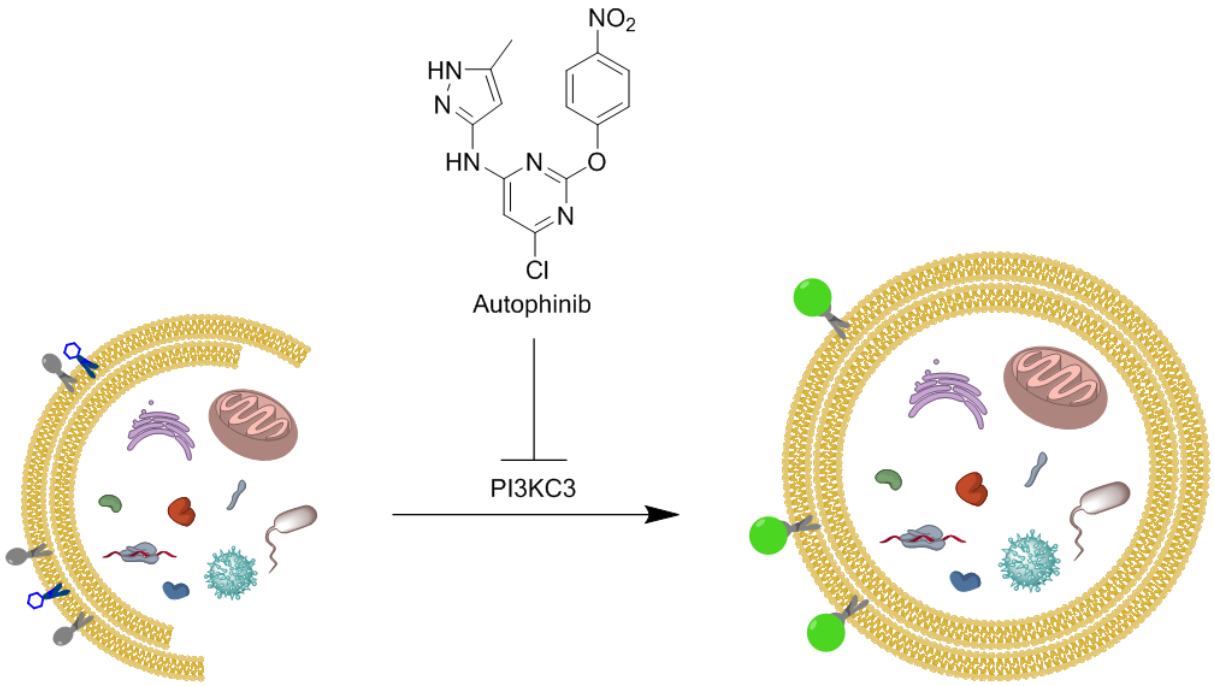

Figure 58: Autophinib represents a novel autophagy inhibiting chemotype that inhibits the lipid kinase PI3KC3 (VPS34) with high potency, disrupting autophagosome biogenesis.

The third chemotype, represented by Aumitin, a diaminopyrimidine based compound was found to inhibit mitochondrial respiration. Further analyses revealed that compounds of this class inhibit the enzymatic activity of complex I within the mitochondrial respiration chain. Subsequent *in vitro* experiments showed that the most active compound of this series inhibits complex I directly, similarly to the natural product Rotenone. The SAR of Aumitin and its analogues correlated strongly between autophagy and mitochondrial flux inhibition. Aumitin killed glucose deprived cells selectively over fed cells. This finding matches the molecular target of Aumitin. Furthermore Aumitin presents a valuable tool for studying autophagy, mitochondria and connected processes, such as neurodegenerative diseases and cancer.

Rotenone has been used for a long time for the study of various pathways and in toxin models of Parkinson's disease. However, it also appears to have activity independent of mitochondrial complex I inhibition, such as the inhibition of microtubule assembly.[202] Thus Aumitin may open up novel opportunities to unravel the role of mitochondrial complex I in (patho)physiological processes. More generally, it was shown that the effect of several other, often used inhibitors of mitochondrial respiration inhibit autophagy. The fact that FCCP shows activity in inhibiting autophagy, but Atractyloside does not, taken together with the fact that mitochondrial flux inhibitors do not lower ATP levels of MCF7 cells, suggests that a deprivation of energy is not the mechanism by which mitochondrial respiration inhibitors act on autophagy. These findings furthermore suggest that the applied compounds presumably act on autophagy by interfering with the proton gradient across the mitochondrial membrane.

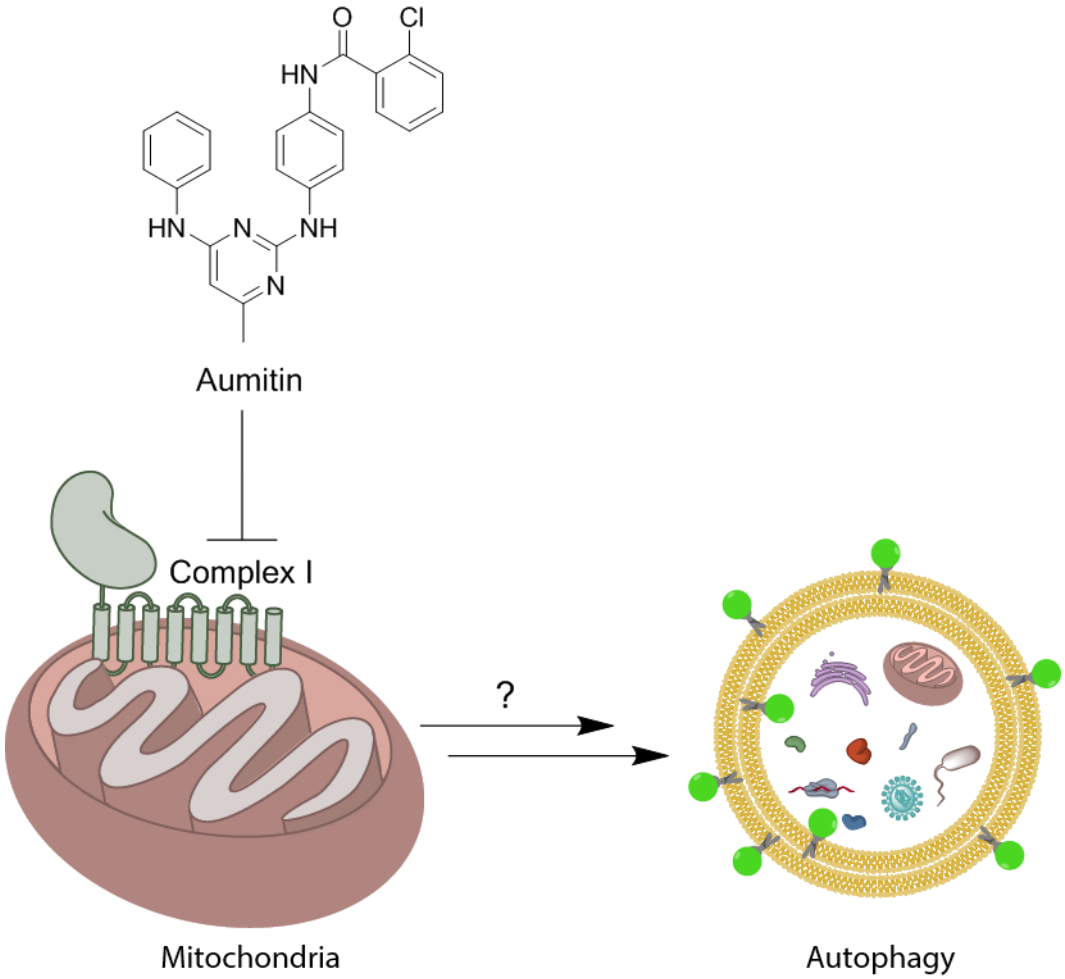

Figure 59: Aumitin represents a novel chemotype to inhibit mitochondrial complex I. The impairment of the proton gradient across the mitochondrial membrane by Aumitin inhibits autophagy.

Overall the work presented within this thesis shows the development of novel autophagy inhibitors which can be applied as useful tools for interrogating this crucial physiological process, which is often misregulated in diseases. It might also present promising starting points for future drug discovery programs.

6 Zusammenfassung

Im Rahmen dieser Arbeit wurden drei neuartige Chemotypen, welche Autophagie inhibieren, mittels eines phänotypischen Screenings identifiziert. Die eingehende Charakterisierung dieser wirkstoffähnlichen Moleküle in Bezug auf ihre Eigenschaft Autophagie zu inhibieren, validiert sie als Testsubstanzen für zukünftige Forschung. So erweitern sie das Repertoire, um diesen konservierten, aber noch nicht vollständig verstandenen zellulären Prozess zu untersuchen, welcher im Falle zahlreicher Krankheiten fehlreguliert ist. Die Aufklärung ihrer zellulären Angriffspunkte hat dazu beigetragen, diesen Prozess weiter zu verstehen und bietet eine noch bessere Grundlage für die Verwendung der präsentierten wirkstoffähnlichen Verbindungen für nachfolgende Forschung oder als Startpunkt für eine Entwicklung in der pharmazeutischen Industrie.

Eine der entdeckten Substanzklassen basiert auf einem Dimethoxypyridin-Grundgerüst und wurde ausgehend von Militarinone-inspirierten MAP4K4-Inhibitoren entwickelt. DMP-1 inhibierte die Nährstoffmangel-, aber nicht Rapamycin-induzierte Autophagie, was darauf hindeutet, dass es oberhalb oder unabhängig von mTOR in der Signalkaskade wirkt. In dem Bemühen, diese Substanzklasse zu optimieren, die Autophagie zu inhibieren, wurden >100 weitere Analoga synthetisiert. Die erhaltenen Informationen bezüglich der SAR erlaubten auch die Synthese einer Pulldown-Sonde, welche biologische Aktivität aufwies. Die nachfolgende Affinitätschromatographie lieferte jedoch keine vielversprechenden Anhaltspunkte bezüglich möglicher zellulärer Angriffspunkte. Aus diesem Grund wurde eine PAL-Sonde synthetisiert, die ein Benzophenon und ein Alkin enthielt. Diese PAL-Sonde wurde in einem PAL-Pulldown verwendet, wobei DMP-1 als freier Kompetitor eingesetzt wurde. In einem dritten Versuch, konnte mittels eines CETSAs ebenfalls kein vielversprechender Kandidat als zellulärer Angriffspunkt identifiziert werden. Schließlich wurde DMP-1 auf Proteom-Ebene mit anderen bioaktiven Molekülen verglichen, jedoch wurden keine signifikanten Ähnlichkeiten gefunden. DMP-1 und dessen Analoga erweitern das Repertoire der pharmakologischen Autophagie-Inhibitoren für das Studium dieses hochgradig regulierten Stoffwechsel-Prozesses. Die Identifizierung zellulärer Angriffspunkte dieser Substanzklasse bleibt jedoch eine Herausforderung.

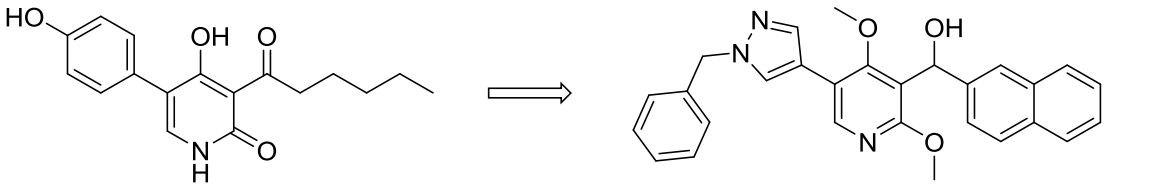

102
Neuritogen
Inaktiv in Autophagie

DMP-1 (116)
Nicht neuritogen
Inhibiert Aminosäuremangel-induzierte Autophagie

Figure 60: Entwicklung des neuartigen Autophagie-Inhibitors DMP-1 aus neuritogenen MAP4K4-Inhibitoren.

Die zweite Verbindungsklasse stellt einen neuartigen Chemotyp für die Inhibierung der Autophagie sowie für die Lipidkinase VPS34 dar. Die SAR dieser Substanzklase wurde durch die Synthese zusätzlicher 46 Verbindungen untersucht. Dem folgte eine Validierung ihrer Wirkung auf die Autophagie. Dabei zeigte sich eine besonders interessante Wirkung von Autophinib, die Bildung von PI3P-haltigen Vesikeln zu inhibieren. PI3P wird hauptsächlich durch die Phosphatidylinositol-Kinase VPS34 dargestellt. Dieser Befund führte zur Identifizierung von VPS34 als verantwortliches Zielprotein für die Inhibition der Autopahgie durch Autophinib.

Strukturell ging Autophinib aus einem TBK1-Inhibitor hervor. Allerdings wird weder der zelluläre Angriffspunkt der Mutterverbindung, noch eine der getesteten Phosphatidylinositol-Kinasen und mTOR von Autophinib inhibiert.
Autophinib zeigt die Inhibierung des zellulären Angriffspunktes in Zell-Lysat, welches die Einsetzbarkeit dieser Testsubstanz für weitere Studien der Autophagie und VPS34 validiert. Darüber hinaus bietet Autophinib eine gute synthetische Zugänglichkeit (3 Stufen, Gesamtausbeute: 45%) und ist damit ein idealer Kandidat für mögliche zukünftige Entwicklungen in der Wirkstoffforschung und für Studien im Bereich der Grundlagenforschung.

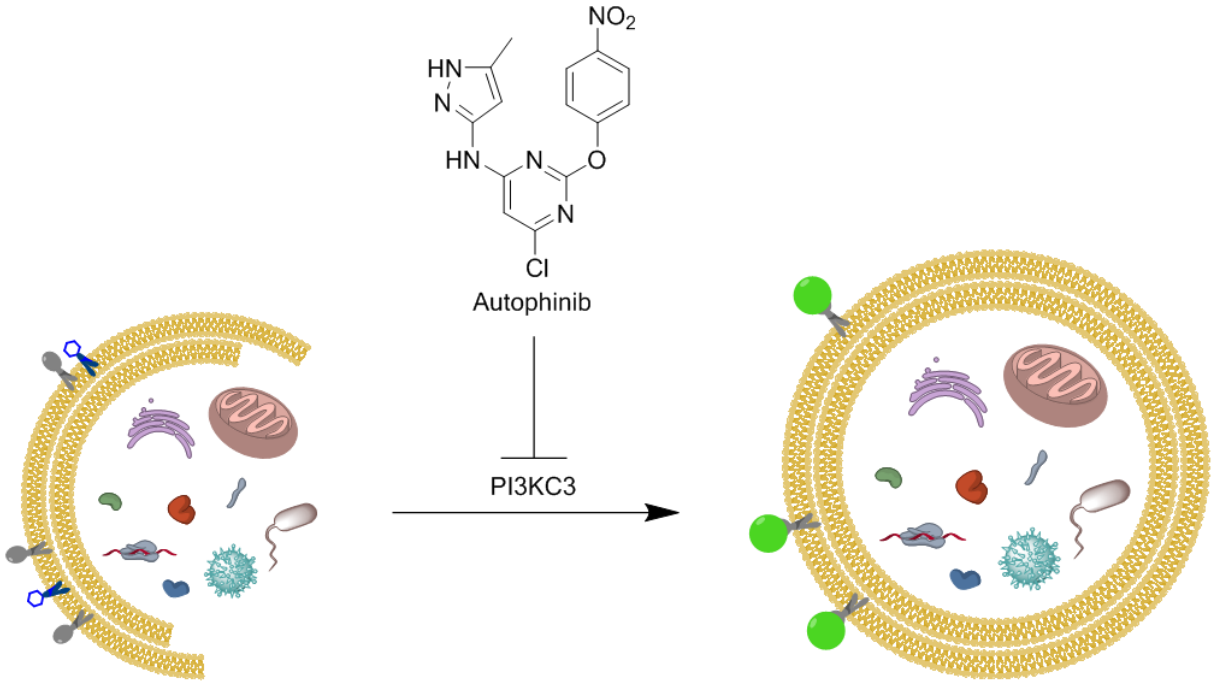

Figure 61: Autophinib stellt einen neuartigen Autophagie-hemmenden Chemotyp dar, der die Lipidkinase PI3KC3 (VPS34) potent inhibiert. Dies führt zu einer Hemmung der Autophagosomen-Biogenese.

Der dritte Chemotyp, Aumitin, eine Verbindung auf Diaminopyrimidin-Basis inhibiert die mitochondriale Atmung. Weitere Analysen zeigten, dass Aumitin die enzymatische Aktivität von Komplex I innerhalb der mitochondrialen Atmungskette hemmt. Nachfolgende *in vitro* Experimente konnten darüber hinaus zeigen, dass Komplex I direkt gehemmt wird und Aumitin daher wie Rotenon wirkt. Die SAR von Aumitin und seiner Analoga korrelierte zwischen Autophagie und mitochondrialer Atmung.

Aumitin stellt eine wertvolle Testsubstanz für das Studium von Autophagie und Mitochondrien und anderen damit verbundenen Prozesses, wie neurodegenerativen Krankheiten und Krebs dar. Rotenon wurde für eine lange Zeit für diese Studien verwendet. Allerdings scheint Rotenon auch eine Aktivität unabhängig von der Mitochondrien-Komplex-I-Inhibition aufzuweisen. Daher bietet Aumitin neue Möglichkeiten, die Rolle des mitochondrialen Komplex I in (patho)physiologischen Prozessen zu entschlüsseln.
Allgemeiner wurde gezeigt, dass mehrere andere, häufig verwendete Inhibitoren der mitochondrialen Atmung die Autophagie hemmen.

Der Befund, dass FCCP die Autophagie inhibiert, aber Atractylosid nicht, zusammen mit der Tatsache, dass Inhibitoren der mitochondrialen Atmung nicht die ATP-Level von MCF7-Zellen senken, deutet darauf hin, dass ein niedriges ATP-Level nicht der Mechanismus ist,

durch den Inhibitoren der mitochondrialen Atmung in unserem Testsystem auf die Autophagie wirken. Vermutlich wirken diese Verbindungen auf die Autophagie, indem sie den Protonengradienten über die mitochondriale Membran stören.

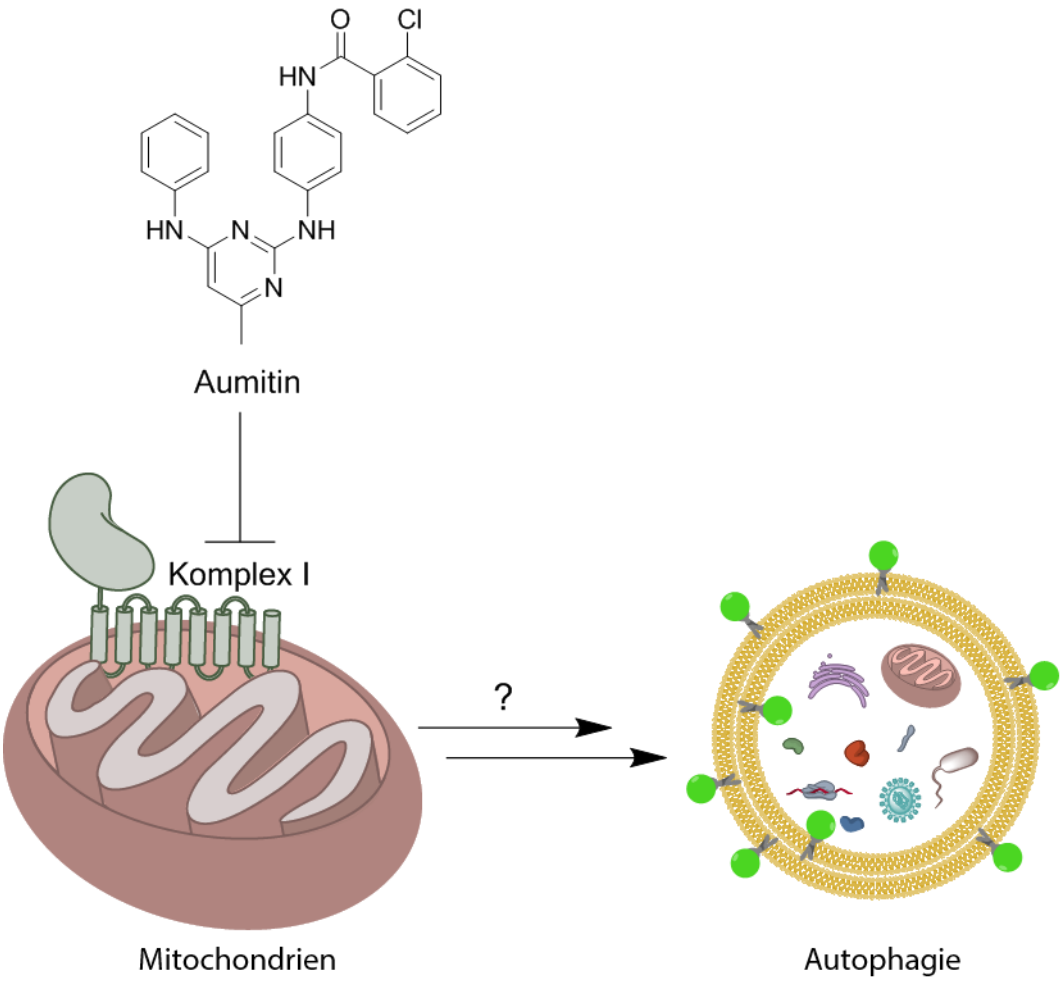

Figure 62: Aumitin stellt einen neuartigen Chemotyp dar, um den mitochondrialen Komplex I zu hemmen. Die Beeinträchtigung des Protonengradienten über die mitochondriale Membran durch Aumitin inhibiert die Autophagie.

Insgesamt wurden im Rahmen dieser Arbeit neuartige Autophagie-Inhibitoren identifiziert und entwickelt. Diese können als nützliche Testsubstanzen für die Untersuchung dieses in Krankheiten oft fehlregulierten Prozesses verwendet werden und könnten vielversprechende Ausgangspunkte für zukünftige Entwicklungen in der Pharmaindustrie darstellen. Darüber hinaus trug die Untersuchung dieser Wirkstoffe und ihrer Wirkungsweisen zum Verständnis dieses hochgradig regulierten Prozesses bei.

7 Methods and Reagents

7.1 Reagents and Material

7.1.1 Buffers and Solutions

Buffer name	Components
Block A solution	0.5 M ethanolamine, 0.5 M NaCl, pH 8.3
Block B solution	0.1 M sodium acetate, 0.5 M NaCl, pH 4.0
Blocking buffer	5% (w/v) milk in TBS-T
Blocking substances	1-5% (w/v) Dry milk powder or BSA in TBS-T buffer
CETSA alkylation solution	375 mM in H_2O
CETSA digestion solution	0.4 µg / mL in 10 mM HCl
CETSA reducing buffer	200 mM TCEP, 0.2 mM TEAB
Coomassie destaining solution	30% (v/v) MeOH, 10% (v/v) acetic acid
Coomassie staining solution	0.25% (w/v) Coomassie brilliant blue G-250, 45% (v/v) MeOH, 10% (v/v) acetic acid
Coupling buffer	0.15 M triethanolamine, 0.5 M NaCl, pH 7
Fixation buffer	3.7% Formaldehyde in PBS
IGD alkylation solution	55 mM iodoacetamide in 25 mM NH_4HCO_3
IGD reducing solution	50 mM DTT in 25 mM NH_4HCO_3
IGD washing solution 1	25 mM NH_4HCO_3 / acetonitrile (3:1)
IGD washing solution 2	25 mM NH_4HCO_3 / acetonitrile (1:1)
Laemmli buffer (2X)	20% (v/v) Glycerol, 120 mM Tris (pH 6.8), 4% (w/v) SDS
Lys-C digestion solution	0.25 µg/µL in H_2O
Lysis buffer	50 mM PIPES, 50 mM NaCl, 5 mM $MgCl_2$, 5 mM EGTA, 0.1% (v/v) NP40, 0.1% (v/v) Triton X-100, 0.1% (v/v) Tween-20, Protease Inhibitor Cocktail, pH 7.4
OBD alkylation buffer	50 mM chloroacetamide in reducing / denaturing buffer
PBS	137 mM NaCl, 2.7 mM KCl, 10 mM Na_2HPO_4, 2.0 mM KH_2PO_4, pH 7.4
Pierce® IP Lysis Buffer	25 mM Tris / HCl, 150 mM NaCl, 1mM EDTA, 1% NP-40, 5% Glycerol, pH 7.4
Reaction Buffer	20 mM Hepes / NaOH, 150 mM NaCl, 0.1% Triton-X-100, pH 7.4
Reducing/denaturing buffer	8 M urea in 50 mM Tris, pH 7.9
RIPA buffer	50 mM Tris / HCl, 150 mM NaCl, 0.1% (w/v) SDS, 1% (v/v) NP40, 0.5% (w/v) Deoxycholate, pH 8.0
SDS gels	According to Harlow and Lane, 1988
SDS loading buffer	10% (v/v) Glycerol, 50 mM Tris (pH 6.8), 2% (w/v) SDS, 500 mM DTT, 360 µM bromophenol blue
SDS loading buffer (5X)	50% (v/v) Glycerol, 250 mM Tris (pH 6.8), 10% (w/v) SDS, 500 mM DTT, 360 µM bromophenol blue
SDS running buffer (10X)	2.5 M Glycine, 250 mM Tris, 35 mM SDS
STAGE elution buffer	0.1% (v/v) formic acid, 80% (v/v) acetonitrile in H_2O
STAGE equilibration buffer	0.1% (v/v) formic acid in H_2O
TBS	10 mM Tris / HCl, 150 mM NaCl, pH 7.4
TBS-T	10 mM Tris / HCl, 150 mM NaCl, 0.1% (v/v) Triton-X100, pH 7.4
Transfer buffer	14.41 g/L glycine, 3.03 g/L Tris and 20% (semi dry) or 10% (wet transfer) (v/v) MeOH
Trypsin digestion solution	µg/mL trypsin (proteomic grade) in 25 mM NH_4HCO_3

7.1.2 Antibodies for Western Blotting

Target	Host	Cat#	Manufacturer	Dilution	Incubation Conditions
Anti-rabbit-HRP	goat	31460	Pierce	1:10,000	5% (w/v) milk in TBS-T
β-actin	rabbit	ab8227	Abcam	1:10,000	5% (w/v) milk in TBS-T
p62	rabbit	PM045	MBL international	1:10,000	5% (w/v) milk in TBS-T
LC3-B	rabbit	2775	Cell Signaling	1:1,000	5% (w/v) milk in TBS-T
VPS34	rabbit	3358	Cell Signaling	1:1,000	5% (w/v) BSA in TBS-T

7.1.3 Software

- EnsoChemLab Version 5.0.8 Enso Software GmbH, Erbach, Germany
- Image Studio™ Version 5.2 LI-COR Biosciences GmbH, Bad Homburg vor der Höhe, Germany
- IncuCyte ZOOM Version 2016A, Essen BioScience, Ann Arbor, USA
- MaxQuant Version 1.4.1.2 MaxQuant; Cox & Mann, 2008[205]
- MestReNova Version 6.0.3-5604, Mestrelab Research, Santiago de Compostela, Spain
- MetaMorph Offline Version 7.7.0.0 Molecular Devices, Biberach, Germany
- MetaXpress Version 5.0.0.26 Molecular Devices, Biberach, Germany
- Tecan i-control Version 3.4.2.0 Tecan AG, Männedorf, CH

7.2 Cell Culture

All cell culture work involving living mammalian cells was performed with sterile equipment, media, and solutions in cell culture-approved benches. Waste was autoclaved for 15 min at 134 °C.

MCF7 cells stably transfected with eGFP-LC3 (MCF7-eGFP-LC3 cells) were cultured at 37 °C with 5% CO_2 using Eagle's MEM (Gibco cat# 21090-022) containing 10% (v/v) FBS (Invitrogen cat# 10500-084), 1 mM L-Glutamine (Invitrogen cat# 25030-081), 1 mM sodium pyruvate (PAN Biotech cat# P04-43100), 1% (v/v) NEAA (PAN Biotech cat# P08-32100), 0.01 mg/ml bovine insulin (Sigma Aldrich cat# I9278) and 200 µg/ml G418. Untransfected MCF7 cells were incubated in Eagle's MEM including the same additives as used for transfected cells except for G418.

HeLa cells were cultured in standard DMEM (PAN Biotech, cat# P04-03500) supplemented with 10% (v/v) FBS (Invitrogen cat# 10500-084), 1 mM sodium pyruvate (PAN Biotech, cat# P04-43100) and 1% (v/v) NEAA (PAN Biotech, cat# P08-32100) at 37 °C with 5% CO_2.

7.2.1 Thawing and Freezing Cryo-Conserved Cells

Thawing of frozen cells was performed by transferring the vial with the cells into a 37 °C warm water bath. The thawed cells were then diluted with 10 mL of the respective medium and the resulting suspension was transferred into a T-75 flask. The cells were incubated as described above. On the next day the DMSO-containing medium was replaced by DMSO-free medium.

For cryo-conservation of mammalian cells, these were grown until reaching 80–95% confluence and then detached by trypsinization. The detached cells were suspended in the respective cell media to inactivate the trypsin, and the cell number was determined. The suspension was centrifuged (room temperature, 150 g, 5 min) and the medium replaced by an appropriate volume of DMSO-containing medium (5% v/v) to reach a final concentration of around 1 x 10^6 cells per cryo-vial). The vials were frozen in a cell freezing container (CoolCell® LX) at -80 °C overnight, to ensure a temperature decrease of 1 °C/min, and then stored in liquid nitrogen.

7.2.2 Passaging Mammalian Cells

MCF7, MCF7-eGFP-LC3 and HeLa cells were grown to a maximum confluence of 80–90%. The medium was removed, cells were washed with PBS (1X, 5 mL for 75 cm^2 (T-75), 10 mL for 175 cm^2 (T-175) tissue culture flasks) and then detached from the flasks by trypsinization (Trypsin/EDTA, 1 mL for T-75 flask, 3 mL for T-175 flask flasks, 6 min incubation at the conditions described above). After the incubation with trypsin, medium was added.

7.2.3 Determination of Cell Number

The concentration or number of cells were determined with the help of the Invitrogen™ Countess™ II Automated Cell Counter (Thermo Fisher Scientific, cat# AMQAX1000) together with Countess® Cell Counting Chamber Slides (Thermo Fisher Scientific, cat# C10228) according to the manufacturer's instructions.

7.2.4 Check for Mycoplasma Contaminations in Cultured Cells

All used cells were checked for mycoplasma contamination using the MycoAlert™ Mycoplasma Detection Kit (Lonza) (cat# LT07) according to manufacturer's instructions.

7.2.5 Cell Treatment with Small Molecules

If not stated otherwise all small molecules were dissolved in DMSO (Bioreagent, Sigma Aldrich, cat# D8418). Cells were seeded into vessels in a cell number that allowed 75–90% confluence at the end of the experiment. Cells were incubated for 12-24 hours as described above and then treated with compounds, which were pre-diluted in the given medium. The final DMSO concentration did not exceed 0.5% (v/v).

7.3 Autophagy Assay

7.3.1 High-content Screening for Autophagy Inhibitors

The phenotypic autophagy screen utilizes a MCF7 cell line stably expressing eGFP-tagged LC3 protein (MCF7-eGFP-LC3 cells). 4,000 cells per well were seeded in 25 µl medium in a 384-well Greiner µclear plate (cat# 781080, lid cat# 656191) and incubated (37 °C, 5% CO_2) overnight. Cells were then washed by a plate washer (Biotek, ELx405) three times with PBS followed by a final aspiration of the washing buffer. The addition of 25 nl of compound solution (10 mM stock solution in DMSO) was then carried out with an echo dispenser (Labcyte, Echo 520 dispenser). Addition of medium to induce autophagy was carried out with a Multidrop Combi (Thermo Scientific). 25 µl EBSS (Sigma Aldrich, cat# E3024-500ml) containing 50 µM Chloroquine (Sigma Aldrich, cat# C6628-25g) was used for starvation-induced autophagy and 25 µl medium containing 50 µM Chloroquine and 100 nM Rapamycin (Biomol, cat# Cay13346) was used for rapamycin-induced autophagy screening. After incubation (37 °C, 5% CO_2) for three hours cells were fixed by addition of 25 µl 1:4 formaldehyde in PBS + 1:500 Hoechst (stock:

1 mg/ml, Sigma Aldrich cat# B2261-25mg) and incubation for 20 min at room temperature. Cells were then washed three times with 1X PBS. Four images per well were taken with ImageXpress Micro XL (Molecular Devices) at 20x. Automated image analysis was performed using the granularity setting of MetaXpress Software (Molecular Devices). The most significant analysis parameter was granule area; with resulting signal-to-background ratios around 40 and Z' values around 0.7. The screening of 160,000 compounds yielded ca. 7,000 hit compounds which suppressed the autophagosome content by more than 50%.

7.3.2 Low-Content Screening for Autophagy Inhibitors

The low-content version utilizes the same MCF7-eGFP-LC3 cell line as the above described high-content version. 10,000 cells per well were seeded in 100 µL medium in 96-well Corning® CellBIND® plates (cat# 3340) and incubated overnight. Cells were washed with 50 µL 1X PBS followed by an aspiration of the washing buffer. Autophagy was induced by addition of 100 µL EBSS (100 µL) containing 50 µM Chloroquine prior to compound addition (20 µL, diluted in EBSS). After incubation (37 °C, 5% CO_2) for 3 h cells were washed with PBS and subsequently fixed by addition of 25 µL 4% formaldehyde in PBS + 1:500 Hoechst (stock: 1 mg/ml, Sigma Aldrich, cat# B2261-25mg) for 20 min at room temperature. Cells were then washed twice with 100 µL and stored in 100 µL PBS. Four images per well were taken with an automated AxioVert 200M fluorescence microscope (Zeiss) at 20X. Automated image analysis was performed using a modified configuration of the granularity assay (approx. granule min. and max. width: 0.4 and 5 µm resp.; approx. nuclei min. and max. width: 6 and 20 µm resp.; intensity of granules and nuclei above background: 300 and 40 gray levels resp.) of MetaMorph Cell Analysis Software (Molecular Devices). Inhibition of autophagy was quantified by calculating the number of granules per nucleus, normalized to the DMSO-treated controls.

7.4 Protein Concentration Determination

Routine determination of protein concentration was performed using the Bradford method with the Bradford reagent (Bio-Rad laboratories) in the linear range of a BSA control (0.3 – 10 mg/mL). The absorbance was measured at 595 nm using a BioPhotometer (Eppendorf).
For a large number of samples or low protein concentrations, a DC protein assay (Bio-Rad laboratories, cat# 500-0116) was performed in 96-well plates according to the manufacturer's instructions. The absorbance was measured at 650–750 nm using a Tecan microplate reader (Tecan Infinite M200) and the concentration calculated using a BSA standard curve.

7.5 Detection of p62 Conversion and LC3-I to LC3-II Ratios by means of Immunoblotting

200,000 MCF7-eGFP-LC3 cells in 2 ml media were seeded in 6-well plates and incubated (37 °C, 5% CO_2) overnight. The media was removed and the cells were washed with PBS (one time), before adding test compounds at the required concentrations in EBSS (2 mL). Cells were incubated (37 °C, 5% CO_2) for 3 h before removing the media, washing with PBS (one time), and lysing in 100 µL SDS loading buffer without bromophenol blue and DTT. Protein concentrations were determined using the DC Assay (Bio-rad) according to the manufacturer's instructions. . After addition of bromophenol blue (1:1000 from a 1% bromophenol blue stock solution) and DTT (final concentration of 50 mM from a 1 M Stock solution) the samples were boiled at 95 °C for 5 min. SDS-PAGE was carried out using self-cast 15% polyacrylamide gels run at a constant voltage of 80 V for 15 min followed by 120 V for approximately 2 h. Semi-dry transfer onto a PVDF membrane (Immobillion-FL, prod# IPFL00010) was performed at 25 V for 45 min. Membranes were blocked in 5% (w/v) powdered milk in TBS-T (blocking buffer) for 1 h at room temperature. The membrane was incubated with the primary antibody in blocking buffer overnight at 4 °C. After washing with TBS-T (3 x 5 min) the membrane was incubated with a HRP-coupled secondary antibody in blocking buffer for one hour at room temperature. Signals were visualized using the SuperSignal West Pico Chemiluminescent Substrate or the SuperSignal West Femto Maximum Sensitivity Substrate (Thermo Fischer) and an Odyssey® FC Imaging System (LICOR). Work was conducted as proposed by the guidelines for the use and interpretation of assays for monitoring autophagy.[163]

7.6 Detection of Cell Death and Apoptosis by Fluorescence Live Cell Imaging

7.6.1 Induction of Cell Death

This method uses the CellTox™ Green Cytotoxicity dye (Promega, cat# G873A), which stains dead cells. It enters cells with damaged cell membranes as a result of cytotoxicity and binds DNA, which causes an enhanced fluorescent signal. Using automated image analysis, fluorescent cells can be quantified and are directly proportional to the number of dead cells.
30,000 (for fed conditions) or 100,000 (for starved conditions) MCF7 cells in 100 µL medium were seeded in a clear flat-bottomed 96-well plate and incubated overnight. The medium was removed carefully, and cells were washed with PBS (50 µL), and 100 µL of medium (DMEM for fed, EBSS for starved conditions) containing 1.2% (v/v) CellTox™ Green Cytotoxicity dye.

Test compounds in a DMSO stock solution were prediluted in the appropriate medium (DMEM or EBSS) at a concentration of 6x the desired final concentration, while keeping the DMSO content constant. Of this solution, 20 µL were added to the cells, and the cells were incubated at 37 °C and 5% CO_2 for 72 h in the Incucyte™ Zoom (Essen Bioscience). Images were acquired at 10X magnification in both the phase contrast and green channel every hour. Images were analyzed using automated image analysis with the Incucyte™ Zoom Control Software. The key parameter was green fluorescence confluence as a percentage of phase contrast confluence (%). Data was expressed as a percentage of the DMSO-treated sample.

7.6.2 Induction of Apoptosis

This method consists of cell treatment with IncuCyte™ Caspase-3/7 Apoptosis Assay Reagent (Essen Bioscience, cat# 4440), a fluorescently-tagged peptide that is recognized and cleaved by the apoptotic caspases 3 and 7. This triggers the release of a DNA-intercalating fluorophore which stains nuclei. Using automated image analysis, fluorescent nuclei can be quantified and are directly proportional to the number of apoptotic cells.
30,000 (for fed conditions) or 100,000 (for starved conditions) MCF7 cells in 100 µL medium were seeded in a clear flat-bottomed 96-well plate and incubated overnight. The medium was removed carefully, and cells were washed with PBS (50 µL), and 100 µL of medium (DMEM for fed, EBSS for starved conditions) containing 1.2% (v/v) IncuCyte™ Kinetic Caspase-3/7 Apoptosis Assay Reagent. Test compounds in a DMSO stock solution were prediluted in the appropriate medium (MEM or EBSS) at a concentration of 6x the desired final concentration, while keeping the DMSO content constant. Of this solution, 20 µL were added to the cells, and the cells were incubated at 37 °C and 5% CO_2 between 24 and 72 h in the Incucyte™ Zoom. Images were acquired at 10X magnification in both the phase and green channel every hour. Images were analyzed using automated image analysis with the Incucyte™ Zoom Control Software. The key parameter was green fluorescence confluence as a percentage of phase contrast confluence (%). Data was expressed as a percentage of the DMSO-treated sample.

7.7 Viability Assay, WST-1 Assay

4,000 MCF7-eGFP-LC3 cells in 100 µl MEM were seeded in a clear flat-bottomed 96-well plate and incubated overnight. For starved conditions, 7000 cells in 100 µL EBSS were used. The medium was removed gently, and cells were washed with PBS (100 µL). The PBS was replaced with 100 µL of media. The test compounds were added at a concentration of 6X the desired final concentration in 20 µl of the appropriate medium. Cells were incubated at 37 °C for 48 h. At this point 10 µl of WST-1 reagent (Roche) were added to each well. The absorbance was measured with a Beckman DTX-880 (Beckman Coulter, Germany) plate reader at 450/690 nm. Absorbance measurements were performed after 20, 30, 40, 50, 60 min of addition. Good measurements are considered when absorbance of the negative control is around 1.00. Growth inhibition values (GI_{50}) were calculated using Graphpad Prism using DMSO (negative) and Nocodazole (10 µM, positive) as controls.

7.8 CellTiter-Glo® Luminescent Cell Viability Assay

The assay is a Luciferin based measurement of ATP-levels. The ATP-levels are considered to be proportional to the amount of viable and metabolically active cells.
300 MCF7 cells were seeded in 25 µL MEM (without phenol red and G418) per well in a 384-well plate (Greiner, cat# 781080) and incubated for 24 hours (37 °C, 5% CO_2). Cells were then washed by a plate washer (Biotek, ELx405) three times with PBS followed by a final aspiration of the washing buffer. The addition of 25 nL of compound solution (10 mM stock solution in DMSO, highest final compound concentration was 10 µM) was then carried out with an echo dispenser (Labcyte, Echo 520 dispenser). Addition of 25 µL medium was carried out with a Multidrop Combi (Thermo Scientific). The plate was then incubated as described above for the respective time and afterwards 15 µL CellTiter-Glo® Reagent (Promega, cat# G7570) were added into each well. The chemiluminescent signal was read out by a Spectramax Paradigm (Molecular Devices) with its high sensitivity luminescence cassette. For the selective viability version of this assay, MEM (Gibco, cat# 21090-022), EBSS (Sigma Aldrich, cat# E3024-500ml) or DMEM w/o glucose (PAN Biotech, cat# P04-01548S1) were added according to the assay protocol.

7.9 Confocal Live Cell Imaging of mCherry-eGFP-LC3/MCF7 and EGFP-WIPI2b/HEK293A Cells

400,000 stable MCF7-mCherry-eGFP-LC3 or HEK293A-eGFP-WIPI2b (kind gift of Sharon Tooze) cells were seeded in glass bottom dishes (MatTek, Ashland) and incubated overnight (37 °C, 5% CO_2). On the next day the medium was removed and replaced with 2 mL of the indicated treatment medium containing the appropriate compounds. After incubation (37 °C, 5% CO_2) for three hours live cell imaging was performed in MEM without phenol red (Invitrogen, cat# 51200-046) or EBSS (Sigma Aldrich, cat# E3024-500ml) by using an inverted confocal microscope Leica SP5 AOBS equipped with a 63×/1.4 HCX Plan Apo oil imMersion lens and a temperature-controlled hood at 37°C and 5% CO_2. The ImageJ software was used to quantify eGFP-WIPI2b puncta and Green and Red Puncta Colocalization macro to analyze mCherry-eGFP-LC3 puncta (Ruben K. Dagda, University of Nevada School of Medicine, Pharmacology Department; Daniel Shiwarski, Carneggie Mellon University; Charleen T Chu, University of Pittsburgh).[134]

7.10 Determination of Induction of Reactive Oxygen Species (ROS)

7.10.1 Cell Culture

HeLa cells and U-2 OS cells were cultured in standard DMEM (PAN Biotech, cat# P04-03500) supplemented with 10% (v/v) FBS (Invitrogen cat# 10500-084), 1 mM sodium pyruvate (PAN Biotech, cat# P04-43100) and 1% (v/v) NEAA (PAN Biotech, cat# P08-32100) at 37 °C with 5% CO_2.

7.10.2 Measurement of Cellular Reactive Oxygen Species (ROS) Levels

Cellular ROS levels were determined using the general ROS indicator CM-H2DCFDA (ThermoFisher Scientific, cat# C6827). HeLa cells were seeded into black 96 well plates with clear flat bottom (Corning) and incubated at 37 °C, 5% CO_2 overnight. Test compounds were added followed by 60 min of incubation. The medium was exchanged for DMEM (without additives) containing 5 µM CM-H2DCFDA and 5 µg/µL Hoechst-33342 (ThermoFisher Scientific, cat# H3570) and cells were incubated for 30 min at 37°C. Cells were fixed with 0.5% paraformaldehyde in phosphate-buffered saline (PBS) for 10 min at room temperature. Afterwards, cells were washed three times with PBS. Cells were imaged at 10x magnification using an Axiovert 200M automated fluorescence microscope (Carl Zeiss, Germany). CM-H2DCFDA-stained area per cell was quantified using MetaMorph 7.7.8.0 (Visitron, Germany). Data was normalized to cells treated with DMSO (= 0%) or 10 µM of CDNB (= 100%). Mean values of three individual experiments are shown.

7.10.3 Measurement of Mitochondrial Reactive Oxygen Species (ROS) Levels

For the determination of mitochondrial superoxide levels the indicator MitoSOX Red (ThermoFisher Scientific, cat# M36008) was used. HeLa cells were seeded and incubated, as described above. Cells were incubated in DMEM (without additives) containing 5 µM MitoSOX Red and 5 µg/µL Hoechst-33342 for 30 min at 37°C, 5% CO2. The supernatant was removed and test compound-containing medium was added, followed by 60 min of incubation at 37°C, 5% CO2. Cells were fixed, washed and imaged as described above. MitoSOX Red-stained area was quantified using CellProfiler.[206] Data was normalized as described above. Mean values of three individual experiments are shown.

7.10.4 High-content ROS Screening

For screening for ROS-inducing compounds U-2 OS cells were plated into black 384 well plates with clear bottom (Corning) and incubated at 37°C, 5% CO2 overnight. Compounds were added using the ECHO 520 acoustic dispenser (Labcyte Inc., USA) and cells were incubated for 60 min at 37°C, 5% CO2. Medium containing 2.5 µM CM-H2DCFDA and 5 µg/µL Hoechst-33342 was added and cells were incubated for 30 min at 37°C, 5% CO2. Cells were fixed and washed as described before. Cells were imaged at 10x magnification using an Image Xpress XL High-Content analysis system in combination with the MetaXpress software (Molecular Devices, USA).

7.11 Detection of Mitochondrial Respiration Inhibition

7.11.1.1 Cell culture

The human cervix epidermoid carcinoma cell line HeLa and the human breast adenocarcinoma cell line MCF7 were obtained from RIKEN Cell Bank and verified to be free of mycoplasma contamination by Hoechst staining. Both cell lines were cultured at 37 °C in DMEM (Thermo Fisher Scientific), supplemented with 10% (v/v) FBS (Sigma-Aldrich).

7.11.1.2 Measurement of Mitochondrial Respiration

The oxygen consumption rate (OCR) and the extracellular acidification rate (ECAR) were measured by the Seahorse XFe96 analyzer (Agilent). HeLa cells (1×10^4 cells/well) or MCF7 cells (0.8 1×10^4 cells/well) plated in XFe96 microplates (Agilent) were preincubated in DMEM-based assay medium (Agilent) supplemented with 25 mM glucose, 2 mM GlutaMAX (Thermo Fisher Scientific), and 1 mM sodium pyruvate (Sigma-Aldrich) for 1 h at 37 °C in a CO_2 free incubator. After the baseline measurements of OCR/ECAR, a test sample was injected from port A. The changes in OCR/ECAR values were recorded in triplicate ten times every 6 minutes, followed by the measurements of XF Cell Mito Stress Test (Agilent), i.e. sequential injections of oligomycin A (1 µM) from port B, FCCP (125 nM) from port C, and antimycin A (1 µM) plus rotenone (1 µM) from port D.

7.11.1.3 Semi-intact Assay for Mitochondrial Respiration

The semi-intact assay for mitochondrial respiration was carried out by the established method[189] with some modifications in the concentrations of digitonin and substrates. HeLa cells (1×10^4 cells/well) were preincubated in MAS buffer (220 mM mannitol, 70 mM sucrose, 10 mM KH_2PO_4, 5 mM $MgCl_2$, 2 mM HEPES-KOH and 1 mM EGTA; pH 7.2) for 15 min at 37 °C in a CO_2 free incubator. After three baseline measurements of OCR, digitonin (20 μg/ml), sodium succinate (10 mM), Rotenone (1 μM), ADP (1 mM), and test samples were injected from port A to start the reaction, followed by sequential treatments of Oligomycin A (1 μM) from port B and Antimycin A (1 μM) or sodium azide (20 mM) from port C. Succinate plus Rotenone were replaced with malate (1 mM) plus pyruvate (10 mM) for the assessment of complex I, duroquinol (0.5 mM) for complex III, or TMPD (0.5 mM) plus sodium ascorbate (2 mM) for complex IV.

7.11.1.4 NADH-CoQ reductase activity test

The enzymatic activity of complex I was determined with a MitoCheck complex I assay kit (Cayman, cat# 700930) according to the manufacturer's instructions.

7.12 Proteomic Profiling by means of ChemProteoBase Analysis

7.12.1 WST-8 Assay

HeLa cells were cultured at 37 °C in DMEM (ThermoFisher), supplemented with 10% (v/v) FBS (Sigma-Aldrich). HeLa cells were seeded into a 96-well plate (2 x 10^3 cells/well) and then exposed to test compounds. After 48-h incubation, cell proliferation was determined using a Cell Count Reagent SF (Nacalai Tesque). Briefly, a 1/10 volume of WST-8 solution was added to each well, and the plates were incubated at 37 °C for 1h. Then, the absorbance at 450 nm was measured in a microplate reader (Perkin Elmer). The assay and the analysis was performed as previously described.[145–148]

7.12.2 ChemProteoBase Analysis

ChemProteoBase profiling was performed as previously described.[145–148] Briefly, HeLa cells were treated with test compounds for 18 h. Proteome analysis of cell lysates was performed using a 2-D DIGE system (GE Healthcare), and images of the gels were analyzed using Progenesis SameSpots (Nonlinear Dynamics). Out of more than 1000 spots detectable in each gel, 296 spots that were found in comMon between gels of reference compound-treated cells were selected. Next, the volume of each spot was normalized using the average of the corresponding control values from DMSO-treated HeLa cells.

Using the normalized volume of the 296 spots, cosine similarity between compounds was calculated, and hierarchical clustering analysis was performed using Gene Cluster 3.0 (clustering method; centroid linkage with the means of uncentered correlation). The predictive dendrogram was visualized using Java Treeview 1.1.3.

7.13 Detection of Target Engagement Using the ActivX ATP Probe

The experiment was carried out very similarly to the producers recommendations and as previously described in the literature.[175,176] For all proteomic experiments LoBind tubes (Eppendorf, cat# 022431081 (1.5 mL) or cat# 022431102 (2 mL)) were used.

7.13.1 Lysate Preparation

Lysates were prepared as recommended by the producer and as previously described in the literature.[175,176] In brief: 2 x 10^7 dissociated and PBS-washed cells were lysed in Pierce® IP Lysis Buffer (25 mM Tris (HCl, pH 7.4), 150 mM NaCl, 1mM EDTA, 1% (v/v) NP-40, 5% (v/v) Glycerol) (Thermo Scientific, Prod# 87787) containing 1:100 protease and phosphatase inhibitors (Thermo Scientific, Prod# 1861281). The lysate was then desalted by means of passing it through a Zeba™ Spin Desalting Column (Thermo Sientific, Prod# 89892) according to the provider's recommendation. The protein concentration was measured and the lysate finally stored at -80°C.

7.13.2 Covalent Labeling of Target Kinases

1 mg HeLa or MCF7 cell lysate was thawed on ice and filled up to 485 µL with Reaction Buffer (20 mM Hepes (NaOH, pH 7.4), 150 mM NaCl, 0.1% Triton-X-100) (Thermo Scientific, Prod #1862510) before 10 µL of a 1 M $MgCl_2$ stock solution were added to each sample. Samples were then inverted five times and incubated for 1 min at room temperature. Afterwards 5 µL DMSO containing a 100X concentration of the respective final compound concentration were added to the samples. After an incubation of 60 min, the samples were treated with a 1 mM solution of the ActivX ATP probes (Thermo Scientific, Prod# 88311, Lot# QG221344; stored at -80°C) in water to give a final concentration of 20 µM ActivX ATP per sample. The samples were inverted five times and again incubated for another 10 min before 490 µL of a 8 M solution of urea in Pierce® IP Lysis Buffer and 50 µL of a 50% high capacity streptavidin agarose resin slurry (Thermo Scientific, Prod # 20357) were added. The resulting suspension was incubated at room temperature for one hour while gently mixing. The samples were centrifuged at 1000 g for 1 min to pellet the resin and the supernatant was replaced by 500 µL of 4 M urea in Pierce® IP Lysis Buffer. The suspension was transferred to a Pierce® Spin Column (Thermo Scientific, Prod# 69705) which itself was placed in a 2 mL tube before. The tube was centrifuged at 1000 g for 1

min. This washing step with the same 4 M urea solution was repeated two more times before the resin was washed in the same manner five times with PBS. The proteins were then eluted by either of the two following methods. 1. 40 µL SDS loading buffer were added to the resin in the bottom-closed Spin Columns and the tubes were heated for 10 min to 95°C.
The content of the Spin Columns was then collected in a new vial by centrifugation at 5000 g for 3 min. The samples were then analyzed by means of immunoblotting or in-gel digestion followed by mass spectrometry analysis. 2. The resin was submitted to on-bead digestion followed by mass spectrometry analysis.

7.13.3 Immunoblotting of VPS34

Anti-VPS34 was obtained from Cell Signaling Technology (cat# 3358). SDS-PAGE was carried out using 10% polyacrylamide gels run at a constant voltage of 90 V for 30 min followed by 130 V for further 45 min. Wet-transfer onto a PVDF membrane was performed at 70 V for 90 min. Membranes were blocked in 5% (w/v) powdered milk in TBS-T and washed 4 times with TBS-T. The membrane was incubated with the primary antibody (1:1000) overnight at 4 °C in 5% (w/v) BSA in TBS-T. After washing with TBS-T for 4 times the membrane was incubated with the secondary antibody (anti-rabbit HRP, purchased from Pierce [Thermo Scientific], cat# 31460) in a dilution of 1:10,000 in 5% (w/v) BSA in TBS-T for one hour at room temperature. Signals were visualized using the Super Signal® West Femto Maximum Sensitivity Substrate (Thermo Scientific, cat# 34096) and an Odyssey® FC Imaging System (LICOR).

7.14 Pulldown via PEG-linked Small Molecules to NHS Activated Sepharose

7.14.1 Cell Lysate Preparation

MCF7-eGFP-LC3 cells were cultured as described above until reaching around 90% confluence After washing with PBS and trypsinization for 6 min. at 37 °C, they were resuspended in PBS. The cell suspension was centrifuged (150 g, 5 min, 4 °C) and the supernatant discarded. The cell pellet was washed twice with PBS, followed by centrifugation (150 g, 5 min, 4 °C) and resuspension in lysis buffer (50 mM PIPES (pH 7.4), 50 mM NaCl, 5 mM $MgCl_2$, 5 mM EGTA, 0.1% NP40, 0.1% Triton X-100, 0.1% Tween 20, 0.1% (w/v) DTT, protease inhibitors). The suspension was incubated for 30 min at 4 °C, while gentle vortexing every 10 min. The lysate was homogenized by passing them 10 times through a 20 G needle and centrifuged for 20 °C at 18,500 g and 4 °C. The supernatant was collected, the protein concentration determined by means of a Bradford assay, and the lysate stored at -80 °C until further use.

7.14.2 Generation of MCF7-eGFP-LC3-SILAC Cell Line

In order to label MCF7-eGFP-LC3 cells with light or heavy amino acids for SILAC, the cells were grown in two different MEM SILAC media. Each medium was supplied with amino acids consisting of either light / normal ($^{12}C_6$-L-lysine and $^{12}C_6{}^{14}N_4$-L-arginine) or heavy isotopes ($^{13}C_6$-L-lysine and $^{13}C_6{}^{15}N_4$-L-arginine). Both media contained dialyzed FBS, and were prepared as normal MEM medium. For verifying the incorporation efficiency, samples of light, heavy, and light + heavy (mixed in a 1:1 ratio of protein concentration) lysates, together with a BSA control (5 pmol) were subjected to in-gel digestion and subsequently submitted for MS/MS analysis.

7.14.3 Pulldown and Isolation of Binding Proteins

NHS magnetic sepharose beads (GE Healthcare®, cat# 28951380, 25 µL) were equilibrated with ice-cold HCl (aq., 1 mM) and incubated with the respective pulldown probe, bearing a PEG-linker with an unprotected amine, in coupling buffer (0.15 M triethanolamine, 0.5 M NaCl, pH 7, 500 µL; compound concentration: 10 µM) overnight at 4 °C with overhead rotation. Residual unreacted groups were quenched in an alternating blocking and alkylation sequence with block A (0.5 M ethanolamine, 0.5 M NaCl, pH 7) and block B solutions (0.5 M NaOAc, 0.5 M NaCl, pH 4) three times respectively (500 µL, room temperature, 15 min the second time with A, otherwise 2 min, with overhead rotation). The beads were equilibrated with lysis buffer (500 µL, 2 min), protein lysate was added (500 µL) and the suspension incubated at 4 °C for 2 h while rotating overhead. The supernatant was removed and the beads washed with lysis buffer with increasing $MgCl_2$ concentrations (5 – 75 mM) in order to remove unspecific binding (5 min, 4 °C). The beads were washed with PBS (3 x 500 µL, 5 min, 4 °C). The sample was further processed by on-bead digest or SDS-PAGE.

7.16 Photo affinity Labeling Pulldown

The experiment consisted of five different sample types, labeled sample A – E. Sample A was the positive experimental sample. Sample B and C were negative samples by means of competition controls with different concentrations of the competitor. Sample D was the negative UV-irradiation control and sample E was the negative click chemistry control.

7.16.1 Protein Labeling and Lysate Preparation

MCF7-eGFP-LC3 cells were seeded in 10 mL MEM per 10 cm cell culture dish. Upon reaching a confluence of 90%, the medium was removed and replaced by EBSS containing 3 µM of the photo-affinity-labeling (PAL) probe. For the competition controls B and C the EBSS also contained the desired concentration of the free competitor in 10X and 5X of the PAL probe concentration respectively. The DMSO concentration was adjusted to be the same in every sample. After treating the cells with the aforementioned compound containing medium, all samples except for sample D were incubated for 2.5 hours in the incubator (37 °C, 5% CO_2) and afterwards irradiated with UV light (365 nm, 5 times 8 W lamps, ca. 15 cm distance to sample) for 1 h on ice. Subsequently the EBSS of all samples was transferred into a 15 mL falcon tube and the cells were detached from the dishes by treating them with 1 mL trypsin for 5 min. The detached cells were then transferred into the same respective falcon and the dishes washed with 3 mL of ice-cold PBS. Manual scraping was used in cases in which the cells were not completely detached by trypsin treatment.

Afterwards the cell suspensions were centrifuged at 500 g for 5 minutes at 4 °C. The supernatant was removed and the cell pellet washed by resuspending it in 2 mL ice-cold PBS buffer. Before pelleting the cells in a second wash step the cell suspension was transferred into a 1.5 mL eppendorf tube.

The supernatant was then removed and 500 µL protease inhibitor containing RIPA buffer was added to each sample for lysis. The samples were incubated for 15 minutes on ice. The cells were lysed by vortexing and ultra-sonication.

The lysates were centrifuged at 4 °C for 15 minutes at 12000 g and the protein concentration of the supernatant was afterwards measured by means of a BCA assay. Lysates were adjusted to a concentration of 1 mg/mL and stored at -80 °C until further use.

7.16.2 Click Reaction

500 µL of the beforehand described lysates were treated for one hour at room temperature with, each in a final concentration, 40 µM azide-TAMRA-biotin (Jena Bioscience cat# CLK-1048-5), 100 µM Tris(benzyltriazolylmethyl)amine (TBTA), 1 mM Tris(2-carboxyethyl)phosphine (TCEP), 5% *tert*-butanol and, for all samples except sample E, 1 mM $CuSO_4$. Subsequently 500 µL ice-cold acetone were added to the reaction and the reaction mixture was vortexed briefly before storing it at -20 °C over night. On the next day the solution was centrifuged at 1 °C for 15 minutes at 20000g. The supernatant was discarded and the precipitate washed twice with ice cold acetone (vortexing and ultra-sonication) followed by storing them at -20 °C for one hour.

The pellet was resuspended depending on the further use: For examining the success of the labeling as well as of the click reaction SDS-PAGE was performed for all samples. For this purpose 5x SDS buffer was added to each sample and the samples were incubated at 95 °C for 6 minutes. For these lysates the SDS-PAGE was performed and the gel was washed three times for 10 minutes with water before detection of TAMRA-labeled proteins using a gel imager (excitation wavelength: 532 nm, emission wavelength: 580 nm).

For a pulldown of the labeled proteins the pellet of samples A and B was taken up in 100 µL PBS (+1% (w/v) SDS) and sonicated until it completely dissolved. Afterwards a further 400 µL SDS detergent free PBS were added.

7.16.3 Pulldown of Biotin-labeled Proteins

Streptavidin Magnetic Beads (NEB [New England Biolabs] cat# S1420) were homogenized and 500 µL of the suspension was transferred into a new eppendorf tube. The beads were washed twice with PBS and 500 µL of the beforementioned 1 mg/mL "clicked lysate" were added. The suspension was then incubated for one hour at room temperature while constantly rotating.

The beads were then washed in the following order: Twice for 4 minutes each with lysis buffer (50 mM PIPES (pH 7.4), 50 mM NaCl, 5 mM $MgCl_2$, 5 mM EGTA, 0.1% NP40, 0.1% Triton X-100, 0.1% Tween 20, 0.1% DTT, protease inhibitors), twice for 4 minutes each with lysis buffer containing 1 M $MgCl_2$, twice for 4 minutes each with PBS containing 0.4% SDS, twice for 3 minutes each with 6 M urea in water and finally four times for 3minutes each with PBS. The proteins were then eluted by either of the two following methods. 1. 35 µL 1X SDS were added to the beads and the tubes were heated for 10 min to 95°C. The eluted proteins were then collected and analysed by means of in-gel digestion followed by mass spectrometry analysis. 2. The beads were submitted to on-bead digestion followed by mass spectrometry analysis.

7.17 Chemical Proteomics

7.17.1 In-gel Digestion

The protocol follows a previously reported procedure.[176] In addition to the samples, a bovine serum albumin (BSA) control was prepared by denaturing 1 µL of 5 pmol / µL BSA solution in a separate tube with 1X SDS buffer. All samples were loaded onto a Mini-PROTEAN® TGX Stain-Free Gel (4-20 %) (BIO RAD, cat# 456-8094). 40 µL 1X SDS buffer were loaded into a separate well as a gel control sample. Proteins were separated for 15 min at 80 V. The gel was transferred to a glass petri dish and shortly rinsed with fixation solution (water:EtOH:acetic acid = 5:4:1). The bands were cut out of the gel and transferred into separate tubes. The gel pieces were then shaken at room temperature in 500 µL fixation solution overnight. On the next day the fixation solution was replaced by 200 µL washing solution 1 (25 mM NH_4HCO_3 3:1 in acetonitrile) and shaken at 37°C for 30 min. The supernatant was removed and the gel pieces shaken at 37°C for 15 min in washing solution 2 (25 mM NH_4HCO_3 1:1 in acetonitrile). The solution was removed and 200 µL reducing solution (50 mM DTT in 25 mM NH_4HCO_3) were added. The tubes were then shaken at 37°C for 45 min. The reducing solution was then exchanged for 200 µL alkylation solution (55 mM chloroacetamide in 25 mM NH_4HCO_3) and shaken in it for 60 min at room temperature. Afterwards the gel pieces were washed with washing solution 2 for 15 min at room temperature. All liquid was removed and 100 µL acetonitrile were added. The tubes were left open for 30 min in order to allow the acetonitrile to evaporate. Subsequently, 75 µL digestion solution (0.1 µg/ml Trypsin/10 mM HCl 1:10 in 25 mM NH_4HCO_3) were added and the tube shaken for 15 min at room temperature before another 75 µL 25 mM NH_4HCO_3 were added and the resulting mixture shaken over night at 30°C. On the next day 10 µL 10 % trifluoroacetic acid (TFA) were added to each sample and the samples were sonicated for 30 min on ice. 75 µL acetonitrile were added and the samples shaken for 15 min at room temperature. The supernatant was transferred into new vials and another 75 µL acetonitrile were added to the gel pieces before the tubes containing the gel pieces were shaken again for 15 min at room temperature. The supernatants were combined and concentrated in vacuo. The samples were stored until mass spectrometry analysis at -20 °C.

7.17.2 On-bead Digestion

The protocol for the on-bead digestions follows a reported procedure.[207] In addition to the samples a bovine serum albumin (BSA) control was prepared by diluting 5 µL of a 2 g/L BSA solution in water with 75 µL buffer (50 mM Tris (HCl, pH 7.5)). 6.6 µL thereof were used as the digestion control and treated like the other samples.

To the tubes containing the washed resin/beads 50 µL denaturing/reducing buffer (1mM DTT, 8 M urea, 50 mM Tris (HCl, pH 7.9)) were added and the tubes were shaken at room temperature for 30 min. Subsequently 5 µL alkylation solution (50 mM chloroacetamide in denaturing/reducing buffer) were added and the mixture shaken for 30 min at room temperature. Afterwards 2µL of a 0.5 µg/µL solution of LysC (Wako, cat# 125-05061) in water were added. The resulting mixture was shaken at 37°C for 60 min. The supernatant was then transferred into a new tube. 150 µL buffer (50 mM Tris (HCl, 7.5)) containing 1 µg trypsin were added to the beads and the suspension shaken for 60 min at 37 °C. The supernatants from the LysC and trypsin digestions were combined and another 2 µg of trypsin were added before the solution was shaken overnight at 37°C. The digestion was stopped by addition of 2 µL trifluoroacetic acid (TFA).

The digested samples were subsequently purified with the help of stage tips. The stage tips were prepared by trumping out two layers of octadecyl (C18) high performance extraction disks (3M, cat# 2215) and transferring them into a 2-200 µL pipette tip (Eppendorf, Order# 0030000.870). First the stage tips were activated with 100 µL methanol and centrifuged until there was no solution left on top of the tip. Second the stage tips were washed with 100 µL buffer B (20% water, 80% acetonitrile containing 0.1% formic acid) and twice with 100 µL buffer A (water containing 0.1% formic acid) by centrifuging them until there was no solution left on top of the stage tip after each sequential step. Third, after the washing steps, the samples were loaded onto the tips and incubated on the tips for 1 min. The solution was removed by centrifugation and the stage tip washed with 100 µL buffer A. The peptides were eluted into a new tube by using 2 times 20 µL buffer B. For this purpose the tips were incubated with the buffer for 1 minute before centrifuging the buffer through the stage tip. The collected samples were concentrated in vacuo and stored at -20°C before mass spectrometric analysis.

7.17.3 Mass Spectrometric Analysis

For protein identification tryptic peptides were separated and analyzed by nano-HPLC/MS/MS. The separations were carried out on UltiMateTM 3000 RSLCnano system (Dionex, Germany). The MS and MS/MS experiments were carried out on a Q Exactive Plus™ Hybrid Quadrupole-Orbitrap Mass Spectrometer equipped with a nano-spray source (Nanospray Flex Ion Source, Thermo Scientific). All solvents were LC-MS grade. The lyophilized tryptic peptides were dissolved in 20 µL 0.1 % TFA in water. 3 µL of sample were injected onto a pre-column cartridge (5 µm, 100 Å, 300 µm ID * 5 mM, Dionex, Germany) using 0.1 % TFA in water as eluent with a flow rate of 30 µL/min. Desalting was performed for 5 min with eluent flow to waste followed by back-flushing of the sample during the whole analysis from the pre-column to the PepMap100 RSLC C18 nano-HPLC column (2 µm, 100 Å, 75 µm ID × 50 cm, nanoViper, Dionex, Germany) using a linear gradient starting with 95 % water containing 0.1 % formic acid / 5 % acetonitrile containing 0.1 % formic acid and increasing to 70 % water containing 0.1 % formic acid / 30 % acetonitrile containing 0.1 % formic acid after 95 min using a flow rate of 300 nL / min.
The nano-HPLC was online coupled to the Quadrupole-Orbitrap Mass Spectrometer using a standard coated SilicaTip (ID 20 µm, Tip-ID 10 µM, New Objective, Woburn, MA, USA). Mass range of m/z 300 to 1650 was acquired with a resolution of 70000 for full scan, followed by up to ten high energy collision dissociation (HCD) MS / MS scans of the most intense at least doubly charged ions.

Data evaluation was performed using MaxQuant software[205] (v.1.5.3.30) including the Andromeda search algorithm and searching the human reference proteome of the Uniprot database. The search was performed for full enzymatic trypsin cleavages allowing two miscleavages. For protein modifications carbamidomethylation was chosen as fixed and oxidation of methionine and acetylation of the N-terminus as variable modifications. The mass accuracy for full mass spectra was set to 4.5 ppm and for MS/MS spectra 20 ppm. The false discovery rates for peptide and protein identification were set to 1 %. Only proteins for which at least two peptides were quantified were chosen for further validation. Relative quantification of proteins was carried out using the label-free quantification algorithm implemented in MaxQuant. All experiments were performed in technical triplicates. Label-free quantification (LFQ) intensities were logarithmized (log2) and proteins which were not three times quantified in at least one of the groups were filtered off. Missing values were imputed using small normal distributed values and a t-test was performed. Proteins which were statistically significant outliers in at least one of the three experiments were considered as hits.

7.18 CETSA

7.18.1 TPP

7.18.1.1 Lysate Preparation

For CETSA and TPP experiments, MCF7-eGFP-LC3 cells were cultivated according to the above-described procedures. For one T175 flask, the cells were tripsinized with 3 mL trypsin/EDTA, resuspended in MEM medium (10 mL), and centrifuged at 150 x g and 4 °C for 5 min. The medium was removed and the cell pellet washed with ice-cold 1X PBS (2 x 25 mL and 1 x 10 mL, centrifugation at 150 *x g* and 4 °C for 5 min each time). The pellet was resuspended in PBS containing NP-40 alternative (1.5 mL, 0.4% v/v), in order to enhance membrane protein solubilization. The cells were lysed via a freeze-thaw cycle (4 times). The insoluble components were separated by centrifugation for 20 min 4 °C and 100,000 g using polycarbonate tubes in an ultra-centrifuge. Protein concentration was determined using a Bradford assay. After diluting the lysate to 2 mg/mL, aliquots were snap-frozen and stored at -80 °C until further use.

7.18.1.2 Thermal Shift Assay

The cell lysate was thawed and split into two vials (1.4 mL each). One sample was treated with the respective compound of interest and the other with DMSO, resulting in a final concentration of 2.5 µM and 1% (v/v) DMSO. The samples were incubated at room temperature for 30 min, each split into 10 aliquots of 120 µL and subjected to heating at different temperatures in a PCR cycler (Eppendorf, Mastercycler, ep*gradient* S) for 3 min. The temperature gradient ranged from 37–67 °C, while one vehicle sample was always heated in parallel with its respective compound sample. The samples were then cooled to 4 °C, centrifuged for 20 min at 4 °C and 100,000 g. The supernatant (100 µL) was transferred into low-binding Eppendorf tubes.

7.18.1.3 Trypsin Digest

After the thermal shift assay, 75 µL of each aliquot were treated with 75 µL freshly prepared TEAB buffer (100 mM) and 7.5 µL CETSA buffer (200 mM TCEP, 0.2 mM TEAB) and incubated for 1 h at 55 °C and 350 rpm. A freshly prepared solution of chloroacetamide in water (375 mM, 7.5 µL) was added to each sample, and incubation was continued for 30 minutes. Afterwards, pre-chilled acetone (ca. 900 µL) was added, and the proteins were allowed to precipitate overnight at -20 °C.

The samples were centrifuged for 10 min at 4 °C and 8,000 x g, and the supernatant was removed carefully. The pellets were air-dried for 45 min and resuspended in TEAB buffer (100 µL, 100 mM) and 7.5 µL trypsin (0.4 µg/mL in 10 mM HCl). The digestion reaction was performed at 37 °C overnight.

7.18.1.4 TMT-labeling

The tryptic peptide solution was centrifuged and labeled with TMT according to the manufacturer's description, with the exception of using only half of the recommended amount of labeling reagent. 82 µL of anhydrous acetonitrile were added to each 0.8 mg of TMT label reagent aliquot (TMT10plex, Thermo Fisher Scientific, cat# 90110). 41 µL of the respective TMT reagent solution were transferred to the peptide sample of the respective DMSO control (V1-10). Directly after addition, samples were briefly vortexed. For the compound-treated samples, 100 µL were transferred to the respective remaining TMT reagent. Directly after addition, samples were briefly vortexed. Samples were incubated for 2 hours at room temperature. Afterwards, 8 µL of 5% hydroxylamine in water were added to the samples, and the reaction was quenched by incubating the samples for 15 min. 120 µL of each compound-treated, labeled sample were combined into one sample and 120 µL of each DMSO-treated, labeled sample were combined to a second one. All samples were concentrated *in vacuo*.

7.18.1.5 Peptide Identification by Nano-LC-MS/MS

Prior to nanoHPLC-MS/MS analysis, samples were fractionated into 10 fractions on a C18 column using high pH conditions to reduce the complexity of the samples and thereby increase the number of quantified proteins. For this purpose, both samples were dissolved in 120 µL of 20 mM ammonium formate (NH_4HCO_2) at pH 11, followed by incubation in an ultra-sonicator for around 2 min, vortexing for 1 min, and centrifugation at 13,000 rpm for 3 min at room temperature 50 µL of supernatant were injected onto an XBridge C18 column (130 Å, 3.5 µm, 1mM x 150 mM) using a U3000 capHPLC- System (Thermo Fisher Scientific, Germany). Separation was performed at a flow rate of 50 µL/min using 20 mM aq. NH_4HCO_2 (pH 11) as solvent A and a mixture of aq. 20 mM NH_4HCO_2 (pH 11) with acetonitrile (2:3) as solvent B. Separation conditions were 95% solvent A / 5% solvent B for the 15 min, to desalt the samples, followed by a linear gradient up to 25% for 5 min and a second linear gradient up to 100% solvent B for 60 min. Afterwards, the column was washed with 100% solvent B for 20 min and re-equilibrated to the starting conditions. Detection was carried out at a valve length of 214 nm. The eluate between 10 and 80 min was fractionated into 10 (1^{st} fraction 20 min, 2^{nd} fraction 10 min, 3^{rd}–8^{th} fraction 5 min each, 9^{th} fraction 10 min, 10^{th} fraction 25 min).

Each fraction was concentrated by vacuum centrifugation (30 °C, max. speed) until complete dryness and subsequently subjected to nanoHPLC-MS/MS analysis. For nanoHPLC-MS/MS analysis, samples were dissolved in 10 µL of 0.1% aq. TFA. 4 µL of this solution were injected into a UltiMate™ 3000 RSLCnano system (Thermo Fisher Scientific, Germany) online-coupled to a Q Exactive™ Plus Hybrid Quadrupole-Orbitrap Mass Spectrometer, which was equipped with a nanospray source (Nanospray Flex Ion Source, Thermo Fisher Scientific), using a standard coated SilicaTip (ID 20 µm, Tip-ID 10 µM, New Objective, Woburn, MA, USA). All solvents were LC-MS grade. For desalting the samples, these were injected into a pre-column cartridge (5 µm, 100 Å, 300 µm ID * 5 mM, Dionex, Germany) using 0.1% TFA in water as eluent at a flow rate of 30 µL/min. Desalting was performed for 5 min with eluent flow to waste followed by back-flushing of the sample during the whole analysis from the pre-column to the PepMap100 RSLC C18 nano-HPLC column (2 mM, 100 Å, 75 mM ID × 50 cm, nanoViper, Dionex, Germany) using a linear gradient of water/ACN (containing 0.1% (v/v) HCOOH) 95:5 → 60:40 during 125 min using a flow rate of 300 nL/min. Afterwards, the column was washed (95% solvent B) and re- equilibrated to starting conditions.

Mass range of m/z = 300–1650 was acquired with a resolution of 70,000 for full scan, followed by up to ten high energy collision dissociation (HCD) MS/MS scans of the most intense at least doubly charged ion peaks using a resolution of 35,000 and a NCE energy of 35%.

7.18.1.6 MS-Data Evaluation

Data evaluation was performed using MaxQuant software[205] (v.1.5.3.30) including the Andromeda search algorithm and searching the human reference proteome of the Uniprot database. The search was performed for full enzymatic trypsin cleavages allowing two miscleavages. For protein modifications carbamidomethylation was chosen as fixed and oxidation of methionine and acetylation of the N-terminus as variable modifications. For relative quantification, the type "reporter ion MS2" was chosen and for all lysines and peptide N-termini 10plex TMT labels were defined. The mass accuracy for first and second search of full mass spectra was set to 20 ppm and 4.5 ppm, respectively and to 20 ppm for MS/MS spectra. The false discovery rates for peptide and protein identification were set to 1%. Only proteins for which at least two peptides were quantified were chosen for further validation. Relative quantification of proteins was carried out using the reporter ion MS2 algorithm implemented in MaxQuant. All experiments were performed in biological triplicates.

7.18.1.7 Melting Curve Calculation

To determine the melting point shifts between compound- and DMSO-treated samples of each protein, an in-house developed Excel-Macro was used. Briefly, melting changes at different temperatures were tracked using the reporter ion intensity and observed in relation to the lowest temperature; the reporter ion intensity for lowest temperature was normalized to 1. The relative fold changes of melting temperatures were calculated as a function of temperature using the Boltzmann equation:

$$y = bottom\ plateau + \frac{top\ plateau - \ bottom\ plateau}{1 + e^{-\left(\frac{a}{T}\right) - b}}$$

The sigmoidal trend of the measured intensities was fitted with the following equation using an iterative working macro in Microsoft Excel. Top plateau was fixed to one; bottom plateau was a protein specific constant that defines the maximal denaturation; a and b are constants which describe the curve progression. The melting point of a protein was defined as the temperature at which half of the protein has been denatured. This point corresponds to the inflection point of the curve, the highest slope of the curve which was defined as the value of the first derivative. For hit identification, following requirements were defined and had to be fulfilled for all replicates: (1) the protein was identified with at least two unique peptides, (2) the average shift of the melting point was at least 2 °C, while showing either a stabilization of destabilization for all replicates, and/or (3) the relative difference in the peak intensities of the two highest temperatures between the DMSO control and the compound-treated sample was at least 10% of the maximum intensity.

7.18.2 Isothermal Dose-Response Fingerprint (ITDRF)

The isothermal dose-response fingerprint has been described in the literature previously.[122,123,208] A T-175 flask of MCF7-eGFP-LC3 cells was washed twice with cold PBS buffer and treated with trypsin. The detached cells were collected and transferred into a tube and washed three times with cold PBS, centrifuging at 500 g in between washes. The cell pellet was dissolved in 1 mL PBS containing 0.4% (v/v) NP-40 and lysed by multiple freeze and thaw cycles with liquid nitrogen. After centrifugation for 25 min at 100.000 x g and 4 °C, the supernatant was collected and diluted to a final concentration of 2 g/L with PBS containing 0.4% (v/v) NP-40. The diluted lysate (100 µL) was treated either with Autophinib at different concentrations or DMSO and incubated for 15 min at room temperature. The thermal treatment was performed in a PCR-Cycler to obtain an equal temperature transfer to the samples. After temperature treatment the samples were cooled down to 4 °C and centrifuged for 25 min at 200.000 x g. The supernatant (80 µL) was mixed with 20 µL 5x LaemMli buffer and 40 µL of this mixture was loaded onto a gel to perform SDS-PAGE. The samples were then further analyzed by means of imMunoblotting.

7.19 Detection of Biochemical Kinase Inhibition

The biochemical inhibition of VPS34 as well as the full panel including > 460 kinases were carried out by Life Technologies (Thermo Fisher Scientific) using the Select Screen® kinase profiling service. Procedures and conditions can be found online. Measurements were performed in duplicate according to the supplier's standards. Unless stated otherwise the inhibition of VPS34 was measured at an ATP concentration of 10 μM (K_M).

Kinases identified as hits in the binding assay of the full panel were retested at either Eurofins (Eurofins Pharma Discovery Services UK Limited) or Reaction Biology (Reaction Biology Corporation). The respective ATP concentrations are mentioned in the supplementary file.

7.20 Synthesis

7.20.1 General Methods and Reagents

Techniques: All reactions involving air or moisture sensitive reagents or intermediates were carried out following standard Schlenk line technique under an argon atmosphere and all the glassware was dried by heat gun under high vacuum prior to use. Concentration of the reaction mixture was performed under reduced pressure at 40°C at the appropriate pressure. Purified compounds were further dried under high vacuum.

Microwave: Reactions performed in the microwave were carried out in the CEM Focused Microwave™ Synthesis System, Discover® SP. The reaction mixture was stirred for one minute before the start of the irradiation, in order to ensure a homogenous mixture. Pressure stable vessels with air vent caps were used. If not stated otherwise 200 Watt were applied to the vessel / the reaction mixture, in order to heat it.

Solvents and reagents: Dry solvents were received from Acros in anhydrous quality and used without any further purification. Acetone was dried by stirring it over anhydrous potassium carbonate or magnesium sulfate for 1 hour. All other solvents or reagents were purified according to standard procedures or were used as received from Sigma Aldrich, Alfa Aesar, Acros, Activate Scientific, Matrix Scientific, Combi Blocks, Fisher Scientific, Merck and TCI. Milli-Q grade water was used for all experiments.

TLC: TLC was performed using pre-coated Merck silica gel 60 F254 glass plates, detection of compounds were performed by UV254 light and/or dipping into a solution of KMnO4 (1.5 g in 400 mL H_2O, 5 g $NaHCO_3$) followed by heating with a heat gun.

Column chromatography: Column chromatography was performed using silica gel from Acros Organics (40 – 65 µm, 230 – 400 mesh). The overpressure was between 0.2 and 0.5 bar. Eluent mixtures are shown in parentheses and stated in volume percent for the polar solvent (X% V_1 / V_2) or in volume percent plus total volume percent (X% V_1 / V_2 + Y% V_3). Used eluents are stated in each section.

^{1}H-NMR and ^{13}C-NMR: Were recorded on devices from Bruker (AMX 400 MHz, AMX 500 MHz and AMX 600 MHz) and on a device from Varian (Mercury 400 MHz), using $CDCl_3$ or DMSO-d_6, CD_2Cl_2, $(CD_3)_2CO$, CD_3CN or CD_3OD as solvent. Data are reported in the following order: chemical shift (δ) values are reported in ppm with the solvent resonance as

internal standard ($CDCl_3$: δ = 7.26 ppm for ^1H, δ = 77.16 ppm for ^{13}C), (DMSO-d_6: δ = 2.50 ppm for ^1H, δ = 39.52 for ^{13}C), (CD_2Cl_2: δ = 5.32 ppm for ^1H, δ = 53.84 for ^{13}C), ($(CD_3)_2CO$: δ = 2.05 ppm for ^1H, δ = 29.84 ppm for ^{13}C), (CD_3CN: δ = 1.94 ppm for ^1H, δ = 1.32 ppm for ^{13}C), (CD_3OD: δ = 3.31 ppm for ^1H, δ = 49.00 ppm for ^{13}C) multiplicities are indicated bs (broadened singlet), s (singlet), d (doublet), t (triplet), q (quartet), m (multiplet), dd (doublet of doublet), dt (doublet of triplet); coupling constants (*J*) are given in Hertz (Hz). Unless stated otherwise all NMRs were measured at room temperature. Where possible, structural assignments were attempted using standard 2-D NMR techniques (gCOSY, gHSQC, gHMBC). For some analogues of Autophinib a mixture of rotameres was observed. This was confirmed by measuring NMR spectra at elevated temperatures. For the majority of the analogues of Autophinib synthesized, some quaternary carbons were not detected by NMR even with increased number of scans.

Analytical HPLC-MS: Data were recorded on one of the following three systems.
1: HPLC system (Ultimate 3000 by Thermo Fisher) with a *Nucleodur* EC 125/3 C4 or a *Nucleodur* EC 50/3 C18 reverse column (Macherey & Nagel) coupled to an ESI spectrometer (LCQ Fleet, Thermo Fisher).
2: HPLC system (Agilent Series 1100 by Agilent Technologies). A CC 125/4 C4 column (Nucleodur) or a CC 125/4 C18-column (Macherey & Nagel) coupled to an ESI spectrometer (LCQ Advantage MAX, Thermo Fisher).
3: uHPLC System (1290 Infinity by Agilent Technologies) with a C18 column (Zorbax Eclipse C18 Rapid Resolution, 2.1*50mM*1.8µm) coupled to an ESI spectrometer (6150 Agilent Technologies).

HRMS (ESI): Spectra were recorded on a LTQ Orbitrap (Thermo Fisher) mass spectrometer coupled to an Accela HPLC-System (HPLC column: Hypersyl GOLD, 50 mM x 1 mM, particle size 1.9 µm), ionization method: electron spray ionization.

GC-MS: GC-MS spectra were recorded on a gas chromatograph (Agilent 7890 A, column DB-5MS) with downstream mass spectrometer (Agilent 5975 inert XL MSD).

Preparative HPLC-MS: Separations were carried out using a preparative mass-directed HPLC (Agilent Series, 1100/LC/MSD VL, Agilent Series) with a reversed-phase C4 or C18 column (RP C4 / C18), flow 20.0 mL/min. If not stated otherwise the solvents used were as follows: Solvent A: 0.1% (v/v) TFA in water, solvent B: 0.1% (v/v) TFA in acetonitrile, from 10% B to 100% B in 20 min.

7.20.2 Synthetic Procedures

7.20.2.1 Synthesis of DMP-1 and Analogues Thereof

3,5-dibromo-2,4-dimethoxypyridine (107)

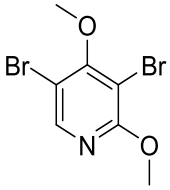

A suspension of 2,4-dimethoxypyridine (5 g, 35.93 mMol), sodium acetate (8.84 g, 107.80 mMol) and bromine (5.52 mL, 107.80 mMol) in 30 mL acetic acid was heated for 16 h to 80 °C and subsequently cooled down to rt 50 mL 10% NaOH (aq.) and 250 mL sat. sodium thiosulfate (aq.) were added to the reaction mixture. The aqueous layer was extracted with EtOAc (5 x 50 mL) and the combined organic layers were dried over anhydrous magnesium sulfate. The product was dried *in vacuo*. Purification of the crude was performed by silica gel column chromatography (1% EtOAc/*n*-pentane) to obtain the product (10.24 g, 34.47 mMol, 96%) as a white solid.

R_f: 0.28 (2% EtOAc/PE).

^{1}H-NMR (400 MHz, $CDCl_3$): δ = 3.95 (s, 3H), 3.99 (s, 3H), 8.14 (s, 1H). ^{13}C-NMR (126 MHz, $CDCl_3$): δ = 55.19, 60.90, 102.49, 107.92, 147.29, 161.53, 162.55.

ESI-MS: m/z = 296.15, 298.01, 299.96 $[M+H]^+$.

3,5-dibromo-4-methoxypyridine (172)

3,5-dibromopyridin-4(1H)-one (170)

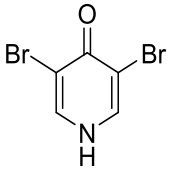

A solution of pyridin-4(1H)-one (2 g, 21.03 mMol) in 48% hydrobromic acid (23 ml) was cooled to 0 °C and bromine (2.37 ml, 46.27 mMol) was added. The mixture was brought to rt and stirred for 1.5 h. After addition of water (60 mL) and a further 30 min of stirring, the precipitated solid was filtered off, washed with small portions of water and then dried in *in vacuo*. The product (1.85 g, 7.3 mMol, 35%) was obtained as a colorless solid.

R_f: 0.65 (15% MeOH/DCM).

^{1}H-NMR (500 MHz, DMSO-d_6) δ = 12.26 (s, 1H), 8.24 (s, 2H).

^{13}C-NMR (126 MHz, DMSO-d_6) δ = 167.49, 138.18, 111.80.

ESI-MS: m/z = 254.14 $[M+H]^+$.

HRMS (ESI): calculated for $C_5H_4ON\ ^{79}Br_2$: m/z = 251.86542 $[M+H]^+$,
found: m/z = 251.86557 $[M+H]^+$.
calculated for $C_5H_4ON\ ^{79}Br\ ^{81}Br$: m/z = 253.86337 $[M+H]^+$,
found: m/z = 253.86284 $[M+H]^+$.
calculated for $C_5H_4ON\ ^{81}Br_2$: m/z = 255.86132 $[M+H]^+$,
found: m/z = 255.86030 $[M+H]^+$.

3,5-dibromo-4-chloropyridine (171)

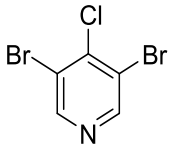

3,5-dibromopyridin-4-ol (170) (1.00 g, 3.95 mMol) was combined with phosphoryl chloride (921.45 µl, 9.89 mMol) in a pressure stable vessel. The vessel was closed and the solution heated to 140 °C under stirring for 2.5 h. Afterwards the reation vessel was cooled down to rt and the reaction solution combined with ice cold water (75 mL). The aqueous layer was extracted with EtOAc (5 x 15 mL) and the combined organic layers were dried over anhydrous magnesium sulfate. The product was dried *in vacuo*. Purification of the crude was performed by silica gel column chromatography (1% EtOAc/*n*-pentane) to obtain the product (805 mg, 2.97 mMol, 75%) as a white solid.

R_f: 0.32 (5% EtOAc/PE).

^{1}H NMR (500 MHz, $CDCl_3$) δ = 8.63 (s, 2H). ^{13}C NMR (126 MHz, $CDCl_3$) δ = 150.97, 144.13, 121.93.

GC-MS: t_R = 4.59 min; m/z = 268.8, 270.8, 272.8, 274.8 $[M^{\bullet}]^+$.

HRMS (ESI): calculated for $C_5H_3N\ ^{79}Br_2\ ^{35}Cl$: m/z = 269.83153 $[M+H]^+$,
found: m/z = 269.83155 $[M+H]^+$.
calculated for $C_5H_3N\ ^{79}Br_2\ ^{37}Cl$: m/z = 271.82858 $[M+H]^+$,
found: m/z = 271.82878 $[M+H]^+$.
calculated for $C_5H_3N\ ^{79}Br\ ^{81}Br\ ^{37}Cl$: m/z = 273.82653 $[M+H]^+$,
found: m/z = 273.82597 $[M+H]^+$.
calculated for $C_5H_3N\ ^{81}Br_2\ ^{35}Cl$: m/z = 275.82449 $[M+H]^+$,
found: m/z = 275.82316 $[M+H]^+$.

3,5-dibromo-4-methoxypyridine(120)

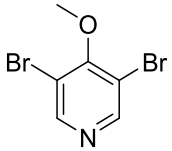

A solution of 3,5-dibromo-4-chloropyridine (171) (249 mg, 918 µmol) and sodium methoxide (198 mg, 3.67 mMol) in 10 mL of MeOH was stirred for six days at rt Subsequently, the reaction mixture was admixed with 10 mL of water and the aqueous layer was then extracted three times with 30 ml of EtOAc. The combined organic layers were dried over anhydrous magnesium sulfate and the solvent was subsequently removed *in vacuo*. The purification was carried out by silica gel column chromatography (5% EtOAc/PE). The product (192 mg, 721 µmol, 79%) was obtained as a white solid.

R_f: 0.44 (5% EtOAc/PE).

^{1}H NMR (500 MHz, $CDCl_3$) δ = 8.54 (s, 2H), 3.95 (s, 3H). ^{13}C NMR (126 MHz, $CDCl_3$) δ = 160.84, 152.13, 116.00, 60.95.

ESI-MS: m/z = 268.00 $[M+H]^+$.

HRMS (ESI): calculated for $C_6H_6ON\ ^{79}Br_2$: m/z = 265.88107 $[M+H]^+$,
found: m/z = 265.88105 $[M+H]^+$.
calculated for $C_6H_6ON\ ^{79}Br\ ^{81}Br$: m/z = 267.87902 $[M+H]^+$,
found: m/z = 267.87831 $[M+H]^+$.
calculated for $C_6H_6ON\ ^{81}Br_2$: m/z = 269.87697 $[M+H]^+$,
found: m/z = 269.87574 $[M+H]^+$.

(±)-(3-bromo-2,6-dimethoxyphenyl)(naphthalen-2-yl)methanol (162)

1,3-dibromo-2,4-dimethoxybenzene (161)

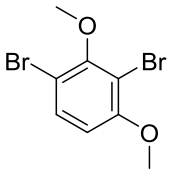

A solution of 2-bromo-1,3-dimethoxybenzene (2.00 g, 9.21 mMol) in 20 mL of acetonitrile was brought to 0 °C and *N*-bromosuccinimide (2.05 g, 11.52 mMol) was added. After the addition, the reaction mixture was brought to rt and stirred overnight. Subsequently, the reaction mixture was concentrated *in vacuo* and the resulting orange solid was redissolved in 70 mL of DCM and washed with half-saturated sodium thiosulfate solution (2 x 20 mL), 15 mL sat. sodium chloride solution and 30 mL of water in the stated order and subsequently dried over magnesium sulfate. The orange oil obtained was dried in a high vacuum and subsequently purified on silica gel by flash chromatography (10% EtOAc/PE). The product (2.17 g, 7.34 mMol, 80%) was obtained as a colorless oil.

R_f: 0.48 (20% EtOAc/PE).

^{1}H NMR (500 MHz, $CDCl_3$) δ = 7.33 (d, ^3J = 8.9 Hz, 1H), 6.50 (d, ^3J = 8.9 Hz, 1H), 3.81 (s, 3H), 3.79 (s, 3H).

^{13}C NMR (126 MHz, $CDCl_3$) δ = 156.59, 154.82, 131.55, 108.59, 108.44, 108.14, 60.34, 56.55.

GC-MS: t_R = 6.02 min; m/z = 293.9, 295.9, 297.9 $[M^\bullet]^+$.

HRMS (EI): calculated for $C_8H_8O_2\ ^{79}Br_2$: m/z = 293.88856 $[M^\bullet]^+$,
found: m/z = 293.88896 $[M^\bullet]^+$.
calculated for $C_8H_8O_2\ ^{79}Br\ ^{81}Br$: m/z = 295.88651 $[M^\bullet]^+$,
found: m/z = 295.88582 $[M^\bullet]^+$.
calculated for $C_8H_8O_2\ ^{81}Br_2$: m/z = 297.88446 $[M^\bullet]^+$,
found: m/z = 297.88565 $[M^\bullet]^+$.

(±)-(3-bromo-2,6-dimethoxyphenyl)(naphthalen-2-yl)methanol (162)

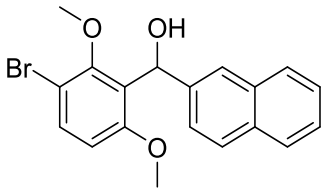

To a solution of 1,3-dibromo-2,4-dimethoxybenzene (161) (375 mg, 1.27 mMol) in 10 mL of abs. THF, *n*-BuLi (1.6 M in hexane, 792 µL, 1.27 mMol) was added slowly at -78 °C and the mixture was stirred at this temperature for a further 2 h. Subsequently, at -78 ° C., a -78 ° C cold solution of 2-naphthalenehyde (495 mg, 3.17 mMol) in 2 mL of abs. THF was added. The reaction mixture was stirred at the same temperature for 1 h and slowly brought to rt overnight. The reaction mixture was washed successively with 4 mL of water, 4 mL of sat. ammonium chloride solution and 30 mL EtOAc. After stirring for 10 min, the organic layer was separated off and the aqueous phase was extracted three times with in each case 10 mL of EtOAc.

The combined organic layers were washed with 15 mL sat. sodium chloride solution and then dried over anhydrous magnesium sulfate. The solvent was completely removed *in vacuo* and the residue was purified by flash chromatography on silica gel (10% EtOAc/PE). The product (404 mg, 1.08 mMol, 85%) was obtained as a colorless oil.

R_f: 0.14 (10% EtOAc/PE).

^{1}H NMR (400 MHz, $CDCl_3$) δ = 7.82 – 7.78 (m, 4H), 7.50 – 7.45 (m, 4H), 6.65 (d, ^3J = 8.9 Hz, 1H), 6.44 (s, 1H), 3.74 (s, 3H), 3.63 (s, 3H). ^{13}C NMR (101 MHz, $CDCl_3$) δ = 157.57, 155.50, 141.88, 133.28, 132.91, 132.60, 128.10, 127.87, 127.64, 127.31, 126.05, 125.71, 124.42, 123.71, 109.06, 108.83, 69.34, 61.67, 56.17.

ESI-MS: m/z = 354.90, 356.90 $[(M-H_2O)+H]^+$.

HRMS (ESI): calculated for $C_{19}H_{16}O_2$ ^{79}Br: m/z = 355.03282 $[M+H]^+$,
found: m/z = 355.03317 $[M+H]^+$.
calculated for $C_{19}H_{16}O_2$ ^{81}Br: m/z = 357.03077 $[M+H]^+$,
found: m/z = 357.03049 $[M+H]^+$.

(±)-(5-bromopyridin-3-yl)(naphthalen-2-yl) methanol (166)

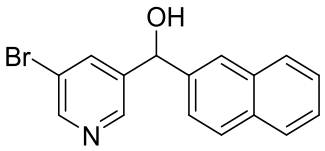

A solution of 3,5-dibromopyridine (300 mg, 1.27 mMol) in 7 mL of abs. THF was slowly treated with isopropyl-magnesium chloride lithium chloride (1.3 M in THF, 1.02 mL, 1.33 mMol) at -78 °C and stirred at this temperature for 1 h. Afterwards a solution of 2-naphthalene (494 mg, 3.17 mMol) in 2 mL of abs. THF was added. The reaction mixture was stirred at the same temperature for 2 h and slowly brought to rt overnight. The reaction mixture was subsequently mixed successively with 4 mL of water, 4 mL of sat. ammonium chloride (aq.) and 30 mL of EtOAc. After stirring for 10 min, the organic layer was separated and the aqueous layer was extracted three times with in each case 10 mL of EtOAc. The combined organic layer were washed with sat. sodium chloride solution and dried over anhydrous magnesium sulfate. The solvent was completely removed under reduced pressure and the residue was purified by flash chromatography on silica gel (20% EtOAc/PE). The product (121 mg, 384 µmol, 30%) was obtained as a yellow oil.

R_f: 0.28 (4% MeOH/DCM).

^{1}H NMR (500 MHz, $CDCl_3$) δ = 8.69 (s, 1H), 8.63 (d, *J* = 5.4, 1H), 8.05 (d, *J* = 5.4 Hz, 1H), 7.83 – 7.79 (m, 4H), 7.52 – 7.49 (m, 2H), 7.40 (d, ^3J = 8.5 Hz, 1H), 6.23 (s, 1H). ^{13}C NMR (126 MHz, $CDCl_3$) δ = 156.39, 148.12, 144.61, 136.88, 133.42, 133.25, 129.21, 128.27, 127.90, 127.26, 127.03, 126.89, 124.77, 124.24, 121.58, 74.48.

ESI-MS: m/z = 313.97, 315.94 $[M+H]^+$.

HRMS (ESI): calculated for $C_{16}H_{13}ON\ ^{79}Br$: m/z = 314.01750 $[M+H]^+$,
found: m/z = 314.01788 $[M+H]^+$.
calculated for $C_{16}H_{13}ON\ ^{81}Br$: m/z = 316.01546 $[M+H]^+$,
found: m/z = 316.01505 $[M+H]^+$.

(±)-(5-bromo-2-methoxypyridin-3-yl)(naphthalen-2-yl)methanol (168)

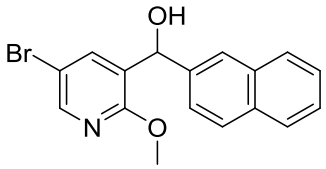

3,5-dibromo-2-methoxypyridine (560 mg, 2.01 mMol) was dissolved in dry Et_2O (7.5 ml) and the mixture was treated dropwise with *s*-BuLi solution (1.4 M in cyclohexane, 1.54 mL, 2.16 mMol) at -100 °C. After stirring at the same temperature for 1 h, a cold solution of 2-naphthalene (819 mg, 5.25 mMol) in dry THF (3 mL) was added and the reaction mixture was subsequently slowly brought to rt overnight. After addition of a mixture of water (6 mL), sat. ammonium chloride solution (aq., 6 mL) and EtOAc (30 mL) were added to the heterogeneous mixture, stirred briefly and the organic layer was separated off. The aqueous layer was then extracted twice with EtOAc (20 mL). The combined organic layers were washed with sat. sodium chloride solution (20 mL) and dried over anhydrous magnesium sulfate. The solvent was completely removed under reduced pressure and the crude product was purified by means of chromatography on silica gel (10% EtOAc/PE). The product (579 mg, 1.68 mMol, 80%) was obtained as a yellow oil.

R_f: 0.18 (10% EtOAc/PE).

^{1}H NMR (500 MHz, $CDCl_3$) δ = 8.15 (d, ^4J = 1.9 Hz, 1H), 7.94 (s, 1H), 7.88 – 7.83 (m, 3H), 7.81 (d, ^3J = 8.5 Hz, 1H), 7.55 – 7.51 (m, 2H), 7.48 (d, ^3J = 8.5 Hz, 1H), 6.81 (s, 1H), 6.07 (s, 1H), 3.91 (s, 3H).

^{13}C NMR (126 MHz, $CDCl_3$) δ = 159.37, 146.00, 139.07, 137.99, 133.11, 132.91, 128.26, 128.21, 128.02, 127.62, 126.15, 126.04, 125.46, 124.54, 112.19, 70.24, 53.78.

ESI-MS: m/z = 344.01, 345,97 $[M+H]^+$.

HRMS (ESI): calculated for $C_{17}H_{15}O_2N\,^{79}Br$: m/z = 344.02807 $[M+H]^+$,
found: m/z = 344.02953 $[M+H]^+$.
calculated for $C_{17}H_{15}O_2N\,^{81}Br$: m/z = 346.02602 $[M+H]^+$,
found: m/z = 346.02657 $[M+H]^+$.

(±)-(2,4-dimethoxy-5-morpholinopyridin-3-yl) (naphthalen-2-yl)methanol (147)

4-(5-bromo-4,6-dimethoxypyridin-3-yl)morpholine (501)

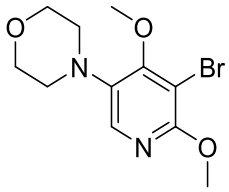

3,5-dibromo-2,4-dimethoxypyridine (25) (200 mg, 674 µmol) was dissolved together with morpholine (59 µL, 674 mMol), tris (dibenzylideneacetone) dipalladium (0) (70 mg, 67 µmol), (±) BINAP (168 mg, 269 µmol) and sodium *tert*-butoxide (129 mg, 1.35 mMol) in degassed toluene (1 mL). The reaction mixture was heated to 80 °C with stirring for 20 h. After the reaction was complete, the solvent was removed *in vacuo* and the crude product was isolated by means of HPLC (without using TFA) without prior work-up. The product (30 mg, 98 µmol, 14%) was obtained as a yellow oil.

^{1}H NMR (500 MHz, $CDCl_3$) δ = 7.84 (s, 1H), 4.09 (s, 1H), 4.07 (s, 1H), 4.00 – 3.94 (m, 4H), 3.21 – 3.14 (m, 4H). ^{13}C NMR (126 MHz, $CDCl_3$) δ = 159.65, 158.00, 136.83, 134.97, 102.22, 67.17, 59.69, 54.93, 51.48.

ESI-MS: m/z = 303.06, 305.00 $[M+H]^+$.

HRMS (ESI): calculated for $C_{11}H_{16}O_3N_2\,^{79}Br$: m/z = 303.03388 $[M+H]^+$,

found: m/z = 303.03453 $[M+H]^+$.

calculated for $C_{11}H_{16}O_3N_2\,^{81}Br$: m/z = 305.03183 $[M+H]^+$,

found: m/z = 305.03179 $[M+H]^+$.

(±)-(2,4-dimethoxy-5-morpholinopyridin-3-yl)(naphthalen-2-yl) methanol (147)

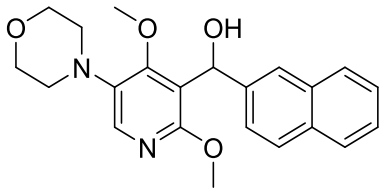

4-(5-bromo-4,6-dimethoxypyridin-3-yl) morpholine (501) (30 mg, 98 µmol) was dissolved in dry THF (1 mL) and the mixture was treated dropwise with *s*-BuLi solution (1.4 M in cyclohexane, 91 µL, 127 µmol) at 78 °C. After stirring at the same temperature for 1 h, the reaction mixture was treated with 2-naphthalene (38 mg, 244 µmol) and afterwards slowly brought to rt overnight. After addition of water (2 mL), sat. ammonium chloride solution (aq., 2 mL) and EtOAc (15 mL) the heterogeneous mixture was stirred briefly before the organic layer was separated off. The aqueous layer was then extracted twice with EtOAc (10 mL).The combined organic layers were washed with sat. sodium chloride solution (10 mL) and dried over anhydrous magnesium sulfate. The solvent was completely removed under reduced pressure and the crude product was purified by means of flash chromatography on silica gel (30% EtOAc/PE). The product (35 mg, 92 µmol, 94%) was obtained as a yellowish oil.

R_f: 0.19 (4% MeOH/DCM).

^{1}H NMR (500 MHz, $CDCl_3$) δ = 7.86 (s, 1H), 7.82 – 7.77 (m, 3H), 7.75 (s, 1H), 7.50 – 7.39 (m, 3H), 6.35 (s, 1H), 4.00 (s, 3H), 3.90 – 3.80 (m, 4H), 3.77 (s, 3H), 3.20 – 2.92 (m, 4H). ^{13}C NMR (126 MHz, $CDCl_3$) δ = 160.46, 158.19, 140.99, 136.83, 134.73, 133.33, 132.80, 128.18, 128.14, 127.75, 126.30, 125.99, 124.19, 123.82, 119.95, 68.45, 67.21, 59.62, 55.19, 51.12.

ESI-MS: m/z = 381.15 $[M+H]^+$.

HRMS (ESI): calculated for $C_{22}H_{25}O_4N_2$: m/z = 381.18088 $[M+H]^+$,
found: m/z = 381.18156 $[M+H]^+$.

3-((trimethylsilyl)ethynyl)benzaldehyde (203)

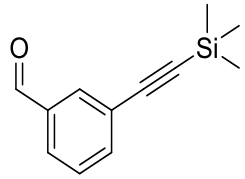

A solution of (3-bromophenylethynyl) trimethylsilane (2.10 mL, 9.87 mMol) in 10 mL of abs. THF was treated slowly with *s*-BuLi (9.87 mL, 13.8 mMol, 1.4 M in cyclohexane) at -78 °C and stirred at this temperature for 1 h. DMF (7.60 mL, 98.7 mMol) was then added at -78 ° C. The reaction mixture was stirred at the same temperature for 1 h and slowly brought to rt overnight. Afterwards the reaction mixture was washed successively with 4 mL of water, 4 mL of saturated ammonium chloride solution (aq.) and 30 mL of EtOAc. After stirring for 10 min, the aqueous layer was extracted three times with in each case 10 mL of EtOAc. The combined organic layers were washed with sat. sodium chloride solution (aq.) and dried over magnesium sulfate. The solvent was completely removed under reduced pressure and the residue was purified by flash chromatography on silica gel (0.5% EtOAc/*n*-pentane). The product (817 mg, 4.04 mMol, 41%) was obtained as a colorless oil.

R_f: 0.19 (1% EtOAc/n-Pentan).

^{1}H NMR (500 MHz, $CDCl_3$) δ = 9.88 (s, 1H), 7.85 (s, 1H), 7.76 – 7.65 (m, 1H), 7.62 – 7.54 (m, 1H), 7.36 (t, ^{3}J = 7.7 Hz, 1H), 0.20 (s, 9H). ^{13}C NMR (126 MHz, $CDCl_3$) δ = 191.08, 137.21, 136.37, 133.15, 128.99, 128.90, 124.30, 103.40, 96.09, -0.19.

GC-MS: t_R = 4.914 min; m/z = 187.1 $[M-O]^+$, 202.1 $[M^{\bullet}]^+$.

HRMS (ESI): calculated for $C_{12}H_{15}OSi$: m/z = 203.8867 $[M+H]^+$,
found: m/z = 203.08891 $[M+H]^+$.

(6-(((*tert*-butyldimethylsilyl)oxy)methyl)naphthalen-2-yl)methanol (184)

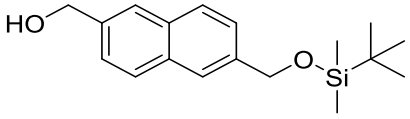

A mixture of naphthalene-2,6-diyldimethanol (1.93 g, 10.25 mMol) and imidazole (271 mg, 3.98 mMol) in dry. THF (85 mL) was treated with *tert*-butylchlorodimethylsilane (618 mg, 4.10 mMol) at 0 °C while stirring vigorously. The mixture was slowly brought to rt and stirred overnight. After adding sat. sodium chloride solution (aq., 30 mL), the heterogeneous mixture was extracted four times with a mixture (4:1) of PE/diethyl ether (30 mL). The combined organic layers were washed with sat. sodium chloride solution (30 mL) and dried over anhydrous magnesium sulfate. The solvent was completely removed under reduced pressure and the crude product was purified by means of flash chromatography on silica gel (30% EtOAc/PE). The product (289 mg, 955 µmol) was obtained as a colorless solid. Unreacted naphthalene-2,6-diyldimethanol (1.68 g, 8.93 mMol, 87%) was reisolated.

R_f: 0.38 (30% EtOAc/PE).

^{1}H NMR (500 MHz, $CDCl_3$) δ = 7.85 – 7.76 (m, 4H); 7.49 – 7.42 (m, 2H); 4.90 (s, 2H); 4.85 (s, 2H); 0.98 (s, 9H), 0.14 (s, 6H). ^{13}C NMR (126 MHz, $CDCl_3$) δ = 139.22, 138.10, 133.06, 132.78, 128.45, 128.01, 125.48, 125.44, 125.15, 124.38, 65.70, 65.29, 26.14, 18.64, -5.03.

ESI-MS: m/z = 285.17 $[M\text{-}H_20+H]^+$.

HRMS (ESI): calculated for $C_{18}H_{25}OSi$: m/z = 285.16692 $[M\text{-}H_20+H]^+$,
found: m/z = 285.16732 $[M+H]^+$.

6-(((*tert*-butyldimethylsilyl)oxy)methyl)-2-naphthaldehyde (185)

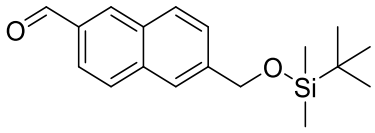

To a solution of (6 - (((tert-butyldimethylsilyl) oxy) methyl) naphthalen-2-yl) methanol (290 mg, 958.73 µmol) in DCM (12 mL) was added dropwise at rt a DMP solution (0.3 M in DCM, 4.79 mL, 1.44 mMol) and the resulting reaction mixture was stirred for 1 h. After adding sat. sodium hydrogencarbonate solution (aq., 15 mL) and EtOAc (40 mL), the heterogeneous mixture was mixed with sodium thiosulfate (1.5 g, 9.5 mMol) and stirred until both phases appear clear. The organic layer was separated off and the aqueous phase was extracted with EtOAc (20 mL). The combined organic layers were washed with sat. sodium chloride solution (aq.) and dried over anhydrous magnesium sulfate. The solvent was completely removed under reduced pressure and the crude product was purified by means of flash chromatography on silica gel (5% EtOAc/PE). The product (261 mg, 869 µmol, 90%) was obtained as a colorless solid.

R_f: 0.38 (10% EtOAc/PE).

^{1}H NMR (400 MHz, $CDCl_3$) δ = 10.15 (d, 2H), 8.32 (s, 1H), 7.99 – 7.90 (m, 3H), 7.85 (s, 1H), 7.54 (d, ^3J = 8.41 Hz, 1H), 4.93 (s, 2H), 0.99 (s, 9H), 0.15 (s, ^4J = 3.1 Hz, 6H). ^{13}C NMR (126 MHz, $CDCl_3$): δ = 192.38, 142.96, 136.72, 134.43, 134.01, 132.02, 129.61, 129.15, 125.81, 124.46, 123.17, 65.02, 26.11, 18.62, -5.07.

GC-MS: m/z = 300.3 $[M^{\bullet}]^+$.

HRMS (ESI): calculated for $C_{18}H_{25}O_2Si$: m/z = 301.16183 $[M\text{-}H_20+H]^+$,
found: m/z = 301.16226 $[M+H]^+$.

Synthesis of 3,5-functionalized pyridines

General procedure I (GP I): Regioselective Br/Li exchange with subsequent addition of aldehydes and isocyanates.

A solution of the pyridine (1.0 eq.) in dry. THF (0.1 M) was treated dropwise with *s*-BuLi solution (1.4 M in cyclohexane, 1 eq.) at 78 °C and stirred at this temperature for 1 h. The reaction solution was then treated with a solution of the aldehyde or the isocyanate (2.5 eq.) in dry THF (1.2 M), and the reaction mixture was slowly warmed to rt overnight. After the addition of water and sat. ammonium chloride solution, the heterogeneous mixture was extracted three times with EtOAc. The combined organic layers were washed with sat. sodium chloride solution, dried over anhydrous magnesium sulfate, and the crude product was concentrated *in vacuo*. The product was isolated by means of flash chromatography on silica gel.

Representative example:

(±)-(5-bromo-2,4-dimethoxypyridin-3-yl)(4-isopropylphenyl) methanol (502)

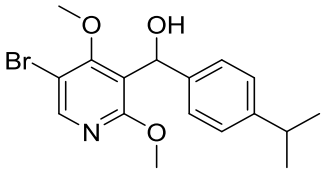

A solution of 3,5-dibromo-2,4-dimethoxypyridine (300 mg, 1.01 mMol) in dry. THF (10 ml) was treated dropwise with *s*-BuLi solution (1.4 M in cyclohexane, 722 µl, 1.01 mMol) at 78 °C and stirred at this temperature for 1 h. The reaction solution was then treated with a solution of cuminaldehyde (374 mg, 2.53 mMol) in dry THF (2 mL) and the reaction mixture was slowly warmed to rt overnight. After the addition of water (4 mL) and sat. ammonium chloride solution (aq., 4 mL), the heterogeneous mixture was extracted three times with EtOAc (15 mL). The combined organic layers were washed with sat. sodium chloride solution (15 mL) and dried over magnesium sulfate. The crude product was concentrated *in vacuo* and then purified by flash chromatography on silica gel (10% EtOAc/PE). The product (268 mg, 733 µmol, 73%) was obtained as a colorless oil.

R_f: 0.27 (20% EtOAc/PE).

^{1}H-NMR (600 MHz, $CDCl_3$): δ = 8.19 (s, 1H), 7.25 (d, ^3J = 8.1 Hz, 2H), 7.17 (d, ^3J = 8.2 Hz, 2H), 6.15 (s, 1H), 3.92 (s, 3H), 3.74 (s, 3H), 2.88 (hept, ^3J = 6,9 Hz, 1H), 1.23 (d, ^3J = 6.9 Hz, 6H). ^{13}C-NMR (151 MHz, $CDCl_3$): δ = 162.49, 162.06, 148.48, 147.93, 140.61, 126.36, 125.60, 120.87, 107.91, 68.40, 61.59, 54.25, 33.79, 24.05. ESI-MS: *m/z* 366.07, 368.07 $[M+H]^+$.

HRMS (ESI): calculated for $C_{17}H_{21}O_3N\,^{79}Br$ m/z = 366.06993 $[M+H]^+$,
found m/z = 366.07078 $[M+H]^+$.
calculated for $C_{17}H_{21}O_3N\,^{81}Br$ m/z = 368.06789 $[M+H]^+$,
found m/z = 368.06777 $[M+H]^+$.

(±)-[1,1'-biphenyl]-4-yl(5-bromo-2,4-dimethoxypyridin-3-yl) methanol (503)

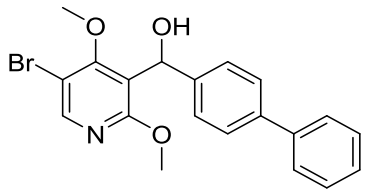

3,5-dibromo-2,4-dimethoxypyridine (300 mg, 1.01 mMol) was reacted according to GP I with [1,1'-biphenyl]-4-aldehyde. The product (307.70 mg, 768 µmol, 76%) was isolated by flash chromatography on silica gel (10% EtOAc/PE) and obtained as a colorless oil.

R_f: 0.22 (20% EtOAc/PE).

^{1}H NMR (500 MHz, $CDCl_3$) δ = 8.20 (s, 1H), 7.56 – 7.52 (m, 4H), 7.42 – 7.37 (m, 4H), 7.32 – 7.29 (m, 1H), 6.20 (s, 1H), 5.27 (s, 1H), 3.93 (s, 3H), 3.77 (s, 3H). ^{13}C NMR (126 MHz, $CDCl_3$) δ = 162.64, 162.01, 148.58, 142.32, 140.76, 140.16, 128.83, 127.36, 127.07, 127.03, 126.02, 120.70, 107.90, 68.21, 61.71, 54.42.

ESI-MS: m/z = 400.00, 402.00 $[M+H]^+$.

HRMS (ESI): calculated for $C_{20}H_{19}O_3N\,^{79}Br$: m/z = 400.05428 $[M+H]^+$,
found: m/z = 400.05353 $[M+H]^+$.
calculated for $C_{20}H_{19}O_3N\,^{81}Br$: m/z = 402.05050 $[M+H]^+$,
found: m/z = 402.05224 $[M+H]^+$.

(±)-(5-bromo-2,4-dimethoxypyridin-3-yl)(4-methoxyphenyl) methanol (504)

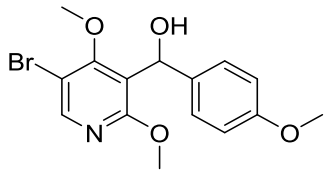

3,5-dibromo-2,4-dimethoxypyridine (200 mg, 674 µmol) was reacted according with GP I with 4-methoxy-benzaldehyde. The product (163 mg, 460 µmol, 68%) was isolated by flash chromatography on silica gel (10% EtOAc/PE) and obtained as a yellow oil.

Rf: 0.25 (20% EtOAc/PE).

1H NMR (500 MHz, $CDCl_3$) δ = 8.18 (s, 1H), 7.23 (d, ^3J = 8.6 Hz, 2H), 6.83 (d, ^3J = 8.7 Hz, 2H), 6.11 (s, 1H), 3.91 (s, 3H), 3.77 (s, 3H), 3.74 (s, 3H). 13C NMR (126 MHz, $CDCl_3$) δ = 162.45, 162.02, 158.85, 148.48, 135.40, 126.87, 120.85, 113.70, 107.94, 68.16, 61.63, 55.30, 54.27.

ESI-MS: m/z = 353.99 $[M+H]^+$.

HRMS (ESI): calculated for $C_{15}H_{17}O_4N\,^{79}Br$: m/z = 354.03355 $[M+H]^+$,
found: m/z = 354.03402 $[M+H]^+$.
calculated for $C_{15}H_{17}O_4N\,^{81}Br$: m/z = 356.03150 $[M+H]^+$,
found: m/z = 356.03108 $[M+H]^+$.

(±)-(5-bromo-2,4-dimethoxypyridin-3-yl)(naphthalen-1-yl) methanol (505)

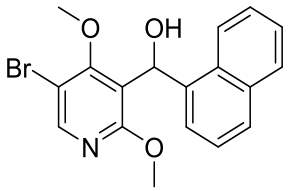

3,5-dibromo-2,4-dimethoxypyridines (300 mg, 1.01 mMol) was reacted according to GP I with 1-naphthaldehyde. The product (309 mg, 827 µmol, 82%) was isolated by flash chromatography on silica gel (10% EtOAc/PE) and obtained as a yellow oil.

Rf: 0.21 (20% EtOAc/PE).

1H NMR (500 MHz, CDCl3) δ = 8.42 (d, ^{3}J = 8.5 Hz, 1H), 8.27 (s, 1H), 7.88 (d, ^{3}J = 8.1 Hz, 1H), 7.80 (d, ^{3}J = 8.2 Hz, 1H), 7.59 – 7.56 (m, 1H), 7.53 – 7.50 (m, 1H), 7.40 – 7.37 (m, 1H), 7.24 (d, ^{3}J = 7.2 Hz, 1H), 6.88 (s, 1H), 3.97 (s, 3H), 3.66 (s, 3H). 13C NMR (126 MHz, CDCl3) δ = 162.80, 162.50, 148.73, 137.38, 134.11, 131.59, 128.79, 128.72, 126.42, 125.81, 124.93, 124.63, 123.91, 119.65, 108.32, 66.77, 61.65, 54.34.

ESI-MS: m/z = 374.07 [M+H]+.

HRMS (ESI): calculated for C18H17O3N ^{79}Br: m/z = 374.03863 [M+H]+,
found: m/z = 374.03957 [M+H]+.
calculated for C18H17O3N ^{81}Br: m/z = 376.03659 [M+H]+,
found: m/z = 376.03661 [M+H]+.

(±)-(5-bromo-2,4-dimethoxypyridin-3-yl)(3,5-dimethoxyphenyl) methanol (506)

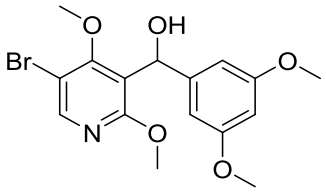

3,5-dibromo-2,4-dimethoxypyridine (300 mg, 1.01 mMol) was reacted according to GP I with 3,5-dimethoxy-benzaldehyde. The product (222 mg, 579 µmol, 57%) was isolated by flash chromatography on silica gel (20% EtOAc/PE) and obtained as a yellow oil.

R_f: 0.18 (30% EtOAc/PE).

^{1}H NMR (500 MHz, $CDCl_3$) δ = 8.19 (s, 1H), 6.48 (d, ^{3}J = 2.1 Hz, 2H), 6.34 (t, ^{4}J = 2.1 Hz, 1H), 6.08 (s, 1H), 3.92 (s, 3H), 3.75 (s, 9H). ^{13}C NMR (126 MHz, $CDCl_3$) δ = 162.65, 162.01, 160.87, 148.67, 146.05, 120.61, 107.85, 103.92, 98.84, 77.41, 77.16, 76.91, 68.35, 61.69, 55.42, 54.39.

ESI-MS: m/z = 384.03 $[M+H]^+$.

HRMS (ESI): calculated for $C_{16}H_{19}O_5N$ ^{79}Br: m/z = 384.04411 $[M+H]^+$,
found: m/z = 384.04560 $[M+H]^+$.
calculated for $C_{16}H_{19}O_5N$ ^{81}Br: m/z = 386.04207 $[M+H]^+$,
found: m/z = 386.04265 $[M+H]^+$.

(±)-(5-bromo-2,4-dimethoxypyridin-3-yl)(4-(trifluoromethyl) phenyl) methanol (507)

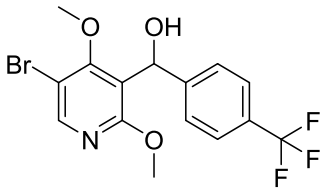

3,5-dibromo-2,4-dimethoxypyridine (325 mg, 1.09 mMol) was reacted according to GP I with 4-(trifluoromethyl) benzaldehyde. The product (269 mg, 685 µmol, 63%) was isolated by flash chromatography on silica gel (10% EtOAc/PE) and obtained as a colorless oil.

R_f: 0.16 (20% EtOAc/PE).

^{1}H NMR (500 MHz, $CDCl_3$) δ = 8.20 (s, 1H), 7.55 (d, ^3J = 8.3 Hz, 2H), 7.44 (d, ^3J = 8.3 Hz, 2H), 6.20 (s, 1H), 3.89 (s, 3H), 3.78 (s, 3H). ^{13}C NMR (126 MHz, $CDCl_3$) δ = 162.66, 161.88, 149.16, 147.45, 129.46 (q, ^2J (C,F) = 32.2 Hz), 125.80, 125.24 (q, ^3J (C,F) = 3.6 Hz), 124.25 (q, ^1J (C,F) = 271.9 Hz), 120.01, 107.78, 67.87, 61.70, 54.35.

ESI-MS: m/z = 392.00, 394.00 $[M+H]^+$.

HRMS (ESI):calculated for $C_{15}H_{14}O_3N\,^{79}BrF_3$: m/z = 392.01037 $[M+H]^+$,
found: m/z = 392.01040 $[M+H]^+$.
calculated for $C_{15}H_{14}O_3N\,^{81}BrF_3$: m/z = 394.00832 $[M+H]^+$,
found: m/z = 394.00742 $[M+H]^+$.

(±)-(5-bromo-4-methoxypyridin-3-yl)(naphthalen-2-yl)methanol (173)

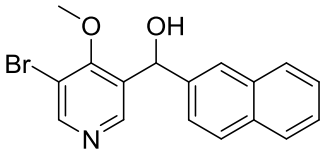

3,5-dibromo-4-methoxypyridine (93 mg, 348 µmol) was reacted according to GP I with 2-naphthalene. The product (113 mg, 327 µmol, 94%) was isolated by flash chromatography on silica gel (30% EtOAc/PE) and obtained as a colorless oil.

R_f: 0.34 (50% EtOAc/PE).

^{1}H NMR (500 MHz, $CDCl_3$) δ = 8.61 (s, 1H), 8.51 (s, 1H), 7.83 – 7.76 (m, 4H), 7.50 – 7.44 (m, 2H), 7.40 (dd, $^{3,4}J$ = 8.5 , 1.7 Hz, 1H), 6.18 (s, 1H), 3.65 (s, 3H). ^{13}C NMR (126 MHz, $CDCl_3$) δ = 161.56, 152.76, 148.55, 140.05, 134.99, 133.29, 133.07, 128.63, 128.15, 127.81, 126.51, 126.37, 125.52, 124.64, 114.44, 70.51, 61.22.

ESI-MS: m/z = 344.07 $[M+H]^+$.

HRMS (ESI): calculated for $C_{17}H_{15}O_2N\,^{79}Br$: m/z = 344.02807 $[M+H]^+$,
found: m/z = 344.02935 $[M+H]^+$.
calculated for $C_{17}H_{15}O_2N\,^{81}Br$: m/z = 346.02602 $[M+H]^+$,
found: m/z = 346.02653 $[M+H]^+$.

(±)-(5-bromo-2,4-dimethoxypyridin-3-yl)(1-methyl-1H-indol-3-yl) methanol (508)

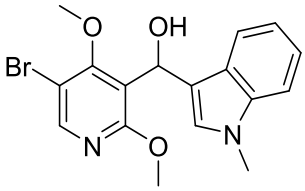

3,5-dibromo-2,4-dimethoxypyridine (200 mg, 674 µmol) was reacted according to GP I with 1-methyl-1H-indole-3-aldehyde. The product (52 mg, 137 µmol, 20%) was isolated by flash chromatography on silica gel (30% EtOAc/PE) and obtained as a red oil.

R_f: 0.45 (50% EtOAc/PE).

^{1}H NMR (500 MHz, $CDCl_3$) δ = 8.17 (s, 1H), 7.42 – 7.37 (m, 2H), 7.05 – 6.99 (m, 3H), 6.81 (s, 1H), 6.43 (s, 1H), 4.04 (s, 3H), 4.00 (s, 3H), 3.71 (s, 3H). ^{13}C NMR (126 MHz, $CDCl_3$) δ = 187.72, 166.24, 165.02, 153.98, 146.15, 137.10, 128.32, 127.70, 121.49, 119.55, 118.91, 115.53, 109.22, 108.44, 63.12, 54.81, 32.87.

ESI-MS: m/z = 376.91 $[M+H]^+$.

HRMS (ESI): calculated for $C_{17}H_{18}O_3N_2$ ^{79}Br: m/z = 377.04953 $[M+H]^+$,
found: m/z = 377.04993 $[M+H]^+$.
calculated for $C_{17}H_{18}O_3N_2$ ^{81}Br: m/z = 379.04748 $[M+H]^+$,
found: m/z = 379.04760 $[M+H]^+$.

(±)-(5-bromo-2,4-dimethoxypyridin-3-yl)(quinoxalin-2-yl) methanol (509)

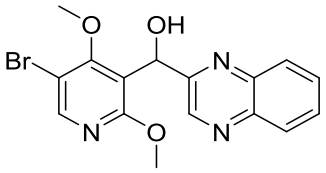

3,5-dibromo-2,4-dimethoxypyridine (275 mg, 926 µmol) was reacted according to GP I with quinoxaline-2-aldehyde. The product (265 mg, 704 µmol, 76%) was isolated by flash chromatography on silica gel (30% EtOAc/PE) and obtained as a yellow oil.

R_f: 0.16 (30% EtOAc/PE).

^{1}H NMR (500 MHz, $CDCl_3$) δ = 8.84 (s, 1H), 8.22 (s, 1H), 8.16 – 8.10 (m, 1H), 8.10 – 8.04 (m, 1H), 7.81 – 7.72 (m, 2H), 6.46 (s, 1H), 3.88 (s, 3H), 3.82 (s, 3H). ^{13}C NMR (126 MHz, $CDCl_3$) δ = 163.87, 162.48, 155.82, 149.69, 143.29, 141.49, 140.91, 130.55, 129.93, 129.15, 128.95, 118.61, 107.91, 67.04, 62.21, 54.41.

ESI-MS: m/z = 375.89, 377.91 $[M+H]^+$.

HRMS (ESI): calculated for $C_{16}H_{15}O_3N_3$ ^{79}Br: m/z = 376.02913 $[M+H]^+$,
found: m/z = 376.03053 $[M+H]^+$.
calculated for $C_{16}H_{15}O_3N_3$ ^{81}Br: m/z = 378.02708 $[M+H]^+$,
found: m/z = 378.02774 $[M+H]^+$.

(±)-Benzofuran-2-yl(5-bromo-2,4-dimethoxypyridin-3-yl) methanol (510)

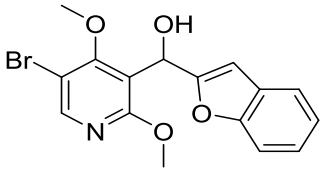

3,5-dibromo-2,4-dimethoxypyridine (359 mg, 1.21 mMol) was reacted according to GP I with benzofuran-2-aldehyde. The product (365 mg, 1.00 mMol, 83%) was isolated by means of flash chromatography on silica gel (10% EtOAc/PE) and obtained as a yellow oil.

R_f: 0.30 (20% EtOAc/PE).

^{1}H NMR (500 MHz, $CDCl_3$) δ = 8.25 (s, 1H), 7.53 – 7.50 (m, 1H), 7.42 (d, ^3J = 8.1 Hz, 1H), 7.26 – 7.17 (m, 2H), 6.59 (s, 1H), 6.30 (d, ^4J = 0.7 Hz, 1H), 3.96 (s, 3H), 3.90 (s, 3H). ^{13}C NMR (126 MHz, $CDCl_3$) δ = 162.90, 162.19, 157.86, 154.92, 149.14, 128.20, 124.13, 122.83, 121.00, 117.57, 111.26, 107.76, 103.02, 63.68, 61.98, 54.36.

ESI-MS: m/z = 363.98, 365.94 $[M+H]^+$.

HRMS (ESI): calculated for $C_{16}H_{15}O_4N\,^{79}Br$: m/z = 364.01790 $[M+H]^+$,
found: m/z = 364.01906 $[M+H]^+$.
calculated for $C_{16}H_{15}O_4N\,^{81}Br$: m/z = 366.01585 $[M+H]^+$,
found: m/z = 366.01585 $[M+H]^+$.

(±)-*tert*-butyl4-(4-((5-bromo-2,4-dimethoxypyridin-3-yl)(hydroxy)methyl)phenyl) piperazine-1-carboxylate (511)

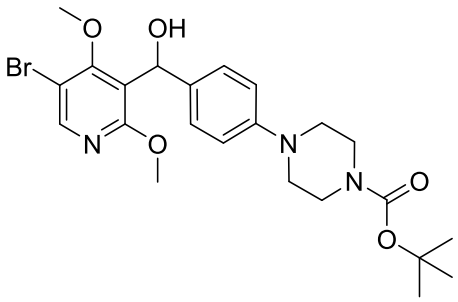

3,5-dibromo-2,4-dimethoxypyridine (522 mg, 1.76 mMol) was reacted according to GP I with tert-butyl-4-(4-formylphenyl)piperazine-1-carboxy-late. The product (642 mg, 1.26 mMol, 72%) was isolated by flash chromatography on silica gel (20% EtOAc/PE) and obtained as a yellow oil.

R_f: 0.13 (30% EtOAc/PE).

^{1}H NMR (500 MHz, $CDCl_3$) δ = 8.07 (s, 1H), 7.13 (d, ^3J = 8.3 Hz, 2H), 6.76 (d, ^3J = 8.4 Hz, 2H), 6.03 (s, 1H), 3.80 (s, 3H), 3.64 (s, 3H), 3.53 – 3.41 (m, 4H), 3.06 – 2.94 (m, 4H), 1.39 (s, 9H).^{13}C NMR (126 MHz, $CDCl_3$) δ = 162.20, 161.77, 154.37, 149.98, 148.04, 134.64, 126.32, 120.72, 115.96, 107.66, 79.54, 67.65, 61.30, 53.91, 49.10, 28.20.

ESI-MS: m/z = 507.76, 509.81 $[M+H]^+$.

HRMS (ESI): calculated for $C_{23}H_{31}O_5N_3\,^{79}Br$: m/z = 508.14416 $[M+H]^+$,
found: m/z = 508.14558 $[M+H]^+$;
calculated for $C_{23}H_{31}O_5N_3\,^{81}Br$: m/z = 510.14211 $[M+H]^+$,
found: m/z = 510.14243 $[M+H]^+$.

(±)-(5-bromo-2,6-dimethoxypyridin-3-yl)(naphthalen-2-yl)methanol (164)

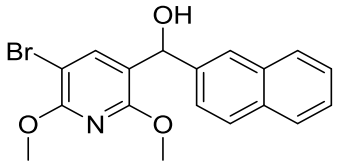

3,5-dibromo-2,4-dimethoxypyridine (310 mg, 1.04 mMol) was reacted according to GP I with 2-naphthaldehyde. The product (320 mg, 855 mMol, 82%) was isolated by flash chromatography on silica gel (1 - 50% EtOAc/PE) and obtained as a yellow oil.

R_f: 0.45 (10% EtOAc/PE).

^{1}H NMR (500 MHz, $CDCl_3$) δ = 7.89 – 7.77 (m, 4H), 7.66 (bs, 1H), 7.52 – 7.42 (m, 3H), 6.10 (s, 1H), 3.99 (s, 3H), 3.95 (s, 3H).

ESI-MS: m/z = 356.34, 358.23 $[M\text{-}OH]^+$.

HRMS (ESI): calculated for $C_{18}H_{15}O_2N\,^{79}Br$: m/z = 356.02807 $[M\text{-}OH]^+$,
found: m/z = 356.02936 $[M\text{-}OH]^+$.
calculated for $C_{18}H_{15}O_2N\,^{81}Br$: m/z = 358.02602 $[M\text{-}OH]^+$,
found: m/z = 358.02728 $[M\text{-}OH]^+$.

(±)-(5-bromo-2,4-dimethoxypyridin-3-yl)(naphthalen-2-yl)methanol (512)

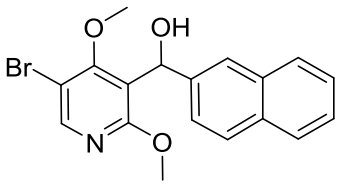

3,5-dibromo-2,4-dimethoxypyridine (535 mg, 1.80 mMol) was reacted according to GP I with 2-naphthaldehyde. The product (568 mg, 1.52 mMol, 84%) was isolated by flash chromatography on silica gel (10% EtOAc/PE) and obtained as a yellow oil.

R_f: 0.17 (10% EtOAc/PE).

^{1}H NMR (600 MHz, $CDCl_3$) δ = 8.26 (s, 1H), 7.84 – 7.78 (m, 4H), 7.50 – 7.44 (m, 3H), 6.40 (s, 1H), 3.92 (s, 3H), 3.74 (s, 3H). ^{13}C NMR (151 MHz, $CDCl_3$) δ = 162.63, 162.01, 148.67, 140.67, 133.15, 132.63, 128.01, 127.99, 127.59, 126.11, 125.82, 124.09, 123.74, 120.60, 107.87, 68.34, 61.59, 54.26.

ESI-MS: m/z = 373.95, 375.91 $[M+H]^+$.

HRMS (ESI): calculated for $C_{18}H_{17}O_3N\,^{79}Br$: m/z = 374.03863 $[M+H]^+$,
found: m/z = 374.03985 $[M+H]^+$;
calculated for $C_{18}H_{17}O_3N\,^{81}Br$: m/z = 376.03659 $[M+H]^+$,
found: m/z = 376.03699 $[M+H]^+$.

(±)-[1,1'-biphenyl]-3-yl(5-bromo-2,4-dimethoxypyridin-3-yl)methanol (513)

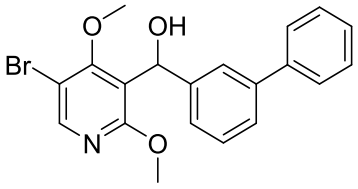

3,5-dibromo-2,4-dimethoxypyridine (302 mg, 1.02 mMol) was reacted according to GP I with [1,1'-biphenyl]-3-carbaldehyde. The product (568 mg, 1.52 mMol, 95%) was isolated by flash chromatography on silica gel (10% EtOAc/PE) and obtained as a yellow oil.

R_f: 0.17 (20% EtOAc/PE).

^{1}H NMR (500 MHz, $CDCl_3$) δ = 8.24 (s, 1H), 7.68 (s, 1H), 7.64 – 7.56 (m, 2H), 7.51 (d, ^3J = 7.6 Hz, 1H), 7.45 (t, ^3J = 7.6 Hz, 2H), 7.43 – 7.34 (m, 2H), 7.31 (d, ^3J = 7.3 Hz, 1H), 6.30 (s, 1H), 3.95 (s, 3H), 3.80 (s, 3H). ^{13}C NMR (126 MHz, $CDCl_3$) δ = 162.63, 162.02, 148.72, 143.85, 141.26, 141.11, 128.81, 128.71, 127.40, 127.18, 126.09, 124.45, 124.30, 120.70, 107.87, 68.35, 61.62, 54.30.

ESI-MS: m/z = 399.90, 401.90 $[M+H]^+$.

HRMS (ESI): calculated for $C_{20}H_{19}O_3N\,^{79}Br$: m/z = 400.05428 $[M+H]^+$,
found: m/z = 400.05463 $[M+H]^+$;
calculated for $C_{20}H_{19}O_3\,^{81}BrSi$: m/z = 402.05224 $[M+H]^+$,
found: m/z = 402.05162 $[M+H]^+$.

(±)-(5-bromo-2,4-dimethoxypyridin-3-yl)(3-((trimethylsilyl)ethynyl)phenyl)meth-anol (204)

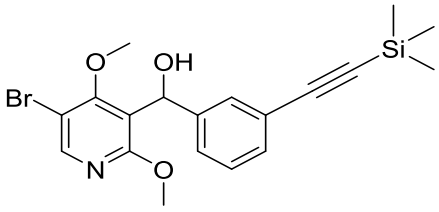

3,5-dibromo-2,4-dimethoxypyridine (500 mg, 1.68 mMol) was reacted according to GP I with 3-((trimethylsilyl) ethynyl) benzaldehyde. The product (568 mg, 1.52 mMol, 77%) was isolated by flash chromatography on silica gel (10% EtOAc/PE) and obtained as a yellow oil. R_f: 0.25 (20% EtOAc/PE).

^{1}H NMR (500 MHz, $CDCl_3$) δ = 8.22 – 8.13 (m, 1H), 7.43 (s, 1H), 7.33 (d, ^3J = 6.9 Hz, 1H), 7.26 – 7.19 (m, 2H), 6.11 (s, 1H), 3.90 – 3.86 (m, 3H), 3.74 – 3.69 (m, 3H), 0.23 (s, ^4J = 2.0 Hz, 9H). ^{13}C NMR (126 MHz, $CDCl_3$) δ = 162.65, 161.95, 148.86, 143.55, 130.89, 128.87, 128.16, 125.63, 123.13, 120.38, 107.80, 105.16, 94.25, 67.83, 61.63, 54.30, 0.04.

ESI-MS: m/z = 419.92, 421.84 $[M+H]^+$.

HRMS (ESI): calculated for $C_{19}H_{23}O_3N\,^{79}BrSi$: m/z = 420.06251 $[M+H]^+$,
found: m/z = 420.06335 $[M+H]^+$;
calculated for $C_{19}H_{23}O_3N\,^{81}BrSi$: m/z = 422.06046 $[M+H]^+$,
found: m/z = 422.06024 $[M+H]^+$.

(±)-(5-bromo-2,4-dimethoxypyridin-3-yl)(3-fluoro-4-(trifluoromethyl)phenyl) methanol (514)

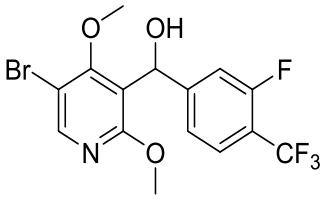

3,5-dibromo-2,4-dimethoxypyridine (301 mg, 1.02 mMol) was reacted according to GP I with 3-fluoro-4- (trifluoromethyl) benzaldehyde. The product (279 mg, 680 µmol, 67%) was isolated by flash chromatography on silica gel (20% EtOAc/PE) and obtained as a colorless oil.

R_f: 0.20 (20% EtOAc/PE).

^{1}H NMR (400 MHz, $CDCl_3$) δ = 8.21 (s, 1H), 7.56 – 7.48 (m, 1H), 7.24 – 7.13 (m, 2H), 6.16 (s, 1H), 3.90 (s, 3H), 3.83 (s, 3H).

^{13}C NMR (101 MHz, $CDCl_3$) δ = 162.70, 161.77, 161.19, 161.17, 161.15, 161.13, 158.64, 158.62, 158.60, 158.58, 150.83, 150.83, 150.76, 150.76, 149.48, 127.12, 127.10, 127.07, 127.06, 126.77, 126.76, 124.06, 124.05, 121.36, 121.35, 120.96, 120.93, 119.34, 118.66, 118.66, 117.59, 117.47, 117.26, 117.14, 116.94, 116.81, 116.61, 116.48, 114.17, 113.95, 107.73, 67.43, 61.83, 61.80, 54.47, 54.44.

ESI-MS: m/z = 409.94, 411.92 $[M+H]^+$.

HRMS (ESI): calculated for $C_{15}H_{13}O_3N\,^{79}BrF_4$: m/z = 410.00095 $[M+H]^+$,
found: m/z = 410.00151 $[M+H]^+$;
calculated for $C_{15}H_{13}O_3N\,^{81}BrF_4$: m/z = 411.99890 $[M+H]^+$,
found: m/z = 411.99835 $[M+H]^+$.

(5-bromo-2,4-dimethoxypyridin-3-yl)(6-(((tert-butyldimethylsilyl)oxy)methyl) naphthalene-2-yl)methanol (186)

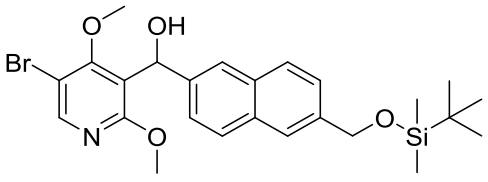

3,5-dibromo-2,4-dimethoxypyridine (258 mg, 869 µmol) was reacted according to GP I with 6-(((tert-butyldimethylsilyl) oxy) methyl) -2-naphthaldehyde. The product (374 mg, 721 µmol, 83%) was isolated by flash chromatography on silica gel (10% EtOAc/PE) and obtained as a white solid.

R_f: 0.10 (10% EtOAc/PE).

^{1}H NMR (500 MHz, $CDCl_3$) δ = 8.24 (s, 1H), 7.78 (dd, $^{3,4}J$ = 8.5, 3.1 Hz, 2H), 7.76 (s, 2H), 7.46-7.42 (m, 2H), 6.34 (s, 1H), 4.90 (s, 2H), 3.92 (s, 3H), 3.73 (s, 3H), 0.98 (s, 9H), 0.14 (s, 6H). ^{13}C NMR (126 MHz, $CDCl_3$) δ = 162.71, 162.15, 148.79, 140.43, 139.14, 132.72, 132.54, 128.13, 128.09, 125.08, 124.31, 124.25, 123.70, 120.75, 107.97, 68.57, 65.24, 61.71, 54.37, 26.11, 18.60, -5.06.

ESI-MS: m/z = 518.0, 520.0 $[M+H]^+$.

HRMS (ESI): calculated for $C_{25}H_{33}O_4N\,^{79}BrSi$: m/z = 518.13567 $[M+H]^+$,
found: m/z = 518.13617 $[M+H]^+$;
calculated for $C_{25}H_{33}O_4N\,^{81}BrSi$: m/z = 520.13363 $[M+H]^+$,
found: m/z = 520.13327 $[M+H]^+$.

5-bromo-2,4-dimethoxy-*N*-phenylnicotinamide (515)

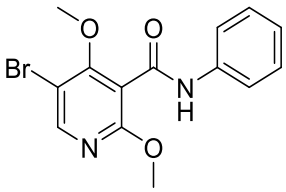

3,5-dibromo-2,4-dimethoxypyridine (151 mg, 509 µmol) was reacted according to GP I with phenyl isocyanate. The product (51 mg, 152 µmol, 30%) was isolated by flash chromatography on silica gel (20% EtOAc/PE) and obtained as a white solid.

R_f: 0.24 (20% EtOAc/PE).

^{1}H NMR (500 MHz, $CDCl_3$) δ = 8.21 (s, 1H), 7.95 (s, 1H), 7.61 (d, ^3J = 7.8 Hz, 2H), 7.40 – 7.32 (m, 2H), 7.20 – 7.12 (m, 1H), 4.02 (s, 3H), 3.94 (s, 3H). ^{13}C NMR (126 MHz, $CDCl_3$) δ = 162.22, 161.53, 161.51, 149.72, 137.76, 129.26, 125.02, 120.05, 113.32, 107.14, 61.57, 54.77.

ESI-MS: m/z = 336.94 $[M+H]^+$.

HRMS (ESI): calculated for $C_{14}H_{14}O_3N_2\,^{79}Br$: m/z = 337.01823 $[M+H]^+$,
found: m/z = 337.01912 $[M+H]^+$.
calculated for $C_{14}H_{14}O_3N_2\,^{81}Br$: m/z = 339.01618 $[M+H]^+$,
found: m/z = 339.01646 $[M+H]^+$.

***N*-benzyl-5-bromo-2,4-dimethoxynicotinamide (516)**

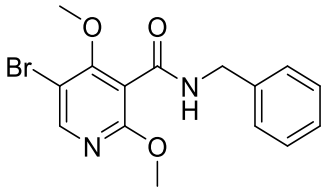

3,5-dibromo-2,4-dimethoxypyridine (302 mg, 1.02 mMol) was reacted according to GP I with benzyl isocyanate. The product (232 mg, 661 µmol, 65%) was isolated by flash chromatography on silica gel (10% EtOAc/PE) and obtained as a white solid.

R_f: 0.42 (30% EtOAc/PE).

^{1}H NMR (500 MHz, $CDCl_3$) δ = 8.11 (s, 1H), 7.34 – 7.24 (m, 5H), 6.86 (s, 1H), 4.52 (d, J = 5.9 Hz, 2H), 3.87 (s, 3H), 3.86 (s, 3H). ^{13}C NMR (126 MHz, $CDCl_3$) δ = 163.42, 161.60, 161.27, 149.17, 137.66, 128.52, 127.65, 127.42, 113.15, 106.74, 61.06, 54.26, 43.78.

ESI-MS: m/z = 350.95, 352.92 $[M+H]^+$.

HRMS (ESI): calculated for $C_{15}H_{16}O_3N_2\,^{79}Br$: m/z = 351.03388 $[M+H]^+$,
found: m/z = 351.03543 $[M+H]^+$.
calculated for $C_{15}H_{16}O_3N_2\,^{81}Br$: m/z = 353.03183 $[M+H]^+$,
found: m/z = 353.03264 $[M+H]^+$.

5-bromo-2,4-dimethoxy-*N*-(naphthalen-1-yl)nicotinamid (517)

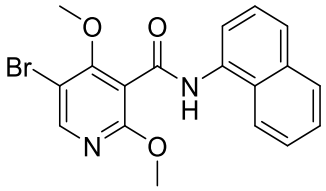

3,5-dibromo-2,4-dimethoxypyridine (320 mg, 1.08 mMol) was reacted according to GP I with 1-isocyanato-naphthalene. The product (115 mg, 299 µmol, 28%) was isolated by flash chromatography on silica gel (10% EtOAc/PE) and obtained as a white solid.

R_f: 0.22 (20% EtOAc/PE).

^{1}H NMR (500 MHz, $CDCl_3$) δ = 8.25 (s, 1H), 7.97 (d, ^3J = 7.4 Hz, 2H), 7.90 – 7.85 (m, 1H), 7.74 (d, ^3J = 8.2 Hz, 1H), 7.54 – 7.47 (m, 3H), 4.07 (s, 3H), 4.01 (s, 3H).

^{13}C NMR (126 MHz, $CDCl_3$) δ = 162.62, 162.21, 161.53, 149.82, 134.27, 131.90, 128.82, 127.55, 126.60, 126.52, 126.22, 125.79, 121.45, 120.94, 113.56, 107.43, 61.79, 54.81.

ESI-MS: m/z = 386.92, 388.96 $[M+H]^+$.

HRMS (ESI): calculated for $C_{18}H_{16}O_3N_2\,^{79}Br$: m/z = 387.03388 $[M+H]^+$,
found: m/z = 387.03546 $[M+H]^+$.
calculated for $C_{18}H_{16}O_3N_2\,^{81}Br$: m/z = 389.03183 $[M+H]^+$,
found: m/z = 389.03281 $[M+H]^+$.

General procedure VI (GP VI): Synthesis of benzylpyrazoleboronic acid pinacol esters for the Suzuki coupling

A solution of 4- (4,4,5,5-tetramethyl-1,3,2-dioxaborolan-2-yl) -1H-pyrazole (1.0 eq.), the functionalized benzyl bromide (1.1 eq.) and caesium carbonate (3 eq.) in acetonitrile (0.1 M with respect to the pyrazole) was stirred at rt for 16 h. By the addition of hydrochloric acid (aq., 0.35 M, 1 eq.) and EtOAc, the reaction was stopped. The aqueous layer was extracted three times with EtOAc and the combined organic layers were dried over anhydrous magnesium sulfate. By concentrating under reduced pressure, the product was obtained as a solid and used without further purification.

Representative example:

1-((perfluorophenyl)methyl)-4-(4,4,5,5-tetramethyl-1,3,2-dioxaborolan-2-yl)-1H-pyrazole (518)

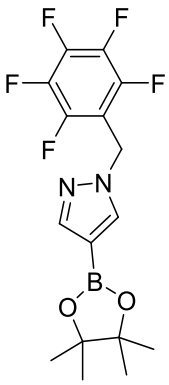

A solution of 4-(4,4,5,5-tetramethyl-1,3,2-dioxaborolan-2-yl)-1H-pyrazole (500,00 mg, 2,58 mMol), perfluorobenzylbromid (1,01 g, 3,87 mMol) and cesium carbonate (1,50 g, 7,73 mMol) in acetonitrile (25 mL) was stirred at rt for 16 h before the reaction was stopped by the addition of HCl (aq, 0.35 M, 50 mL). The aqueous layer was extracted with EtOAc (3 x 40 mL). The combined organic layers were washed with sat. sodium chloride solution (aq., 3 x 30 mL) and dried over anhydrous magnesium sulfate, filtered and concentrated *in vacuo*. The crude residue was used without further purification.

ESI-MS: m/z = 375.0 $[M+H]^+$.

HRMS (ESI): calculated for $C_{16}H_{17}O_2N_2BF_5$: m/z = 375.12978 $[M+H]^+$,
found: m/z = 375.13065 $[M+H]^+$.

1-(3-methoxybenzyl)-4-(4,4,5,5-tetramethyl-1,3,2-dioxaborolan-2-yl)-1H-pyrazole (519)

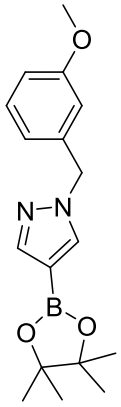

4- (4,4,5,5-tetramethyl-1,3,2-dioxaborolan-2-yl) -1H-pyrazole (500 mg, 2.58 mMol) was treated with 1-(bromomethyl)-3-methoxybenzene according to GP VI. The product was used without further purification for subsequent reactions.

ESI-MS: m/z = 315.0 $[M+H]^+$.

HRMS (ESI): calculated for $C_{17}H_{24}O_3N_2B$: m/z = 315.18745 $[M+H]^+$,
found: m/z = 315.18796 $[M+H]^+$.

1-(4-nitrobenzyl)-4-(4,4,5,5-tetramethyl-1,3,2-dioxaborolan-2-yl)-1H-pyrazole (520)

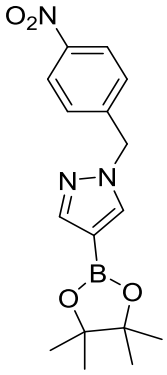

4- (4,4,5,5-tetramethyl-1,3,2-dioxaborolan-2-yl) -1H-pyrazole (1.00 g, 5.15 mMol) was prepared according to GP VI with 1-(bromomethyl)-4-nitrobenzene. The product was used without further purification for subsequent reactions.

ESI-MS: m/z = 330.0 $[M+H]^+$.

HRMS (ESI): calculated for $C_{16}H_{21}O_4N_3B$: m/z = 330.16196 $[M+H]^+$,
found: m/z = 330.16283 $[M+H]^+$.

Phenyl(4-((4-(4,4,5,5-tetramethyl-1,3,2-dioxaborolan-2-yl)-1H-pyrazol-1-yl)methyl)phenyl)methanone (201)

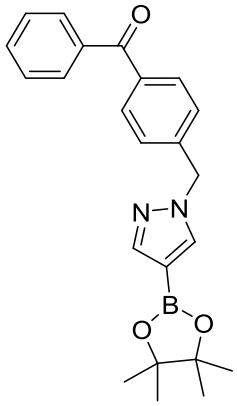

A solution of 4-(4,4,5,5-tetramethyl-1,3,2-dioxaborolan-2-yl)-1H-pyrazole (200 mg), (4-(bromomethyl)phenyl)(phenyl)methanone (312 mg) and caesium carbonate (600 mg, 3.09 mMol) in acetonitrile (10 mL) was stirred at room temperature for 16 h and the reaction was stopped. HCl (aq, 0.35 M, 10 mL) was added into the reaction mixture and the aqueous layer was extracted with ethyl acetate (3 x 16 mL). The combined organic layers were washed with brine (3 x 60 mL), dried over anhydrous magnesiumsulfate, filtered and concentrated *in vacuo*. The crude residue was used without further purification.

ESI-MS: m/z = 389.14 $[M+H]^+$.

HRMS (ESI): calculated for $C_{23}H_{26}O_3N_2B$: m/z = 389.20310 $[M+H]^+$,
found: m/z = 389.20429 $[M+H]^+$.

General procedure II (GP II): Suzuki coupling with C3-functionalized 5-bromo aromatic compounds

The functionalized 5-bromopyridine (1.0 eq.) was dissolved together with the corresponding boronic acid or a corresponding boronic acid ester (2.0 eq.), tetrakis(triphenylphosphine)palladium (0) (10 mol%) and 1,1'bis(diphenylphosphino) ferrocene (20 mol%) in a mixture of toluene/ethanol (4:1, 0.05 M based on the 5-bromopyridine) and sodium carbonate solution (aq., 2 M, 70% by volume of the organic solvents) was added. The reaction mixture was degassed and refluxed (oil bath temperature 110 °C) for 16-20 h. After bringing the reaction mixture to rt, it was diluted with EtOAc and separated from the aqueous layer. The organic layer was washed with sat. sodium chloride solution (aq.), dried over anhydrous magnesium sulfate and filtered over celite. The filtrate was concentrated *in vacuo* and the crude product was purified by means of flash chromatography on silica gel.

Representative example:

(±)-(2,4-dimethoxy-5-(2-methoxyphenyl)pyridin-3-yl)(4-methoxy phenyl)methanol (521)

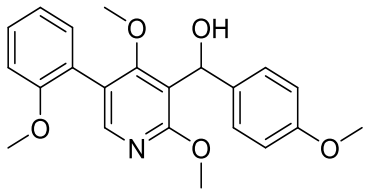

Pyridine **504** (60 mg, 169 µmol), (2-methoxyphenyl) boronic acid (51 mg, 339 µmol), tetrakis (triphenylphosphine) palladium (20 mg, 17 µmol, 10 mol%) and 1,1'bis(diphenylphosphino)ferrocene (19 mg, 34 µmol, 20 mol%) are dissolved in a mixture of toluene/ethanol (4: 1.4 mL) and mixed with sodium carbonate solution (aq., 2 M, 2.5 mL). The reaction mixture was degassed and refluxed for 16 h (oil bath temperature 110 °C). After bringing the reaction mixture to rt, it was diluted with EtOAc (50 mL) and separated from the aqueous layer. The organic layer was washed with sat. sodium chloride solution (aq., 15 mL), dried over anhydrous magnesium sulfate and filtered through celite. The filtrate was concentrated *in vacuo* and the crude product was purified by means of flash chromatography on silica gel (20% EtOAc/PE). The product (63 mg, 164 µmol, 97%) was obtained as a yellow oil.

R_f: 0.25 (30% EtOAc/PE).

^{1}H NMR (500 MHz, $CDCl_3$) δ = 7.99 (s, 1H), 7.38 – 7.35 (m, 1H), 7.31 (d, ^3J = 8.7 Hz, 2H), 7.27 (dd, $^{3,4}J$ = 7.5, 1.6 Hz, 1H), 7.03 – 7.00 (m, 1H), 6.98 (d, ^3J = 8.3 Hz, 1H), 6.86 (d, ^3J = 8.7 Hz, 2H), 6.20 (d, ^3J = 10.9 Hz, 1H), 3.99 (s, 3H), 3.79 (s, 3H), 3.79 (s, 3H), 3.24 (s, 3H). ^{13}C NMR (126 MHz, $CDCl_3$) δ = 164.19, 161.72, 158.72, 157.19, 148.51, 136.41, 131.53, 129.62, 127.04, 124.63, 121.30, 120.84, 117.27, 113.65, 111.20, 68.25, 60.56, 55.78, 55.40, 54.15.

ESI-MS: m/z = 382.15 $[M+H]^+$.

HRMS (ESI): calculated for $C_{22}H_{24}O_5N$: m/z = 382.16490 $[M+H]^+$,
found: m/z = 382.16567 $[M+H]^+$.

(±)-(5-(benzo[d][1,3]dioxol-5-yl)-2,4-dimethoxypyridin-3-yl) (naphthalen-2-yl)methanol (131)

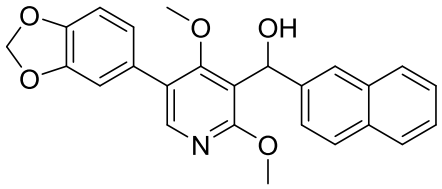

Pyridine **512** (75 mg, 200 µmol) was reacted with benzo[d][1,3]dioxole-5-boronic acid according to GP II. The crude product was purified by flash chromatography on silica gel (20% EtOAc/PE). The product (29 mg, 70 µmol, 35%) was obtained as a yellow oil.

R_f: 0.31 (30% EtOAc/PE).

^{1}H NMR (500 MHz, $CDCl_3$) δ = 8.07 (s, 1H), 7.82 – 7.79 (m, 4H), 7.49 (d, ^3J = 8.5 Hz, 1H), 7.47 – 7.43 (m, 2H), 6.99 (s, 1H), 6.95 (dd, $^{3,4}J$ = 8.0, 1.7 Hz, 1H), 6.88 (d, ^3J = 8.0 Hz, 1H), 6.41 (s, 1H), 6.01 (dd, $^{3,4}J$ = 4.0 Hz, 1.4, 2H), 5.30 (s, 1H), 4.03 (s, 3H), 3.23 (s, 3H). ^{13}C NMR (126 MHz, $CDCl_3$) δ = 164.24, 161.56, 148.16, 147.54, 147.17, 141.38, 133.35, 132.76, 128.71, 128.16, 128.11, 127.74, 126.22, 125.90, 125.15, 124.36, 123.83, 122.43, 118.42, 109.36, 108.83, 101.40, 68.50, 60.86, 54.76.

ESI-MS: m/z = 416.13 $[M+H]^+$.

HRMS (ESI): calculated for $C_{25}H_{22}O_5N$: m/z = 416.14925 $[M+H]^+$,
found: m/z = 416.14830 $[M+H]^+$.

(±)-tert-butyl 4-(4-((2,4-dimethoxy-5-(quinolin-3-yl)pyridin-3-yl)(hydroxy)methyl) phenyl)piperazin-1-carboxylat (522)

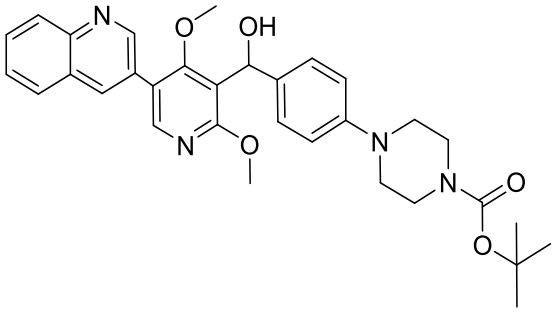

Pyridine **511** (105 mg, 207 µmol) was reacted according to GP II with 3-(4,4,5,5-tetramethyl-1,3,2-dioxaborolan-2-yl) quinoline. The crude product was purified by means of flash chromatography on silica gel (2% MeOH/DCM). The product (109 mg, 196 µmol, 95%) was obtained as a yellow oil.

R_f: 0.22 (4% MeOH/DCM).

^{1}H NMR (500 MHz, $CDCl_3$) δ = 9.07 (s, 1H), 8.29 (s, 1H), 8.18 – 8.13 (m, 2H), 7.86 (d, ^3J = 8.2 Hz, 1H), 7.73 (t, ^3J = 7.6 Hz, 1H), 7.58 (t, ^3J = 7.5 Hz, 1H), 7.29 (d, ^3J = 8.6 Hz, 2H), 6.88 (d, ^3J = 8.5 Hz, 2H), 6.22 (s, 1H), 3.99 (s, 3H), 3.57 – 3.52 (m, 4H), 3.23 (s, 3H), 3.12 – 3.07 (m, 4H), 1.45 (s, 9H). ^{13}C NMR (126 MHz, $CDCl_3$) δ = 163.86, 162.73, 154.75, 150.51, 150.35, 147.84, 147.12, 135.34, 135.22, 129.95, 129.20, 128.52, 128.00, 127.99, 127.30, 126.74, 122.04, 118.89, 116.34, 79.95, 68.02, 61.34, 54.18, 49.45, 28.49, 24.93.

ESI-MS: m/z = 556.97 $[M+H]^+$.

HRMS (ESI): calculated for $C_{32}H_{37}O_5N_4$: m/z = 557.27585 $[M+H]^+$,
found: m/z = 557.27671 $[M+H]^+$.

(±)-(5-(1-benzyl-1H-pyrazol-4-yl)-2,4-dimethoxypyridin-3-yl)(3-((trimethylsilyl) ethynyl)phenyl)methanol (523)

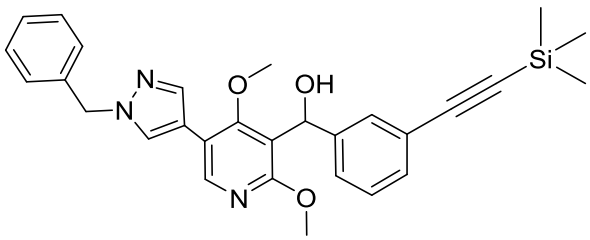

Pyridine **204** (133 mg, 316 µmol) was reacted according to GP II with 1-benzyl-4-(4,4,5,5-tetramethyl-1,3,2-dioxaborolan-2-yl) -1H-pyrazole. The crude product was purified by means of flash chromatography on silica gel (50% EtOAc/PE) followed by HPLC (without using TFA). The product (71 mg, 142 µmol, 45%) was obtained as a colorless oil.

R_f: 0.45 (50% EtOAc/PE).

^{1}H NMR (500 MHz, $CDCl_3$) δ = 8.17 (s, 1H), 7.81 (s, 1H), 7.68 (s, 1H), 7.49 (s, 1H), 7.38 – 7.29 (m, 4H), 7.29 – 7.19 (m, 4H), 6.16 (s, 1H), 5.35 (s, 2H), 3.92 (s, 3H), 3.36 (s, 3H), 0.24 (s, 9H).

^{13}C NMR (126 MHz, $CDCl_3$) δ = 163.07, 161.51, 146.17, 144.15, 138.19, 136.42, 130.79, 129.11, 129.00, 128.32, 128.14, 128.00, 127.79, 125.86, 123.07, 118.44, 117.38, 115.72, 105.32, 94.17, 67.76, 60.68, 56.38, 54.02, 0.09.

ESI-MS: m/z = 498.2 $[M+H]^+$.

HRMS (ESI): calculated for $C_{29}H_{32}O_3N_3Si$: m/z = 498.22074 $[M+H]^+$,
found: m/z = 498.22013 $[M+H]^+$.

(±)-(5-(1-benzyl-1H-pyrazol-4-yl)-2,6-dimethoxypyridin-3-yl)(naphthalen-2-yl)methanol (178)

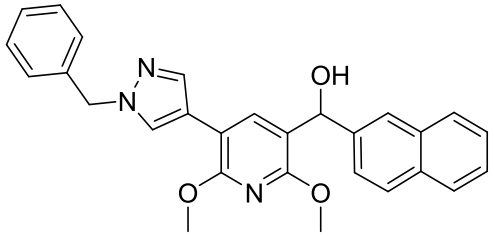

Pyridine **164** (100 mg, 267 µmol) was reacted according to GP II with 1-benzyl-4- (4,4,5,5-tetramethyl-1,3,2-dioxaborolan-2-yl) -1H-pyrazole. The crude product was purified by means of flash chromatography on silica gel (10-50% EtOAc/PE) followed by HPLC (without using TFA). The product (32 mg, 71 µmol, 27%) was obtained as a colorless oil.

R_f: 0.65 (50% EtOAc/PE).

^{1}H NMR (600 MHz, CD_3CN) δ = 8.00 (d, *J* = 0.6 Hz, 1H), 7.97 (d, *J* = 0.5 Hz, 1H), 7.89 (s, 1H), 7.87 – 7.82 (m, 3H), 7.80 (d, *J* = 8.6 Hz, 1H), 7.52 – 7.49 (m, 1H), 7.49 – 7.44 (m, 2H), 7.36 – 7.33 (m, 2H), 7.31 – 7.27 (m, 1H), 7.27 – 7.25 (m, 2H), 6.07 (d, *J* = 4.7, 1H), 5.29 (s, 2H), 4.00 (s, 3H), 3.92 (s, 3H). ^{13}C NMR (151 MHz, CD_3CN) δ = 158.21, 157.91, 142.77, 138.65, 138.35, 136.60, 134.18, 133.60, 129.57, 129.11, 128.82, 128.70, 128.66, 128.57, 128.45, 127.02, 126.71, 126.00, 125.65, 119.08, 118.07, 108.06, 70.22, 56.35, 54.07, 53.98.

ESI-MS: m/z = 452.32 $[M+H]^+$.

HRMS (ESI): calculated for $C_{28}H_{26}O_3N_3$: m/z = 452.19687 $[M+H]^+$,
found: m/z = 452.19779 $[M+H]^+$.

(±)-(5-(1-benzyl-1H-pyrazol-4-yl)-2,4-dimethoxypyridin-3-yl)(6-(((tert-butyldimethylsilyl)oxy)methyl)naphthalen-2-yl)methanol (187)

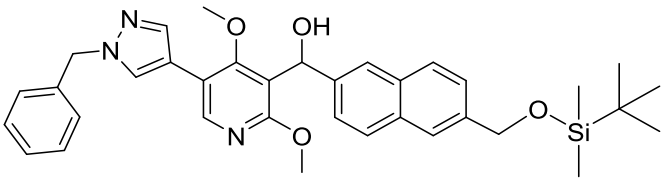

Pyridine **186** (124 mg, 239 µmol) was reacted according to GP II with 1-benzyl-4- (4,4,5,5-tetramethyl-1,3,2-dioxaborolan-2-yl) -1H-pyrazole. The crude product was purified by means of flash chromatography on silica gel (10-50% EtOAc/PE). The product (85 mg, 143 µmol, 60%) was obtained as a colorless wax.

R_f: 0.17 (30% EtOAc/PE).

^{1}H NMR (500 MHz, $CDCl_3$) δ = 8.20 (s, 1H), 7.83 (s, 1H), 7.79 – 7.67 (m, 5H), 7.50 – 7.21 (m, 7H), 6.36 (s, 1H), 5.36 (s, 2H), 4.88 (s, 2H), 3.94 (s, 3H), 3.35 (s, 3H), 0.96 (s, 9H), 0.13 (s, 6H).

^{13}C NMR (126 MHz, $CDCl_3$) δ = 163.14, 161.69, 146.07, 141.00, 139.04, 138.24, 136.46, 132.69, 132.59, 129.03, 128.35, 128.15, 128.06, 128.01, 127.82, 125.01, 124.60, 124.27, 123.79, 118.74, 117.46, 115.81, 68.44, 65.28, 60.73, 56.42, 54.08, 26.12, 18.61, -5.05.

ESI-MS: m/z = 596.2 $[M+H]^+$.

HRMS (ESI): calculated for $C_{35}H_{42}O_4N_3$:Si m/z = 596.29391 $[M+H]^+$,
found: m/z = 596.29426 $[M+H]^+$.

(±)-[1,1'-biphenyl]-3-yl(5-(1-benzyl-1H-pyrazol-4-yl)-2,4-dimethoxypyridin-3-yl)methanol (524)

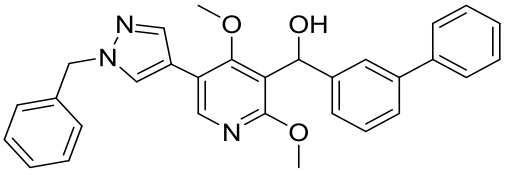

Pyridine **513** (98 mg, 245 µmol) was reacted according to GP II with 1-benzyl-4- (4,4,5,5-tetramethyl-1,3,2-dioxaborolan-2-yl) -1H-pyraz-ole. The crude product was purified by means of flash chromatography on silica gel (30% EtOAc/PE) followed by HPLC (without using TFA). The product (94 mg, 197 µmol, 80%) was obtained as a colorless oil.

R_f: 0.36 (30% EtOAc/PE).

^{1}H NMR (500 MHz, $CDCl_3$) δ = 8.21 (s, 1H), 7.85 (s, 1H), 7.72 (s, 1H), 7.68 (s, 1H), 7.62 – 7.57 (m, 2H), 7.54 – 7.13 (m, 11H), 6.32 (s, 1H), 5.38 (s, 2H), 3.99 (s, 3H), 3.43 (s, 3H). ^{13}C NMR (126 MHz, $CDCl_3$) δ = 163.10, 161.55, 145.98, 144.44, 141.29, 141.23, 138.21, 137.18, 136.42, 129.00, 128.84, 128.70, 128.32, 128.03, 127.79, 127.26, 126.01, 124.68, 124.53, 118.76, 117.42, 115.74, 68.28, 60.70, 56.36, 54.10.

ESI-MS: m/z = 478.38 $[M+H]^+$.

HRMS (ESI): calculated for $C_{30}H_{28}O_3N_3$: m/z = 478.21190 $[M+H]^+$,
found: m/z = 478.21309 $[M+H]^+$.

(±)-(5-(1-benzyl-1H-pyrazol-4-yl)-2,4-dimethoxypyridin-3-yl)(3-fluoro-4-(trifluoromethyl)phenyl)methanol (148)

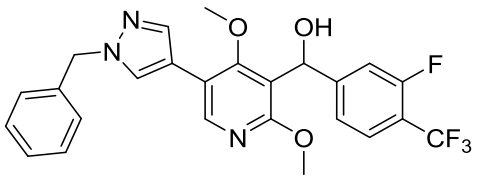

Pyridine **514** (61 mg, 149 µmol) was reacted according to GP II with 1-benzyl-4- (4,4,5,5-tetramethyl-1,3,2-dioxaborolan-2-yl) -1H-pyraz-ole. The crude product was purified by means of flash chromatography on silica gel (30% EtOAc/PE) followed by HPLC (without using TFA). The product (74 mg, 151 µmol, quantitative) was obtained as a colorless oil.

R_f: 0.24 (30% EtOAc/PE).

^{1}H NMR (500 MHz, $CDCl_3$) δ = 8.21 (s, 1H), 7.84 (s, 1H), 7.71 (s, 1H), 7.55 (t, ^3J = 7.6 Hz, 1H), 7.43 – 7.18 (m, 7H), 6.22 (s, 1H), 5.40 (s, 2H), 3.96 (s, 3H), 3.48 (s, 3H). ^{13}C NMR (126 MHz, $CDCl_3$) δ = 163.05, 161.22, 151.45, 146.73, 138.24, 136.37, 129.06, 128.42, 128.08, 127.85, 127.04, 121.11, 121.08, 117.48, 115.54, 114.28, 114.11.

ESI-MS: m/z = 488.31 $[M+H]^+$.

HRMS (ESI): calculated for $C_{xx}H_{37}O_5N_4$: m/z = 488.15982 $[M+H]^+$,
found: m/z = 488.15856 $[M+H]^+$.

(±)-(2,4-dimethoxy-5-(quinolin-3-yl)pyridin-3-yl)(4-(trifluoromethyl)phenyl)methanol (525)

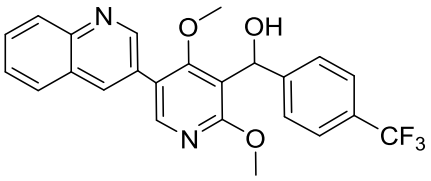

Pyridine **507** (59 mg, 150 µmol) was reacted according to GP II with 3- (4,4,5,5-tetramethyl-1,3,2-dioxaborolan-2-yl)quinoline. The crude product was purified by flash chromatography on silica gel (30% EtOAc/PE). The product (65 mg, 148 µmol, 98%) was obtained as a colorless oil.

R_f: 0.22 (50% EtOAc/PE).

^{1}H NMR (500 MHz, $CDCl_3$) δ = 9.07 (d, ^4J = 2.2, 1H), 8.29 (d, ^4J = 2.0 Hz, 1H), 8.20 (s, 1H), 8.16 (d, ^3J = 8.5 Hz, 1H), 7.88 (d, ^3J = 8.1 Hz, 1H), 7.79 – 7.73 (m, 1H), 7.62 – 7.58 (m, 3H), 7.54 (d, ^3J = 8.3 Hz, 2H), 6.34 (s, 1H), 4.00 (s, 3H), 3.26 (s, 3H). ^{13}C NMR (126 MHz, $CDCl_3$) δ = 164.04, 162.54, 150.65, 148.62, 147.97, 147.52, 135.13, 130.14, 130.05, 129.61, 129.49, 129.36, 129.10, 128.35, 128.23, 128.06, 128.01, 127.55, 127.40, 125.94, 125.40, 125.33 (q, ^3J (C,F) = 3.7 Hz), 123.24, 122.17, 118.13, 67.83, 61.44, 54.35.

ESI-MS: m/z = 441.12 $[M+H]^+$.

HRMS (ESI): calculated for $C_{24}H_{20}O_3N_2F_3$: m/z = 441.14205 $[M+H]^+$,
found: m/z = 441.14231 $[M+H]^+$.

(±)-benzofuran-2-yl(6'-(benzyloxy)-4,6-dimethoxy-[3,3'-bipyridin]-5-yl)methanol (526)

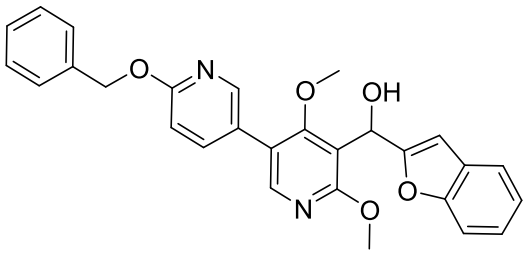

Pyridine **510** (93 mg, 256 µmol) was reacted according to GP II with 2- (benzyloxy) -5- (4,4,5,5-tetramethyl-1,3,2-dioxaborolan-2-yl) pyridines. The crude product was purified by flash chromatography on silica gel (20% EtOAc/PE). The product (116 mg, 248 µmol, 97%) was obtained as a yellowish oil.

R_f: 0.33 (30% EtOAc/PE).

^{1}H NMR (500 MHz, $CDCl_3$) δ = 8.32 (d, ^4J = 2.3 Hz, 1H), 8.10 (s, 1H), 7.80 (dd, $^{3,4}J$ = 8.6, 2.5 Hz, 1H), 7.54 – 7.48 (m, 3H), 7.45 – 7.37 (m, 3H), 7.36 – 7.31 (m, 1H), 7.26 – 7.18 (m, 2H), 6.91 (d, ^3J = 8.6 Hz, 1H), 6.59 (s, 1H), 6.36 (s, 1H), 5.44 (s, 2H), 4.03 (s, 3H), 3.45 (s, 3H). ^{13}C NMR (126 MHz, $CDCl_3$) δ = 164.14, 163.39, 162.47, 158.46, 155.09, 147.96, 146.17, 139.38, 137.25, 128.63, 128.38, 128.14, 128.06, 124.37, 124.17, 122.89, 122.05, 121.08, 115.49, 111.44, 111.39, 103.00, 68.00, 63.72, 61.41, 54.26.

ESI-MS: m/z = 468.97 $[M+H]^+$.

HRMS (ESI): calculated for $C_{28}H_{25}O_5N_2$: m/z = 469.17580 $[M+H]^+$,
found: m/z = 469.17570 $[M+H]^+$.

(±)-(2,4-dimethoxy-5-(quinolin-3-yl)pyridin-3-yl)(naphthalen-2-yl)methanol (120)

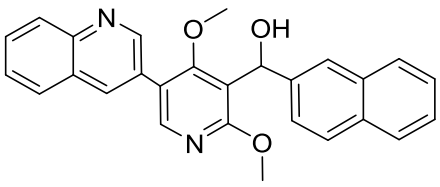

Pyridine **512** (345 mg, 922 µmol) was reacted according to GP II with 3- (4,4,5,5-tetramethyl-1,3,2-dioxaborolan-2-yl) quinoline. The crude product was purified by flash chromatography on silica gel (30% EtOAc/PE). The product (214 mg, 508 µmol, 55%) was obtained as a colorless oil.

R_f: 0.26 (50% EtOAc/PE).

^{1}H NMR (600 MHz, $CDCl_3$) δ = 9.10 (d, ^4J = 2.2 Hz, 1H), 8.29 (d, ^4J = 2.2 Hz, 1H), 8.21 (s, 1H), 8.16 (d, ^3J = 8.4 Hz, 1H), 7.89 (s, 1H), 7.85 (d, ^3J = 8.1 Hz, 1H), 7.83 – 7.78 (m, 3H), 7.74 – 7.71 (m, 1H), 7.59 – 7.53 (m, 2H), 7.46 – 7.41 (m, 2H), 4.00 (s, 3H), 3.17 (s, 3H). ^{13}C NMR (151 MHz, $CDCl_3$) δ = 164.11, 162.72, 150.55, 148.15, 147.20, 141.19, 135.06, 133.23, 132.63, 129.87, 129.20, 128.40, 128.03, 128.00, 127.96, 127.92, 127.62, 127.22, 126.12, 125.78, 124.28, 123.81, 122.05, 118.76, 68.15, 61.26, 54.22.

ESI-MS: m/z = 423.15 $[M+H]^+$.

HRMS (ESI): calculated for $C_{27}H_{23}O_3N_2$: m/z = 423.17032 $[M+H]^+$,
found: m/z = 423.17022 $[M+H]^+$.

(±)-(2,4-dimethoxy-5-(pyrimidin-5-yl)pyridin-3-yl)(naphthalen-2-yl)methanol (135)

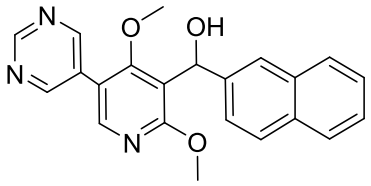

Pyridine **512** (62 mg, 164 µmol) was reacted according to GP II with pyrimidin-5-ylboronic acid. The crude product was purified by means of flash chromatography on silica gel (4% MeOH/DCM) followed by HPLC (without using TFA). The product (3 mg, 9 µmol, 5%) was obtained as a yellow oil.

R_f: 0.14 (4% MeOH/DCM).

^{1}H NMR (600 MHz, $CDCl_3$) δ = 9.26 (s, 1H), 9.01 (s, 2H), 8.16 (s, 1H), 7.85 – 7.76 (m, 4H), 7.52 – 7.42 (m, 3H), 6.42 (s, 1H), 4.01 (s, 3H), 3.29 (s, 3H). ^{13}C NMR (151 MHz, $CDCl_3$) δ = 163.94, 163.66, 157.23, 156.22, 147.62, 140.66, 133.31, 132.84, 129.70, 128.31, 128.17, 127.78, 126.39, 126.12, 124.25, 123.98, 119.26, 118.67, 68.36, 61.92, 54.60.

ESI-MS: m/z = 374.09 $[M+H]^+$.

HRMS (ESI): calculated for $C_{22}H_{20}O_3N_3$: m/z = 374.14992 $[M+H]^+$,
found: m/z = 374.15025 $[M+H]^+$.

(±)-(5-(2-aminopyrimidin-5-yl)-2,4-dimethoxypyridin-3-yl)(naphthalen-2-yl)methanol (136)

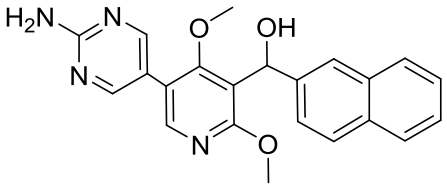

Pyridine **512** (90 mg, 240 µmol) was reacted according to GP II with 5- (4,4,5,5-tetramethyl-1,3,2-dioxaborolan-2-yl) pyrimidin-2-amine. The crude product was purified by means of flash chromatography on silica gel (4% MeOH/DCM) followed by HPLC (without using TFA). The product (4 mg, 11 µmol, 4%) was obtained as a white amorphous solid.

R_f: 0.39 (10% MeOH/DCM).

^{1}H NMR (600 MHz, acetone) δ = 8.49 (s, 2H), 8.12 (s, 1H), 7.97 (s, 1H), 7.89 – 7.84 (m, 2H), 7.83 (d, ^3J = 8.6 Hz, 1H), 7.55 (dd, $^{3,4}J$ = 8.6, 1.7 Hz, 1H), 7.49 – 7.43 (m, 2H), 6.41 (s, 1H), 3.91 (s, 3H), 3.42 (s, 3H). ^{13}C NMR (151 MHz, acetone) δ = 164.95, 163.52, 163.11, 158.24, 147.93, 143.02, 134.36, 133.61, 128.89, 128.51, 128.43, 126.91, 126.47, 125.44, 124.72, 120.91, 120.21, 119.17, 68.03, 61.68, 54.28.

ESI-MS: m/z = 389.14 $[M+H]^+$.

HRMS (ESI): calculated for $C_{22}H_{21}O_3N_4$: m/z = 389.16082 $[M+H]^+$,
found: m/z = 389.16180 $[M+H]^+$.

(±)-(4,6-dimethoxy-[3,3'-bipyridin]-5-yl)(4-isopropylphenyl) methanol (528)

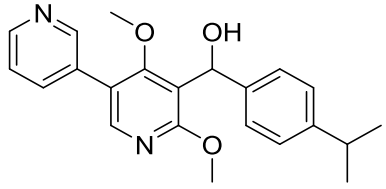

Pyridine **502** (98 mg, 536 µmol) was reacted according to GP II with pyridin-3-ylboronic acid. The crude product was purified by means of flash chromatography on silica gel (3% MeOH/DCM) followed by HPLC (without using TFA). The product (50 mg, 138 µmol, 51%) was obtained as a yellow oil.

R_f: 0.12 (2% MeOH/DCM).

^{1}H NMR (500 MHz, $CDCl_3$) δ = 8.81 (s, 1H), 8.66 (s, 1H), 8.08 (s, 1H), 7.94 (d, ^3J = 7.8 Hz, 1H), 7.46 – 7.43 (m, 1H), 7.28 (d, ^3J = 8.0 Hz, 2H), 7.18 (d, ^3J = 8.2 Hz, 2H), 6.23 (s, 1H), 4.00 (s, 3H), 3.23 (s, 3H), 2.88 (hept, ^3J = 6.9 Hz, 1H), 1.22 (d, ^3J = 6.9 Hz, 6H). ^{13}C NMR (126 MHz, $CDCl_3$) δ = 163.76, 162.92, 148.58, 148.10, 147.99, 147.56, 140.95, 137.27, 131.91, 126.45, 125.71, 124.12, 121.60, 119.00, 68.29, 61.36, 54.28, 33.85, 24.11.

ESI-MS: m/z = 365.27 $[M+H]^+$.

HRMS (ESI): calculated for $C_{22}H_{25}O_3N_2$: m/z = 365.18597 $[M+H]^+$,
found: m/z = 365.18585 $[M+H]^+$.

(±)-(4-isopropylphenyl)(2',4,6-trimethoxy-[3,3'-bipyridin]-5-yl) methanol (529)

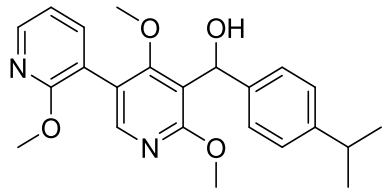

Alcohol **502** (49 mg, 134 µmol) was reacted according to GP II with 2-methoxy-3-pyridineboronic acid. The crude product was purified by flash chromatography on silica gel (20% EtOAc/PE) and the product (51 mg, 129 µmol, 96%) was obtained as a colorless oil.

R_f: 0.18 (20% EtOAc/PE).

^{1}H-NMR (600 MHz, $CDCl_3$): δ = 8.19 (dd, $^{3,4}J$ = 5.0, 1.9 Hz, 1H), 7.84 (d, ^3J = 8.4 Hz, 2H), 8.08 (s, 1H), 7.58 (dd, $^{3,4}J$ = 7.2, 1.9 Hz, 1H), 7.32 (d, ^3J = 8.1 Hz, 2H), 6.96 (dd, ^3J = 7.3, 5.0 Hz, 1H), 3.94 (s, 3H), 3.88 (s, 3H), 3.44 (s, 3H), 2.97 (hept, ^3J = 6.9 Hz, 1H), 1.28 (d, ^3J = 6.9 Hz, 6H). ^{13}C-NMR (151 MHz, $CDCl_3$): δ = 193.60, 163.65, 162.13, 161.64, 155.54, 149.43, 146.72, 139.81, 135.40, 129.94, 126.96, 119.44, 118.53, 116.67, 113.82, 60.95, 54.20, 53.77, 34.51, 23.88.

ESI-MS: m/z = 393.20 $[M+H]^+$.

HRMS (ESI): calculated for $C_{23}H_{25}O_4N_2$ m/z = 393.18088 $[M+H]^+$,
found m/z = 393.18004 $[M+H]^+$.

(±)-[1,1'-biphenyl]-4-yl(2,4-dimethoxy-5-(2-methoxyphenyl) pyridin-3-yl)methanol (530)

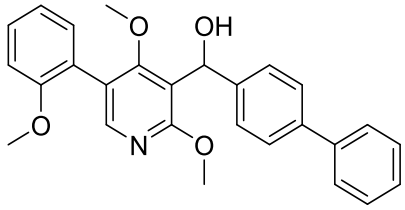

Alcohol **503** (52 mg, 129 µmol) was reacted according to GP II with (2-methoxyphenyl) boronic acid. The crude product was purified by flash chromatography on silica gel (20% EtOAc/PE) and the product (53 mg, 124 µmol, 96%) was obtained as a colorless oil.

R_f: 0.24 (30% EtOAc/PE).

^{1}H NMR (500 MHz, $CDCl_3$) δ = 8.02 (s, 1H), 7.60 – 7.56 (m, 4H), 7.47 (d, ^3J = 8.1 Hz, 2H), 7.44 – 7.41 (m, 1H), 7.39 – 7.36 (m, 2H), 7.34 – 7.31 (m, 1H), 7.30 (dd, $^{3,4}J$ = 7.4, 1.3 Hz, 1H), 6.99 (d, ^3J = 8.3 Hz, 1H), 7.04 – 7.01 (m, 1H), 6.32 (s, 1H), 4.03 (s, 3H), 3.81 (s, 3H), 3.27 (s, 3H). ^{13}C NMR (126 MHz, $CDCl_3$) δ = 164.35, 161.67, 157.17, 148.57, 143.27, 141.03, 139.90, 131.49, 129.69, 128.85, 127.29, 127.15, 126.99, 126.18, 124.53, 121.26, 120.85, 117.09, 111.19, 68.32, 60.56, 55.77, 54.31.

ESI-MS: m/z = 428.18 $[M+H]^+$.

HRMS (ESI): calculated for $C_{27}H_{26}O_4N$: m/z = 428.18563 $[M+H]^+$,
found: m/z = 428.18493 $[M+H]^+$.

(±)-(2,4-dimethoxy-5-(2-methoxyphenyl)pyridin-3-yl)
(4-isopropylphenyl)methanol (531)

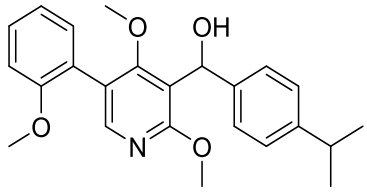

Alcohol **502** (90 mg, 246 µmol) was reacted according to GP II with (2-methoxyphenyl) boronic acid. The crude product was purified by flash chromatography on silica gel (20% EtOAc/PE) and the product (72 mg, 181 µmol, 74%) was obtained as a colorless oil.

R_f: 0.30 (30% EtOAc/PE).

^{1}H NMR (500 MHz, $CDCl_3$) δ = 7.99 (s, 1H), 7.38 – 7.35 (m, 1H), 7.32 (d, ^3J = 8.1 Hz, 2H), 7.28 (dd, $^{3,4}J$ = 7.5, 1.6 Hz, 1H), 7.18 (d, ^3J = 8.2 Hz, 2H), 7.03 – 6.97 (m, 2H), 6.24 (s, 1H), 3.99 (s, 3H), 3.80 (s, 3H), 3.24 (s, 3H), 2.89 (hept, ^3J = 6.9 Hz, 1H), 1.24 (d, ^3J = 6.9 Hz, 6H). ^{13}C NMR (126 MHz, $CDCl_3$) δ = 164.19, 161.75, 157.17, 148.50, 147.59, 141.50, 131.50, 129.58, 126.27, 125.76, 121.23, 120.80, 117.25, 111.18, 68.46, 60.49, 55.74, 33.85, 24.13, 17.62, 17.42.

ESI-MS: m/z = 394.19 $[M+H]^+$.

HRMS (ESI): calculated for $C_{24}H_{28}O_4N$: m/z = 394.20128 $[M+H]^+$,
found: m/z = 394.19948 $[M+H]^+$.

(±)-(5-(benzo[c][1,2,5]oxadiazol-5-yl)-2,4-dimethoxypyridin-3-yl) (4-isopropylphenyl)methanol (532)

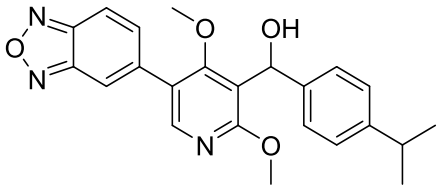

Alcohol **502** (52 mg, 143 µmol) was reacted with 5-(4,4,5,5-tetramethyl-1,3,2-dioxaborolan-2-yl) benzo[c][1,2,5]oxadiazole. The crude product was purified by flash chromatography on silica gel (30% EtOAc/PE) and the product (56 mg, 137 µmol, 96%) was obtained as a yellow oil.

R_f: 0.19 (30% EtOAc/PE).

^{1}H NMR (500 MHz, $CDCl_3$) δ = 8.18 (s, 1H), 7.93 (s, 1H), 7.89 (d, ^3J = 9.3 Hz, 1H), 7.65 (d, ^3J = 9.3 Hz, 1H), 7.29 (d, ^3J = 8.1 Hz, 2H), 7.20 (d, ^3J = 8.1 Hz, 2H), 6.25 (s, 1H), 4.03 (s, 3H), 3.32 (s, 3H), 2.89 (hept, ^3J = 6.9 Hz, 1H), 1.23 (d, ^3J = 6.9 Hz, 6H). ^{13}C NMR (126 MHz, $CDCl_3$) δ = 163.83, 163.20, 149.57, 148.49, 148.12, 147.47, 140.78, 139.33, 133.82, 126.51, 125.67, 123.39, 119.17, 116.74, 114.51, 68.27, 61.54, 54.55, 33.87, 24.12.

ESI-MS: m/z = 406.13 $[M+H]^+$.

HRMS (ESI): calculated for $C_{23}H_{24}O_4N_3$: m/z = 406.17613 $[M+H]^+$,
found: m/z = 406.17463 $[M+H]^+$.

(±)-(5-(3,5-dimethylisoxazol-4-yl)-2,4-dimethoxypyridin-3-yl) (naphthalen-2-yl)methanol (137)

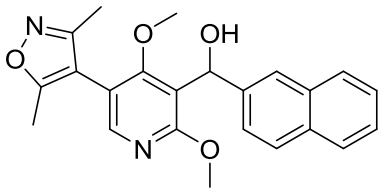

Pyridine **512** (88 mg, 235 µmol) was reacted with isoxazol-4-ylboronic acid according to GP II. The crude product was purified by means of flash chromatography on silica gel (30% EtOAc/PE) followed by HPLC (without using TFA). The product (11 mg, 27 µmol, 12%) was obtained as a yellow oil.

R_f: 0.15 (30% EtOAc/PE).

^{1}H NMR (500 MHz, $CDCl_3$) δ = 7.93 (s, 1H), 7.83 – 7.79 (m, 4H), 7.48 - 7.46 (m, 3H), 6.40 (s, 1H), 4.01 (s, 3H), 3.30 (s, 3H), 2.37 (s, 3H), 2.22 (s, 3H). ^{13}C NMR (126 MHz, $CDCl_3$) δ = 164.67, 162.73, 148.68, 141.11, 133.34, 132.78, 128.18, 128.12, 127.76, 126.32, 126.01, 124.19, 123.84, 118.70, 113.97, 110.39, 110.14, 68.43, 60.99, 54.47, 11.67, 10.72.

ESI-MS: m/z = 391.12 $[M+H]^+$.

HRMS (ESI): calculated for $C_{23}H_{23}O_4N_2$: m/z = 391.16523 $[M+H]^+$,
found: m/z = 391.16709 $[M+H]^+$.

(±)-(5-(1-benzyl-1H-pyrazol-4-yl)-2,4-dimethoxypyridin-3-yl) (naphthalen-2-yl) methanol (116)

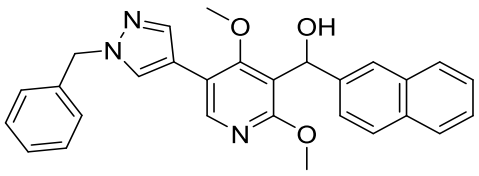

Pyridine 512 (76 mg, 203 µmol) was reacted according to GP II with 1-benzyl-4- (4,4,5,5- Tetramethyl-1,3,2-dioxaborolan-2-yl) -1H-pyraz-ole. The crude product was purified by means of flash chromatography on silica gel (50% EtOAc/PE) followed by HPLC (without using TFA). The product (25 mg, 55 µmol, 27%) was obtained as a yellow oil.

R_f: 0.22 (50% EtOAc/PE).

^{1}H NMR (500 MHz, $CDCl_3$) δ = 8.20 (s, 1H), 7.83 (s, 1H), 7.82 – 7.75 (m, 4H), 7.69 (s, 1H), 7.48 (d, ^3J = 8.8 Hz, 1H), 7.46 – 7.41 (m, 2H), 7.39 – 7.29 (m, 3H), 7.29 – 7.23 (m, 2H), 6.36 (s, 1H), 5.36 (s, 2H), 3.95 (s, 3H), 3.37 (s, 3H). ^{13}C NMR (126 MHz, $CDCl_3$) δ = 163.25, 161.61, 145.94, 141.30, 138.24, 136.44, 133.32, 132.76, 129.05, 128.38, 128.17, 128.08, 128.07 127.83, 127.72, 126.19, 125.90, 124.49, 123.94, 118.75, 117.52, 115.74, 68.43, 60.78, 56.44, 54.25.

ESI-MS: m/z = 452.20 $[M+H]^+$.

HRMS (ESI): calculated for $C_{28}H_{26}O_3N_3$: m/z = 452.19687 $[M+H]^+$,
found: m/z = 452.19654 $[M+H]^+$.

(±)-(5-(1H-indol-5-yl)-2,4-dimethoxypyridin-3-yl)([1,1'-biphenyl]4-yl)methanol (533)

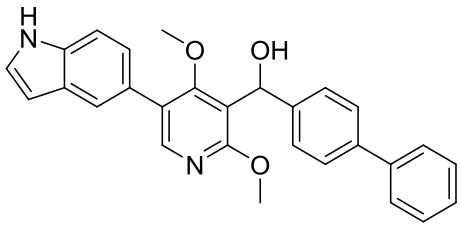

Alcohol **503** (61 mg, 153 µmol) was reacted with (1H-indol-5-yl) boronic acid according to GP II. The crude product was purified by means of flash chromatography on silica gel (20% EtOAc/PE) followed by HPLC (without using TFA). The product (22 mg, 51 µmol, 33%) was obtained as a yellow oil.

R_f: 0.20 (30% EtOAc/PE).

^{1}H NMR (500 MHz, $CDCl_3$) δ = 8.29 (s, 1H), 8.08 (s, 1H), 7.67 (s, 1H), 7.52 - 7.50 (m, 4H), 7.42 - 7.34 (m, 4H), 7.27 – 7.25 (m, 2H), 7.19 (s, 1H), 6.53 (s, 1H), 6.27 (s, 1H), 3.99 (s, 3H), 3.15 (s, 3H). ^{13}C NMR (126 MHz, $CDCl_3$) δ = 164.25, 161.20, 147.73, 143.27, 140.99, 139.99, 135.47, 128.88, 128.35, 127.34, 127.16, 127.07, 126.76, 126.40, 126.15, 125.10, 123.31, 121.08, 118.03, 111.45, 103.06, 68.40, 60.73, 60.54.

ESI-MS: m/z = 437.20 $[M+H]^+$.

HRMS (ESI): calculated for $C_{28}H_{25}O_3N_2$: m/z = 437.18597 $[M+H]^+$,
found: m/z = 437.18574 $[M+H]^+$.

(±)-(6'-isopropoxy-4,6-dimethoxy-[3,3'-bipyridin]-5-yl) (naphthalen-1-yl)methanol (534)

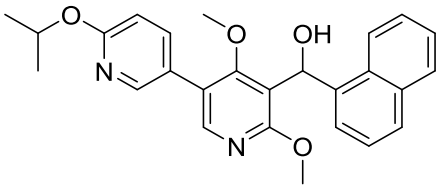

Alcohol **505** (50 mg, 134 µmol) was reacted with (6-isopropoxypyridin-3-yl) boronic acid according to GP II. The crude product was isolated by means of flash chromatography on silica gel (20% EtOAc/PE). The product (57 mg, 133 µmol, 99%) was obtained as a colorless oil.

R_f: 0.10 (20% EtOAc/PE).

^{1}H NMR (500 MHz, $CDCl_3$) δ = 8.50 (d, ^3J = 8.5 Hz, 1H), 8.27 (d, ^4J = 2.3 Hz, 1H), 8.11 (s, 1H), 7.87 (d, ^3J = 8.1 Hz, 1H), 7.79 (d, ^3J = 8.2 Hz, 1H), 7.74 (dd, $^{3,4}J$ = 8.6, 2.4 Hz, 1H), 7.60 - 7.59 (m, 1H), 7.53 – 7.50 (m, 1H), 7.39 – 7.36 (m, 1H), 7.27 - 7.26 (m, 1H), 6.94 (s, 1H), 6.76 (d, ^3J = 8.6 Hz, 1H), 5.35 (hept, ^3J = 6.2 Hz, 1H), 4.02 (s, 3H), 3.23 (s, 3H), 1.38 (d, ^3J = 6.2 Hz, 6H). ^{13}C NMR (126 MHz, $CDCl_3$) δ = 164.02, 163.09, 162.69, 147.44, 146.07, 139.42, 137.90, 134.18, 131.81, 128.72, 128.71, 126.35, 125.80, 124.98, 124.89, 123.98, 123.76, 122.39, 117.37, 111.67, 68.57, 66.71, 61.07, 54.15, 22.22.

ESI-MS: m/z = 431.04 $[M+H]^+$.

HRMS (ESI): calculated for $C_{26}H_{27}O_4N_2$: m/z = 431.19653 $[M+H]^+$,
found: m/z = 431.19614 $[M+H]^+$.

(±)-(5-(3-(dimethylamino)phenyl)-2,4-dimethoxypyridin-3-yl)
(4-methoxyphenyl)methanol (535)

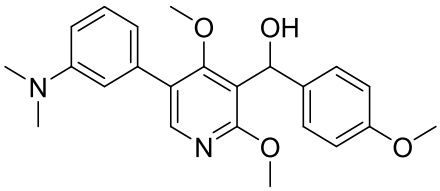

Alcohol **504** (38 mg, 106 µmol) was reacted according to GP II with (3 (dimethylamino) phenyl) boronic acid. The crude product was purified by means of flash chromatography on silica gel (30% EtOAc/PE) followed by HPLC (without using TFA). The product (33 mg, 85 µmol, 80%) was obtained as a colorless oil.

R_f: 0.20 (30% EtOAc/PE).

^{1}H NMR (500 MHz, $CDCl_3$) δ = 8.07 (s, 1H), 7.30 – 7.26 (m, 3H), 6.86 – 6.83 (m, 4H), 6.76 – 6.75 (m, 1H), 6.20 (s, 1H), 3.97 (s, 3H), 3.77 (s, 3H), 3.24 (s, 3H), 2.96 (s, 6H).

^{13}C NMR (126 MHz, $CDCl_3$) δ = 162.52, 160.60, 157.58, 146.67, 135.23, 135.17, 128.34, 127.99, 127.18, 125.83, 125.45, 124.65, 124.26, 116.80, 112.51, 67.07, 59.58, 54.21, 52.87, 39.73.

ESI-MS: m/z = 395.20 $[M+H]^+$.

HRMS (ESI): calculated for $C_{23}H_{27}O_4N_2$: m/z = 395.19653 $[M+H]^+$,
found: m/z = 395.19506 $[M+H]^+$.

(±)-[1,1'-biphenyl]-4-yl(5-(3-(dimethylamino)phenyl)-2,4-dimethoxypyridin-3-yl)methanol (536)

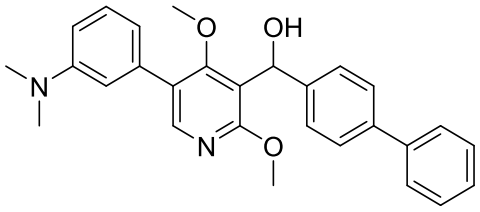

Alcohol **503** (57 mg, 141 µmol) was reacted according to GP II with (3 (dimethylamino) phenyl) boronic acid. The crude product was purified by means of flash chromatography on silica gel (20% EtOAc/PE) followed by HPLC (without using TFA). The product (18 mg, 41 µmol, 29%) was obtained as a yellow oil.

R_f: 0.13 (20% EtOAc/PE).

^{1}H NMR (500 MHz, $CDCl_3$) δ = 8.10 (s, 1H), 7.59 – 7.56 (m, 5H), 7.46 (d, ^3J = 8.1 Hz, 2H), 7.44 - 7.41 (m, 2H), 7.36 – 7.31 (m, 2H), 7.05 - 6.96 (m, 2H), 6.31 (s, 1H), 4.01 (s, 3H), 3.27 (s, 3H), 3.02 (s, 6H).

ESI-MS: m/z = 441.27 $[M+H]^+$.

HRMS (ESI): calculated for $C_{28}H_{29}O_3N_2$: m/z = 441.21727 $[M+H]^+$,
found: m/z = 441.21682 $[M+H]^+$.

(±)-naphthalen-1-yl(4,5',6-trimethoxy-[3,3'-bipyridin]-5-yl) methanol (537)

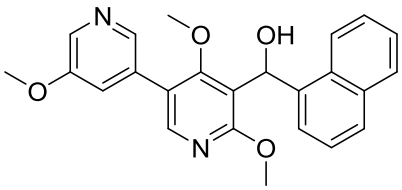

Alcohol **505** (55 mg, 147 µmol) was reacted according to GP II with (5-methoxypyridin-3-yl) boronic acid. The crude product was purified by means of flash chromatography on silica gel (50% EtOAc/PE) followed by HPLC (without using TFA). The product (13 mg, 32 µmol, 22%) was obtained as a colorless oil.

R_f: 0.27 (4% MeOH/DCM).

^{1}H NMR (500 MHz, $CDCl_3$) δ = 8.48 – 8.42 (m, 2H), 8.35 (s, 1H), 8.16 (s, 1H), 7.88 (d, ^3J = 8.0 Hz, 1H), 7.80 (d, ^3J = 8.2 Hz, 1H), 7.62 – 7.56 (m, 2H), 7.54 – 7.49 (m, 1H), 7.41 – 7.36 (m, 1H), 7.28 – 7.24 (m, 1H), 6.93 (s, 1H), 4.04 (s, 3H), 3.94 (s, 3H), 3.22 (s, 3H). ^{13}C NMR (126 MHz, $CDCl_3$) δ = 163.91, 163.79, 156.60, 147.81, 138.63, 137.49, 134.22, 133.37, 131.73, 128.91, 128.82, 126.50, 125.92, 124.99, 124.72, 124.21, 123.99, 120.91, 117.94, 110.14, 66.62, 61.72, 56.39, 54.44.

ESI-MS: m/z = 403.27 $[M+H]^+$.

HRMS (ESI): calculated for $C_{24}H_{23}O_4N_2$: m/z = 403.16523 $[M+H]^+$,
found: m/z = 403.16378 $[M+H]^+$.

(±)-[1,1'-biphenyl]-4-yl(5-(1-benzyl-1H-pyrazol-4-yl)-2,4-dimethoxypyridin-3-yl)methanol (153)

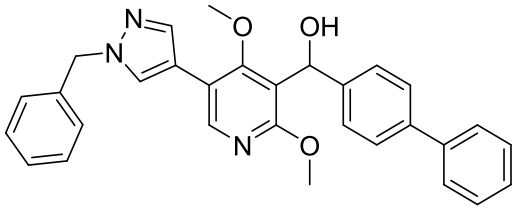

Alcohol **503** (83 mg, 208 µmol) was reacted according to GP II with 1-benzyl-4- (4,4,5,5-tetramethyl-1,3,2-dioxaborolan-2-yl) -1H-pyrazole. The crude product was isolated by means of flash chromatography on silica gel (30% EtOAc/PE). The product (53 mg, 110 µmol, 53%) was obtained as a yellow oil.

R_f: 0.17 (50% EtOAc/PE).

^{1}H NMR (500 MHz, $CDCl_3$) δ = 8.20 (s, 1H), 7.83 (s, 1H), 7.70 (s, 1H), 7.58 – 7.55 (m, 4H), 7.44 – 7.41 (m, 4H), 7.38 – 7.32 (m, 4H), 7.27 - 7.26 (m, 2H), 6.26 (s, 1H), 5.37 (s, 2H), 3.99 (s, 3H), 3.43 (s, 3H). ^{13}C NMR (126 MHz, $CDCl_3$) δ = 163.31, 161.47, 145.62, 142.81, 140.89, 140.12, 138.21, 136.38, 129.06, 128.89, 128.40, 128.11, 127.86, 127.39, 127.14, 127.08, 126.21, 118.91, 117.55, 115.67, 68.19, 60.82, 56.44, 54.46.

ESI-MS: m/z = 478.23 $[M+H]^+$.

HRMS (ESI): calculated for $C_{30}H_{28}O_3N_3$: m/z = 478.21252 $[M+H]^+$,
found: m/z = 478.21228 $[M+H]^+$.

(±)-(2,4-dimethoxy-5-(2-methoxyphenyl)pyridin-3-yl)(3,5-dimethoxyphenyl)methanol (538)

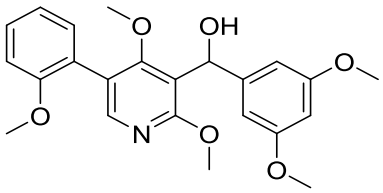

Alcohol **506** (55 mg, 143 µmol) was reacted according to GP II with (2-methoxyphenyl) boronic acid. The crude product was purified by flash chromatography on silica gel (50% EtOAc/PE) and the product (50 mg, 121 µmol, 85%) was obtained as a colorless oil.

R_f: 0.39 (50% EtOAc/PE).

^{1}H NMR (500 MHz, $CDCl_3$) δ = 7.99 (s, 1H), 7.39 – 7.36 (m, 1H), 7.28 (dd, $^{3,4}J$ = 7.5, 1.6 Hz, 1H), 7.04 – 7.01 (m, 1H), 6.98 (d, ^3J = 8.3 Hz, 1H), 6.59 (d, ^4J = 1.8 Hz, 2H), 6.35 (t, ^4J = 2.0 Hz, 1H), 6.20 (s, 1H), 3.99 (s, 3H), 3.80 (s, 3H), 3.79 (s, 6H), 3.26 (s, 3H). ^{13}C NMR (126 MHz, $CDCl_3$) δ = 164.19, 161.71, 160.77, 157.19, 148.72, 146.98, 131.47, 129.60, 124.61, 121.20, 120.79, 116.92, 111.15, 104.05, 98.68, 68.40, 60.53, 55.70, 55.41, 54.08.

ESI-MS: m/z = 412.15 $[M+H]^+$.

HRMS (ESI): calculated for $C_{23}H_{26}O_6N$: m/z = 412.17546 $[M+H]^+$,
found: m/z = 412.17463 $[M+H]^+$.

(±)-(5-(1-benzyl-1H-pyrazol-4-yl)-2,4-dimethoxypyridin-3-yl)
(3,5-dimethoxyphenyl)methanol (155)

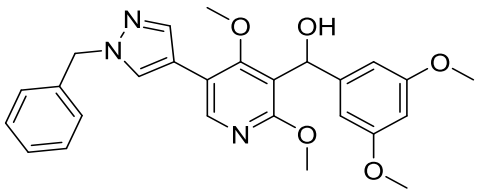

Alcohol **506** (58 mg, 151 µmol) was reacted according to GP II with 1-benzyl-4- (4,4,5,5-tetramethyl-1,3,2-dioxaborolan-2-yl) -1H-pyraz-ole. The crude product was isolated by means of flash chromatography on silica gel (2% MeOH/DCM). The product (39 mg, 84 µmol, 56%) was obtained as a colorless oil.

R_f: 0.12 (2% MeOH/DCM).

^{1}H NMR (500 MHz, $CDCl_3$) δ = 8.17 (s, 1H), 7.82 (s, 1H), 7.69 (s, 1H), 7.38 – 7.33 (m, 3H), 7.28 – 7.26 (m, 2H), 6.54 (d, ^4J = 2.0 Hz, 2H), 6.35 (t, ^4J = 2.1 Hz, 1H), 6.14 (s, 1H), 5.37 (s, 2H), 3.96 (s, 3H), 3.77 (s, 6H), 3.41 (s, 3H). ^{13}C NMR (126 MHz, $CDCl_3$) δ = 163.04, 161.51, 160.82, 146.61, 145.94, 138.21, 136.43, 129.00, 128.32, 128.01, 127.78, 118.60, 117.36, 115.74, 104.08, 98.73, 68.22, 60.68, 56.36, 55.41, 54.08.

ESI-MS: m/z = 462.20 $[M+H]^+$.

HRMS (ESI): calculated for $C_{26}H_{28}O_3N_3$: m/z = 462.20235 $[M+H]^+$,
found: m/z = 462.20218 $[M+H]^+$.

(±)-(2,4-dimethoxy-5-(2-methoxyphenyl)pyridin-3-yl)
(naphthalen-1-yl)methanol (539)

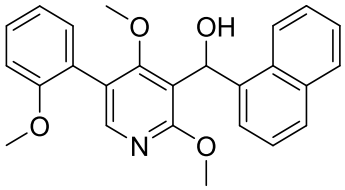

Alcohol **505** (61 mg, 164 µmol) was reacted according to GP II with (2-methoxyphenyl) boronic acid. The crude product was purified by flash chromatography on silica gel (20% EtOAc/PE) and the product (48 mg, 119 µmol, 72%) was obtained as a yellowish oil.

R_f: 0.14 (20% EtOAc/PE).

^{1}H NMR (500 MHz, $CDCl_3$) δ = 8.53 (d, ^3J = 8.5 Hz, 1H), 8.07 (s, 1H), 7.88 (d, ^3J = 8.1 Hz, 1H), 7.79 (d, ^3J = 8.1 Hz, 1H), 7.60 – 7.57 (m, 1H), 7.53 – 7.50 (m, 1H), 7.40 - 7.36 (m, 2H), 7.30 (d, ^3J = 7.3 Hz, 2H), 7.04 – 7.01 (m, 1H), 6.98 (d, ^3J = 8.3 Hz, 1H), 6.95 (s, 1H), 4.02 (s, 3H), 3.80 (s, 3H), 3.24 (s, 3H). ^{13}C NMR (126 MHz, $CDCl_3$) δ = 164.71, 162.10, 157.21, 148.54, 138.08, 134.19, 131.93, 131.51, 129.67, 128.66, 128.56, 126.23, 125.70, 125.04, 125.00, 124.57, 124.04, 121.49, 120.82, 115.86, 111.15, 66.85, 60.70, 55.76, 54.29.

ESI-MS: m/z = 402.20 $[M+H]^+$.

HRMS (ESI): calculated for $C_{25}H_{24}O_4N$: m/z = 402.16998 $[M+H]^+$,
found: m/z = 402.16844 $[M+H]^+$.

(±)-(2,4-dimethoxy-5-(quinolin-3-yl)pyridin-3-yl)(naphthalen-1-yl) methanol (540)

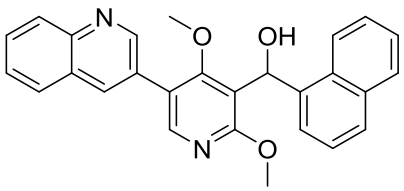

Alcohol **505** (56 mg, 150 µmol) was reacted according to GP II with 3- (4,4,5,5-tetramethyl-1,3,2-dioxaborolan-2-yl) quinoline. The crude product was purified by flash chromatography on silica gel (50% EtOAc/PE) and the product (59 mg, 139 µmol, 93%) was obtained as a colorless oil.

R_f: 0.19 (50% EtOAc/PE).

^{1}H NMR (500 MHz, $CDCl_3$) δ = 9.10 (d, ^4J = 2.1 Hz, 1H), 8.51 (d, ^3J = 8.6 Hz, 1H), 8.34 (d, ^4J = 1.6 Hz, 1H), 8.25 (s, 1H), 8.20 (d, ^3J = 8.5 Hz, 1H), 7.88 (d, ^3J = 7.4 Hz, 2H), 7.81 (d, ^3J = 8.2 Hz, 1H), 7.79 – 7.76 (m, 1H), 7.63 – 7.59 (m, 2H), 7.54 – 7.51 (m, 1H), 7.41 – 7.38 (m, 1H), 7.30 (d, ^3J = 7.2 Hz, 1H), 6.99 (d, ^3J = 6.8 Hz, 1H), 4.06 (s, 3H), 3.20 (s, 3H). ^{13}C NMR (126 MHz, $CDCl_3$) δ = 164.18, 163.30, 150.39, 148.18, 137.74, 135.68, 134.22, 131.79, 130.22, 129.05, 128.83, 128.78, 128.58, 128.10, 128.08, 127.50, 126.45, 125.88, 125.01, 124.84, 124.00, 122.27, 117.70, 110.15, 66.71, 61.53, 54.33.

ESI-MS: m/z = 423.26 $[M+H]^+$.

HRMS (ESI): calculated for $C_{27}H_{23}O_3N_2$: m/z = 423.17032 $[M+H]^+$,
found: m/z = 423.16964 $[M+H]^+$.

(±)-(5-(isoquinolin-4-yl)-2,4-dimethoxypyridin-3-yl)(naphthalen-1-yl)methanol (541)

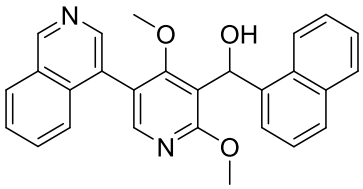

Alcohol **505** (66 mg, 175 µmol) was reacted according to GP II with isoquinolin-4-ylboronic acid. The crude product was purified by flash chromatography on silica gel (2% MeOH/DCM) and the product (16 mg, 37 µmol, 21%) was obtained as a colorless oil.

R_f: 0.42 (2% MeOH/DCM).

^{1}H NMR (500 MHz, $CDCl_3$) δ = 9.34 – 9.32 (m, 1H), 8.56 – 8.48 (m, 2H), 8.15 – 8.08 (m, 2H), 7.89 (d, ^3J = 8.2 Hz, 1H), 7.82 – 7.80 (m, 1H), 7.77 – 7.76 (m, 1H), 7.73 – 7.64 (m, 5H), 7.29 – 7.27 (m, 1H), 7.02 – 6.96 (m, 1H), 5.29 (s, 1H), 4.03 (s, 3H), 3.13 (s, 3H).

ESI-MS: m/z = 423.22 $[M+H]^+$.

HRMS (ESI): calculated for $C_{27}H_{23}O_3N_2$: m/z = 423.17032 $[M+H]^+$,
found: m/z = 423.16976 $[M+H]^+$.

(±)-(2,4-dimethoxy-5-(thiophen-2-yl)pyridin-3-yl)(3,5-dimethoxy phenyl)methanol (542)

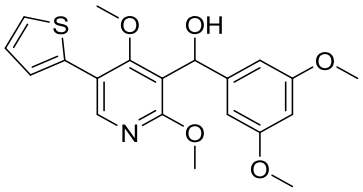

Alcohol **506** (98 mg, 254 µmol) was reacted with thiophen-2-ylboronic acid according to GP II. The crude product was purified by flash chromatography on silica gel (2% MeOH/DCM) and the product (14 mg, 37 µmol, 15%) was obtained as a yellow oil.

R_f: 0.41 (2% MeOH/DCM).

^{1}H NMR (500 MHz, $CDCl_3$) δ = 8.25 (s, 1H), 7.37 (d, ^3J = 5.1 Hz, 1H), 7.29 (d, ^3J = 3.5 Hz, 1H), 7.11 – 7.09 (m, 1H), 6.54 (d, ^4J = 2.0 Hz, 2H), 6.35 (t, ^4J = 2.1, 1H), 6.16 (s, 1H), 3.98 (s, 3H), 3.77 (s, 6H), 3.44 (s, 3H).

^{13}C NMR (126 MHz, $CDCl_3$) δ = 163.21, 162.11, 160.89, 147.11, 146.54, 135.86, 127.54, 126.32, 126.20, 119.36, 118.52, 104.09, 98.85, 68.31, 61.23, 55.48, 54.29.

ESI-MS: m/z = 388.11 $[M+H]^+$.

HRMS (ESI): calculated for $C_{20}H_{22}O_5NS$: m/z = 388.12132 $[M+H]^+$,
found: m/z = 388.12194 $[M+H]^+$.

(±)-naphthalen-2-yl(2,2',4-trimethoxy-[1,1'-biphenyl]-3-yl) methanol (543)

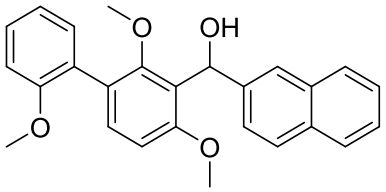

Alcohol **162** (43 mg, 114 µmol) was reacted according to GP II with (2-methoxyphenyl) boronic acid for 32 h instead of the usual 16-20 h. The crude product was purified by flash chromatography on silica gel (10% EtOAc/PE) and the product (43 mg, 107 µmol, 94%) was obtained as a colorless oil.

R_f: 0,13 (20% EtOAc/PE).

^{1}H NMR (500 MHz, $CDCl_3$) δ = 7.91 (s, 1H), 7.86 – 7.80 (m, 3H), 7.58 (dd, $^{3,4}J$ = 8.5, 1.6 Hz, 1H), 7.49 – 7.44 (m, 2H), 7.38 – 7.34 (m, 2H), 7.28 (d, ^3J = 8.3 Hz, 1H), 7.05 – 7.00 (m, 2H), 6.83 (d, ^3J = 8.6 Hz, 1H), 6.53 (s, 1H), 4.53 (s, 1H), 3.87 (s, 3H), 3.83 (s, 3H), 3.09 (s, 3H). ^{13}C NMR (126 MHz, $CDCl_3$) δ = 157.19, 156.99, 142.87, 133.41, 132.58, 131.87, 131.62, 128.87, 128.15, 127.70, 127.66, 125.88, 125.50, 124.84, 124.80, 123.75, 120.66, 111.32, 106.76, 77.41, 77.16, 76.91, 69.22, 60.88, 56.03, 55.85.

ESI-MS: m/z = 383.00 $[(M-H_2O)+H]^+$, 423.00 $[M+Na]^+$.

HRMS (ESI): calculated for $C_{26}H_{23}O_3$: m/z = 383.16417 $[(M-H_2O)+H]^+$,
found: m/z = 383.16446 $[(M-H_2O)+H]^+$.
calculated for $C_{26}H_{24}O_4Na$: m/z = 423.15668 $[M+Na]^+$,
found: m/z = 423.15646 $[M+Na]^+$.

(±)-(3-(1-benzyl-1H-pyrazol-4-yl)-2,6-dimethoxyphenyl) (naphthalen-2-yl)methanol (177)

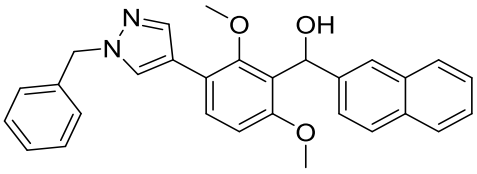

Alcohol **162** (41 mg, 109 µmol) was treated with 1-benzyl-4- (4,4,5,5-tetramethyl-1,3,2-dioxaborolan- 2-yl) -1H-pyrazole. The crude product was purified by flash chromatography on silica gel (20% EtOAc/PE) and the product (44 mg, 97 µmol, 89%) was obtained as a colorless oil.

R_f: 0.30 (50% EtOAc/PE).

^{1}H NMR (500 MHz, $CDCl_3$) δ = 7.86 (s, 1H), 7.81 – 7.75 (m, 5H), 7.75 (s, 2H), 7.50 (dd, $^{3,4}J$ = 8.6, 1.5 Hz, 1H), 7.44 – 7.42 (m, 2H), 7.39 (d, ^3J = 8.6 Hz, 1H), 7.36 – 7.30 (m, 3H), 7.26 – 7.25 (m, 2H), 6.78 (d, ^3J = 8.7 Hz, 1H), 6.44 (s, 1H), 5.36 (s, 2H), 3.77 (s, 3H), 3.28 (s, 3H). ^{13}C NMR (126 MHz, $CDCl_3$) δ = 157.00, 155.65, 142.44, 138.13, 136.55, 133.36, 132.62, 129.00, 128.69, 128.29, 128.23, 128.16, 127.82, 127.67, 125.99, 125.73, 125.64, 124.75, 123.84, 119.60, 118.88, 108.02, 69.24, 60.73, 56.30, 56.10.

ESI-MS: m/z = 451.07 $[M+H]^+$.

HRMS (ESI): calculated for $C_{29}H_{27}O_3N_2$: m/z = 451.20162 $[M+H]^+$,
found: m/z = 451.20161 $[M+H]^+$.

(±)-(5-(1-benzyl-1H-pyrazol-4-yl)pyridin-3-yl)(naphthalen-2-yl) methanol (176)

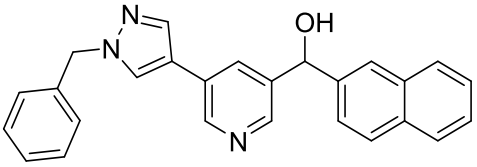

Alcohol **166** (100 mg, 318 µmol) was reacted according to GP II with 1-benzyl-4- (4,4,5,5-tetramethyl-1,3,2-dioxaborolan-2-yl) -1H-pyrazoles. The crude product was purified by flash chromatography on silica gel (4% MeOH/DCM) and the product (118 mg, 302 µmol, 95%) was obtained as a yellow oil.

R_f: 0.17 (4% MeOH/DCM).

^{1}H NMR (500 MHz, $CDCl_3$) δ = 7.82 – 7.71 (m, 6H), 7.65 (s, 1H), 7.44 – 7.42 (m, 3H), 7.36 (d, ^3J = 8.4 Hz, 1H), 7.31 – 7.29 (m, 4H), 7.16 (d, ^3J = 7.0 Hz, 2H), 5.92 (s, 1H), 5.19 (s, 1H), 1.21 (s, 2H). ^{13}C NMR (126 MHz, $CDCl_3$) δ = 145.50, 144.86, 140.88, 136.99, 136.02, 133.21, 132.91, 131.01, 129.01, 128.91, 128.58, 128.43, 128.26, 128.07, 127.83, 127.71, 127.67, 126.75, 126.34, 126.16, 125.34, 124.73, 119.71, 75.01, 73.71.

ESI-MS: m/z = 392.24 $[M+H]^+$.

HRMS (ESI): calculated for $C_{26}H_{22}ON_3$: m/z = 392.17574 $[M+H]^+$,
found: m/z = 392.17416 $[M+H]^+$.

(±)-(5-(1-benzyl-1H-pyrazol-4-yl)-2,4-dimethoxypyridin-3-yl)(4-(trifluoromethyl)phenyl)methanol (149)

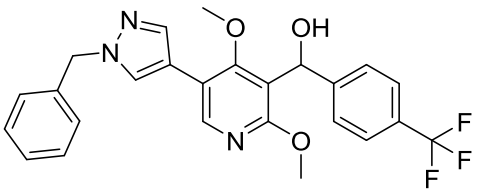

Alcohol **507** (86 mg, 219 µmol) was reacted according to GP II with 1-benzyl-4- (4,4,5,5-tetramethyl-1,3,2-dioxaborolan-2-yl) -1H-pyraz-ole. The crude product was purified by means of flash chromatography on silica gel (30% EtOAc/PE) followed by HPLC (without using TFA). The product (51 mg, 108 µmol, 49%) was obtained as a colorless oil.

R_f: 0.19 (50% EtOAc/PE).

^{1}H NMR (500 MHz, $CDCl_3$) δ = 8.18 (s, 1H), 7.82 (s, 1H), 7.68 (s, 1H), 7.56 (d, ^3J = 8.3 Hz, 2H), 7.47 (d, ^3J = 8.3 Hz, 2H), 7.38 – 7.30 (m, 3H), 7.28 – 7.24 (m, 2H), 6.23 (s, 1H), 5.37 (s, 2H), 3.94 (s, 3H), 3.41 (s, 3H).

ESI-MS: m/z = 470.12 $[M+H]^+$.

HRMS (ESI): calculated for $C_{25}H_{23}O_3N_3F_3$: m/z = 470.16860 $[M+H]^+$,
found: m/z = 470.16837 $[M+H]^+$.

(±)-(2,4-dimethoxy-5-(1-((perfluorophenyl)methyl)-1H-pyrazol-4-yl)pyridin-3-yl)(naphthalen-2-yl)methanol (134)

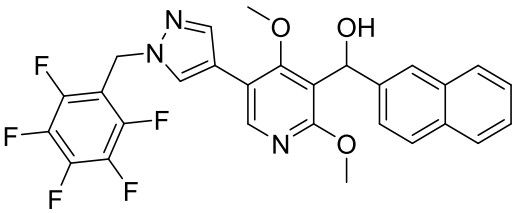

Alcohol **512** (65 mg, 174 µmol) was reacted according to GP II with 1 - ((perfluorophenyl) methyl) -4- (4,4,5,5-tetramethyl-1,3,2-dioxaborolan-2-yl) -1H -pyrazole. The crude product was purified by HPLC (without using TFA) and the product (8 mg, 14 µmol, 8%) was obtained as a colorless amorphous solid.

^{1}H NMR (400 MHz, DMSO-*d6*) δ = 8.31 (s, 1H), 8.21 (s, 1H), 7.91 – 7.77 (m, 4H), 7.49 – 7.32 (m, 4H), 6.34 (d, ^3J = 5.6, 1H), 5.81 (d, ^3J = 5.8 Hz, 1H), 5.52 (s, 2H), 3.79 (s, 3H), 3.49 (s, 3H).

ESI-MS: m/z = 542.47 $[M+H]^+$.

HRMS (ESI): calculated for $C_{28}H_{21}O_3N_3F_5$: m/z = 542.14976 $[M+H]^+$,
found: m/z = 542.15038 $[M+H]^+$.

(±)-(2,4-dimethoxy-5-(1-(3-methoxybenzyl)-1H-pyrazol-4-yl)pyridin-3-yl)(naphthalen-2-yl)methanol (128)

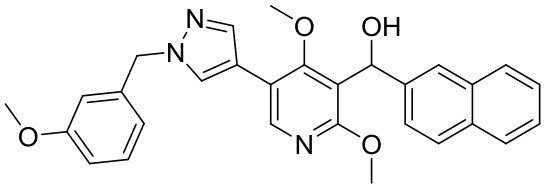

Alcohol **512** (65 mg, 174 µmol) was reacted with 1- (3-methoxybenzyl) -4- (4,4,5,5-tetramethyl-1,3,2-dioxaborolan-2-yl) -1H- pyrazole. The crude product was purified by HPLC (without using TFA) and the product (20 mg, 42 µmol, 24%) was obtained as a colorless wax.

^{1}H NMR (400 MHz, $CDCl_3$) δ = 8.23 (s, 1H), 7.91 (s, 1H), 7.84 – 7.70 (m, 5H), 7.49 – 7.40 (m, 3H), 7.30 (s, 1H), 6.90 – 6.75 (m, 3H), 6.39 (s, 1H), 5.36 (s, 2H), 3.97 (s, 3H), 3.78 (s, 3H), 3.38 (s, 3H). ^{13}C NMR (101 MHz, $CDCl_3$) δ = 163.70, 161.77, 160.21, 145.57, 140.86, 137.70, 137.08, 133.29, 132.81, 130.24, 128.79, 128.20, 128.18, 127.73, 126.28, 126.02, 124.34, 123.97, 120.11, 119.14, 117.17, 114.03, 113.68, 68.44, 61.00, 56.17, 55.39, 54.69.

ESI-MS: m/z = 482.30 $[M+H]^+$.

HRMS (ESI): calculated for $C_{29}H_{28}O_4N_3$: m/z = 482.20743 $[M+H]^+$,
found: m/z = 482.20901 $[M+H]^+$.

(±)-(2,4-dimethoxy-5-(1-(4-nitrobenzyl)-1H-pyrazol-4-yl)pyridin-3-yl)(naphthalen-2-yl)methanol (115)

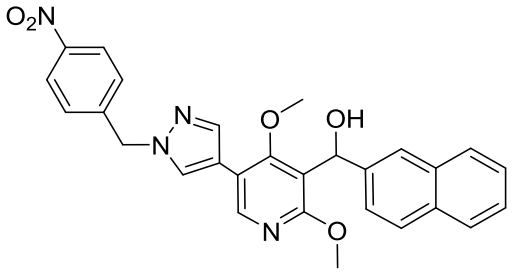

Alcohol **512** (65 mg, 174 µmol) was reacted according with GP II with 1- (4-nitrobenzyl) -4- (4,4,5,5-tetramethyl-1,3,2-dioxaborolan-2-yl) -1H- Pyrazole. The crude product was purified by means of flash chromatography on silica gel (50% EtOAc/PE) followed by HPLC (without using TFA). The product (31 mg, 61 µmol, 15%) was obtained as a colorless amorphous solid.

R_f: 0.15 (50% EtOAc/*n*-pentane).

^{1}H NMR (400 MHz, $CDCl_3$) δ = 8.23 (s, 1H), 8.22 – 8.18 (m, 2H), 7.88 (s, 1H), 7.82 – 7.76 (m, 5H), 7.49 – 7.42 (m, 3H), 7.36 (d, ^3J = 8.7 Hz, 2H), 6.38 (s, 1H), 5.46 (s, 2H), 3.98 (s, 3H), 3.41 (s, 3H). ^{13}C NMR (101 MHz, $CDCl_3$) δ = 163.57, 161.63, 147.92, 145.47, 143.67, 141.02, 139.02, 133.30, 132.78, 128.42, 128.26, 128.15, 128.14, 127.73, 126.27, 125.99, 124.36, 124.27, 123.95, 119.13, 117.26, 116.22, 68.36, 60.98, 55.43, 54.69.

ESI-MS: m/z = 497.43 $[M+H]^+$.

HRMS (ESI): calculated for $C_{28}H_{25}O_5N_4$: m/z = 497.18195 $[M+H]^+$,
found: m/z = 497.18280 $[M+H]^+$.

(±)-naphthalen-2-yl(4,4',6-trimethoxy-[3,3'-bipyridin]-5-yl)methanol (544)

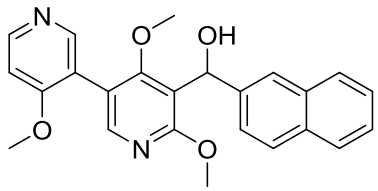

Alcohol **512** (100 mg, 267 µmol) was reacted according to GP II with (4-methoxypyridin-3-yl) boronic acid monohydrate. The crude product was purified by flash chromatography on silica gel (2% MeOH/DCM) and the product (79 mg, 195 µmol, 73%) was obtained as a colorless wax.

R_f: 0.28 (4% MeOH/DCM).

^{1}H NMR (500 MHz, $CDCl_3$) δ = 8.63 (d, ^3J = 6.1 Hz, 1H), 8.53 (s, 1H), 8.03 (s, 1H), 7.84 – 7.78 (m, 4H), 7.50 – 7.43 (m, 3H), 7.19 (d, ^3J = 6.2 Hz, 1H), 6.38 (s, 1H), 4.03 (s, 3H), 3.99 (s, 3H), 3.27 (s, 3H).

ESI-MS: m/z = 403.31 $[M+H]^+$.

HRMS (ESI): calculated for $C_{24}H_{23}O_4N_2$: m/z = 403.16523 $[M+H]^+$,
found: m/z = 403.16642 $[M+H]^+$.

(±)-(5-(1-benzyl-1H-pyrazol-4-yl)-4-methoxypyridin-3-yl) (naphthalen-2-yl)methanol (175)

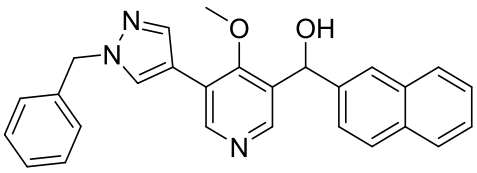

Alcohol **512** (54 mg, 156 µmol) was reacted according to GP II with 1-benzyl-4- (4,4,5,5-tetramethyl-1,3,2-dioxaborolan-2-yl) -1H-pyrazole. The crude product was purified by means of flash chromatography on silica gel (2% MeOH/DCM) followed by HPLC (without using TFA). The product (41 mg, 98 µmol, 63%) was obtained as a colorless oil.

R_f: 0.26 (4% MeOH/DCM).

^{1}H NMR (500 MHz, $CDCl_3$) δ = 9.03 (s, 1H), 8.55 (s, 1H), 7.79 – 7.70 (m, 6H), 7.45 – 7.41 (m, 2H), 7.38 (d, ^3J = 8.4 Hz, 1H), 7.36 – 7.29 (m, 3H), 7.24 – 7.20 (m, 2H), 6.31 (s, 1H), 5.30 (s, 2H), 3.38 (s, 3H). ^{13}C NMR (126 MHz, $CDCl_3$) δ = 166.55, 162.15, 161.86, 141.45, 139.38, 138.77, 138.71, 138.29, 135.41, 133.26, 133.25, 129.20, 129.02, 128.76, 128.17, 128.01, 127.82, 126.70, 126.37, 125.24, 124.67, 112.69, 69.57, 60.89, 56.69.

ESI-MS: m/z = 422.20 $[M+H]^+$.

HRMS (ESI): calculated for $C_{27}H_{24}O_2N_3$: m/z = 422.18630 $[M+H]^+$,
found: m/z = 422.18613 $[M+H]^+$.

(5-(1-benzyl-1H-pyrazol-4-yl)-2,4-dimethoxypyridin-3-yl) (quinoxalin-2-yl)methanone (545)

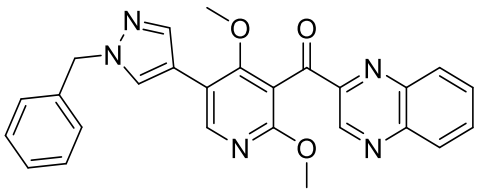

Alcohol **509** (78 mg, 207 µmol) was reacted according to GP II with 1-benzyl-4- (4,4,5,5-tetramethyl-1,3,2-dioxaborolan-2-yl) -1H-pyrazole. In the course of the cross-coupling, oxidation took place, so that instead of the secondary alcohol the corresponding ketone was obtained as the main product. This product was purified by means of flash chromatography on silica gel (2% MeOH/DCM) followed by HPLC (without using TFA). The product (76 mg, 169 µmol, 82%) was obtained as a yellow oil.

R_f: 0.35 (4% MeOH/DCM).

^{1}H NMR (500 MHz, $CDCl_3$) δ = 8.88 (s, 1H), 8.21 (s, 1H), 8.18 – 8.13 (m, 1H), 8.11 – 8.06 (m, 1H), 7.91 – 7.88 (m, 1H), 7.81 (s, 1H), 7.80 – 7.76 (m, 1H), 7.68 (s, 1H), 7.39 – 7.29 (m, 3H), 7.29 – 7.23 (m, 2H), 5.35 (s, 2H), 3.89 (s, 3H), 3.54 (s, 3H).

ESI-MS: m/z = 452.14 $[M+H]^+$.

HRMS (ESI): calculated for $C_{26}H_{22}O_3N_5$: m/z = 452.17172 $[M+H]^+$,
found: m/z = 452.17212 $[M+H]^+$.

***N*-benzyl-5-(1-benzyl-1H-pyrazol-4-yl)-2,4-dimethoxynicotinamide (158)**

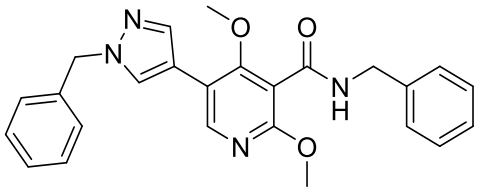

Amide **517** (61 mg, 174 µmol) was reacted according to GP II with 1-benzyl-4- (4,4,5,5-tetramethyl-1,3,2-dioxaborolan-2-yl) -1H-pyraz-ole. The crude product was purified by means of flash chromatography on silica gel (1% MeOH/DCM) followed by HPLC (without using TFA). The product (54 mg, 127 µmol, 73%) was obtained as a colorless amorphous solid.

R_f: 0.14 (2% MeOH/DCM).

^{1}H NMR (500 MHz, $CDCl_3$) δ = 8.15 (s, 1H), 7.75 (s, 1H), 7.64 (s, 1H), 7.40 – 7.24 (m, 8H), 7.22 (d, ^3J = 7.1 Hz, 2H), 6.55 (s, 1H), 5.29 (s, 2H), 4.63 (d, J = 5.7 Hz, 2H), 3.92 (s, 3H), 3.75 (s, 3H).

^{13}C NMR (126 MHz, $CDCl_3$) δ = 164.56, 162.53, 160.71, 145.98, 137.97, 137.92, 136.37, 128.96, 128.75, 128.27, 128.14, 127.93, 127.77, 127.64, 116.57, 115.29, 112.12, 60.60, 56.24, 54.31, 44.09.

ESI-MS: m/z = 429.10 $[M+H]^+$.

HRMS (ESI): calculated for $C_{25}H_{25}O_3N_4$: m/z = 429.19212 $[M+H]^+$,
found: m/z = 429.19197 $[M+H]^+$.

5-(1-benzyl-1H-pyrazol-4-yl)-2,4-dimethoxy-*N*-phenylnicotinamide (159)

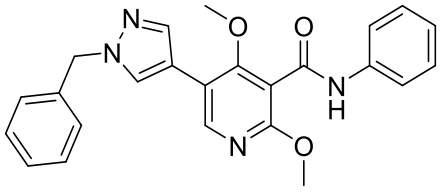

Amide **516** (67 mg, 199 µmol) was reacted according to GP II with 1-benzyl-4- (4,4,5,5-tetramethyl-1,3,2-dioxaborolan-2-yl) -1H-pyrazole. The crude product was purified by means of flash chromatography on silica gel (30% EtOAc/PE) followed by HPLC (without using TFA). The product (36 mg, 87 µmol, 44%) was obtained as a colorless amorphous solid.

R_f: 0.26 (50% EtOAc/PE).

^{1}H NMR (500 MHz, $CDCl_3$) δ = 8.21 (s, 1H), 8.09 (s, 1H), 7.80 (s, 1H), 7.69 – 7.64 (m, 3H), 7.40 – 7.29 (m, 5H), 7.28 – 7.22 (m, 2H), 7.16 (t, ^3J = 7.4 Hz, 1H), 5.32 (s, 2H), 3.99 (s, 3H), 3.86 (s, 3H). ^{13}C NMR (126 MHz, $CDCl_3$) δ = 162.86, 162.47, 160.67, 145.74, 138.05, 136.33, 129.27, 129.04, 128.38, 128.29, 127.89, 124.87, 120.00, 116.83, 115.17, 112.15, 60.77, 56.36, 54.79.

ESI-MS: m/z = 415.12 $[M+H]^+$.

HRMS (ESI): calculated for $C_{24}H_{23}O_3N_4$: m/z = 415.17647 $[M+H]^+$,
found: m/z = 415.17653 $[M+H]^+$.

(±)-(5-(1-benzyl-1H-pyrazol-4-yl)-2-methoxypyridin-3-yl) (naphthalen-2-yl)methanol (174)

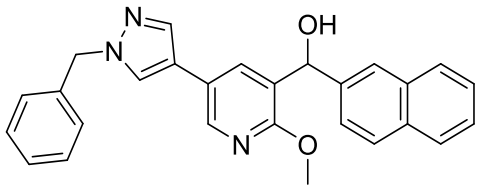

Alcohol **168** (134 mg, 389 µmol) was reacted according to GP II with 1-benzyl-4- (4,4,5,5-tetramethyl-1,3,2-dioxaborolan-2-yl) -1H-pyraz-ole. The crude product was purified by means of flash chromatography on silica gel (30% EtOAc/PE) followed by HPLC (without using TFA). The product (65 mg, 153 µmol, 39%) was obtained as a yellowish oil.

R_f: 0.35 (50% EtOAc/PE).

^{1}H NMR (500 MHz, $CDCl_3$) δ = 8.18 (d, ^4J = 2.4 Hz, 1H), 7.85 (s, 1H), 7.83 – 7.79 (m, 2H), 7.78 (s, 1H), 7.77 (d, ^4J = 2.3 Hz, 1H), 7.73 (s, 1H), 7.52 (s, 1H), 7.50 – 7.44 (m, 3H), 7.38 – 7.29 (m, 3H), 7.25 – 7.20 (m, 2H), 6.15 (s, 1H), 5.29 (s, 2H), 3.94 (s, 3H). ^{13}C NMR (126 MHz, $CDCl_3$) δ = 159.72, 142.23, 139.79, 136.70, 136.14, 133.81, 133.36, 133.06, 129.03, 128.38, 128.30, 128.21, 127.86, 127.78, 126.50, 126.28, 126.13, 125.47, 124.88, 122.34, 120.16, 71.21, 56.27, 53.88.

ESI-MS: m/z = 422.15 $[M+H]^+$.

(2,4-dimethoxy-5-(quinolin-3-yl)pyridin-3-yl)(1-methyl-1H-indol-3-yl)methanone (546)

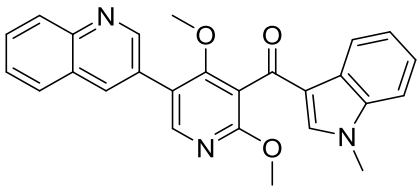

Alcohol **508** (56 mg, 142 µmol) was reacted according to GP II 3- (4,4,5,5-tetramethyl-1,3,2-dioxaborolan-2-yl) quinoline. In the course of the cross-coupling, oxidation took place, so that instead of the secondary alcohol the corresponding ketone was obtained as the main product of the reaction. This product was purified by means of flash chromatography on silica gel (30% EtOAc/PE) followed by HPLC (without using TFA). The product (23 mg, 55 µmol, 39%) was obtained as a red oil.

R_f: 0.25 (50% EtOAc/PE).

ESI-MS: m/z = 424.12 $[M+H]^+$.

HRMS (ESI): calculated for $C_{26}H_{22}O_3N_3$: m/z = 424.16557 $[M+H]^+$,
found: m/z = 424.16533 $[M+H]^+$.

(±)-benzofuran-2-yl(2,4-dimethoxy-5-(quinolin-3-yl)pyridin-3-yl) methanol (547)

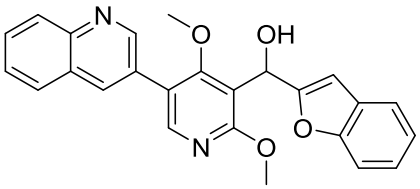

Alcohol **510** (89 mg, 244 µmol) was reacted according to GP II with 3- (4,4,5,5-tetramethyl-1,3,2-dioxaborolan-2-yl) quinoline. The crude product was purified by flash chromatography on silica gel (50% EtOAc/PE) and the product (74 mg, 181 µmol, 74%) was obtained as a yellow oil.

R_f: 0.30 (50% EtOAc/PE).

^{1}H NMR (500 MHz, $CDCl_3$) δ = 9.12 (d, ^4J = 2.0 Hz, 1H), 8.34 (d, ^4J = 1.8 Hz, 1H), 8.25 (s, 1H), 8.20 (d, ^3J = 8.6 Hz, 1H), 7.90 (d, ^3J = 8.0 Hz, 1H), 7.81 – 7.75 (m, 1H), 7.64 – 7.60 (m, 1H), 7.54 (d, ^3J = 7.2 Hz, 1H), 7.44 (d, ^3J = 8.1 Hz, 1H), 7.27 – 7.18 (m, 2H), 6.65 (s, 1H), 6.43 (s, 1H), 4.06 (s, 3H), 3.43 (s, 3H). ^{13}C NMR (126 MHz, $CDCl_3$) δ = 164.33, 162.92, 158.32, 155.03, 150.47, 148.59, 147.18, 135.35, 130.08, 129.19, 128.39, 128.34, 128.05, 128.02, 127.39, 124.15, 122.88, 122.02, 121.06, 115.75, 111.33, 103.03, 63.59, 61.78, 54.36.

ESI-MS: m/z = 413.17 $[M+H]^+$.

HRMS (ESI): calculated for $C_{25}H_{21}O_4N_2$: m/z = 413.14958 $[M+H]^+$,
found: m/z = 413.14940 $[M+H]^+$.

5-(1-benzyl-1H-pyrazol-4-yl)-2,4-dimethoxy-*N*-(naphthalen-1-yl) nicotinamide (152)

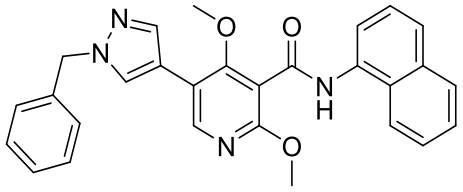

Amide **517** (69 mg, 177 µmol) was reacted according to GP II with 1-benzyl-4- (4,4,5,5-tetramethyl-1,3,2-dioxaborolan-2-yl) -1H-pyrazole. The crude product was purified by means of flash chromatography on silica gel (30% EtOAc/PE) followed by HPLC (without using TFA). The product (41 mg, 98 µmol, 50%) was obtained as a colorless solid.

R_f: 0.20 (50% EtOAc/PE).

^{1}H NMR (500 MHz, $CDCl_3$) δ = 8.44 (s, 1H), 8.26 (s, 1H), 8.08 – 8.01 (m, 2H), 7.92 – 7.86 (m, 1H), 7.83 (s, 1H), 7.77 – 7.71 (m, 2H), 7.55 – 7.48 (m, 3H), 7.39 – 7.29 (m, 3H), 7.25 (d, ^3J = 6.7 Hz, 2H), 5.33 (s, 2H), 4.06 (s, 3H), 3.92 (s, 3H). ^{13}C NMR (126 MHz, $CDCl_3$) δ = 163.19, 160.71, 146.08, 138.05, 136.35, 134.30, 132.20, 129.01, 128.84, 128.33, 127.84, 127.51, 126.56, 126.33, 126.19, 125.87, 121.23, 121.00, 117.01, 115.21, 112.19, 60.91, 56.33, 54.75.

ESI-MS: m/z = 465.08 $[M+H]^+$.

HRMS (ESI): calculated for $C_{28}H_{25}O_3N_4$: m/z = 465.19212 $[M+H]^+$,
found: m/z = 465.19246 $[M+H]^+$.

(±)-*N*-(4-(5-(hydroxy(4-isopropylphenyl)methyl)-4,6-dimethoxy pyridin-3-yl)phenyl)methanesulfonamide (548)

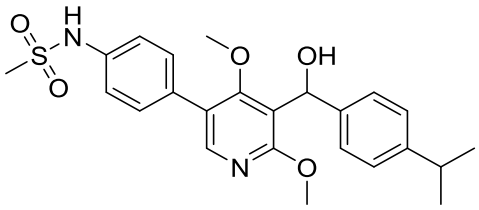

Alcohol **502** (105 mg, 288 µmol) was reacted according to GP II with (4 (methylsulfonamido) phenyl) boronic acid. The crude product was isolated by means of flash chromatography on silica gel (30% EtOAc/PE). The product (12 mg, 27 µmol, 9%) was obtained as a yellow oil.

R_f: 0.27 (50% EtOAc/PE).

^{1}H NMR (500 MHz, $CDCl_3$) δ = 8.06 (s, 1H), 7.56 – 7.42 (m, 3H), 7.32 – 7.27 (m, 3H), 7.24 – 7.15 (m, 2H), 6.83 (s, 1H), 6.23 (s, 1H), 4.03 (s, 3H), 3.22 (s, 3H), 3.07 (s, 3H), 2.96 – 2.81 (m, 1H), 1.22 (d, ^3J = 7.0 Hz, 6H). ^{13}C NMR (126 MHz, $CDCl_3$) δ = 164.13, 161.90, 158.66, 147.98, 147.06, 141.08, 136.61, 132.13, 130.28, 126.47, 125.75, 124.46, 120.78, 118.88, 68.37, 61.13, 54.89, 39.95, 33.86, 24.12.

ESI-MS: m/z = 457.04 $[M+H]^+$.

HRMS (ESI): calculated for $C_{24}H_{29}O_5N_2S$: m/z = 457.17917 $[M+H]^+$,
found: m/z = 457.17935 $[M+H]^+$.

(±)-tert-butyl-4-(5'-(hydroxy(4-isopropylphenyl)methyl)-4',6'-dimethoxy-[3,3'-bipyridin]-6-yl)piperazine-1-carboxylate (549)

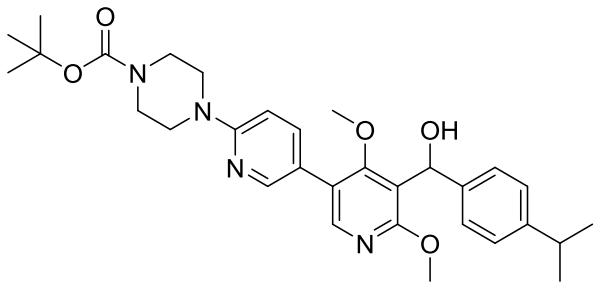

Alcohol **502** (429 mg, 1.17 mol) was reacted with (6- (4- (tert-butoxycarbonyl) piperazin-1-yl) pyridin-3-yl) boronic acid according to GP II. The crude product was purified by means of flash chromatography on silica gel (2% MeOH/DCM) followed by HPLC (without using TFA). The product (152 mg, 276 µmol, 24%) was obtained as a colorless amorphous solid.

R_f: 0.20 (2% MeOH/DCM).

^{1}H NMR (500 MHz, $CDCl_3$) δ = 8.36 (s, 1H), 8.04 (s, 1H), 7.96 (d, ^3J = 8.8 Hz, 1H), 7.25 (d, ^3J = 8.1 Hz, 2H), 7.17 (d, ^3J = 8.1 Hz, 2H), 6.93 (d, ^3J = 9.1 Hz, 1H), 6.19 (s, 1H), 3.98 (d, ^3J = 9.9 Hz, 3H), 3.74 (s, 4H), 3.65 (s, 4H), 3.29 (s, 3H), 2.87 (hept, ^3J = 6.9 Hz, 1H), 1.48 (s, 9H), 1.21 (d, ^3J = 6.9 Hz, 6H). ^{13}C NMR (126 MHz, $CDCl_3$) δ = 163.56, 162.96, 154.61, 153.93, 148.05, 146.94, 142.62, 140.76, 140.27, 126.46, 125.73, 121.30, 120.07, 119.13, 110.14, 80.85, 68.22, 61.36, 54.31, 46.20, 33.83, 28.49, 24.08, 24.07.

ESI-MS: m/z = 549.02 $[M+H]^+$.

HRMS (ESI): calculated for $C_{31}H_{41}O_5N_4$: m/z = 549.30715 $[M+H]^+$,
found: m/z = 549.30671 $[M+H]^+$.

General procedure III (GP III): Buchwald-Hartwig amination of substituted 5-bromopyridines

The corresponding 5-bromopyridine (1 eq.) was dissolved together with the respective amine (5 eq), tris (dibenzylideneacetone) dipalladium (0 mol%), *t*-BuXPhos (40 mol%) and sodium *tert*-butanolate (2 eq.) in degassed toluene (125 mM with respect to 5-bromopyridine). The reaction mixture was heated to 80 °C with stirring for 16-20 h. After the reaction was complete, the solvent was removed *in vacuo* and the crude product was purified by means of flash chromatography on silica gel without prior work-up.

Representative example:

(2,4-dimethoxy-5-morpholinopyridin-3-yl)(4-isopropylphenyl) methanone (550)

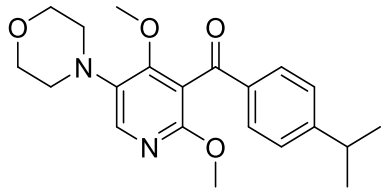

Ketone 139 (88 mg, 241 µmol) was dissolved together with morpholine (105 µL, 1.20 mMol), tris (dibenzylideneacetone) dipalladium (25 mg, 24 µmol), *t*-BuXPhos (41 mg, 481 µmol) in degassed toluene (1.93 mL). The reaction mixture was heated to 80 ° C with stirring for 20 h. After the reaction was complete, the solvent was removed *in vacuo* and the crude product was purified on silica gel without prior work-up by means of flash chromatography (30% EtOAc/PE). The product (85.35 mg, 230 µmol, 96%) was obtained as a yellow oil.

R_f: 0.22 (30% EtOAc/PE).

^{1}H NMR (500 MHz, $CDCl_3$) δ = 7.81 (s, 1H), 7.74 (d, ^3J = 8.3 Hz, 1H), 7.28 (d, ^3J = 8.3 Hz, 1H), 3.84 – 3.81 (m, 1H), 3.81 (s, 1H), 3.79 (s, 1H), 3.07 – 3.03 (m, 1H), 2.94 (d, ^3J = 6.9 Hz, 1H), 1.25 (d, ^3J = 6.9 Hz, 1H).

^{13}C NMR (126 MHz, $CDCl_3$) δ = 193.05, 158.91, 157.94, 155.38, 137.39, 135.74, 135.25, 129.77, 126.83, 116.09, 67.27, 59.95, 53.81, 51.28, 34.41, 23.68.

ESI-MS: m/z = 371.09 $[M+H]^+$.

HRMS (ESI): calculated for $C_{21}H_{27}O_4N_2$: m/z = 371.19653 $[M+H]^+$,
found: m/z = 371.19717 $[M+H]^+$.

(2,4-dimethoxy-5-(octahydroisoquinolin-2(1H)-yl)pyridin-3-yl)(4-isopropylphenyl)methanone (551)

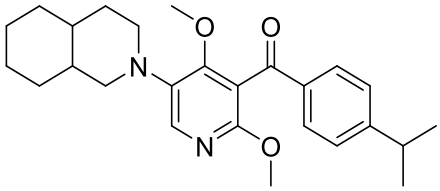

Ketone 139 (92 mg, 253 µmol) was reacted according to GP III with decahydroisoquinoline. The crude product was purified by means of flash chromatography on silica gel (10% EtOAc/PE). The product (27 mg, 63 µmol, 25%) was obtained as a colorless oil.

R_f: 0.24 (10% EtOAc/PE).

ESI-MS: m/z = 423.27 $[M+H]^+$.

HRMS (ESI): calculated for $C_{26}H_{35}O_3N_2$: m/z = 423.26422 $[M+H]^+$,
found: m/z = 423.26370 $[M+H]^+$.

(5-(4-benzylpiperazin-1-yl)-2,4-dimethoxypyridin-3-yl)(4-isopropylphenyl)methanone (552)

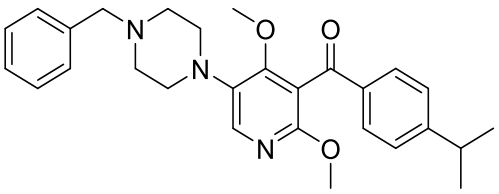

Ketone 139 (90 mg, 248 µmol) was reacted according to GP III with twelve equivalents of sodium *tert*-butoxide instead of the usual two equivalents with 1-benzylpiperazine dihydrochloride. The crude product was purified by means of flash chromatography on silica gel (30% EtOAc/PE + 2% Et_3N) followed by HPLC (without using TFA). The product (94 mg, 205 µmol, 83%) was obtained as a colorless amorphous solid.

R_f: 0.23 (30% EtOAc/PE + 2% Et_3N).

^{1}H NMR (500 MHz, $CDCl_3$) δ = 7.80 (s, 1H), 7.71 (d, ^3J = 8.2 Hz, 2H), 7.45 – 7.38 (m, 5H), 7.28 (d, ^3J = 8.2 Hz, 2H), 4.25 (s, 2H), 3.76 (s, 3H), 3.73 (s, 3H), 3.59 (bs, 2H), 3.37 (bs, 4H), 2.99 (bs, 2H), 2.95 (hept, ^3J = 6.9 Hz, 1H), 1.25 (d, ^3J = 6.9 Hz, 6H). ^{13}C NMR (126 MHz, $CDCl_3$) δ = 192.88, 159.22, 158.99, 155.73, 138.59, 135.13, 133.63, 131.18, 130.39, 129.76, 129.50, 128.02, 126.97, 115.01, 60.82, 60.48, 54.03, 51.84, 47.87, 34.41, 23.63.

ESI-MS: m/z = 460.09 $[M+H]^+$.

HRMS (ESI): calculated for $C_{28}H_{34}O_3N_3$: m/z = 460.25947 $[M+H]^+$,
found: m/z = 460.25933 $[M+H]^+$.

benzofuran-2-yl(2,4-dimethoxy-5-(pyrazin-2-ylamino)pyridin-3-yl)methanone (553)

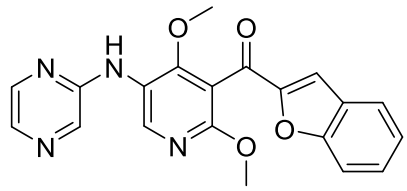

Ketone 139 (92 mg, 253 µmol) was reacted according to GP III for 72 h at 60 ° C. with pyrazine-2-amine. The product (27 mg, 63 µmol, 63%) was purified by HPLC (without using TFA) and obtained as a yellow oil.

^{1}H NMR (500 MHz, $CDCl_3$) δ = 8.71 (s, 1H), 8.51 (s, 1H), 8.26 (s, 1H), 8.10 (d, ^{4}J = 2.1 Hz, 1H), 8.04 (d, ^{4}J = 3.0 Hz, 1H), 7.72 (d, ^{3}J = 7.9 Hz, 1H), 7.61 (d, ^{3}J = 8.4 Hz, 1H), 7.53 (t, ^{3}J = 7.6 Hz, 1H), 7.46 (s, 1H), 7.34 (t, ^{3}J = 7.5 Hz, 1H), 3.89 (s, 3H), 3.85 (s, 3H). ^{13}C NMR (126 MHz, $CDCl_3$) δ = 182.27, 160.41, 158.61, 156.74, 153.41, 151.82, 143.05, 138.76, 133.88, 132.69, 129.56, 127.44, 124.67, 124.12, 121.41, 116.99, 113.13, 111.77, 61.61, 54.88.

ESI-MS: m/z = 376.92 $[M+H]^+$.

HRMS (ESI): calculated for $C_{20}H_{17}O_4N_4$: m/z = 377.12443 $[M+H]^+$,
found: m/z = 377.12449 $[M+H]^+$.

General procedure IV (GP IV): Oxidation of the secondary 3 pyridinyl alcohols with manganese (IV) oxide

The secondary alcohol (1.0 eq.) was dissolved in DCM (20 mM), and mixed with manganese (IV) oxide (15 eq.) and stirred at rt for 2 days. The suspension was then diluted with DCM and filtered over Celite. The filtrate was concentrated *in vacuo* and the crude product was purified by means of flash chromatography on silica gel.

Representative example:

(2,4-dimethoxy-5-(2-methoxyphenyl)pyridin-3-yl)(4-isopropyl phenyl)methanone (554)

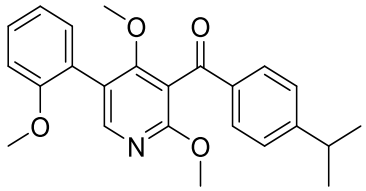

Alcohol **531** (10 mg, 25 µmol) was dissolved in DCM (1.25 ml), mixed with manganese (IV) oxide (33 mg, 381 µmol) and stirred at rt for 2 days. The suspension was then diluted with DCM and filtered through celite. The filtrate was concentrated *in vacuo* and the crude product was purified by means of flash chromatography (15% EtOAc/PE) on silica gel. The product (9 mg, 24 µmol, 90%) was obtained as a colorless oil.

R_f: 0.31 (15% EtOAc/PE).

^{1}H NMR (500 MHz, $CDCl_3$) δ = 8.08 (s, 1H), 7.85 (d, ^3J = 8.3 Hz, 2H), 7.38 – 7.35 (m, 1H), 7.32 (d, ^3J = 8.3 Hz, 2H), 7.29 (dd, $^{3,4}J$ = 7.5, 1.6 Hz, 1H), 7.04 – 7.01 (m, 1H), 6.97 (d, ^3J = 8.2 Hz, 1H), 3.90 (s, 3H), 3.80 (s, 3H), 3.39 (s, 3H), 2.98 (hept, ^3J = 6.9 Hz, 1H), 1.28 (d, ^3J = 6.9 Hz, 6H).

^{13}C NMR (126 MHz, $CDCl_3$) δ = 193.68, 163.95, 161.60, 157.33, 155.37, 149.57, 135.44, 131.54, 129.92, 129.62, 126.90, 124.35, 120.80, 120.77, 113.99, 111.05, 60.76, 55.74, 54.24, 34.49, 23.77.

ESI-MS: m/z = 392.20 $[M+H]^+$.

HRMS (ESI): calculated for $C_{24}H_{26}O_4N$: m/z = 392.18563 $[M+H]^+$,
found: m/z = 392.18390 $[M+H]^+$.

(5-(1-benzyl-1H-pyrazol-4-yl)pyridin-3-yl)(naphthalen-2-yl) methanone (181)

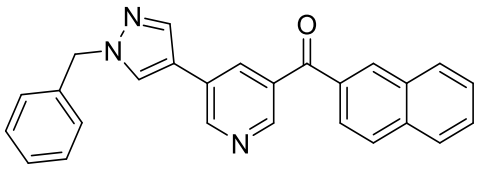

Alcohol **176** (27 mg, 69 µmol) was reacted according to GP IV. The crude product was purified by flash chromatography on silica gel (2% MeOH/DCM) and the product (24 mg, 61 µmol, 89%) was obtained as a colorless oil.

R_f: 0.19 (2% MeOH/DCM).

^{1}H NMR (500 MHz, $CDCl_3$) δ = 9.02 (s, 1H), 8.84 (s, 1H), 8.41 (s, 1H), 8.27 (s, 1H), 7.99 (d, ^3J = 8.5 Hz, 1H), 7.97 – 7.91 (m, 4H), 7.83 (s, 1H), 7.69 – 7.64 (m, 1H), 7.62 – 7.57 (m, 1H), 7.41 – 7.33 (m, 3H), 7.32 – 7.28 (m, 2H), 5.38 (s, 2H). ^{13}C NMR (126 MHz, $CDCl_3$) δ = 193.25, 146.08, 144.78, 137.27, 136.03, 135.91, 135.54, 135.14, 133.39, 132.49, 132.36, 130.84, 129.78, 129.33, 129.23, 129.22, 128.73, 128.11, 128.06, 127.48, 127.43, 125.12, 118.03, 56.77.

ESI-MS: m/z = 390.23 $[M+H]^+$.

HRMS (ESI): calculated for $C_{26}H_{20}ON_3$: m/z = 390.16009 $[M+H]^+$,
found: m/z = 390.16139 $[M+H]^+$.

(5-(1-benzyl-1H-pyrazol-4-yl)-4-methoxypyridin-3-yl) (naphthalen-2-yl)methanone (180)

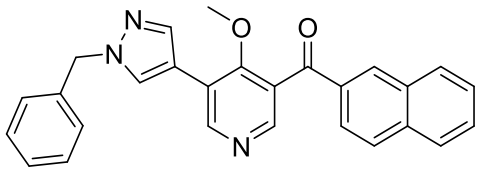

Alcohol **175** (16 mg, 38 µmol) was reacted according to GP IV. The crude product was purified by flash chromatography on silica gel (2% MeOH/DCM) and the product (14 mg, 35 µmol, 91%) was obtained as a colorless oil.

R_f: 0.16 (2% MeOH/DCM).

^{1}H NMR (500 MHz, $CDCl_3$) δ = 8.84 (s, 1H), 8.43 (s, 1H), 8.28 (s, 1H), 8.06 (dd, ^3J = 8.6, 1.4 Hz, 1H), 8.00 (s, 1H), 7.97 (d, ^3J = 8.6 Hz, 1H), 7.92 (dd, $^{3,4}J$ = 8.1, 3.5 Hz, 2H), 7.89 (s, 1H), 7.69 – 7.63 (m, 1H), 7.61 – 7.55 (m, 1H), 7.40 – 7.31 (m, 3H), 7.28 (d, ^3J = 6.9 Hz, 2H), 5.38 (s, 2H), 3.75 (s, 3H). ^{13}C NMR (126 MHz, $CDCl_3$) δ = 193.62, 162.12, 146.76, 138.66, 136.28, 136.09, 134.13, 133.39, 132.48, 130.02, 129.56, 129.30, 129.23, 129.13, 128.52, 128.07, 127.96, 127.41, 127.01, 124.59, 114.61, 109.73, 61.63, 56.58.

ESI-MS: m/z = 420.18 $[M+H]^+$.

HRMS (ESI): calculated for $C_{27}H_{22}O_2N_3$: m/z = 420.17065 $[M+H]^+$,
found: m/z = 420.17039 $[M+H]^+$.

(5-(benzo[c][1,2,5]oxadiazol-5-yl)-2,4-dimethoxypyridin-3-yl)(4-isopropylphenyl)methanone (555)

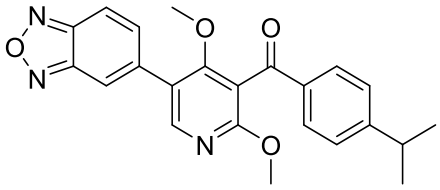

Alcohol **532** (29 mg, 72 µmol) was reacted according to GP IV. The crude product was purified by flash chromatography on silica gel (15% EtOAc/PE) and the product (27 mg, 67 µmol, 93%) was obtained as a colorless wax.

R_f: 0.32 (20% EtOAc/PE).

^{1}H NMR (500 MHz, $CDCl_3$) δ = 8.17 (s, 1H), 7.84 (s, 1H), 7.80 – 7.76 (m, 3H), 7.54 (dd, $^{3,4}J$ = 9.3, 1.1 Hz, 1H), 7.28 (d, ^3J = 8.3 Hz, 2H), 3.84 (s, 3H), 3.50 (s, 3H), 2.93 (hept, ^3J = 6.9 Hz, 1H), 1.22 (d, ^3J = 6.9 Hz, 6H). ^{13}C NMR (126 MHz, $CDCl_3$) δ = 193.07, 163.04, 155.93, 149.58, 148.50, 148.39, 139.13, 135.27, 134.32, 129.91, 127.13, 122.46, 116.20, 114.98, 113.99, 110.14, 61.30, 54.57, 34.53, 23.75.

ESI-MS: m/z = 404.20 $[M+H]^+$.

HRMS (ESI): calculated for $C_{23}H_{22}O_4N_3$: m/z = 404.16048 $[M+H]^+$,
found: m/z = 404.15893 $[M+H]^+$.

benzofuran-2-yl(5-bromo-2,4-dimethoxypyridin-3-yl)methanone (556)

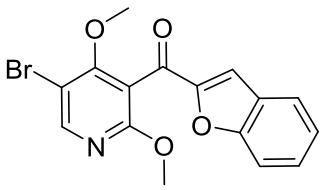

Alcohol **510** (160 mg, 439 µmol) was reacted according to GP IV. The crude product was purified by flash chromatography on silica gel (10% EtOAc/PE) and the product (141 mg, 390 µmol, 88%) was obtained as a colorless oil.

R_f: 0.25 (20% EtOAc/PE).

^{1}H NMR (500 MHz, $CDCl_3$) δ = 8.31 (s, 1H), 7.68 (d, ^3J = 7.9 Hz, 1H), 7.58 (d, ^3J = 8.4 Hz, 1H), 7.49 (t, ^3J = 7.7 Hz, 1H), 7.37 (s, 1H), 7.31 (t, ^3J = 7.5 Hz, 1H), 3.88 (s, 3H), 3.86 (s, 3H). ^{13}C NMR (126 MHz, $CDCl_3$) δ = 181.48, 162.34, 162.06, 156.39, 152.87, 150.47, 129.08, 127.14, 124.25, 123.72, 116.60, 114.64, 112.79, 106.60, 62.03, 54.52.

ESI-MS: m/z = 361.92, 363.94 $[M+H]^+$.

HRMS (ESI): calculated for $C_{16}H_{13}O_4N\,^{79}Br$: m/z = 362.00225 $[M+H]^+$,
found: m/z = 362.00292 $[M+H]^+$;
calculated for $C_{16}H_{13}O_4N\,^{81}Br$: m/z = 364.00020 $[M+H]^+$,
found: m/z = 364.00018 $[M+H]^+$.

(5-bromo-2,4-dimethoxypyridin-3-yl)(4-(trifluoromethyl)phenyl)methanone (557)

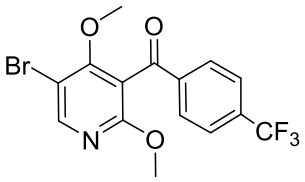

Alcohol **507** (1.50 mg, 3.82 mMol) was reacted according to GP IV. The crude product was purified by flash chromatography on silica gel (5% EtOAc/PE) and the product (1.22 g, 3.14 mMol, 82%) was obtained as a colorless wax.

R_f: 0.22 (5% EtOAc/PE).

^{1}H NMR (500 MHz, $CDCl_3$) δ = 8.32 (s, 1H), 7.97 – 7.92 (m, 2H), 7.74 (d, ^3J = 8.2 Hz, 2H), 3.82 (s, 3H), 3.81 (s, 3H).^{13}C NMR (126 MHz, $CDCl_3$) δ = 191.69, 162.34, 161.72, 150.56, 139.65, 135.35, 135.09, 129.83, 126.01, 125.98, 124.74, 122.57, 115.05, 106.81, 62.01, 54.53.

ESI-MS: m/z = 389.97, 391.97 $[M+H]^+$.

HRMS (ESI): calculated for $C_{15}H_{12}O_3N\,^{79}BrF_3$: m/z = 389.99472 $[M+H]^+$,
found: m/z = 389.99478 $[M+H]^+$;
calculated for $C_{15}H_{12}O_3N\,^{81}BrF_3$: m/z = 391.99267 $[M+H]^+$,
found: m/z = 391.99133 $[M+H]^+$.

(2,4-dimethoxy-5-(quinolin-3-yl)pyridin-3-yl)(naphthalen-2-yl)methanone (121)

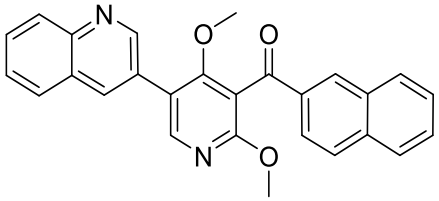

Alcohol **120** (146 mg, 346 µmol) was reacted according to GP IV. The crude product was purified by flash chromatography on silica gel (30% EtOAc/PE) and the product (112 mg, 266 µmol, 77%) was obtained as a colorless oil.

R_f: 0.38 (50% EtOAc/PE).

^{1}H NMR (500 MHz, $CDCl_3$) δ 9.12 (d, ^4J = 2.1 Hz, 1H), 8.37 (s, 1H), 8.35 – 8.30 (m, 2H), 8.15 (d, ^3J = 8.4 Hz, 1H), 8.09 (dd, $^{3,4}J$ = 8.6, 1.1 Hz, 1H), 7.95 (d, ^3J = 8.3 Hz, 2H), 7.88 (t, ^3J = 9.7 Hz, 2H), 7.74 (t, ^3J = 7.5 Hz, 1H), 7.64 – 7.51 (m, 3H), 3.90 (s, 3H), 3.53 (s, 3H). ^{13}C NMR (126 MHz, $CDCl_3$) δ 193.62, 163.45, 162.58, 151.04, 149.13, 147.32, 136.17, 135.48, 134.88, 132.68, 132.26, 129.91, 129.84, 129.35, 129.04, 128.84, 128.22, 128.04, 127.96, 127.16, 126.99, 124.35, 121.33, 114.11, 61.27, 54.33.

ESI-MS: m/z = 421.14 $[M+H]^+$.

HRMS (ESI): calculated for $C_{27}H_{21}O_3N_2$: m/z = 421.15467 $[M+H]^+$,
found: m/z = 421.15436 $[M+H]^+$.

(4,6-dimethoxy-[3,3'-bipyridin]-5-yl)(4-isopropylphenyl) methanone (558)

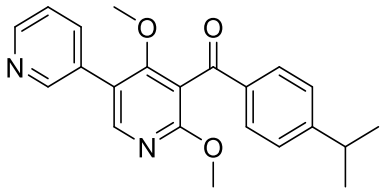

Alcohol **528** (18 mg, 49 µmol) was reacted according to GP IV. The crude product was purified by flash chromatography on silica gel (4% MeOH/DCM) and the product (16 mg, 44 µmol, 90%) was obtained as a colorless wax.

R_f: 0.33 (4% MeOH/DCM).

^{1}H NMR (400 MHz, $CDCl_3$) δ = 8.77 (s, 1H), 8.62 (d, ^3J = 4.8 Hz, 1H), 8.16 (s, 1H), 7.92 – 7.89 (m, 1H), 7.83 (d, ^3J = 8.2 Hz, 2H), 7.42 (dd, $^{3,3}J$ = 7.9, 4.9 Hz, 1H), 7.34 (d, ^3J = 8.2 Hz, 2H), 3.89 (s, 3H), 3.51 (s, 3H), 2.99 (hept, ^3J = 6.9 Hz, 1H), 1.28 (d, ^3J = 6.9 Hz, 6H). ^{13}C NMR (101 MHz, $CDCl_3$) δ = 193.30, 163.02, 162.67, 155.80, 148.94, 148.55, 147.88, 137.45, 135.31, 131.50, 129.92, 127.09, 123.79, 120.72, 114.13, 61.24, 54.38, 34.53, 23.76.

ESI-MS: m/z = 363.15 $[M+H]^+$.

HRMS (ESI): calculated for $C_{22}H_{23}O_3N_2$: m/z = 363.17032 $[M+H]^+$,
found: m/z = 363.17028 $[M+H]^+$.

(5-(1-benzyl-1H-pyrazol-4-yl)-2,4-dimethoxypyridin-3-yl)
(3,5-dimethoxyphenyl)methanone (156)

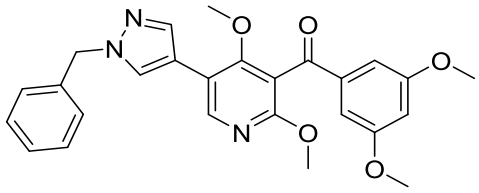

Alcohol **155** (23 mg, 50 µmol) was reacted according to GP IV. The crude product was purified by flash chromatography on silica gel (2% MeOH/DCM) and the product (17 mg, 38 µmol, 76%) was obtained as a colorless oil.

R_f: 0.16 (2% MeOH/DCM).

^{1}H NMR (400 MHz, $CDCl_3$) δ = 8.29 (s, 1H), 7.84 (s, 1H), 7.70 (s, 1H), 7.38 – 7.31 (m, 3H), 7.27 – 7.25 (m, 2H), 6.96 (d, ^4J = 2.2 Hz, 2H), 6.68 (t, ^4J = 2.2 Hz, 1H), 5.35 (s, 2H), 3.87 (s, 3H), 3.74 (s, 6H), 3.61 (s, 3H). ^{13}C NMR (101 MHz, $CDCl_3$) δ = 193.63, 162.33, 161.14, 160.99, 146.24, 139.43, 138.11, 136.40, 129.05, 128.36, 128.27, 127.89, 116.32, 115.44, 114.14, 107.45, 106.25, 60.92, 56.41, 55.77, 54.45.

ESI-MS: m/z = 460.13 $[M+H]^+$.

HRMS (ESI): calculated for $C_{26}H_{26}O_5N_3$: m/z = 460.18670 $[M+H]^+$,
found: m/z = 460.18634 $[M+H]^+$.

(5-(isoquinolin-4-yl)-2,4-dimethoxypyridin-3-yl)(naphthalen-1-yl) methanone (559)

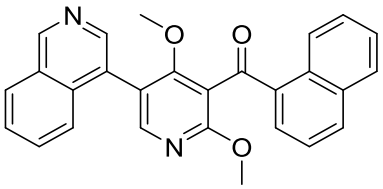

Alcohol **541** (11 mg, 26 µmol) was reacted according to GP IV. The crude product was purified by flash chromatography on silica gel (2% MeOH/DCM) and the product (10 mg, 24 µmol, 93%) was obtained as a colorless oil.

R_f: 0.11 (2% MeOH/DCM).

^{1}H NMR (600 MHz, DMSO-d_6) δ = 9.47 (s, 1H), 9.07 (d, ^3J = 8.6 Hz, 1H), 8.57 (s, 1H), 8.26 (m, 3H), 8.08 (d, ^3J = 8.0 Hz, 1H), 8.04 (dd, $^{3,4}J$ = 7.2, 1.1 Hz, 1H), 7.87 (m, 1H), 7.78 (m, 1H), 7.73 (m, 2H), 7.65 (m, 2H), 3.83 (s, 3H), 3.14 (s, 3H). ^{13}C NMR (151 MHz, DMSO-d_6) δ = 194.64, 163.17, 161.78, 152.08, 149.85, 134.76, 134.45, 133.62, 133.28, 133.08, 132.01, 131.48, 129.90, 128.91, 128.83, 128.43, 128.13, 127.64, 126.76, 125.65, 125.21, 125.12, 124.49, 118.76, 115.14, 60.50, 54.12.

ESI-MS: m/z = 421.16 $[M+H]^+$.

HRMS (ESI): calculated for $C_{27}H_{21}O_3N_2$: m/z = 421.15467 $[M+H]^+$,
found: m/z = 421.15417 $[M+H]^+$.

(2,4-dimethoxy-5-(2-methoxyphenyl)pyridin-3-yl)(4-methoxy phenyl)methanone (560)

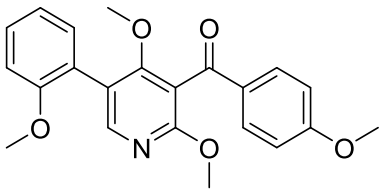

Alcohol **521** (34 mg, 88 µmol) was reacted according to GP IV. The crude product was purified by flash chromatography on silica gel (30% EtOAc/PE) and the product (31 mg, 83 µmol, 94%) was obtained as a yellow wax.

R_f: 0.37 (30% EtOAc/PE).

^{1}H NMR (500 MHz, $CDCl_3$) δ = 8.07 (s, 1H), 7.89 (d, ^3J = 8.8 Hz, 2H), 7.38 – 7.35 (m, 1H), 7.28 (dd, $^{3,4}J$ = 6.4, 3.2 Hz, 1H), 7.03 – 7.00 (m, 1H), 6.97 (d, ^3J = 8.4 Hz, 1H), 6.95 (d, ^3J = 8.8 Hz, 2H), 3.90 (s, 3H), 3.88 (s, 3H), 3.80 (s, 3H), 3.40 (s, 3H). ^{13}C NMR (126 MHz, $CDCl_3$) δ = 192.50, 164.20, 163.92, 161.59, 157.35, 149.47, 132.05, 131.54, 130.86, 129.62, 124.39, 120.86, 120.78, 114.02, 113.99, 111.08, 60.71, 55.75, 55.65, 54.26.

ESI-MS: m/z = 380.20 $[M+H]^+$.

HRMS (ESI): calculated for $C_{22}H_{22}O_5N$: m/z = 380.14925 $[M+H]^+$,
found: m/z = 380.14980 $[M+H]^+$.

[1,1'-biphenyl]-4-yl(5-(1-benzyl-1H-pyrazol-4-yl)-2,4-dimethoxy pyridin-3-yl)methanone (154)

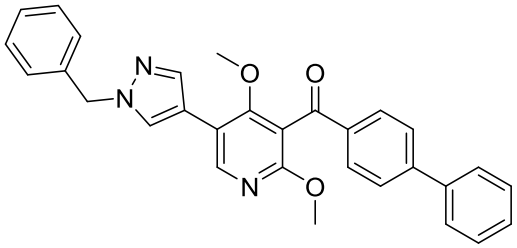

Alcohol **153** (24 mg, 49 µmol) was reacted according to GP IV. The crude product was purified by flash chromatography on silica gel (30% EtOAc/PE) and the product (23 mg, 48 µmol, 97%) was obtained as a colorless oil.

R_f: 0.12 (30% EtOAc/PE).

^{1}H NMR (500 MHz, $CDCl_3$) δ = 8.33 (s, 1H), 7.95 (d, ^3J = 8.3 Hz, 2H), 7.87 (s, 1H), 7.72 (s, 1H), 7.69 (d, ^3J = 8.3 Hz, 2H), 7.63 (d, ^3J = 7.5 Hz, 2H), 7.49 – 7.46 (m, 2H), 7.42 - 7.41 (m, 1H), 7.38 – 7.30 (m, 3H), 7.27 (d, ^3J = 7.8 Hz, 2H), 5.36 (s, 2H), 3.90 (s, 3H), 3.64 (s, 3H). ^{13}C NMR (126 MHz, $CDCl_3$) δ = 193.37, 162.55, 160.98, 146.76, 139.92, 138.08, 136.36, 136.15, 130.23, 129.13, 129.06, 128.54, 128.39, 128.30, 127.92, 127.58, 127.47, 116.49, 115.40, 114.35, 110.14, 61.07, 56.43, 54.60.

ESI-MS: m/z = 476.22 $[M+H]^+$.

HRMS (ESI): calculated for $C_{30}H_{26}O_3N_3$: m/z = 476.19687 $[M+H]^+$,
found: m/z = 476.19657 $[M+H]^+$.

(6'-isopropoxy-4,6-dimethoxy-[3,3'-bipyridin]-5-yl)(naphthalen-1-yl)methanone (561)

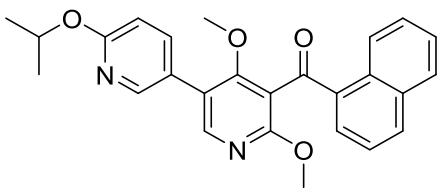

Alcohol **534** (32 mg, 73 µmol) was reacted according to GP IV. The crude product was purified by flash chromatography on silica gel (30% EtOAc/PE) and the product (30 mg, 69 µmol, 94%) was obtained as a colorless wax.

R_f: 0.44 (30% EtOAc/PE).

^{1}H NMR (500 MHz, $CDCl_3$) δ = 9.23 (d, ^3J = 8.7 Hz, 1H), 8.28 (d, ^4J = 1.9 Hz, 1H), 8.15 (s, 1H), 8.06 (d, ^3J = 8.2 Hz, 1H), 7.93 (d, ^3J = 8.1 Hz, 1H), 7.84 (dd, $^{3,4}J$ = 7.2 Hz, 1.0, 1H), 7.75 (dd, $^{3,4}J$ = 8.6, 2.4 Hz, 1H), 7.73 – 7.69 (m, 1H), 7.61 – 7.58 (m, 1H), 7.49 – 7.45 (m, 1H), 6.75 (d, ^3J = 8.6 Hz, 1H), 5.35 (hept, ^3J = 6.2 Hz, 1H), 3.87 (s, 3H), 3.47 (s, 3H), 1.38 (d, ^3J = 6.2 Hz, 6H). ^{13}C NMR (126 MHz, $CDCl_3$) δ = 195.58, 163.15, 163.03, 162.00, 148.42, 146.17, 139.71, 134.66, 134.21, 134.18, 132.94, 130.94, 128.97, 128.66, 126.83, 126.31, 124.55, 123.53, 121.42, 116.64, 111.56, 68.66, 61.10, 54.28, 22.24.

ESI-MS: m/z = 429.01 $[M+H]^+$.

HRMS (ESI): calculated for $C_{26}H_{25}O_4N_2$: m/z = 429.18088 $[M+H]^+$,
found: m/z = 429.18046 $[M+H]^+$.

(2,4-dimethoxy-5-(2-methoxyphenyl)pyridin-3-yl)(3,5-dimethoxy phenyl)methanone (562)

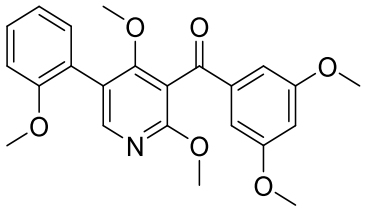

Alcohol **538** (25 mg, 62 µmol) was reacted according to GP IV. The crude product was purified by flash chromatography on silica gel (50% EtOAc/PE) and the product (24 mg, 58 µmol, 94%) was obtained as a colorless wax.

R_f: 0.56 (50% EtOAc/PE).

^{1}H NMR (500 MHz, $CDCl_3$) δ = 8.06 (s, 1H), 7.38 – 7.35 (m, 1H), 7.28 (dd, $^{3,4}J$ = 7.5, 1.6 Hz, 1H), 7.07 (d, ^4J = 2.3 Hz, 2H), 7.03 – 7.00 (m, 1H), 6.97 (d, ^3J = 8.2 Hz, 1H), 6.68 (t, ^4J = 2.2 Hz, 1H), 3.91 (s, 3H), 3.83 (s, 6H), 3.80 (s, 3H), 3.39 (s, 3H). ^{13}C NMR (126 MHz, $CDCl_3$) δ = 193.74, 164.02, 161.50, 161.06, 157.34, 149.70, 139.50, 131.47, 129.68, 124.28, 120.76, 120.65, 113.59, 111.02, 107.47, 106.09, 60.69, 55.73, 55.69, 54.35.

ESI-MS: m/z = 410.17 $[M+H]^+$.

HRMS (ESI): calculated for $C_{23}H_{24}O_6N$: m/z = 410.15981 $[M+H]^+$,
found: m/z = 410.15889 $[M+H]^+$.

(5-(1-benzyl-1H-pyrazol-4-yl)-2,4-dimethoxypyridin-3-yl) (naphthalen-2-yl)methanone (117)

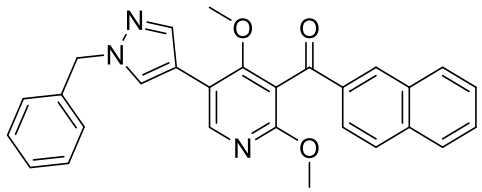

Alcohol **116** (26 mg, 58 µmol) was reacted according to GP IV. The crude product was purified by flash chromatography on silica gel (50% EtOAc/PE) and the product (26 mg, 57 µmol, 98%) was obtained as a colorless oil.

R_f: 0.33 (50% EtOAc/PE).

^{1}H NMR (500 MHz, $CDCl_3$) δ = 8.36 (s, 1H), 8.28 (s, 1H), 8.04 (dd, $^{3,4}J$ = 8.6, 1.5 Hz, 1H), 7.94 – 7.88 (m, 4H), 7.74 (s, 1H), 7.63 – 7.60 (m, 1H), 7.55 – 7.52 (m, 1H), 7.37 – 7.31 (m, 3H), 7.27 (d, ^3J = 8.1 Hz, 2H), 5.36 (s, 2H), 3.87 (s, 3H), 3.64 (s, 3H). ^{13}C NMR (126 MHz, $CDCl_3$) δ = 193.75, 162.61, 161.06, 145.95, 138.07, 136.34, 136.21, 134.91, 132.70, 132.35, 129.97, 129.08, 129.04, 128.86, 128.38, 128.33, 127.99, 127.90, 127.01, 124.34, 116.48, 115.40, 114.23, 60.98, 56.41, 54.64.

ESI-MS: m/z = 450.20 $[M+H]^+$.

HRMS (ESI): calculated for $C_{28}H_{24}O_3N_3$: m/z = 450.18122 $[M+H]^+$,
found: m/z = 450.18090 $[M+H]^+$.

(5-(1-benzyl-1H-pyrazol-4-yl)-2,4-dimethoxypyridin-3-yl)
(4-(trifluoromethyl)phenyl)methanone (150)

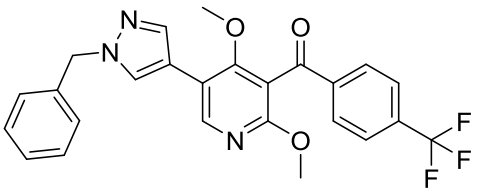

Alcohol **149** (27 mg, 58 µmol) was reacted according to GP IV. The crude product was purified by flash chromatography on silica gel (30% EtOAc/PE) and the product (25 mg, 53 µmol, 92%) was obtained as a colorless oil.

R_f: 0.22 (30% EtOAc/PE).

^{1}H NMR (500 MHz, $CDCl_3$) δ = 8.33 (s, 1H), 7.98 (d, *J* = 8.2 Hz, 2H), 7.85 (s, 1H), 7.73 (d, *J* = 8.3 Hz, 2H), 7.70 (s, 1H), 7.38 – 7.29 (m, 3H), 7.29 – 7.23 (m, *J* = 5.7 Hz, 2H), 5.36 (s, 2H), 3.85 (s, 3H), 3.58 (s, 3H).

ESI-MS: m/z = 468.14 $[M+H]^+$.

HRMS (ESI): calculated for $C_{25}H_{21}O_3N_3F_3$: m/z = 468.15295 $[M+H]^+$,
found: m/z = 468.15250 $[M+H]^+$.

(2,4-dimethoxy-5-(thiophen-2-yl)pyridin-3-yl)(3,5-dimethoxy phenyl)methanone (563)

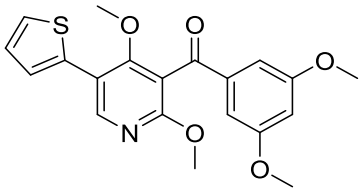

Alcohol **542** (14 mg, 36 µmol) was reacted according to GP IV. The crude product was purified by flash chromatography on silica gel (30% EtOAc/PE) and the product (13 mg, 35 µmol, 96%) was obtained as a yellow oil.

R_f: 0.48 (30% EtOAc/PE).

^{1}H NMR (400 MHz, $CDCl_3$) δ = 8.40 (s, 1H), 7.37 (dd, $^{3,4}J$ = 5.1, 1.2 Hz, 1H), 7.35 (dd, $^{3,4}J$ = 3.7, 1.2 hz, 1H), 7.10 (dd, $^{3,3}J$ = 5.1, 3.7 Hz, 1H), 7.04 (d, ^4J = 2.3 Hz, 2H), 6.70 (t, ^4J = 2.3 Hz, 1H), 3.90 (s, 3H), 3.82 (s, 6H), 3.66 (s, 3H). ^{13}C NMR (101 MHz, $CDCl_3$) δ = 190.89, 161.16, 158.55, 147.34, 147.25, 140.85, 139.33, 135.51, 127.35, 126.28, 125.95, 118.40, 107.47, 106.35, 61.23, 55.79, 54.61.

ESI-MS: m/z = 386.07 $[M+H]^+$.

HRMS (ESI): calculated for $C_{20}H_{20}O_5NS$: m/z = 386.10567 $[M+H]^+$,
found: m/z = 386.10625 $[M+H]^+$.

(3-(1-benzyl-1H-pyrazol-4-yl)-2,6-dimethoxyphenyl)(naphthalen-2-yl)methanone (182)

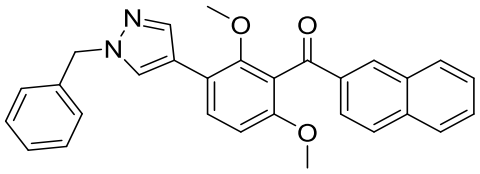

Alcohol **177** (21 mg, 47 µmol) was reacted according to GP IV. The crude product was purified by flash chromatography on silica gel (30% EtOAc/PE) and the product (20 mg, 44 µmol, 94%) was obtained as a colorless oil.

R_f: 0.18 (30% EtOAc/PE).

^{1}H NMR (500 MHz, $CDCl_3$) δ = 8.27 (s, 1H), 8.05 (dd, $^{3,4}J$ = 8.6, 1.6 Hz, 1H), 7.92 – 7.86 (m, 4H), 7.78 (s, 1H), 7.60 – 7.56 (m, 1H), 7.55 (d, ^3J = 8.7 Hz, 1H), 7.52 – 7.48 (m, 1H), 7.36 – 7.28 (m, 3H), 7.27 – 7.23 (m, 2H), 6.82 (d, ^3J = 8.7 Hz, 1H), 5.35 (s, 2H), 3.72 (s, 3H), 3.49 (s, 3H).

^{13}C NMR (126 MHz, $CDCl_3$) δ = 195.05, 156.29, 154.62, 137.72, 135.98, 134.96, 132.62, 132.06, 129.81, 129.54, 129.03, 128.89, 128.58, 128.43, 128.24, 128.22, 127.79, 126.58, 124.41, 124.15, 118.99, 118.30, 107.47, 61.44, 56.14, 56.01, 45.98.

ESI-MS: m/z = 449.05 $[M+H]^+$.

HRMS (ESI): calculated for $C_{29}H_{25}O_3N_2$: m/z = 449.18597 $[M+H]^+$,
found: m/z = 449.18563 $[M+H]^+$.

(5-(1H-indol-5-yl)-2,4-dimethoxypyridin-3-yl)([1,1'-biphenyl]-4-yl) methanone (564)

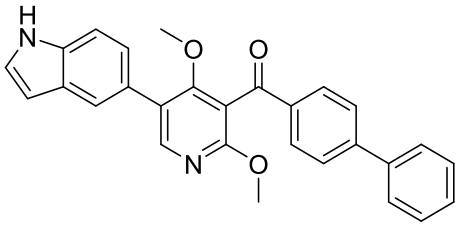

Alcohol **533** (15 mg, 35 µmol) was reacted according to GP IV. The crude product was purified by flash chromatography on silica gel (30% EtOAc/PE) and the product (15 mg, 34 µmol, 96%) was obtained as a red-orange oil.

^{1}H NMR (400 MHz, $CDCl_3$) δ = 8.28 (s, 1H), 7.99 (d, ^3J = 8.2 Hz, 2H), 7.77 (s, 1H), 7.73 (d, ^3J = 8.2 Hz, 2H), 7.65 (d, ^3J = 7.6 Hz, 2H), 7.52 – 7.46 (m, 3H), 7.43 – 7.39 (m, 1H), 7.33 (d, J = 8.4 Hz, 1H), 7.29 – 7.25 (m, 1H), 6.63 – 6.61 (m, 1H), 4.04 (s, 3H), 3.46 (s, 3H).

ESI-MS: m/z = 435.18 $[M+H]^+$.

HRMS (ESI): calculated for $C_{28}H_{23}O_3N_2$: m/z = 435.17032 $[M+H]^+$,
found: m/z = 435.16994 $[M+H]^+$.

(2,4-dimethoxy-5-(quinolin-3-yl)pyridin-3-yl)(naphthalen-1-yl) methanone (565)

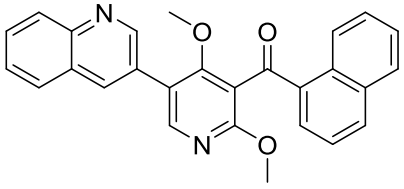

Alcohol **540** (30 mg, 70 µmol) was reacted according to GP IV. The crude product was purified by flash chromatography on silica gel (50% EtOAc/PE) and the product (27 mg, 65 µmol, 92%) was obtained as a colorless wax.

^{1}H NMR (400 MHz, $CDCl_3$) δ = 9.26 (d, ^{3}J = 8.6 Hz, 1H), 9.13 (d, ^{4}J = 2.2 Hz, 1H), 8.37 (d, ^{4}J = 1.7 Hz, 1H), 8.29 (s, 1H), 8.23 (d, ^{3}J = 8.4 Hz, 1H), 8.09 (d, ^{3}J = 8.2 Hz, 1H), 7.95 (d, ^{3}J = 8.1 Hz, 1H), 7.91 (d, ^{3}J = 7.8 Hz, 1H), 7.90 (dd, $^{3,4}J$ = 7.2, 1.2 Hz, 1H), 7.81 – 7.77 (m, 1H), 7.75 – 7.71 (m, 1H), 7.65 – 7.59 (m, 2H), 7.53 – 7.49 (m, 1H), 3.90 (s, 3H), 3.52 (s, 3H). ^{13}C NMR (101 MHz, $CDCl_3$) δ = 195.38, 167.89, 163.10, 162.70, 150.37, 149.05, 140.84, 136.41, 134.90, 134.23, 134.07, 133.19, 130.96, 130.42, 129.11, 128.73, 128.67, 128.46, 128.14, 127.61, 126.92, 126.28, 124.60, 121.05, 116.26, 61.32, 54.46.

ESI-MS: m/z = 421.20 $[M+H]^+$.

HRMS (ESI): calculated for $C_{27}H_{21}O_3N_2$: m/z = 421.15467 $[M+H]^+$,
found: m/z = 421.15404 $[M+H]^+$.

(2,4-dimethoxy-5-(2-methoxyphenyl)pyridin-3-yl)(naphthalen-1-yl)methanone (566)

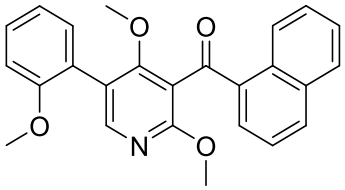

Alcohol **539** (21 mg, 53 µmol) was reacted according to GP IV. The crude product was purified by flash chromatography on silica gel (20% EtOAc/PE) and the product (19 mg, 48 µmol, 91%) was obtained as a colorless oil.

R_f: 0.21 (20% EtOAc/PE).

^{1}H NMR (500 MHz, $CDCl_3$) δ = 9.22 (d, ^{3}J = 8.7 Hz, 1H), 8.10 (s, 1H), 8.04 (d, ^{3}J = 8.2 Hz, 1H), 7.91 (d, ^{3}J = 8.1 Hz, 1H), 7.87 (d, ^{3}J = 7.2 Hz, 1H), 7.71 – 7.68 (m, 1H), 7.60 – 7.57 (m, 1H), 7.49 – 7.46 (m, 1H), 7.38 – 7.35 (m, 1H), 7.31 (d, ^{3}J = 7.5 Hz, 1H), 7.04 – 7.01 (m, 1H), 6.98 (d, ^{3}J = 8.3 Hz, 1H), 3.89 (s, 3H), 3.81 (s, 3H), 3.35 (s, 3H). ^{13}C NMR (126 MHz, $CDCl_3$) δ = 195.87, 163.91, 161.64, 157.29, 149.82, 134.45, 134.36, 134.15, 132.72, 131.56, 130.99, 129.65, 128.77, 128.57, 126.69, 126.42, 124.57, 124.29, 120.92, 120.79, 116.09, 111.08, 60.72, 55.76, 54.28.

ESI-MS: m/z = 400.20 $[M+H]^+$.

HRMS (ESI): calculated for $C_{25}H_{22}O_4N$: m/z = 400.15433 $[M+H]^+$,
found: m/z = 400.15281 $[M+H]^+$.

General procedure V (GP V): Oxidation of the secondary 3 pyridinyl alcohols using Dess-Martin-Periodinane (DMP)

A 20 mM solution of the secondary alcohol (1.0 eq.) in DCM was admixed at rt with a DMP solution (15% in DCM, 2.0 eq.) and stirred for 1 h (reaction control). After the reaction was completed EtOAc, sat. sodium hydrogencarbonate solution (aq.) and solid sodium thiosulfate (75 mg/100 µL of the DMP solution used) were admixed to the reaction solution, and the mixture was stirred briefly until both layers clarified. After separating the two layers, the aqueous layer was extracted with EtOAc and the combined organic layers were washed with sat. sodium chloride solution (aq.) and subsequently dried over anhydrous magnesium sulfate. The product was obtained by flash chromatography of the crude product which has been concentrated *in vacuo*.

Representative example:

(5-(benzo[d][1,3]dioxol-5-yl)-2,4-dimethoxypyridin-3-yl) (naphthalen-2-yl)methanone (132)

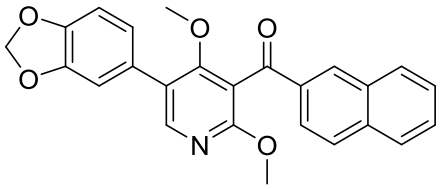

A solution of alcohol **131** (12 mg, 28 µmol) in DCM (1.40 mL) was admixed at rt with DMP solution (15% in DCM, 157 µL, 55 µmol). After stirring for 2 h, the reaction solution was washed successively with EtOAc (30 mL), sat. sodium hydrogencarbonate solution (aq.) (10 mL) and solid sodium thiosulfate (120 mg) and the mixture was stirred briefly until both phases appeared clear. After separation of the two layers, the aqueous layer was extracted with EtOAc (20 mL), the combined organic layers were washed with sat. sodium chloride solution (15 mL) and then dried over anhydrous magnesium sulfate. The solvent was completely removed *in vacuo* and the crude productwas purified by means of flash chromatography on silica gel (20% EtOAc/PE). The product (9 mg, 22 µmol, 80%) was obtained as a yellow wax.

R_f: 0.40 (30% EtOAc/PE).

^{1}H NMR (500 MHz, $CDCl_3$) δ = 8.31 (s, 1H), 8.18 (s, 1H), 8.06 (d, ^3J = 8.6 Hz, 1H), 7.94 (d, ^3J = 8.4 Hz, 2H), 7.90 (d, ^3J = 8.1 Hz, 1H), 7.63 – 7.60 (m, 1H), 7.56 – 7.53 (m, 1H), 7.03 (s, 1H), 6.99 (d, ^3J = 7.9 Hz, 1H), 6.90 (d, ^3J = 8.0 Hz, 1H), 6.01 (s, 2H), 3.90 (s, 3H), 3.47 (s, 3H). ^{13}C NMR (126 MHz, $CDCl_3$) δ = 193.69, 163.63, 161.54, 148.60, 148.04, 147.53, 136.23, 134.96, 132.76, 132.26, 129.97, 129.00, 128.79, 128.58, 128.02, 126.98, 124.46, 122.71, 114.77, 109.72, 108.73, 101.39, 61.14, 54.54, 29.86.

ESI-MS: m/z = 414.20 $[M+H]^+$.

HRMS (ESI): calculated for $C_{25}H_{20}O_5N$: m/z = 414.13360 $[M+H]^+$,
found: m/z = 414.13277 $[M+H]^+$.

[1,1'-biphenyl]-4-yl(2,4-dimethoxy-5-(2-methoxyphenyl)pyridin-3-yl)methanone (567)

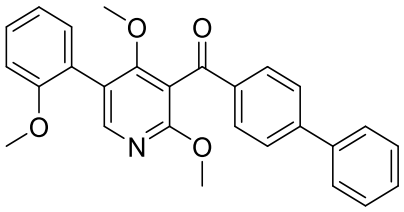

Alcohol **530** (32 mg, 74 µmol) was reacted according to GP V. The crude product was purified by flash chromatography on silica gel (30% EtOAc/PE) and the product (23 mg, 53 µmol, 72%) was obtained as a colorless wax.

R_f: 0.38 (30% EtOAc/PE).

^{1}H NMR (500 MHz, $CDCl_3$) δ = 8.10 (s, 1H), 8.00 (d, ^3J = 8.3 Hz, 2H), 7.70 (d, ^3J = 8.3 Hz, 2H), 7.64 (d, ^3J = 7.5 Hz, 2H), 7.49 – 7.46 (m, 2H), 7.42 – 7.36 (m, 2H), 7.31 (dd, $^{3,4}J$ = 7.4, 1.4 Hz, 1H), 7.05 – 7.02 (m, 1H), 6.99 (d, ^3J = 8.3 Hz, 1H), 3.93 (s, 3H), 3.82 (s, 3H), 3.42 (s, 3H). ^{13}C NMR (126 MHz, $CDCl_3$) δ = 193.60, 164.11, 161.64, 157.36, 149.82, 146.47, 140.11, 136.34, 131.54, 130.24, 129.69, 129.09, 128.42, 127.46, 124.35, 120.82, 113.85, 111.10, 60.79, 55.77, 54.29.

ESI-MS: m/z = 426.20 $[M+H]^+$.

HRMS (ESI): calculated for $C_{27}H_{24}O_4N$: m/z = 426.16998 $[M+H]^+$,
found: m/z = 426.16939 $[M+H]^+$.

***tert*-butyl 4-(4-(2,4-dimethoxy-5-(quinolin-3-yl)nicotinoyl)phenyl)piperazin-1-carboxylate (568)**

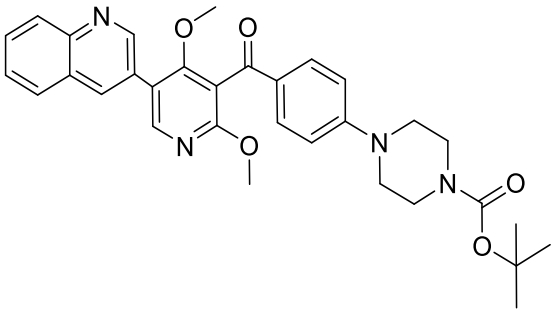

Alcohol **522** (63 mg, 112 µmol) was reacted according to GP V. The crude product was purified by flash chromatography on silica gel (2% MeOH/DCM) and the product (42 mg, 76 µmol, 68%) was obtained as a yellow wax.

R_f: 0.27 (4% MeOH/DCM).

^{1}H NMR (500 MHz, $CDCl_3$) δ = 9.35 (s, 1H), 8.65 (s, 1H), 8.46 (d, ^3J = 8.6 Hz, 1H), 8.24 (s, 1H), 8.06 (d, ^3J = 8.0 Hz, 1H), 7.97 – 7.92 (m, 1H), 7.82 (d, ^3J = 8.8 Hz, 2H), 7.79 (d, ^3J = 7.5 Hz, 1H), 6.88 (d, ^3J = 9.1 Hz, 2H), 3.91 (s, 3H), 3.66 (s, 3H), 3.62 – 3.57 (m, 4H), 3.43 – 3.39 (m, 4H), 1.48 (s, 9H). ^{13}C NMR (126 MHz, $CDCl_3$) δ = 191.27, 163.61, 162.28, 154.79, 154.62, 148.20, 147.44, 141.03, 132.90, 132.05, 129.64, 129.38, 128.72, 128.44, 127.93, 124.30, 118.71, 113.61, 113.07, 80.45, 60.91, 54.58, 47.04, 28.55.

ESI-MS: m/z = 555.01 $[M+H]^+$.

HRMS (ESI): calculated for $C_{32}H_{35}O_5N_4$: m/z = 555.26020 $[M+H]^+$,
found: m/z = 555.26014 $[M+H]^+$.

benzofuran-2-yl(6'-(benzyloxy)-4,6-dimethoxy-[3,3'-bipyridin]-5-yl)methanone (569)

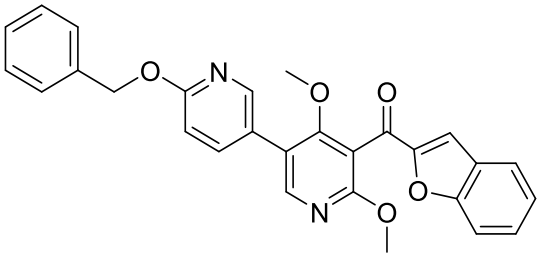

Alcohol **526** (21 mg, 45 µmol) was reacted according to GP V. The crude product was purified by flash chromatography on silica gel (20% EtOAc/PE) and the product (18 mg, 39 µmol, 86%) was obtained as a yellow oil.

R_f: 0.26 (20% EtOAc/PE).

^{1}H NMR (500 MHz, $CDCl_3$) δ = 8.31 (d, ^4J = 2.4 Hz, 1H), 8.17 (s, 1H), 7.78 (dd, $^{3,4}J$ = 8.6, 2.5 Hz, 1H), 7.71 (d, ^3J = 7.8 Hz, 1H), 7.61 (d, ^3J = 8.5 Hz, 1H), 7.53 – 7.47 (m, 3H), 7.43 (s, 1H), 7.42 – 7.37 (m, 2H), 7.36 – 7.30 (m, 2H), 6.90 (d, ^3J = 8.6 Hz, 1H), 5.44 (s, 2H), 3.92 (s, 3H), 3.58 (s, 3H). ^{13}C NMR (126 MHz, $CDCl_3$) δ = 182.74, 163.81, 163.34, 162.34, 156.40, 153.29, 149.11, 146.40, 139.71, 137.29, 128.96, 128.65, 128.16, 128.08, 127.28, 124.22, 124.09, 123.71, 121.26, 116.28, 113.54, 112.85, 111.27, 68.03, 61.49, 54.36

ESI-MS: m/z = 466.97 $[M+H]^+$.

HRMS (ESI): calculated for $C_{28}H_{23}O_5N_2$: m/z = 476.16015 $[M+H]^+$,
found: m/z = 476.16122 $[M+H]^+$.

(2,4-dimethoxy-5-(quinolin-3-yl)pyridin-3-yl)(4-(trifluoromethyl)phenyl)methanone (570)

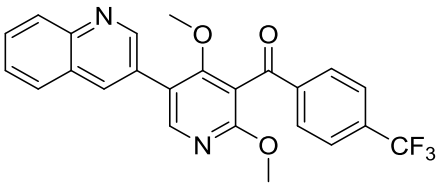

Alcohol **525** (21 mg, 45 µmol) was reacted according to GP V. The crude product was purified by flash chromatography on silica gel (30% EtOAc/PE) and the product (18 mg, 39 µmol, 85%) was obtained as a colorless oil.

R_f: 0.14 (30% EtOAc/PE).

^{1}H NMR (500 MHz, $CDCl_3$) δ = 9.08 (d, ^4J = 2.2 Hz, 1H), 8.31 (s, 1H), 8.30 (d, ^4J = 1.9 Hz, 1H), 8.18 (d, ^3J = 8.5 Hz, 1H), 8.05 (d, ^3J = 8.1 Hz, 2H), 7.89 (d, ^3J = 8.2 Hz, 1H), 7.80 – 7.75 (m, 3H), 7.64 – 7.59 (m, 1H), 3.92 (s, 3H), 3.50 (s, 3H). ^{13}C NMR (126 MHz, $CDCl_3$) δ = 192.69, 163.82, 162.45, 150.79, 149.78, 147.28, 140.00, 135.72, 135.32, 135.06, 131.03, 130.14, 129.87, 129.33, 128.11, 128.04, 128.02, 127.41, 126.03 (q, ^3J (C,F) = 3.6 Hz), 124.80, 122.63, 121.46, 113.67, 61.62, 54.45.

ESI-MS: m/z = 439.12 $[M+H]^+$.

HRMS (ESI): calculated for $C_{24}H_{18}O_3N_2F_3$: m/z = 439.12640 $[M+H]^+$,
found: m/z = 439.12617 $[M+H]^+$.

benzofuran-2-yl(2,4-dimethoxy-5-(quinolin-3-yl)pyridin-3-yl) methanone (571)

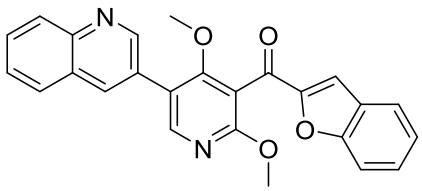

Alcohol **547** (44 mg, 106 µmol) was reacted according to GP V. The crude product was purified by flash chromatography on silica gel (30% EtOAc/PE) and the product (35 mg, 86 µmol, 81%) was obtained as a yellow wax.

R_f: 0.20 (30% EtOAc/PE).

^{1}H NMR (500 MHz, $CDCl_3$) δ = 9.11 (d, ^4J = 2.1 Hz, 1H), 8.36 (d, ^4J = 1.7 Hz, 1H), 8.30 (s, 1H), 8.24 (d, ^3J = 8.5 Hz, 1H), 7.91 (d, ^3J = 8.1 Hz, 1H), 7.82 – 7.76 (m, 1H), 7.73 (d, ^3J = 7.9 Hz, 1H), 7.66 – 7.60 (m, 2H), 7.54 – 7.49 (m, 1H), 7.48 (s, 1H), 7.36 – 7.31 (m, 1H), 3.95 (s, 3H), 3.61 (s, 3H). ^{13}C NMR (126 MHz, $CDCl_3$) δ = 182.59, 163.74, 162.95, 156.43, 153.25, 150.24, 149.66, 136.46, 130.48, 129.07, 128.65, 128.27, 128.14, 128.11, 127.65, 127.24, 124.29, 123.76, 120.92, 116.37, 113.15, 112.85, 61.64, 54.51.

ESI-MS: m/z = 411.13 $[M+H]^+$.

HRMS (ESI): calculated for $C_{25}H_{19}O_4N_2$: m/z = 411.13393 $[M+H]^+$,
found: m/z = 411.13378 $[M+H]^+$.

(5-(1-benzyl-1H-pyrazol-4-yl)-2-methoxypyridin-3-yl) (naphthalen-2-yl)methanone (179)

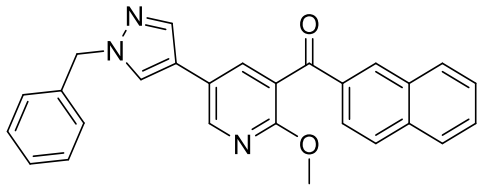

Alcohol **174** (24 mg, 58 µmol) was reacted according to GP V. The crude product was purified by flash chromatography on silica gel (30% EtOAc/PE) and the product (22 mg, 52 µmol, 90%) was obtained as a yellow oil.

R_f: 0.21 (30% EtOAc/PE).

^{1}H NMR (500 MHz, $CDCl_3$) δ = 8.47 (d, ^4J = 2.4 Hz, 1H), 8.24 (s, 1H), 7.97 – 7.93 (m, 1H), 7.92 – 7.87 (m, 3H), 7.83 (d, ^4J = 2.4 Hz, 1H), 7.80 (s, 1H), 7.64 – 7.59 (m, 2H), 7.56 – 7.51 (m, 1H), 7.39 – 7.30 (m, 3H), 7.29 – 7.23 (m, 1H), 7.19 – 7.13 (m, 1H), 5.35 (s, 2H), 3.88 (s, 3H). ^{13}C NMR (126 MHz, $CDCl_3$) δ = 194.68, 159.96, 145.74, 136.77, 136.46, 135.96, 134.65, 132.60, 132.28, 129.84, 129.18, 129.11, 128.85, 128.48, 128.37, 128.01, 127.97, 126.92, 126.24, 125.00, 123.07, 122.36, 119.43, 56.55, 54.11.

ESI-MS: m/z = 420.04 $[M+H]^+$.

HRMS (ESI): calculated for $C_{27}H_{22}O_2N_3$: m/z = 420.17065 $[M+H]^+$,
found: m/z = 420.17080 $[M+H]^+$.

(5-bromo-2,4-dimethoxypyridin-3-yl)(4-isopropylphenyl) methanone (572)

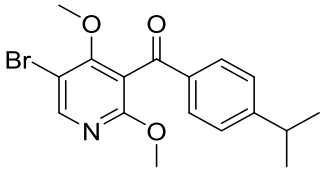

Alcohol **502** (380 mg, 1.04 mMol) was reacted according to GP V. The crude product was purified by flash chromatography on silica gel (10% EtOAc/PE) and the product (306 mg, 839 µmol, 81%) was obtained as a colorless wax.

R_f: 0.27 (10% EtOAc/PE).

^{1}H NMR (500 MHz, $CDCl_3$) δ = 8.27 (s, 1H), 7.76 (d, ^3J = 8.3 Hz, 2H), 7.30 (d, ^3J = 8.3 Hz, 2H), 3.80 (s, 3H), 3.78 (s, 3H), 2.95 (hept, ^3J = 6.9 Hz, 1H), 1.25 (d, ^3J = 6.9 Hz, 6H). ^{13}C NMR (126 MHz, $CDCl_3$) δ = 191.99, 161.65, 161.61, 155.63, 149.53, 134.94, 129.75, 126.90, 115.51, 106.53, 61.49, 54.24, 34.34, 23.57.

ESI-MS: m/z = 364.05, 365.99 $[M+H]^+$.

HRMS (ESI): calculated for $C_{17}H_{19}O_3N\,^{79}Br$: m/z = 364.05428 $[M+H]^+$,
found: m/z = 364.05568 $[M+H]^+$.
calculated for $C_{17}H_{19}O_3N\,^{81}Br$: m/z = 366.05224 $[M+H]^+$,
found: m/z = 366.05284 $[M+H]^+$.

(±)-5'-((4-isopropylphenyl)(methoxy)methyl)-2,4',6'-trimethoxy-3,3'-bipyridine (573)

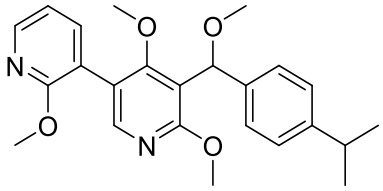

A solution of alcohol **529** (18 mg, 46 µmol) in dry THF (2 mL) was treated with sodium hydride (60% in mineral oil, 11 mg, 461 µmol) and stirred for 3 h at rt Subsequently trimethyloxonium tetrafluoro-borate (68 mg, 461 µmol) was added to the solution and the mixture was stirred for a further 16 h at rt. Ammonium chloride sol. (aq., 10 mL) and sodium carbonate sol. (aq., 2 M, 10 mL) were added to the reaction mixture and the two layers were separated. The aqueous layer was extracted three times with EtOAc (20 mL) and the combined organic layers were dried over magnesium sulfate. The solvent was removed under reduced pressure and the residue purified by flash chromatography (20% EtOAc/PE) on silica gel. The product (19 mg, 46 µmol, quantitative) was obtained as a colorless oil.

R_f: 0.32 (30% EtOAc/PE).

^{1}H NMR (500 MHz, $CDCl_3$) δ = 8.19 – 8.17 (m, 1H), 8.05 (s, 1H), 7.61 – 7.59 (m, 1H), 7.34 (d, ^3J = 8.1 Hz, 2H), 7.16 (d, ^3J = 8.2 Hz, 2H), 6.95 – 6.92 (m, 1H), 5.90 (s, 1H), 3.99 (s, 3H), 3.93 (s, 3H), 3.47 (d, ^4J = 1.8 Hz, 3H), 3.09 (s, 3H), 2.87 (hept, ^3J = 6.9 Hz, 1H), 1.22 (d, ^3J = 6.9 Hz, 6H). ^{13}C NMR (126 MHz, $CDCl_3$) δ = 165.67, 163.09, 161.37, 148.77, 147.46, 146.59, 140.04, 139.15, 126.11, 126.03, 120.04, 118.67, 116.93, 116.33, 76.55, 60.59, 57.78, 54.35, 53.83, 33.90, 24.18.

ESI-MS: m/z = 409.20 $[M+H]^+$.

HRMS (ESI): calculated for $C_{24}H_{29}O_4N_2$: m/z = 409.21218 $[M+H]^+$,
found: m/z = 409.21112 $[M+H]^+$.

(±)-3-(fluoro(4-isopropylphenyl)methyl)-
2,4-dimethoxy-5-(2-methoxyphenyl)pyridine (574)

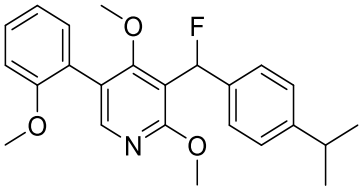

A solution of Alcohol **531** (12 mg, 29 µmol) in dry DCM (3 mL) was slowly admixed with DAST (15 µL, 117 µmol) at -78 °C and stirred at this temperature for 1 h. The reaction mixture was then brought to rt overnight. The reaction mixture was subsequently treated successively with 5 mL of water and 15 mL of EtOAc. After stirring for 15 min, the aqueous layer was extracted three times with in each case 7 mL of EtOAc. The combined organic layers were washed with 4 mL sat. sodium chloride solution (aq.) followed by drying over anhydrous magnesium sulfate. The solvent was completely removed under reduced pressure and the crude product purified by flash chromatography (20% EtOAc/PE) on silica gel. The product (12 mg, 28 µmol, 95%) was obtained as a colorless oil.

R_f: 0.15 (20% EtOAc/PE).

^{1}H NMR (400 MHz, $CDCl_3$) δ = 8.04 (d, J = 1.1 Hz, 1H), 7.34 (d, ^3J = 8.3 Hz, 3H), 7.20 (d, ^3J = 8.2 Hz, 2H), 7.03 (d, ^2J (H,F) = 35.2 Hz, 1H), 7.02 – 7.00 (m, 2H), 6.96 (d, ^4J = 2.8 Hz, 1H), 3.98 (s, 3H), 3.79 (s, 3H), 3.21 (s, 3H), 2.90 (hept, ^3J = 6.9 Hz, 1H), 1.24 (d, ^3J = 6.9 Hz, 6H).

ESI-MS: m/z = 396.13 $[M+H]^+$.

HRMS (ESI): calculated for $C_{24}H_{27}O_3NF$: m/z = 396.19695 $[M+H]^+$,
found: m/z = 396.19509 $[M+H]^+$.

(±)-5'-(fluoro(4-isopropylphenyl)methyl)-2,4',6'-trimethoxy-3,3'-bipyridine (575)

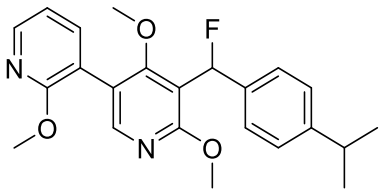

A solution of alcohol **529** (18 mg, 46 µmol) in dry DCM (3 mL) was slowly admixed with DAST (24 µL, 185 µmol) at -78 °C and stirred at this temperature for 1 h. The reaction mixture was then brought to rt overnight. The reaction mixture was subsequently treated successively with 5 ml of water and 15 ml of EtOAc. After stirring for 15 min, the aqueous layer was extracted three times with in each case 7 ml of EtOAc. The combined organic layers were washed with 4 mL sat. sodium chloride solution (aq.) and then dried over anhydrous magnesium sulfate. The solvent was completely removed under reduced pressure and the crude product purified by flash chromatography (10% EtOAc/PE) on silica gel. The product (18 mg, 42 µmol, 92%) was obtained as a colorless oil.

R_f: 0.17 (20% EtOAc/PE). ^{1}H NMR (400 MHz, $CDCl_3$) δ = 8.24 – 8.22 (m, 1H), 8.05 (s, 1H), 7.63 (dd, $^{3,4}J$ = 7.3 Hz, 1.8, 1H), 7.29 (d, ^3J = 8.2 Hz, 2H), 7.19 (d, ^3J = 8.2 Hz, 2H), 7.01 – 6.97 (m, 1H), 6.12 (d, ^2J (H,F) = 37.7 Hz, 1H), 4.03 (s, 3H), 3.97 (s, 3H), 3.26 (s, 3H), 2.89 (hept, ^3J = 6.9 Hz, 1H), 1.23 (d, ^3J = 6.9 Hz, 6H).

ESI-MS: m/z = 397.13 $[M+H]^+$.

HRMS (ESI): calculated for $C_{23}H_{26}O_3N_2F$: m/z = 397.19220 $[M+H]^+$,
found: m/z = 397.19059 $[M+H]^+$.

(±)-3-(5-(azido(naphthalen-2-yl)methyl)-4,6-dimethoxypyridin-3-yl)quinoline (576)

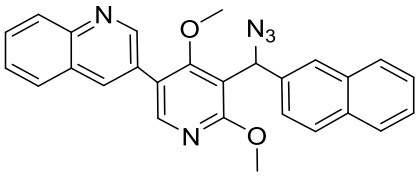

DBU (68 µL, 454 µmol) was added to a solution of alcohol **120** (32 mg, 76 µmol) and DPPA (98 µL, 454 µmol) in 1 mL toluene at 0 °C. After the addition was complete, the reaction solution was stirred at 0 °C for 1 h and then brought to rt and stirred overnight. The next day it was heated to 60 °C and stirred at this temperature for a further 16 h. The reaction was then stopped by the addition of 3 mL of water and 3 mL of EtOAc. The two layers were separated from one another and the aqueous layer was extracted three times with in each case 3 mL EtOAc. The combined organic layers were dried over anhydrous magnesium sulfate and concentrated *in vacuo*. The crude was purified by flash chromatography on silica gel (30% EtOAc/PE). The product was obtained as a white solid (32 mg, 72 µmol, 95%).

R_f: 0.42 (50% EtOAc/PE).

^{1}H NMR (500 MHz, $CDCl_3$) δ = 9.09 (s, 1H), 8.31 (s, 1H), 8.25 (s, 1H), 8.16 (d, ^3J = 8.4 Hz, 1H), 7.91 (s, 1H), 7.89 – 7.80 (m, 4H), 7.76 (t, ^3J = 7.6 Hz, 1H), 7.60 (t, ^3J = 7.5 Hz, 1H), 7.51 – 7.44 (m, 3H), 6.51 (s, 1H), 4.03 (s, 3H), 3.14 (s, 3H). ^{13}C NMR (126 MHz, $CDCl_3$) δ = 165.24, 163.30, 150.59, 149.27, 147.38, 136.29, 135.27, 133.31, 132.82, 130.01, 129.41, 128.49, 128.24, 128.19, 128.07, 128.02, 127.76, 127.36, 126.43, 126.19, 125.43, 124.81, 122.00, 114.81, 61.32, 59.14, 54.47.

ESI-MS: m/z = 447.91 $[M+H]^+$.

HRMS (ESI): calculated for $C_{27}H_{22}O_2N_5$: m/z = 488.17680 $[M+H]^+$,
found: m/z = 448.17761 $[M+H]^+$.

(2-methoxy-4-methyl-5-(quinolin-3-yl)pyridin-3-yl)(naphthalen-2-yl)methanol (577)

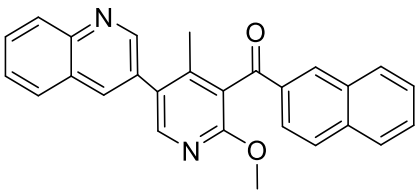

A solution of ketone **121** (24 mg, 57 µmol) in 1 mL abs. THF was treated slowly with methylmagnesium bromide (27 µL, 80 µmol, 3M in diethyl ether) at 0 °C and stirred at this temperature for 1 h. The reaction mixture was then brought to rt and stirred for 3 h. Thereafter, the reaction mixture was washed successively with 4 mL of water, 4 mL of sat. ammonium chloride solution and 30 mL of EtOAc. After stirring for 10 min, the aqueous layer was extracted three times with in each case 10 ml of EtOAc. The combined organic layers were washed with. sat. sodium chloride solution (aq.) and dried over magnesium sulfate. The solvent was removed under reduced pressure and the residue was purified by flash chromatography on silica gel (20% EtOAc/PE). The product (24 mg, 58 µmol, quantitative) was obtained as a yellow oil.

R_f: 0.35 (50% EtOAc/PE).

^{1}H NMR (600 MHz, $CDCl_3$) δ = 8.96 (d, ^{4}J = 1.9 Hz, 1H), 8.28 (s, 1H), 8.26 – 8.19 (m, 3H), 8.06 (dd, $^{3,4}J$ = 8.6, 1.7 Hz, 1H), 7.95 (t, ^{3}J = 7.9 Hz, 2H), 7.91 (d, ^{3}J = 8.2 Hz, 2H), 7.84 – 7.78 (m, 1H), 7.68 – 7.61 (m, 2H), 7.59 – 7.54 (m, 1H), 3.91 (s, 3H), 2.16 (s, 3H). ^{13}C NMR (151 MHz, $CDCl_3$) δ = 195.91, 160.91, 150.79, 147.97, 145.32, 137.01, 136.30, 134.27, 132.77, 132.19, 130.75, 130.46, 129.95, 129.16, 129.03, 128.93, 128.49, 128.07, 128.06, 127.89, 127.72, 127.07, 124.29, 123.35, 77.16, 54.12, 17.41.

ESI-MS: m/z = 405.10 $[M+H]^+$.

HRMS (ESI): calculated for $C_{27}H_{21}O_2N_2$: m/z = 405.15975 $[M+H]^+$,
found: m/z = 405.15936 $[M+H]^+$.

(±)-(4,6-dimethoxy-6'-(piperazin-1-yl)-[3,3'-bipyridin]-5-yl)(4-isopropylphenyl)methanol (578)

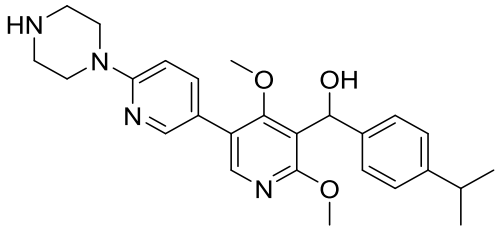

Alcohol **549** (13 mg, 23 µmol) was dissolved in DCM (5 mL) and TFA (5 mL, 65 mMol) was added dropwise at rt. After 20 min, the reaction mixture was concentrated with the aid of an argon stream and the crude product was subsequently purified by means of HPLC (without using TFA). The product (8 mg, 18 µmol, 77%) was obtained as a yellow oil.

R_f: 0.25 (10% MeOH/DCM).

^{1}H NMR (500 MHz, $CDCl_3$) δ = 8.19 – 7.97 (m, 3H), 7.25 – 7.12 (m, 6H), 6.25 – 6.13 (m, 1H), 4.15 – 3.97 (m, 4H), 3.93 (s, 3H), 3.69 – 3.39 (m, 4H), 3.27 (s, 3H), 2.84 (hept, ^{3}J = 6.9 Hz, 1H), 1.19 (d, ^{3}J = 6.9 Hz, 6H). ^{13}C NMR (126 MHz, $CDCl_3$) δ = 163.82, 163.33, 151.96, 148.23, 146.72, 144.85, 140.24, 126.52, 125.68, 122.53, 119.47, 119.04, 117.22, 114.87, 68.07, 61.54, 54.60, 43.63, 42.86, 33.82, 24.02.

ESI-MS: m/z = 449.17 $[M+H]^+$.

HRMS (ESI): calculated for $C_{26}H_{33}O_3N_4$: m/z = 449.25472 $[M+H]^+$,
found: m/z = 449.25443 $[M+H]^+$.

(±)-3-(4,6-dimethoxy-5-(4-(piperazin-1-yl)benzyl)pyridin-3-yl)quinolone (579)

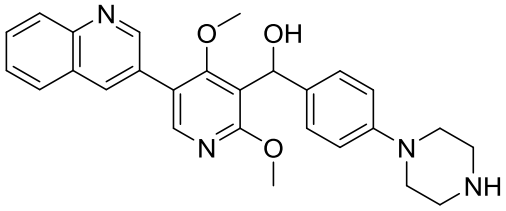

Alcohol **522** (43 mg, 77 µmol) was dissolved in DCM (5 mL) and TFA (5 mL, 65 mMol) was added dropwise at rt After 20 min, the reaction mixture was concentrated to dryness with the aid of an argon stream and the crude product was subsequently purified by means of HPLC (without using TFA). The product (35 mg, 77 µmol, quantitative) was obtained as a yellow oil.

R_f: 0.13 (15% MeOH/DCM).

ESI-MS: m/z = 457.08 $[M+H]^+$.

HRMS (ESI): calculated for $C_{27}H_{29}O_3N_4$: m/z = 457.22342 $[M+H]^+$,
found: m/z = 457.22293 $[M+H]^+$.

(2,4-dimethoxy-5-(quinolin-3-yl)pyridin-3-yl)(4-(piperazin-1-yl)phenyl)methanone (580)

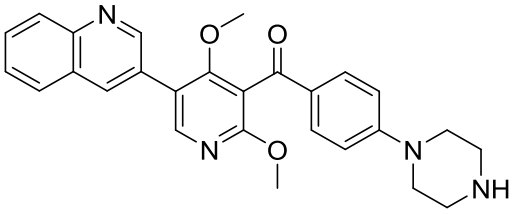

Alcohol **568** (25 mg, 63 µmol) was dissolved in DCM (5 mL) and TFA (5 mL, 65 mMol) was added dropwise at rt After 20 min, the reaction mixture was concentrated to dryness with the aid of an argon stream and the crude product was subsequently purified by means of HPLC (without using TFA). The product (29 mg, 63 µmol, quantitative) was obtained as a red oil.

R_f: 0.15 (10% MeOH/DCM).

^{1}H NMR (500 MHz, MeOD) δ = 10.56 (d, ^4J = 2.1 Hz, 1H), 10.06 (d, ^4J = 1.6 Hz, 1H), 9.89 (s, ^4J = 7.4 Hz, 1H), 9.63 (d, ^3J = 8.5 Hz, 1H), 9.58 (d, ^3J = 8.1 Hz, 1H), 9.40 – 9.34 (m, 3H), 9.26 – 9.19 (m, 1H), 8.62 (d, ^3J = 9.1 Hz, 2H), 5.45 (s, 3H), 5.18 – 5.13 (m, 4H), 5.08 (s, 3H), 4.83 – 4.78 (m, 4H). ^{13}C NMR (126 MHz, MeOD) δ = 221.52, 192.61, 191.87, 183.93, 180.06, 178.18, 175.87, 165.69, 161.09, 159.54, 158.02, 157.79, 157.72, 157.63, 157.15, 156.71, 150.59, 143.76, 143.32, 89.81, 82.78, 74.75, 73.08.

ESI-MS: m/z = 455.12 $[M+H]^+$.

HRMS (ESI): calculated for $C_{27}H_{27}O_3N_4$: m/z = 455.20777 $[M+H]^+$,
found: m/z = 455.20726 $[M+H]^+$.

(±)-(2,4-dimethoxy-5-(quinolin-3-yl)pyridin-3-yl)(naphthalen-2-yl)methanamine (581)

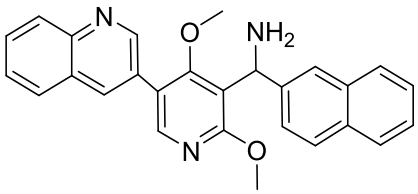

A suspension of azide **576** (16 mg, 36 µmol) in 5 mL abs. MeOH was treated with 200 µL of AcOH and then brought into solution for 30 min by means of ultrasound. The addition of Pd (100 mg, 15% on charcoal) was then carried out. The reaction mixture was placed under a hydrogen atmosphere at atmospheric pressure and stirred at rt for 3 h. The reaction mixture was then filtered through celite and the filtrate was concentrated under reduced pressure. The product (15 mg, 35 µmol, 97%) was isolated by HPLC (without using TFA).

R_f: 0.39 (10% MeOH/DCM).

ESI-MS: m/z = 404.91 $[M\text{-}NH_2]^+$.

HRMS (ESI): calculated for $C_{27}H_{21}O_2N_2$: m/z = 405.15975 $[M\text{-}NH_2]^+$,
found: m/z = 405.15951 $[M+H]^+$.

(±)-(5-(1-benzyl-1H-pyrazol-4-yl)-2,4-dimethoxypyridin-3-yl)(3-ethynylphenyl)methanol (151)

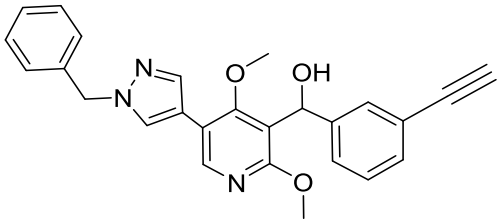

A solution of alcohol **523** (30 mg, 60 µmol) and potassium carbonate (42 mg, 301 µmol) in MeOH (2 ml) was stirred at rt until complete conversion of the reaction (reaction control). The reaction was terminated by addition of 2 mL of water and 6 mL of EtOAc. After separation of the two layers, the aqueous layer was extracted three times with in each case 6 mL EtOAc and the combined organic layers were then dried over magnesium sulfate and then concentrated under reduced pressure. The crude product was purified by flash chromatography on silica gel (50% EtOAc/PE). The product (25 mg, 59 µmol, 97%) was obtained as a colorless wax.

R_f: 0.42 (50% EtOAc/PE).

1H NMR (500 MHz, CDCl3) δ = 8.17 (s, 1H), 7.81 (s, 1H), 7.68 (s, 1H), 7.48 (s, 1H), 7.40 – 7.29 (m, 5H), 7.26 (t, ^3J = 7.6 Hz, 3H), 6.17 (s, 1H), 5.36 (s, 2H), 3.93 (s, 3H), 3.38 (s, 3H), 3.04 (s, 1H). ^{13}C NMR (126 MHz, $CDCl_3$) δ = 163.10, 161.46, 146.19, 144.31, 138.24, 136.44, 130.94, 129.35, 129.04, 128.37, 128.33, 128.07, 127.82, 126.27, 122.06, 118.37, 117.44, 115.71, 83.90, 77.20, 67.82, 60.73, 56.42, 54.14.

ESI-MS: m/z = 426.28 $[M+H]^+$.

HRMS (ESI): calculated for $C_{26}H_{24}O_3N_3$: m/z = 426.18122 $[M+H]^+$,
found: m/z = 426.18119 $[M+H]^+$.

(5-(1-(4-aminobenzyl)-1H-pyrazol-4-yl)-2,4-dimethoxypyridin-3-yl)(naphthalen-2-yl)methanol (125)

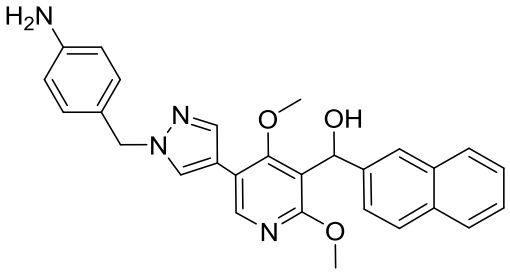

Ammonium formate (18.44 mg, 604 µmol) and 5% Pd/C (11 mg, 10 µmol) were added to a solution of alcohol **115** (25 mg, 50 µmol) in EtOH (4 mL). The suspension was heated for 1 h to 95 °C (oil bath temperature). Afterwards the reaction mixture was filtered over celite and the filtrate was concentrated *in vacuo*. HPLC (without using TFA) provided the product (10 mg, 15 µmol, 29%).

^{1}H NMR (600 MHz, DMSO-d_6) δ = 8.32 (d, J = 0.7 Hz, 1H), 8.17 (s, 1H), 7.91 – 7.77 (m, 5H), 7.48 – 7.38 (m, 3H), 7.32 – 7.26 (m, 2H), 7.18 – 7.12 (m, 2H), 6.34 (s, 1H), 5.33 (s, 2H), 3.80 (s, 3H), 3.48 (s, , 3H). ^{13}C NMR (151 MHz, DMSO-d_6) δ = 163.12, 161.24, 145.13, 142.16, 137.49, 132.71, 131.84, 128.94, 128.64, 127.75, 127.40, 127.04, 125.89, 125.31, 124.35, 123.26, 119.63, 117.28, 114.53, 65.42, 60.57, 53.55.

ESI-MS: m/z = 467.39 $[M+H]^+$.

HRMS (ESI): calculated for $C_{28}H_{27}O_3N_4$: m/z = 467.20777 $[M+H]^+$,
found: m/z = 467.20828 $[M+H]^+$.

***tert*-butyl (3-(2-(2-(3-aminopropoxy)ethoxy)ethoxy)propyl)carbamate (190)**

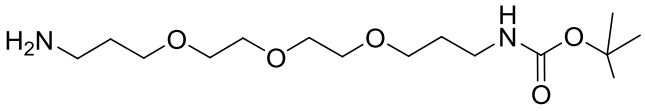

To a vigorously stirred solution of 3,3'-((oxybis(ethane-2,1-diyl))bis(oxy))bis(propan-1-amine) (9.9 mL, 44 mMol) in DCM (200 mL) at room temperature, a solution of Boc_2O (5 g, 23 mMol) in DCM (100 mL) was added using a dropping funnel over a period of 1 hour. The solution was stirred at room temreprature for 16 h and washed with HCl (aq., 0.1 M, 2 x 100 mL). The aqueous layer was extracted with DCM (5 x 50 mL). The combined organic layers were dried over anhydrous magnesium sulfate and dried *in vacuo*. The crude product (containing 60 % of the desired product according to NMR) was used without further purification.

tert-butyl (1-bromo-2-oxo-7,10,13-trioxa-3-azahexadecan-16-yl)carbamate (191)

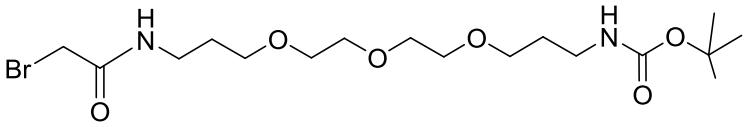

A solution of bromoacetylbromide (272 µl, 3.12 mMol) in abs. THF (20 mL) was cooled to 0°C and to this was added a solution of linker **190** (1.00 g, 1.87 mMol, containing 60 % of the desired starting material according to NMR) and DIPEA (265 µl, 1.56 mMol) in abs. THF (16 mL) over 1 h. The mixture was then warmed to room temperatuer, and stirred for another 1 h. At this point it was diluted with EtOAc (20 mL), and washed with half sat. ammonium chloride solution (aq., 20 mL) and half sat. sodium hydrogen carbonate (aq., 20 mL) and brine (20 mL) The organic layer was dried over anhydrous magnesium sulfate and the solvent removed *in vacuo*. The crude product was purified by silica column chromatography (50% - 100% EtOAc/cyclohexane) to yield the product (777 mg, 1.76 mMol, 94%) as a brown oil.

R_f: 0.23 (EtOAc), R_f: 0.05 (50% EtOAc/cyclohexane).

^{1}H NMR (500 MHz, $CDCl_3$) δ = 7.19 (s, 1H), 4.92 (s, 1H), 3.84 (s, 2H), 3.68 – 3.55 (m, 10H), 3.52 (t, ^3J = 5.9 Hz, 2H), 3.40 (q, ^3J = 5.8 Hz, 2H), 3.20 (t, ^3J = 6.4 Hz, 2H), 1.84 – 1.77 (m, 2H), 1.74 (p, ^3J = 6.2 Hz, 2H), 1.42 (s, 9H). ^{13}C NMR (126 MHz, $CDCl_3$) δ = 165.63, 156.17, 79.16, 70.69, 70.67, 70.50, 70.46, 70.35, 69.64, 39.14, 38.81, 29.82, 29.38, 28.67, 28.58.

ESI-MS: m/z = 440.89 $[M+H]^+$.

HRMS (ESI): calculated for $C_{17}H_{34}O_6N_2\,^{79}Br$: m/z = 441.15948 $[M+H]^+$,
found: m/z = 441.16087 $[M+H]^+$;
calculated for $C_{17}H_{34}O_6N_2\,^{81}Br$: m/z = 443.15743 $[M+H]^+$,
found: m/z = 443.15891 $[M+H]^+$.

(±)-(5-(1-benzyl-1H-pyrazol-4-yl)-2,4-dimethoxypyridin-3-yl)(6-(hydroxymethyl)naphthalen-2-yl)methanol (157)

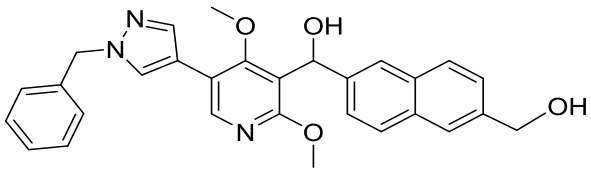

Alcohol **187** (100 mg, 168 µmol) was dissolved in THF (7 mL) and tetra-n-butylammonium fluoride solution (1M in THF, 504 µL, 504 µmol) was added dropwise at 0 °C. The solution was first stirred at 0 °C for 30 min and then at rt until a complete reaction of the starting material took place (reaction control). Subsequently, the reaction solution was mixed with a mixture of sat. sodium chloride solution (aq., 3 mL) and sodium hydrogencarbonate solution (5% w/v, 3 mL). After addition of EtOAc (20 mL), the organic layer was separated off and the aqueous layer was extracted with EtOAc (20 mL). The combined organic layers were washed with sat. sodium chloride solution (20 mL) and dried over anhydrous magnesium sulfate. The solvent was completely removed under reduced pressure and the crude product was purified by means of flash chromatography on silica gel (50% EtOAc/PE). The product (57 mg, 119 µmol, 71%) was obtained as a colorless oil.

R_f: 0.20 (50% EtOAc/PE).

^{1}H NMR (400 MHz, $CDCl_3$) δ = 8.17 (s, 1H), 7.84 – 7.72 (m, 5H), 7.67 (s, 1H), 7.51 – 7.41 (m, 2H), 7.38 – 7.19 (m, 5H), 6.35 (s, 1H), 5.34 (s, 2H), 4.82 (s, 2H), 3.92 (s, 3H), 3.34 (s, 3H). ^{13}C NMR (126 MHz, $CDCl_3$) δ = 163.15, 161.64, 146.08, 141.39, 138.51, 138.18, 136.39, 132.79, 132.67, 129.02, 128.56, 128.35, 128.07, 128.04, 127.81, 125.54, 125.27, 124.80, 123.77, 118.67, 117.44, 115.75, 68.37, 65.47, 60.72, 56.37, 54.12.

ESI-MS: m/z = 482.13 $[M+H]^+$.

HRMS (ESI): calculated for $C_{29}H_{28}O_4N_3$: m/z = 482.20719 $[M+H]^+$,
found: m/z = 482.20767 $[M+H]^+$.

(±)-*tert*-Butyl(1-(6-((5-(1-benzyl-1H-pyrazol-4-yl)-2,4-dimethoxypyridin-3-yl)(hydroxy)methyl)naphthalen-2-yl)-4-oxo-2,9,12,15-tetraoxa-5-azaoctadecan-18-yl)carbamate (192) and (±)-*tert*-butyl(1-(5-(1-benzyl-1H-pyrazol-4-yl)-2,4-dimethoxypyridin-3-yl)-1-(6-(hydroxymethyl)naphthalen-2-yl)-4-oxo-2,9,12,15-tetraoxa-5-azaoctadecan-18-yl)carbamate (193)

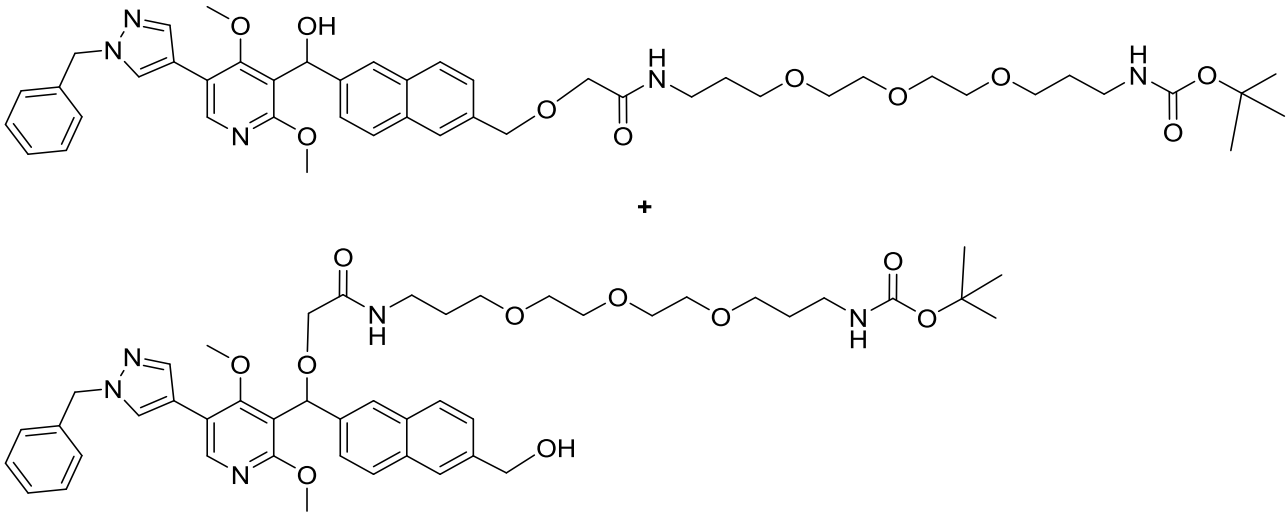

A 0.1 M solution of diol XYZ (LR203A) (180 mg, 374 µmol) in abs. THF (3.8 mL) is admixed dropwise at 0 ° C with a 0.2 M solution of NaH (33 mg, 822 µmol) in abs. THF (4.1 mL). After five minutes the ice bath was removed and the reaction stirred for a further 30 minutes. This was followed by the dropwise addition of a 0.1 M solution of the PEG linker (82 mg, 187 µmol) in abs. THF (1.8 mL) to the reaction mixture, which was beforehand cooled down to -78 ° C. After the addition was complete, the reaction mixture was brought to room temperature with stirring overnight in the cooling bath. Subsequently, the reaction was terminated by adding sat. ammonium chloride solution (aq., 2 mL), water (2 mL) and ethyl acetate (10 mL). The aqueous layer was separated and extracted with ethyl acetate (3 x 10 mL). The combined organic layers were dried over anhydrous magnesium sulfate and the concentrated *in vacuo*. Purification of the crude products was carried out by flash chromatography on silica gel (2 - 4% MeOH/DCM) to give (±)-*tert*-Butyl(1-(6-((5-(1-benzyl-1H-pyrazol-4-yl)-2,4-dimethoxypyridin-3-yl)(hydroxy)methyl)naphthalen-2-yl)-4-oxo-2,9,12,15-tetraoxa-5-azaoctadecan-18-yl)carbamate (LR257S3) (42 mg, 50 µmol, 27%) as a colorless wax and (±)-*tert*-butyl(1-(5-(1-benzyl-1H-pyrazol-4-yl)-2,4-dimethoxypyridin-3-yl)-1-(6-(hydroxymethyl)naphthalen-2-yl)-4-oxo-2,9,12,15-tetraoxa-5-azaoctadecan-18-yl)carbamate (LR257S4) (55 mg, 66 µmol , 35%) as a colorless wax.

(±)-*tert*-Butyl(1-(6-((5-(1-benzyl-1H-pyrazol-4-yl)-2,4-dimethoxypyridin-3-yl)(hydroxy)methyl)naphthalen-2-yl)-4-oxo-2,9,12,15-tetraoxa-5-azaoctadecan-18-yl)carbamate (192):

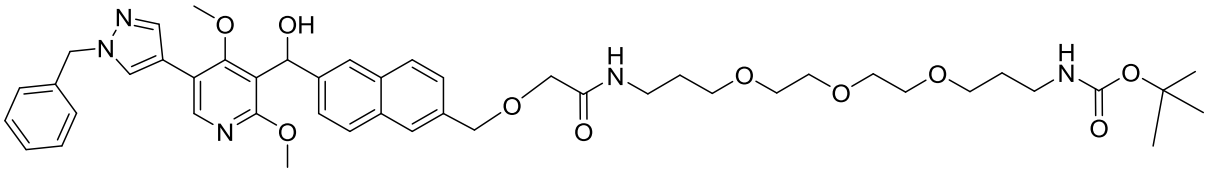

R_f: 0.39 (4% MeOH/DCM).

^{1}H NMR (600 MHz, $CDCl_3$) δ = 8.19 (s, 1H), 7.83 – 7.74 (m, 5H), 7.73 (s, 1H), 7.69 (s, 1H), 7.48 (dd, $^{3,4}J$ = 8.6, 1.6 Hz, 1H), 7.42 (dd, ^3J = 8.4, 1.6 Hz, 1H), 7.36 – 7.28 (m, 3H), 7.26 – 7.21 (m, 2H), 7.01 (s, 1H), 6.35 (s, 1H), 5.35 (s, 2H), 4.99 (s, 1H), 4.70 (s, 2H), 3.98 (s, 2H), 3.93 (s, 3H), 3.56 – 3.46 (m, 12H), 3.42 – 3.37 (m, 2H), 3.36 (s, 3H), 3.21 – 3.16 (m, 2H), 1.83 – 1.75 (m, 2H), 1.75 – 1.68 (m, 2H), 1.42 (s, 9H). ^{13}C NMR (151 MHz, $CDCl_3$) δ = 169.56, 163.25, 161.51, 156.14, 145.92, 141.81, 138.18, 136.38, 134.38, 133.01, 132.45, 129.01, 128.71, 128.34, 128.03, 127.79, 127.77, 126.83, 126.03, 124.95, 123.72, 118.69, 117.50, 115.64, 73.70, 70.60, 70.42, 70.26, 69.88, 69.65, 68.25, 60.76, 56.38, 54.25, 38.62, 37.16, 29.75, 29.34, 28.56.

ESI-MS: m/z = 842.00 $[M+H]^+$, 864.41 $[M+Na]^+$.

HRMS (ESI): calculated for $C_{46}H_{60}O_{10}N_5$: m/z = 842.43347 $[M+H]^+$,
found: m/z = 842.43677 $[M+H]^+$.
calculated for $C_{46}H_{60}O_{10}N_5Na$: m/z = 864.41541 $[M+Na]^+$,
found: m/z = 864.41785 $[M+Na]^+$.

(±)-*tert*-butyl(1-(5-(1-benzyl-1H-pyrazol-4-yl)-2,4-dimethoxypyridin-3-yl)-1-(6-(hydroxymethyl)naphthalen-2-yl)-4-oxo-2,9,12,15-tetraoxa-5-azaoctadecan-18-yl)carbamate (193):

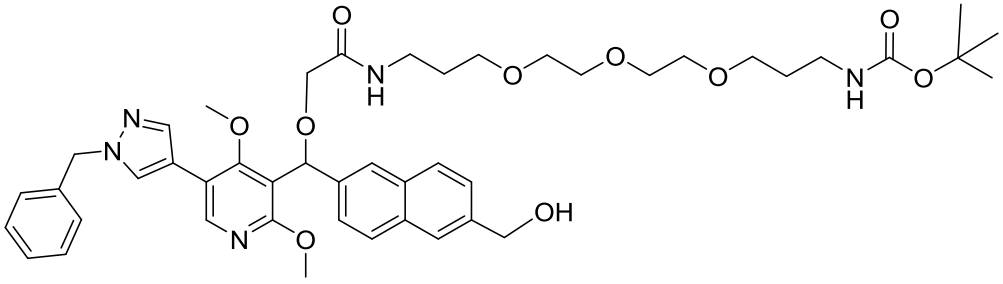

R_f: 0.20 (4% MeOH/DCM).

^{1}H NMR (600 MHz, $CDCl_3$) δ = 8.16 (s, 1H), 7.82 (s, 1H), 7.80 – 7.72 (m, 4H), 7.62 (s, 1H), 7.48 – 7.42 (m, 2H), 7.34 – 7.26 (m, 3H), 7.21 (d, ^{3}J = 7.2 Hz, 2H), 7.13 (t6, ^{3}J = 5.6 Hz, 1H), 6.20 (s, 1H), 5.31 (s, 2H), 5.02 (s, 1H), 4.81 (s, 2H), 4.18, 4.01 (AB system, ^{2}J = 15.2 Hz, 2H), 3.92 (s, 3H), 3.50 – 3.31 (m, 14H), 3.20 (s, 3H), 3.18 – 3.14 (m, 1H), 1.77 (p, ^{3}J = 6.5 Hz, 2H), 1.73 – 1.66 (m, 2H), 1.41 (s, 9H). ^{13}C NMR (151 MHz, $CDCl_3$) δ = 169.90, 164.68, 162.24, 147.22, 138.85, 138.17, 138.15, 136.34, 132.68, 132.61, 128.97, 128.35, 128.30, 128.06, 127.85, 127.73, 125.65, 125.18, 124.65, 124.39, 117.43, 115.66, 115.49, 77.37, 77.16, 76.95, 75.51, 70.50, 70.31, 70.20, 69.33, 69.01, 65.20, 60.37, 56.31, 54.25, 36.79, 29.55, 28.54, 21.13, 14.28.

ESI-MS: m/z = 841.90 $[M+H]^+$.

HRMS (ESI): calculated for $C_{46}H_{60}O_{10}N_5$: m/z = 842.43347 $[M+H]^+$,
found: m/z = 842.43646 $[M+H]^+$.

(±)-*N*-(3-(2-(2-(3-aminopropoxy)ethoxy)ethoxy)propyl)-2-((6-((5-(1-benzyl-1H-pyrazol-4-yl)-2,4-dimethoxypyridin-3-yl)(hydroxy)methyl)naphthalen-2-yl)methoxy)acetamide • TFA (194)

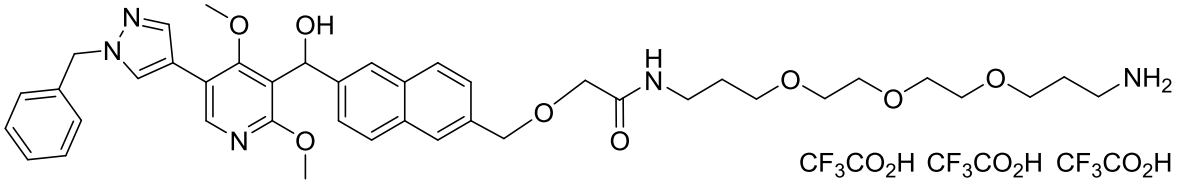

192 (42 mg, 50 µmol) was dissolved in a 1:1 mixture of DCM:water (10 mL) at room temperature. To this solution was added dropwise TFA until a final concentration of 5vol/vol% TFA. The reaction progress was analyzed by means of thin layer chromatography and the reaction was stopped by evaporating the solvent with an argon stream after the reaction was complete. The crude product was purified via preparative HPLC to yield the product (11 mg, 10 µmol, 20 %) as a yellow wax.

^{1}H NMR (600 MHz, $CDCl_3$) δ = 8.20 (s, 1H), 7.85 – 7.69 (m, 5H), 7.49 (dd, $^{3,4}J$ = 8.5, 1.6 Hz, 1H), 7.43 (dd, $^{3,4}J$ = 8.4, 1.3 Hz, 1H), 7.37 – 7.30 (m, 3H), 7.27 – 7.25 (m, 2H), 6.95 (t, ^{3}J = 6.0 Hz, 1H), 6.36 (s, 1H), 5.37 (s, 2H), 4.71 (s, 2H), 4.01 (s, 2H), 3.94 (s, 3H), 3.71 (t, ^{3}J = 5.1 Hz, 2H), 3.64 – 3.61 (m, 2H), 3.60 – 3.58 (m, 2H), 3.57 – 3.53 (m, 4H), 3.44 (t, J = 5.2 Hz, 2H), 3.38 – 3.35 (m, 5H), 3.19 (s, 2H), 2.66 (s, 4H), 1.94 (s, 2H), 1.75 – 1.70 (m, 2H). ^{13}C NMR (151 MHz, $CDCl_3$) δ = 171.00, 163.19, 161.65, 146.11, 141.88, 138.14, 136.27, 134.23, 133.10, 132.50, 129.09, 128.83, 128.45, 128.16, 127.87, 127.08, 126.18, 125.02, 123.77, 118.64, 117.41, 73.93, 71.00, 70.57, 69.81, 69.66, 69.61, 69.38, 68.37, 68.11, 60.83, 56.40, 54.21, 40.72, 36.22, 29.82, 26.07.

ESI-MS: m/z = 742.32 $[M+H]^+$.

HRMS (ESI): calculated for $C_{41}H_{52}O_8N_5$: m/z = 742.38104 $[M+H]^+$,
found: m/z = 742.38324 $[M+H]^+$.
calculated for $C_{41}H_{51}O_8N_5Na$: m/z = 764.36298 $[M+Na]^+$,
found: m/z = 764.36613 $[M+Na]^+$.

(±)-*N*-(3-(2-(2-(3-aminopropoxy)ethoxy)ethoxy)propyl)-2-((5-(1-benzyl-1H-pyrazol-4-yl)-2,4-dimethoxypyridin-3-yl)(6-(hydroxymethyl)naphthalen-2-yl)methoxy)acetamide • TFA (195)

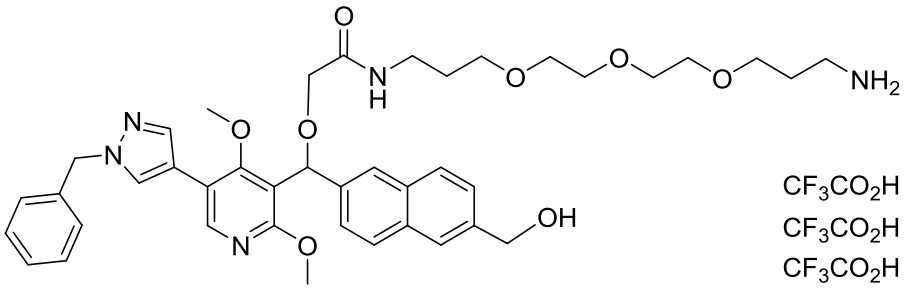

193 (55 mg, 66 µmol) was dissolved in a 1:1 mixture of DCM:water (10 mL) at room temperature. To this solution was added dropwise TFA until a final concentration of 5vol/vol% TFA. The reaction progress was analyzed by means of thin layer chromatography and the reaction was stopped by evaporating the solvent with an argon stream after the reaction was complete. The crude product was purified via preparative HPLC to yield the product (10 mg, 9 µmol, 14 %) as a yellow wax.

^{1}H NMR (600 MHz, $CDCl_3$) δ = 8.19 (s, 1H), 7.91 – 7.75 (m, 5H), 7.71 – 7.61 (m, 1H), 7.52 – 7.42 (m, 2H), 7.38 – 7.28 (m, 3H), 7.25 – 7.21 (m, 2H), 6.22 (s, 1H), 5.50 (s, 1H), 5.36 (s, 2H), 4.85 (s, 2H), 4.24, 4.02 (AB System, ^2J = 15.4 Hz, 2H), 3.95 (s, 3H), 3.74 – 3.32 (m, 14H), 3.22 (s, 3H), 3.18 (bs, 1H), 2.03 – 1.92 (m, 2H), 1.85 – 1.68 (m, 2H).

ESI-MS: m/z = 742.39 $[M+H]^+$.

HRMS (ESI): calculated for $C_{41}H_{52}O_8N_5$: m/z = 742.38104 $[M+H]^+$,
found: m/z = 742.38354 $[M+H]^+$.
calculated for $C_{41}H_{51}O_8N_5Na$: m/z = 764.36298 $[M+Na]^+$,
found: m/z = 764.36645 $[M+Na]^+$.

***tert*-butyl(1-(naphthalen-2-yl)-4-oxo-2,9,12,15-tetraoxa-5-azaoctadecan-18-yl)carbamate (197)**

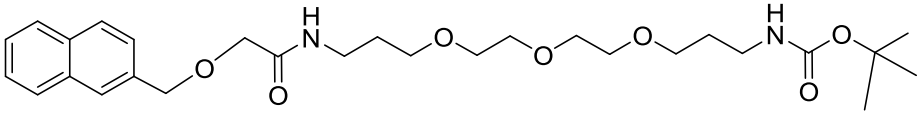

A 0.1 M solution naphthalen-2-ylmethanol (100 mg, 632 µmol) in abs. THF (6.3 mL) is admixed dropwise at 0 ° C with a 0.2 M solution of NaH (51 mg, 1.26 µmol) in abs. THF (6.3 mL). After five minutes the ice bath was removed and the reaction stirred for a further 30 minutes. This was followed by the dropwise addition of a 0.1 M solution of the PEG linker **191** (279 mg, 632 µmol) in abs. THF (6.3 mL) to the reaction mixture, which was beforehand cooled down to 0 °C. After the addition was complete, the reaction mixture was brought to room temperature with stirring overnight in the cooling bath. Subsequently, the reaction was terminated by adding sat. ammonium chloride solution (aq., 10 mL), water (10 mL) and ethyl acetate (25 mL). The aqueous layer was separated and extracted with ethyl acetate (3 x 10 mL). The combined organic layers were dried over anhydrous magnesium sulfate and the concentrated *in vacuo*. The product (241 mg, 465 µmol, 74%) was obtained as a brownish wax.

***N*-(3-(2-(2-(3-aminopropoxy)ethoxy)ethoxy)propyl)-2-(naphthalen-2-ylmethoxy)acetamide • TFA (198)**

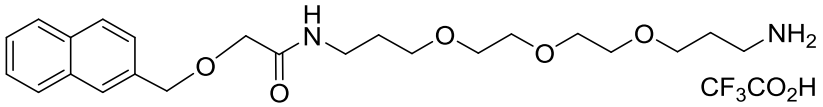

197 (80 mg, 154 µmol) was dissolved in 4 mL DCM and the solution was cooled down to 0 °C. At this temperature 2 mL TFA were added dropwise. The reaction progress was determined by means of thin layer chromatography and after completion the solvent was evaporated with the help of an argon stream. Purification of the crude product was performed via preparative HPLC, yielding the product (48 mg, 91 µmol, 59%) as a yellowish-white wax.

^{1}H NMR (600 MHz, $CDCl_3$) δ = 7.94 – 7.87 (m, 2H), 7.87 – 7.80 (m, 3H), 7.78 (s, 1H), 7.54 – 7.42 (m, 2H), 7.45 (dd, *J* = 8.4, 1.6 Hz, 1H), 6.97 (t, *J* = 5.8 Hz, 1H), 4.73 (s, 2H), 4.02 (s, 2H), 3.70 (t, *J* = 5.3 Hz, 2H), 3.65 – 3.49 (m, 9H), 3.46 – 3.42 (m, 1H), 3.37 (q, *J* = 6.8 Hz, 2H), 3.18 (dd, *J* = 10.5, 5.3 Hz, 2H), 1.94 (dt, *J* = 10.7, 5.4 Hz, 2H), 1.78 – 1.68 (m, 2H). ^{13}C NMR (151 MHz, $CDCl_3$) δ = 170.79, 134.30, 133.32, 133.31, 128.68, 128.08, 127.88, 127.32, 126.55, 126.45, 125.92, 73.93, 70.86, 70.53, 69.81, 69.65, 69.43, 68.24, 40.48, 36.26, 29.74, 26.11.

ESI-MS: m/z = 419.53 $[M+H]^+$.

HRMS (ESI): calculated for $C_{23}H_{35}O_5N_2$: m/z = 419.25409 $[M+H]^+$,
found: m/z = 419.25526 $[M+H]^+$.

(±)-(4-((4-(5-((3-ethynylphenyl)(hydroxy)methyl)-4,6-dimethoxypyridin-3-yl)-1H-pyrazol-1-yl)methyl)phenyl)(phenyl)methanone (205)

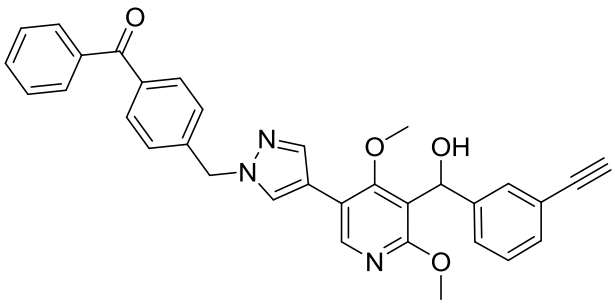

A solution of **204** (90 mg, 214 µmol), **201** (166 mg, 428 µmol), tetrakis (triphenylphosphine) palladium (0) (24 mg, 43 µmol) and 1,1'-bis (diphenylphosphino) ferrocene (25 mg, 21 µmol) in 4.3 mL dioxane, was admixed with 3 mL of a sodium carbonate solution (aq., 2 M) and degassed. The reaction mixture was heated to 120 °C for 1 h in the microwave. After cooling to room temperature, the solution was diluted with 20 mL of ethyl acetate. The organic layer was separated off and washed with 15 mL of water and 15 mL of saturated sodium chloride solution (aq.). After drying over anhydrous magnesium sulfate, the organic layer was filtered over celite and the solvent was completely removed *in vacuo*. The crude product was purified by flash chromatography on silica gel (30% EtOAc/PE). The product (98 mg, 184 µmol, 86%) was obtained as a colorless wax.

^{1}H NMR (600 MHz, $CDCl_3$) δ = 8.13 (s, 1H), 7.77 (s, 1H), 7.72 (s, 1H), 7.71 – 7.67 (m, 4H), 7.50 (t, *J* = 7.4 Hz, 1H), 7.39 (t, *J* = 7.7 Hz, 3H), 7.32 – 7.23 (m, 3H), 7.23 – 7.15 (m, 2H), 6.10 (s, 1H), 5.37 (s, 2H), 3.90 (s, 3H), 3.34 (s, 3H), 2.97 (s, 1H). ^{13}C NMR (151 MHz, $CDCl_3$) δ = 196.20, 163.54, 161.29, 145.54, 144.03, 140.90, 138.63, 137.56, 137.44, 132.73, 131.05, 130.83, 130.15, 129.27, 128.48, 128.41, 128.37, 127.43, 126.20, 122.09, 118.78, 117.44, 115.79, 83.80, 77.33, 67.72, 60.91, 55.96, 54.75.

ESI-MS: m/z = 530.52 $[M+H]^+$.

HRMS (ESI): calculated for $C_{33}H_{28}O_4N_3$: m/z = 530.20743 $[M+H]^+$,
found: m/z = 530.20829 [M+H]+.

(±)-(4-((4-(5-(hydroxy(3-(1-(2-(2-(2-hydroxyethoxy)ethoxy)ethoxy)ethyl)-1H-1,2,3-triazol-4-yl)phenyl)methyl)-4,6-dimethoxypyridin-3-yl)-1H-pyrazol-1-yl)methyl)phenyl)(phenyl)methanone • TFA (207)

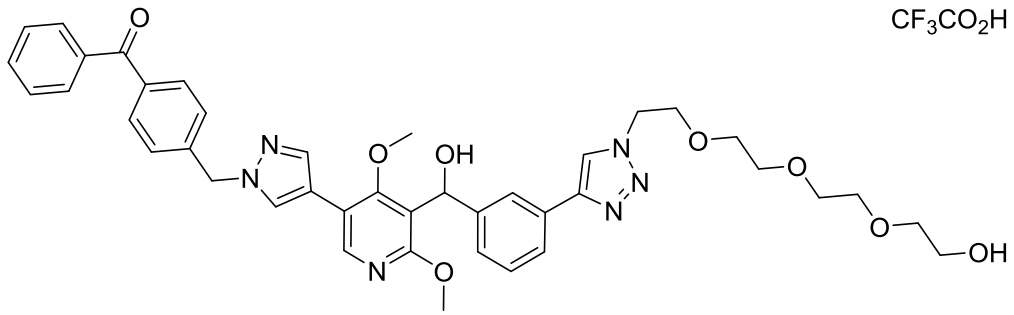

205 (15 mg, 28.3 µmol), (+)-sodium L-ascorbate (560 µg, 283 nmol), $CuSO_4$ (140 µg, 570 nmol), TBTA (150 µg, 283 nmol) and 2-(2-(2-(2-azidoethoxy)ethoxy)ethoxy)ethan-1-ol (621 µg, 28.3 µmol) were dissolved in 1.5 mL of 1:1 solution of water and *tert*-butanol. The reaction mixture was stirred at rt overnight and afterwards stopped by adding 15 mL EtOAc and 5 mL water to the solution. The layers were separated and the aqueous layer was extracted thrice with in each case 5 mL EtOAc. The combined organic layers were dried over anhydrous magnesium sulfate and concentrated *in vacuo*. Purification of the crude product was performed by preparative HPLC to yield the product (6 mg, 7 µmol, 24 %) as an amorphous white solid.

^{1}H NMR (600 MHz, $CDCl_3$) δ = 8.20 (s, 1H), 8.03 (s, 1H), 7.93 (s, 1H), 7.87 (s, 1H), 7.81 – 7.75 (m, 5H), 7.71 (d, *J* = 7.7 Hz, 1H), 7.58 (t, *J* = 7.4 Hz, 1H), 7.47 (t, *J* = 7.8 Hz, 2H), 7.38 – 7.32 (m, 3H), 7.23 (d, *J* = 7.7 Hz, 1H), 6.26 (s, 1H), 5.46 (s, 2H), 4.64 – 4.55 (m, 2H), 3.95 (s, 3H), 3.94 – 3.86 (m, 2H), 3.76 – 3.67 (m, 2H), 3.67 – 3.50 (m, 10H), 3.43 (s, 3H). ^{13}C NMR (151 MHz, $CDCl_3$) δ = 196.25, 163.26, 161.71, 147.67, 146.02, 144.52, 140.85, 138.55, 137.57, 137.45, 132.75, 130.84, 130.62, 130.17, 128.88, 128.52, 128.49, 127.44, 125.53, 124.76, 123.13, 121.57, 118.82, 117.20, 116.12, 72.50, 70.64, 70.48, 70.28, 69.64, 68.12, 61.75, 60.90, 55.89, 54.29, 50.62.

ESI-MS: m/z = 749.56 $[M+H]^+$.

HRMS (ESI): calculated for $C_{41}H_{45}O_8N_6$: m/z = 749.32934 $[M+H]^+$,
found: m/z = 749.33074 $[M+H]^+$.

7.20.2.2 Synthesis of Autophinib and Analogues Thereof

4,6-dichloro-2-(methylsulfonyl)pyrimidine (320)

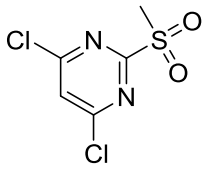

The synthesis was carried out as described in the literature.[152]

^{1}H NMR (400 MHz, DMSO-d_6) δ = 8.38 (s, 1H), 3.44 (s, 3H).

^{13}C NMR (101 MHz, DMSO-d_6) δ = 164.86, 162.67, 125.28, 39.22.

GC-MS: t_R = 5.697 min; m/z = 146.9 [M-$(SO_2CH_3)^-$]$^+$, 210.9 [M-$(CH_3)^-$]$^+$. HRMS (ESI): Calculated for $C_5H_5O_2N_2{}^{35}Cl_2S$: m/z = 226.94433 [M+H]$^+$, found: m/z = 226.94429 [M+H]$^+$. Calculated for $C_5H_5O_2N_2{}^{35}Cl{}^{37}ClS$: m/z = 228.94138 [M+H]$^+$, found: m/z = 228.94135 [M+H]$^+$.

4,6-dichloro-2-(4-nitrophenoxy)pyrimidine (322a)

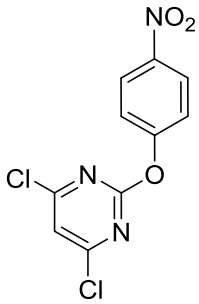

The synthesis was carried out as described in the literature.[152]

^{1}H NMR (500 MHz, DMSO-d_6) δ = 8.36 (d, ^{3}J = 9.1 Hz, 2H), 7.85 (s, 1H), 7.60 (d, ^{3}J = 9.1 Hz, 2H). ^{13}C NMR (126 MHz, DMSO-d_6) δ = 162.65, 162.59, 156.62, 145.09, 125.63, 122.68, 117.05.

GC-MS: t_R = 6.891 min; m/z =250.0 [M-Cl^-]$^+$. HRMS (ESI): Calculated for $C_{10}H_6O_3N_3{}^{35}Cl_2$: m/z = 285.97807 [M+H]$^+$, found: m/z = 285.97761 [M+H]$^+$. Calculated for $C_{10}H_6O_3N_3{}^{35}Cl{}^{37}Cl$: m/z = 287.97512 [M+H]$^+$, found: m/z = 287.97457 [M+H]$^+$.

6-chloro-*N*-(5-methyl-1H-pyrazol-3-yl)-2-(4-nitrophenoxy)pyrimidin-4-amine (313)

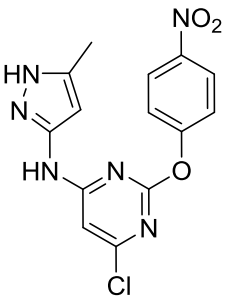

The synthesis was carried out as described in the literature.[152]

R_f: 0.30 (50% EtOAc/n-Pentane).

^{1}H NMR (600 MHz, DMSO-d_6, 50 °C) δ = 12.00 (s, 1H), 10.27 (s, 1H), 8.33 (d, ^{3}J = 8.9 Hz, 2H), 7.53 (d, ^{3}J = 9.1 Hz, 2H), 6.63 (s, 1H), 5.69 (s, 1H), 2.06 (s, 3H). ^{13}C NMR (151 MHz, DMSO-d_6, 50 °C) δ = 157.63, 144.48, 125.18, 122.96, 99.91, 95.48, 10.16.

ESI-MS: m/z = 347.35 [M+H]$^+$. HRMS (ESI): Calculated for $C_{14}H_{12}O_3N_6{}^{35}Cl$: m/z = 347.06539 [M+H]$^+$, found: m/z = 347.06582 [M+H]$^+$. Calculated for $C_{14}H_{12}O_3N_6{}^{37}Cl$: m/z = 349.06244 [M+H]$^+$, found: m/z = 349.06252 [M+H]$^+$.

6-chloro-*N*-(5-methyl-1H-pyrazol-3-yl)-2-(methylthio)pyrimidin-4-amine (323a)

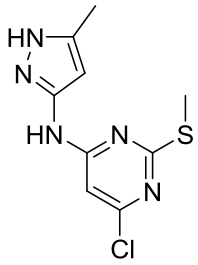

A stirred solution of 4,6-dichloro-2-(thiomethyl)pyrimidine (5 g, 25.6 mMol), DIPEA (4.64 g, 35.9 mMol) und 5-methyl-1H-pyrazol-3-amine (3.49 g, 35.9 mMol) was heated to 50 °C for 16 h. Subsequently the mixture was cooled to ambient and poured into water (50 mL). The precipitate was filtered and the wet solid was dissolved EtOAc (60 mL), filtered again and eventually taken up MeOH (20 mL). The product (4.53 g, 17.7 mMol, 69%) was dried *in vacuo* and obtained as a white solid which was used without further purification.

^{1}H NMR (400 MHz, DMSO-d_6) δ = 12.10 (s, 1H), 10.17 (s, 1H), 6.00 – 7-50 (br m, 2H), 3.31 (s, 3H), 2.22 (s, 3H). ^{13}C NMR (101 MHz, DMSO-d_6) δ = 159.73, 147.48, 138.75, 112.84, 99.70, 78.15, 62.12, 13.53, 10.61.

ESI-MS: m/z = 256.16 $[M+H]^+$. HRMS (ESI): Calculated for $C_9H_{11}N_5$ ^{35}ClS: m/z = 256.04182 $[M+H]^+$, found: m/z = 256.04285 $[M+H]^+$. Calculated for $C_9H_{11}N_5$ ^{37}ClS: m/z = 258.03887 $[M+H]^+$, found: m/z = 258.03889 $[M+H]^+$.

6-chloro-*N*-(5-methyl-1H-pyrazol-3-yl)-2-(methylsulfonyl)pyrimidin-4-amine (324a)

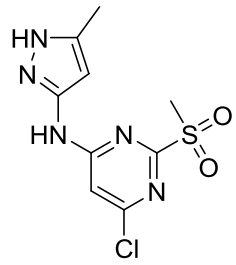

To a stirred solution of 6-chloro-N-(5-methyl-1H-pyrazol-3-yl)-2-(methylthio)pyrimidin-4-amine (**32a**) (3 g, 11.7 mMol) in MeOH (75 mL) cooled in an ice bath was added portionwise a slurry of oxone (16.6 g, 27 mMol) in water (40 mL) over 10 min. The reaction mixture was stirred at this temperature for a further 30 min before being allowed to warm up to room temperature for two hours. The solid, isolated by filtration, was stirred vigorously in a 1:1 mixture of water and saturated bicarbonate solution. The solid was then filtrated and dried in vacuo to afford the title compound as a yellow solid (2 g, 6.97 mMol, 59%).

^{1}H NMR (400 MHz, DMSO-d_6) δ = 12.27 (s, 1H), 10.93 (s, 1H), 8.12 – 5.69 (m, 2H), 3.34 (s, 3H), 2.23 (s, 3H).

ESI-MS: m/z = 287.9 $[M+H]^+$. HRMS (ESI): Calculated for $C_9H_{11}O_2N_5$ ^{35}ClS: m/z = 288.03156 $[M+H]^+$, found: m/z = 288.03182 $[M+H]^+$. Calculated for $C_9H_{11}O_2N_5$ ^{37}ClS: m/z = 290.02870 $[M+H]^+$, found: m/z = 290.02818 $[M+H]^+$.

General procedure A:

A stirred solution of 6-chloro-*N*-(5-methyl-1H-pyrazol-3-yl)-2-(methylsulfonyl)pyrimidin-4-amine (**324a**) (1 eq), potassium *tert*-butoxide (1.15 eq) and the phenol (1.1 eq) in *tert*-butanol (0.05 M with respect to the pyrimidine) was heated to 50 °C until complete conversion as indicated by uHPLC/MS or TLC (at least 16 h). The reaction was quenched by the addition of water and EtOAc. The organic layer was separated and the aqueous layer was extracted with EtOAc (3x). The combined organic layers were dried over magnesium sulfate and concentrated *in vacuo*. The resulting crude was then purified by silica gel column chromatography or mass-directed preparative HPLC to obtain the desired compound.

4-((4-chloro-6-((5-methyl-1H-pyrazol-3-yl)amino)pyrimidin-2-yl)oxy) benzenesulfonamide • TFA (360)

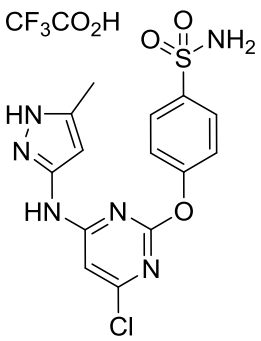

324a (50 mg, 174 µmol) was reacted with 4-hydroxybenzenesulfonamide following general procedure A. Purification by mass-directed preparative HPLC yielded the product (61 mg, 123 µmol, 71%) as a white amorphous solid.

^{1}H NMR (400 MHz, DMSO-d_6, 80 °C) δ = 10.02 (s, 1H), 7.94 – 7.88 (m, 2H), 7.44 – 7.36 (m, 2H), 7.19 (bs, 2H), 7.07 – 6.87 (m, 1H), 5.77 (s, 1H), 2.15 (s, 3H).

ESI-MS: m/z = 381.27, 383.24 $[M+H]^+$. HRMS (ESI): Calculated for $C_{14}H_{14}O_3N_6$ ^{35}ClS: m/z = 381.05311 $[M+H]^+$, found: m/z = 381.05218 $[M+H]^+$. Calculated for $C_{14}H_{14}O_3N_6$ ^{37}ClS: m/z = 383.05016 $[M+H]^+$, found: m/z = 383.05002 $[M+H]^+$.

6-chloro-2-(3-fluoro-4-nitrophenoxy)-*N*-(5-methyl-1H-pyrazol-3-yl)pyrimidin-4-amine • TFA (349)

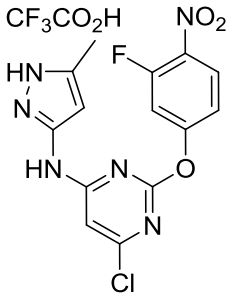

324a (50 mg, 174 µmol) was reacted with 3-fluoro-4-nitrophenol following general procedure A. Purification by mass-directed preparative HPLC yielded the product (34 mg, 71 µmol, 41%) as a white amorphous solid. ^{1}H NMR (400 MHz, DMSO-d_6) δ = 10.47 (s, 1H), 8.29 (t, J = 8.4 Hz, 1H), 7.72 (d, J = 12.2 Hz, 1H), 7.38 (d, J = 8.9 Hz, 1H), 6.61 (s, 1H), 5.72 (s, 1H), 2.15 – 2.01 (m, 3H).

ESI-MS: m/z = 365.36 $[M+H]^+$. HRMS (ESI): Calculated for $C_{14}H_{11}O_3N_6$ ^{35}ClF: m/z = 365.05597 $[M+H]^+$, found: m/z = 365.05587 $[M+H]^+$.

4-((4-chloro-6-((5-methyl-1H-pyrazol-3-yl)amino)pyrimidin-2-yl)oxy)benzonitrile • TFA (350)

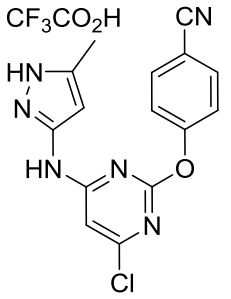

324a (50 mg, 174 µmol) was reacted with 4-hydroxybenzonitrile following general procedure A. Purification by mass-directed preparative HPLC yielded the product (62 mg, 141 µmol, 81%) as a white amorphous solid. ^{1}H NMR (500 MHz, DMSO-d_6) δ = 12.16 (s, 1H), 10.47 (s, 1H), 7.99 (bs, 2H), 7.49 (d, ^{3}J = 8.5 Hz, 2H), 6.54 (s, 1H), 5.50 (s, 1H), 2.10 (bs, 3H). ^{13}C NMR (126 MHz, DMSO-d_6) δ = 164.02, 161.14, 158.36, 156.32, 146.95, 138.23, 134.30, 123.96, 118.57, 108.31, 99.92, 95.80, 10.53.

ESI-MS: m/z = 327.38 $[M+H]^+$. HRMS (ESI): Calculated for $C_{15}H_{12}ON_6$ ^{35}Cl: m/z = 327.07556 $[M+H]^+$, found: m/z = 327.07569 $[M+H]^+$.

6-chloro-*N*-(5-methyl-1H-pyrazol-3-yl)-2-(2-(pyridin-4-yl)ethoxy)pyrimidin-4-amine • TFA (359)

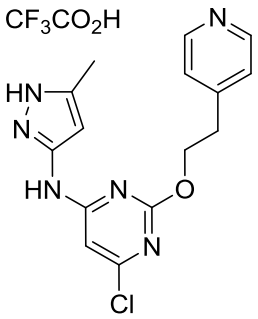

324a (50 mg, 174 µmol) was reacted with 2-(pyridin-4-yl)ethan-1-ol following general procedure A. Purification by mass-directed preparative HPLC yielded the product (24 mg, 54 µmol, 31%) as a white amorphous solid.

^{1}H NMR (400 MHz, DMSO-d_6) δ = 10.16 (s, 1H), 8.82 (d, J = 6.6 Hz, 2H), 7.96 (d, J = 6.6 Hz, 2H), 4.62 (t, J = 6.2 Hz, 2H), 3.33 (t, J = 6.2 Hz, 2H), 2.21 (s, 3H).

ESI-MS: m/z = 226.19 $[M+H-(4\text{-ethylpyridine})]^+$. HRMS (ESI): Calculated for $C_{15}H_{16}ON_6{}^{35}Cl$: m/z = 331.10686 $[M+H]^+$, found: m/z = 331.10727 $[M+H]^+$. Calculated for $C_8H_9ON_5{}^{35}Cl$: m/z = 226.04901 $[M+H-(4\text{-ethylpyridine})]^+$, found: m/z = 226.04918 $[M+H-(4\text{-ethylpyridine})]^+$.

6-chloro-*N*-(5-methyl-1H-pyrazol-3-yl)-2-((4-nitrobenzyl)oxy)pyrimidin-4-amine • TFA (352)

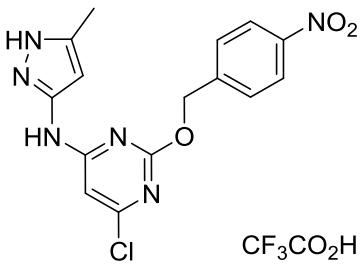

324a (50 mg, 174 µmol) was reacted with (4-nitrophenyl)MeOH following general procedure A. Purification by mass-directed preparative HPLC yielded the product (61 mg, 136 µmol, 78%) as an off-white amorphous solid.

R_f: 0.32 (2% MeOH/DCM).

^{1}H NMR (400 MHz, DMSO-d_6) δ = 12.09 (s, 1H), 10.20 (s, 1H), 8.26 (d, ^3J = 8.7 Hz, 2H), 7.71 (d, ^3J = 8.7 Hz, 2H), 5.50 (s, 2H), 2.20 (s, 3H).

ESI-MS: m/z = 361.30 $[M+H]^+$. HRMS (ESI): Calculated for $C_{15}H_{14}O_3N_6{}^{35}Cl$: m/z = 361.08104 $[M+H]^+$, found: m/z = 361.08088 $[M+H]^+$.

6-chloro-2-(2-fluoro-4-nitrophenoxy)-*N*-(5-methyl-1H-pyrazol-3-yl)pyrimidin-4-amine • TFA (351)

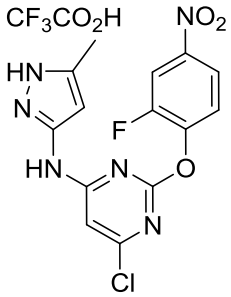

324a (50 mg, 174 µmol) was reacted with 2-fluoro-4-nitrophenol following general procedure A. Purification by mass-directed preparative HPLC yielded the product (16 mg, 33 µmol, 19%) as a white amorphous solid. ^{1}H NMR (400 MHz, DMSO-d_6) δ = 10.53 (s, 1H), 8.41 (d, J = 9.2 Hz, 1H), 8.23 (d, J = 8.1 Hz, 1H), 7.76 (t, J = 8.4 Hz, 1H), 6.60 (s, 1H), 5.52 (s, 1H), 1.99 (s, 3H). ^{13}C NMR (101 MHz, DMSO-d_6) δ = 158.44, 145.37, 145.25, 125.46, 121.01, 120.98, 113.15, 112.91, 100.46, 95.46, 62.15, 10.31.

ESI-MS: m/z = 365.38 $[M+H]^+$. HRMS (ESI): Calculated for $C_{14}H_{11}O_3N_6$ ^{35}ClF: m/z = 365.05597 $[M+H]^+$, found: m/z = 365.05590 $[M+H]^+$.

6-chloro-2-(2-chloro-4-nitrophenoxy)-*N*-(5-methyl-1H-pyrazol-3-yl)pyrimidin-4-amine • TFA (353)

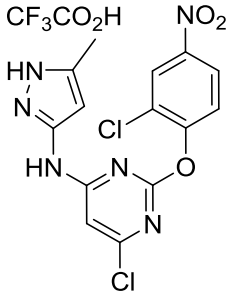

324a (50 mg, 174 µmol) was reacted with 2-chloro-4-nitrophenol following general procedure A. Purification by mass-directed preparative HPLC yielded the product (58 mg, 116 µmol, 67%) as a white amorphous solid. ^{1}H NMR (400 MHz, DMSO-d_6) δ = 10.49 (s, 1H), 8.53 (s, 1H), 8.32 (d, J = 8.3 Hz, 1H), 7.74 (d, J = 9.0 Hz, 1H), 6.57 (s, 1H), 5.42 (s, 1H), 2.25 – 1.77 (m, 3H).

ESI-MS: m/z = 381.39 $[M+H]^+$. HRMS (ESI): Calculated for $C_{14}H_{11}O_3N_6$ $^{35}Cl_2$: m/z = 381.02642 $[M+H]^+$, found: m/z = 381.02725 $[M+H]^+$.

6-chloro-*N*-(5-methyl-1H-pyrazol-3-yl)-2-(3-methyl-4-nitrophenoxy)pyrimidin-4-amine • TFA (354)

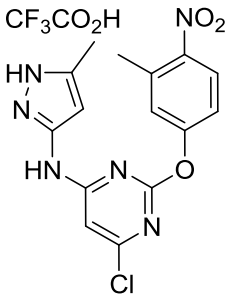

324a (50 mg, 174 µmol) was reacted with 3-methyl-4-nitrophenol following general procedure A. Purification by mass-directed preparative HPLC yielded the product (31 mg, 64 µmol, 37%) as a white amorphous solid.

^{1}H NMR (400 MHz, DMSO-d_6) δ = 10.42 (s, 1H), 8.12 (d, ^3J = 8.8 Hz, 1H), 7.44 (s, 1H), 7.34 (dd, ^3J = 8.9 Hz, 2.6 Hz, 1H), 6.57 (s, 1H), 5.65 (s, 1H), 2.55 (s, 3H), 2.07 (s, 3H).

ESI-MS: m/z = 361.39 $[M+H]^+$. HRMS (ESI): Calculated for $C_{15}H_{14}O_3N_6$ ^{35}Cl: m/z = 361.08104 $[M+H]^+$, found: m/z = 361.08091 $[M+H]^+$.

6-chloro-2-(4-methoxyphenoxy)-*N*-(5-methyl-1H-pyrazol-3-yl)pyrimidin-4-amine • TFA (355)

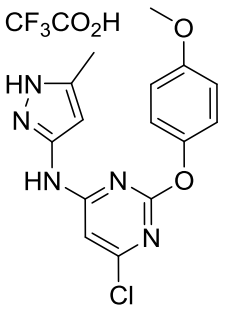

324a (50 mg, 174 µmol) was reacted with 4-methoxyphenol following general procedure A. Purification by silica gel column chromatography (4% MeOH/DCM) followed by mass-directed preparative HPLC yielded the product (50 mg, 151 µmol, 87%) as a white amorphous solid.

R_f: 0.27 (4% MeOH/DCM).

^{1}H NMR (400 MHz, DMSO-d_6) δ = 11.98 (s, 1H), 10.29 (s, 1H), 7.16 – 7.10 (m, 2H), 7.00 (d, ^3J = 8.6 Hz, 2H), 6.77 – 6.64 (m, 1H), 5.67 (s, 1H), 3.78 (s, 3H), 2.07 (s, 3H).

ESI-MS: m/z = 332.21 $[M+H]^+$. HRMS (ESI): Calculated for $C_{15}H_{15}O_2N_5$ ^{35}Cl: m/z = 332.09088 $[M+H]^+$, found: m/z = 332.09216 $[M+H]^+$. Calculated for $C_{15}H_{15}O_2N_5$ ^{37}Cl: m/z = 334.08793 $[M+H]^+$, found: m/z = 334.08883 $[M+H]^+$.

6-chloro-*N*-(5-methyl-1H-pyrazol-3-yl)-2-((4-nitrophenyl)thio)pyrimidin-4-amine • TFA (356)

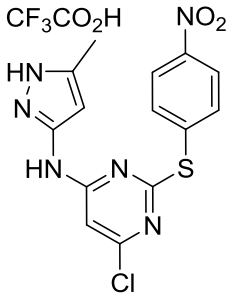

324a (100 mg, 410 µmol) was reacted with 4-nitrobenzenethiol following general procedure A. Purification by mass-directed preparative HPLC yielded the product (46 mg, 98 µmol, 24%) as a yellow amorphous solid.

ESI-MS: m/z = 363.39 $[M+H]^+$. HRMS (ESI): Calculated for $C_{14}H_{12}O_2N_6$ ^{35}ClS: m/z = 363.04255 $[M+H]^+$, found: m/z = 363.04327 $[M+H]^+$. Calculated for $C_{14}H_{12}O_2N_6$ ^{37}ClS: m/z = 366.04221 $[M+H]^+$, found: m/z = 366.04267 $[M+H]^+$.

6-chloro-*N*-(5-methyl-1H-pyrazol-3-yl)-2-(2-methyl-4-nitrophenoxy)pyrimidin-4-amine • TFA (357)

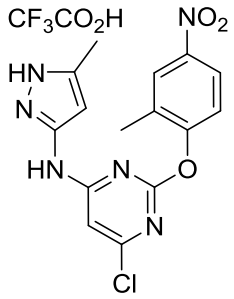

324a (50 mg, 174 µmol) was reacted with 2-methyl-4-nitrophenol following general procedure A. Purification by mass-directed preparative HPLC yielded the product (82 mg, 172 µmol, quant.) as a white amorphous solid.

^1H NMR (500 MHz, DMSO-d_6) δ = 12.29 – 11.86 (m, 1H), 10.49 (s, 1H), 8.34 (s, 1H), 8.19 (bs, 1H), 7.49 (d, ^3J = 8.8 Hz, 1H), 6.54 (s, 1H), 5.36 (s, 1H), 2.22 (s, 3H), 1.92 (s, 3H).

ESI-MS: m/z = 361.41 $[M+H]^+$. HRMS (ESI): Calculated for $C_{15}H_{14}O_3N_6$ ^{35}Cl: m/z = 361.08104 $[M+H]^+$, found: m/z = 361.08168 $[M+H]^+$.

6-chloro-*N*-(5-methyl-1H-pyrazol-3-yl)-2-(4-nitro-2-(trifluoromethyl)phenoxy) pyrimidin-4-amine • TFA (358)

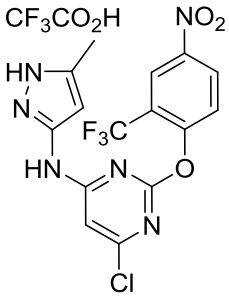

324a (50 mg, 174 µmol) was reacted with 4-nitro-2-(trifluoromethyl)phenol following general procedure A. Purification by mass-directed preparative HPLC yielded the product (14 mg, 26 µmol, 15%) as an off-white amorphous solid.

^{1}H NMR (400 MHz, DMSO-d_6, 50°C) δ = 10.35 (s, 1H), 8.62 (dd, J = 9.0 Hz, 2.6, 1H), 8.57 (d, J = 2.5 Hz, 1H), 8.35 (dd, J = 9.1 Hz, 2.8, 1H), 7.87 (d, J = 9.0 Hz, 1H), 7.27 – 7.21 (m, 1H), 5.64 (s, 1H), 2.09 (s, 3H). ^{13}C NMR (101 MHz, DMSO-d_6) δ = 161.84, 154.84, 138.81, 129.67, 129.29, 124.11, 123.29, 123.23, 122.86, 122.81, 121.40, 117.78, 115.82, 100.52, 95.42, 10.37.

ESI-MS: m/z = 415.38 $[M+H]^+$. HRMS (ESI): Calculated for $C_{15}H_{11}O_3N_6$ $^{35}ClF_3$: m/z = 415.05278 $[M+H]^+$, found: m/z = 415.05335 $[M+H]^+$.

6-chloro-*N*-(5-methyl-1H-pyrazol-3-yl)-2-(4-(trifluoromethyl)phenoxy)pyrimidin-4-amine (361)

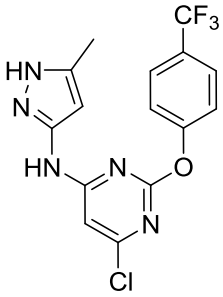

The synthesis was carried out as described in and by the authors of the literature.[152]

6-chloro-2-(4-chloro-3-fluorophenoxy)-*N*-(5-methyl-1H-pyrazol-3-yl)pyrimidin-4-amine (362)

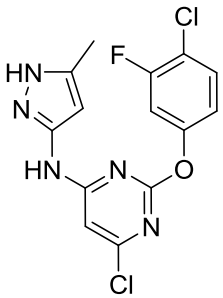

The synthesis was carried out as described in and by the authors of the literature.[152]

6-chloro-2-(4-chlorophenoxy)-*N*-(5-methyl-1H-pyrazol-3-yl)pyrimidin-4-amine (363)

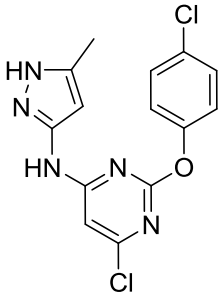

The synthesis was carried out as described in and by the authors of the literature.[152]

1-(4-((4-chloro-6-((5-methyl-1H-pyrazol-3-yl)amino)pyrimidin-2-yl)oxy)phenyl) ethan-1-one • TFA (364)

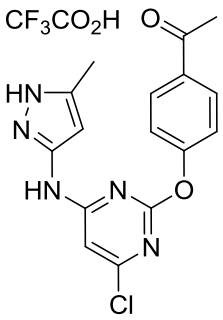

324a (50 mg, 174 µmol) was reacted with 1-(4-hydroxyphenyl)ethan-1-one following general procedure A. Purification by mass-directed preparative HPLC yielded the product (34 mg, 75 µmol, 43%) as a white amorphous solid.

^{1}H NMR (400 MHz, DMSO-d_6) δ = 10.34 (s, 1H), 8.06 (d, ^{3}J = 8.5 Hz, 2H), 7.37 (d, ^{3}J = 8.6 Hz, 2H), 6.64 (bs, 1H), 5.64 (s, 1H), 2.61 (s, 3H), 2.04 (s, 3H).

^{13}C NMR (101 MHz, DMSO-d_6) δ = 196.84, 161.42, 158.18, 156.45, 134.08, 130.09, 122.32, 99.72, 95.73, 62.17, 26.70, 10.43.

ESI-MS: m/z = 344.42 $[M+H]^+$. HRMS (ESI): Calculated for $C_{16}H_{15}O_2N_5$ ^{35}Cl: m/z = 344.09088 $[M+H]^+$, found: m/z = 344.08983 $[M+H]^+$.

6-methyl-*N*-(5-methyl-1H-pyrazol-3-yl)-2-(4-(methylsulfonyl)phenoxy)pyrimidin-4-amine • TFA (365)

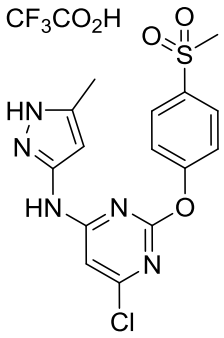

324a (50 mg, 174 µmol) was reacted with 4-(methylsulfonyl)phenol following general procedure A. Purification by silica column chromatography (2% MeOH/DCM) followed by mass-directed preparative HPLC yielded the product (61 mg, 162 µmol, 93%) as an off-white amorphous solid.

R_f: 0.32 (2% MeOH/DCM).

^{1}H NMR (500 MHz, DMSO-d_6) δ = 12.06 (s, 1H), 10.48 – 10.18 (m, 1H), 8.02 (d, ^3J = 7.5 Hz, 2H), 7.52 (d, ^3J = 8.6 Hz, 2H), 6.59 (s, 1H), 5.64 (s, 1H), 3.27 (s, 3H), 2.08 (s, 3H).

ESI-MS: m/z = 380.25 $[M+H]^+$. HRMS (ESI): calculated for $C_{15}H_{15}O_3N_5$ ^{35}ClS: m/z = 380.05786 $[M+H]^+$, found: m/z = 380.05938 $[M+H]^+$. Calculated for $C_{15}H_{15}O_3N_5$ ^{37}ClS: m/z = 382.05491 $[M+H]^+$, found: m/z = 382.05617 $[M+H]^+$.

2-((1H-indazol-5-yl)oxy)-6-chloro-*N*-(5-methyl-1H-pyrazol-3-yl)pyrimidin-4-amine • TFA (366)

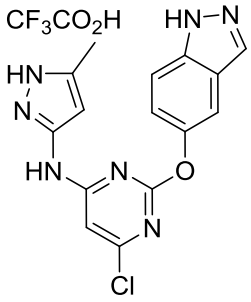

324a (50 mg, 174 µmol) was reacted with 1H-indazol-5-ol following general procedure A. Purification by mass-directed preparative HPLC yielded the product (41 mg, 90 µmol, 52%) as a white amorphous solid.

^{1}H NMR (600 MHz, DMSO-d_6) δ = 10.31 (s, 1H), 8.08 (s, 1H), 7.61 (d, J = 8.8 Hz, 1H), 7.58 (d, J = 1.9 Hz, 1H), 7.20 (dd, J = 8.9 Hz, 2.2 Hz, 1H), 6.49 (s, 1H), 5.37 (s, 1H), 1.70 (s, 3H). ^{13}C NMR (151 MHz, DMSO-d_6) δ = 165.24, 161.19, 158.42 (q, J = 37.8 Hz) 147.10, 146.44, 138.29, 137.97, 133.54, 123.04, 121.96, 115.32 (d, J = 285.5 Hz), 112.43, 111.07, 99.04, 95.93, 10.14.

ESI-MS: m/z = 342.33 $[M+H]^+$. HRMS (ESI): Calculated for $C_{15}H_{13}ON_7$ ^{35}Cl: m/z = 342.08646 $[M+H]^+$, found: m/z = 342.08754 $[M+H]^+$.

6-chloro-*N*-(5-methyl-1H-pyrazol-3-yl)-2-(2-nitrophenoxy)pyrimidin-4-amine (367)

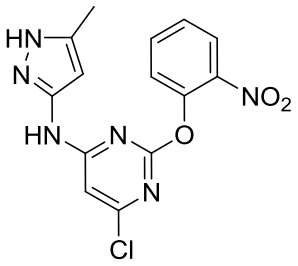

The synthesis was carried out as described in and by the authors of the literature.[152]

6-chloro-2-((1,1,1,3,3,3-hexafluoropropan-2-yl)oxy)-*N*-(5-methyl-1H-pyrazol-3-yl)pyrimidin-4-amine • TFA (368)

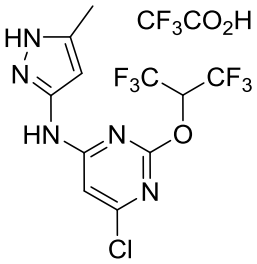

324a (50 mg, 174 µmol) was reacted with hexafluoropropan-2-ol following general procedure A. Purification by mass-directed preparative HPLC yielded the product (85 mg, 174 µmol, quant.) as a white amorphous solid.

^{1}H NMR (400 MHz, DMSO-d_6, 90 °C) δ = 10.16 (s, 1H), 7.12 (s, 1H), 6.70 – 6.58 (m, 1H), 6.04 (s, 1H), 2.25 (s, 3H).

ESI-MS: m/z = 376.39 $[M+H]^+$. HRMS (ESI): Calculated for $C_{11}H_9ON_5ClF_6$: m/z = 376.03943 $[M+H]^+$, found: m/z = 376.03940 $[M+H]^+$.

4-((4-chloro-6-((5-methyl-1H-pyrazol-3-yl)amino)pyrimidin-2-yl)oxy)benzamide • TFA (369)

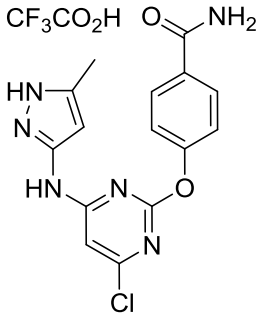

324a (50 mg, 174 µmol) was reacted with 4-hydroxybenzamide following general procedure A. Purification by mass-directed preparative HPLC yielded the product (59 mg, 130 µmol, 75%) as a white amorphous solid.

^{1}H NMR (400 MHz, DMSO-d_6, 100 °C) δ = 9.87 (s, 1H), 8.01 – 7.89 (m, 2H), 7.28 – 7.24 (m, 2H), 6.92 (s, 1H), 5.73 (s, 1H), 2.56 – 2.42 (m, J = 3.6 Hz, 1.7, 2H), 2.12 (s, 3H). ^{13}C NMR (101 MHz, DMSO-d_6, 100 °C) δ = 166.81, 163.43, 161.55, 158.77, 154.70, 146.61, 138.45, 130.98, 128.56, 120.80, 99.10, 95.49, 9.86.

ESI-MS: m/z = 345.35, 347.23 $[M+H]^+$. HRMS (ESI): Calculated for $C_{15}H_{14}O_2N_6{}^{35}Cl$: m/z = 345.08613 $[M+H]^+$, found: m/z = 345.08597 $[M+H]^+$. Calculated for $C_{15}H_{14}O_2N_6{}^{37}Cl$: m/z = 347.08318 $[M+H]^+$, found: m/z = 347.08319 $[M+H]^+$.

6-chloro-*N*-(5-methyl-1H-pyrazol-3-yl)-2-(3-nitrophenoxy)pyrimidin-4-amine (370)

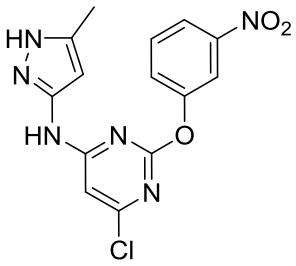

The synthesis was carried out as described in and by the authors of the literature.[152]

6-chloro-*N*-(5-methyl-1H-pyrazol-3-yl)-2-((5-nitropyridin-2-yl)oxy)pyrimidin-4-amine • TFA (371)

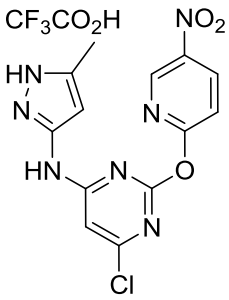

324a (50 mg, 174 µmol) was reacted with 5-nitropyridin-2-ol following general procedure A. Purification by mass-directed preparative HPLC yielded the product (23 mg, 49 µmol, 28%) as a white amorphous solid. ^{1}H NMR (400 MHz, DMSO-d_6, 50°C) δ = 10.62 (s, 1H), 9.24 (d, *J* = 3.1 Hz, 1H), 8.23 (dd, *J* = 10.2 Hz, 3.2, 1H), 7.72 (s, 1H), 6.64 (d, *J* = 10.2 Hz, 1H), 6.04 (s, 1H), 2.22 (s, 3H). ^{13}C NMR (151 MHz, DMSO-d_6) δ = 161.47, 160.19, 159.75, 158.35 (q, *J* = 37.5 Hz), 147.38, 139.56, 134.53, 130.40, 119.91, 115.37 (q, *J* = 289.9 Hz), 104.91, 103.75, 96.04, 95.10, 10.49.

ESI-MS: m/z = 348.39 $[M+H]^+$.

HRMS (ESI): Calculated for $C_{13}H_{11}O_3N_7{}^{35}Cl$: m/z = 348.06064 $[M+H]^+$,
found: m/z = 348.05982 $[M+H]^+$.

6-chloro-2-(4-chloro-3-(trifluoromethyl)phenoxy)-*N*-(5-methyl-1H-pyrazol-3-yl)pyrimidin-4-amine (372)

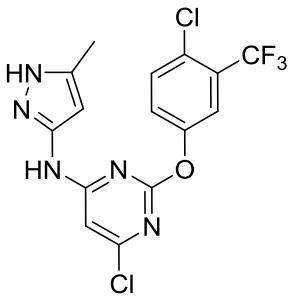

The synthesis was carried out as described in and by the authors of the literature.[152]

6-chloro-*N*-(5-methyl-1H-pyrazol-3-yl)-2-(pyridin-4-ylmethoxy)pyrimidin-4-amine • TFA (373)

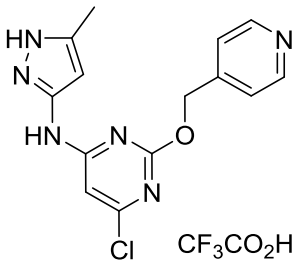

324a (50 mg, 174 µmol) was reacted with pyridin-4-ylmethanol following general procedure A. Purification by mass-directed preparative HPLC yielded the product (75 mg, 174 µmol, quant.) as a white amorphous solid.

^{1}H NMR (400 MHz, DMSO-d_6) δ = 10.25 (s, 1H), 8.82 (dd, J = 5.1 Hz, 1.4, 2H), 7.87 (d, J = 6.4 Hz, 2H), 5.60 (s, 2H), 2.20 (s, 3H).

ESI-MS: m/z = 317.28 $[M+H]^+$. HRMS (ESI): Calculated for $C_{14}H_{14}ON_6$ ^{35}Cl: m/z = 317.09121 $[M+H]^+$, found: m/z = 317.09149 $[M+H]^+$.

6-chloro-*N*-(5-methyl-1H-pyrazol-3-yl)-2-(pyridin-3-ylmethoxy)pyrimidin-4-amine • TFA (374)

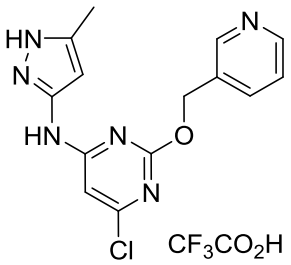

324a (50 mg, 174 µmol) was reacted with pyridin-3-ylmethanol following general procedure A. Purification by mass-directed preparative HPLC yielded the product (63 mg, 155 µmol, 89%) as a white amorphous solid.

^{1}H NMR (400 MHz, DMSO-d_6) δ = 10.23 (s, 1H), 8.90 (s, 1H), 8.76 (d, J = 5.1 Hz, 1H), 8.34 (d, J = 7.8 Hz, 1H), 7.81 (dd, J = 7.8 Hz, 5.4, 1H), 5.47 (s, 2H), 2.21 (s, 3H). ^{13}C NMR (101 MHz, DMSO-d_6) δ = 164.21, 162.41, 159.15, 158.79, 145.71, 145.60, 145.59, 141.86, 135.27, 126.15, 104.59, 66.03, 62.83, 11.33.

ESI-MS: m/z = 317.16 $[M+H]^+$. HRMS (ESI): Calculated for $C_{14}H_{14}ON_6$ ^{35}Cl: m/z = 317.09121 $[M+H]^+$, found: m/z = 317.09188 $[M+H]^+$.

7.20.2.2.1 General procedure B:

A solution of the amine (1.1 eq), DIPEA (1.2 eq) and 4,6-Dichloro-2-(4-nitrophenoxy)pyrimidine **31a** (1 eq) in DMF (0.05 M with respect to the amine) was stirred at 85 °C until complete conversion was observed by uHPLC/MS or TLC. EtOAc was added to the reaction mixture before the organic layer was washed with water. The aqueous layer was extracted with EtOAc (2x) and the combined organic layers were dried over $MgSO_4$ and filtered. The solvent was removed *in vacuo* and the mixture was purified by silica gel column chromatography or mass-directed preparative HPLC.

***N*-(5-(tert-butyl)-1H-pyrazol-3-yl)-6-chloro-2-(4-nitrophenoxy)pyrimidin-4-amine • TFA (338)**

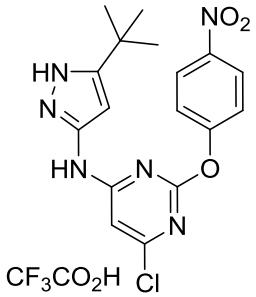

31a (50 mg, 175 µmol) was reacted with 5-(*tert*-butyl)-1H-pyrazol-3-amine according to general procedure B. Purification of the crude was performed by silica gel column chromatography (30% EtOAc/n-Pentane + 3% Et_3N) followed by mass-directed preparative HPLC to obtain the product (31 mg, 79 µmol, 45%) as a white amorphous solid.

R_f: 0.14 (30% EtOAc/Petrolether + 3% Et_3N).

^{1}H NMR (400 MHz, DMSO-d_6) δ = 12.06 (s, 1H), 10.49 (s, 1H), 8.35 (d, ^3J = 8.7 Hz, 2H), 7.56 (d, ^3J = 8.8 Hz, 2H), 6.59 (s, 1H), 5.56 (s, 1H), 1.01 (s, 9H).

ESI-MS: m/z = 389.28, 391.21 $[M+H]^+$. HRMS (ESI): Calculated for $C_{17}H_{18}O_3N_6{}^{35}Cl$: m/z = 389.11234 $[M+H]^+$, found: m/z = 389.11387 $[M+H]^+$. Calculated for $C_{17}H_{18}O_3N_6{}^{37}Cl$: m/z = 391.10939 $[M+H]^+$, found: m/z = 391.11045 $[M+H]^+$.

6-chloro-*N*-(5-cyclopropyl-1H-pyrazol-3-yl)-2-(4-nitrophenoxy)pyrimidin-4-amine • TFA (336)

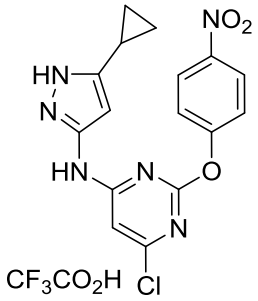

31a (50 mg, 175 µmol) was reacted with 5-cyclopropyl-1H-pyrazol-3-amine according to general procedure B. Purification of the crude was performed by mass-directed preparative HPLC to obtain the product (54 mg, 145 µmol, 83%) as a white amorphous solid.

^{1}H NMR (400 MHz, DMSO-d_6, 100°C) δ = 9.98 (s, 1H), 8.35 – 8.29 (m, 2H), 7.53 – 7.48 (m, 2H), 6.92 (s, 1H), 5.61 (s, 1H), 1.76 (td, J = 8.5 Hz, 4.3, 1H), 0.88 – 0.81 (m, 2H), 0.52 – 0.45 (m, 2H). ^{13}C NMR (101 MHz, DMSO-d_6, 100°C) δ = 162.83, 161.48, 158.68, 157.39, 146.25, 145.66, 144.28, 124.66, 122.23, 99.71, 92.22, 6.64, 5.87.

ESI-MS: m/z = 373.40, 375.30 $[M+H]^+$. HRMS (ESI): Calculated for $C_{16}H_{14}O_3N_6{}^{35}Cl$: m/z = 373.08104 $[M+H]^+$, found: m/z = 373.08134 $[M+H]^+$. Calculated for $C_{16}H_{14}O_3N_6{}^{37}Cl$: m/z = 375.07809 $[M+H]^+$, found: m/z = 375.07796 $[M+H]^+$.

6-chloro-*N*-methyl-2-(4-nitrophenoxy)pyrimidin-4-amine (343)

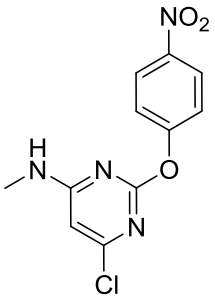

31a (50 mg, 175 µmol) was reacted with methylamine hydrochloride according to general procedure B. Purification of the crude was performed by silica gel column chromatography (20% EtOAc/n-Pentane + 3% Et_3N) to obtain the product (37 mg, 133 µmol, 76%) as an off-white amorphous solid. R_f: 0.24 (30% EtOAc/n-Pentane + 3% Et_3N).

^{1}H NMR (500 MHz, DMSO-d_6) δ = 8.29 (d, ^{3}J = 9.0 Hz, 2H), 8.00 – 7.85 (bs, 1H), 7.48 (d, ^{3}J = 8.9 Hz, 2H), 6.37 (bs, 1H), 2.74 (d, ^{3}J = 4.8 Hz, 3H).

ESI-MS: m/z = 281.15, 283.08 $[M+H]^+$. HRMS (ESI): Calculated for $C_{11}H_{10}O_3N_4{}^{35}Cl$: m/z = 281.04359 $[M+H]^+$, found: m/z = 281.04438 $[M+H]^+$. Calculated for $C_{11}H_{10}O_3N_4{}^{37}Cl$: m/z = 283.04064 $[M+H]^+$, found: m/z = 283.04102 $[M+H]^+$.

4-chloro-2-(4-nitrophenoxy)-6-(pyrrolidin-1-yl)pyrimidine (344)

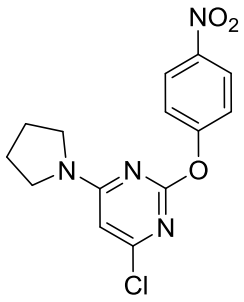

31a (50 mg, 175 µmol) was reacted with pyrrolidine according to general procedure B. Purification of the crude was performed by silica gel column chromatography (5% EtOAc/n-Pentane) to obtain the product (52 mg, 161 µmol, 92%) as a white amorphous solid.

R_f: 0.17 (10% EtOAc/n-Pentane).

^{1}H NMR (400 MHz, DMSO-d_6) δ = 8.32 – 8.27 (m, 2H), 7.51 – 7.45 (m, 2H), 6.45 (s, 1H), 3.36 (t, ^3J = 6.8 Hz, 2H), 2.08 (s, ^3J = 2.7 Hz, 1H), 2.00 – 1.79 (m, 4H). ^{13}C NMR (101 MHz, DMSO-d_6) δ = 162.48, 161.63, 158.42, 157.71, 144.14, 125.22, 122.37, 98.22, 46.68, 46.51, 24.86, 24.17.

ESI-MS: m/z = 321.20, 323.13 $[M+H]^+$. HRMS (ESI): Calculated for $C_{14}H_{14}O_3N_4{}^{35}Cl$: m/z = 321.07489 $[M+H]^+$, found: m/z = 321.07584 $[M+H]^+$. Calculated for $C_{14}H_{14}O_3N_4{}^{37}Cl$: m/z = 323.07194 $[M+H]^+$, found: m/z = 323.07249 $[M+H]^+$.

6-chloro-2-(4-nitrophenoxy)-*N*-phenylpyrimidin-4-amine (342)

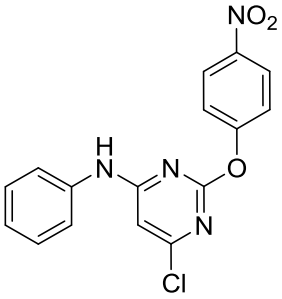

31a (50 mg, 175 µmol) was reacted with aniline according to general procedure B. Purification of the crude was performed by silica gel column chromatography (20% EtOAc/n-Pentane) to obtain the product (60 mg, 175 µmol, quant.) as an off-white amorphous solid.

R_f: 0.26 (20% EtOAc/n-Pentane).

^{1}H NMR (500 MHz, DMSO-d_6) δ = 10.05 (s, 1H), 8.34 (d, ^3J = 9.1 Hz, 2H), 7.55 (d, ^3J = 9.1 Hz, 2H), 7.36 (d, ^3J = 7.8 Hz, 2H), 7.18 (t, ^3J = 7.6 Hz, 2H), 7.02 (t, ^3J = 7.2 Hz, 1H), 6.59 (s, 1H).

ESI-MS: m/z = 343.18 $[M+H]^+$. HRMS (ESI): Calculated for $C_{11}H_{10}O_3N_4{}^{35}Cl$: m/z = 343.05924 $[M+H]^+$, found: m/z = 343.06049 $[M+H]^+$.

_N_-(6-chloro-2-(4-nitrophenoxy)pyrimidin-4-yl)-5-methylisoxazol-3-amine • TFA (348)

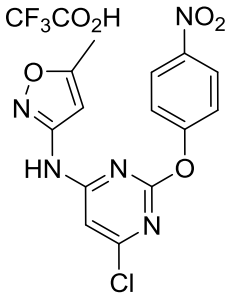

31a (50 mg, 175 µmol) was reacted with 5-methylisoxazol-3-amine according to general procedure B**.** Purification of the crude was performed by mass-directed preparative HPLC to obtain the product (7 mg, 16 µmol, 9%) as a white amorphous solid.

^{1}H NMR (600 MHz, DMSO-d_6) δ = 10.93 (s, 1H), 8.36 (d, J = 9.1 Hz, 2H), 7.59 – 7.56 (m, 2H), 7.04 (bs, 1H), 6.03 (s, 1H), 2.26 (s, 3H). ^{13}C NMR (101 MHz, DMSO-d_6) δ = 169.23, 162.65, 162.60, 157.41, 156.62, 145.10, 125.64, 125.52, 123.16, 122.69, 117.06, 19.54, 11.82.

ESI-MS: m/z = 348.39 $[M+H]^+$. HRMS (ESI): Calculated for $C_{14}H_{11}O_4N_5$ ^{35}Cl: m/z = 348.04941 $[M+H]^+$, found: m/z = 348.04985 $[M+H]^+$.

_N_-(6-chloro-2-(4-nitrophenoxy)pyrimidin-4-yl)-1H-indazol-3-amine • TFA (337)

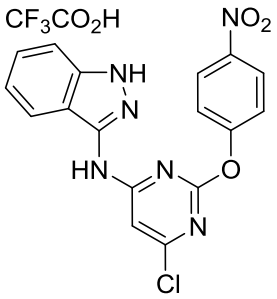

31a (50 mg, 175 µmol) was reacted with 1H-indazol-3-amine according to general procedure B. Purification of the crude was performed by mass-directed preparative HPLC to obtain the product (73 mg, 147 µmol, 84%) as a white amorphous solid.

^{1}H NMR (400 MHz, DMSO-d_6, 50°C) δ = 12.64 (s, 1H), 10.64 (s, 1H), 8.26 (d, J = 8.9 Hz, 2H), 8.38 – 7.57 (m, 1H), 7.87 (d, J = 6.8 Hz, 1H), 7.52 (d, J = 9.1 Hz, 2H), 7.47 (d, J = 8.4 Hz, 1H), 7.39 – 7.33 (m, 1H), 7.05 (t, J = 7.5 Hz, 1H). ^{13}C NMR (151 MHz, DMSO-d_6) δ = 163.01, 162.72, 157.70, 156.69, 145.15, 144.44, 140.62, 125.73, 125.48, 122.78, 122.64, 119.77, 117.12, 110.13, 100.49.

ESI-MS: m/z = 383.42 $[M+H]^+$. HRMS (ESI): Calculated for $C_{17}H_{12}O_3N_6$ ^{35}Cl: m/z = 383.06539 $[M+H]^+$, found: m/z = 383.06543 $[M+H]^+$.

4-chloro-6-((5-methyl-1H-pyrazol-3-yl)oxy)-2-(4-nitrophenoxy)pyrimidine • TFA (339)

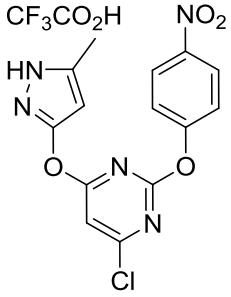

31a (50 mg, 175 µmol) was reacted with 5-methyl-1H-pyrazol-3-ol according to general procedure B. Purification of the crude was performed by mass-directed preparative HPLC to obtain the product (21 mg, 45 µmol, 26%) as a white amorphous solid.

^{1}H NMR (600 MHz, DMSO-d_6) δ = 12.34 (s, 1H), 8.35 – 8.29 (m, 2H), 7.60 – 7.53 (m, 2H), 7.10 (s, 1H), 5.80 (s, 1H), 2.18 (s, 3H). ^{13}C NMR (151 MHz, DMSO-d_6) δ = 171.06, 162.96, 162.17, 156.91, 155.56, 144.90, 140.23, 125.48, 122.95, 102.74, 94.09, 10.96.

ESI-MS: m/z = 348.31 $[M+H]^+$. HRMS (ESI): Calculated for $C_{14}H_{11}O_4N_5$ ^{35}Cl: m/z = 348.04941 $[M+H]^+$, found: m/z = 348.04965 $[M+H]^+$.

***N*-(6-chloro-2-(4-nitrophenoxy)pyrimidin-4-yl)-1H-benzo[d]imidazol-2-amine • TFA (340)**

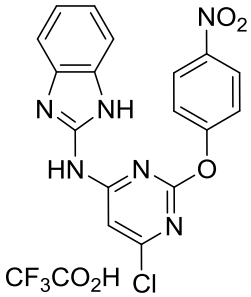

31a (50 mg, 175 µmol) was reacted with 1H-benzo[d]imidazol-2-amine according to general procedure B. Purification of the crude was performed by mass-directed preparative HPLC to obtain the product (41 mg, 82 µmol, 47%) as a white amorphous solid.

^{1}H NMR (600 MHz, DMSO-d_6) δ = 8.55 – 8.45 (m, 1H), 8.42 – 8.38 (m, 2H), 7.89 (s, 1H), 7.74 – 7.70 (m, 1H), 7.70 – 7.67 (m, 2H), 7.53 (d, J = 8.1 Hz, 1H), 7.38 (d, J = 7.8 Hz, 1H), 7.34 – 7.16 (m, 2H).

ESI-MS: m/z = 383.45 $[M+H]^+$. HRMS (ESI): Calculated for $C_{17}H_{12}O_3N_6$ ^{35}Cl: m/z = 383.06539 $[M+H]^+$, found: m/z = 383.06695 $[M+H]^+$. Calculated for $C_{17}H_{12}O_3N_6$ ^{37}Cl: m/z = 385.06396 $[M+H]^+$, found: m/z = 385.06399 $[M+H]^+$.

6-chloro-*N*-(2-chlorophenyl)-2-(4-nitrophenoxy)pyrimidin-4-amine • TFA (341)

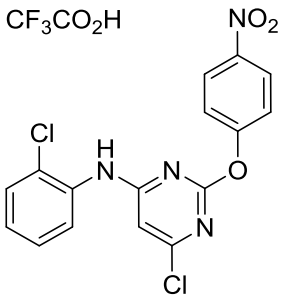

31a (50 mg, 175 µmol) was reacted with 2-chloroaniline according to general procedure B. Purification of the crude was performed by mass-directed preparative HPLC to obtain the product (70 mg, 142 µmol, 81%) as a white amorphous solid.

^{1}H NMR (400 MHz, DMSO-d_6) δ = 9.75 (s, 1H), 8.31 – 8.24 (m, 2H), 7.55 (dd, J = 7.6 Hz, 1.9 Hz, 1H), 7.52 – 7.46 (m, 3H), 7.25 – 7.16 (m, 2H), 6.64 (s, 1H). ^{13}C NMR (101 MHz, DMSO-d_6) δ = 163.57, 163.10, 159.18, 157.40, 144.45, 134.42, 129.68, 127.33, 127.05, 126.96, 125.24, 122.80, 100.34.

ESI-MS: m/z = 377.41 $[M+H]^+$. HRMS (ESI): Calculated for $C_{16}H_{11}O_3N_4\,^{35}Cl_2$: m/z = 377.02027 $[M+H]^+$, found: m/z = 377.02023 $[M+H]^+$. Calculated for $C_{16}H_{11}O_3N_4\,^{37}Cl_2$: m/z = 379.01708 $[M+H]^+$, found: m/z = 379.01713 $[M+H]^+$.

1-(6-chloro-2-(4-nitrophenoxy)pyrimidin-4-yl)indoline (345)

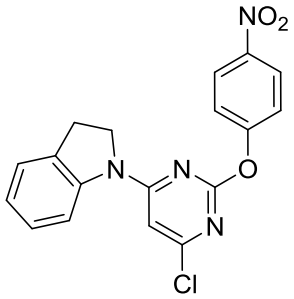

31a (50 mg, 175 µmol) was reacted with indoline according to general procedure B. Purification of the crude was performed by silica gel column chromatography (20% EtOAc/n-Pentane) to obtain the product (65 mg, 175 µmol, quant.) as an off-white amorphous solid.

R_f: 0.39 (20% EtOAc/n-Pentane).

^{1}H NMR (500 MHz, DMSO-d_6) δ = 8.39 (d, ^{3}J = 9.1 Hz, 2H), 7.59 (d, ^{3}J = 9.1 Hz, 2H), 7.46 (d, ^{3}J = 8.1 Hz, 1H), 7.22 (d, ^{3}J = 7.3 Hz, 1H), 6.93 (t, ^{3}J = 7.4 Hz, 1H), 6.79 – 6.73 (m, 2H), 4.04 (t, ^{3}J = 8.5 Hz, 2H), 3.18 (t, ^{3}J = 8.4 Hz, 2H).

ESI-MS: m/z = 369.23 $[M+H]^+$. HRMS (ESI): Calculated for $C_{18}H_{14}O_3N_4\,^{35}Cl$: m/z = 369.07489 $[M+H]^+$, found: m/z = 369.07607 $[M+H]^+$. Calculated for $C_{18}H_{14}O_3N_4\,^{37}Cl$: m/z = 371.07194 $[M+H]^+$, found: m/z = 371.07295 $[M+H]^+$.

3-((6-chloro-2-(4-nitrophenoxy)pyrimidin-4-yl)amino)-1H-pyrazol-5-ol • TFA (346)

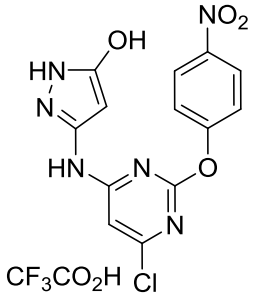

31a (50 mg, 175 µmol) was reacted with 3-amino-1H-pyrazol-5-ol according to general procedure B. Purification of the crude was performed by mass-directed preparative HPLC to obtain the product (18 mg, 38 µmol, 22%) as a white amorphous solid.

^{1}H NMR (600 MHz, DMSO-d_6) δ = 8.37 – 8.30 (m, 2H), 7.62 – 7.52 (m, 2H), 7.04 (s, 1H), 5.12 (s, 1H). ^{13}C NMR (151 MHz, DMSO-d_6) δ = 171.29, 162.94, 162.10, 156.90, 154.92, 148.89, 144.88, 125.59, 125.54, 123.06, 122.76, 102.61.

ESI-MS: m/z = 349.30 $[M+H]^+$. HRMS (ESI): Calculated for $C_{13}H_{10}O_4N_6{}^{35}Cl$: m/z = 349.04466 $[M+H]^+$, found: m/z = 349.04579 $[M+H]^+$.

4-(6-chloro-2-(4-nitrophenoxy)pyrimidin-4-yl)morpholine (347)

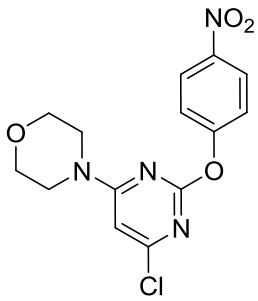

31a (50 mg, 175 µmol) was reacted with morpholine according to general procedure B. The addition of water to the crude led to the precipitation of pure product (54 mg, 160 µmol, 91%) as a white amorphous solid.

^{1}H NMR (400 MHz, DMSO-d_6) δ = 8.32 – 8.28 (m, 2H), 7.50 – 7.46 (m, 2H), 6.83 (s, 1H), 3.65 – 3.58 (m, 4H), 3.58 – 3.52 (m, 4H).

ESI-MS: m/z = 337.37, 339.24 $[M+H]^+$. HRMS (ESI): Calculated for $C_{14}H_{14}O_4N_4{}^{35}Cl$: m/z = 337.06981 $[M+H]^+$, found: m/z = 337.07000 $[M+H]^+$. Calculated for $C_{14}H_{14}O_4N_4{}^{37}Cl$: m/z = 339.06686 $[M+H]^+$, found: m/z = 339.06679 $[M+H]^+$.

_N_-(5-methyl-1H-pyrazol-3-yl)-6-(4-methylpiperazin-1-yl)-2-(4-nitrophenoxy) pyrimidin-4-amine (302)

The synthesis was carried out as described in and by the authors of the literature.[152]

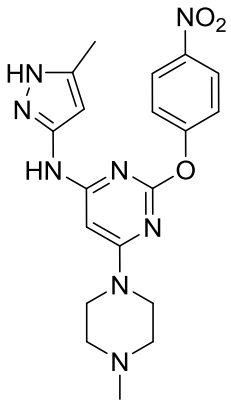

1H NMR (500 MHz, DMSO-d_6) δ 11.83 (s, 1H), 9.33 (s, 1H), 8.29 (d, J = 9.0 Hz, 2H), 7.43 (d, J = 9.0 Hz, 2H), 6.36 (s, 1H), 5.64 (s, 1H), 3.43 (s, 4H), 2.34 (s, 4H), 2.20 (s, 3H), 2.07 (s, 3H). 13C NMR (126 MHz, DMSO-d_6) δ 164.29, 161.42, 158.85, 148.81, 143.66, 138.49, 138.05, 125.15, 122.47, 94.97, 79.63, 54.03, 45.66, 43.70, 9.96.

ESI-MS: m/z = 411.40 $[M+H]^+$. HRMS (ESI): Calculated for $C_{19}H_{23}O_3N_8$: m/z = 411.18876 $[M+H]^+$, found: m/z = 411.18820 $[M+H]^+$.

_N_-(5-methyl-1H-pyrazol-3-yl)-6-morpholino-2-(4-nitrophenoxy)pyrimidin-4-amine • TFA (332)

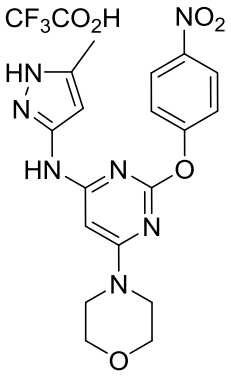

2 (50 mg, 144 µmol) was dissolved in morpholine (3 ml) and the resulting reaction mixture was stirred at 110 °C for 30 min. Subsequently the reaction mixture was cooled to rt and a saturated aqueous solution of $NaHCO_3$ followed by EtOAc was added. The aqueous layer was extracted with EtOAc (3 times 50 ml) and the combined organic layers were dried over magnesium sulfate before the volatiles were removed under reduced pressure. Purification of the crude was performed by preparative HPLC to yield the product (5 mg, 11 µmol, 7%) as a white amorphous solid.

^{1}H NMR (400 MHz, CD_3CN) δ = 9.88 (s, 1H), 8.31 (d, J = 8.9 Hz, 2H), 7.45 (d, J = 8.5 Hz, 2H), 6.20 (s, 1H), 5.89 (s, 1H), 3.66 – 3.61 (m, 4H), 3.48 – 3.43 (m, 4H), 2.25 (s, 3H).

ESI-MS: m/z = 398.48 $[M+H]^+$. HRMS (ESI): Calculated for $C_{18}H_{20}O_4N_7$: m/z = 398.15713 $[M+H]^+$, found: m/z = 398.15627 $[M+H]^+$.

N^4,N^4-dimethyl-N^6-(5-methyl-1H-pyrazol-3-yl)-2-(4-nitrophenoxy)pyrimidine-4,6-diamine • TFA (333)

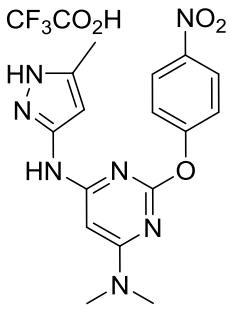

2 (30 mg, 87 µmol), dimethylamine hydrochloride (141 mg, 1.73 mMol) and caesium carbonate (142 mg, 433 µmol) were dissolved in NMP (1.5 ml) and the resulting reaction mixture was stirred at 110 °C for 16 h. Subsequently the reaction mixture was cooled to rtT and a saturated aqueous solution of $NaHCO_3$ followed by EtOAc was added. The aqueous layer was extracted with EtOAc (3 x 50 ml) and the combined organic layers were dried over magnesium sulfate before the volatiles were removed under reduced pressure. Purification of the crude was performed by mass-directed preparative HPLC to yield the product (7 mg, 15 µmol, 17%) as a white amorphous solid.

^{1}H NMR (400 MHz, DMSO-d_6) δ = 9.35 (s, 1H), 8.32 – 8.26 (m, 2H), 7.46 – 7.40 (m, 2H), 6.19 (s, 1H), 5.67 (s, 1H), 2.95 (s, 6H), 2.08 (s, 3H).

ESI-MS: m/z = 356.41 $[M+H]^+$. HRMS (ESI): Calculated for $C_{16}H_{18}O_3N_7$: m/z = 356.14656 $[M+H]^+$, found: m/z = 356.14703 $[M+H]^+$.

2-chloro-*N*-(5-methyl-1H-pyrazol-3-yl)-6-(trifluoromethyl)pyrimidin-4-amine (328a)

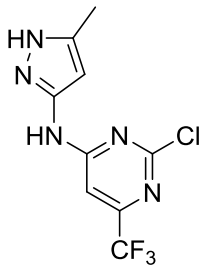

To a stirred solution of 2,4-dichloro-6-(trifluoromethyl)pyrimidine (200 mg, 922 µmol) in DMF (2 mL) was added DIPEA (219 µl, 1.29 mMol) followed by 5-methyl-1H-pyrazol-3-amin (125 mg, 1.29 mMol). The solution was stirred at rt for 16 h. The mixture was cooled to rt and water (5 mL) and EtOAc (15 mL) were added. The organic layer was separated and the aqueous layer was extracted with EtOAc (2x). The combined organic layers were then washed with sat $NaHCO_3$ (3x) and then with brine (2x) and then dried over anhydrous magnesium sulfate. The product was dried *in vacuo*. The solid was then washed with 50 mL of EtOAc/n-Pentanee (1:1) and the off-white solid (225 mg, 812 µmol, 88%) was then dried in Vacuo again.

^{1}H NMR (400 MHz, DMSO-d_6) δ = 12.29 (d, J = 23.3 Hz, 2H), 10.97 (s, 2H), 8.15 – 5.78 (m, 2H), 2.24 (s, 3H). ^{13}C NMR (101 MHz, DMSO-d_6) δ = 184.61, 161.72, 160.72, 147.16, 146.39, 140.43, 139.53, 138.84, 121.56, 118.87, 112.86, 102.83, 101.05, 96.24, 95.28, 78.17, 39.52, 19.56.
ESI-MS: m/z = 278.0 $[M+H]^+$. HRMS (ESI): Calculated for $C_9H_8N_5\,^{35}ClF_3$: m/z = 278.04148 $[M+H]^+$, found: m/z = 278.04197 $[M+H]^+$. Calculated for $C_9H_8N_5\,^{37}ClF_3$: m/z = 280.03853 $[M+H]^+$, found: m/z = 280.03837 $[M+H]^+$.

N-(5-methyl-1H-pyrazol-3-yl)-2-(4-nitrophenoxy)-6-(trifluoromethyl) pyrimidin-4-amine • TFA (331)

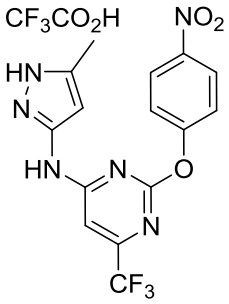

A stirred solution of 4-nitrophenol (50 mg, 359 µmol), caesiumcarbonate (70 mg, 216 µmol) and 2-chloro-N-(5-methyl-1H-pyrazol-3-yl)-6-(trifluoromethyl)pyrimidin-4-amine (**37a**) (50 mg, 180 µmol) in DMF (3 mL) was heated to 100 °C for 16 h. The mixture was cooled to ambient and diluted with water (5 mL) and EtOAc (5 mL). The aqueous solution was extracted with EtOAc (2 x 5 mL) und dried over magnesiumsulfate. Silica column chromatography (50% EtOAc/n-Pentane) followed by mass-directed preparative HPLC yielded the product (23 mg, 47 µmol, 13%) as a white amorphous solid.

R_f: 0.20 (50% EtOAc/n-Pentane).

^{1}H NMR (400 MHz, DMSO-d_6, 100°C) δ = 10.34 (s, 1H), 8.37 – 8.22 (m, 2H), 7.60 – 7.44 (m, 2H), 7.29 (s, 1H), 5.77 (s, 1H), 2.11 (s, 3H). ^{13}C NMR (101 MHz, DMSO-d_6, 100 °C) δ = 164.88, 162.74, 158.42, 147.26, 145.30, 139.39, 125.67, 123.29, 99.61, 96.59, 10.75.

ESI-MS: m/z = 381.23 $[M+H]^+$. HRMS (ESI): Calculated for $C_{15}H_{12}O_3N_6F_3$: m/z = 381.09175 $[M+H]^+$, found: m/z = 381.09273 $[M+H]^+$.

2-chloro-6-methyl-*N*-(5-methyl-1H-pyrazol-3-yl)pyrimidin-4-amine (328b)

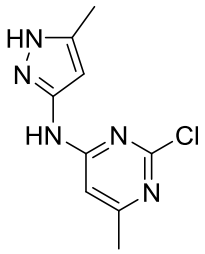

A solution of 5-methyl-1H-pyrazol-3-amine (2.98 g, 30.7 mMol) in EtOH (150 mL) was added dropwise to a solution of 2,4-dichloro-6-methylpyrimidine (5 g, 30,67 mMol) in EtOH (150 mL). The resulting solution was stirred at rt for 7 d. After completion the mixture was diluted with water (150 mL) and EtOAc (150 mL). The organic layer was separated and the aqueous layer was extracted with EtOAc (2 x 75 mL). The combined organic layers were washed with sat. $NaHCO_3$ (3x) and brine (2x) and afterwards dried over anhydrous magnesium sulfate. The product (2.33 g, 10.43 mMol, 34%) was obtained as a white solid after being dried *in vacuo*.

^{1}H NMR (500 MHz, DMSO-d_6) δ = 10.24 (s, 1H), 7.00 (s, 1H), 6.07 (s, 1H), 2.27 (s, 3H), 2.22 (s, 3H).

ESI-MS: m/z = 224.0 $[M+H]^+$. HRMS (ESI): Calculated for $C_9H_{11}N_5$ ^{35}Cl: m/z = 224.06975 $[M+H]^+$, found: m/z = 224.07072 $[M+H]^+$. Calculated for $C_9H_{11}N_5$ ^{37}Cl: m/z = 226.06680 $[M+H]^+$, found: m/z = 226.06713 $[M+H]^+$.

6-methyl-*N*-(5-methyl-1H-pyrazol-3-yl)-2-(4-nitrophenoxy)pyrimidin-4-amine • TFA (330)

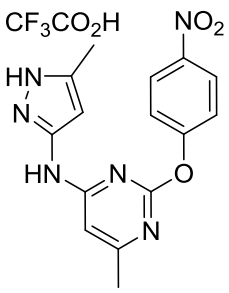

A stirred solution of 4-nitrophenol (124 mg, 894 µmol), caesiumcarbonate (161 mg, 492 µmol) and 2-chloro-N-(5-methyl-1H-pyrazol-3-yl)-6-(trifluoromethyl)pyrimidin-4-amine (**37b**) (100 mg, 447 µmol) in DMF (3 mL) was heated to 100 °C for 3 d. The mixture was cooled to ambient and diluted with water (5 mL) and EtOAc (5 mL). The aqueous solution was extracted with EtOAc (2 x 5 mL) und dried over magnesiumsulfate. Silica column chromatography (50% EtOAc/n-Pentane) followed by HPLC yielded the product (175 mg, 398 µmol, 89%) as a white amorphous solid.

^{1}H NMR (400 MHz, DMSO-d_6, 100 °C) δ = 9.49 (s, 1H), 8.28 (d, ^3J = 8.9 Hz, 2H), 7.44 (d, ^3J = 8.9 Hz, 2H), 6.75 (s, 1H), 5.79 (s, 1H), 2.26 (s, 3H), 2.12 (s, 3H).

ESI-MS: m/z = 327.27 $[M+H]^+$. HRMS (ESI): Calculated for $C_{15}H_{15}O_3N_6$: m/z = 327.12001 $[M+H]^+$, found: m/z = 327.12064 $[M+H]^+$.

***N*4-(5-methyl-1H-pyrazol-3-yl)-*N*2-(4-nitrophenyl)-6-(trifluoromethyl)pyrimidine-2,4-diamine • TFA (335)**

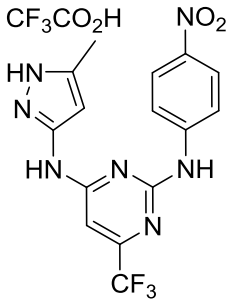

37a (100 mg, 360 µmol), 4-nitroaniline (75 mg, 540 µmol) and 4-methylbenzenesulfonic acid hydrate (69 mg, 360 µmol) were dissolved in *tert*-Butanol. The resulting reaction mixrure was heated to 50 °C for 16 h and afterwards cooled to room temperature. The reaction was quenched by the addition of saturated aqueous $NaHCO_3$ solution and EtOAc. The aqueous layer was extracted with EtOAc (3 times 50 ml) and the combined organic layers were dried over magnesium sulfate before the volatiles were removed under reduced pressure. Purification of the crude was performed by preparative HPLC to yield the product (37 mg, 76 µmol, 21%) as a yellow amorphous solid.

^{1}H NMR (500 MHz, DMSO-d_6, 50 °C) δ = 10.25 (s, 1H), 10.19 (s, 1H), 8.19 – 8.14 (m, 2H), 8.06 (d, J = 9.2 Hz, 2H), 7.24 – 6.88 (m, 1H), 6.26 (s, 1H), 2.26 (s, 3H).

ESI-MS: m/z = 380.35 $[M+H]^+$. HRMS (ESI): Calculated for $C_{15}H_{13}O_2N_7F_3$: m/z = 380.10773 $[M+H]^+$, found: m/z = 380.10759 $[M+H]^+$.

_N_-(5-methyl-1H-pyrazol-3-yl)-2-((4-nitrophenyl)thio)-6-(trifluoromethyl) pyrimidin-4-amine • TFA (334)

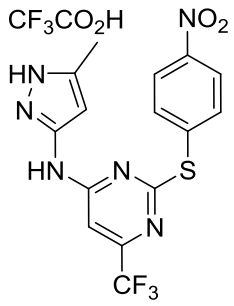

37a (50 mg, 180 µmol), 4-nitrophenol (70 mg, 360 µmol) and caesium carbonate (118 mg, 360 µmol) were dissolved in NMP (1.5 ml) and the resulting reaction mixture was stirred at 110 °C for 16 h. Subsequently the reaction mixture was cooled to rt and a saturated aqueous solution of $NaHCO_3$ followed by EtOAc was added. The aqueous layer was extracted with EtOAc (3 times 50 ml) and the combined organic layers were dried over magnesium sulfate before the volatiles were removed under reduced pressure. Purification of the crude was performed by preparative HPLC to yield the product (32 mg, 63 µmol, 35%) as a yellow-white amorphous solid.

^{1}H NMR (400 MHz, DMSO-d_6) δ = 10.66 (s, 1H), 8.35 (d, J = 7.5 Hz, 2H), 7.96 (d, J = 8.6 Hz, 2H), 6.90 (s, 1H), 5.27 (s, 1H), 1.91 (s, 3H).

ESI-MS: m/z = 397.36 $[M+H]^+$. HRMS (ESI): Calculated for $C_{15}H_{12}O_2N_6F_3S$: m/z = 397.06891 $[M+H]^+$, found: m/z = 397.06727 $[M+H]^+$.

7.20.2.3 Synthesis of Aumitin

2-chloro-6-methyl-*N*-phenylpyrimidin-4-amine (422)

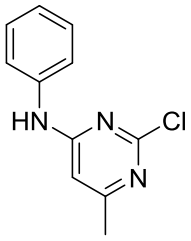

2,4-dichloro-6-methylpyrimidine (8.00 g, 49.1 mMol), aniline (5.60 mL, 61.4 mMol) and DIPEA (10.69 mL, 61.4 mMol) were dissolved in cold *n*-butanol (80 mL) and slowly brought to rt over 3 days. Subsequently, 100 mL of EtOAc and 40 mL of water were added to the reaction solution. The aqueous layer was extracted three times with 40 mL of EtOAc and the combined organic layers were dried over anhydrous magnesium sulfate and then concentrated *in vacuo*. The crude was purified by column chromatography on silica gel (0 – 50% EtOAc/cyclohexane). The product (4.50 g, 20.5 mMol, 42%) was obtained as an off-white solid.

^{1}H NMR (600 MHz, DMSO-d_6) δ = 9.89 (s, 1H), 7.55 (d, *J* = 7.8 Hz, 2H), 7.36 (t, *J* = 7.9 Hz, 2H), 7.08 (t, *J* = 7.4 Hz, 1H), 6.58 (s, 1H), 2.27 (s, 3H). ^{13}C NMR (151 MHz, DMSO) δ = 167.24, 161.89, 159.02, 138.84, 128.98, 123.40, 120.53, 103.44, 23.20.

ESI-MS: m/z = 220.23, 222.11 $[M+H]^+$.

HRMS (ESI): calculated for $C_{11}H_{11}N_3{}^{35}Cl$: m/z = 220.06360 $[M+H]^+$,
found: m/z = 220.06424 $[M+H]^+$.
calculated for $C_{11}H_{11}N_3{}^{37}Cl$: m/z = 222.06065 $[M+H]^+$,
found: m/z = 222.06086 $[M+H]^+$.

***N*2-(4-aminophenyl)-6-methyl-*N*4-phenylpyrimidine-2,4-diamine (423)**

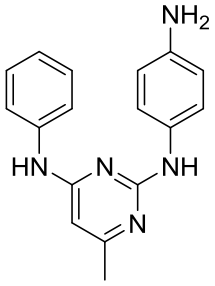

2-chloro-6-methyl-*N*-phenylpyrimidin-4-amine (422) (1.00 g, 4.55 mMol) and *p*-phenylenediamine (492 mg, 4.55 mMol) were dissolved in 15 mL EtOH and heated to 50 °C under microwave irradiation for 1 h. Afterwards the ethanol was removed *in vacuo* and the product used without further purification.

^{1}H NMR (600 MHz, CD_3CN) δ = 7.62 (bs, 2H), 7.52 (d, *J* = 7.8 Hz, 2H), 7.27 – 7.19 (m, 4H), 6.96 (t, *J* = 7.4 Hz, 1H), 6.58 – 6.54 (m, 2H), 5.93 (s, 1H), 3.77 (bs, 2H), 2.13 (s, 3H). ^{13}C NMR (151 MHz, CD_3CN) δ = 167.06, 162.47, 161.52, 144.36, 141.00, 131.77, 129.64, 123.67, 123.42, 121.43, 115.55, 96.57, 24.05.

ESI-MS: m/z = 292.30 $[M+H]^+$.

HRMS (ESI): calculated for $C_{17}H_{18}N_5$: m/z = 292.15567 $[M+H]^+$,
found: m/z = 292.15597 $[M+H]^+$.

2-chloro-*N*-(4-((4-methyl-6-(phenylamino)pyrimidin-2-yl)amino)phenyl)benz-amide (Aumitin)

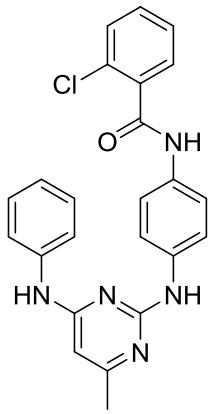

*N*2-(4-aminophenyl)-6-methyl-*N*4-phenylpyrimidines-2,4-diamine (423) (54 mg, 185 µmol), 2-chlorobenzoic acid (29 mg, 185 µmol), DIPEA (32 µL, 185 µmol) and PyBOP (96 mg, 185 µmol) were dissolved in 2 mL DMF at 0 °C. The reaction mixture was brought to room temperature overnight. The reaction was then quenched by the addition of 10 mL of water and 15 mL of EtOAc. The organic layer was washed twice with 4 mL of HCl (aq., 1M), twice with 4 mL of sodium carbonate solution (saturated, aq.) and eventually dried over anhydrous magnesium sulfate and concentrated *in vacuo*. The product (42 mg, 77 µmol, 42%) was isolated by chromatography on silica gel (0-50% EtOAc/cyclohexane). Rf: 0.13 (50% EtOAc/cyclohexane)

^{1}H NMR (600 MHz, CD_3CN) δ = 8.64 (s, 1H), 7.92 (s, 1H), 7.65 (d, *J* = 8.9 Hz, 2H), 7.61 – 7.55 (m, 5H), 7.51 (dd, *J* = 8.0, 0.9 Hz, 1H), 7.46 (td, *J* = 7.7, 1.7 Hz, 1H), 7.42 (td, *J* = 7.4, 1.2 Hz, 1H), 7.34 (t, *J* = 7.9 Hz, 2H), 7.10 (t, *J* = 7.4 Hz, 1H), 6.08 (s, 1H), 2.26 (s, 3H). ^{13}C NMR (151 MHz, CD_3CN) δ = 165.93, 162.69, 158.93, 140.07, 137.64, 137.15, 134.37, 132.18, 131.46, 130.84, 129.98, 129.82, 128.15, 124.57, 122.29, 121.72, 121.33, 97.56, 22.65.

ESI-MS: m/z = 430.45, 432.38 $[M+H]^+$.

HRMS (ESI): calculated for $C_{24}H_{21}N_5{}^{35}Cl$: m/z = 430.14291 $[M+H]^+$,

found: m/z = 430.14394 $[M+H]^+$.

calculated for $C_{24}H_{21}N_5{}^{37}Cl$: m/z = 432.13996 $[M+H]^+$,

found: m/z = 432.14105 $[M+H]^+$.

7.20.2.4 Synthesis and Origin of Literature Reported, Not Commercially Acquired Kinase Inhibitors

PI4KB inhibitor 1 (421)

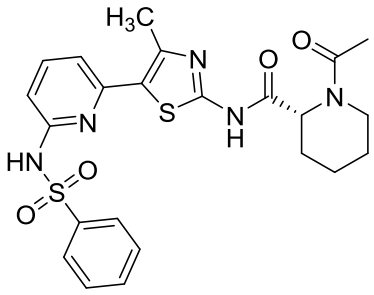

The thiazole based PI4KB inhibitor was obtained as a kind donation by Astra Zeneca.[183]

PI4KB inhibitor 2[181]

4-bromo-6-chloropyridazin-3-amine (763)

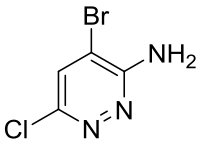

4-bromo-6-chloropyridazin-3-amine was synthesized as described in the literature.[181]

ESI-MS: m/z = 208.24, 209.98 $[M+H]^+$.

HRMS (ESI): calculated for $C_4H_4N_3Br\ ^{35}Cl$: m/z = 207.92716 $[M+H]^+$,
found: m/z = 207.92688 $[M+H]^+$.
calculated for $C_4H_4N_3Br\ ^{37}Cl$: m/z = 209.92421 $[M+H]^+$,
found: m/z = 209.92447 [M+H]+.

6,8-dichloro-2-methylimidazo[1,2-b]pyridazine (764)

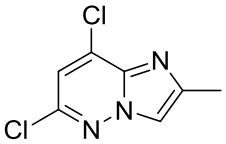

6,8-dichloro-2-methylimidazo[1,2-b]pyridazine was synthesized as described in the literature.[181]

^{1}H NMR (500 MHz, $CDCl_3$) δ = 7.74 (s, 1H), 7.12 (s, 1H), 2.51 (s, 3H).
^{13}C NMR (126 MHz, $CDCl_3$) δ = 145.45, 145.15, 135.73, 133.59, 117.23, 116.27, 14.98.

ESI-MS: m/z = 202.22, 203.93 $[M+H]^+$.

HRMS (ESI): calculated for $C_7H_6N_3\ ^{35}Cl_2$: m/z = 201.99333 $[M+H]^+$,
found: m/z = 201.99234 $[M+H]^+$.
calculated for $C_7H_6N_3\ ^{35}Cl\ ^{37}Cl$: m/z = 203.99038 $[M+H]^+$,
found: m/z = 203.98923 $[M+H]^+$.

_N_-(2-((6-chloro-2-methylimidazo[1,2-b]pyridazin-8-yl)amino)ethyl)acetamide (765)

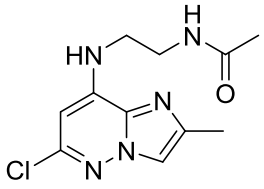

N-(2-((6-chloro-2-methylimidazo[1,2-b]pyridazin-8-yl)amino) ethyl) acetamide was synthesized as described in the literature.[181]

^{1}H NMR (600 MHz, DMSO) δ = 8.22 (s, 1H), 8.04 (t, *J* = 5.4, 1H), 7.79 (t, *J* = 5.8 Hz, 1H), 7.75 – 7.72 (m, 2H), 6.20 (s, 1H), 3.26 – 3.21 (m, 2H), 2.31 (s, 3H), 1.79 (s, 3H).

ESI-MS: m/z = 268.28, 270.14 $[M+H]^+$.

HRMS (ESI): calculated for $C_{11}H_{15}ON_5{}^{35}Cl$: m/z = 268.09596 $[M+H]^+$,
found: m/z = 268.09534 $[M+H]^+$.
calculated for $C_{11}H_{15}ON_5{}^{37}Cl$: m/z = 270.09301 $[M+H]^+$,
found: m/z = 270.09222 $[M+H]^+$.

_N_-(2-((6-chloro-3-iodo-2-methylimidazo[1,2-b]pyridazin-8-yl)amino)ethyl)acetamide (766)

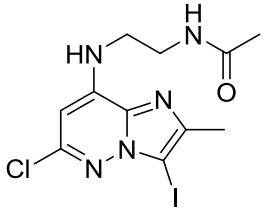

N-(2-((6-chloro-3-iodo-2-methylimidazo[1,2-b]pyridazin-8-yl)amino) ethyl)acetamide was synthesized as described in the literature.[181]

^{1}H NMR (600 MHz, DMSO) δ = 8.03 (t, *J* = 5.5 Hz, 1H), 7.89 (t, *J* = 5.9 Hz, 1H), 6.31 (s, 1H), 3.33 (bs, 2H), 3.23 (q, *J* = 6.1 Hz, 2H), 2.34 (s, 3H), 1.79 (s, 3H).

ESI-MS: m/z = 394.36 $[M+H]^+$.

HRMS (ESI): calculated for $C_{11}H_{14}ON_5{}^{35}ClI$: m/z = 393.99261 $[M+H]^+$,
found: m/z = 393.99317 $[M+H]^+$.

_N_-(2-((6-chloro-3-(3-(N,N-dimethylsulfamoyl)phenyl)-2-methylimidazo[1,2-b]pyridazin-8-yl)amino)ethyl)acetamide (422)

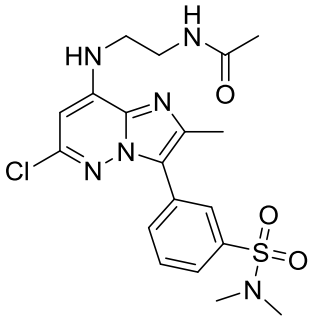

N-(2-((6-chloro-3-(3-(N,N-dimethylsulfamoyl)phenyl)-2-methyl-imidazo[1,2-b]pyridazin-8-yl)amino)ethyl)acetamide was synthesized as described in the literature.[181]

^{1}H NMR (600 MHz, $CDCl_3$) δ = 9.41 (s, 1H), 8.11 (s, 1H), 7.94 (d, *J* = 7.7 Hz, 1H), 7.82 – 7.75 (m, 2H), 7.71 (t, *J* = 5.4 Hz, 1H), 6.44 (s, 1H), 3.68 (dd, *J* = 10.5, 5.7 Hz, 2H), 3.50 (dd, *J* = 9.8, 4.6 Hz, 2H), 2.81 (s, 6H), 2.69 (s, 3H), 2.01 (s, 3H). ^{13}C NMR (151 MHz, $CDCl_3$) δ = 171.70, 152.02, 140.59, 136.75, 133.61, 131.92, 129.97, 129.52, 129.02, 128.42, 125.84, 125.48, 97.96, 43.81, 38.18, 37.68, 23.07, 11.14.

ESI-MS: m/z = 451.55, 453.27 $[M+H]^+$.

HRMS (ESI): calculated for $C_{19}H_{24}O_3N_6{}^{35}ClS$: m/z = 451.13136 $[M+H]^+$,
found: m/z = 451.13241 $[M+H]^+$,
calculated for $C_{19}H_{24}O_3N_6{}^{37}ClS$: m/z = 453.12841 $[M+H]^+$,
found: m/z = 453.12916 $[M+H]^+$.

PI3KC2G inhibitors[182]

***N*²-(3,5-dimethoxyphenyl)pyrazine-2,3-diamine (767)**

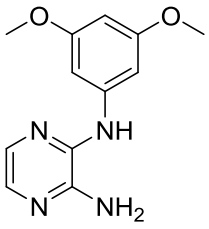

A suspension of 3-chloropyrazin-2-amine (500 mg, 3.86 mMol) and 3,5-dimethoxyaniline (621 mg, 4.05 mMol) in 20 mL HCl (aq., 0.1 M) was heated in the micro wave to 120 °C for 2 hours. After bringing the reaction mixture to room temperature it was diluted and thereafter stirred for 5 minutes with 20 mL EtOAC before the two layers were separated. The aqueous layer was extraceted three times with in each case 20 mL EtOAc and the combined organic layers were dried over anhydrous magnesium sulfate. The crude was purified by flash column chromatography on silica gel (10-60% EtOAc / Cyclohexane) to yield the product (293 mg, 1.19 mMol, 31%) as an off-white wax.

^{1}H NMR (600 MHz, $CDCl_3$) δ = 7.69 (d, *J* = 2.8 Hz, 1H), 7.64 (d, *J* = 2.9 Hz, 1H), 6.52 (d, *J* = 2.0 Hz, 2H), 6.17 (t, *J* = 2.0 Hz, 1H), 4.43 (s, 2H), 3.78 (s, 6H). ^{13}C NMR (151 MHz, $CDCl_3$) δ = 161.45, 145.44, 141.94, 140.96, 133.96, 132.85, 97.86, 94.87, 55.50.

ESI-MS: m/z = 247.24 $[M+H]^+$.

HRMS (ESI): calculated for $C_{12}H_{15}O_2N_4$: m/z = 247.11895 $[M+H]^+$,
found: m/z = 247.11874 $[M+H]^+$.

***N*-(3-((3,5-dimethoxyphenyl)amino)pyrazin-2-yl)-3-nitrobenzenesulfonamide (425)**

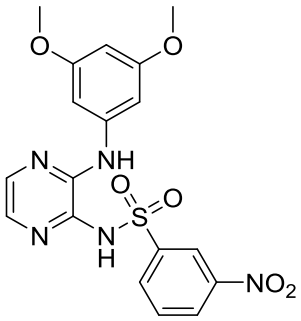

N-(3-((3,5-dimethoxyphenyl)amino)pyrazin-2-yl)-3-nitrobenzene sulfonamide was synthesized as described in the literature. [182]

^{1}H NMR (500 MHz, $CDCl_3$) δ = 12.02 (s, 1H), 8.82 (s, 1H), 8.41 (d, *J*=6.9, 1H), 8.32 (d, *J*=6.8, 1H), 8.11 (s, 1H), 7.73 (t, *J*=7.5, 1H), 7.46 (s, 1H), 6.94 (d, *J*=1.7, 2H), 6.91 (s, 1H), 6.22 (s, 1H), 3.79 (s, 6H). ^{13}C NMR (126 MHz, $CDCl_3$) δ = 161.19, 148.29, 146.81, 144.39, 140.32, 139.61, 132.04, 130.61, 128.26, 127.17, 121.72, 113.21, 98.52, 96.20, 55.58.

ESI-MS: m/z = 432.24 $[M+H]^+$.

HRMS (ESI): calculated for $C_{18}H_{18}O_6N_5S$: m/z = 432.09723 $[M+H]^+$,
found: m/z = 432.09694 $[M+H]^+$.

3-amino-*N*-(3-((3,5-dimethoxyphenyl)amino)pyrazin-2-yl)benzenesulfonamide (423)

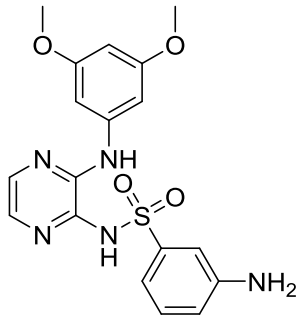

3-amino-N-(3-((3,5-dimethoxyphenyl)amino)pyrazin-2-yl)benzene sulfonamide sulfonamide was synthesized as described in the literature.[182]

^{1}H NMR (500 MHz, $CDCl_3$) δ = 11.87 (s, 1H), 8.12 (s, 1H), 7.63 – 7.56 (m, 1H), 7.40 (td, *J* = 7.5, 2.9 Hz, 1H), 7.28 (d, *J* = 4.2 Hz, 1H), 7.25 (d, *J* = 8.1 Hz, 1H), 7.22 – 7.16 (m, 2H), 6.90 (d, *J* = 2.2 Hz, 2H), 6.78 – 6.70 (m, 2H), 6.14 (t, *J* = 2.2 Hz, 1H), 3.73 (s, 6H).

ESI-MS: m/z = 402.23 $[M+H]^+$.

HRMS (ESI): calculated for $C_{18}H_{20}O_4N_5S$: m/z = 402.12305 $[M+H]^+$,

found: m/z = 402.12286 $[M+H]^+$.

calculated for $C_{12}H_{13}N_3{}^{37}Cl$: m/z = 236.07630 $[M+H]^+$,

found: m/z = 236.07627 $[M+H]^+$.

***N*-(3-(*N*-(3-((3,5-dimethoxyphenyl)amino)pyrazin-2-yl)sulfamoyl)phenyl)acetamide (424)**

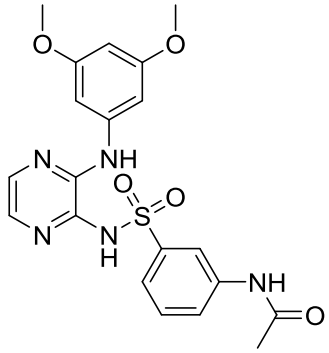

N-(3-(N-(3-((3,5-dimethoxyphenyl)amino)pyrazin-2-yl)sulf amoyl)phenyl)acetamide was synthesized as described in the literature.[182]

^{1}H NMR (500 MHz, $CDCl_3$) δ = 11.91 (s, 1H), 8.15 (d, *J* = 6.3 Hz, 1H), 7.84 (d, *J* = 8.1 Hz, 1H), 7.76 (s, 1H), 7.72 – 7.63 (m, 1H), 7.50 – 7.42 (m, 1H), 7.36 (d, *J* = 4.1 Hz, 1H), 6.94 (d, *J* = 2.1 Hz, 2H), 6.83 (d, *J* = 3.7 Hz, 1H), 6.20 (t, *J* = 2.0 Hz, 1H), 3.78 (s, 6H), 2.18 (s, 3H).

ESI-MS: m/z = 444.30 $[M+H]^+$.

HRMS (ESI): calculated for $C_{20}H_2O_5N_5S$: m/z = 444.13362 $[M+H]^+$,

found: m/z = 444.13320 $[M+H]^+$.

methyl 3-(*N*-(3-((3,5-dimethoxyphenyl)amino)pyrazin-2-yl)sulfamoyl)benzoate (426)

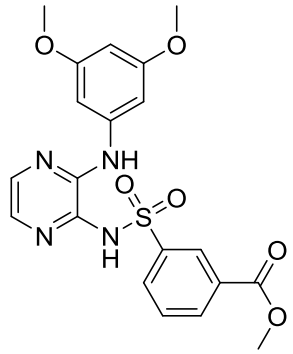

methyl 3-(N-(3-((3,5-dimethoxyphenyl)amino)pyrazin-2-yl)sulfamoyl)benzoate was synthesized as described in the literature.[182]

^{1}H NMR (400 MHz, $CDCl_3$) δ = 11.97 (s, 1H), 8.63 (s, 1H), 8.24 (d, *J* = 7.8 Hz, 1H), 8.21 – 8.09 (m, 2H), 7.61 (t, *J* = 7.8 Hz, 1H), 7.41 (d, *J* = 4.2 Hz, 1H), 6.96 (d, *J* = 2.2 Hz, 2H), 6.83 (d, *J* = 4.1 Hz, 1H), 6.22 (t, *J* = 2.1 Hz, 1H), 3.95 (s, 3H), 3.79 (s, 6H). ^{13}C NMR (126 MHz, $CDCl_3$) δ = 161.16, 147.15, 146.90, 143.03, 140.55, 139.95, 132.27, 130.11, 128.72, 127.09, 119.03, 115.93, 112.12, 98.39, 96.06, 55.58, 31.10.

ESI-MS: m/z = 445.26 $[M+H]^+$.

HRMS (ESI): calculated for $C_{20}H_{21}O_6N_4S$: m/z = 445.11763 $[M+H]^+$,

found: m/z = 445.11635 $[M+H]^+$.

8 Appendix

8.1 DMP-1

Appendix-Table 1: Inhibition of starvation-induced autophagy by dimethoxypyridines varying R^1 and R^2 whilst keeping the bridging ketone between the core and R^2 in place. Activity > 10 = no inhibition at a test concentration > 10 µM. Data is mean ± SD, n ≥ 3; for SD = na, data is mean, n = 2.

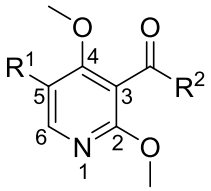

Entry	Number	R^1	R^2	IC_{50} [µM]	SD [µM]
1	**582**			1.8	na
2	**565**			2.2	0.5
3	**583**			2.5	0.7
4	**571**			2.6	0.3
5	**584**			2.8	na
6	**585**			2.8	na
7	**144**			3.0	na
8	**586**			3.4	0.4
9	**587**	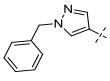		3.5	0.3
10	**558**			3.7	0.4
11	**121**			3.9	0.4
12	**119**			4.1	na
13	**146**			4.2	na
14	**130**			4.4	1.6

15	**555**			5.1	0.6
16	**559**			5.5	2.7
17	**545**	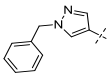		6.2	2.6
18	**150**	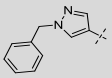		6.4	0.6
19	**117**	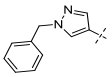		6.5	3.2
20	**588**			6.6	na
21	**105**			6.9	na
22	**589**			7.3	2.1
23	**570**			7.9	0.9
24	**132**			8.3	0.8
25	**127**			8.8	0.1
26	**568**		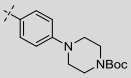	8.8	0.7
27	**566**			9.5	0.5
28	**561**	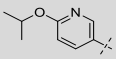		9.9	0.1
29	**154**	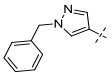	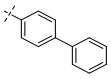	>10	na
30	**569**	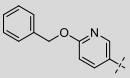		>10	na
31	**546**			>10	na
32	**564**		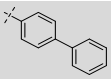	>10	na
33	**563**			>10	na
34	**562**			>10	na
35	**554**			>10	na
36	**567**			>10	na

37	**590**			>10	na
38	**591**			>10	na
39	**592**			>10	na
40	**593**			>10	na
41	**594**			>10	na
42	**595**			>10	na
43	**596**	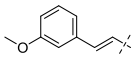		>10	na
44	**597**			>10	na
45	**598**			>10	na
46	**599**			>10	na
47	**600**			>10	na
48	**601**			>10	na
49	**602**			>10	na
50	**140**			>10	na
51	**603**			>10	na
52	**604**			>10	na
53	**605**	**Br**		>10	na
54	**606**			>10	na
55	**607**			>10	na
56	**608**			>10	na
57	**609**			>10	na
58	**610**			>10	na

59	**611**			>10	na
60	**612**			>10	na
61	**613**	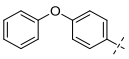		>10	na
62	**614**			>10	na
63	**615**	**Br**		>10	na
64	**616**			>10	na
65	**617**	**Br**		>10	na
66	**618**	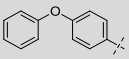		>10	na
67	**619**			>10	na
68	**620**			>10	na
69	**621**			>10	na
70	**622**			>10	na
71	**623**			>10	na
72	**624**			>10	na
73	**625**			>10	na
74	**626**			>10	na
75	**627**			>10	na
76	**628**			>10	na
77	**560**			>10	na

Appendix-Table 2: Inhibition of starvation-induced autophagy with varying R^1 and R^2 whilst keeping the bridging hydroxymethyl group between the core and R^2 in place. Activity > 10 = no inhibition at a test concentration > 10 µM. Data is mean ± SD, n ≥ 3; for SD = na, data is mean, n = 2.

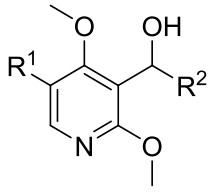

Entry	Number	R^1	R^2	IC_{50} [µM]	SD [µM]
1	**115**	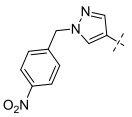		1.3	0.5
2	**205**	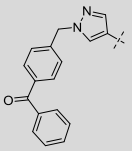		1.4	0.4
3	**116**	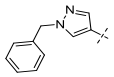		1.9	0.8
4	**148**	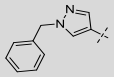		2.2	2.0
5	**118**			2.2	2.4
6	**149**	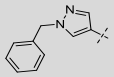		2.4	0.6
7	**120**			2.5	0.5
8	**547**			3.0	0.2
9	**526**	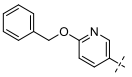		3.2	0.6
10	**541**			3.2	0.7
11	**629**			3.2	0.2
12	**151**	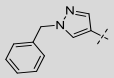		3.3	2.5
13	**525**			3.4	0.3
14	**630**			3.8	na
15	**122**			3.8	1.0
16	**123**			3.9	na
17	**153**	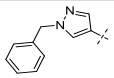	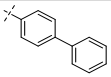	4.2	1.4

18	**125**	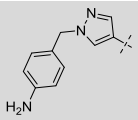		4.4	0.7
19	**540**			4.4	1.1
20	**126**			4.6	0.6
21	**522**		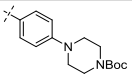	5.0	0.3
22	**631**			5.4	0.9
23	**128**	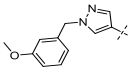		5.5	1.4
24	**524**	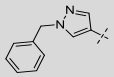	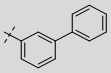	5.5	1.5
25	**155**	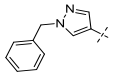		5.9	1.8
26	**129**			6.5	1.6
27	**534**	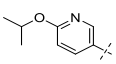		6.6	2.2
28	**131**	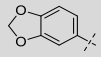		6.6	1.0
29	**632**			6.8	0.4
30	**532**			6.8	2.1
31	**133**			7.0	0.6
32	**633**			7.2	na
33	**549**	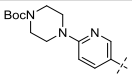		7.3	1.9
34	**634**			9.0	na
35	**134**	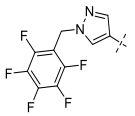		9.2	1.0
36	**104**			9.3	na
37	**530**		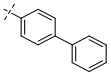	9.5	0.5
38	**548**			9.7	0.3
39	**635**			9.8	na
40	**157**			10	6.0

41	**544**			>10	na
42	**533**		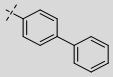	>10	na
43	**523**	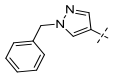	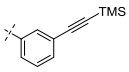	>10	na
44	**135**			>10	na
45	**136**			>10	na
46	**579**		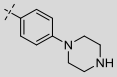	>10	na
47	**578**	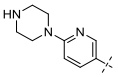		>10	na
48	**542**			>10	na
49	**539**			>10	na
50	**537**			>10	na
51	**536**		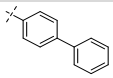	>10	na
52	**535**			>10	na
53	**137**			>10	na
54	**528**			>10	na
55	**538**			>10	na
56	**521**			>10	na
57	**531**			>10	na
58	**636**			12	4.0
59	**637**	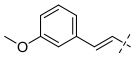		>10	na
60	**638**	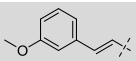		>10	na
61	**639**			>10	na
62	**640**			>10	na
63	**641**			>10	na
64	**642**			>10	na

65	**643**			>10	na
66	**644**	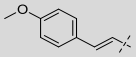		>10	na
67	**645**	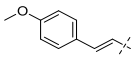		>10	na
68	**138**	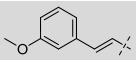		>10	na
69	**646**			>10	na
70	**647**			>10	na
71	**648**			>10	na
72	**649**			>10	na
73	**650**			>10	na
74	**651**			>10	na
75	**652**			>10	na
76	**653**			>10	na
77	**654**			>10	na
78	**655**			>10	na
79	**656**			>10	na
80	**141**	**Br**		>10	na
81	**657**	**Br**		>10	na
82	**658**			>10	na
83	**659**			>10	na
84	**660**			>10	na
85	**661**			>10	na
86	**662**			>10	na
87	**663**			>10	na
88	**664**	**Br**		>10	na
89	**665**			>10	na
90	**666**			>10	na
91	**667**	**Br**		>10	na

92	**668**	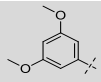		>10	na
93	**669**			>10	na
94	**143**			>10	na
95	**670**	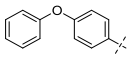		>10	na
96	**145**			>10	na
97	**671**			>10	na
98	**672**			>10	na
99	**673**			>10	na
100	**674**			>10	na
101	**675**		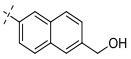	>10	na
102	**676**			>10	na
103	**677**			>10	na
104	**678**			>10	na
105	**679**			>10	na
106	**680**	**Br**		>10	na
107	**681**			>10	na
108	**682**			>10	na

Appendix-Table 3: Inhibition of starvation-induced autophagy with varying R^1 and R^2 whilst keeping the bridging amide between the core and R^2 in place. Activity > 10 = no inhibition at a test concentration > 10 µM. Data is mean ± SD, n ≥ 3.

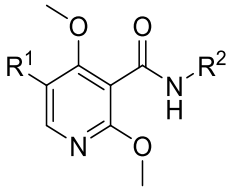

Entry	Number	R^1	R^2	IC_{50} [µM]	SD [µM]
1	**152**	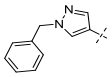		4.0	1.0
2	**159**	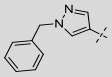		>10	na
3	**158**	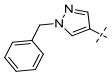		>10	na

Appendix-Table 4: Inhibition of starvation-induced autophagy with varying R^1 and R^2. The substituent for R^2 was introduced by means of a Buchwald-Hartwig coupling. Activity > 10 = no inhibition at a test concentration > 10 µM. Data is mean ± SD, n ≥ 3.

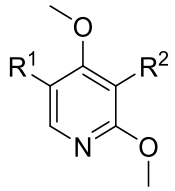

Entry	Number	R^1	R^2	IC_{50} [µM]	SD [µM]
1	**552**	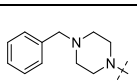	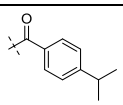	4.6	1.2
2	**553**			9.8	0.3
3	**550**		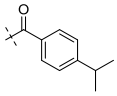	>10	na
4	**551**		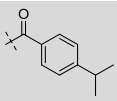	>10	na
5	**147**		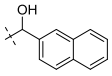	>10	na

Appendix-Table 5: Inhibition of starvation induced autophagy with varying R^1 and R^2, in order to examine the SAR of the core, while keeping the bridging ketone constant. Activity > 10 = no inhibition at a test concentration > 10 µM. Data is mean ± SD, n ≥ 3.

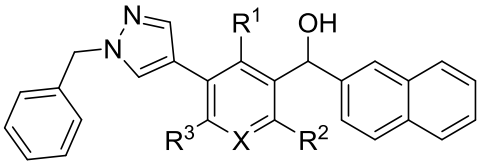

Entry	Number	R^1	R^2	R^3	X	IC_{50} [µM]	SD [µM]
1	**116**	OMe	OMe	H	N	1.9	0.8
2	**174**	H	OMe	H	N	3.7	1.5
3	**175**	OMe	H	H	N	6.2	1.2
4	**176**	H	H	H	N	6.2	2.2
5	**177**	OMe	OMe	H	C	1.8	0.8
6	**178**	H	OMe	OMe	N	>10	na

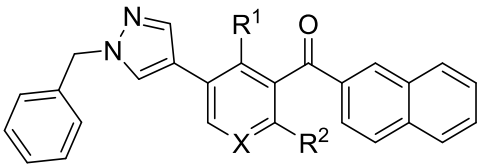

Entry	Number	R^1	R^2	X	IC_{50} [µM]	SD [µM]
7	**117**	OMe	OMe	N	6.5	3.2
8	**179**	H	OMe	N	5.1	3.3
9	**180**	OMe	H	N	5.8	3.3
10	**181**	H	H	N	>10	na
11	**182**	OMe	OMe	C	>10	na

Appendix-Table 6: Inhibition of starvation induced autophagy for additional compounds, which do not fall into one of the above mentioned categories. Activity > 10 = no inhibition at a test concentration > 10 µM. Data is mean ± SD, n ≥ 3.

Entry	Number	Structure	IC_{50} [µM]	SD [µM]
1	**581**	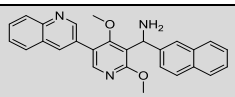	>10	na
2	**577**	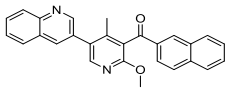	4.0	0.7
3	**543**	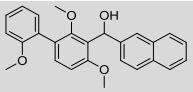	6.1	0.9
4	**576**	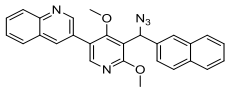	>10	na
5	**573**	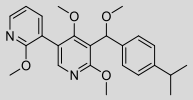	>10	na
6	**574**	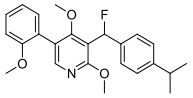	>10	na
7	**575**	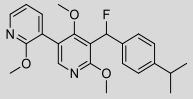	>10	na
8	**683**	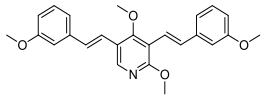	>10	na
9	**684**	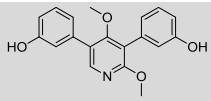	>10	na
10	**207**	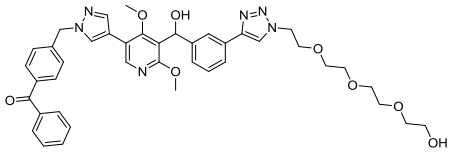	2.2	1.2
11	**193**	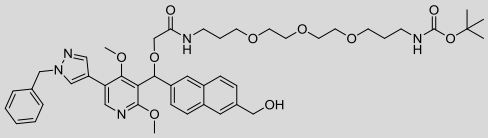	>10	na
12	**192**	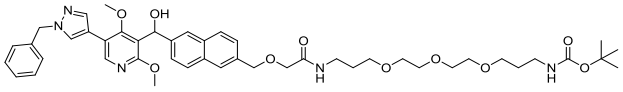	3.2	2.4
13	**195**	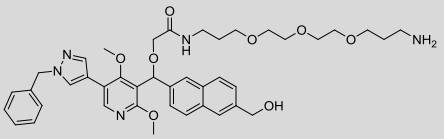	>10	na
14	**194**	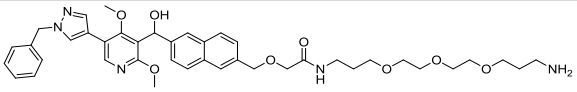	>10	na
15	**198**	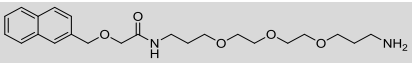	>10	na
16	**197**	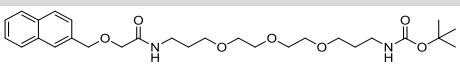	>10	na

Appendix-Table 7: Combined protein outliers of four independent PAL pulldown experiments of which two were performed by on-bead digestion and two by in-gel digestion. Count represents how many times a protein has been identified as an outlier out of the four experiments.

Protein name	Gene name	Count
Acetoacetyl-CoA synthetase	AACS	1
Cytoplasmic aconitate hydratase	ACO1	1
Adenosylhomocysteinase	AHCY	1
AH receptor-interacting protein	AIP	1
Coatomer subunit delta	ARCN1	1
Armadillo repeat-containing protein 10	ARMC10	2
Actin-related protein 2/3 complex subunit 1B	ARPC1B	1
ATPase ASNA1	ASNA1	1
V-type proton ATPase catalytic subunit A	ATP6V1A	1
T-complex protein 1 subunit gamma	CCT3	1
Cyclin-dependent kinase 7	CDK7	1
Cytoskeleton-associated protein 5	CKAP5	1
Cellular retinoic acid-binding protein 2	CRABP2	1
Probable ATP-dependent RNA helicase DDX5	DDX5	1
Derlin-1	DERL1	1
Cytoplasmic dynein 1 heavy chain 1	DYNC1H1	1
Elongation factor 2	EEF2	1
Eukaryotic translation initiation factor 3 subunit B	EIF3B	1
Eukaryotic initiation factor 4A-II; Eukaryotic initiation factor 4A-II, N-terminally processed	EIF4A2	1
Gem-associated protein 2	GEMIN2	1
Guanine nucleotide-binding protein subunit beta-2-like 1;Guanine nucleotide-binding protein subunit beta-2-like 1, N-terminally processed	GNB2L1	1
Glutamate-rich WD repeat-containing protein 1	GRWD1	1
Heterogeneous nuclear ribonucleoproteins A2/B1	HNRNPA2B1	1

Interferon-induced transmembrane protein 3; Interferon-induced transmembrane protein 1; Interferon-induced transmembrane protein 2	IFITM3; IFITM2; IFITM1	2
Malate dehydrogenase, cytoplasmic	MDH1	1
Malate dehydrogenase, mitochondrial;Malate dehydrogenase	MDH2	1
Nuclear protein localization protein 4 homolog	NPLOC4	1
Polyadenylate-binding protein;Polyadenylate-binding protein 1;Polyadenylate-binding protein 3	PABPC1; PABPC3	1
Protein deglycase DJ-1	PARK7	1
Prenylcysteine oxidase 1	PCYOX1	1
Choline-phosphate cytidylyltransferase A;Choline-phosphate cytidylyltransferase B	PCYT1A;PCYT1B	1
ATP-dependent 6-phosphofructokinase, liver type	PFKL	2
6-phosphogluconate dehydrogenase, decarboxylating	PGD	1
26S proteasome non-ATPase regulatory subunit 1	PSMD1	1
Glutamine--tRNA ligase	QARS	1
Transforming protein RhoA; Rho-related GTP-binding protein RhoC	RHOA; RHOC	1
60S ribosomal protein L36	RPL36	1
Secretory carrier-associated membrane protein 1	SCAMP1	1
4F2 cell-surface antigen heavy chain	SLC3A2	1
Choline transporter-like protein 2	SLC44A2	1
Putative protein FAM10A4; Hsc70-interacting protein;Putative protein FAM10A5	ST13; ST13P4; ST13P5	1
Sulfotransferase 1A1-2	SULT1A1; SULT1A2	1
Synaptojanin-2-binding protein	SYNJ2BP	1
Transcription elongation factor B polypeptide 2	TCEB2	1
Delta(14)-sterol reductase	TM7SF2	1
Ubiquitin-fold modifier 1	UFM1	1
UDP-glucose 6-dehydrogenase	UGDH	1

Appendix-Table 8: List of protein spots in the ChemProteoBase that were significantly changed by DMP-1. "p-value" indicates that of Student's t-test between control and samples. Among the identified spots, the spots with p-value less than 0.03 were listed.

Spot Number	Fold ratio	p-value	GENE	Protein Name
837	1.71	0.017	HSPA5	78 kDa glucose-regulated protein
1144	1.29	0.011	WARS	Tryptophanyl-tRNA synthetase, cytoplasmic
1910	0.69	0.026	DUT	Deoxyuridine 5'-triphosphate nucleotidohydrolase, mitochondrial
2164	1.39	0.021	GARS	Glycyl-tRNA synthetase

Appendix-Table 9: Histogramm for Table 9 for the similarity of DMP-1 to the 83 compounds in the ChemProteoBase library.

Cosine similarity	Number of compounds
0.9 ～ 1.0	
0.8 ～ 0.9	
0.7 ～ 0.8	
0.6 ～ 0.7	
0.5 ～ 0.6	
0.4 ～ 0.5	**
0.3 ～ 0.4	**********
0.2 ～ 0.3	**********
0.1 ～ 0.2	**********
0.0 ～ 0.1	**********
-0.1 ～ 0.0	*******
-0.2 ～ -0.1	
-0.3 ～ -0.2	
-0.4 ～ -0.3	
-0.5 ～ -0.4	
-0.6 ～ -0.5	
-0.7 ～ -0.6	
-0.8 ～ -0.7	
-0.9 ～ -0.8	
-1.0 ～ -0.9	

8.2 Autophinib

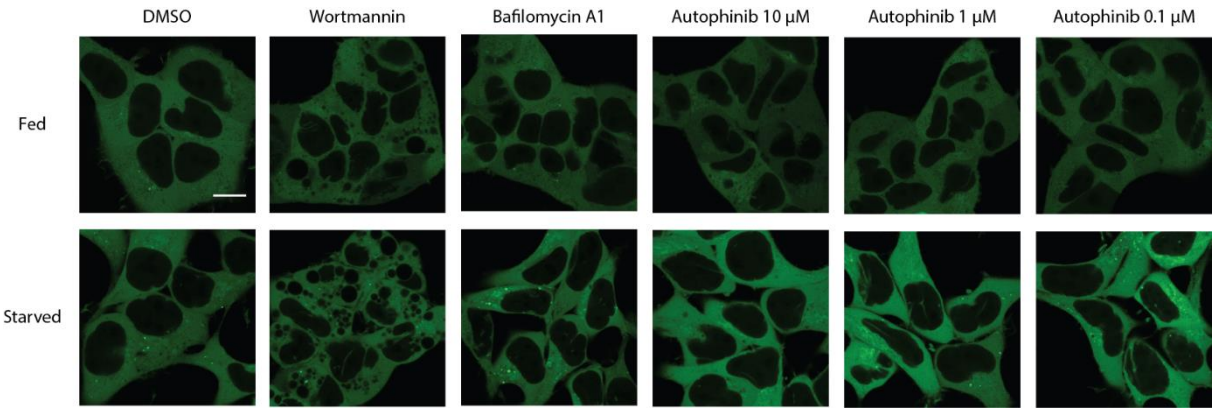

Appendix-Figure 1: Autophinib inhibits the formation of starvation induced WIPI2-eGFP puncta. HEK293A cells stably expressing eGFP-WIPI-2. The WIPI-2 domain binds to PI3P leading to fluorescent puncta when PI3P is enriched in certain regions. Starvation induces autophagy leading to vesicles that contain higher levels of PI3P. This is observed as an increased number of green fluorescent dots in the microscopy images. Autophinib reverts the phenotype showing a similar effect as Wortmannin (Wort., 500 nM) and the opposite effect of Bafilomycin A1 (Baf. A1, 50 nM). Scale bar = 10 µm.

Appendix-Table 10: List of spots that were significantly changed by Autophinib. "p-value" indicates that of t-test between control and samples. Among the identified spots, the spots with p-value less than 0.03 were listed.

Spot Number	Fold ratio	p-value	GENE	Protein Name
588	1.33	0.011	HSP90AB1	Heat shock protein HSP 90-beta
990	0.68	0.002	HNRPL	Heterogeneous nuclear ribonucleoprotein L
1016	0.68	0.018	HNRPK	Heterogeneous nuclear ribonucleoprotein K
1177	1.22	0.008	HNRPH1	Heterogeneous nuclear ribonucleoprotein H
1382	1.22	0.004	DNAJB11	DnaJ homolog subfamily B member 11
1453	0.79	0.020	OXCT1	Succinyl-CoA:3-ketoacid-coenzyme A transferase 1, mitochondrial
1579	0.85	0.022	PPA1	Inorganic pyrophosphatase
1668	1.25	0.002	PHB	Prohibitin
1737	1.71	0.010	ERP29	Endoplasmic reticulum protein ERp29

Appendix-Table 11: Histogramm for Table 16 for the similarity of Autophinib to the 83 compounds in the ChemProteoBase library.

Cosine similarity	Number of compounds
0.9 ~ 1.0	
0.8 ~ 0.9	
0.7 ~ 0.8	
0.6 ~ 0.7	
0.5 ~ 0.6	
0.4 ~ 0.5	*
0.3 ~ 0.4	**********
0.2 ~ 0.3	*********
0.1 ~ 0.2	**********
0.0 ~ 0.1	**********
-0.1 ~ 0.0	****
-0.2 ~ -0.1	*
-0.3 ~ -0.2	
-0.4 ~ -0.3	
-0.5 ~ -0.4	
-0.6 ~ -0.5	
-0.7 ~ -0.6	
-0.8 ~ -0.7	
-0.9 ~ -0.8	
-1.0 ~ -0.9	

Appendix-Table 12: Biochemical Inhibition of kinases by Autophinib. The detection of biochemical inhibition of overall 467 kinases was carried out by Life Technologies. The screen were performed in three different assays formats: Adapta (activity based), Z-Lyte (activity based) and Lantha (binding based) at a concentration of 1 µM for Autophinib. For seleceted kinases an IC_{50} was determined.

Method	[ATP] Tested / µM	Kinase Tested	% Inhibition Point 1	% Inhibition Point 2	% Inhibition mean	IC_{50} / nM 1.	IC_{50} / nM 2.
Adapta	10	CAMK1 (CaMK1)	7	10	9		
Adapta	Km app	CDK7/cyclin H/MNAT1	63	69	66	2620	765
Adapta	Km app	CDK9/cyclin T1	85	85	85	425	188
Adapta	Km app	CHUK (IKK alpha)	22	8	15		
Adapta	Km app	DAPK1	32	31	32		
Adapta	Km app	GSG2 (Haspin)	11	23	17		
Adapta	Km app	IRAK1	9	5	7		
Adapta	Km app	LRRK2 FL	89	87	88	134	180
Adapta	Km app	LRRK2 G2019S FL	79	81	80		
Adapta	Km app	LRRK2 G2019S	82	78	80		
Adapta	Km app	LRRK2 I2020T	81	84	82		
Adapta	Km app	LRRK2 R1441C	90	89	89		
Adapta	Km app	LRRK2	84	89	86		
Adapta	Km app	NUAK1 (ARK5)	92	91	91	40.7	46.1
Adapta	10	PI4K2A (PI4K2 alpha)	2	1	2		
Adapta	10	PI4K2B (PI4K2 beta)	-13	8	-3		
Adapta	10	PI4KA (PI4K alpha)	-4	1	-1		
Adapta	Km app	PI4KB (PI4K beta)	33	15	24		
Adapta	Km app	PIK3C2A (PI3K-C2 alpha)	20	19	19		
Adapta	10	PIK3C2B (PI3K-C2 beta)	-58	-51	-55		
Adapta	10	PI3KC2G (PI3K-C2 gamma)	65	69	67	188	
Adapta	Km app	PIK3C3 (hVPS34)	97	97	97	Refer to Results and discussion	
Adapta	10	PIK3CA E545K/PIK3R1 (p110 alpha E545K/p85 alpha)	14	5	9		
Adapta	Km app	PIK3CA/PIK3R1 (p110 alpha/p85 alpha)	10	19	15		
Adapta	10	PIK3CA/PIK3R3 (p110 alpha/p55 gamma)	7	14	10		
Adapta	Km app	PIK3CB/PIK3R1 (p110 beta/p85 alpha)	7	-4	1		
Adapta	10	PIK3CB/PIK3R2 (p110 beta/p85 beta)	11	17	14		
Adapta	Km app	PIK3CD/PIK3R1 (p110 delta/p85 alpha)	36	24	30		

Adapta	Km app	PIK3CG (p110 gamma)	12	7	10		
Adapta	Km app	SPHK1	12	-2	5		
Adapta	10	SPHK2	-17	-6	-12		
Z-Lyte	Km app	ABL1 E255K	29	23	26		
Z-Lyte	Km app	ABL1 F317I	4	2	3		
Z-Lyte	Km app	ABL1 G250E	13	12	13		
Z-Lyte	Km app	ABL1 T315I	52	52	52		
Z-Lyte	Km app	ABL1 Y253F	15	20	17		
Z-Lyte	Km app	ABL1	54	58	56		
Z-Lyte	Km app	ABL2 (Arg)	33	43	38		
Z-Lyte	Km app	ACVR1B (ALK4)	5	-2	1		
Z-Lyte	Km app	ADRBK1 (GRK2)	6	0	3		
Z-Lyte	Km app	ADRBK2 (GRK3)	-1	7	3		
Z-Lyte	Km app	AKT1 (PKB alpha)	-11	-5	-8		
Z-Lyte	Km app	AKT2 (PKB beta)	4	4	4		
Z-Lyte	Km app	AKT3 (PKB gamma)	-4	0	-2		
Z-Lyte	Km app	ALK	3	3	3		
Z-Lyte	Km app	AMPK (A1/B2/G3)	29	24	27		
Z-Lyte	Km app	AMPK (A2/B1/G2)	35	29	32		
Z-Lyte	Km app	AMPK (A2/B1/G3)	27	28	27		
Z-Lyte	Km app	AMPK (A2/B2/G3)	23	27	25		
Z-Lyte	Km app	AMPK A1/B1/G1	10	17	13		
Z-Lyte	Km app	AMPK A2/B1/G1	35	40	37		
Z-Lyte	Km app	AURKA (Aurora A)	82	83	82	101	
Z-Lyte	Km app	AURKB (Aurora B)	43	47	45		
Z-Lyte	Km app	AURKC (Aurora C)	47	52	49		
Z-Lyte	Km app	AXL	-14	-12	-13		
Z-Lyte	Km app	BLK	-5	-9	-7		
Z-Lyte	Km app	BMX	13	9	11		
Z-Lyte	100	BRAF V599E	53	54	54		
Z-Lyte	100	BRAF	63	65	64		
Z-Lyte	Km app	BRSK1 (SAD1)	30	41	36		
Z-Lyte	Km app	BTK	21	14	17		
Z-Lyte	Km app	CAMK1D (CaMKI delta)	5	1	3		
Z-Lyte	Km app	CAMK1G (CAMKI gamma)	-14	5	-4		
Z-Lyte	Km app	CAMK2A (CaMKII alpha)	0	-1	0		
Z-Lyte	Km app	CAMK2B (CaMKII beta)	0	-4	-2		
Z-Lyte	Km app	CAMK2D (CaMKII delta)	4	10	7		
Z-Lyte	Km app	CAMK4 (CaMKIV)	-11	-13	-12		
Z-Lyte	Km app	CDC42 BPA (MRCKA)	-5	5	0		
Z-Lyte	Km app	CDC42 BPB (MRCKB)	1	1	1		
Z-Lyte	Km app	CDC42 BPG (MRCKG)	0	-8	-4		
Z-Lyte	Km app	CDK1/cyclin B	90	81	85	186	206
Z-Lyte	Km app	CDK17/cyclin Y	77	73	75	667	519

Z-Lyte	Km app	CDK18/cyclin Y	50	52	51		
Z-Lyte	Km app	CDK2/cyclin A	99	98	98	23.4	26.7
Z-Lyte	Km app	CDK5/p25	99	101	100	27.4	23.8
Z-Lyte	Km app	CDK5/p35	98	101	99	27.4	33.5
Z-Lyte	Km app	CDKL5	92	89	90	215	224
Z-Lyte	Km app	CHEK1 (CHK1)	-4	12	4		
Z-Lyte	Km app	CHEK2 (CHK2)	3	-11	-4		
Z-Lyte	Km app	CLK1	14	12	13		
Z-Lyte	Km app	CLK2	8	19	13		
Z-Lyte	Km app	CLK3	-5	-2	-3		
Z-Lyte	Km app	CSF1R (FMS)	32	35	34		
Z-Lyte	Km app	CSK	2	2	2		
Z-Lyte	Km app	CSNK1A1 (CK1 alpha 1)	-2	5	2		
Z-Lyte	Km app	CSNK1A1L	10	6	8		
Z-Lyte	Km app	CSNK1D (CK1 delta)	-3	-1	-2		
Z-Lyte	Km app	CSNK1E (CK1 epsilon)	9	7	8		
Z-Lyte	Km app	CSNK1G1 (CK1 gamma 1)	11	7	9		
Z-Lyte	Km app	CSNK1G2 (CK1 gamma 2)	-5	-1	-3		
Z-Lyte	Km app	CSNK1G3 (CK1 gamma 3)	-14	-17	-16		
Z-Lyte	Km app	CSNK2A1 (CK2 alpha 1)	15	22	19		
Z-Lyte	Km app	CSNK2A2 (CK2 alpha 2)	4	0	2		
Z-Lyte	Km app	DAPK3 (ZIPK)	1	15	8		
Z-Lyte	Km app	DCAMKL1 (DCLK1)	3	-2	1		
Z-Lyte	Km app	DCAMKL2 (DCK2)	9	9	9		
Z-Lyte	Km app	DNA-PK	35	38	36		
Z-Lyte	Km app	DYRK1A	24	24	24		
Z-Lyte	Km app	DYRK1B	92	90	91	398	250
Z-Lyte	Km app	DYRK3	2	5	4		
Z-Lyte	Km app	DYRK4	-4	-7	-6		
Z-Lyte	Km app	EEF2K	2	5	3		
Z-Lyte	Km app	EGFR (ErbB1) L858R	-1	1	0		
Z-Lyte	Km app	EGFR (ErbB1) L861Q	4	-7	-1		
Z-Lyte	Km app	EGFR (ErbB1) T790M L858R	-10	-16	-13		
Z-Lyte	Km app	EGFR (ErbB1) T790M	6	5	6		
Z-Lyte	Km app	EGFR (ErbB1)	3	6	4		
Z-Lyte	Km app	EPHA1	44	34	39		
Z-Lyte	Km app	EPHA2	5	8	6		
Z-Lyte	Km app	EPHA4	20	23	22		
Z-Lyte	Km app	EPHA5	20	13	17		
Z-Lyte	Km app	EPHA8	13	12	12		
Z-Lyte	Km app	EPHB1	32	29	31		
Z-Lyte	Km app	EPHB2	22	18	20		
Z-Lyte	Km app	EPHB3	7	5	6		
Z-Lyte	Km app	EPHB4	9	7	8		

Z-Lyte	Km app	ERBB2 (HER2)	-7	-2	-4		
Z-Lyte	Km app	ERBB4 (HER4)	6	1	4		
Z-Lyte	Km app	FER	14	19	16		
Z-Lyte	Km app	FES (FPS)	7	0	3		
Z-Lyte	Km app	FGFR1	37	40	38		
Z-Lyte	Km app	FGFR2	73	63	68		
Z-Lyte	Km app	FGFR3 K650E	36	37	37		
Z-Lyte	Km app	FGFR3	19	28	24		
Z-Lyte	Km app	FGFR4	-2	15	7		
Z-Lyte	Km app	FGR	23	23	23		
Z-Lyte	Km app	FLT1 (VEGFR1)	9	27	18		
Z-Lyte	Km app	FLT3 D835Y	70	69	69		
Z-Lyte	Km app	FLT3	61	63	62		
Z-Lyte	Km app	FLT4 (VEGFR3)	75	77	76	1300	716
Z-Lyte	Km app	FRAP1 (mTOR)	19	29	24		
Z-Lyte	Km app	FRK (PTK5)	2	2	2		
Z-Lyte	Km app	FYN	6	6	6		
Z-Lyte	Km app	GRK4	-2	-15	-8		
Z-Lyte	Km app	GRK5	1	2	1		
Z-Lyte	Km app	GRK6	-7	0	-3		
Z-Lyte	Km app	GRK7	4	8	6		
Z-Lyte	Km app	GSK3A (GSK3 alpha)	100	99	100	1.69	
Z-Lyte	Km app	GSK3B (GSK3 beta)	103	104	103	1.3	
Z-Lyte	Km app	HCK	16	16	16		
Z-Lyte	Km app	HIPK1 (Myak)	3	5	4		
Z-Lyte	Km app	HIPK2	7	9	8		
Z-Lyte	Km app	HIPK3 (YAK1)	4	5	4		
Z-Lyte	Km app	HIPK4	-1	2	1		
Z-Lyte	Km app	IGF1R	-6	-7	-6		
Z-Lyte	Km app	IKBKB (IKK beta)	14	20	17		
Z-Lyte	Km app	IKBKE (IKK epsilon)	1	3	2		
Z-Lyte	Km app	INSR	3	3	3		
Z-Lyte	Km app	INSRR (IRR)	19	24	22		
Z-Lyte	Km app	IRAK4	-3	-4	-3		
Z-Lyte	Km app	ITK	18	20	19		
Z-Lyte	Km app	JAK1	37	35	36		
Z-Lyte	Km app	JAK2 JH1 JH2 V617F	27	31	29		
Z-Lyte	Km app	JAK2 JH1 JH2	35	34	35		
Z-Lyte	Km app	JAK2	62	65	64		
Z-Lyte	Km app	JAK3	65	51	58		
Z-Lyte	Km app	KDR (VEGFR2)	42	56	49		
Z-Lyte	Km app	KIT T670I	40	44	42		
Z-Lyte	Km app	KIT V559D V654A	4	11	7		
Z-Lyte	Km app	KIT V559D	10	10	10		

Z-Lyte	Km app	KIT V560G	-15	-9	-12		
Z-Lyte	Km app	KIT	1	16	8		
Z-Lyte	Km app	KSR2	7	8	7		
Z-Lyte	Km app	LCK	28	19	23		
Z-Lyte	Km app	LTK (TYK1)	14	16	15		
Z-Lyte	Km app	LYN A	26	27	26		
Z-Lyte	Km app	LYN B	11	14	12		
Z-Lyte	100	MAP2K1 (MEK1)	56	45	50		
Z-Lyte	100	MAP2K2 (MEK2)	50	53	51		
Z-Lyte	100	MAP2K6 (MKK6)	72	74	73	1820	564
Z-Lyte	Km app	MAP3K19 (YSK4)	5	11	8		
Z-Lyte	100	MAP3K8 (COT)	40	37	39		
Z-Lyte	Km app	MAP3K9 (MLK1)	22	11	17		
Z-Lyte	Km app	MAP4K2 (GCK)	-19	-2	-11		
Z-Lyte	Km app	MAP4K4 (HGK)	11	1	6		
Z-Lyte	Km app	MAP4K5 (KHS1)	41	36	38		
Z-Lyte	Km app	MAPK1 (ERK2)	44	54	49		
Z-Lyte	100	MAPK10 (JNK3)	35	29	32		
Z-Lyte	Km app	MAPK11 (p38 beta)	3	6	5		
Z-Lyte	Km app	MAPK12 (p38 gamma)	13	19	16		
Z-Lyte	Km app	MAPK13 (p38 delta)	29	26	27		
Z-Lyte	100	MAPK14 (p38 alpha)	-8	-8	-8		
Z-Lyte	Km app	MAPK14 (p38 alpha)	-2	1	-1		
Z-Lyte	Km app	MAPK3 (ERK1)	59	64	62	3150	5212
Z-Lyte	Km app	MAPK7 (ERK5)	1	-1	0		
Z-Lyte	100	MAPK8 (JNK1)	30	26	28		
Z-Lyte	100	MAPK9 (JNK2)	19	13	16		
Z-Lyte	Km app	MAPKAPK2	11	6	8		
Z-Lyte	Km app	MAPKAPK3	-1	4	2		
Z-Lyte	Km app	MAPKAPK5 (PRAK)	-2	-1	-2		
Z-Lyte	Km app	MARK1 (MARK)	22	31	26		
Z-Lyte	Km app	MARK2	39	40	40		
Z-Lyte	Km app	MARK3	26	31	28		
Z-Lyte	Km app	MARK4	42	41	42		
Z-Lyte	Km app	MATK (HYL)	-6	-12	-9		
Z-Lyte	Km app	MELK	32	44	38		
Z-Lyte	Km app	MERTK (cMER)	14	10	12		
Z-Lyte	Km app	MET (cMet)	6	7	6		
Z-Lyte	Km app	MET M1250T	8	10	9		
Z-Lyte	Km app	MINK1	11	6	9		
Z-Lyte	Km app	MKNK1 (MNK1)	-1	-1	-1		
Z-Lyte	Km app	MST1R (RON)	-1	-4	-3		
Z-Lyte	Km app	MST4	19	13	16		
Z-Lyte	Km app	MUSK	32	42	37		

Z-Lyte	Km app	MYLK2 (skMLCK)	32	23	28
Z-Lyte	Km app	NEK1	4	-6	-1
Z-Lyte	Km app	NEK2	2	23	13
Z-Lyte	Km app	NEK4	12	9	10
Z-Lyte	Km app	NEK6	-1	-11	-6
Z-Lyte	Km app	NEK7	1	2	1
Z-Lyte	Km app	NEK9	-3	2	-1
Z-Lyte	Km app	NIM1K	5	10	7
Z-Lyte	Km app	NTRK1 (TRKA)	39	32	35
Z-Lyte	Km app	NTRK2 (TRKB)	51	47	49
Z-Lyte	Km app	NTRK3 (TRKC)	40	54	47
Z-Lyte	Km app	PAK1	26	24	25
Z-Lyte	Km app	PAK2 (PAK65)	0	8	4
Z-Lyte	Km app	PAK3	30	18	24
Z-Lyte	Km app	PAK4	-3	12	4
Z-Lyte	Km app	PAK6	13	21	17
Z-Lyte	Km app	PAK7 (KIAA1264)	27	7	17
Z-Lyte	Km app	PASK	2	-4	-1
Z-Lyte	Km app	PDGFRA (PDGFR alpha)	9	0	5
Z-Lyte	Km app	PDGFRA D842V	18	8	13
Z-Lyte	Km app	PDGFRA T674I	18	11	15
Z-Lyte	Km app	PDGFRA V561D	26	28	27
Z-Lyte	Km app	PDGFRB (PDGFR beta)	10	22	16
Z-Lyte	100	PDK1	8	4	6
Z-Lyte	Km app	PDK1	21	12	17
Z-Lyte	Km app	PEAK1	1	4	3
Z-Lyte	Km app	PHKG1	-2	10	4
Z-Lyte	Km app	PHKG2	2	2	2
Z-Lyte	Km app	PIM1	-15	-15	-15
Z-Lyte	Km app	PIM2	-1	-16	-9
Z-Lyte	Km app	PIM3	-13	-8	-11
Z-Lyte	Km app	PKN1 (PRK1)	-6	5	-1
Z-Lyte	Km app	PLK1	1	12	6
Z-Lyte	Km app	PLK2	13	8	10
Z-Lyte	Km app	PLK3	-19	-21	-20
Z-Lyte	Km app	PRKACA (PKA)	4	5	4
Z-Lyte	Km app	PRKCA (PKC alpha)	13	16	14
Z-Lyte	Km app	PRKCB1 (PKC beta I)	20	20	20
Z-Lyte	Km app	PRKCB2 (PKC beta II)	13	24	19
Z-Lyte	Km app	PRKCD (PKC delta)	16	15	15
Z-Lyte	Km app	PRKCE (PKC epsilon)	-18	5	-7
Z-Lyte	Km app	PRKCG (PKC gamma)	-4	20	8
Z-Lyte	Km app	PRKCH (PKC eta)	-9	13	2
Z-Lyte	Km app	PRKCI (PKC iota)	0	-18	-9

Z-Lyte	Km app	PRKCN (PKD3)	56	56	56
Z-Lyte	Km app	PRKCQ (PKC theta)	9	12	11
Z-Lyte	Km app	PRKCZ (PKC zeta)	-4	-8	-6
Z-Lyte	Km app	PRKD1 (PKC mu)	45	45	45
Z-Lyte	Km app	PRKD2 (PKD2)	8	18	13
Z-Lyte	Km app	PRKG1	-12	-9	-11
Z-Lyte	Km app	PRKG2 (PKG2)	-1	9	4
Z-Lyte	Km app	PRKX	8	11	10
Z-Lyte	Km app	PTK2 (FAK)	7	20	13
Z-Lyte	Km app	PTK2B (FAK2)	2	3	2
Z-Lyte	Km app	PTK6 (Brk)	-2	0	-1
Z-Lyte	100	RAF1 (cRAF) Y340D Y341D	39	27	33
Z-Lyte	Km app	RET S891A	49	37	43
Z-Lyte	Km app	RET V804L	69	66	67
Z-Lyte	Km app	RET Y791F	58	54	56
Z-Lyte	Km app	RET	65	70	68
Z-Lyte	Km app	ROCK1	-12	6	-3
Z-Lyte	Km app	ROCK2	-3	1	-1
Z-Lyte	Km app	ROS1	37	41	39
Z-Lyte	Km app	RPS6KA1 (RSK1)	11	9	10
Z-Lyte	Km app	RPS6KA2 (RSK3)	23	28	26
Z-Lyte	Km app	RPS6KA3 (RSK2)	-4	2	-1
Z-Lyte	Km app	RPS6KA4 (MSK2)	0	0	0
Z-Lyte	Km app	RPS6KA5 (MSK1)	9	10	10
Z-Lyte	Km app	RPS6KA6 (RSK4)	15	23	19
Z-Lyte	Km app	RPS6KB1 (p70S6K)	-6	-2	-4
Z-Lyte	Km app	RPS6KB2 (p70S6Kb)	-9	-11	-10
Z-Lyte	Km app	SBK1	-3	0	-1
Z-Lyte	Km app	SGK (SGK1)	8	6	7
Z-Lyte	Km app	SGK2	2	2	2
Z-Lyte	Km app	SGKL (SGK3)	18	2	10
Z-Lyte	Km app	SNF1LK2	12	17	14
Z-Lyte	Km app	SRC N1	6	13	10
Z-Lyte	Km app	SRC	19	17	18
Z-Lyte	Km app	SRMS (Srm)	-4	-4	-4
Z-Lyte	Km app	SRPK1	7	7	7
Z-Lyte	Km app	SRPK2	-10	-5	-7
Z-Lyte	Km app	STK22B (TSSK2)	8	7	7
Z-Lyte	Km app	STK22D (TSSK1)	8	10	9
Z-Lyte	Km app	STK23 (MSSK1)	-1	9	4
Z-Lyte	Km app	STK24 (MST3)	26	23	25
Z-Lyte	Km app	STK25 (YSK1)	13	21	17
Z-Lyte	Km app	STK3 (MST2)	10	24	17
Z-Lyte	Km app	STK4 (MST1)	22	29	25

Z-Lyte	Km app	SYK	11	3	7
Z-Lyte	Km app	TAOK2 (TAO1)	66	65	66
Z-Lyte	Km app	TBK1	8	5	6
Z-Lyte	Km app	TEK (TIE2) Y897S	-2	1	-1
Z-Lyte	Km app	TEK (Tie2)	0	5	3
Z-Lyte	Km app	TNK1	25	24	24
Z-Lyte	Km app	TXK	7	0	3
Z-Lyte	Km app	TYK2	70	60	65
Z-Lyte	Km app	TYRO3 (RSE)	-11	-11	-11
Z-Lyte	Km app	YES1	35	32	34
Z-Lyte	Km app	ZAP70	16	17	17
Lantha	NA	AAK1	25	30	28
Lantha	NA	ABL1 H396P	73	65	69
Lantha	NA	ABL1 M351T	59	62	60
Lantha	NA	ABL1 Q252H	50	49	50
Lantha	NA	ACVR1 (ALK2) R206H	86	84	85
Lantha	NA	ACVR1 (ALK2)	74	78	76
Lantha	NA	ACVR1C (ALK7)	36	34	35
Lantha	NA	ACVR2A	5	11	8
Lantha	NA	ACVR2B	32	18	25
Lantha	NA	ACVRL1 (ALK1)	73	86	80
Lantha	NA	ADCK3	20	7	13
Lantha	NA	ALK C1156Y	9	9	9
Lantha	NA	ALK F1174L	15	11	13
Lantha	NA	ALK L1196M	9	1	5
Lantha	NA	ALK R1275Q	6	3	4
Lantha	NA	AMPK (A1/B1/G2)	45	47	46
Lantha	NA	AMPK (A1/B1/G3)	50	57	53
Lantha	NA	AMPK (A1/B2/G1)	64	59	61
Lantha	NA	AMPK (A2/B2/G1)	49	49	49
Lantha	NA	AMPK (A2/B2/G2)	51	50	51
Lantha	NA	ANKK1	2	8	5
Lantha	NA	AXL R499C	7	2	5
Lantha	NA	BMPR1A (ALK3)	-8	-6	-7
Lantha	NA	BMPR1B (ALK6)	57	62	60
Lantha	NA	BMPR2	100	103	101
Lantha	NA	BRAF V599E	-3	-1	-2
Lantha	NA	BRAF	22	15	18
Lantha	NA	BRSK2	23	23	23
Lantha	NA	CAMK2G (CaMKII gamma)	10	8	9
Lantha	NA	CAMKK1 (CAMKKA)	65	63	64
Lantha	NA	CAMKK2 (CaMKK beta)	31	28	30
Lantha	NA	CASK	20	14	17
Lantha	NA	CDC7/DBF4	50	37	44

Lantha	NA	CDK1/cyclin A2	94	100	97
Lantha	NA	CDK11 (Inactive)	11	8	9
Lantha	NA	CDK14 (PFTK1)/cyclin Y	85	84	84
Lantha	NA	CDK16 (PCTK1)/cyclin Y	90	90	90
Lantha	NA	CDK2/cyclin A1	98	97	98
Lantha	NA	CDK2/cyclin E1	114	109	111
Lantha	NA	CDK2/cyclin O	103	102	102
Lantha	NA	CDK3/cyclin E1	99	100	99
Lantha	NA	CDK5 (Inactive)	107	107	107
Lantha	NA	CDK8/cyclin C	54	51	53
Lantha	NA	CDK9 (Inactive)	78	85	81
Lantha	NA	CDK9/cyclin K	75	76	76
Lantha	NA	CLK4	76	79	77
Lantha	NA	DAPK2	26	40	33
Lantha	NA	DDR1	8	3	6
Lantha	NA	DDR2 N456S	32	37	35
Lantha	NA	DDR2 T654M	60	56	58
Lantha	NA	DDR2	3	-1	1
Lantha	NA	DMPK	25	24	25
Lantha	NA	DYRK2	37	26	31
Lantha	NA	EGFR (ErbB1) d746-750	6	-1	2
Lantha	NA	EIF2AK2 (PKR)	31	8	19
Lantha	NA	EPHA3	17	6	11
Lantha	NA	EPHA6	37	48	43
Lantha	NA	EPHA7	31	24	27
Lantha	NA	ERN1	64	60	62
Lantha	NA	ERN2	63	55	59
Lantha	NA	FGFR1 V561M	84	84	84
Lantha	NA	FGFR3 G697C	45	46	45
Lantha	NA	FGFR3 K650M	74	67	70
Lantha	NA	FLT3 ITD	43	50	47
Lantha	NA	FYN A	18	15	16
Lantha	NA	GAK	3	4	4
Lantha	NA	GRK1	15	8	11
Lantha	NA	HUNK	30	16	23
Lantha	NA	ICK	98	99	99
Lantha	NA	IRAK3	18	3	10
Lantha	NA	KIT A829P	24	31	27
Lantha	NA	KIT D816H	49	44	47
Lantha	NA	KIT D816V	80	71	75
Lantha	NA	KIT D820E	24	19	22
Lantha	NA	KIT N822K	13	22	18
Lantha	NA	KIT T670E	27	19	23
Lantha	NA	KIT V559D T670I	40	34	37

Lantha	NA	KIT V654A	4	1	3
Lantha	NA	KIT Y823D	9	6	8
Lantha	NA	LATS1	-25	-17	-21
Lantha	NA	LATS2	7	5	6
Lantha	NA	LIMK1	56	46	51
Lantha	NA	LIMK2	23	30	26
Lantha	NA	MAP2K1 (MEK1) S218D S222D	8	8	8
Lantha	NA	MAP2K1 (MEK1)	7	5	6
Lantha	NA	MAP2K2 (MEK2)	2	1	2
Lantha	NA	MAP2K3 (MEK3)	98	97	97
Lantha	NA	MAP2K4 (MEK4)	98	97	97
Lantha	NA	MAP2K5 (MEK5)	12	9	10
Lantha	NA	MAP2K6 (MKK6) S207E T211E	86	89	87
Lantha	NA	MAP2K6 (MKK6)	73	70	72
Lantha	NA	MAP3K10 (MLK2)	38	30	34
Lantha	NA	MAP3K11 (MLK3)	21	17	19
Lantha	NA	MAP3K14 (NIK)	21	22	22
Lantha	NA	MAP3K2 (MEKK2)	61	56	59
Lantha	NA	MAP3K3 (MEKK3)	32	25	28
Lantha	NA	MAP3K5 (ASK1)	20	15	17
Lantha	NA	MAP3K7/MAP3K7IP1 (TAK1-TAB1)	73	72	72
Lantha	NA	MAP4K1 (HPK1)	87	82	85
Lantha	NA	MAP4K3 (GLK)	30	24	27
Lantha	NA	MAPK10 (JNK3)	94	90	92
Lantha	NA	MAPK15 (ERK7)	99	99	99
Lantha	NA	MAPK8 (JNK1)	86	81	83
Lantha	NA	MAPK9 (JNK2)	68	63	66
Lantha	NA	MASTL	24	11	18
Lantha	NA	MERTK (cMER) A708S	3	3	3
Lantha	NA	MET D1228H	6	9	7
Lantha	NA	MKNK2 (MNK2)	7	-10	-2
Lantha	NA	MLCK (MLCK2)	85	88	87
Lantha	NA	MLK4	14	11	12
Lantha	NA	MYLK (MLCK)	10	9	10
Lantha	NA	MYLK4	99	89	94
Lantha	NA	MYO3A (MYO3 alpha)	49	53	51
Lantha	NA	MYO3B (MYO3 beta)	43	46	45
Lantha	NA	NEK8	8	4	6
Lantha	NA	NLK	78	81	79
Lantha	NA	NUAK2	96	87	92
Lantha	NA	OXSR1	1	-11	-5
Lantha	NA	PKMYT1	-6	12	3
Lantha	NA	PKN2 (PRK2)	24	21	22

Lantha	NA	PLK4	64	65	64
Lantha	NA	PRKACB (PRKAC beta)	16	13	14
Lantha	NA	PRKACG (PRKAC gamma)	4	-7	-1
Lantha	NA	RAF1 (cRAF) Y340D Y341D	2	-5	-2
Lantha	NA	RET G691S	68	70	69
Lantha	NA	RET M918T	56	58	57
Lantha	NA	RET V804M	81	75	78
Lantha	NA	RIPK2	9	3	6
Lantha	NA	RIPK3	18	16	17
Lantha	NA	SIK1	0	1	1
Lantha	NA	SIK3	7	12	9
Lantha	NA	SLK	55	54	54
Lantha	NA	STK16 (PKL12)	70	73	72
Lantha	NA	STK17A (DRAK1)	31	23	27
Lantha	NA	STK17B (DRAK2)	52	40	46
Lantha	NA	STK32B (YANK2)	21	7	14
Lantha	NA	STK32C (YANK3)	4	7	6
Lantha	NA	STK33	7	4	6
Lantha	NA	STK38 (NDR)	10	-7	1
Lantha	NA	STK38L (NDR2)	-16	-10	-13
Lantha	NA	STK39 (STLK3)	-8	5	-2
Lantha	NA	TAOK1	94	97	96
Lantha	NA	TAOK3 (JIK)	59	54	57
Lantha	NA	TEC	13	7	10
Lantha	NA	TEK (TIE2) R849W	9	11	10
Lantha	NA	TEK (TIE2) Y1108F	4	11	7
Lantha	NA	TESK1	11	10	11
Lantha	NA	TESK2	-5	5	0
Lantha	NA	TGFBR1 (ALK5)	58	58	58
Lantha	NA	TGFBR2	85	88	86
Lantha	NA	TLK1	41	34	38
Lantha	NA	TLK2	89	89	89
Lantha	NA	TNIK	25	26	26
Lantha	NA	TNK2 (ACK)	4	5	5
Lantha	NA	TTK	24	33	29
Lantha	NA	ULK1	8	2	5
Lantha	NA	ULK2	7	17	12
Lantha	NA	ULK3	12	22	17
Lantha	NA	VRK2	5	10	7
Lantha	NA	WEE1	-2	-6	-4
Lantha	NA	WNK2	3	9	6
Lantha	NA	WNK3	-1	-12	-7
Lantha	NA	ZAK	18	21	19

Appendix-Table 13: Kinases identified as hits for Autophinib in the Lantha binding assay of the full panel were retested at either Eurofins or Reaction Biology. When available the retest was first performed at a single concentration of 1 µM, followed by an IC_{50} in the case of confirmed kinase inhibition by the retest. When single dose retest was not available an IC_{50} was performed directly.

Kinase Tested	IC_{50} / nM		IC_{50} / retest tested at	% Inhibition for retest		% Inhibition mean	[ATP] Retest / µM
	1.	2.		Point 1	Point 2		
ACVR1 (ALK2)			Eurofins	14	18	16	10
ACVRL1 (ALK1)			Eurofins	-1	1	0	10
BMPR2	3040	1940	Reaction Biology				10; 15
CDK1/cyclin A2	351	197	Eurofins	28	28	28	45
CDK14 (PFTK1)/cyclin Y	778	741	Reaction Biology				15
CDK16 (PCTK1)/cyclin Y	657	508	Reaction Biology				10
CDK2/cyclin A1	22	66	Eurofins	93	89	91	45
CDK2/cyclin E1			Eurofins	91	95	93	120
CDK3/cyclin E1	79	66	Eurofins	92	92	92	200
CDK9 (Inactive)	174	151	Eurofins	82	82	82	45
CLK4			Eurofins	31.5	28.5	30	15
ICK	134	120	Eurofins	85	85	85	90
MAP2K3 (MEK3)	306	156	Reaction Biology				1
MAP2K4 (MEK4)	110	106	Lifetechnologies				NA
MAP2K5 (MEK5)	6140	8050	Reaction Biology				5
MAP2K6 (MKK6)			Eurofins	45	37	41	10
MAP3K2 (MEKK2)			Eurofins	-0.5	2.5	1	15
MAP3K7/MAP3K7IP1 (TAK1-TAB1)	21440	16230	Reaction Biology				20
MAP4K1 (HPK1)			Eurofins	25	29	27	15
MAPK10 (JNK3)			Eurofins	64	68	66	10
MAPK15 (ERK7)	123	208	Reaction Biology				20
MAPK8 (JNK1)			Eurofins	11	3	7	45
MAPK9 (JNK2)			Eurofins	0	-4	-2	45
MYLK4	423	314	Reaction Biology				50
NLK	2850	2110	Eurofins	46	38	42	200
NUAK2			Eurofins	34	46	40	15
STK16 (PKL12)	2970		Reaction Biology				5
TAOK1	1380	1260	Reaction Biology				30
TGFBR2	33540	37700	Reaction Biology				1
TLK2			Eurofins	16	8	12	10
MKK7			Eurofins	31	27	29	10

Appendix-Table 14: Examination of the off-target effects of Autophinib by the employment of literature reported kinase inhibitors. Bought or synthesized literature reported kinase inhibitors, their known targets and their effect in our autophagy assay are shown. Inactive = No autophagy inhibition at an assay concentration of 10 µM. Starvation = starvation induced autophagy assay; Rapamycin = Rapamycin induced autophagy assay. Inactive = no inhibition at a test concentration > 10 µM. Data is mean ± SD, n ≥ 3 for all autophagy inhibition values.

Entry	Inhibitor name (Number)	Structure	Known targets	Autophagy Inhibition	
				Starvation IC_{50} [µM]	Rapamycin IC_{50} [µM]
1	PHA-793887 [209–211] (**685**)	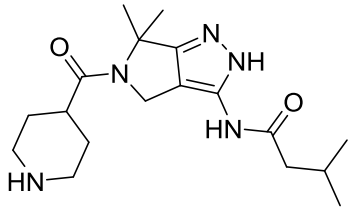	CDK2, -5, -7	Inactive	Inactive
2	LDC-000067[212] (**686**)	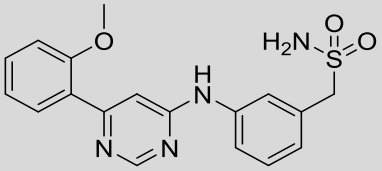	CDK9	Inactive	Inactive
3	AZ191[213] (**687**)	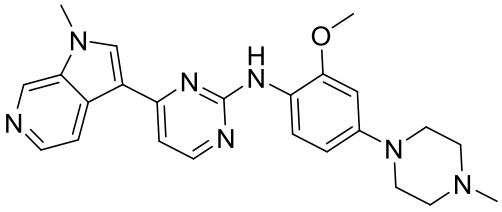	DYRK1B, DYRK1A, DYRK2	Inactive	Inactive
4	GNE-7915[214] (**688**)	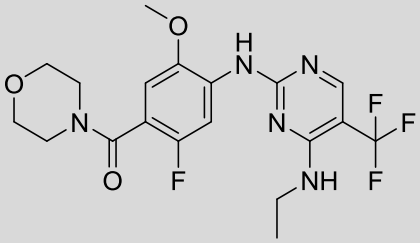	LRRK2	Inactive	Inactive
5	MK-5108[215,216] (**689**)	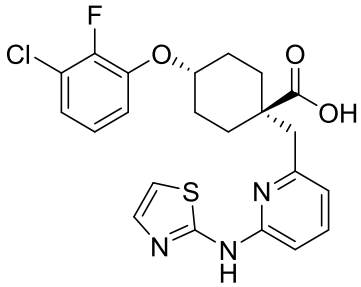	Aurora A	6.2 ± 3.0	Inactive

6	CGP-74514A[217] (**690**)	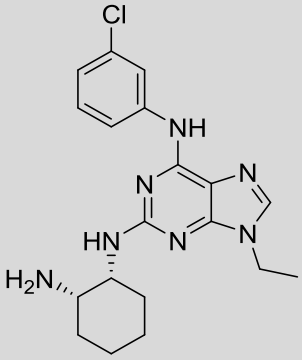	CDK1	Inactive	Inactive
7	WZ4003 [218,219] (**691**)	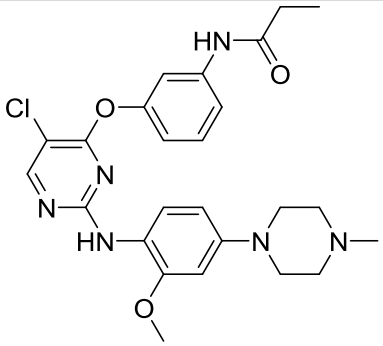	NUAK1, -2	Inactive	Inactive
8	HTH 01-015[218,220] (**692**)	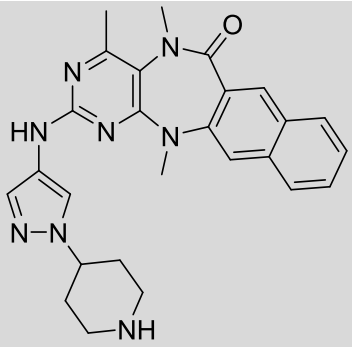	NUAK1	Inactive	Inactive
9	CHIR-99021[221] (**693**)	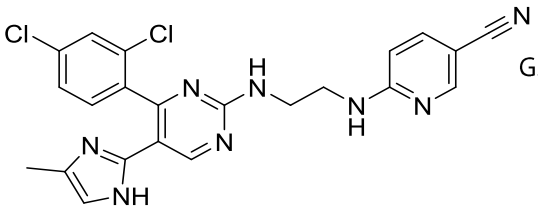	GSK3A, -B	Inactive	Inactive
10	BMS-265246 [222,223] (**694**)	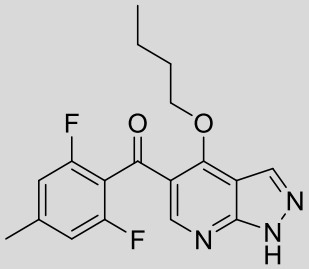	CDK1, -2	Inactive	Inactive

11	Olomoucine[224] (**695**)	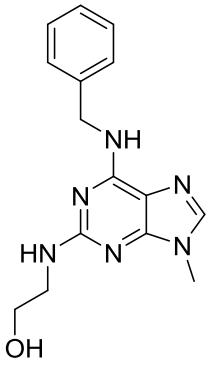	CDK1, -2; Erk1	Inactive	Inactive
12	NU6027 [225,226] (**696**)	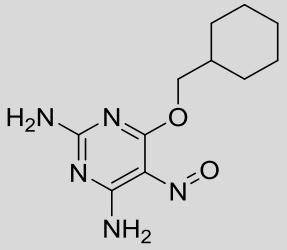	CDK2	Inactive	Inactive
13	Kenpaullone[227] (**697**)	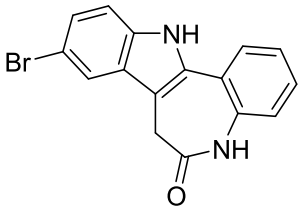	CDK1, -2, 5; GSK3B	Inactive	Inactive
14	Roscovitine[228] (**698**)	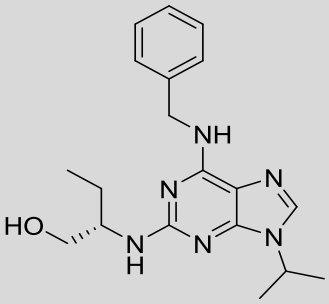	CDK1, -2, 5; (little effect on CDK4, -6)	Inactive	Inactive
15	Tozasertib[154] (**699**)	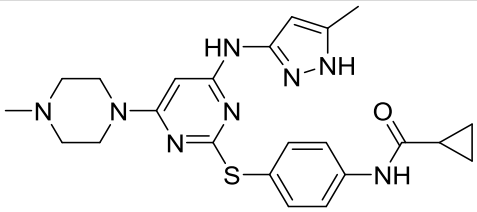	Aurora A, B, C; FLT3, Bcr-Abl	Inactive	Inactive
16	JNK-IN-8[229,230] (**700**)	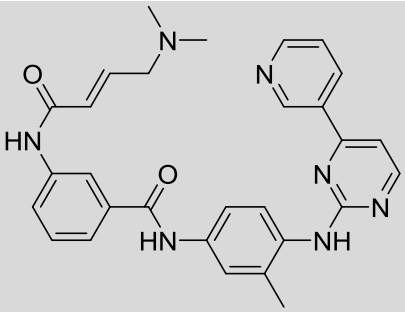	JNK1, -2, -3	Inactive	Inactive

17	Crizotinib [231,232] (**701**)	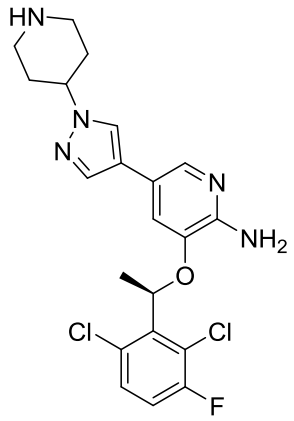	c-Met, ALK1	Inactive	Inactive
18	Dorso-morphin [233] (**702**)	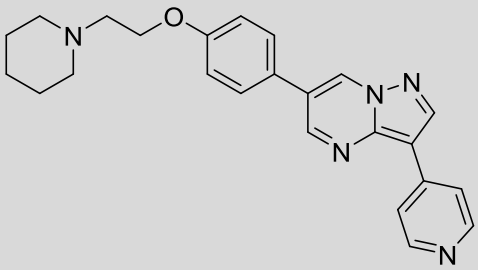	ALK2, -3, -6; AMPK	Inactive	Inactive
19	SAR405[99,105] (**17**)	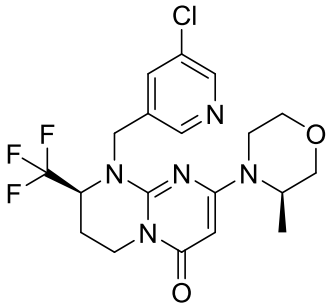	VPS34	0.053 ± 0.025	0.020 ± 0.000
20	VPS34-IN1[100,106] (**18**)	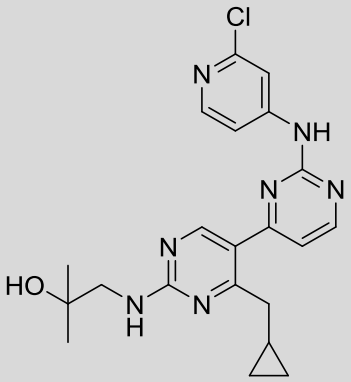	VPS34	0.013 ± 0.005	0.015 ± 0.005
21	Ro 31-8220[234–236] (**703**)	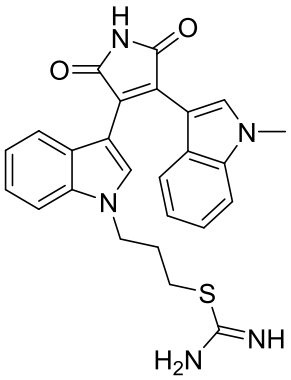	MAPK15	Inactive	Inactive

22	RGB-286147[237] (**704**)	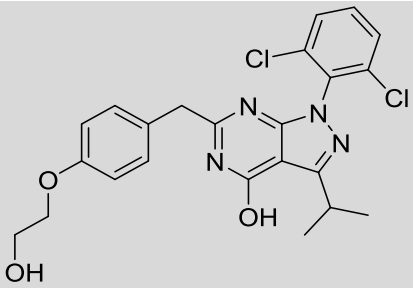	CDK1, -2, -3, -4, -5, -7, -9	Inactive	Inactive
23	TMCB [238,239] (**705**)	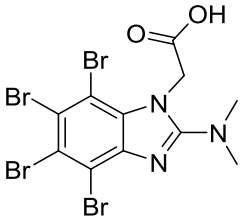	MAPK15	Inactive	Inactive
24	PIK3C2g inhibitor 1[182,184] (**423**)	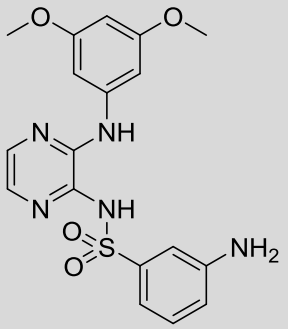	PIK3C2g	Inactive	Inactive
25	PIK3C2g inhibitor 2[182,184] (**424**)	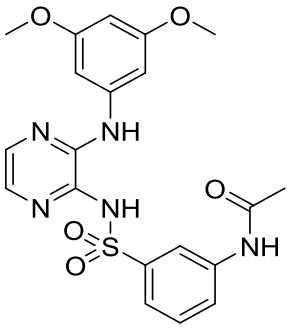	PIK3C2g	Inactive	Inactive
26	PIK3C2g inhibitor 3[182,184] (**425**)	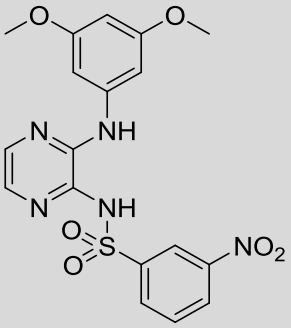	PIK3C2g	2.40 ± 1.50	Inactive
27	PIK3C2g inhibitor 4[182,184] (**426**)	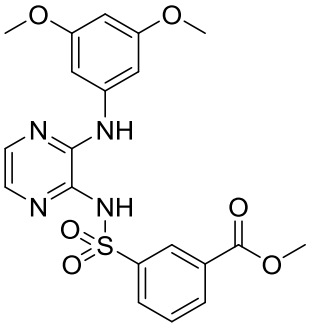	PIK3C2g	Inactive	Inactive

8.3 Aumitin

Appendix-Table 15: Structure activity relationship of the diaminopyrimidines. Starvation = starvation induced autophagy assay; Rapamycin = Rapamycin induced autophagy assay. > 10 = no inhibition at a test concentration of 10 µM. Data is mean; SD = ± standard deviation; n ≥ 3 for all autophagy IC_{50} values.

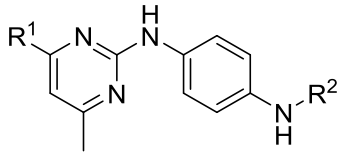

Entry	Number	R^1	R^2	Starvation (IC_{50} [µM])	SD [µM] (Starvation)	Rapamycin (IC_{50} [µM])	SD [µM] (Rapamycin)
1	Aumitin (**405**)			0.12	0.07	0.24	0.20
2	**406**		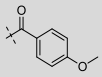	0.37	0.18	1.8	0.9
3	**407**			0.38	0.23	1.8	2.0
4	**706**		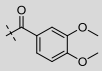	0.73	0.06	3.4	0.8
5	**408**			0.75	0.11	1.7	0.5
6	**409**			0.80	0.30	0.81	0.68
7	**410**		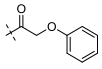	0.81	0.16	0.29	0.18
8	**411**			0.97	0.47	0.16	0.08
9	**707**			1.1	0.1	1.1	0.2
10	**708**		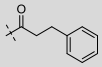	1.3	0.1	na	na
11	**709**		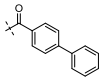	1.3	1.5	na	na
12	**710**		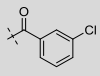	1.5	0.2	4.0	0.3
13	**711**		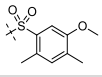	1.6	0.2	3.3	0.8
14	**412**		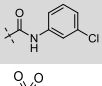	1.6	0.6	4.1	3.0
15	**712**			1.8	0.3	3.4	1.7
16	**713**		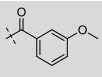	1.8	0.9	na	na

17	**714**			1.9	0.7	0.38	0.05
18	**715**		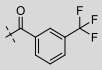	2.0	0.1	2.2	0.2
19	**716**			2.0	0.3	3.6	0.5
20	**717**			2.0	0.3	1.9	1.1
21	**718**			2.1	0.3	5.7	1.7
22	**719**			2.2	0.4	1.7	1.1
23	**413**			2.3	1.2	1.3	0.7
24	**720**		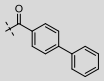	2.4	1.3	2.0	1.7
25	**721**		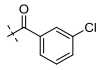	2.4	0.7	1.1	0.3
26	**722**			2.5	0.3	2.4	1.0
27	**414**		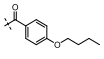	2.7	0.1	1.1	0.5
28	**723**		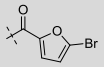	2.8	0.2	3.6	1.1
29	**724**		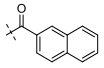	2.8	1.6	3.1	2.1
30	**725**		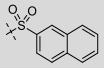	3.0	1.0	3.9	1.3
31	**726**		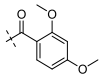	3.1	0.7	1.4	0.6
32	**727**		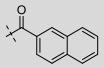	3.5	0.4	3.4	0.7
33	**728**			3.6	0.3	7.0	0.8
34	**729**		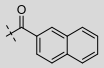	4.0	0.2	2.8	0.3
35	**730**		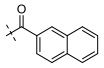	4.1	1.4	5.4	0
36	**731**		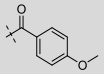	6.9	0.7	2.6	0.9
37	**732**			7.0	2.7	na	na
38	**733**			7.8	3.0	2.7	1.1
39	**734**			8.6	0.9	na	na

40	**735**		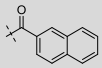	8.6	1.5	na	na
41	**736**		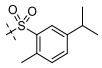	8.8	0.4	3.8	4.1
42	**416**		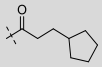	9.45	0.77	4.7	0.3
43	**737**		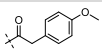	9.4	0	na	na
44	**738**		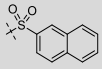	9.9	0	na	na
45	**417**		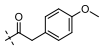	>10	na	na	na
46	**739**		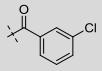	>10	na	na	na
47	**418**			>10	na	na	na
48	**740**		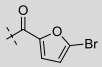	>10	na	na	na
49	**741**			>10	na	na	na
50	**419**			>10	na	na	na
51	**742**		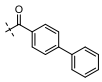	>10	na	na	na
52	**743**		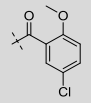	>10	na	na	na
53	**744**		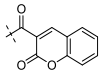	>10	na	na	na
54	**745**		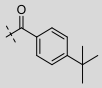	>10	na	na	na
55	**746**			>10	na	na	na
56	**747**		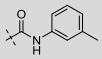	>10	na	na	na
57	**420**		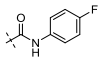	>10	na	na	na
58	**748**		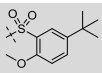	>10	na	9.1	0.7
59	**749**		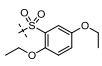	>10	na	na	na
60	**750**			>10	na	na	na
61	**751**			>10	na	na	na
62	**752**			>10	na	na	na
63	**753**			>10	na	na	na

64	**754**			>10	na	na	na
65	**755**		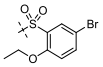	>10	na	na	na
66	**756**			>10	na	na	na
67	**757**		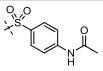	>10	na	na	na
68	**758**		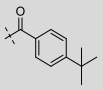	>10	na	na	na
69	**759**		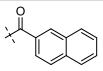	>10	na	na	na
70	**760**		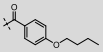	>10	na	3.7	2.2
71	**761**		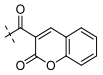	>10	na	na	na
72	**762**		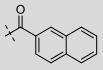	>10	na	0.53	0

Appendix-Table 16: Biochemical Inhibition of kinases by Aumitin. The detection of biochemical inhibition of overall 419 kinases was carried out by Life Technologies. The screen were performed in three different assays formats: Adapta (activity based), Z-Lyte (activity based) and Lantha (binding based) at a concentration of 1 µM for Aumitin. Only PI4KB was inhibited more than 40 % in the screen and thus tested for in dose response. PI3KC2G was not tested in the initial screen but tested later on directly in dose response.

Method	[ATP] Tested / µM	Kinase Tested	% Inhibition Point 1	% Inhibition Point 2	% Inhibition mean	IC_{50} / nM 1.	IC_{50} / nM 2.
Adapta	10	CAMK1 (CaMK1)	-13	-3	-8		
Adapta	Km app	CDK7/cyclin H/MNAT1	-6	13	3		
Adapta	Km app	CDK9/cyclin T1	5	11	8		
Adapta	Km app	CHUK (IKK alpha)	-8	-12	-10		
Adapta	Km app	DAPK1	32	5	18		
Adapta	Km app	GSG2 (Haspin)	-5	-2	-3		
Adapta	Km app	IRAK1	-17	-12	-15		
Adapta	Km app	LRRK2 FL	-3	12	4		
Adapta	Km app	LRRK2 G2019S FL	-8	7	-1		
Adapta	Km app	LRRK2 G2019S	-5	16	6		
Adapta	Km app	LRRK2 I2020T	-4	-6	-5		
Adapta	Km app	LRRK2 R1441C	-14	3	-5		
Adapta	Km app	LRRK2	-9	10	0		
Adapta	Km app	NUAK1 (ARK5)	0	26	13		
Adapta	10	PI4KA (PI4K alpha)	-1	6	2		
Adapta	Km app	PI4KB (PI4K beta)	43	45	44	301	426
Adapta	Km app	PIK3C2A (PI3K-C2 alpha)	3	3	3		
Adapta	10	PIK3C2B (PI3K-C2 beta)	24	20	22		
Adapta	10	PI3KC2G (PI3K-C2 gamma)	NA	NA	NA	2610	3670
Adapta	Km app	PIK3C3 (hVPS34)	4	23	14		
Adapta	Km app	PIK3CA/PIK3R1 (p110 alpha/p85 alpha)	0	12	6		
Adapta	Km app	PIK3CB/PIK3R1 (p110 beta/p85 alpha)	17	3	10		
Adapta	Km app	PIK3CD/PIK3R1 (p110 delta/p85 alpha)	-6	15	5		
Adapta	Km app	PIK3CG (p110 gamma)	7	4	5		
Adapta	10	PIP4K2A	-1	-3	-2		
Adapta	10	PIP5K1A	11	8	9		
Adapta	10	PIP5K1B	-18	-11	-14		
Adapta	10	PIP5K1C	-3	7	2		
Adapta	Km app	SPHK1	2	-2	0		
Adapta	10	SPHK2	5	-4	1		
Z-Lyte	Km app	ABL1 E255K	8	0	4		
Z-Lyte	Km app	ABL1 G250E	0	-3	-1		

Z-Lyte	Km app	ABL1 T315I	0	1	1
Z-Lyte	Km app	ABL1 Y253F	5	3	4
Z-Lyte	Km app	ABL1	19	-1	9
Z-Lyte	Km app	ABL2 (Arg)	8	6	7
Z-Lyte	Km app	ACVR1B (ALK4)	11	12	11
Z-Lyte	Km app	ADRBK1 (GRK2)	0	3	2
Z-Lyte	Km app	ADRBK2 (GRK3)	-3	-2	-2
Z-Lyte	Km app	AKT1 (PKB alpha)	-6	-10	-8
Z-Lyte	Km app	AKT2 (PKB beta)	8	12	10
Z-Lyte	Km app	AKT3 (PKB gamma)	12	1	7
Z-Lyte	Km app	ALK	5	-5	0
Z-Lyte	Km app	AMPK A1/B1/G1	4	1	3
Z-Lyte	Km app	AMPK A2/B1/G1	21	12	17
Z-Lyte	Km app	AURKA (Aurora A)	17	16	16
Z-Lyte	Km app	AURKB (Aurora B)	9	7	8
Z-Lyte	Km app	AURKC (Aurora C)	-6	-3	-5
Z-Lyte	Km app	AXL	-6	-4	-5
Z-Lyte	Km app	BLK	18	6	12
Z-Lyte	Km app	BMX	6	3	5
Z-Lyte	100	BRAF V599E	17	13	15
Z-Lyte	100	BRAF	11	5	8
Z-Lyte	Km app	BRSK1 (SAD1)	1	-6	-2
Z-Lyte	Km app	BTK	12	2	7
Z-Lyte	Km app	CAMK1D (CaMKI delta)	6	4	5
Z-Lyte	Km app	CAMK2A (CaMKII alpha)	7	9	8
Z-Lyte	Km app	CAMK2B (CaMKII beta)	1	-2	-1
Z-Lyte	Km app	CAMK2D (CaMKII delta)	6	10	8
Z-Lyte	Km app	CAMK4 (CaMKIV)	-14	-14	-14
Z-Lyte	Km app	CDC42 BPA (MRCKA)	4	-9	-3
Z-Lyte	Km app	CDC42 BPB (MRCKB)	18	3	11
Z-Lyte	Km app	CDK1/cyclin B	4	8	6
Z-Lyte	Km app	CDK2/cyclin A	3	4	4
Z-Lyte	Km app	CDK5/p25	-1	-8	-4
Z-Lyte	Km app	CDK5/p35	0	0	0
Z-Lyte	Km app	CHEK1 (CHK1)	-16	-14	-15
Z-Lyte	Km app	CHEK2 (CHK2)	-15	-5	-10
Z-Lyte	Km app	CLK1	8	8	8
Z-Lyte	Km app	CLK2	6	6	6
Z-Lyte	Km app	CLK3	10	0	5
Z-Lyte	Km app	CSF1R (FMS)	3	2	2
Z-Lyte	Km app	CSK	0	2	1
Z-Lyte	Km app	CSNK1A1 (CK1 alpha 1)	9	8	9
Z-Lyte	Km app	CSNK1D (CK1 delta)	2	4	3
Z-Lyte	Km app	CSNK1E (CK1 epsilon)	6	6	6

Z-Lyte	Km app	CSNK1G1 (CK1 gamma 1)	-1	1	0
Z-Lyte	Km app	CSNK1G2 (CK1 gamma 2)	1	1	1
Z-Lyte	Km app	CSNK1G3 (CK1 gamma 3)	8	0	4
Z-Lyte	Km app	CSNK2A1 (CK2 alpha 1)	3	6	4
Z-Lyte	Km app	CSNK2A2 (CK2 alpha 2)	3	0	2
Z-Lyte	Km app	DAPK3 (ZIPK)	-10	-1	-6
Z-Lyte	Km app	DCAMKL2 (DCK2)	22	6	14
Z-Lyte	Km app	DNA-PK	6	1	3
Z-Lyte	Km app	DYRK1A	1	0	1
Z-Lyte	Km app	DYRK1B	-2	-2	-2
Z-Lyte	Km app	DYRK3	18	-2	8
Z-Lyte	Km app	DYRK4	4	1	3
Z-Lyte	Km app	EEF2K	1	0	0
Z-Lyte	Km app	EGFR (ErbB1) L858R	-10	-17	-14
Z-Lyte	Km app	EGFR (ErbB1) L861Q	-3	2	-1
Z-Lyte	Km app	EGFR (ErbB1) T790M L858R	-3	-3	-3
Z-Lyte	Km app	EGFR (ErbB1) T790M	7	1	4
Z-Lyte	Km app	EGFR (ErbB1)	3	-2	0
Z-Lyte	Km app	EPHA1	5	7	6
Z-Lyte	Km app	EPHA2	16	3	9
Z-Lyte	Km app	EPHA4	21	5	13
Z-Lyte	Km app	EPHA5	6	2	4
Z-Lyte	Km app	EPHA8	11	6	8
Z-Lyte	Km app	EPHB1	0	4	2
Z-Lyte	Km app	EPHB2	2	2	2
Z-Lyte	Km app	EPHB3	19	9	14
Z-Lyte	Km app	EPHB4	6	4	5
Z-Lyte	Km app	ERBB2 (HER2)	-29	-23	-26
Z-Lyte	Km app	ERBB4 (HER4)	2	-7	-2
Z-Lyte	Km app	FER	-2	-1	-1
Z-Lyte	Km app	FES (FPS)	6	-5	0
Z-Lyte	Km app	FGFR1	9	7	8
Z-Lyte	Km app	FGFR2	-1	-6	-4
Z-Lyte	Km app	FGFR3 K650E	-11	-2	-6
Z-Lyte	Km app	FGFR3	-1	4	2
Z-Lyte	Km app	FGFR4	-8	-9	-8
Z-Lyte	Km app	FGR	14	14	14
Z-Lyte	Km app	FLT1 (VEGFR1)	-3	-7	-5
Z-Lyte	Km app	FLT3 D835Y	26	20	23
Z-Lyte	Km app	FLT3	5	4	4
Z-Lyte	Km app	FLT4 (VEGFR3)	12	6	9
Z-Lyte	Km app	FRAP1 (mTOR)	-14	0	-7
Z-Lyte	Km app	FRK (PTK5)	-1	6	2
Z-Lyte	Km app	FYN	9	8	8

Z-Lyte	Km app	GRK4	7	8	7
Z-Lyte	Km app	GRK5	1	5	3
Z-Lyte	Km app	GRK6	1	2	1
Z-Lyte	Km app	GRK7	2	-3	0
Z-Lyte	Km app	GSK3A (GSK3 alpha)	6	4	5
Z-Lyte	Km app	GSK3B (GSK3 beta)	9	16	12
Z-Lyte	Km app	HCK	7	10	8
Z-Lyte	Km app	HIPK1 (Myak)	11	7	9
Z-Lyte	Km app	HIPK2	1	2	2
Z-Lyte	Km app	HIPK3 (YAK1)	4	-1	1
Z-Lyte	Km app	HIPK4	4	-1	2
Z-Lyte	Km app	IGF1R	-6	-3	-4
Z-Lyte	Km app	IKBKB (IKK beta)	6	1	3
Z-Lyte	Km app	IKBKE (IKK epsilon)	15	4	10
Z-Lyte	Km app	INSR	5	8	6
Z-Lyte	Km app	INSRR (IRR)	8	15	12
Z-Lyte	Km app	IRAK4	-9	-1	-5
Z-Lyte	Km app	ITK	-8	-9	-9
Z-Lyte	Km app	JAK1	-1	-2	-2
Z-Lyte	Km app	JAK2 JH1 JH2 V617F	2	-6	-2
Z-Lyte	Km app	JAK2 JH1 JH2	6	-3	2
Z-Lyte	Km app	JAK2	0	-1	0
Z-Lyte	Km app	JAK3	9	1	5
Z-Lyte	Km app	KDR (VEGFR2)	1	0	0
Z-Lyte	Km app	KIT T670I	-2	-4	-3
Z-Lyte	Km app	KIT	-5	-5	-5
Z-Lyte	Km app	LCK	6	2	4
Z-Lyte	Km app	LTK (TYK1)	-8	0	-4
Z-Lyte	Km app	LYN A	2	2	2
Z-Lyte	Km app	LYN B	19	5	12
Z-Lyte	100	MAP2K1 (MEK1)	-17	7	-5
Z-Lyte	100	MAP2K2 (MEK2)	-16	0	-8
Z-Lyte	100	MAP2K6 (MKK6)	9	5	7
Z-Lyte	100	MAP3K8 (COT)	12	2	7
Z-Lyte	Km app	MAP3K9 (MLK1)	-9	-14	-12
Z-Lyte	Km app	MAP4K2 (GCK)	-10	-6	-8
Z-Lyte	Km app	MAP4K4 (HGK)	11	-5	3
Z-Lyte	Km app	MAP4K5 (KHS1)	15	9	12
Z-Lyte	Km app	MAPK1 (ERK2)	27	10	18
Z-Lyte	100	MAPK10 (JNK3)	6	2	4
Z-Lyte	Km app	MAPK11 (p38 beta)	12	10	11
Z-Lyte	Km app	MAPK12 (p38 gamma)	16	10	13
Z-Lyte	Km app	MAPK13 (p38 delta)	8	12	10
Z-Lyte	Km app	MAPK14 (p38 alpha) Direct	7	6	6

Z-Lyte	100	MAPK14 (p38 alpha)	-2	-11	-6
Z-Lyte	Km app	MAPK3 (ERK1)	4	4	4
Z-Lyte	100	MAPK8 (JNK1)	3	-15	-6
Z-Lyte	100	MAPK9 (JNK2)	-7	-3	-5
Z-Lyte	Km app	MAPKAPK2	23	20	21
Z-Lyte	Km app	MAPKAPK3	1	2	1
Z-Lyte	Km app	MAPKAPK5 (PRAK)	3	1	2
Z-Lyte	Km app	MARK1 (MARK)	1	-2	-1
Z-Lyte	Km app	MARK2	14	12	13
Z-Lyte	Km app	MARK3	-8	9	0
Z-Lyte	Km app	MARK4	-1	-3	-2
Z-Lyte	Km app	MATK (HYL)	-2	-2	-2
Z-Lyte	Km app	MELK	-9	-2	-6
Z-Lyte	Km app	MERTK (cMER)	4	1	3
Z-Lyte	Km app	MET (cMet)	7	13	10
Z-Lyte	Km app	MET M1250T	-4	0	-2
Z-Lyte	Km app	MINK1	-17	-5	-11
Z-Lyte	Km app	MKNK1 (MNK1)	-12	1	-5
Z-Lyte	Km app	MST1R (RON)	-1	-3	-2
Z-Lyte	Km app	MST4	-3	-5	-4
Z-Lyte	Km app	MUSK	-1	4	1
Z-Lyte	Km app	MYLK2 (skMLCK)	-5	-9	-7
Z-Lyte	Km app	NEK1	-16	-12	-14
Z-Lyte	Km app	NEK2	-6	-11	-9
Z-Lyte	Km app	NEK4	-3	13	5
Z-Lyte	Km app	NEK6	-3	-4	-3
Z-Lyte	Km app	NEK7	-8	-3	-6
Z-Lyte	Km app	NEK9	-4	-9	-6
Z-Lyte	Km app	NTRK1 (TRKA)	-3	0	-1
Z-Lyte	Km app	NTRK2 (TRKB)	0	-2	-1
Z-Lyte	Km app	NTRK3 (TRKC)	-3	0	-1
Z-Lyte	Km app	PAK1	-11	3	-4
Z-Lyte	Km app	PAK2 (PAK65)	7	3	5
Z-Lyte	Km app	PAK3	19	-5	7
Z-Lyte	Km app	PAK4	16	3	10
Z-Lyte	Km app	PAK6	-25	-11	-18
Z-Lyte	Km app	PAK7 (KIAA1264)	-13	-3	-8
Z-Lyte	Km app	PASK	0	-2	-1
Z-Lyte	Km app	PDGFRA (PDGFR alpha)	-4	-3	-3
Z-Lyte	Km app	PDGFRA D842V	2	-3	0
Z-Lyte	Km app	PDGFRA T674I	9	6	7
Z-Lyte	Km app	PDGFRA V561D	9	-1	4
Z-Lyte	Km app	PDGFRB (PDGFR beta)	1	2	2
Z-Lyte	Km app	PDK1 Direct	-11	-21	-16

Z-Lyte	100	PDK1	13	13	13
Z-Lyte	Km app	PHKG1	1	-14	-7
Z-Lyte	Km app	PHKG2	0	0	0
Z-Lyte	Km app	PIM1	-8	-21	-15
Z-Lyte	Km app	PIM2	-14	-16	-15
Z-Lyte	Km app	PKN1 (PRK1)	2	-3	-1
Z-Lyte	Km app	PLK1	13	8	11
Z-Lyte	Km app	PLK2	2	7	4
Z-Lyte	Km app	PLK3	-3	0	-2
Z-Lyte	Km app	PRKACA (PKA)	-3	-1	-2
Z-Lyte	Km app	PRKCA (PKC alpha)	0	6	3
Z-Lyte	Km app	PRKCB1 (PKC beta I)	-10	5	-2
Z-Lyte	Km app	PRKCB2 (PKC beta II)	-12	-6	-9
Z-Lyte	Km app	PRKCD (PKC delta)	-14	-9	-12
Z-Lyte	Km app	PRKCE (PKC epsilon)	-12	-8	-10
Z-Lyte	Km app	PRKCG (PKC gamma)	-2	-18	-10
Z-Lyte	Km app	PRKCH (PKC eta)	-2	1	0
Z-Lyte	Km app	PRKCI (PKC iota)	-2	-1	-1
Z-Lyte	Km app	PRKCN (PKD3)	10	9	10
Z-Lyte	Km app	PRKCQ (PKC theta)	5	-7	-1
Z-Lyte	Km app	PRKCZ (PKC zeta)	8	3	6
Z-Lyte	Km app	PRKD1 (PKC mu)	2	-1	0
Z-Lyte	Km app	PRKD2 (PKD2)	-6	-3	-5
Z-Lyte	Km app	PRKG1	-2	0	-1
Z-Lyte	Km app	PRKG2 (PKG2)	1	-1	0
Z-Lyte	Km app	PRKX	12	0	6
Z-Lyte	Km app	PTK2 (FAK)	6	6	6
Z-Lyte	Km app	PTK2B (FAK2)	10	0	5
Z-Lyte	Km app	PTK6 (Brk)	7	7	7
Z-Lyte	100	RAF1 (cRAF) Y340D Y341D	18	5	12
Z-Lyte	Km app	RET V804L	4	5	4
Z-Lyte	Km app	RET Y791F	6	9	8
Z-Lyte	Km app	RET	7	7	7
Z-Lyte	Km app	ROCK1	20	7	14
Z-Lyte	Km app	ROCK2	9	17	13
Z-Lyte	Km app	ROS1	1	-1	0
Z-Lyte	Km app	RPS6KA1 (RSK1)	3	8	5
Z-Lyte	Km app	RPS6KA2 (RSK3)	0	6	3
Z-Lyte	Km app	RPS6KA3 (RSK2)	7	9	8
Z-Lyte	Km app	RPS6KA4 (MSK2)	0	4	2
Z-Lyte	Km app	RPS6KA5 (MSK1)	5	6	6
Z-Lyte	Km app	RPS6KA6 (RSK4)	-4	1	-2
Z-Lyte	Km app	RPS6KB1 (p70S6K)	-5	1	-2
Z-Lyte	Km app	SGK (SGK1)	2	5	4

Z-Lyte	Km app	SGK2	-7	8	1
Z-Lyte	Km app	SGKL (SGK3)	-2	4	1
Z-Lyte	Km app	SNF1LK2	15	0	7
Z-Lyte	Km app	SRC N1	15	11	13
Z-Lyte	Km app	SRC	21	7	14
Z-Lyte	Km app	SRMS (Srm)	2	4	3
Z-Lyte	Km app	SRPK1	1	4	2
Z-Lyte	Km app	SRPK2	-12	-13	-13
Z-Lyte	Km app	STK22B (TSSK2)	6	5	5
Z-Lyte	Km app	STK22D (TSSK1)	-2	0	-1
Z-Lyte	Km app	STK23 (MSSK1)	0	4	2
Z-Lyte	Km app	STK24 (MST3)	-3	-2	-2
Z-Lyte	Km app	STK25 (YSK1)	8	-10	-1
Z-Lyte	Km app	STK3 (MST2)	-6	-9	-8
Z-Lyte	Km app	STK4 (MST1)	-8	-7	-7
Z-Lyte	Km app	SYK	1	-1	0
Z-Lyte	Km app	TAOK2 (TAO1)	2	-6	-2
Z-Lyte	Km app	TBK1	-4	-10	-7
Z-Lyte	Km app	TEK (Tie2)	10	14	12
Z-Lyte	Km app	TXK	2	-1	1
Z-Lyte	Km app	TYK2	-7	-6	-6
Z-Lyte	Km app	TYRO3 (RSE)	7	3	5
Z-Lyte	Km app	YES1	13	10	11
Z-Lyte	Km app	ZAP70	5	2	3
Lantha	NA	ABL1 H396P	1	1	1
Lantha	NA	ABL1 M351T	4	10	7
Lantha	NA	ABL1 Q252H	-2	-2	-2
Lantha	NA	ACVR1 (ALK2) R206H	-11	-22	-16
Lantha	NA	ACVR1 (ALK2)	-1	0	-1
Lantha	NA	ACVR2A	4	0	2
Lantha	NA	ACVR2B	5	8	7
Lantha	NA	ACVRL1 (ALK1)	0	-6	-3
Lantha	NA	ALK C1156Y	12	8	10
Lantha	NA	ALK F1174L	2	3	3
Lantha	NA	ALK L1196M	-2	5	2
Lantha	NA	ALK R1275Q	1	1	1
Lantha	NA	AMPK (A1/B1/G2)	0	-7	-4
Lantha	NA	AMPK (A1/B1/G3)	2	-3	0
Lantha	NA	AMPK (A1/B2/G1)	1	-1	0
Lantha	NA	AMPK (A2/B2/G1)	1	10	5
Lantha	NA	AMPK (A2/B2/G2)	1	2	1
Lantha	NA	AXL R499C	3	3	3
Lantha	NA	BMPR1A (ALK3)	1	-2	-1
Lantha	NA	BMPR1B (ALK6)	1	-9	-4

Lantha	NA	BMPR2	-6	-3	-5
Lantha	NA	BRAF V599E	-5	1	-2
Lantha	NA	BRAF	-2	7	3
Lantha	NA	BRSK2	5	4	5
Lantha	NA	CAMK2G (CaMKII gamma)	-1	5	2
Lantha	NA	CAMKK1 (CAMKKA)	-10	-5	-8
Lantha	NA	CAMKK2 (CaMKK beta)	-1	2	1
Lantha	NA	CASK	-10	3	-4
Lantha	NA	CDC7/DBF4	0	0	0
Lantha	NA	CDK1/cyclin A2	-8	4	-2
Lantha	NA	CDK11 (Inactive)	14	19	17
Lantha	NA	CDK14 (PFTK1)/cyclin Y	6	2	4
Lantha	NA	CDK16 (PCTK1)/cyclin Y	11	3	7
Lantha	NA	CDK2/cyclin A1	0	4	2
Lantha	NA	CDK2/cyclin E1	-2	-1	-1
Lantha	NA	CDK2/cyclin O	-2	2	0
Lantha	NA	CDK3/cyclin E1	4	9	6
Lantha	NA	CDK5 (Inactive)	-1	8	3
Lantha	NA	CDK8/cyclin C	-1	-3	-2
Lantha	NA	CDK9 (Inactive)	11	-3	4
Lantha	NA	CDK9/cyclin K	1	1	1
Lantha	NA	CLK4	-3	3	0
Lantha	NA	DAPK2	0	1	0
Lantha	NA	DDR1	-1	-1	-1
Lantha	NA	DDR2 N456S	4	-3	0
Lantha	NA	DDR2 T654M	-7	0	-3
Lantha	NA	DDR2	-1	-5	-3
Lantha	NA	DMPK	12	5	9
Lantha	NA	DYRK2	13	3	8
Lantha	NA	EGFR (ErbB1) d746-750	-2	-1	-2
Lantha	NA	EIF2AK2 (PKR)	-6	-4	-5
Lantha	NA	EPHA3	-4	2	-1
Lantha	NA	EPHA6	-10	3	-4
Lantha	NA	EPHA7	-4	-9	-6
Lantha	NA	FGFR1 V561M	-1	-5	-3
Lantha	NA	FGFR3 G697C	-6	-1	-3
Lantha	NA	FGFR3 K650M	-4	5	0
Lantha	NA	FLT3 ITD	-1	-4	-2
Lantha	NA	FYN A	3	5	4
Lantha	NA	GRK1	2	-1	1
Lantha	NA	ICK	0	2	1
Lantha	NA	KIT A829P	1	1	1
Lantha	NA	KIT D816H	-3	2	0
Lantha	NA	KIT D816V	2	2	2

Lantha	NA	KIT D820E	2	2	2
Lantha	NA	KIT N822K	-1	-1	-1
Lantha	NA	KIT T670E	1	-4	-1
Lantha	NA	KIT V559D T670I	3	2	3
Lantha	NA	KIT V654A	-4	2	-1
Lantha	NA	KIT Y823D	0	6	3
Lantha	NA	LATS1	2	-6	-2
Lantha	NA	LATS2	-3	-5	-4
Lantha	NA	LIMK1	1	-2	0
Lantha	NA	LIMK2	-6	-4	-5
Lantha	NA	MAP2K1 (MEK1) S218D S222D	-4	2	-1
Lantha	NA	MAP2K1 (MEK1)	-3	-3	-3
Lantha	NA	MAP2K2 (MEK2)	-3	1	-1
Lantha	NA	MAP2K3 (MEK3)	4	7	5
Lantha	NA	MAP2K6 (MKK6) S207E T211E	-2	-4	-3
Lantha	NA	MAP2K6 (MKK6)	1	1	1
Lantha	NA	MAP3K10 (MLK2)	1	2	1
Lantha	NA	MAP3K11 (MLK3)	-1	1	0
Lantha	NA	MAP3K14 (NIK)	-3	-3	-3
Lantha	NA	MAP3K2 (MEKK2)	4	-4	0
Lantha	NA	MAP3K3 (MEKK3)	-2	6	2
Lantha	NA	MAP3K5 (ASK1)	-10	-1	-6
Lantha	NA	MAP3K7/MAP3K7IP1 (TAK1-TAB1)	-3	2	-1
Lantha	NA	MAP4K1 (HPK1)	0	-1	0
Lantha	NA	MAP4K3 (GLK)	-4	3	0
Lantha	NA	MAPK10 (JNK3)	5	6	6
Lantha	NA	MAPK15 (ERK7)	-2	-2	-2
Lantha	NA	MAPK8 (JNK1)	10	4	7
Lantha	NA	MAPK9 (JNK2)	5	3	4
Lantha	NA	MERTK (cMER) A708S	3	-2	1
Lantha	NA	MET D1228H	3	1	2
Lantha	NA	MKNK2 (MNK2)	1	-1	0
Lantha	NA	MLCK (MLCK2)	-4	-3	-3
Lantha	NA	MYLK (MLCK)	-2	-2	-2
Lantha	NA	MYO3B (MYO3 beta)	0	2	1
Lantha	NA	NLK	2	6	4
Lantha	NA	NUAK2	1	0	1
Lantha	NA	PKN2 (PRK2)	-4	-3	-4
Lantha	NA	PLK4	2	5	3
Lantha	NA	PRKACB (PRKAC beta)	5	1	3
Lantha	NA	PRKACG (PRKAC gamma)	-1	-3	-2
Lantha	NA	RAF1 (cRAF) Y340D Y341D	-2	0	-1
Lantha	NA	RET G691S	1	7	4

Lantha	NA	RET M918T	2	-8	-3
Lantha	NA	RET V804M	15	23	19
Lantha	NA	RIPK2	0	2	1
Lantha	NA	RIPK3	0	0	0
Lantha	NA	SIK1	0	0	0
Lantha	NA	SIK3	6	9	8
Lantha	NA	SLK	-1	-3	-2
Lantha	NA	STK16 (PKL12)	1	3	2
Lantha	NA	STK17A (DRAK1)	12	7	9
Lantha	NA	STK17B (DRAK2)	1	2	2
Lantha	NA	STK32B (YANK2)	0	3	1
Lantha	NA	STK32C (YANK3)	4	3	3
Lantha	NA	STK33	0	-2	-1
Lantha	NA	STK38 (NDR)	-2	7	3
Lantha	NA	STK38L (NDR2)	4	7	6
Lantha	NA	STK39 (STLK3)	-2	8	3
Lantha	NA	TAOK1	14	19	17
Lantha	NA	TAOK3 (JIK)	3	-1	1
Lantha	NA	TEC	-3	-3	-3
Lantha	NA	TEK (TIE2) R849W	4	3	4
Lantha	NA	TEK (TIE2) Y1108F	-1	-3	-2
Lantha	NA	TESK2	9	11	10
Lantha	NA	TGFBR1 (ALK5)	-5	-2	-4
Lantha	NA	TGFBR2	1	-4	-1
Lantha	NA	TLK1	-1	-4	-2
Lantha	NA	TLK2	-2	-3	-3
Lantha	NA	TNIK	-3	-6	-4
Lantha	NA	TNK2 (ACK)	1	1	1
Lantha	NA	TTK	0	-4	-2
Lantha	NA	ULK1	3	-3	0
Lantha	NA	ULK2	4	3	4
Lantha	NA	ULK3	8	0	4
Lantha	NA	WEE1	1	-1	0
Lantha	NA	WNK2	9	3	6
Lantha	NA	WNK3	6	7	6
Lantha	NA	ZAK	0	0	0

9 Abbreviations

Abbreviation	Meaning
(e)GFP	(enhanced)Green Fluorescent Protein
AC	Adenylyl Cyclase
ADP	Adenosine Di Phosphate
AMP	Adenosine Mono Phosphate
AMPK	AMP-activated protein kinase
Atg	AuTophaGy related gene / protein
ATP	Adenosine Tri Phosphate
BSA	Bovine Serum Albumin
BuLi	Butyl Lithium
cAMP	Cyclic AMP
CETSA	Cellular Thermal Shift Assay
DCM	Dichlormethane
DMEM	Dulbecco's modified Eagle's medium
DMP	DiMethoxyPyridine
DMSO	Dimethylsulfoxide
DNA	DeoxyriboNucleic Acid
DTT	Dithiothreitol
EBSS	Earle's Balanced Salt Solution
ECAR	Extra Cellular Acidification Rate
EDTA	Ethylenediaminetetraacetic acid
EGTA	(ethylene glycol-bis(β-aminoethyl ether)-N,N,N',N'-tetraacetic acid)
EPAC	Exchange protein directly activated by cAMP
ER	Endoplasmatic reticulum
EtOAc	Ethylacetate
EtOH	Ethanol
FBS	Fetal Bovine Serum
GC	Gas Chromatography
GPCR	G-protein coupled receptor
$G_{\alpha S}$	α-subunit of the heterotrimeric G-protein of the S-subfamily
HCD	high energy collision dissociation
HEPES	(4-(2-hydroxyethyl)-1-piperazineethanesulfonic acid)
HPLC	High Pressure Liquid Chromatography
HRP	Horse Radish Peroxidase
i-	iso-
iBAQ	Intensity-Based Absolute Quantification
IGD	In-gel digestion
IP	Inositol Phosphate
ITDRF	Isothermal Dose Response Fingerprint
LC3	Microtubule-associated protein 1A/1B-light chain 3
LFQ	Label Free Quantification
MEM	Eagle's minimal essential medium
MeOH	Methanol
MS	Mass Spectrometry
mTOR	Mammalian / Mechanistic Target Of Rapamycin

NHS	*N*-hydroxysuccinimide
NMR	Nuclear magnetic resonance
OBD	On-bead digestion
OCR	Oxygen Consumption Rate
p62	Sequestosome-1 or ubiquitin-binding protein p62
PAGE	Poly Acrylamide Gel Electrophoresis
PAL	Photo Affinity Labeling
PBS	Phosphate buffered saline
PCR	Polymerase Chain Reaction
PE	Petroleum ether
PEG	Poly Ethylene Glycol
PIK	Phosphatidyl Inositol Kinase
PIP	Phosphatidyl Inositol Phosphate
PIPES	piperazine-N,N′-bis(2-ethanesulfonic acid)
PKA	Protein Kinase A
PKB	Protein Kinase B
PKC	Protein Kinase C
PLCε	Phospholipase Cε
PVDF	Polyvinylidene fluoride
Rap-2B	Ras-related protein 2B
Rheb	Ras homolog enriched in brain
RIPA	radioimmunoprecipitation assay
RNA	RiboNucleic Acid
ROS	Reactive Oxygen Species
RTK	Receptor tyrosine kinase
s-	sec-
SDS	Sodium dodecylsulfate
SILAC	stable isotope labeling by/with amino acids in cell culture
STAGE	STop And Go Extraction
t-	tert-
TAMRA	Carboxytetramethylrhodamine
TBS	Tris buffered saline
TBTA	Tris(benzyltriazolylmethyl)amine
TCEP	(tris(2-carboxyethyl)phosphine)
TEAB	Triethylammoniumbicarbonate
TFA	Trifluoroacetic Acid
TLC	Thin Layer Chromatograpy
TMT	Tandem mass tags
TPP	Thermal Proteome Profiling
TSC	Tuberous sclerosis complex
ULK1	Unc-51 like kinase 1
UV	Ultraviolet
VPS34	Vacuolar Protein Sorting 34

10 References

1. Capasso, L. 5300 years ago, the Ice Man used natural laxatives and antibiotics. *Lancet* **352,** 1864 (1998).
2. Drews, J. Drug Discovery: A Historical Perspective. *Science* **287,** 1960–1964 (2000).
3. Galluzzi, L., Bravo-San Pedro, J. M., Levine, B., Green, D. R. & Kroemer, G. Pharmacological modulation of autophagy: therapeutic potential and persisting obstacles. *Nat. Rev. Drug Discov.* (2017).
4. Wetzel, S., Bon, R. S., Kumar, K. & Waldmann, H. Biology-oriented synthesis. *Angew. Chem. Int. Ed.* **50,** 10800–10826 (2011).
5. Klionsky, D. J. Autophagy revisited. A conversation with Christian de Duve. *Autophagy* **4,** 740–743 (2014).
6. Christian de Duve & Robert Wattiaux. Functions of Lysosomes. *Annu. Rev. Physiol.* **28,** 435–492 (1966).
7. Ashford, T. P. & Porter, K. R. Cytoplasmic components in hepatic cell lysosomes. *J. Cell Biol.* **12,** 198–202 (1962).
8. Sam L. Clark Jr. Cellular differentiation in the kidney of newborn mice studied with the electron microscope. *J. Biophys. Biochem. Cytol.* **3,** 349–362 (1957).
9. Kazuhiko Takeshige, Misuzu Baba, Shigeru Tsuboi, Takeshi Noda, and Yoshinori Ohsumi. Autophagy in Yeast Demonstrated with Proteinase-deficient Mutants and Conditions for its Induction. *J. Cell Biol.* **152,** 657–668 (2001).
10. Miki Tsukada, Y. O. Isolation and characterization of autophagy-defective mutants of Saccharomyces cerevisiae. *FEBS Lett.* **333,** 169–174 (1993).
11. Matsuura, A., Tsukada, M., Wada, Y. & Ohsumi, Y. Apg1p, a novel protein kinase required for the autophagic process in Saccharomyces cerevisiae. *Gene* **192,** 245–250 (1997).
12. Yao, Z., Delorme-Axford, E., Backues, S. K. & Klionsky, D. J. Atg41/Icy2 regulates autophagosome formation. *Autophagy* **11,** 2288–2299 (2015).
13. Yorimitsu, T. & Klionsky, D. J. Autophagy: molecular machinery for self-eating. *Cell Death Differ.* **12,** 1542–1552 (2005).
14. Kunz, J. B., Schwarz, H. & Mayer, A. Determination of four sequential stages during microautophagy in vitro. *J. Biol. Chem.* **279,** 9987–9996 (2004).
15. Majeski, A. E. & Dice, J. F. Mechanisms of chaperone-mediated autophagy. *Int. J. Biochem. Cell Biol.* **36,** 2435–2444 (2004).
16. Ashrafi, G. & Schwarz, T. L. The pathways of mitophagy for quality control and clearance of mitochondria. *Cell Death Differ.* **20,** 31–42 (2013).
17. Rubinsztein, D. C., Shpilka, T. & Elazar, Z. Mechanisms of autophagosome biogenesis. *Curr. Biol.* **22,** R29-34 (2012).
18. Xie, Z. & Klionsky, D. J. Autophagosome formation: core machinery and adaptations. *Nat. Cell. Biol.* **9,** 1102–1109 (2007).
19. Suzuki, K. & Ohsumi, Y. Current knowledge of the pre-autophagosomal structure (PAS). *FEBS Lett.* **584,** 1280–1286 (2010).

20. Webber, J. L. & Tooze, S. A. New insights into the function of Atg9. *FEBS Lett.* **584,** 1319–1326 (2010).

21. Mizushima, N. The role of the Atg1/ULK1 complex in autophagy regulation. *Curr. Opin. Cell Biol.* **22,** 132–139 (2010).

22. Jaber, N. *et al.* Class III PI3K Vps34 plays an essential role in autophagy and in heart and liver function. *Proc. Natl. Acad. Sci. U.S.A.* **109,** 2003–2008 (2012).

23. Russell, R. C. *et al.* ULK1 induces autophagy by phosphorylating Beclin-1 and activating VPS34 lipid kinase. *Nat. Cell. Biol.* **15,** 741–750 (2013).

24. Backer, J. M. The intricate regulation and complex functions of the Class III phosphoinositide 3-kinase Vps34. *Biochem. J.* **473,** 2251–2271 (2016).

25. Lindmo, K. & Stenmark, H. Regulation of membrane traffic by phosphoinositide 3-kinases. *J. Cell. Sci.* **119,** 605–614 (2006).

26. Dooley, H. C. *et al.* WIPI2 links LC3 conjugation with PI3P, autophagosome formation, and pathogen clearance by recruiting Atg12-5-16L1. *Mol. cell* **55,** 238–252 (2014).

27. Yoshinobu Ichimura *et al.* A ubiquitin-like system mediates protein lipidation. *Nature* **408,** 488–492 (2000).

28. Hemelaar, J., Lelyveld, V. S., Kessler, B. M. & Ploegh, H. L. A single protease, Apg4B, is specific for the autophagy-related ubiquitin-like proteins GATE-16, MAP1-LC3, GABARAP, and Apg8L. *J. Biol. Chem.* **278,** 51841–51850 (2003).

29. Bjorkoy, G. *et al.* p62/SQSTM1 forms protein aggregates degraded by autophagy and has a protective effect on huntingtin-induced cell death. *J. Cell Biol.* **171,** 603–614 (2005).

30. Chen, Y. & Yu, L. Autophagic lysosome reformation. *Exp. Cell. Res.* **319,** 142–146 (2013).

31. Mindell, J. A. Lysosomal acidification mechanisms. *Annu. Rev. Physiol.* **74,** 69–86 (2012).

32. Boya, P., Reggiori, F. & Codogno, P. Emerging regulation and functions of autophagy. *Nat. Cell Biol.* **15,** 1017 (2013).

33. Klionsky, D. J. Autophagy as a Regulated Pathway of Cellular Degradation. *Science* **290,** 1717–1721 (2000).

34. Lewis C. Cantley. The Phosphoinositide 3-Kinase Pathway. *Science* **296,** 1655–1657 (2002).

35. Gao, X. *et al.* Tsc tumour suppressor proteins antagonize amino-acid-TOR signalling. *Nat. Cell Biol.* **4,** 699–704 (2002).

36. Do-Hyung Kim *et al.* mTOR Interacts with Raptor to Form a Nutrient-Sensitive Complex that Signals to the Cell Growth Machinery. *Cell* **110,** 163–175 (2002).

37. Papandreou, I., Lim, A. L., Laderoute, K. & Denko, N. C. Hypoxia signals autophagy in tumor cells via AMPK activity, independent of HIF-1, BNIP3, and BNIP3L. *Cell Death Differ.* **15,** 1572–1581 (2008).

38. S. Sarkar, B. Ravikumar, R. A. Floto & D. C. Rubinsztein. Rapamycin and mTOR-independent autophagy inducers ameliorate toxicity of polyglutamineexpanded huntingtin and related proteinopathies. *Cell Death. Differ.* **16,** 46–56 (2009).

39. Xia, H.-G. *et al.* Control of basal autophagy by calpain1 mediated cleavage of ATG5. *Autophagy* **6,** 61–66 (2014).

40. Williams, A. *et al.* Novel targets for Huntington's disease in an mTOR-independent autophagy pathway. *Nat. Chem. Biol.* **4,** 295–305 (2008).

41. He, C. & Klionsky, D. J. Regulation mechanisms and signaling pathways of autophagy. *Annu. Rev. Genet.* **43,** 67–93 (2009).

42. Cherra, S. J. 3. *et al.* Regulation of the autophagy protein LC3 by phosphorylation. *J. Cell Biol.* **190,** 533–539 (2010).

43. Stephan, J. S., Yeh, Y.-Y., Ramachandran, V., Deminoff, S. J. & Herman, P. K. The Tor and PKA signaling pathways independently target the Atg1/Atg13 protein kinase complex to control autophagy. *Proc. Natl. Acad. Sci. U.S.A.* **106,** 17049–17054 (2009).

44. Torres-Quiroz, F., Filteau, M. & Landry, C. R. Feedback regulation between autophagy and PKA. *Autophagy* **11,** 1181–1183 (2015).

45. Ravikumar, B. *et al.* Regulation of mammalian autophagy in physiology and pathophysiology. *Physiol. Rev.* **90,** 1383–1435 (2010).

46. Schenck, M., Carpinteiro, A., Grassme, H., Lang, F. & Gulbins, E. Ceramide: physiological and pathophysiological aspects. *Arch. Biochem. Biophys.* **462,** 171–175 (2007).

47. Harvald, E. B., Olsen, A. S. B. & Faergeman, N. J. Autophagy in the light of sphingolipid metabolism. *Apoptosis* **20,** 658–670 (2015).

48. Villena, J. *et al.* Ceramide-induced formation of ROS and ATP depletion trigger necrosis in lymphoid cells. *Free Radic. Biol. Med.* **44,** 1146–1160 (2008).

49. Schieber, M. & Chandel, N. S. ROS function in redox signaling and oxidative stress. *Curr. Biol.* **24,** R453-62 (2014).

50. Ruth Scherz-Shouval *et al.* Reactive oxygen species are essential for autophagy and specifically regulate the activity of Atg4. *EMBO J.* **26,** 1749–1760 (2007).

51. Lee, J., Giordano, S. & Zhang, J. Autophagy, mitochondria and oxidative stress: cross-talk and redox signalling. *Biochem. J.* **441,** 523–540 (2012).

52. Okamoto, K. & Kondo-Okamoto, N. Mitochondria and autophagy: critical interplay between the two homeostats. *Biochim. Biophys. Acta* **1820,** 595–600 (2012).

53. Kim, I., Rodriguez-Enriquez, S. & Lemasters, J. J. Selective degradation of mitochondria by mitophagy. *Arch. Biochem. Biophys.* **462,** 245–253 (2007).

54. Deretic, V., Saitoh, T. & Akira, S. Autophagy in infection, inflammation and immunity. *Nat. Rev. Immunol.* **13,** 722–737 (2013).

55. Sarkar, S. *et al.* Complex inhibitory effects of nitric oxide on autophagy. *Mol. cell* **43,** 19–32 (2011).

56. Deretic, V. Autophagy as an innate immunity paradigm: expanding the scope and repertoire of pattern recognition receptors. *Curr. Opin. Immunol.* **24,** 21–31 (2012).

57. Webb, J. L., Ravikumar, B., Atkins, J., Skepper, J. N. & Rubinsztein, D. C. Alpha-Synuclein is degraded by both autophagy and the proteasome. *J. Biol. Chem.* **278,** 25009–25013 (2003).

58. Levine, B. & Kroemer, G. Autophagy in the pathogenesis of disease. *Cell* **132,** 27–42 (2008).

59. Kiriyama, Y. & Nochi, H. The Function of Autophagy in Neurodegenerative Diseases. *Int. J. Mol. Sci.* **16,** 26797–26812 (2015).

60. Ravikumar, B. Aggregate-prone proteins with polyglutamine and polyalanine expansions are degraded by autophagy. *Hum. Mol. Genet.* **11,** 1107–1117 (2002).

61. Berger, Z. *et al.* Rapamycin alleviates toxicity of different aggregate-prone proteins. *Hum. Mol. Genet.* **15,** 433–442 (2006).

62. Nixon, R. A. The role of autophagy in neurodegenerative disease. *Nat. Med.* **19,** 983–997 (2013).

63. Yang, Z. & Klionsky, D. J. Eaten alive: a history of macroautophagy. *Nat. Cell Biol.* **12,** 814–822 (2010).

64. Mizushima, N. & Levine, B. Autophagy in mammalian development and differentiation. *Nat. Cell Biol.* **12,** 823–830 (2010).

65. Rubinsztein, D. C., Codogno, P. & Levine, B. Autophagy modulation as a potential therapeutic target for diverse diseases. *Nat Rev. Drug Discov.* **11,** 709–730 (2012).

66. Liu, Y. & Levine, B. Autosis and autophagic cell death: the dark side of autophagy. *Cell Death Differ.* **22,** 367–376 (2015).

67. Marino, G., Niso-Santano, M., Baehrecke, E. H. & Kroemer, G. Self-consumption: the interplay of autophagy and apoptosis. *Nat. Rev. Mol. Cell Biol.* **15,** 81–94 (2014).

68. Maiuri, M. C., Zalckvar, E., Kimchi, A. & Kroemer, G. Self-eating and self-killing: crosstalk between autophagy and apoptosis. *Nat. Rev. Mol. Cell Biol.* **8,** 741–752 (2007).

69. Shintani, T. & Klionsky, D. J. Autophagy in health and disease: a double-edged sword. *Science* **306,** 990–995 (2004).

70. Choi, K. S. Autophagy and cancer. *Exp. Mol. Med.* **44,** 109–120 (2012).

71. Hanahan, D. & Weinberg, R. A. Hallmarks of cancer: the next generation. *Cell* **144,** 646–674 (2011).

72. Kondo, Y. & Kondo, S. Autophagy and Cancer Therapy. *Autophagy* **2,** 85–90 (2014).

73. White, E. & Dipaola, R. S. The double-edged sword of autophagy modulation in cancer. *Clin. Cancer Res.* **15,** 5308–5316 (2009).

74. Amaravadi, R. K. *et al.* Principles and current strategies for targeting autophagy for cancer treatment. *Clin. Cancer Res.* **17,** 654–666 (2011).

75. Chen, N. & Karantza, V. Autophagy as a therapeutic target in cancer. *Cancer Biol. Ther.* **11,** 157–168 (2014).

76. Chen, S. *et al.* Autophagy is a therapeutic target in anticancer drug resistance. *Biochim. Biophys. Acta* **1806,** 220–229 (2010).

77. Kanzawa, T. *et al.* Role of autophagy in temozolomide-induced cytotoxicity for malignant glioma cells. *Cell Death Differ.* **11,** 448–457 (2004).

78. Shingu, T. *et al.* Inhibition of autophagy at a late stage enhances imatinib-induced cytotoxicity in human malignant glioma cells. *Int. J. Cancer* **124,** 1060–1071 (2009).

79. Faivre, S., Kroemer, G. & Raymond, E. Current development of mTOR inhibitors as anticancer agents. *Nat. Rev. Drug Discov.* **5,** 671–688 (2006).

80. Thoreen, C. C. *et al.* An ATP-competitive mammalian target of rapamycin inhibitor reveals rapamycin-resistant functions of mTORC1. *J. Biol. Chem.* **284,** 8023–8032 (2009).

81. Han, W. *et al.* EGFR Tyrosine Kinase Inhibitors Activate Autophagy as a Cytoprotective Response in Human Lung Cancer Cells. *PloS one* **6,** e18691 (2011).

82. Fung, C., Chen, X., Grandis, J. R. & Duvvuri, U. EGFR tyrosine kinase inhibition induces autophagy in cancer cells. *Cancer Biol. Ther.* **13,** 1417–1424 (2012).

83. Kim, J., Yang, G., Kim, Y., Kim, J. & Ha, J. AMPK activators: mechanisms of action and physiological activities. *Exp. Mol. Med.* **48,** e224 (2016).

84. Goransson, O. *et al.* Mechanism of action of A-769662, a valuable tool for activation of AMP-activated protein kinase. *J. Biol. Chem.* **282,** 32549–32560 (2007).

85. Walter, C., Metzger, S., Weiss, A., Riess, O. & Phuc Nguyen, H. M12 A769662 Leads to AMPK Activation, Induces Autophagy and has Beneficial Effects IN HD Cells. *J. Neurol. Neurosurg. Psychiatry* **85,** A98-A98 (2014).

86. Lee, J. W., Park, S., Takahashi, Y. & Wang, H.-G. The association of AMPK with ULK1 regulates autophagy. *PloS one* **5,** e15394 (2010).

87. Rose, C. *et al.* Rilmenidine attenuates toxicity of polyglutamine expansions in a mouse model of Huntington's disease. *Hum. Mol. Genet.* **19,** 2144–2153 (2010).

88. Puls, F. *et al.* Autophagy-enhancing drug carbamazepine diminishes hepatocellular death in fibrinogen storage disease. *J. Hepatol.* **59,** 626–630 (2013).

89. Kania, E. *et al.* Verapamil treatment induces cytoprotective autophagy by modulating cellular metabolism. *FEBS J.* (2017).

90. Ravikumar, B. *et al.* Inhibition of mTOR induces autophagy and reduces toxicity of polyglutamine expansions in fly and mouse models of Huntington disease. *Nat. Genet.* **36,** 585–595 (2004).

91. Yamamoto, A. *et al.* Bafilomycin A1 prevents maturation of autophagic vacuoles by inhibiting fusion between autophagosomes and lysosomes in rat hepatoma cell line, H-4-II-E cells. *Cell Struct. Funct.* **23,** 33–42 (1998).

92. Balic, A. *et al.* Chloroquine targets pancreatic cancer stem cells via inhibition of CXCR4 and hedgehog signaling. *Mol. Cancer Ther.* **13,** 1758–1771 (2014).

93. Eng, C. H. *et al.* Macroautophagy is dispensable for growth of KRAS mutant tumors and chloroquine efficacy. *Proc. Natl. Acad. Sci. U.S.A.* **113,** 182–187 (2016).

94. Nordstrøm, L. U. *et al.* Discovery of autophagy inhibitors with antiproliferative activity in lung and pancreatic cancer cells. *ACS Med. Chem. Lett.* **6,** 134–139 (2015).

95. Arenz, C. Small Molecule Inhibitors of Acid Sphingomyelinase. *Cell. Physiol. Biochem.* **26,** 1–8 (2010).

96. Liu, J. *et al.* Beclin1 controls the levels of p53 by regulating the deubiquitination activity of USP10 and USP13. *Cell* **147,** 223–234 (2011).

97. Wu, Y.-T. *et al.* Dual Role of 3-Methyladenine in Modulation of Autophagy via Different Temporal Patterns of Inhibition on Class I and III Phosphoinositide 3-Kinase. *J. Biol. Chem.* **285,** 10850–10861 (2010).

98. Yang, Y.-p. *et al.* Application and interpretation of current autophagy inhibitors and activators. *Acta Pharmacol. Sin.* **34,** 625–635 (2013).

99. Ronan, B. *et al.* A highly potent and selective Vps34 inhibitor alters vesicle trafficking and autophagy. *Nat. Chem. Biol.* **10,** 1013–1019 (2014).

100. Bago, R. *et al.* Characterization of VPS34-IN1, a selective inhibitor of Vps34, reveals that the phosphatidylinositol 3-phosphate-binding SGK3 protein kinase is a downstream target of class III phosphoinositide 3-kinase. *Biochem. J.* **463,** 413–427 (2014).

101. Dowdle, W. E. *et al.* Selective VPS34 inhibitor blocks autophagy and uncovers a role for NCOA4 in ferritin degradation and iron homeostasis in vivo. *Nat. Cell Biol.* **16,** 1069–1079 (2014).

102. Triola, G. Chemical tools for modulating autophagy. *Tetrahedron* **71,** 387–406 (2015).

103. Fleming, A., Noda, T., Yoshimori, T. & Rubinsztein, D. C. Chemical modulators of autophagy as biological probes and potential therapeutics. *Nat. Chem. Biol.* **7,** 9–17 (2011).

104. Boya, P. *et al.* Inhibition of Macroautophagy Triggers Apoptosis. *Mol. Cell. Biol.* **25,** 1025–1040 (2005).

105. Pasquier, B. *et al.* Discovery of (2 S)-8-[(3 R)-3-Methylmorpholin-4-yl]-1-(3-methyl-2-oxobutyl)-2-(trifluoromethyl)-3,4-dihydro-2 H -pyrimido[1,2- a]pyrimidin-6-one. A Novel Potent and Selective Inhibitor of Vps34 for the Treatment of Solid Tumors. *J. Med. Chem.* **58,** 376–400 (2015).

106. Honda, A. *et al.* Potent, Selective, and Orally Bioavailable Inhibitors of VPS34 Provide Chemical Tools to Modulate Autophagy in Vivo. *ACS Med. Chem. Lett.* (2015).

107. O'Connor, C. J., Laraia, L. & Spring, D. R. Chemical genetics. *Chem. Soc. Rev.* **40,** 4332–4345 (2011).

108. Spring, D. R. Chemical genetics to chemical genomics. Small molecules offer big insights. *Chem. Soc. Rev.* **34,** 472 (2005).

109. Kaiser, M., Wetzel, S., Kumar, K. & Waldmann, H. Biology-inspired synthesis of compound libraries. *Cell. Mol. Life Sci.* **65,** 1186–1201 (2008).

110. Derek S. Tan. Diversity-oriented synthesis: exploring the intersections between chemistry and biology. *Nat. Chem. Biol.* **1,** 74–84 (2005).

111. Ziegler, S., Pries, V., Hedberg, C. & Waldmann, H. Target identification for small bioactive molecules: finding the needle in the haystack. *Angew. Chem. Int. Ed.* **52,** 2744–2792 (2013).

112. Moffat, J. G., Rudolph, J. & Bailey, D. Phenotypic screening in cancer drug discovery - past, present and future. *Nat. Rev. Drug Discov.* **13,** 588–602 (2014).

113. Lee, Y.-C. *et al.* A ligand-directed divergent catalytic approach to establish structural and functional scaffold diversity. *Nat. Commun.* **8,** 14043 (2017).

114. Takayama, H. *et al.* Discovery of inhibitors of the Wnt and Hedgehog signaling pathways through the catalytic enantioselective synthesis of an iridoid-inspired compound collection. *Angew. Chem. Int. Ed.* **52,** 12404–12408 (2013).

115. Ramm P. & Thomas N. Image-Based Screening of Signal Transduction Assays. *Sci. Signal.* **177,** 1–14 (2003).

116. Mullard, A. The phenotypic screening pendulum swings. *Nat. Rev. Drug Discov.* **14,** 807–809 (2015).

117. Ochoa, J. L., Bray, W. M., Lokey, R. S. & Linington, R. G. Phenotype-Guided Natural Products Discovery Using Cytological Profiling. *J. Nat. Prod.* **78,** 2242–2248 (2015).

118. Kang, J. *et al.* Improving drug discovery with high-content phenotypic screens by systematic selection of reporter cell lines. *Nat. Biotech.* **34,** 70–77 (2016).

119. Gough, A., Shun, T. Y., Lansing Taylor, D. & Schurdak, M. A metric and workflow for quality control in the analysis of heterogeneity in phenotypic profiles and screens. *Methods* **96,** 12–26 (2016).

120. Swinney, D. C. & Anthony, J. How were new medicines discovered? *Nat. Rev. Drug Discov.* **10,** 507–519 (2011).

121. Shao-En Onga *et al.* Identifying the proteins to which small-molecule probes and drugs bind in cells. *Proc. Natl. Acad. Sci. U.S.A.* **106,** 4617–4622 (2009).

122. Franken, H. *et al.* Thermal proteome profiling for unbiased identification of direct and indirect drug targets using multiplexed quantitative mass spectrometry. *Nat. protoc.* **10,** 1567–1593 (2015).

123. Jafari, R. *et al.* The cellular thermal shift assay for evaluating drug target interactions in cells. *Nat. protoc.* **9,** 2100–2122 (2014).

124. Laraia, L. & Waldmann, H. Natural product inspired compound collections. Evolutionary principle, chemical synthesis, phenotypic screening, and target identification. *Drug Discov. Today* (2017).

125. Mizushima, N., Levine, B., Cuervo, A. M. & Klionsky, D. J. Autophagy fights disease through cellular self-digestion. *Nature* **451,** 1069–1075 (2008).

126. Rubinsztein, D. C., Codogno, P. & Levine, B. Autophagy modulation as a potential therapeutic target for diverse diseases. *Nat. Rev. Drug Discov.* **11,** 709–730 (2012).

127. Rubinsztein, D. C., Gestwicki, J. E., Murphy, L. O. & Klionsky, D. J. Potential therapeutic applications of autophagy. *Nat. Rev. Drug Discov.* **6,** 304–312 (2007).

128. Lazarus, M. B., Novotny, C. J. & Shokat, K. M. Structure of the human autophagy initiating kinase ULK1 in complex with potent inhibitors. *ACS Chem. Biol.* **10,** 257–261 (2015).

129. Sarkar, S. *et al.* Small molecules enhance autophagy and reduce toxicity in Huntington's disease models. *Nat. Chem. Biol.* **3,** 331–338 (2007).

130. Lebovitz, C. B. *et al.* Precision autophagy: Will the next wave of selective autophagy markers and specific autophagy inhibitors feed clinical pipelines? *Autophagy* **11,** 1949–1952 (2015).

131. Petherick, K. J. *et al.* Autolysosomal β-catenin degradation regulates Wnt-autophagy-p62 crosstalk. *EMBO J.* **32,** 1903–1916 (2013).

132. Kühn, K. *et al.* The interplay of autophagy and β-Catenin signaling regulates differentiation in acute myeloid leukemia. *Cell Death Discov.* **1,** 15031 (2015).

133. Jimenez-Sanchez, M. *et al.* The Hedgehog signalling pathway regulates autophagy. *Nat. Commun.* **3,** 1200 (2012).

134. Pampliega, O. *et al.* Functional interaction between autophagy and ciliogenesis. *Nature* **502,** 194–200 (2013).

135. Balgi, A. D. *et al.* Screen for chemical modulators of autophagy reveals novel therapeutic inhibitors of mTORC1 signaling. *PLoS ONE* **4,** e7124 (2009).

136. Peppard, J. V. *et al.* Identifying Small Molecules which Inhibit Autophagy: a Phenotypic Screen Using Image-Based High-Content Cell Analysis. *Curr. Chem. Genom. Transl. Med.* **8,** 3–15 (2014).

137. Mizushima, N., Yoshimori, T. & Ohsumi, Y. The role of Atg proteins in autophagosome formation. *Annu. Rev. Cell Dev. Biol.* **27,** 107–132 (2011).

138. Schröder, P. *et al.* Neuritogenic militarinone-inspired 4-hydroxypyridones target the stress pathway kinase MAP4K4. *Angew. Chem. Int. Ed.* **54,** 12398–12403 (2015).

139. Bhutia, S. K. *et al.* Astrocyte elevated gene-1 induces protective autophagy. *Proc. Natl. Acad. Sci. U.S.A.* **107,** 22243–22248 (2010).

140. Park, J., Koh, M., Koo, J. Y., Lee, S. & Park, S. B. Investigation of Specific Binding Proteins to Photoaffinity Linkers for Efficient Deconvolution of Target Protein. *ACS Chem. Biol.* **11,** 44–52 (2016).

141. Lee, S. *et al.* A small molecule binding HMGB1 and HMGB2 inhibits microglia-mediated neuroinflammation. *Nat. Chem. Biol.* **10,** 1055–1060 (2014).

142. Smits, A. H., Jansen, Pascal W T C, Poser, I., Hyman, A. A. & Vermeulen, M. Stoichiometry of chromatin-associated protein complexes revealed by label-free quantitative mass spectrometry-based proteomics. *Nucleic Acids Res.* **41,** e28 (2013).

143. Lu, P., Vogel, C., Wang, R., Yao, X. & Marcotte, E. M. Absolute protein expression profiling estimates the relative contributions of transcriptional and translational regulation. *Nat. Biotech.* **25,** 117–124 (2007).

144. Ishihama, Y. *et al.* Exponentially modified protein abundance index (emPAI) for estimation of absolute protein amount in proteomics by the number of sequenced peptides per protein. *Mol. Cell. Proteomics* **4,** 1265–1272 (2005).

145. Kawamura, T. *et al.* Proteomic profiling of small-molecule inhibitors reveals dispensability of MTH1 for cancer cell survival. *Sci. Rep.* **6,** 26521 (2016).

146. Kawatani, M. *et al.* Identification of a small-molecule inhibitor of DNA topoisomerase II by proteomic profiling. *Chem. Biol.* **18,** 743–751 (2011).

147. Minegishi, H. *et al.* Methyl 3-((6-methoxy-1,4-dihydroindeno1,2-cpyrazol-3-yl)amino)benzoate (GN39482) as a tubulin polymerization inhibitor identified by MorphoBase and ChemProteoBase profiling methods. *J. Med. Chem.* **58,** 4230–4241 (2015).

148. Muroi, M., Futamura, Y. & Osada, H. Integrated profiling methods for identifying the targets of bioactive compounds: MorphoBase and ChemProteoBase. *Nat. Prod. Rep.* **33,** 621–625 (2016).

149. Futamura, Y. *et al.* Identification of a molecular target of a novel fungal metabolite, pyrrolizilactone, by phenotypic profiling systems. *Chembiochem* **14,** 2456–2463 (2013).

150. Futamura, Y. *et al.* Morphobase, an encyclopedic cell morphology database, and its use for drug target identification. *Chem. Biol.* **19,** 1620–1630 (2012).

151. Robke, L. *et al.* Phenotypic Identification of a Novel Autophagy Inhibitor Chemotype Targeting Lipid Kinase VPS34. *Angew. Chem. Int. Ed.* (2017).

152. Richters, A. *et al.* Identification and further development of potent TBK1 inhibitors. *ACS Chem. Biol.* **10,** 289–298 (2015).

153. Pilli, M. *et al.* TBK-1 promotes autophagy-mediated antimicrobial defense by controlling autophagosome maturation. *Immunity* **37,** 223–234 (2012).

154. Harrington, E. A. *et al.* VX-680, a potent and selective small-molecule inhibitor of the Aurora kinases, suppresses tumor growth in vivo. *Nat. Med.* **10,** 262–267 (2004).

155. Bebbington, D. *et al.* The discovery of the potent aurora inhibitor MK-0457 (VX-680). *Bio. Org. Med. Chem. Lett.* **19,** 3586–3592 (2009).

156. Engel, J. *et al.* Targeting Drug Resistance in EGFR with Covalent Inhibitors: A Structure-Based Design Approach. *J. Med. Chem.* **58,** 6844–6863 (2015).

157. Chang, J. W. *et al.* Highly Selective Inhibitors of Monoacylglycerol Lipase Bearing a Reactive Group that Is Bioisosteric with Endocannabinoid Substrates. *Chem. Biol.* **19,** 579–588 (2012).

158. Patterson, S. & Wyllie, S. Nitro drugs for the treatment of trypanosomatid diseases: past, present, and future prospects. *Trends Parasitol.* **30,** 289–298 (2014).

159. Im, J.-Y. *et al.* DNA damage-induced apoptosis suppressor (DDIAS), a novel target of NFATc1, is associated with cisplatin resistance in lung cancer. *Biochim. Biophys. Acta* **1863,** 40–49 (2016).

160. Moore, C. E. J. *et al.* Elongation factor 2 kinase promotes cell survival by inhibiting protein synthesis without inducing autophagy. *Cell. Signal.* **28,** 284–293 (2016).

161. Komatsu, M. & Ichimura, Y. Physiological significance of selective degradation of p62 by autophagy. *FEBS Lett.* **584,** 1374–1378 (2010).

162. Pankiv, S. *et al.* p62/SQSTM1 binds directly to Atg8/LC3 to facilitate degradation of ubiquitinated protein aggregates by autophagy. *J. Biol. Chem.* **282,** 24131–24145 (2007).

163. Klionsky, D. J. *et al.* Guidelines for the use and interpretation of assays for monitoring autophagy (3rd edition). *Autophagy* **12,** 1–222 (2016).

164. Laraia, L. *et al.* Discovery of Novel Cinchona-Alkaloid-Inspired Oxazatwistane Autophagy Inhibitors. *Angew. Chem. Int. Ed.* **56,** 2145–2150 (2017).

165. Lamb, C. A., Yoshimori, T. & Tooze, S. A. The autophagosome: origins unknown, biogenesis complex. *Nat. Rev. Mol. Cell Biol.* **14,** 759–774 (2013).

166. Dall'Armi, C., Devereaux, K. A. & Di Paolo, G. The role of lipids in the control of autophagy. *Curr. Biol.* **23,** R33-45 (2013).

167. Orsi, A. *et al.* Dynamic and transient interactions of Atg9 with autophagosomes, but not membrane integration, are required for autophagy. *Mol. Biol. Cell* **23,** 1860–1873 (2012).

168. Backer, J. M. The regulation and function of Class III PI3Ks. Novel roles for Vps34. *Biochem. J.* **410,** 1–17 (2008).

169. Devereaux, K. *et al.* Regulation of mammalian autophagy by class II and III PI 3-kinases through PI3P synthesis. *PLoS ONE* **8,** e76405 (2013).

170. Yuan, H.-X., Russell, R. C. & Guan, K.-L. Regulation of PIK3C3/VPS34 complexes by MTOR in nutrient stress-induced autophagy. *Autophagy* **9,** 1983–1995 (2014).

171. Bechtel, W. *et al.* The class III phosphatidylinositol 3-kinase PIK3C3/VPS34 regulates endocytosis and autophagosome-autolysosome formation in podocytes. *Autophagy* **9,** 1097–1099 (2013).

172. Funderburk, S. F., Wang, Q. J. & Yue, Z. The Beclin 1–VPS34 complex – at the crossroads of autophagy and beyond. *Trends Cell Biol.* **20,** 355–362 (2010).

173. Kim, J. *et al.* Differential regulation of distinct Vps34 complexes by AMPK in nutrient stress and autophagy. *Cell* **152,** 290–303 (2013).

174. Marsh, T. & Debnath, J. Ironing out VPS34 inhibition. *Nat. Cell. Biol.* **17,** 1–3 (2014).

175. Patricelli, M. P. *et al.* Functional interrogation of the kinome using nucleotide acyl phosphates. *Biochemistry* **46,** 350–358 (2007).

176. Ursu, A. *et al.* Epiblastin A Induces Reprogramming of Epiblast Stem Cells Into Embryonic Stem Cells by Inhibition of Casein Kinase 1. *Cell Chem. Biol.* **23,** 494–507 (2016).

177. Huang, Z. *et al.* Approaching the active conformation of 1,3-diaminopyrimidine based covalent inhibitors of Bruton's tyrosine kinase for treatment of Rheumatoid arthritis. *Bioorg. Med. Chem. Lett.* **26,** 1954–1957 (2016).

178. Lawrence, H. R. *et al.* Development of o-chlorophenyl substituted pyrimidines as exceptionally potent aurora kinase inhibitors. *J. Med. Chem.* **55,** 7392–7416 (2012).

179. Vicinanza, M. *et al.* PI(5)P regulates autophagosome biogenesis. *Mol. Cell* **57,** 219–234 (2015).

180. Yamashita, S.-i., Oku, M. & Sakai, Y. Functions of PI4P and Sterol Glucoside Necessary for the Synthesis of a Nascent Membrane Structure During Pexophagy. *Autophagy* **3,** 35–37 (2014).

181. Mejdrová, I. *et al.* Highly Selective Phosphatidylinositol 4-Kinase IIIβ Inhibitors and Structural Insight into Their Mode of Action. *J. Med. Chem.* **58,** 3767–3793 (2015).

182. Freitag, A. *et al.* Development of first lead structures for phosphoinositide 3-kinase-C2γ inhibitors. *J. Med. Chem.* **58,** 212–221 (2015).

183. Waring, M. J. *et al.* Potent, selective small molecule inhibitors of type III phosphatidylinositol-4-kinase α- but not β-inhibit the phosphatidylinositol signaling cascade and cancer cell proliferation. *Chem. Commun.* **50,** 5388–5390 (2014).

184. Mountford, S. J. *et al.* Class II but Not Second Class-Prospects for the Development of Class II PI3K Inhibitors. *ACS Med. Chem. Lett.* **6,** 3–6 (2015).

185. Galluzzi, L., Pietrocola, F., Levine, B. & Kroemer, G. Metabolic control of autophagy. *Cell* **159,** 1263–1276 (2014).

186. Rabinowitz, J. D. & White, E. Autophagy and Metabolism. *Science* **330,** 1344–1348 (2010).

187. Russell, R. C., Yuan, H.-X. & Guan, K.-L. Autophagy regulation by nutrient signaling. *Cell Res.* **24,** 42–57 (2014).

188. Yamamoto, N., Sato, T., Kawasaki, K., Murosaki, S. & Yamamoto, Y. A nonradioisotope, enzymatic assay for 2-deoxyglucose uptake in L6 skeletal muscle cells cultured in a 96-well microplate. *Anal. Biochem.* **351,** 139–145 (2006).

189. Salabei, J. K., Gibb, A. A. & Hill, B. G. Comprehensive measurement of respiratory activity in permeabilized cells using extracellular flux analysis. *Nat. protoc.* **9,** 421–438 (2014).

190. Dagda, R. K., Das Banerjee, T. & Janda, E. How Parkinsonian toxins dysregulate the autophagy machinery. *Int. J. Mol. Sci.* **14,** 22163–22189 (2013).

191. Giordano, S. *et al.* Bioenergetic adaptation in response to autophagy regulators during rotenone exposure. *J. Neurochem.* **131,** 625–633 (2014).

192. Schockel, L. *et al.* Targeting mitochondrial complex I using BAY 87-2243 reduces melanoma tumor growth. *Cancer Metab.* **3,** 11 (2015).

193. Ellinghaus, P. *et al.* BAY 87-2243, a highly potent and selective inhibitor of hypoxia-induced gene activation has antitumor activities by inhibition of mitochondrial complex I. *Cancer Med.* **2,** 611–624 (2013).

194. Xiong, N. *et al.* The role of autophagy in Parkinson's disease: rotenone-based modeling. *Behav. Brain Funct.* **9,** 13 (2013).

195. Tettamanti, G. *et al.* Oligomycin A induces autophagy in the IPLB-LdFB insect cell line. *Cell Tissue Res.* **326,** 179–186 (2006).

196. Mader, B. J. *et al.* Rotenone inhibits autophagic flux prior to inducing cell death. *ACS Chem. Neurosci.* **3,** 1063–1072 (2012).

197. Ma, X. *et al.* Mitochondrial electron transport chain complex III is required for antimycin A to inhibit autophagy. *Chem. Biol.* **18,** 1474–1481 (2011).

198. Graef, M. & Nunnari, J. Mitochondria regulate autophagy by conserved signalling pathways. *EMBO J.* **30,** 2101–2114 (2011).

199. Chen, Y., McMillan-Ward, E., Kong, J., Israels, S. J. & Gibson, S. B. Mitochondrial electron-transport-chain inhibitors of complexes I and II induce autophagic cell death mediated by reactive oxygen species. *J. Cell Sci.* **120,** 4155–4166 (2007).

200. Steinberg, B. E. *et al.* A cation counterflux supports lysosomal acidification. *J. Cell Biol.* **189,** 1171–1186 (2010).

201. Berezhnov, A. V. *et al.* Intracellular pH Modulates Autophagy and Mitophagy. *J. Biol. Chem.* **291,** 8701–8708 (2016).

202. Brinkley, B. R., Barham, S. S., Barranco, S. C. & Fuller, G. M. Rotenone inhibition of spindle mcrotubule assembly in mammalian cells. *Exp. Cell. Res.* **85,** 41–46 (1974).

203. Grefte, S., Wagenaars, J. A. L., Jansen, R., Willems, Peter H. G. M. & Koopman, W. J. H. Rotenone inhibits primary murine myotube formation via Raf-1 and ROCK2. *Biochim. Biophys. Acta* **1853,** 1606–1614 (2015).

204. MacDonald, M. L. *et al.* Identifying off-target effects and hidden phenotypes of drugs in human cells. *Nat. Chem. Biol.* **2,** 329–337 (2006).

205. Cox, J. & Mann, M. MaxQuant enables high peptide identification rates, individualized p.p.b.-range mass accuracies and proteome-wide protein quantification. *Nat. Biotech.* **26,** 1367–1372 (2008).

206. Carpenter, A. E. CellProfiler: image analysis software for identifying and quantifying cell phenotypes. *Genome Biol.* **7,** R100 (2006).

207. Hubner, N. C. *et al.* Quantitative proteomics combined with BAC TransgeneOmics reveals in vivo protein interactions. *J. Cell Biol.* **189,** 739–754 (2010).

208. Bradley, W. D. *et al.* EZH2 inhibitor efficacy in non-Hodgkin's lymphoma does not require suppression of H3K27 monomethylation. *Chem. Biol.* **21,** 1463–1475 (2014).

209. Alzani, R. *et al.* Therapeutic efficacy of the pan-cdk inhibitor PHA-793887 in vitro and in vivo in engraftment and high-burden leukemia models. *Exp. Hematol.* **38,** 259-269.e2 (2010).

210. Brasca, M. G. *et al.* Optimization of 6,6-dimethyl pyrrolo3,4-cpyrazoles: Identification of PHA-793887, a potent CDK inhibitor suitable for intravenous dosing. *Bio. Org. Med. Chem.* **18,** 1844–1853 (2010).

211. Massard, C. *et al.* A first in man, phase I dose-escalation study of PHA-793887, an inhibitor of multiple cyclin-dependent kinases (CDK2, 1 and 4) reveals unexpected hepatotoxicity in patients with solid tumors. *Cell Cycle* **10,** 963–970 (2011).

212. Albert, T. K. *et al.* Characterization of molecular and cellular functions of the cyclin-dependent kinase CDK9 using a novel specific inhibitor. *Br. J. Pharmacol.* **171,** 55–68 (2014).

213. Ashford, A. L. *et al.* A novel DYRK1B inhibitor AZ191 demonstrates that DYRK1B acts independently of GSK3beta to phosphorylate cyclin D1 at Thr(286), not Thr(288). *Biochem. J.* **457,** 43–56 (2014).

214. Estrada, A. A. *et al.* Discovery of highly potent, selective, and brain-penetrable leucine-rich repeat kinase 2 (LRRK2) small molecule inhibitors. *J. Med. Chem.* **55,** 9416–9433 (2012).

215. Shan, W. *et al.* A small-molecule inhibitor targeting the mitotic spindle checkpoint impairs the growth of uterine leiomyosarcoma. *Clin. Cancer Res.* **18,** 3352–3365 (2012).

216. Shimomura, T. *et al.* MK-5108, a highly selective Aurora-A kinase inhibitor, shows antitumor activity alone and in combination with docetaxel. *Mol. Cancer Ther.* **9,** 157–166 (2010).

217. Wei, Y. *et al.* CDK1-dependent phosphorylation of EZH2 suppresses methylation of H3K27 and promotes osteogenic differentiation of human mesenchymal stem cells. *Nat. Cell Biol.* **13,** 87–94 (2011).

218. Banerjee, S. *et al.* Characterization of WZ4003 and HTH-01-015 as selective inhibitors of the LKB1-tumour-suppressor-activated NUAK kinases. *Biochem. J.* **457,** 215–225 (2014).

219. Zhou, W. *et al.* Novel mutant-selective EGFR kinase inhibitors against EGFR T790M. *Nature* **462,** 1070–1074 (2009).

220. Banerjee, S. *et al.* Interplay between Polo kinase, LKB1-activated NUAK1 kinase, PP1betaMYPT1 phosphatase complex and the SCFbetaTrCP E3 ubiquitin ligase. *Biochem. J.* **461,** 233–245 (2014).

221. Wu, Y. *et al.* GSK3 inhibitors CHIR99021 and 6-bromoindirubin-3'-oxime inhibit microRNA maturation in mouse embryonic stem cells. *Sci. Rep.* **5,** 8666 (2015).

222. Misra, R. N. *et al.* 1H-Pyrazolo[3,4-b]pyridine inhibitors of cyclin-dependent kinases. Highly potent 2,6-Difluorophenacyl analogues. *Bio. Org. Med. Chem. Lett.* **13,** 2405–2408 (2003).

223. Sutherland, J. J. *et al.* A robust high-content imaging approach for probing the mechanism of action and phenotypic outcomes of cell-cycle modulators. *Mol. Cancer Ther.* **10,** 242–254 (2011).

224. Jaroslav, V. Inhibition of Cyclin-Dependent Kinases by Purine Analogues. *Eur. J. Biochem.* **224,** 771–786 (1994).

225. Peasland, A. *et al.* Identification and evaluation of a potent novel ATR inhibitor, NU6027, in breast and ovarian cancer cell lines. *Br. J. Cancer* **105,** 372–381 (2011).

226. Sultana, R. *et al.* Ataxia telangiectasia mutated and Rad3 related (ATR) protein kinase inhibition is synthetically lethal in XRCC1 deficient ovarian cancer cells. *PloS one* **8,** e57098 (2013).

227. Schultz, C. *et al.* Paullones, a series of cyclin-dependent kinase inhibitors: synthesis, evaluation of CDK1/cyclin B inhibition, and in vitro antitumor activity. *J. Med. Chem.* **42,** 2909–2919 (1999).

228. Cicenas, J. *et al.* Roscovitine in cancer and other diseases. *Ann. Transl. Med.* **3,** 135 (2015).

229. Liu, Q. *et al.* Developing irreversible inhibitors of the protein kinase cysteinome. *Chem. Biol.* **20,** 146–159 (2013).

230. Zhang, T. *et al.* Discovery of potent and selective covalent inhibitors of JNK. *Chem. Biol.* **19,** 140–154 (2012).

231. Chuang, J. C. & Neal, J. W. Crizotinib as first line therapy for advanced ALK-positive non-small cell lung cancers. *Transl. Lung Cancer Res.* **4,** 639–641 (2015).

232. Zou, H. Y. *et al.* An orally available small-molecule inhibitor of c-Met, PF-2341066, exhibits cytoreductive antitumor efficacy through antiproliferative and antiangiogenic mechanisms. *Cancer Res.* **67,** 4408–4417 (2007).

233. Yu, P. B. *et al.* Dorsomorphin inhibits BMP signals required for embryogenesis and iron metabolism. *Nat. Chem. Biol.* **4,** 33–41 (2008).

234. Colecchia, D. *et al.* MAPK15/ERK8 stimulates autophagy by interacting with LC3 and GABARAP proteins. *Autophagy* **8,** 1724–1740 (2012).

235. Colecchia, D. *et al.* MAPK15 mediates BCR-ABL1-induced autophagy and regulates oncogene-dependent cell proliferation and tumor formation. *Autophagy* **11,** 1790–1802 (2015).

236. McCormick, F. The Selective Protein Kinase C Inhibitor, Ro-31-8220, Inhibits Mitogen-activated Protein Kinase Phosphatase-1 (MKP-1) Expression, Induces c-Jun Expression, and Activates Jun N-terminal Kinase. *J. Biol. Chem.* **271,** 27018–27024 (1996).

237. Caligiuri, M. *et al.* A proteome-wide CDK/CRK-specific kinase inhibitor promotes tumor cell death in the absence of cell cycle progression. *Chem. Biol.* **12,** 1103–1115 (2005).

238. Bollacke, A., Nienberg, C., Le Borgne, M. & Jose, J. Toward selective CK2alpha and CK2alpha' inhibitors: Development of a novel whole-cell kinase assay by Autodisplay of catalytic CK2alpha'. *J. Pharm. Biomed. Anal.* **121,** 253–260 (2016).

239. Pagano, M. A. *et al.* The selectivity of inhibitors of protein kinase CK2: an update. *Biochem. J.* **415,** 353–365 (2008).

11 Acknowledgements (Danksagung)

Ich danke Herrn Professor Doktor Waldmann für die Möglichkeit meine Promotion unter seiner Betreuung durchführen zu dürfen, für das ausgezeichnete Arbeitsumfeld und die gewährte Freiheit bezüglich der wissenschaftlichen Herausforderungen. Damit verbunden danke ich ihm für alles was ich in den letzten Jahren lernen konnte.
Herrn Professor Doktor Martin Engelhard danke ich für die Übernahme des Koreferats.
Ein Dank geht auch an Frau Doktor Slava Ziegler, die mir in vielen Gesprächen hilfreiche Denkanstöße gab. Herrn Doktor Yaowen Wu, Herrn Professor Doktor Rauh und Herr Doktor Georgios Konstantinidis danke ich für die erfolgreiche Zusammenarbeit. Frau Doktor Petra Janning und dem gesamten MS-Team danke ich für die Durchführung zahlreicher Analysen, deren Auswertungen und die Diskussionen. Ein enormer Dank gilt auch Frau Doktor Sonja Sievers, Herrn Doktor Claude Ostermann und dem gesamten COMAS-Team für die Messung unzähliger niedermolekularer Verbindungen.
Herrn Professor Doktor Hiroyuki Osada, Herrn Doktor Nobumoto Watanabe, Herrn Doktor Yushi Futamura und Herrn Doktor Makoto Muroi möchte ich für herzliche Betreuung während meines Aufenthalts am RIKEN Center in Japan und die anschließende Zusammenarbeit danken.
Dem Böhringer Ingelheim Fonds möchte ich für die Finanzierung und insbesondere Frau Doktor Claudia Walther, Frau Doktor Anja Hoffmann und Sandra Schedler für die Betreuung danken.
Meinen Labor- und Bürokollegen, ebenso wie allen Arbeitskollegen am Max-Planck-Institut, möchte ich für die Unterstützung und die außerordentlich gute Arbeitsatmosphäre danken. Namentlich möchte ich dabei Michael Winzker, Doktor Philipp Küchler, Doktor Peter Schröder, Marjorie Rummelt, Janine Schulte-Zweckel, Sumersing Patil, Doktor Zhi-Jun Jia, Guillaume Garivet, Melanie Schwalfenberg, Doktor Shobhna Kapoor, Jens Warmers und Marvin von Kölln nennen.
Gesondert hervorzuheben ist mein Dank an Doktor Luca Laraia für seine unablässigen Ratschläge und die exzellente Zusammenarbeit.
Ein großer Dank außerhalb der Wissenschaftswelt gilt Morgane Louarn für die Hilfe und Inspiration an jedem einzelnen Tag der letzten Jahre.
Schlussendlich möchte ich meiner Familie für die Unterstützung während meiner letzten 27 Jahre danken.

12 Contributions

- All high content screenings for autophagy modulation, all ATP-Glo-based assays, the general/cytosolic ROS induction assay and the Glucose uptake inhibition measurement were performed by the compound management and screening center (COMAS), Dortmund.
- The induction of mitochondrial ROS was measured by Julian Wilken.
- All WST-1 assays were performed together with or by Dr. Luca Laraia, Postdoc at the MPI, Dortmund.
- All confocal microscopy-based experiments such as WIPI2b and LC3-mCherry-eGFP assays were performed by Dr. Georgios Konstantinidis, Postdoc at the CGC of the MPG, Dortmund.
- All CETSA, TPP and isothermal shift experiments were performed by Michael Winzker, doctoral student at the MPI, Dortmund.
- The incucyte-based analysis of cell death and apoptosis was performed and analysed together with or by Marjorie Rummelt and Dr. Luca Laraia, doctoral student and postdoc respectively, at the MPI, Dortmund.
- All MS/MS analyses were performed and analyzed by the MS-Team of the MPI Dortmund under guidance of Dr. Petra Janning.
- The proteomic profiling and the associated WST-8 assay and the analyses thereof were performed by Dr. Makoto Muroi and his team at RIKEN, Japan.
- All analyses measuring the effect on mitochondrial respiration were performed by Dr. Yushi Futamura and his team at RIKEN, Japan.
- All kinase profilings were outsourced and performed by external companies. Please refer to the respective section of the methods and reagents for further details.
- The first analogues and the mother compound of Autophinib were synthesized by the group of Prof. Dr. Daniel Rauh. Please refer to the synthesis section of the methods and reagents for further details. Please also refer to the following publication for more information: Richters, A. *et al.* Identification and further development of potent TBK1 inhibitors. *ACS Chem. Biol.* **10,** 289–298 (2015).
- All analogues of the dimethoxypyridine-based compound class, which are not shown in the synthesis part of the methods and reagent were synthesized and the synthetic route thereof developed by Dr. Peter Schröder. The synthetic procedure is described in Dr. Schröder's doctoral thesis. Please also refer to the following publication for more information: Schröder, P. *et al.* Neuritogenic militarinone-inspired 4-hydroxypyridones target the stress pathway kinase MAP4K4. *Angew. Chem. Int. Ed.* **54,** 12398–12403.

13 Curriculum Vitae (Lebenslauf)

Name	Lucas Robke
Date of birth	10.06.1990
Place of birth	Wuppertal (Germany)

Academic career

04/2014 – today	Max Planck Institute of Molecular Physiology, Dortmund PhD: Development and Target Identification of Small Molecule Autophagy Inhibitors
08/2013 – 03/2014	Technical University Dortmund Preparatory training for the fast-track PhD - GPA: 1,0
09/2010 – 07/2013	Technical University Dortmund Bachelor of Science Chemical Biology - GPA: 1,2

International experience

09/2016 – 12/2016	RIKEN Center for Sustainable Resource Sciene, Wako, Japan - Research stay
09/2013 – 12/2013	Hong Kong University of Science & Technology (HKUST) - Semester abroad

Internships & Social Engagement

08/2010 – 09/2010	Intern at Bayer Schering Pharma AG, Wuppertal
04/2010 – 08/2010	Intern at wppt:kommunikation GmbH, Wuppertal
02/2010 – 03/2010	Intern at August Pohli GmbH & Co. KG, Wuppertal
08/2009 – 01/2010	Voluntary social half-year at Johanniter-Unfall-Hilfe e.V, Wuppertal
12/2006	Intern at DuPont Performance Coatings GmbH & Co. KG, Wuppertal

Education

08/2000 – 08/2009	Gymnasium am Kothen, Wuppertal - University entrance diploma (Abitur)

14 Affidavit (Eidesstattliche Versicherung)

Robke, Lucas

Name, Vorname
(Surname, first name)

142003

Matrikel-Nr.
(Enrolment number)

Belehrung:
Wer vorsätzlich gegen eine die Täuschung über Prüfungsleistungen betreffende Regelung einer Hochschulprüfungsordnung verstößt, handelt ordnungswidrig. Die Ordnungswidrigkeit kann mit einer Geldbuße von bis zu 50.000,00 € geahndet werden. Zuständige Verwaltungsbehörde für die Verfolgung und Ahndung von Ordnungswidrigkeiten ist der Kanzler/die Kanzlerin der Technischen Universität Dortmund. Im Falle eines mehrfachen oder sonstigen schwerwiegenden Täuschungsversuches kann der Prüfling zudem exmatrikuliert werden, § 63 Abs. 5 Hochschulgesetz NRW.
Die Abgabe einer falschen Versicherung an Eides statt ist strafbar.
Wer vorsätzlich eine falsche Versicherung an Eides statt abgibt, kann mit einer Freiheitsstrafe bis zu drei Jahren oder mit Geldstrafe bestraft werden, § 156 StGB. Die fahrlässige Abgabe einer falschen Versicherung an Eides statt kann mit einer Freiheitsstrafe bis zu einem Jahr oder Geldstrafe bestraft werden, § 161 StGB.

Die oben stehende Belehrung habe ich zur Kenntnis genommen:

Official notification:
Any person who intentionally breaches any regulation of university examination regulations relating to deception in examination performance is acting improperly. This offence can be punished with a fine of up to EUR 50,000.00. The competent administrative authority for the pursuit and prosecution of offences of this type is the chancellor of the TU Dortmund University. In the case of multiple or other serious attempts at deception, the candidate can also be unenrolled, Section 63, paragraph 5 of the Universities Act of North Rhine-Westphalia.

The submission of a false affidavit is punishable.

Any person who intentionally submits a false affidavit can be punished with a prison sentence of up to three years or a fine, Section 156 of the Criminal Code. The negligent submission of a false affidavit can be punished with a prison sentence of up to one year or a fine, Section 161 of the Criminal Code.

I have taken note of the above official notification.

Dortmund,

Ort, Datum
(Place, date)

Unterschrift
(Signature)

Titel der Dissertation:
(Title of the thesis):

DEVELOPMENT AND TARGET IDENTIFICATION OF SMALL MOLECULE AUTOPHAGY INHIBITORS.

Ich versichere hiermit an Eides statt, dass ich die vorliegende Dissertation mit dem Titel selbstständig und ohne unzulässige fremde Hilfe angefertigt habe. Ich habe keine anderen als die angegebenen Quellen und Hilfsmittel benutzt sowie wörtliche und sinngemäße Zitate kenntlich gemacht.
Die Arbeit hat in gegenwärtiger oder in einer anderen Fassung weder der TU Dortmund noch einer anderen Hochschule im Zusammenhang mit einer staatlichen oder akademischen Prüfung vorgelegen.

I hereby swear that I have completed the present dissertation independently and without inadmissible external support. I have not used any sources or tools other than those indicated and have identified literal and analogous quotations.

The thesis in its current version or another version has not been presented to the TU Dortmund University or another university in connection with a state or academic examination.*

*Please be aware that solely the German version of the affidavit ("Eidesstattliche Versicherung") for the PhD thesis is the official and legally binding version.

Dortmund,

Ort, Datum
(Place, date)

Unterschrift
(Signature)